Texte

Texte
38
08
ISSN
1862-4804

National Implementation of the UNECE Convention on Long-range Transboundary Air Pollution (Effects)

Part 1: Deposition Loads: Methods, modelling and mapping results, trends

Umwelt Bundes Amt
Für Mensch und Umwelt

ENVIRONMENTAL RESEARCH OF THE
FEDERAL MINISTRY OF THE ENVIRONMENT,
NATURE CONSERVATION AND NUCLEAR SAFETY

Research Report 204 63 252
UBA-FB 001189E

Texte
38
08
ISSN
1862-4804

National Implementation of the UNECE Convention on Long-range Transboundary Air Pollution (Effects)

Part 1: Deposition Loads: Methods, modelling and mapping results, trends

by

Thomas Gauger[1,4], Hans-Dieter Haenel[1], Claus Rösemann[1], Ulrich Dämmgen[1], Albert Bleeker[2], Jan Willem Erisman[2], Alex T. Vermeulen[2], Martijn Schaap[3], R.M.A Timmermanns[3], Peter J. H. Builtjes[3], Jan H. Duyzer[3]

[1] Federal Agricultural Research Centre, Institute of Agroecology (FAL-AOE), Braunschweig

[2] Energy research Center of the Netherlands (ECN) - Biomass, Coal & Environmental Research, Air Quality & Climate Change, Petten, NL

[3] Netherlands Organisation for Applied Scientific Research (TNO-B&O), Department of Environmental Quality, Apeldoorn, NL

[4] Institute of Navigation, Universität Stuttgart (INS)

On behalf of the Federal Environmental Agency

This Publication is only available as Download under
http://www.umweltbundesamt.de

Publisher: Federal Environmental Agency (Umweltbundesamt)
P.O.B. 14 06
06813 Dessau-Roßlau
Tel.: +49-340-2103-0
Telefax: +49-340-2103 2285
Internet: http://www.umweltbundesamt.de

Edited by: Section II 4.3
Claudia Neumann

Dessau-Roßlau, September 2008

Contents

List of figures

List of tables

List of maps

1 Introduction

Thomas Gauger
Federal Agricultural Research Centre, Institute of Agroecology (FAL-AOE), Bundesallee 50, D-38116 Braunschweig
Bundesforschungsanstalt für Landwirtschaft, Institut für Agrarökologie (FAL-AOE), Bundesallee 50, 38116 Braunschweig

The research project "National Implementation of the UNECE Convention on Long-range Trans-boundary Air Pollution (Effects): ICP Modelling&Mapping NFC; Heavy Metals (Critical Loads, Deposition); Nitrogen + Acidity (Deposition); Nitrogen (Effects); Material Corrosion; Critical Ozone fluxes" (BMU/UBA FE-No. 204 63 252) is carried out on behalf of Federal Environment Agency, Dessau (Umweltbundesamt, UBA). The aim of the project is to support the German Federal Environmental Agency in calculation and verification of national data to be implemented in European scale Critical Loads and Levels maps. Special interest is put on the detection of long term trends in deposition loads and concentration of air pollutants in Germany, and on risk assessment describing the (potential) effects caused by anthropogenic emission. The results of this research project are gained by working in close co-operation with

(1) Gesellschaft für Ökosystemanalyse und Umweltdatenmanagement mbH (ÖKO-DATA GmbH) located in Strausberg, Germany
(2) Netherlands Organization for Applied Scientific Research (TNO), Institute of Environmental Sciences, Energy Research and Process Innovation (TNO-MEP), Appeldoorn, the Neterlands, and
(3) Netherlands Energy Research Foundation (ECN), Petten, the Netherlands.
(4) Moreover, the part of this project, which is dealing with material corrosion, was carried out in co-operation with Geotechnik Südwest, Bietigheim-Bissingen, Germany.

Within the project national high resolution maps of air concentration levels and deposition loads are generated. The maps are used to calculate exceedances of scientifically derived thresholds, aimed to protect different receptors, the Critical Loads and Critical Levels, respectively, in Germany. The calculation of the maps is based upon measurement network data, additional model estimates and high resolution land use maps. Differences of air pollutant input to several receptors, ecosystems and constructive materials, respectively, on the local scale can be identified and exceedances of Critical Levels and Critical Loads within different regions in Germany are determined.

Moreover time-rows of pollutant maps, or the presentation of an early and a later year, are generated in order to monitor the effects of emission reduction over time and horizontally over Germany. From this ecosystem specific longer-term trends of air pollutants and exceedances, and hence the effect of emission reduction on the receptor level can be derived.

The International Co-operative Programme on Modelling and Mapping of Critical Loads & Levels and Air Pollution Effects, Risks and Trends (ICP Modelling and Mapping), formerly Task Force on Mapping, founded in 1988 under the leadership of the Federal Republic of Germany, has developed an effects-based approach. The concept of critical loads and levels as an effects-based approach allows to monitor, map and evaluate the concentrations and loads of pollutants under various chemical parameters and biological conditions. The critical loads and levels are scientifically derived thresholds, aimed to protect different receptors (ICP Modelling and Mapping, 2002).

The Critical Loads and Levels concept has been successfully applied to strategies for emission reductions under two protocols of the UN/ECE Convention on Long-range Transboundary Air Pollution (CLRTAP, Geneva, 1979): the 1994 Protocol on Further Reductions of Sulphur Emissions and the 1999 Gothenburg-Protocol to Abate Acidification, Eutrophication and Ground-level Ozone ('multi-pollutant/multi-effect protocol'). The 1999 Gothenburg-Protocol for the first time sets the critical loads for acidity, nutrient nitrogen and critical levels or national ambient air quality standards for ozone as emission reduction targets (ICP Modelling and Mapping, 2002). Article 1 of the Gothenburg Protocol defines the terms "Critical Load" and "Critical Levels":

- "Critical load" means a quantitative estimate of an exposure to one or more pollutants below which significant harmful effects on specified sensitive elements of the environment do not occur, according to present knowledge.
- "Critical levels" mean concentrations of pollutants in the atmosphere above which direct adverse effects on receptors, such as human beings, plants, ecosystems or materials, may occur, according to present knowledge.

Objectives of the ICP Modelling and Mapping among others are to

- support the Working Group on Effects (WGE) and the Convention (CLRTAP) by preparing, reviewing and assessing critical load and level maps and by performing data quality control
- continuously update the critical loads and levels methodologies; maintain and update existing data bases
- disseminate information and provide assistance for interpretation and use of critical load and level maps.

In order to provide scientific and technical assistance to the ICP Modelling and Mapping, a Coordination Center for Effects (CCE) was established at the National Institute of Public Health and the Environment (RIVM) in Bilthoven, The Netherlands. The CCE solicits and co-ordinates the data of the 26 participating countries (ICP Modelling and Mapping, 2002; CCE, 2007, http://www.mnp.nl/cce/links/).

On the national scale this research and development is co-ordinated by the National Focal Centers (NFC). The NFC Mapping Germany is established at Federal Environment Agency (Umweltbundesamt), Berlin, its collaborating institutions are ÖKO-DATA, Strausberg, and INS (Institute of Navigation, Universität Stuttgart) (CCE, 2008, http://www.mnp.nl/cce/Images/NFC's13.03.08_tcm42-49654.pdf), from 2003 to 2007 FAL-AOE, Braunschweig (CCE, 2005), respectively.

The outline of the methodologies of modelling and mapping air concentration, total deposition, critical levels and loads was published in the Manual on Methodologies and Criteria for Mapping Critical Levels/Loads ('Mapping Manual', UBA 1996, ICP Modelling and Mapping 2004). The publication of the latest updated and revised version of the Mapping Manual, including several new developments and applications found on the base of international scientific discussion and experiences, is downloadable at ICP Modelling and Mapping web site (http://www.icpmapping.org/). The Mapping Manual and its updates are basic orientation for the work carried out within this project.

The scope of this research and development project is the effect oriented mapping of

- actual high resolution air concentration fields for the years 2000 to 2004 derived from measurements of sulphur dioxide (SO_2), nitrogen oxides (NO, NO_2, and NO_X), and ozone (O_3). Due to the lack of measurements NH_X is not included
- SO_2, NO, NO_2, NO_X, and O_3critical level exceedances for ecosystems (vegetation, lichens, forests, crops, and seminatural vegetation) in Germany (2000 to 2004)
- high resolution receptor specific total deposition fields of heavy metals, base cations, acidifying and eutrophicating compounds in Germany (1995, 1997, and 1999 to 2004), used as input for ecosystem specific calculations of critical loads and critical loads exceedances
- actual corrosion rates for constructive materials (1990 and 2000) in Germany, the Czech Republic, and Switzerland, and in the metropolitan areas of Berlin/Brandenburg, Milano/Lombardia, Paris/Île de France, and Vienna/Niederösterreich

Furthermore the work of the German National Focal Center (NFC) for ICP Modelling & Mapping under the LRTAP Convention is supported by

- calculating critical loads and exceedances for eutrophication and acidification (nitrogen and sulphur) using the simple mass balance approach

The Expert Panel for Heavy Metals (EP-HM) is supported by

- coordination of the work of EP-HM, development of methods and recommendations for ICP Modelling & Mapping
- finalising the respective heavy metal chapter in the Modelling and Mapping Manual
- supporting of the CCE call for data on Critical Loads for heavy metals (Cd, Pb, Hg)
- calculation of the German data set of Critical Loads of the hevy metals, and of Critical Load exceedances for Cd, Pb, and Hg

The implementation of biodiversity aspects using the BERN-Model (Bioindication for Ecosystem Regeneration towards Natural conditions) was carried out, and linked to dynamic modelling of critical loads.

Dynamic modelling of nitrogen and acidifying compounds was further developed and applied.

Emission, in-air transport and conversion of pollutants, air concentration, removal from the atmosphere ('total deposition') by in-cloud scavenging of air pollutants and below cloud scavenging ('wet deposition'), by direct deposition of particles and gases to terrestrial surfaces ('dry deposition'), or direct capture of cloud and/or fog droplets containing airborne pollutants by receptor surfaces ('cloud&fog deposition'), in principle can all be measured directly at certain sample points. There are different measurement networks spread over Germany, where basic measurands are quantified routinely. Additionally applied model calculations can generate fields of atmospheric conditions, atmospheric processes and atmospheric fluxes from basic measurement and successively modelled data.

Within this research and development project the whole chain of processes from emission of air pollutants to estimates of their effects on the receptor level is covered. Whenever possible, however, directly measured data are used as input for mapping and modelling, or for validation of model results.

Air pollution levels and loads as well as critical levels and loads need to be mapped in order to implement regionalized emission control strategies based on a cost-effective minimisation of effects. The risk of damage to ecosystems by air pollutants is determined neither by actual pollutant air concentrations or total deposition fluxes alone, nor by critical levels or critical loads alone. It is determined by the difference between actual and critical values, which is termed exceedance of critical levels and loads (UBA, 1996; Spranger et al. 2001).

Actual air pollutants, receptors and critical levels and loads are conveniently represented on maps (Figure 1.1). This allows the quantification of combined effects of receptor and/or ecosystem specific factors in relation to current pollutant inputs in their spatial distribution.

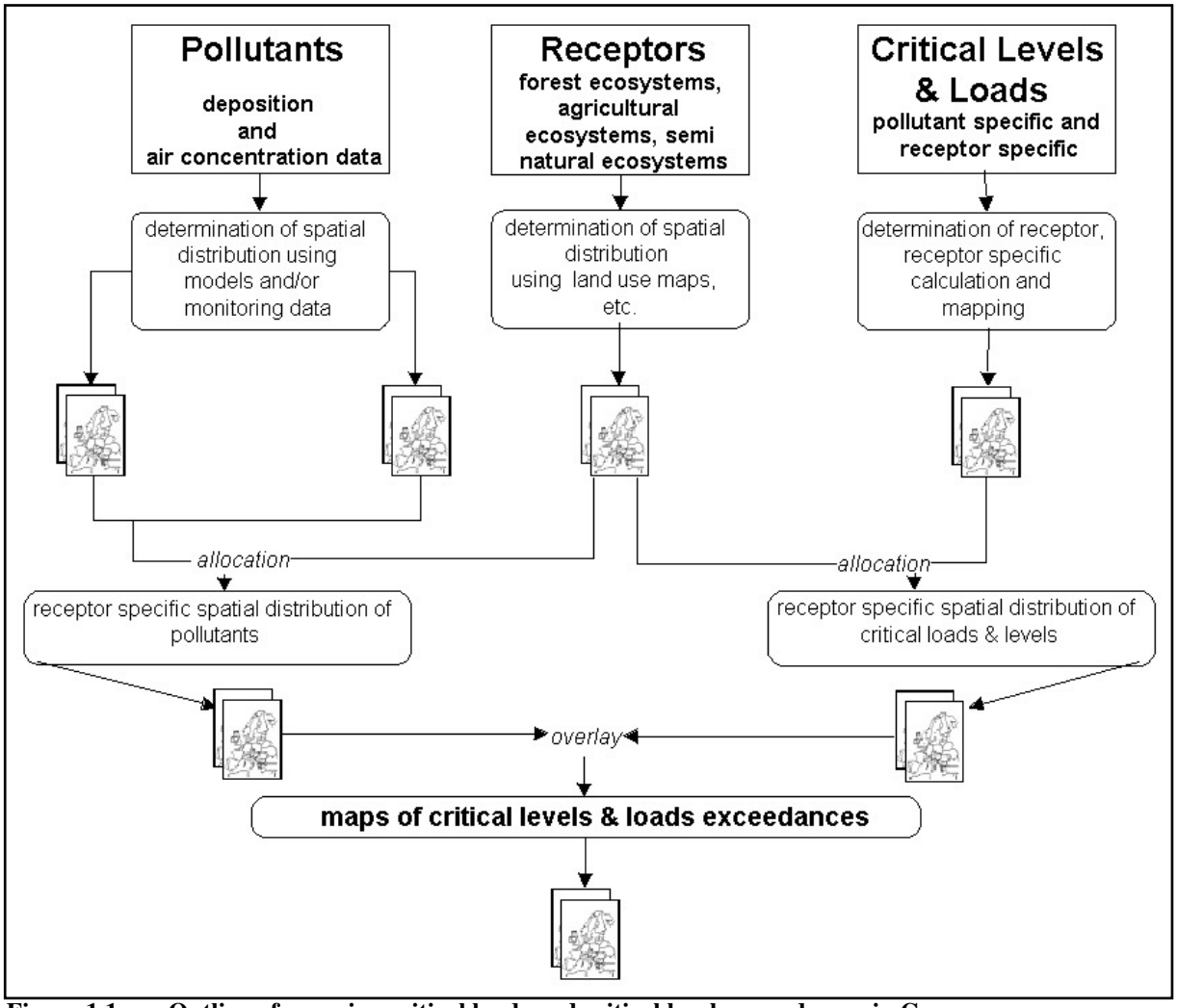

Figure 1.1: Outline of mapping critical loads and critical levels exceedances in Germany

The work carried out in this joint research and development project of FAL-AOE and the sub-contractors ECN, TNO-MEP, ÖKO-DATA, and the co-operation partner Geotechnik Südwest in particular were:

at FAL-AOE, Braunschweig:

Co-ordination of the project and data fluxes

- the co-ordination of the work of the project partners, including data transfer within the project; organisation and presentation of project meetings (July 6th 2005 in Amsterdam, NL; both May 4th to 5th 2006, and December 14th to 15th 2006 in Braunschweig); reporting and permanent contact to Federal Environmental Agency (UBA)
- the support of Federal Environmental Agency (UBA) by:
  - providing data and information needed at UBA or in parallel projects carried out on behalf of UBA
  - providing data and information to other scientific and governmental institutions
  - participating in national and international expert work group sessions and workshops including oral and poster presentations of methods and interim results
- co-ordination and compilation of the final report of the project

Deposition loads

- update of INS/FAL/UBA wet deposition database, including quality checks and preparation (pre-processing) of input data for mapping wet deposition
- update of DWD high resolution data sets of annual precipitation, relative humidity, and temperature via UBA (FG. II 5.2)
- mapping annual wet deposition fields of SO_4-S, NO_3-N, NH_4-N, K, Ca, Mg, Na, Cl, and H for the years 1987 to 2004; calculation of preliminary annual maps of wet deposition fields of Cd and Pb 1994 to 2004
- investigation of errors and uncertainties of wet deposition maps and calculation of map statistics and trends of wet deposition in Germany
- canopy budget model calculations used for validation of the mapping results of dry and total deposition, transfer of data from FAL-AOE to ECN
- calculation of dry deposition map statistics and trends of dry deposition in Germany
- calculation of occult (cloud&fog) deposition map statistics and trends of occult deposition in Germany
- calculation of total deposition fluxes from wet, dry, and occult deposition fluxes, map statistics and trends of total deposition in Germany
- comparison of deposition mapping results with EMEP model estimates
- deposition data transfer to ÖKO-DATA for critical loads and exceedance calculations

Air concentration and critical level exceedance

- update of UBA/INS/FAL air concentration database, provided by UBA Fg. II 4.2
- classification of air concentration monitoring sites, mapping air concentration fields of O_3, SO_2, NO, NO_2 and mapping of critical level exceedances for SO_2, NO_X, O_3 (excluding NH_X due to lack of data)
- calculation of critical level exceedances for ecosystems (vegetation, lichens, forests, crops, and seminatural vegetation) in Germany (2000 to 2004), including modified level I AOT40 for ozone due to changes in the revised Modelling and Mapping Manual
- calculation of map statistics and trends in air concentration and critical levels exceedance over Germany
- providing SO_2 air concentration measurement data to TNO in order to compare it to LOTOS-EUROS model estimates

Material corrosion

- primary input and pre-processing of data for dose-response functions
  - data acquisition of meteorological parameters and pre-processing of the data for the years 1990 and 2000: precipitation data [annual mean in l m^{-2}, raster data], temperature [annual mean in °C, raster data], relative humidity [annual mean in %, raster data]
  - data acquisition of air concentration and concentration in precipitation parameters and pre-processing of the data for the years 1990 and 2000: concentration in precipitation of H^+ [point data at monitoring sites interpolated using kriging technique, annual raster data in mg l^{-1}], air concentration of SO_2, O_3, NO_2 [point data at monitoring sites interpolated using kriging technique, annual mean raster data in µg m^{-3}]
  - data retrieval at EMEP (WebDab download at http://webdab.emep.int/Unified_Model_Results/; EMEP Status Report 1/03 data) for PM_{10} [EMEP modelled annual mean raster data in µg m^{-3}], pre-processing for the years 1990 and 2000
  - data retrieval of NERI modelled data of NO_2 [annual mean raster data in µg m^{-3}] from the previous project (BMU/UBA 299 42 210, Gauger et al. 2002), pre-processing for the years 1990 and 2000
  - retrieval of data covering the area of Switzerland (data delivery by FOEN/Meteotest in 2005) and the Chech Republik (data delivery by CEI/CHMI in 2005)
  - data retrieval for the urban agglomerations of Milan/Lombardy (data delivered by ENEA, 2006), Paris/Île de France (data delivered by LISA, 2006), and Vienna/Lower Austria (annual data reports downloaded from from Vienna at http://www.magwien.gv.at/ma22/luftgue.html, from Umweltbundesamt at http://www.umweltbundesamt.at/umweltschutz/luft/luftguete_aktuell/jahresberichte/, and data downloaded from EEA ETC/ACC AirView at http://airview.mnp.nl/etc-acc/appletstart.html)
- calculation of actual corrosion in the year 1990 and 2000 for the areas of Germany, Switzerland and the Czech Republic, and for the urban agglomeration areas of Berlin/Brandenburg, Milan/Lombardy, Paris/Île de France, and Vienna/Lower Austria for the materials carbon steel, zinc, cast bronze, copper, and Portland limestone
- joint activity between D, CZ, CH, I, F, A; co-operation in mapping with Geotechnik Südwest (see below)

at ECN, Petten:

- update and thorough modification of the IDEM/FACEM model parameterisation modules due to the findings in the previous project (BMU/UBA FE-No. 299 42 210, Gauger et al 2002)
- retrival and update of meteorological input data and pre-processing
- transfer of LOTOS-EUROS modelled air concentration data for 1995, 1997, and 1999 to 2004 from TNO to ECN
- recalculation of dry deposition from the previous project, comparison of mapping and modelling results
- pre-processing of air concentration data sets and use as input for IDEM/FACEM model calculations
- modelling of dry deposition 1995, 1997, and 1999 to 2004 of nitrogen, acidifying compounds, heavy metals, and base cations in Germany
- generation of land use specific maps (receptor specific deposition maps) for 9 land use classes
- preliminary modelling of occult (cloud&fog) deposition 1995, 1997, and 1999 to 2004
- programming of a map and data viewer for Germany
- modelling of dry deposition point data (at forest stands)
- canopy budget model calculations used for validation of the mapping results of dry and total deposition
- reporting

at TNO-MEP, Apeldoorn:

- developments to the model code of LOTOS-EUROS modelling system, as inclusion of a 25m surface layer, and an update of the parameterisation of the dry deposition

- data retrieval (meteorology, emission inventories of SO_x, NO_x, NM-VOC, CO, CH_4, NH_3, land use), pre-processing and use as input to LOTOS-EUROS calculations of air concentraton for acidifying compounds,
- modelling distributions of acidifying components over Europe and Germany in order to derive air concentration fields for 1995, 1997 and 1999 t/m 2004
- generating files with 3 hourly data by sampling the results of the model calculations and data transfer of modelled fields for 1995, 1997 and 1999 t/m 2004 to ECN for deposition calculations
- data validation by comparing the modelled concentrations to observations in Germany and the rest of Europe
- developing the code to perform simulations for lead and cadmium with LOTOS-EUROS
- annual mean distributions of air concentration for lead and cadmium are calculated using the LOTOS-EUROS model
- lead and cadmium concentrations are compared with observed concentrations and to results with ESPREME emissions
- made a considerable effort to incorporate soil derived base cations into the modelling system. Estimates for anthropogenic emissions and an emission module for wind-generated emissions from bare soil have been implemented and are ready to contribute to a future exercise
- reporting

at ÖKO-DATA, Strausberg:

- supporting the Federal Environment Agency (UBA) in all aspects of the actual work according to the medium term work plan of the UNECE Working Group on Effects (WGE) as the support by the German National Focal Centre (NFC) of ICP Modelling and Mapping is concerned, as among others support in organising workshops, co-ordination of updates of the Mapping Manual, regular updates ICP Modelling and Mapping internet presentation co-ordination of internatiomal expert groups, analysis of guidelines (CAFE Strategy, NEC), deduction of recommendations, etc.
- actualisation of the German Critical Load data base (SMB, dynamic modelling), modelling and mapping Critical Loads and exceedances, data delivery to the CCE (calls for data in 2004 to 2007)
- transfer of available data of wet, dry and total deposition estimates from FAL-AOE to ÖKO-DATA for critical loads and exceedance calculations
- calculation of trends to derive estimates of the dynamics in deposition abatement affecting critical loads and exceedance calculation results
- co-ordination of the work on Critical Loads/Limits for heavy metals, further development of methods, calculation of national data sets (Cd, Pb, Hg), risk assessment
- test and application of dynamic models, model comparisons, data retrieval and target load calculations and compilation of national data sets, reporting and data delivery to CCE
- further development of the capabilities and application of the BERN model (Biodiversity)
- participating in national and international expert work group sessions and workshops including oral and poster presentations of methods, data and interim results
- reporting

Co-operation with Geotechnik Südwest, Bietigheim-Bissingen:

Within this research project a close co-operation on the work carried out with respect to mapping of corrosion of materials by airpollutants between FAL-AOE and Geotechnik Südwest, Bietigheim-Bissingen was established in order to assist UBA in compilation of results concered with testing of dose-reponse functions and mapping of risk of material corrosion over time in different spatial scale. The cooperation mainly consisted in:

- transfer of available input data for dose-response functions used as input for mapping material corrosion in the scale of Central Europe (Germany, Chech Republic, Swizerland) and for urban agglomerations (Berlin, Paris, Vienna)
- compilation of data for 1990 and 2000, analysis of data and interpretation of mapping results, and reporting

2 Deposition of air pollutants used as input for critical loads exceedance calculations

Thomas Gauger
Federal Agricultural Research Centre, Institute of Agroecology (FAL-AOE), Bundesallee 50, D-38116 Braunschweig
Bundesforschungsanstalt für Landwirtschaft, Institut für Agrarökologie (FAL-AOE), Bundesallee 50, 38116 Braunschweig

In this chapter only a very brief overview is given on critical loads exceedance calculation in order to illustrate the use of deposition estimates within the critical load concept. Detailes and periodically actualised information on the whole context is given in the Mapping Manual (ICP MODELLING & MAPPING 2004). The extensive description of actual critical loads and exceedance calculation is pesented by NAGEL ET AL. 2008 in Part 2 of this report.

The application of the critical load concept is suitable to describe the threshold below which present loads have to be reduced for ecosystem recovery. By definition, the threshold values are measurable quantitative estimates showing the degree of tolerable exposure to one or more pollutants. These scientifically derived values reflect the state of present knowledge and are subject to revisions as science develops further.

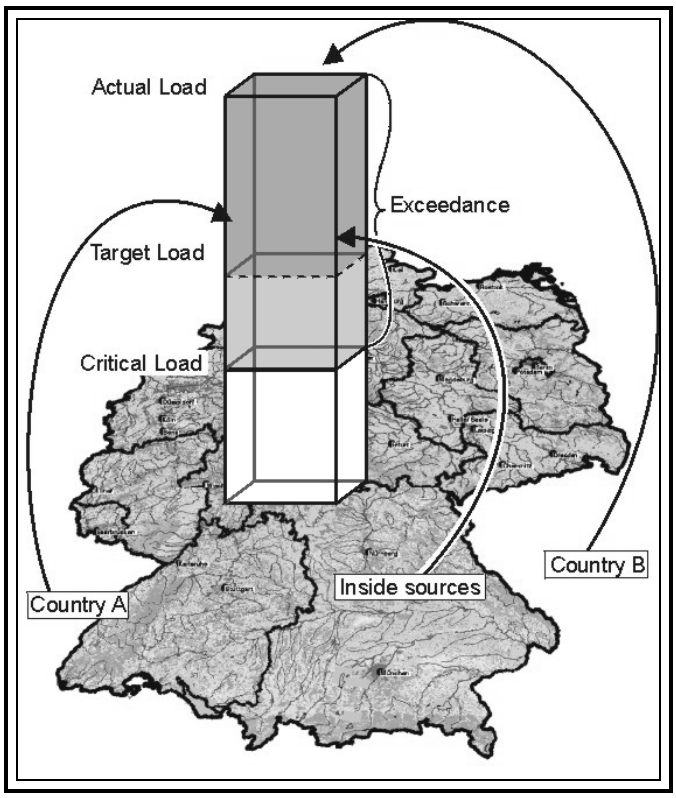

Figure 2.1: Illustration of the critical loads concept (ICP Modelling & Mapping 2002)

Figure 2.1 illustrates the concept on the example of Germany representing a 'receptor'. The arrows stand for the transport of transboundary and inland emitted pollutants, which are deposited into the receptor system (actual load). The column is showing the critical load value in its bottom part. Preliminary emission reduction ceilings (termed 'target load' in Figure 2.1) are standing for a percentage reduction towards achieving critical loads ('gap-closure'). Exceedance is the difference between critical load and actual deposition load. The critical loads represent tolerable, long-term deposition rates of pollutants that do not harm structure and function of ecosystems.

Potential acidifying compounds are mainly emitted as primary gases (SO_2, NO, NO_2, NH_3, HCl). During in-air transport they are chemically converted by oxidation and neurtalisation processes into gaseous acids (HNO_3, H_2SO_4) and are forming secondary particles (e.g. droplets containing HNO_3, particulate SO_4, NH_4NO_3, NH_4Cl, $(NH_4)_2SO_4$, etc.). Once deposited into ecosystems, compounds of sulfur (SO_4-S), oxidised and reduced nitrogen (NO_3-N and NH_4-N, respectively) again are coverted. In the soil acidification process acid deposition provides mobile SO_4^{2-} and NO_3^- anions and a source of protons, which can exchange base cations. Deposition of 1 mol NO_Y equals the release of 1 mol H^+ in the soil, per mol SO_X the release of 2 mol H^+ is accounted for. Nitrogen, deposited as compounds of NH_3-N, NH_4-N, and NO_3-N, has direct and indirect acidifying effects due to nitrogen

transformations in the soil. Assuming that NH_X-N on the long run will completely be nitrified, the release of 1 mol H^+ per mol NH_X in the soil is accounted for. The acidity arising from oxidation processes also happens when emitted gases are deposited on exposed receptor surfaces (vegetation, soil, water, etc.). Moreover gaseous NH_3 is taken up and metabolised by plants, which also sets one hydrogen ion per NH_3 ion free. The contribution of HCl, mainly emitted from coal combustion, is very small compared to S and N compounds and only of local concern.

Acidification hence generally occurs due to the total deposition of sulphur (S) and nitrogen (N) compounds, resulting in destabilisation of soil processes or to direct vegetation damage. Significant damage can be expected to develop when certain chemical parameters of the soil solution, such as base cations, show a marked deviation from the steady-state conditions. The release of heavy metals and aluminium may increase the negative effects of acidification. Eutrophication will occur when nitrogen (N) inputs result in nutrient imbalances. The ecosystem then more likely is affected by climatic and other stresses, and eutrophication often affects the biodiversity of terrestrial and aquatic ecosystems because existing plant and animal communities are unable to adapt to the changes in chemical conditions.

The magnitude of any critical load depends on the structural and functional (geological, hydrological, pedological, biological, economical and ecological) factors and properties of the target ecosystem and receptor respectively, tat builds up the pollution load capacity at a given location. Thus, critical loads are different for each plant community, forest and soil type, climatic condition, etc.

Receptors (c.f. Map 2.1) for critical loads in this project are terrestrial ecosystems, including forests, and (semi-) natural vegetation, covering about 30% of Germany. Mapping of critical loads and their exceedance in Germany is carried out using the 'Level I' or mass-balance approach: A simple mass balance ('SMB') is used to calculate critical loads for acidity and nutrient nitrogen (Figure 2.2).

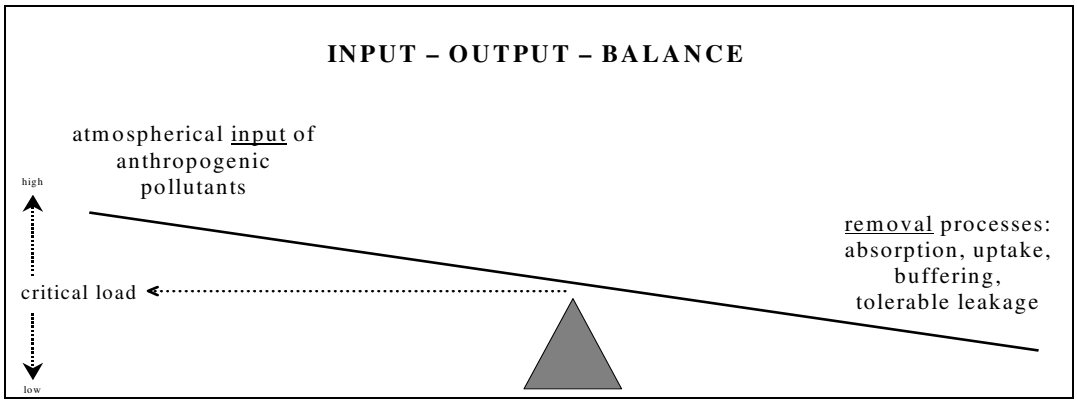

Figure 2.2: Application of a simple quantitative mass balance to derive critical loads

Critical loads for each ecosystem are determined using a simple quantitative mass balance method, where the balance is calculated between the mainly anthropogenic inputs of pollutants (sources) on the one side, and removal processes (sinks) on the other side, which consist in absorption, uptake, buffering or tolerable transfer into other environmental compartments. The critical load for potential acidity ($CL_{(ACpot)}$, Equation (2.1) is set where the acid input can be neutralised by the total acid neutralisation capacity (ANC) of the ecosystem:

$$CL_{(AC_{pot})} = BC_w - BC_u + N_i + N_u + N_{de} - ANC_{le(crit)} \text{ [eq ha}^{-1}\text{ a}^{-1}\text{]} \quad (2.1)$$

where:

$CL_{(ACpot)}$	=	critical load for potential acidity
BC_w	=	base cations weathering derived from soil type and parent material class
BC_u	=	base cations uptake and removal by biomass under steady state conditions
N_i	=	long-term nitrogen immobilisation
N_u	=	nitrogen uptake and removal by biomass under steady state conditions
N_{de}	=	denitrification rate
$ANC_{le(crit)}$	=	acceptable leaching of acid neutralisation capacity

Critical loads for nutrient nitrogen ($CL_{nut(N)}$) are determined by the given properties of the ecosystems. The maximum tolerable deposition (critical load) of nitrogen again is calculated at equilibrium between input and removal. Temporary deviations from equilibrium only are tolerable as long as the ecosystem is capable of recovering (steady state condition). Equation (2.2) shows the nitrogen cycle of terrestrial ecosystems on these terms:

$$CL_{nut}(N) = N_u + N_i + N_{le(acc)} + N_{de} \text{ [eq ha}^{-1}\text{ a}^{-1}\text{]} \quad (2.2)$$

where:

$CL_{nut}(N)$	=	critical load for nutrient nitrogen
N_u	=	nitrogen uptake and removal by biomass under steady state conditions
N_i	=	long-term nitrogen immobilisation
$N_{le(acc)}$	=	acceptable leaching of nitrogen
N_{de}	=	denitrification rate

Details on the equations can be found in the 'Mapping Manual' (ICP Modelling & Mapping 2004) and in NAGEL & GREGOR (1999). The methods applied and current (preliminary) critical loads maps of Germany can be found in the CCE status reports (e.g. CCE, 2007) and in national reports (e.g. NAGEL ET AL. 2008 in Part 2 of this report), respectively.

The comparison of critical loads maps, calculated for a certain receptor-pollutant combination, with current deposition loads of the pollutant provides critical loads exceedance maps. To derive the exceedance of critical loads of nitrogen, $CL_{nut}(N)$ (Equation (2.2)) the difference to total depositions of nitrogen, N_{dep} (Equation (2.3)) is calculated. The exceedance of critical loads of potential acidity is calculated as difference of $CL_{(ACpot)}$ (Equation (2.1)) and total deposition of potential acidity, $AC_{(pot)dep}$ (Eqation. (2.4)).

$$N_{dep} = NO_{ydep} + NH_{xdep} \text{ [eq ha}^{-1}\text{ a}^{-1}\text{]} \quad (2.3)$$

$$AC_{(pot)dep} = (SO_{X(nss)dep} + N_{dep} + Cl_{(nss)dep}) - (Ca_{(nss)dep} + Mg_{(nss)dep} + K_{(nss)dep}) \text{ [eq ha}^{-1}\text{ a}^{-1}\text{]} \quad (2.4)$$

where:

$SO_{X\,(nss)dep}$	=	total deposition of non-sea-salt oxidised sulphur compounds (SO_2, SO_4^{2-})
NO_{Ydep}	=	total deposition of oxidised nitrogen compounds (NO, NO_2, HNO_3, NO_3)
NH_{Xdep}	=	total deposition of reduced nitrogen compounds (NH_3, NH_4^+)
N_{dep}	=	total deposition of nitrogen compounds (NO_{ydep} + NH_{xdep})
$Cl_{(nss)dep}$	=	wet deposition of non-sea-salt chloride (Cl^-)
$Ca_{(nss)dep}$	=	total deposition of non-sea-salt calcium (Ca^{2+})
$Mg_{(nss)dep}$	=	total deposition of non-sea-salt magnesium (Mg^{2+})
$K_{(nss)dep}$	=	total deposition of non-sea-salt potassium (K^+)

In the definition of $\boldsymbol{AC_{(pot)dep}}$ the following **basic assumptions** are made:

- Several oxidative processes, mainly due to fossil fuel combustion, are underlying the acidifying effects of airborne sulphur and nitrogen. The products of in-air chemical reaction are deposited and taken up by the soil e.g. in form of nitric and sulphuric acid. The deposition of 1 mol of oxidised nitrogen (NO_Y) is set equal to 1 mol H^+, the deposition of 1 mol of oxidised sulphur (SO_X) is set equal to 2mol H^+.
- Within the frame of the critical loads concept it is assumed, that on the long run all reduced nitrogen input (NH_X) is completely nitrified and exported from the ecosystem as nitrate (NO_3^-), thereby acidifying the system. Thus, with respect to soil acidification, a net-production of 1mol H^+ per 1mol NH_X is assumed.
- The anthropogenic chloride mainly are emitted as hydrochloric acid (HCl) and equal 1 mol H^+ per 1 mol of deposited chloride (Cl^-). However, the quantitatively most important natural source of deposited Cl^- is sea spray. Emission abatement of course aims at man-made emission. Moreover it can be assumed that all sea salt input is chemically neutral. Deposition originating from sea spray therefore is quantified by assuming that the ratio of Ca^{2+}, K^+, Mg^{2+}, SO_4^{2-} and Cl^- to sodium (Na^+) in bulk sea water is the same as in sea spray and all Na is of marine origin. It then is possible to correct the deposition for the sea-salt contribution accordingly (see Chapter 4.3.1). These corrected deposition values are attributable to predominantly anthropogenic sources and termed 'non-sea-salt' (e.g. $Cl_{(nss)}$). With respect to soil acidification it is assumed that 1 mol H^+ per 1 mol $Cl_{(nss)}$ is formed.
- The non-sea-salt deposition of the base cations calcium (Ca^{2+}), potassium (K^+), and magnesium (Mg^{2+}) – all Na^+ is assumed to be of sea spray origin and not taken into account (see above and Chapter 4.3.1) – are assumed to neutralise the input of potential acidity ($AC_{(pot)dep}$). Natural background deposition of base cations in principle should not be included here. The rates emission reduction of acidifying compounds, negotiated and decided upon within the frame of CLRTAP, is to be deduced from their acidifying effects alone and must not be compensated by other anthropogenic emissions (e.g. base compounds emitted by coal combustion).

Thus only the natural background deposition of base cations, which can be assumed as ecosystem property because it has certain continuity in time and space, may be charged up against potential acid deposition. Unfortunately there is no adequate application quantifying natural and anthropogenic rates of base cation deposition fluxes yet. The total deposition of non-sea-salt base cations (BC_{nss}) representing base cations attributable to natural *and* anthropogenic emission processes excluding neutral salts from sea spray therefore is used in this study to be charged up against potential acid deposition ($AC_{(pot)dep}$). The result is termed deposition of potential net acidity ($AC_{(pot)net}$).

The units used for deposition fluxes as well as for critical loads are ionic equivalents per hectare and year (eq ha^{-1} a^{-1}). The calculation on the base of ionic equivalents facilitates the direct comparison of deposited magnitudes of compounds and of their quantities e.g. with regard of the acid balance.

An important aspect – aside an exact definition of the compounds being processed – is the use of the same spatial geometry for mapping deposition and critical loads. Deposition fluxes as well as critical loads have to be related to the same area and to the same receptor. Calculations of critical loads in Germany presently are carried out for the receptor ecosystems: coniferous forests, deciduous forests and mixed forests, natural grassland, acid fens and heathland wet grassland and mesotrophic peat bogs respectively (Table 2.1). The minimum requirements for gathering receptor specific total deposition are spatial resolutions corresponding to the receptor map used for critical loads calculations and mapping.

Table 2.1: Receptors for critical loads calculations in Germany (CCE Status Report 2003)

Ecosystem type	Percentage of receptor area (total Germany = 100%)	Percentage of total considered receptor area
coniferous forest	16.1 %	53.6 %
deciduous forest	6.4 %	212 %
mixed forest	6.4 %	21.3 %
natural grassland	0.5 %	1.7 %
acid fens and heathland	0.3 %	0.9 %
wet grassland	0.1 %	0.3 %
mesotrophic peat bogs	0.3 %	0.9 %
total:	30 %	100 %

3 Methods applied for mapping total deposition loads

Thomas Gauger
Federal Agricultural Research Centre, Institute of Agroecology (FAL-AOE), Bundesallee 50, D-38116 Braunschweig
Bundesforschungsanstalt für Landwirtschaft, Institut für Agrarökologie (FAL-AOE), Bundesallee 50, 38116 Braunschweig

Detailed information on spatial variation of deposition and on ecosystems and their spatial distribution is needed to determine deposition fluxes on the ecosystem level. The three main different deposition processes of wet, dry and occult (cloud&fog) deposition contribute to total deposition fluxes. Total deposition is the sum of these three fluxes at a certain location. The magnitude of the contribution of each flux to total deposition is varying over time and geographical space, due to pollution gradients, variations in atmospherical properties and surface conditions.

- The removal of pollutants from the atmosphere via precipitation of rain and snow is termed **wet deposition**. The wet deposition process is mainly controlled by the concentration of the pollutants and the precipitation amount. The wet deposition amount is most independent from the structure and surface of the receptor. Briefly, at a given solute concentration, amount and intensity of precipitation, the magnitude of the wet deposition flux (the wet deposition load respectively) into a water surface will be the same as into e.g. a forested area. However, large-scale and regional scale gradients of wet deposition amounts over Germany can be found. The 'rain-out' of pollutants captured in rain droplets (in-cloud scavenging) and 'wash-out' of in-air pollutants by the falling rain (below cloud scavenging) are constitutive processes for measured solute concentrations in precipitation. Thus, by installation of monitoring networks of sufficient spread and density of sampling sites to cover the spatial gradients of variation in solute concentrations, maps of wet deposition fields can be interpolated from these measurements.

- The direct deposition of particles and gases on surfaces of terrestrial ecosystems including stomatal uptake into plant organs happening in periods without precipitation is termed **dry deposition**. Interactions between the receptor surfaces and airborne components strongly determine the load of dry deposition. The dry deposition processes are controlled by atmospheric conditions, the concentration of gaseous and particulate pollutants in ambient air as well as by the shape, area, roughness, and condition of the receptor's surface. There are only few sites in Germany where dry deposition is or was monitored routinely. Moreover the high variability of dry deposition fluxes in time and space does not allow spatial interpolation of measured values. However, the knowledge on deposition processes derived from measurements can be parameterised and is used in inferential deposition models, allowing the mapping of dry deposition fluxes.
- The flux of cloud and fog droplets to the receptor's surfaces in this study is termed occult deposition, or preferably **cloud&fog deposition**. Concentrations in cloud droplets depend on air concentrations of gases and aerosols and their scavenging ratios and have been found highly variable in space and time. Cloud&fog droplet deposition was found to contribute considerably to total deposition at hillsides of mountain regions in Germany (Bleeker et al. 2000).

Wet deposition is measured in local, regional and national monitoring networks in Germany. The wet deposition database which was set up by comprehensive data acquisition at the institutions responsible for the different monitoring programmes (see Chapter 4.1 for further details). The scatter and density of open field wet deposition measurements (Chapter 4.2.4) is appropriate to map the spatial trend of wet deposition fluxes over the area of Germany using kriging technique (see Chapter 4.3 for further details).

Estimates of total deposition into single forested areas may be derived by applying **canopy budget model** (termed **CBM** in this report) calculations (e.g. ULRICH 1983, ULRICH 1991; UBA 1996; DRAAIERS & ERISMAN 1995, DRAAIJERS ET AL. 1996B, DRAAIJERS ET AL. 1998; DE VRIES ET AL. 2001). Basic data in CBM calculations are open space wet deposition and parallel throughfall and stemflow measurements at single forest stand areas. In a CBM the effect of canopy exchange processes (canopy leaching and/or uptake) is accounted for, which is due to atmospheric input as well as to ecosystem properties. Because of inner ecosystem cycling the data of throughfall and stemflow measurements and hence CBM estimates of dry and total deposition are explicitly site specific. Long-term routine measurements of throughfall and stemflow data provided from the Bundesländer Forest Research Centres, from Water Management and Environmental Agencies, respectively, are integral part of INS/FAL/UBA deposition database (see Chapter 4.1).

Total deposition into forests is systematically higher than it is into other ecosystem types. This mainly is due to the structure (height, roughness, large surface area) of forest ecosystems which forms the so called 'filtering effect'. The magnitude of this 'filtering effect' also is conditioned by air pollutant concentrations and meteorological parameters (wind speed, humidity, time of wetness etc.). The spatial variability of these parameters is virtually independent from spatial distribution of land use and ecosystem structure as well as from the spatial patterns of wet deposition rates. The processes controlling the fluxes dry, cloud&fog droplet and wet deposition are virtually independent from each other over space and no constant linear relation between the respective fluxes can be derived. Thus it is strongly recommended not to use e.g. constant 'filtering factors' for total deposition mapping (LÖVBLAD et al. 1993, UBA 1996, NAGEL&GREGOR 1999).

Inferential deposition models are available (ICP Modelling & Mapping 2004), which are used to derive receptor soecific dry and cloud&fog droplet deposition fluxes from information on air concentration data, derived by **chmical transport models** (CTM) using emission inventory data. Both types of models are linked to meteorological data and ecosystem information in high spatial and time resolution, respectively. CTM are using those data for parameterisations of the dispersion, chemical reactions and transport from the emission source into the air. In inferential deposition modelling these data are used for parameterisations of the atmospheric deposition processes at the ecosystem level. However, open field wet deposition measurements, throughfall and stemflow data together with the results of CBM estimates of dry and total deposition, which are only valid for single forest locations, can be used for inferential model evaluation purposes.

In the **German approach mapping total deposition loads** the interpolation of wet deposition measurements to derive wet deposition fields is combined with small scale processing of receptor specific dry and cloud&fog droplet deposition by using the CTM LOTOS-EUROS and the inferential deposition models IDEM/FACEM (Figure 3.1). The application of inferential models using basic data of different scale (i.e. both LRT and small scale air concentration data, meteorological data in high time resolution, small scale emission inventories, small scale receptor information) combined with interpolated measurement data (small scale air concentration, precipitation data and wet deposition) is the most promising method to derive small scale total deposition and critical loads exceedance (UBA 1996, LÖVBLAD ET AL. 1993, ICP MODELLING&MAPPING 2004). Details of the calculation of wet deposition fields are given in Cchapter 4, descriptions on the application of IDEM/FACEM

model can be found in Chapter 6, and the description of modelling air concentration using LOTOS-EUROS is described in Chapter 10 of this report.

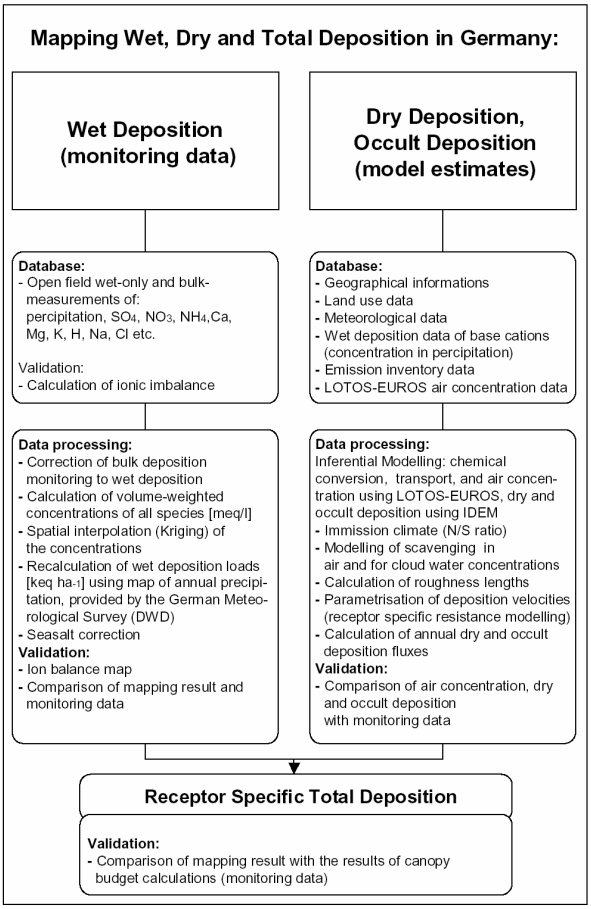

Figure 3.1: Mapping wet, dry, cloud&fog, and total deposition in Germany

4 Mapping wet deposition

Thomas Gauger & Claus Rösemann
Federal Agricultural Research Centre, Institute of Agroecology (FAL-AOE), Bundesallee 50, D-38116 Braunschweig
Bundesforschungsanstalt für Landwirtschaft, Institut für Agrarökologie (FAL-AOE), Bundesallee 50, 38116 Braunschweig

Wet deposition is the vertical chemical input of airborne compounds to a ground surface via precipitation. Airborne pollutants, which are attached to and dissolved in cloud droplets (‘in cloud scavenging’), rain drops, and snow, respectively, are either transported downwards to the ground surface by ‘rain-out’, or they are taken up from the atmosphere by hydrometeors during the precipitation event (‘wash-out’, ‘below cloud scavenging’). Using **wet-only samplers** with funnels open to the atmosphere at precipitation events only to collect hydrometeors, is an adequate method **for measuring wet deposition fluxes**. Open top precipitation collectors permanently exposed to the atmosphere are referred to as **bulk deposition samplers**. **Bulk deposition fluxes** also include a surplus amount of dry deposited matter (particulates and gases) collected in dry periods. Bulk to wet-only conversion factors have been derived using parallel measurements (GAUGER ET AL. 2000) in order to correct measured bulk deposition to wet deposition fluxes (cf. Chapter 4.2.3).

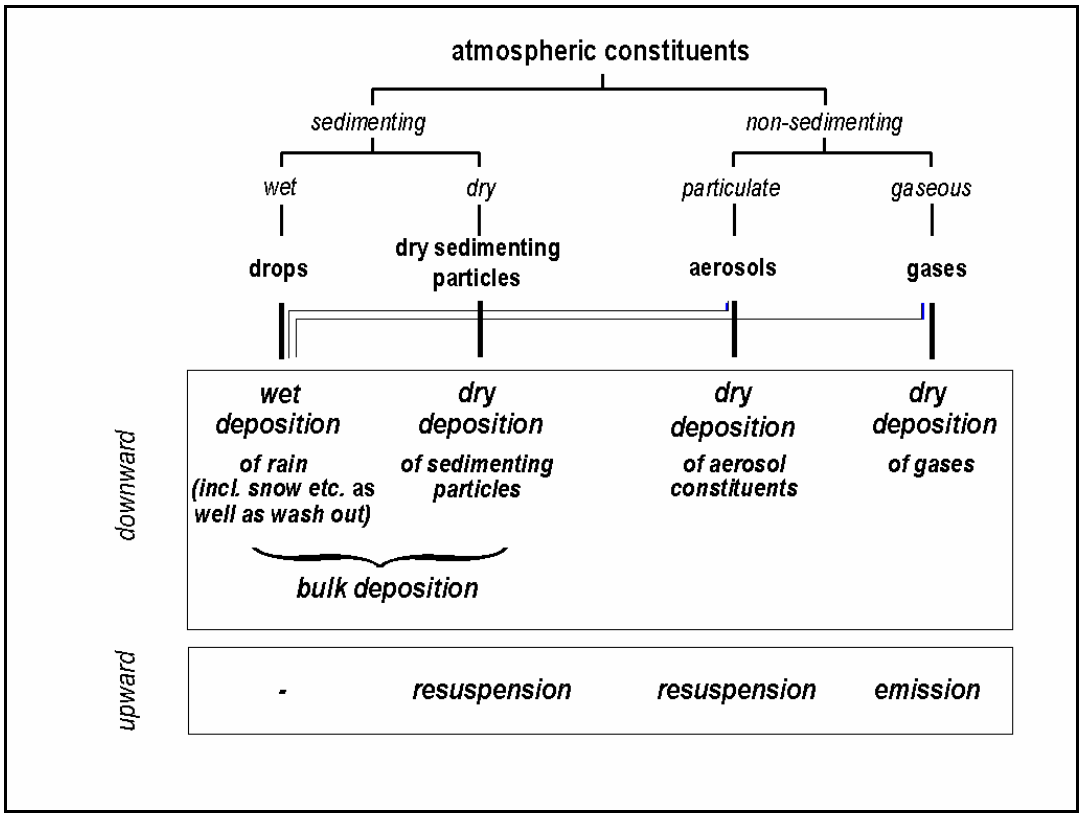

Figure 4.1: (Conceptual) differentiation of air constituents with respect to their deposition properties in order to derive flux detection methods (Grünhage et al. 1993, Dämmgen et al. 2005)

The absence of precipitation is prerequisite for **dry deposition** processes, where gases and particulate matter is transported to and deposited directly on exposed surfaces (cf. Chapter 6). **Cloud&fog deposition** (also termed 'occult' deposition) is the process where cloud and fog water droplets are directly intercepted by surfaces (cf. Chapter 6.2). Sophisticated micrometeorological measurements have to be applied in order to quantify dry and cloud&fog deposition in the field. An outline of main deposition processes, defined as downward flux, is given in Figure 4.1.

Throughfall and stemflow deposition are measured in forest stands and attributed to the deposition fluxes into the forest soil. Rainwater passing the forest canopy downwards to the ground is termed throughfall deposition. The throughfall water hereby is enriched with compounds washed from tree foliage and branches. The water running down tree trunks, also enriched with dissolved matter,, is termed stemflow.

4.1 INS/FAL/UBA wet deposition data base

Wet deposition is mapped using annual wet deposition monitoring data as basic input. Wet deposition in Germany is routinely measured in several local, regional and national monitoring programmes and networks. A wet deposition database has been initially set up at Institute of Navigation, Stuttgart University (INS) by comprehensive data acquisition at the institutions responsible for the monitoring. The database has been transferred to FAL-AOE in 2003 (GAUGER 2005) and several updates of the data base have been carried out (Chapter 4.1.1). The database consists in wet deposition load data of the main components in precipitation SO_4-S, NO_3-N, NH_4-N, K, Ca, Mg, Na, Cl, H, additional data on pH, annual precipitation, and conductivity, as well as data of trace elements (heavy metals and metalloids) Pb, Cd, Zn, Mn, Cu, Al, Cr, Fe, Ni, As, and others (Chapter 4.1.4). The respective location parameters (co-ordinates) and additional information on each sample station provided is stored as meta data linked to the data records.

The German INS/FAL/UBA wet deposition database (Table 4.1) is split into three parts containing

- data from precipitation monitoring, i.e. deposition data analysed from **wet and bulk** samplers exposed in **open field** locations
- deposition data of **bulk throughfall and stemflow from deciduous forests** and
- deposition data of **bulk throughfall from coniferous forests**.

Bulk deposition, throughfall and stemflow fluxes measured in forest stands are basic input for canopy budget

model (CBM) calculations. The application of CBM takes into account canopy exchange processes and allows to calculate estimates of dry, cloud&fog and total deposition data for a certain forest stand. CBM calculation data can be used as evaluation data for modelled dry and total deposition maps. An overview of CBM calculations can be found in DRAAIERS ET AL. 1998. Wet-only and bulk deposition data, corrected to wet deposition fluxes, are used as input for mapping wet concentration fields using kriging technique. From this wet fluxes are derived by multiplication with high resolution maps of precipitation.

4.1.1 Data acquisition and updates of the data base used for mapping wet deposition

Comprehensive and iterative data acquisition has been started in 1993 (GAUGER ET AL. 1997) in order to set up the wet deposition database. In the initial phase data published in literature were compiled to a data pool, consisting of data measured between 1979 and 1992. The authors and institutions responsible for monitoring deposition in a second phase (GAUGER ET AL. 2000) were contacted in order to consolidate all available information on measurement networks and programmes in Germany and in the cross border areas. The monitoring institutions in a third phase (GAUGER ET AL. 2002) were asked to provide annual measured deposition data using open field bulk and wet-only samplers as well as canopy throughfall and stemflow data. During the following fourth phase (GAUGER ET AL. 2005) also data from three neighbouring countries (A, CZ, PL) were included into the data base, and during the last phase special attention was given to gain data of heavy metal analyses.

With the reflux of provided data after data acquisition in the second phase the database serving for wet deposition mapping could be set up. The data pool then included 16718 records of main components in precipitation analysed 1979 to 1994 from open field bulk and wet-only measurements in Germany and Austria, 7.489 records of main components in throughfall measured in coniferous forests, and 2.239 records of main components in throughfall and stemflow sampled in deciduous forests in Germany (GAUGER ET AL. 1997).

In the following time period from 1997 to 1999 updates and thorough revisions of the database were carried out. A questionnaire was sent out to the institutions providing data in order to get more standardised information on the monitoring programmes and networks. The data pool was actualised and extended by about 19685 data records of open field bulk and wet-only measurements to a total of 36403, by about 7441 data records of throughfall measured in coniferous forests to a total of 14930, and 4780 records of throughfall and stemflow sampled in deciduous forests to total 7019 records, respectively. The database then consisted in data analysed within 1979 to 1996, including measurements of heavy metals (GAUGER ET AL. 2000).

In the 1999 to 2002 updates of the wet deposition database the main goal was to acquire monitoring data including the year 1999 and to replace or add revised measurement data for all years covered. After this data acquisition the data pool was extended by about 15242 data records of open field bulk and wet-only measurements to a total of 51645, by about 5303 data records of throughfall measured in coniferous forests to a total of 20233, and by 2909 new records of throughfall and stemflow sampled in deciduous forests to total 9928 records respectively.

The 2003 to 2005 updates of the wet deposition database are reported in GAUGER ET AL. 2005. Focus in data acquisition was set on monitoring data including the year 2002 or 2003. With this the data pool was extended by about 19884 data records of open field bulk and wet-only measurements to a total of 71529.

The recent updates of the wet deposition database in 2005 to 2006 were carried out in this study. The main focus was set on acquisition of monitoring data including the year 2004 and on retrieval of heavy metal data. Also cross border data from monitoring networks of Poland and Czech Republik were integrated into the data base. The update of the database also included revised measurement data for all years covered. After this data acquisition the open field data pool was extended to a total of 97723 data records, to a total of 26193 data records of coniferous forests throughfall, and to total 11511 records of deciduous forest throughfall and stemflow, respectively (Figure 4.2).

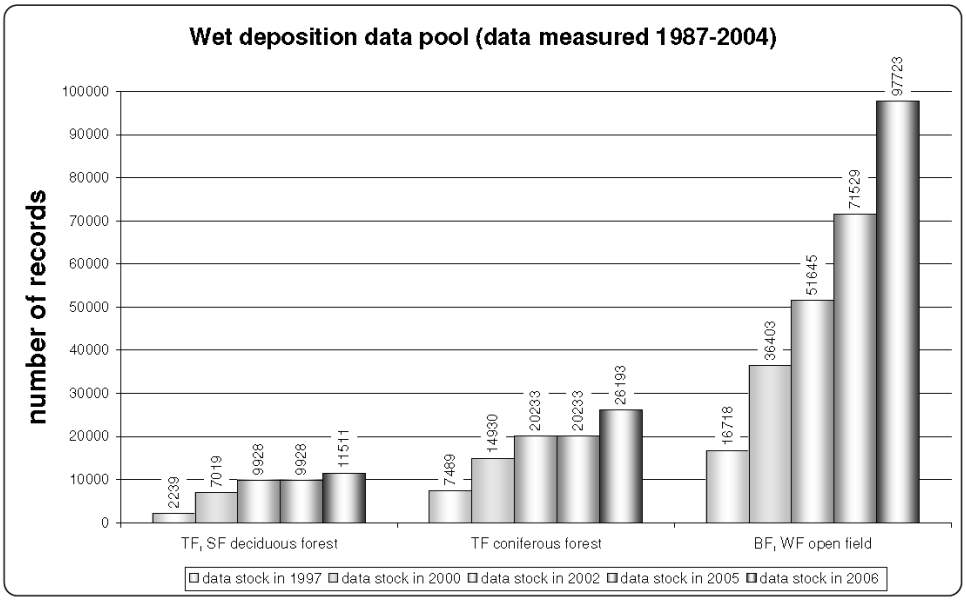

Figure 4.2: Updates of the wet deposition database from 1997 to 2006 (TF = ThroughFall, SF = StemFlow, BF = Bulk Flux, WF = Wet-only Flux)

To meet the requirements of using the provided data for mapping wet deposition the institutions responsible for monitoring deposition were asked to provide measurement data

- of annual fluxes [in g ha^{-1} a^{-1}, kg ha^{-1} a^{-1}, eq ha^{-1} a^{-1}] and/or annual concentrations in precipitation [in mg l^{-1}, g l^{-1}] and annual precipitation amount [in l m^{-2}, mm], respectively, from complete measurements over time (e.g. samples of 52 weeks, 12 months per year, respectively)

and, if analysed

- of pH (H^+ concentrations respectively) and conductivity
- of the main components: SO_4-S, NO_3-N, NH_4-N, K, Ca, Mg, Na, Cl, F, H, PO_4-P
- of trace elements and metalloids: Cd, Pb, Al, As, Br, Co, Cu, Fe, Hg, Mn, Mo, Ni, Si, Tl, V, Zn, and others
- of organic compounds: DOC, TOC, PCB, PAK, HKW and others
- derived from bulk and/or wet-only samplers in the open field and from throughfall and stemflow measurements in deciduous, coniferous, mixed forest stands
- if older data were not already provided and implemented into the wet deposition database beforehand, the data should cover the sampling periods from the beginning of the measurements until 2004
- and additional information (meta data, master data) on the samples, the sampling location (name of the site, co-ordinates, height above sea level, tree species, tree height, tree age, etc.), on the network and programme (beginning and end of measurements, main purpose, objectives and scientific goal of the monitoring), respectively

4.1.2 Wet deposition data sources

In Table 4.1 the 45 data providing institutions are listed, including a listing of main components analysed in the respective network, and the latest data set included into the data base.

Table 4.1: Data sources of deposition monitoring data in Germany and the neighbouring countries Austria, Poland and Czech Republic provided to set up the INS/FAL/UBA deposition data base for wet deposition mapping (10/2006)

Region	Institution	Acronym	SO_4	NO_3	NH_4	Cl	Na	Ca	Mg	K	H	PO_4	Pb	Cd	Nieders	Leitf.	pH	open field monitoring	throughfall, stemflow	year of latest data set
Germany	Umweltbundesamt, Fg. II 6,5 Meßnetz-Datenzentrale; Langen	UBA-b (bulk)	X	X	X	X	X	X	X	X	X	-	-	-	X	X	X	network reduced	n. a.	2003
Germany	Umweltbundesamt, Fg. II 6.5; Meßnetz-Datenzentrale; Langen	UBA-wo (wet-only)	X	X	X	X	X	X	X	X	X		X	X	X	X	X	network terminated	n. a.	2003
Ehem. DDR	Meteorologischer Dienst der DDR (via SLUG)	DDR-MD	X	X	-	X	X	X	X	X	X	-	-	-	X	-	-	network terminated	n.a.	1990
Germany	Institut für Troposphärenforschung e.V., Abt. Chemie; Leipzig (Deutschlandweites Messnetz verkleinert)	IFT	X	X	X	X	X	X	X	X	X				X			network terminated except 1 site	n. a.	1999
Germany	Umweltforschungszentrum Leipzig-Halle GmbH, Sektion Analytik; Leipzig	UFZ	X	X	X	X		X	X	X	X				X		X	network terminated	network terminated	1994
Germany	*Bundesforschundsanstalt für Landwirtschaft BS-Völkenrode, Institut für agrarrelevante Klimaforschung; Müncheberg und Braunschweig; / FAL-IAO, Braunschweig*	*FAL*	*X*	*X*	*X*	*X*	*X*	*X*	*X*	*X*		*X*	*X*	*X*	*X*			network terminated	*n.a.*	*1993, 1996*
Germany	*Bundesforschungsanstalt für Holz- und Forstwirtschaft; Eberswalde (Simon & Westendorff)*	*BFH-EB*	*X*	*X*	*X*	*X*	*X*	*X*	*X*	*X*	*X*	*X*			*X*		*X*	network terminated	network terminated	*1989*
Germany	Bundesforschungsanstalt für Holz- und Forstwirtschaft; Eberswalde	BFH-EB	X	X	X	X	X	X	X	X	X	X			X		X	no data provided	no data provided	- -
Schleswig-Holstein	Staatliches Umweltamt Itzehoe, Lufthygienische Überwachung Schleswig-Holstein Ehem. Gewerbeaufsichtsamt Schleswig-Holstein, Dez. Luftqualitätsüberwachung;	STUA-SH (ehem. GAA-SH)	X	X	X	X	X	X	X	X	X		X	X	X		X	updated	n.a.	wet-only: 2004 HM bulk: 2004
Schleswig-Holstein	Landesamt für Natur und Umwelt des Landes Schleswig-Holstein, Abteilung Gewässer; Flintbek	LANU-SH	X	X	X	X	X	X	X	X	X		X	X	X		X	updated	n.a.	2004
Schleswig-Holstein	*Christian-Albrechts-Universität Kiel, Öklologie-Zentrum (Jensen-Huß; Schimming; Spranger; Branding)*	*Univ. KI*	*X*	*X*	*X*	*X*	*X*	*X*	*X*	*X*	*X*				*X*			no data provided	no data provided	*1989, 1990*
Hamburg	*Freie und Hansestadt Hamburg - Umweltbehörde, Amt für Naturschutz und Landschaftspflege / Universität Hamburg, Institut für Bodenkunde (Lux)*	*Univ. HH*	*X*	*X*	*X*	*X*	*X*	*X*	*X*	*X*	*X*		*X*	*X*	*X*			network terminated	network terminated	*1992*
Hamburg	Deutscher Wetterdienst, Meteorologisches Observatorium Hohenpeißenberg	DWD	X	X	X	X									X		X	network terminated	n.a.	1993
Mecklenburg-Vorpommern	Landesamt für Umwelt und Natur, Abt. Immissionsschutz; Güstrow-Gülzow	LAUN-MV	X	X	X	X	X	X	X	X	X		X	X	X	X	X	updated	n.a.	wet-only: 2004 bulk: 2004
Mecklenburg-Vorpommern	Landesamt für Forstplanung; Schwerin	LAFOP-MV	X	X	X	X	X	X	X	X	X	X	X	X	X	X	X	no data provided	no data provided	- -
Niedersachsen	Niedersächsisches Landesamt für Ökologie, Dez.63 Luftreinhaltung, Dr. K.-P. Giesen; Hannover	NLÖ-H	X	X		X	X		X	X			X	X				updated	n.a.	2004
Niedersachsen	Niedersächsisches Landesamt für Ökologie, Abt. 6 Immissionsschutz; Frau A. Jankowski, Hildesheim	NLÖ-HI	X	X	X	X	X			X					X			updated	updated	2004
Niedersachsen	Niedersächsische Forstliche Versuchsanstalt, Abt. Umweltkontrolle; Göttingen	NFVA	X	X	X	X	X	X	X	X	X				X		X	updated	updated	2004
Niedersachsen	*Bundesanstalt für Geowissenschaften und Rohstoffe; Hannover (Franken et.al)*	*BGR*	*X*	*X*	*X*	*X*	*X*	*X*	*X*	*X*							*X*	network terminated	network terminated	*1995/ 1996*
Brandenburg	Landesumweltamt Brandenburg	LUA-BB	X	X	X	X	X	X	X	X			X	X	X	X	X	updated	n.a.	2004
Brandenburg	Landesanstalt für Forstplanung, Brandenburg; Potsdam	LAFOP-BB	X	X	X	X	X	X	X	X	X				X		X	updated	updated	2004
Berlin	Senatsverwaltung für Stadtentwicklung und Umweltschutz, Abt. III A 31; Berlin	SenV-B.	X	X	X	X	X	X	X	X	X	X	X	X	X			network terminated	network terminated	1998
Sachsen-Anhalt	Landesamt für Umweltschutz Sachsen-Anhalt, Abt.5, Halle	LfU-ST	X	X	X	X	X	X	X	X	X				X	X	X	updated	n.a.	2004
Sachsen-Anhalt	Forstliche Versuchs- und Forschungsanstalt; Flechtingen	FVFA-ST																updated	updated	2002
Nordrhein-Westfalen	Landesanstalt für Ökologie, Bodenordnung und Forsten/Landesamt für Agrarordnung, Dez. Bioindikation, Biomonitoring; Recklinghausen	LÖBF/ LAFAO-NW	X	X	X	X	X	X	X	X	X	X			X			updated	updated	2004
Nordrhein-Westfalen	Landesanstalt für Umweltschutz (LUA, früher LIS), Nordrhein-Westfalen, Abt. 3; Essen	LUA-NW	X	X	X	X	X	X	X	X	X				X			updated	n.a.	2004
Nordrhein-Westfalen	Fraunhofer Gesellschaft für Umweltchemie und Ökotoxikologie, Schmallenberg, Grafschaft	FhG	X	X	X	X	X	X	X	X	X				X	X		network terminated	n.a.	1988
																				...

Region	Institution	Acronym	SO_4	NO_3	NH_4	Cl	Na	Ca	Mg	K	H	PO_4	Pb	Cd	Nieders	Leitf.	pH	open field monitoring	throughfall, stemflow	year of latest data set
Nordrhein-Westfalen	Universität Münster, Inst. f. Didaktik d. Geographie, Münster	Univ-MS	X	X	X	X	X	X	X	X	X				X			updated	updated	2004
Hessen	Hessische Landesanstalt f. Forsteinrichtung, Waldforschung und Waldökologie; Hannoversch Münden	HLFWW	X	X	X	X	X	X	X	X	X		X	X	X		X	updated	updated	2004
Hessen	Universität Frankfurt, Zentrum für Umweltforschung (ZUF)	Univ. F	X	X	X	X	X	X	X	X	X				X			network terminated	network terminated	1989
Hessen	*Hessische Landesanstalt für Umwelt und Geologie (Dämmgen et al. 2003 ff)*	*HLFUG/FAL*	*X*	*X*	*X*	*X*	*X*	*X*	*X*	*X*	*X*				*X*			updated	*n. a.*	2004
Sachsen	Institut für Troposphärenforschung e.V., Abt. Chemie; Leipzig (Germanyweites Messnetz verkleinert)	IFT	X	X	X	X	X	X	X	X	X				X			network terminated except 1 site	n. a.	2003
Sachsen	Sächsische Landesanstalt für Umwelt und Geologie, Radebeul	SLUG	X	X	X	X	X	X	X	X	X				X	X	X	updated	n. a.	2004
Sachsen	Sächsische Landesanstalt für Umwelt und Geologie, Freiberg	SLUG-BDFL						X	X	X			X	X				updated	n. a.	2002
Sachsen	Sächsische Landesanstalt für Forsten; Graupa	SLAF	X	X	X	X	X	X	X	X	X	X	X	X	X			updated	updated	2004
Sachsen	Technische Universität Dresden, Institut für Pflanzen- und Holzchemie; Tharandt	TU-DD	X	X	X	X	X	X	X	X	X				X	X	X	network terminated	network terminated	1996
Thüringen	Landesanstalt für Wald und Forstwirtschaft, Thüringen; Gotha	TLWJF	X	X	X	X	X	X	X	X	X	X	X	X	X	X	X	updated	updated	2004
Thüringen	Thüringer Landesanstalt für Umwelt und Geologie, Geologischer Landesdienst, Grundwasser, Herr Dr. Hauschild, Thüringen; Jena	TLUG																no data provided	no data provided	- -
Thüringen	Thüringer Landesanstalt für Landwirtschaft, Lysimeterstation, Frau Dr. Knoblauch, Thüringen; Buttelstedt	TLL																no data provided	no data provided	- -
Rheinland-Pfalz	Forstliche Versuchsanstalt Rheinland-Pfalz, Abt. Waldschutz; Trippstadt	FVA-RP	X	X	X	X	X	X	X	X	X	X	X	X	X		X	updated (download)	updated (download)	2004
Bayern	Bayerische Landesanstalt für Wald- und Forstwirtschaft, Abt. Forsthydrologie, Freising	BLWF	X	X	X	X	X	X	X	X	X				X			updated	updated	2004
Bayern	Bayerische Landesanstalt für Umweltschutz; Aussenstelle Kulmbach	BLFU	X	X	X								X	X				updated / download	n. a.	2004
Bayern	Bayerisches Landesamt für Wasserwirtschaft; München	BLFW	X	X	X	X	X	X	X	X	X	X	X	X	X	X	X	updated	updated	2004
Bayern	Bayerische Landesanstalt für Geologie; Wunsiedel	BLFG	X	X	X													not yet successfully contacted	n. a.	- -
Saarland	Forstplanungsanstalt des Saarlandes; Saarbrücken/Univ. des Saarlandes, ZFU, AG-Forst; Duttweiler	FPA-SB	X	X	X	X	X	X	X	X	X	X	X		X		X	no actual data provided	no actual data provided	1999
Saarland	Landesanstalt für Umwelt	LFU-SL											X	X				updated (download)	updated (download)	2004
Baden-Württemberg	Forstliche Versuchs- und Forschungsanstalt Baden-Württemberg; Freiburg i. B.	FVA-BW	X	X	X	X	X	X	X	X	X	X	X	X	X			updated	updated	2004
Baden-Württemberg	Landesanstalt für Umweltschutz Baden-Württemberg, Ref. 31 Luftreinhaltung Klima; Karlsruhe / UMEG	LFU-BW	X	X			X								X			no actual data available (download)	n. a.	2002
Österreich	Technische Universität Wien, Institut für Analytische Chemie, Abt. Umweltanalytik	TU Wien	X	X	X	X	X	X	X	X	X				X		X	not successfully contacted	n. a.	1998
Czech Republic	Czech Hydrometeorological Institute et al. (download)	CHMI	X	X	X	X	X	X	X	X	X				X			updated (download)	n. a.	2004
Czech Republic	Czech Hydrometeorological Institute et al. (download)	CGU	X	X	X	X	X	X	X	X	X				X			updated (download)	n. a.	2004
Czech Republic	Czech Hydrometeorological Institute et al. (download)	VUV	X	X	X	X	X	X	X	X	X				X			updated (download)	n. a.	2004
Czech Republic	Czech Hydrometeorological Institute et al. (download)	HBUAVCR	X	X	X	X	X	X	X	X	X				X			updated (download)	n. a.	2004
Czech Republic	Czech Hydrometeorological Institute et al. (download)	VUHLM	X	X	X	X	X	X	X	X	X				X			updated (download)	n. a.	2004
Czech Republic	Czech Hydrometeorological Institute et al. (download)	IFER	X	X	X	X	X	X	X	X	X				X			updated (download)	n. a.	2004
Poland	Czech Hydrometeorological Institute et al. (download)	IMGW	X	X	X	X	X	X	X	X	X				X		X	updated	n. a.	2004
Poland	Institute of Meteorology and Water Management, (IMGW), Wroclaw Branch Glowny Inspektorat Ochrony Srodowiska (GIOS), Departament Monitoringu	IMGW GIOS	X	X	X	X	X	X	X	X	X				X		X	updated	n. a.	2003

Italics: *Data from literature / publication* n.a.: not analysed - - : no data provided

4.1.3 Overview on deposition monitoring networks in Germany including cross boarder sites in neighbouring countries

The 1987 to 2004 monitoring data from different deposition networks and programs were provided by about 45 institutions. A summarised overview of the scatter of the monitoring sites is given in Figure 4.3. The acronyms for the different monitoring networks used in Figure 4.3 are listed in Table 4.1.

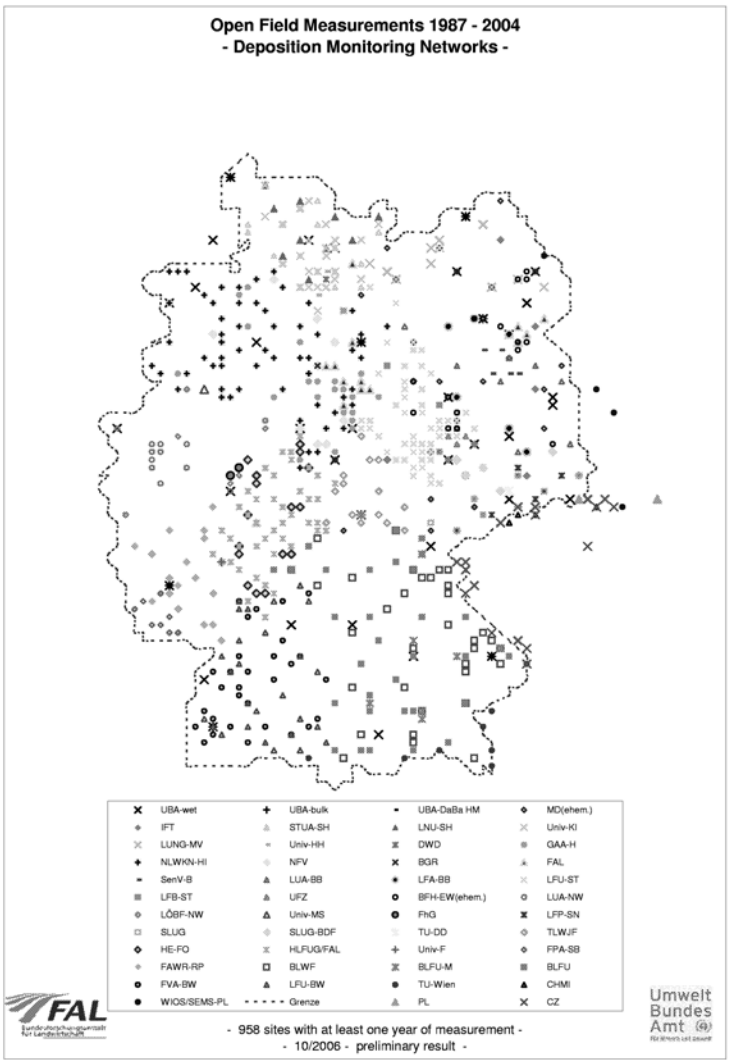

Figure 4.3: Distribution of open field bulk or wet-only deposition measurements (958 sites with at least one year measurement within 1987-2004 at each point)

4.1.4 Deposition monitoring data measured in the open field, in coniferous, and in deciduous forests

The main use of open field measurements is the mapping of wet deposition fluxes using kriging interpolation technique, whereas throughfall and stemflow measurements from forest plots are used to evaluate deposition fluxes calculated using inferential model technique (cf. Chapter 5.51).

Figure 4.4 shows the **open field deposition data stock** for 1987 to 2004 for all components included as at October 2006 in the wet deposition data base (n = 97723) and provided by the institutions responsible for monitoring (listed in Table 4.1). For comparison the smaller and lighter coloured columns in the graph are showing the data stock as at December 2002 (cf. GAUGER ET AL. 2002).

The columns of Figure 4.4 show that, except for Pb and Cd, the number of main components measured in wet

deposition is higher than the number of measurements of e.g. heavy metals, other trace components, or of pH and conductivity, respectively. Data of heavy metal wet deposition in some cases are screening data analysed from some selected samples primarily used for analysis of main components (cf. Chapter 4.4), data of pH in this study is not used, but recalculated to H^+ concentration and wet deposition flux if H+ data are not provided directly. Al, F, and P data, as well as DOC and conductivity are only provided by a smaller number of monitoring networks. The number of data per component is mainly due to different objectives of the different monitoring networks, and due to costs for sampling and analyses. There are also some monitoring programmes included, where only SO_4^{2-}-S and NO_3^--N (and Cl^-) is analysed. Other smaller differences in the total amount of measurements are due to (a) the scale of data analysed, e.g. when some networks were set up base cations were not analysed in the first years, due to (b) sample contamination and analytic errors, where only some components where affected, due to (c) incomplete delivery of data sets and (d) other errors, respectively. This also applies for forest monitoring data (Figures 4.5 and 4.6).

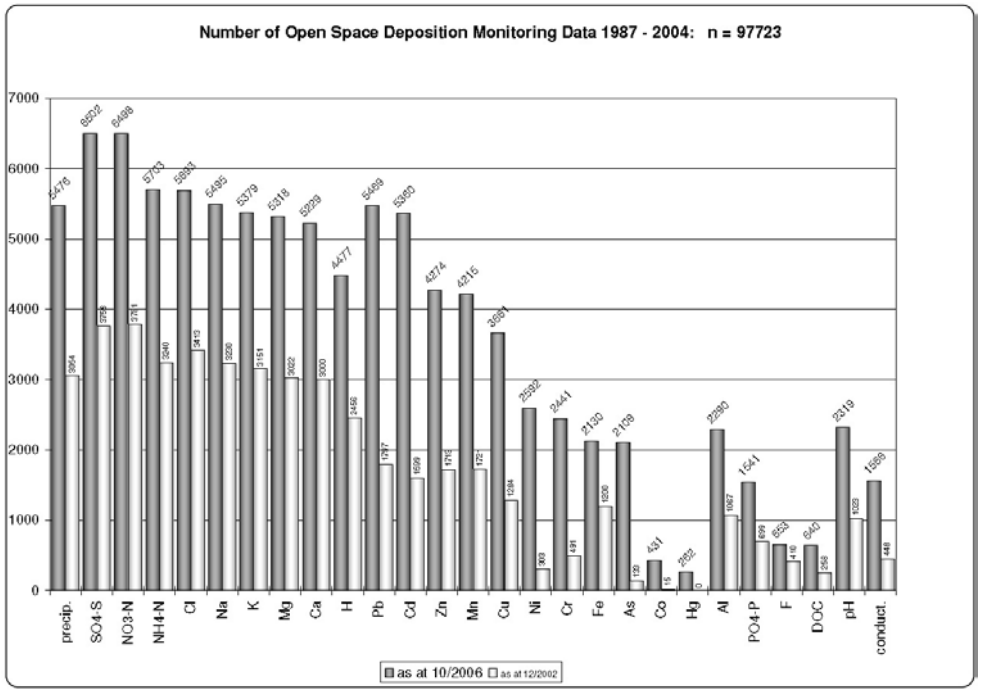

Figure 4.4: Open field wet-only and bulk deposition measurements 1987-2004 (as at 12/2002 and 10/2006)

The **data pool of coniferous forest monitoring data** for the same time period 1987 to 2004 (Figure 4.5) consists of 26193 throughfall data only. More or less the same amount of data for the nine main components and for precipitation ('precip.') can be found in this data pool. Heavy metals, which again are mainly screening data analysed from the same bulk throughfall sample like the main compounds, and other components in throughfall are not analysed at and/or provided from every monitoring site.

The 1987 to 2004 **data pool of deciduous forest wet deposition** monitoring data consists of about 11511 throughfall and stemflow data (Figure 4.6). On the contrary to coniferous forests, where stemflow measurements are scarcely carried out anywhere in Germany because of the high intensity of maintenance and costs compared to the magnitude of fluxes, stemflow fluxes in deciduous forests are remarkable in magnitude and routinely analysed at several sites.

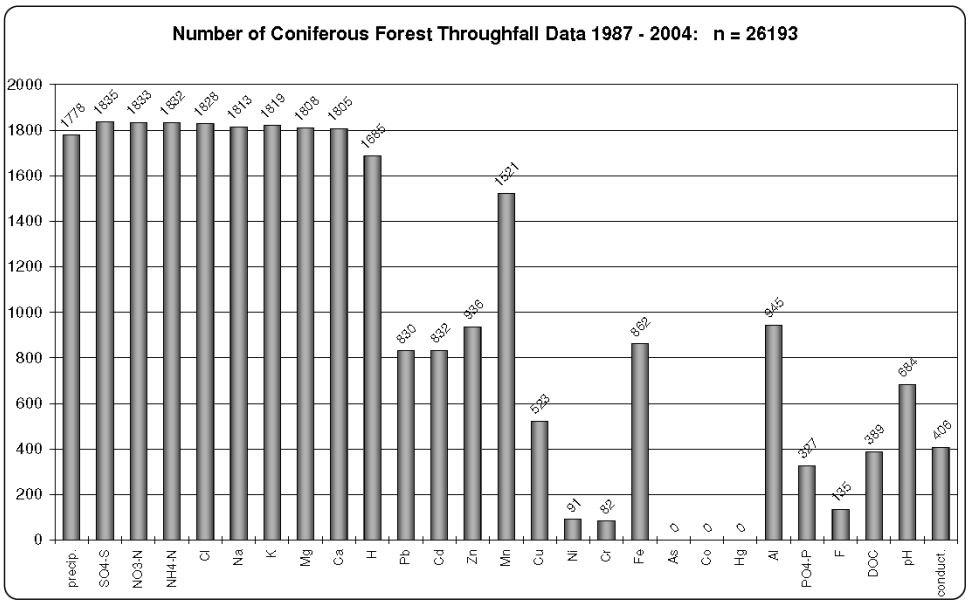

Figure 4.5: Bulk deposition measurements in coniferous forests 1987-2004 (as at 10/2006)

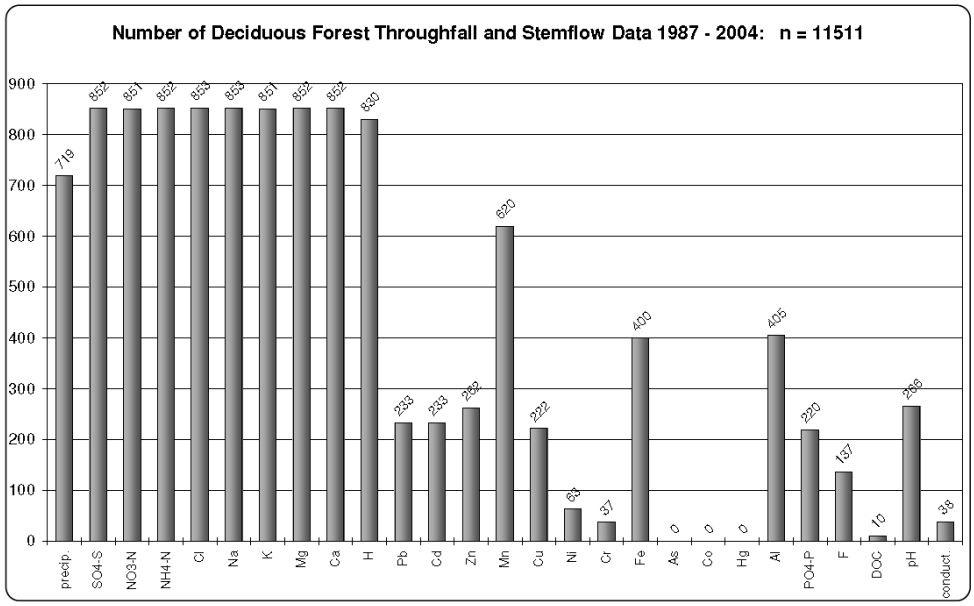

Figure 4.6: Bulk deposition measurements in deciduous forests 1987-2004 (as at 10/2006)

4.2 Data management and preprocessing

The wet deposition data are stored using relational tables of MS Excel. The use of this software application has some technical advantages, since most of the institutions providing data are also using this application for storing their own database and/or for delivering the data. The use of relational tables allow to process most of the data conversions and calculations needed, e.g. for preparation of input data for mapping wet deposition.

4.2.1 Data conversions

Different conversions of data are necessary to realise a consistent data management and largely smooth preparation of measured annual deposition fluxes and concentrations in precipitation to provide input data for mapping wet deposition using GIS ARC/INFO and ArcMap, respectively.

The data provided by the institutions responsible for monitoring wet deposition either are wet deposition fluxes per area and year at the respective sample points [in µg ha^{-1} a^{-1}, mg ha^{-1} a^{-1}, g ha^{-1} a^{-1} or kg ha^{-1} a^{-1}], daily averages per year [in g m^{-2} d^{-1}, mg m^{-2} d^{-1} or µg m^{-2} d^{-1}], concentrations in precipitation [in µg l^{-1} a^{-1}, mg l^{-1} a^{-1}, g l^{-1} a^{-1}] or ion equivalents [in meq l^{-1} a^{-1}, eq l^{-1} a^{-1}, keq l^{-1} a^{-1}; meq ha^{-1} a^{-1}, eq ha^{-1} a^{-1}, keq ha^{-1} a^{-1}]. Fluxes of

nitrogen, sulphur and phosphor compounds are either denoted as sulphate (SO_4^{2-}), nitrate (NO_3^-), ammonium (NH_4^+) and phosphate (PO_4^{2-}), or as phosphor, nitrogen and sulphur (PO_4-P, NO_3-N, NH_4-N, SO_4-S). Data of proton fluxes (H^+) are provided either as loads [e.g. kg ha^{-1} a^{-1} H^+] or as precipitation weighted pH. Precipitation weighted conductivity [in µS cm^{-1}] – if provided – may be used for checking the data quality. Units for precipitation amounts most commonly are mm a^{-1} (= 1 m^{-2} a^{-1}).

Provided data are put into the database as annual wet deposition fluxes [in g ha^{-1} a^{-1}, kg ha^{-1} a^{-1}] of all compounds. With further data processing ion equivalents of each compound [in meq ha^{-1} a^{-1}, eq ha^{-1} a^{-1}] are derived. Finally concentration in precipitation [in meq l^{-1} a^{-1}] is calculated using annual precipitation data at each sample site.

Data conversion keys, factors and equations used are presented in Table 4.2 and 4.3.

Table 4.2: Conversion keys for elements and compounds of S, N, and P

SO_4-S	=	SO_4	·	0,3338
NO_3-N	=	NO_3	·	0,2259
NH_4-N	=	NH_4	·	0,7765
PO_4-P	=	PO_4	·	0,3261
SO_4	=	SO_4-S	·	2,9958
NO_3	=	NO_3-N	·	4,4267
NH_4	=	NH_4-N	·	1,2879
PO_4	=	PO_4-P	·	3,0662

Table 4.3: Conversion of masses and equivalents

	valency	molar mass [g/mol]	equivalent mass [g/eq]	factor keq → kg	factor kg → keq
Ca	2^+	40.08	20.04	20.04	0.050
Cd	2^+	112.40	56.20	56.20	0.018
Cl	1^-	35.45	35.45	35.45	0.028
H	1^+	1.01	1.01	1.01	0.992
K	1^+	39.10	39.10	39.10	0.026
Mg	2^+	24.31	12.15	12.15	0.082
Na	1^+	22.99	22.99	22.99	0.043
NH_4-N	1^+	14.01	14.01	14.01	0.071
NO_3-N	1^-	14.01	14.01	14.01	0.071
PO_4-P	2^-	30.97	15.49	15.49	0.065
Pb	2^+	207.20	103.60	103.60	0.010
SO_4-S	2^-	32.06	16.03	16.03	0.062

4.2.2 Data quality: ion balance and "4-sigma-test"

In a liquid water phase the sum of anions and cations should be of the same magnitude because of the electroneutrality condition. The equilibrium of anion and cation equivalent concentration is commonly used to control the analytical procedures applied when measuring the content of species in precipitation. Hereby the quotient of anions and cations should be smaller than ±20% otherwise outliers due to analytical errors are indicated. The quality of measured open field deposition data used for mapping wet deposition fields is checked

by calculating the ion balance from 9 main components accordingly, using Equation 4.1:

$$Ion\ Balance\ [\%] = \frac{(NH_4^+\text{-}N + Ca^{2+} + Mg^{2+} + K^+ + Na^+ + H^+) - (SO_4^{2-}S + NO_3^-\text{-}N + Cl^-)}{(NH_4^+\text{-}N + Ca^{2+} + Mg^{2+} + K^+ + Na^+ + H^+) + (SO_4^{2-}\text{-}S + NO_3^-\text{-}N + Cl^-)} \cdot 100\ [eq] \qquad (4.1)$$

A more extended Ion balance, including HCO_3 is given in Equation 4.2:

$$Ion\ Balance\ [\%] = \frac{(NH_4^+\text{-}N + Ca^{2+} + Mg^{2+} + K^+ + Na^+ + H^+) - (SO_4^{2-}S + NO_3^-\text{-}N + Cl^- + HCO_3^-)}{(NH_4^+\text{-}N + Ca^{2+} + Mg^{2+} + K^+ + Na^+ + H^+) + (SO_4^{2-}\text{-}S + NO_3^-\text{-}N + Cl^- + HCO_3^-)} \cdot 100\ [eq] \qquad (4.2)$$

HCO_3 usually is not analysed or data are not provided by the monitoring networks. It can be calculated from H^+ concentration using Equation 4.3 (IHLE ET AL. 2001):

$$HCO_3 = 5{,}487 / H^+ \qquad (4.3)$$

For checking the quality of the data also Equation 4.4 is used. Here only 6 main components are included, beeing those species, which are deposited at the same time (by the same processes). Compared to Equation 4.1, Ca and K are not included, since those species are mainly bound to resuspended soil particles and associated with other anions (silicates, carbonates), which are uasually not included in the analyses of the deposition samples (DÄMMGEN 2006).

$$Ion\ Balance\ [\%] = \frac{(NH_4^+\text{-}N + Mg^{2+} + Na^+) - (SO_4^{2-}\text{-}S + NO_3^-\text{-}N + Cl^-)}{(NH_4^+\text{-}N + Mg^{2+} + Na^+) + (SO_4^{2-}\text{-}S + NO_3^-\text{-}N + Cl^-)} \cdot 100\ [eq] \qquad (4.4)$$

Finally Equation 4.5 can be used for calculating an ionic balance from only 4 quantitatively dominating components of wet deposition. Compared to Equation 4.4 also Na and Cl, wich mainly originate from sea salt NaCl, are excluded from the calculation of the ion balance.

$$Ion\ Balance\ [\%] = \frac{(NH_4^+\text{-}N + Mg^{2+}) - (SO_4^{2-}\text{-}S + NO_3^-\text{-}N)}{(NH_4^+\text{-}N + Mg^{2+}) + (SO_4^{2-}\text{-}S + NO_3^-\text{-}N)} \cdot 100\ [eq] \qquad (4.5)$$

The quality of all datasets in the wet deposition data base provided for each year and all components analysed was checked using all the ion balance calculations shown above (Equations 4.1, 4.2, 4.4, and 4.5). A selection of data sets due to the result of the ion balance calculation was carried out using a deviation from the balance calculation of more than ±20% as criterion for excluding the respective data set from further processing. The balance calculations were used that way, that whenever possible, at least one ion balance calculation should be applicable. In the case that not all main components are provided, which are needed as input for Equation 4.2, or 4.1, an application of Equation 4.4 or 4.5 in most cases still would give an estimate of the ion balance. The selection of samples for further processing is based upon the lowest value of deviation within the results of the four different ion balance calculations. The results of quality rating using ion balance calculations are shown in Table 4.4. With application of ion balance calculations 69% to 84% of all bulk/wet deposition data sets are rated for quality in the single years 1987 to 2004, and, in case the ion balance is <20%, selected for further processing.

Table 4.4: Data quality and data set selection using ion balance calculations

Year	Number of data sets Total	Rated using Eq. 4.2	Rated using Eq. 4.1	Rated using Eq. 4.4	Rated using Eq. 4.5	Total rated	Ion balance >20%	Ion balance <20%	Total rated (%)	Excluded from further processing (%)
2004	378	152	43	91	18	304	29	275	80	10
2003	481	193	64	87	14	358	25	333	74	7
2002	463	214	55	67	19	355	45	310	77	13
2001	449	195	59	79	46	379	52	327	84	14
2000	420	209	71	40	9	329	20	309	78	6
1999	450	228	81	37	7	353	24	329	78	7
1998	438	212	37	66	24	339	28	311	77	8
1997	394	182	39	67	30	318	28	290	81	9
1996	416	149	53	75	25	302	44	258	73	15
1995	383	138	74	52	16	280	43	237	73	15
1994	354	159	40	45	7	251	42	209	71	17
1993	330	144	44	38	13	239	47	192	72	20
1992	280	139	22	30	1	192	38	154	69	20
1991	189	95	33	17	8	153	20	133	81	13
1990	281	108	74	21	3	206	16	190	73	8
1989	303	131	87	9	3	230	14	216	76	6
1988	291	87	106	17	10	220	21	199	76	10
1987	252	60	104	10	0	174	17	157	69	10

Another check of the wet deposition input data is made by determining and rejecting outliers of each component in order to exclude high values which are due to very local circumstances or sample contamination. In the analysis carried out both statistical and the regional context of the measurements are taken into account.

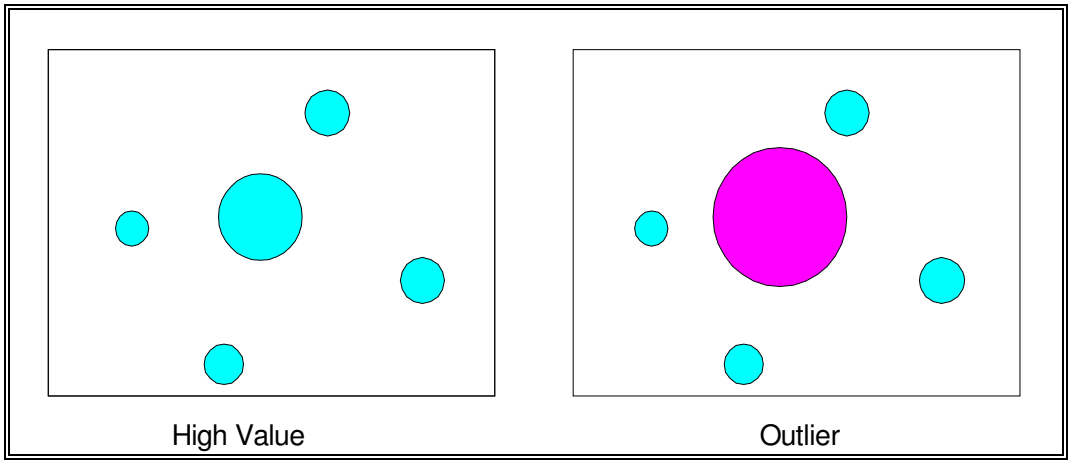

Figure 4.7: Illustration of the detection of outliers in a point map

Point maps were calculated in order to detect high outliers in the regional context of surrounding measurements. The difference between high values and outliers is illustrated in Figure 4.7. Very high values (outliers, respectively) can be attributed to local circumstances, where the measurements either are strongly influenced by local emissions of a certain compound or by contamination of the sample. Where applicable, additional information on the surroundings of the sample site, and/or on certain events near by the site in the respective year (e.g. construction activities or stormy weather conditions in an agrarian area in harvesting periods leading to high deposition of base cations, high sulphate deposition close to a power plant etc.) provided by the institutions

responsible were also taken into account in order to detect suspected outliers.

In addition to this investigation, a statistical analysis was applied. A statistical method applicable for detection of outliers is the "4-sigma-test" (SACHS 1997, p 364), where the mean value ± 4 times the standard deviation of the population, both calculated without the suspected outliers, marks the upper and lower limit beyond which the outliers can be found.

The "4-sigma-test" is carried out for all main components in the wet deposition database in order to detect high outliers before the data are used as input for mapping. All detected outliers in excess of the mean value +4 times the standard deviation of the population are excluded from further processing.

4.2.3 Bulk to wet-only conversion

At those sampling points where bulk deposition samplers are used wet deposition is estimated by correcting bulk deposition fluxes for dry deposition into the funnels. Simultaneous bulk and wet deposition measurements in different parts of Germany (Figure 4.8) were used to derive average conversion factors listed in Table 4.5. The ratios shown in Table 4.5 are used to calculate wet deposition fluxes from bulk deposition fluxes. According to the Mapping Manual (UBA 1996, ICP Modelling & Mapping 2004) only corrected bulk deposition data and measured wet deposition data are used as input for mapping wet deposition in Germany.

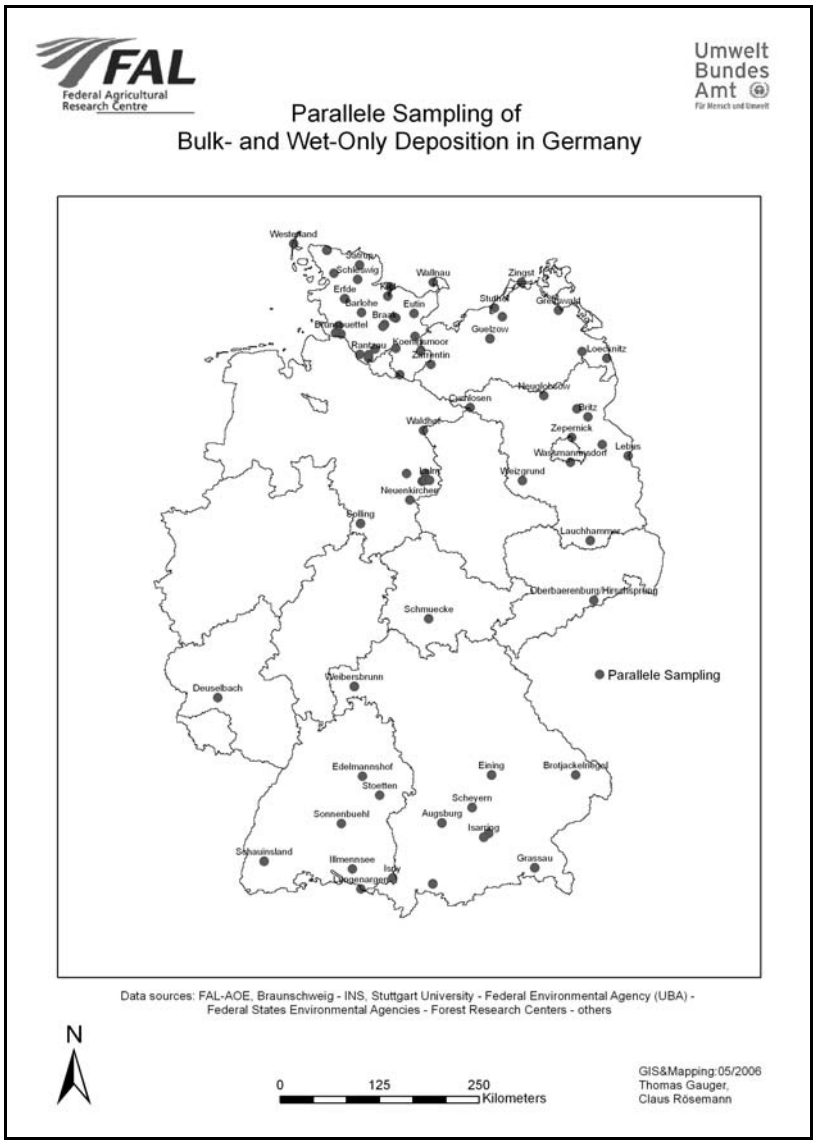

Figure 4.8: Locations of paralelle sampling of wet-only and bulk deposition in Germany

In previous projects (GAUGER ET AL. 2000, 2002) species specific annual mean ratios of wet-only and bulk fluxes derived from data of 23 monitoring sites in Germany were used as factors for correcting bulk deposition fluxes for dry deposition. In this study 97 parallele measurements of wet only and bulk deposition samplers, carried out in the period 1987 to 2003 at 68 locations scattered over Germany (Figure 4.8) are used to derive

average conversion factors listed in Table 4.5 and shown in Figure 4.9.

The average contribution of dry deposited components in bulk deposition varies between 3% for pH and 38% for K^+ (Table 4.5). Wet deposition of H^+ is found to be on average about 34% higher in wet-only deposition samples compared to bulk deposition. This can be attributed to exchange processes with particles in bulk samples. The latter also are in most cases exposed for longer time periods than wet-only samples (e.g. weekly to monthly bulk and daily to weekly wet-only samples), which enhances this exchange process. Precipitation amounts are on average about 3% higher in wet-only samples compared to bulk samples, which either can be attributed to the collecting efficiency of the sampler types (wet-only > bulk sampler), or to evaporation loss in bulk samplers.

Table 4.5: Average ratio of wet-only and bulk fluxes measured in Germany and used as correction factors in order to derive wet deposition from bulk deposition samples

	K	Ca	Mg	Na	SO4-S	Cl	NO3-N	NH4-N	pH	precip.	H
simultaneous measurements, n =	66	65	67	67	87	54	86	79	35	54	37
average ratio wet-only / bulk	**0.62**	**0.63**	**0.76**	**0.81**	**0.82**	**0.85**	**0.90**	**0.95**	**0.97**	**1.03**	**1.34**
Maximum	1.44	1.77	1.36	1.47	1.07	1.42	2.01	1.79	1.06	3.00	3.17
Minimum	0.09	0.21	0.18	0.22	0.26	0.32	0.30	0.29	0.83	0.84	0.48
Standard deviation	0.24	0.24	0.25	0.20	0.17	0.19	0.22	0.25	0.06	0.29	0.62

In the single German regions (9 Bundeslaender, Figure 4.9) the average wet/bulk ratio in most cases and for the single species (with the exception of H^+) ranges from 0.50 to 1.00, meaning that 50% to 100% of the species in bulk deposition can be assumed to be deposited by the wet(-only) deposition flux.

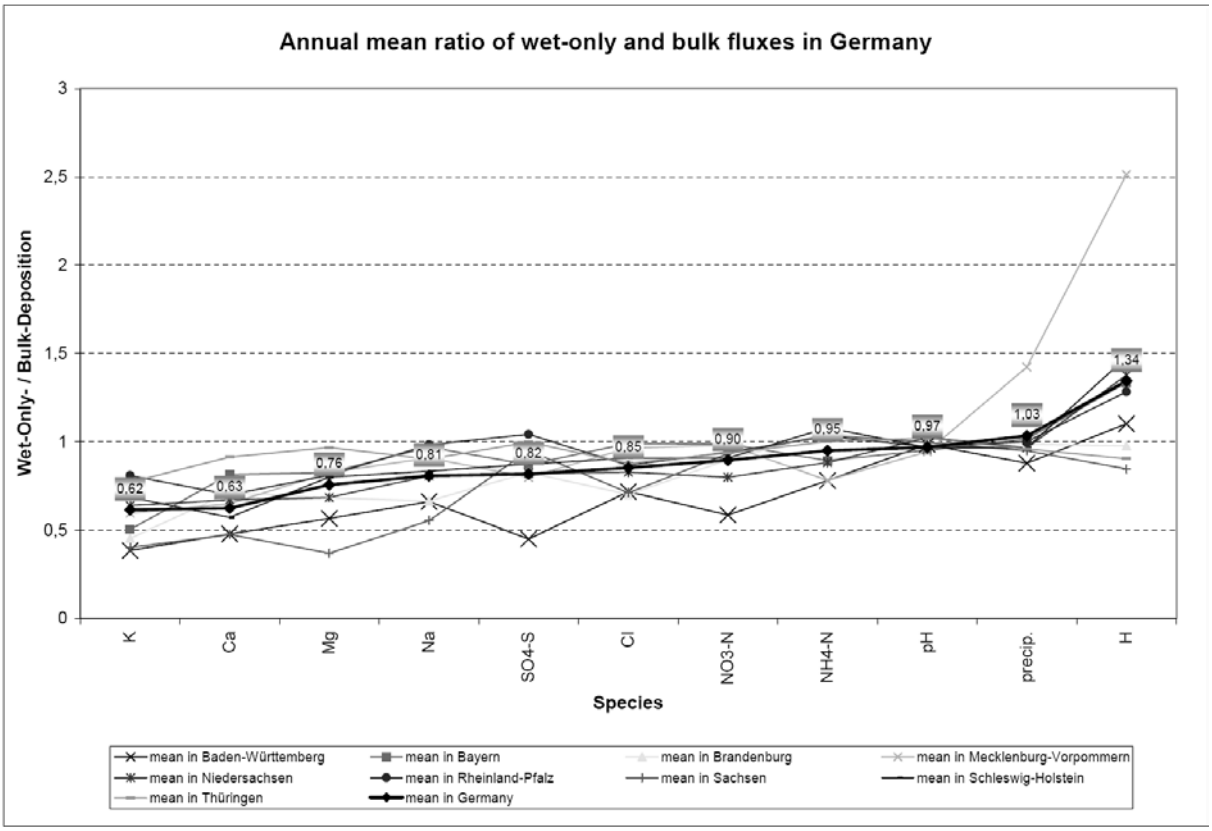

Figure 4.9: Annual mean ratio of wet-only and bulk fluxes measured in Germany

4.2.4 Input data used for mapping wet deposition for 1987 - 2004

After data conversion and quality checks, the input data sets for the mapping procedure are used in the GIS. Table 4.6 shows the respective number of 1987 to 2004 data (1) in the wet deposition database, (2) after data revision is made, and (3) after averaging the values of closely neighbouring sites. The latter step of preprocessing the input data is made in order to accommodate the scatter of the sample points more equally over the whole area, since clustered data points should be avoided when using kriging interpolation technique.

The scatter and density of open field wet deposition measurements is important for spatial representativity. Taking spatial variability of wet deposition fluxes of SO_4-S and NO_3-N into account, it is assumed that the survey area should be covered with one site per 1000km² to 2000km², or, that a wet deposition monitoring network representative for main components should be arranged in a regular 40 km grid to derive spatial average estimates with standard errors of the mean below ±20% for SO_4-S and NO_3-N. Other components, e.g. Mg, Ca, H, and an orographically complex terrain would require a more dense distribution of the network over the geographical area (KALLWEIT 1997, SAGER 1997). This means that a monitoring network covering all Germany with its acreage of about 357000km² should consist of 178 wet deposition sites (one per 2000km²), 233 sites (one per 1600km²), 268 sites (one per 1500km²) or 357 sites (one per 1000km²), respectively, in a more or less regular scatter in order to approach the conventional requirements mentioned above.

The amount of open field wet deposition measurements provided as input to the INS/FAL/UBA wet deposition database and used to derive wet deposition fields (see ‘available data’ and ‘input data’ in Table 4.6) already more or less meets the conventional minimum requirements to derive fields of wet deposition fluxes. The only exception is the year 1991. The sample data are used to derive fields of precipitation weighted annual mean ion concentrations. When the concentration fields are mapped, wet deposition fluxes are calculated as the product of concentrations and the annual precipitation amount provided by Deutscher Wetterdienst (DWD) in 1x1km² grid resolution maps. The precipitation maps are modelled by DWD using a very large network of gauges (more than 3500 sample sites) as primary input (cf. Chapter 4.3.1).

Table 4.6: Quantity of monitoring data used for mapping wet deposition

	1987			1988			1989			1990			1991			1992		
	availabe data(1)	after revision (2)	input data(3)	availabe data[1]	after revision [2]	input data[3]	availabe data[1]	after revision [2]	input data[3]	availabe data[1]	after revision [2]	input data[3]	availabe data[1]	after revision [2]	input data[3]	availabe data[1]	after revision [2]	input data[3]
SO_4-S	252	226	200	300	274	227	311	289	227	279	259	214	189	169	150	268	231	195
NO_3-N	253	231	204	300	284	236	312	297	234	281	263	216	191	171	151	284	246	208
NH_4-N	224	207	184	281	264	216	277	264	210	249	229	189	159	141	124	224	187	162
Ca	188	163	140	234	210	168	241	218	162	210	185	147	159	134	116	217	176	153
Mg	182	158	131	235	217	167	241	226	171	208	191	150	157	136	120	213	173	153
K	185	165	144	266	243	204	279	261	205	245	228	188	157	136	119	237	198	171
Na	181	159	134	265	245	196	275	259	203	246	226	186	157	135	119	228	191	168
Cl	244	218	188	287	266	222	311	295	233	278	253	209	188	163	144	242	200	174
H	172	162	135	202	194	164	224	218	171	185	176	140	132	132	111	177	154	136
precip.			DWD map			DWD map			DWD map			DWD map			DWD map			DWD map

	1993			1994			1995			1996			1997			1998		
	availabe data(1)	after revision (2)	input data(3)	availabe data[1]	after revision [2]	input data[3]	availabe data[1]	after revision [2]	input data[3]	availabe data[1]	after revision [2]	input data[3]	availabe data[1]	after revision [2]	input data[3]	availabe data[1]	after revision [2]	input data[3]
SO_4-S	316	276	238	346	304	264	375	335	288	409	369	313	395	369	317	438	410	353
NO_3-N	320	281	242	348	309	268	367	329	287	405	368	314	393	369	316	436	407	351
NH_4-N	254	213	188	284	242	215	319	276	242	350	310	266	342	317	273	388	358	310
Ca	255	213	182	264	221	186	294	251	210	330	286	240	341	316	273	361	327	283
Mg	248	209	178	262	221	185	310	265	226	347	297	250	347	318	275	372	339	293
K	273	232	198	282	233	196	307	263	223	338	300	250	342	309	268	353	318	274
Na	272	227	195	285	242	204	317	267	229	357	299	253	356	320	275	375	322	276
Cl	282	229	200	291	245	213	314	267	233	341	286	246	350	315	270	376	328	282
H	197	175	156	202	177	155	217	198	172	212	207	178	241	233	205	281	271	236
precip.			DWD map			DWD map			DWD map			DWD map			DWD map			DWD map

	1999			2000			2001			2002			2003			2004		
	availabe data(1)	after revision (2)	input data(3)	availabe data[1]	after revision [2]	input data[3]	availabe data[1]	after revision [2]	input data[3]	availabe data[1]	after revision [2]	input data[3]	availabe data[1]	after revision [2]	input data[3]	availabe data[1]	after revision [2]	input data[3]
SO_4-S	438	413	353	412	394	346	442	390	347	463	413	357	472	439	377	381	355	318
NO_3-N	438	415	354	412	394	347	439	390	347	466	420	363	472	444	383	380	355	318
NH_4-N	389	367	313	363	341	302	394	345	312	415	368	323	421	395	341	369	345	306
Ca	364	329	281	340	316	281	391	339	306	368	313	280	362	330	306	310	277	269
Mg	376	338	289	351	325	289	405	349	316	377	318	284	378	339	314	309	276	266
K	366	333	287	337	315	282	384	332	300	363	312	279	369	334	308	296	263	254
Na	375	330	280	350	315	279	380	310	278	383	320	286	380	336	311	313	269	261
Cl	375	330	280	351	316	279	380	311	279	375	313	285	380	344	318	328	285	276
H	358	338	292	332	312	282	316	280	255	314	279	249	301	291	251	248	235	210
precip.			DWD map			DWD map			DWD map			DWD map			DWD map			DWD map

[1] = quantity of open field sampling data in the wet deposition data base

[2] = quantity of data after data revision (without outliers and ion balance <21%)

[3] = quantity of data input for mapping after averaging closely neighbouring sample points (within each 5x5km² grid cell)

4.3 Calculation and mapping of wet deposition fields

4.3.1 Concept of mapping wet deposition

The concept of mapping wet deposition in Germany follows the recommendations of the Mapping Manual (ICP MODELLING&MAPPING 1996, 2004). The horizontal variation of the chemical composition of precipitation in most cases is much smaller than the horizontal variation of precipitation amount.

Spatial pattern of rainfall composition is monitored in the wet deposition sampling networks (Chapter 4.2). The sample data are used to calculate precipitation weighted annual ion concentration fields for the main species SO_4^{2-}-S, NO_3^--N, NH_4^+-N, K^+, Ca^{2+}, Mg^{2+}, Na^+, Cl^- and H^+ using kriging technique. All concentration maps are calculated in 1x1km² grid resolution for the years 1996 to 2004. For the years 1987 to 1995, due to the poorer amount and scatter of monitoring data (Table 4.6), a coarser 5x5km² grid had to be chosen to derive wet concentration fields covering all Germany.

Though the number and scatter of the measurement data plots is varying from year to year between 1987 and 2004, the monitoring sites cover most areas of Germany, both horizontally (scatter and density) and vertically (orography and exposition). In previous studies it has been proved possible to calculate regional distribution of the main components' ion concentration in precipitation in 5x5km² grids with a minimum number of about 130 sites scattered more or less equally over the whole country (Gauger et al. 1997). For a kriging interpolation in a target 1x1 grid about twice the number of input data per species more or less equally spread over the area of Germany is needed. However, the more equal the scatter of the monitoring sites and the more monitoring data are available, which do represent the spatial trend of wet deposition, the better the kriging interpolation result will be in terms of lower errors and uncertainties (see Chapter 4.3.2).

The outline of data processing using GIS is shown in Figure 4.10. Co-ordinates of the measurement sites and attributed concentration in precipitation are input to derive point maps showing the scatter and measured annual concentration of the different species in precipitation. These maps give an overview on possible horizontal lack of data, which is useful when analysing uncertainties of the mapping result, and they are used for visual identification of outliers in their spatial context (see Chapter 4.2.2). In a second step the concentrations in precipitation of closely neighbouring sample points within each 5x5km² grid cell are averaged to one value and attributed to one point (see Chapter 4.2.4). These points are input for kriging interpolation procedure.

A **sea salt correction** is calculated for SO_4^{2-}-S, Cl^-, Ca^{2+}, K^+ and Mg^{2+}, using sodium (Na^+) as a tracer. The sea salt correction is calculated with the interpolated fields, because sodium deposition is not measured at each monitoring site. Rainwater contains ions originating from sea water which is transported into the continent by sea spray. The sea salt correction is used to correct the measured ion content from a sample for the sea salt contribution. It is assumed that the ratio of Na^+ to SO_4^{2-}-S, Cl^-, Ca^{2+}, K^+ and Mg^{2+} in the sample is the same as in sea water and that all Na^+ is of marine origin. Table 4.7 shows the Na-ratios in sea water and the calculation of the sea salt correction.

Table 4.7: S, Cl, Ca, K, and Mg to Na ratios in sea water [eq/eq] and the calculation of the sea salt correction (ICP MODELLING&MAPPING 2004)

Na_{sw}/Na_{sw}	Ca_{sw}/Na_{sw}	Mg_{sw}/Na_{sw}	K_{sw}/Na_{sw}	S_{sw}/Na_{sw}	Cl_{sw}/Na_{sw}
1	*0,043*	*0,278*	*0,021*	*0,120*	*1,166*
- -	$Ca_{nss} = Ca_{dep} - (Na_{dep} \cdot 0{,}043)$	$Mg_{nss} = Mg_{dep}\ (Na_{dep} \cdot 0{,}278)$	$K_{nss} = K_{dep} - (Na_{dep} \cdot 0{,}021)$	$S_{nss} = S_{dep} - (Na_{dep} \cdot 0{,}120)$	$Cl_{nss} = Cl_{dep} - (Na_{dep} \cdot 1{,}166)$

The fluxes of SO_4^{2-}-S, Cl^-, Ca^{2+}, K^+ and Mg^{2+} corrected for sea salt are termed '<u>n</u>on <u>s</u>ea <u>s</u>alt' ('nss', e.g. $K_{(nss)}$ for non sea salt potassium). They are representing the deposition flux mainly attributable to anthropogenic processes excluding the natural sea spray input.

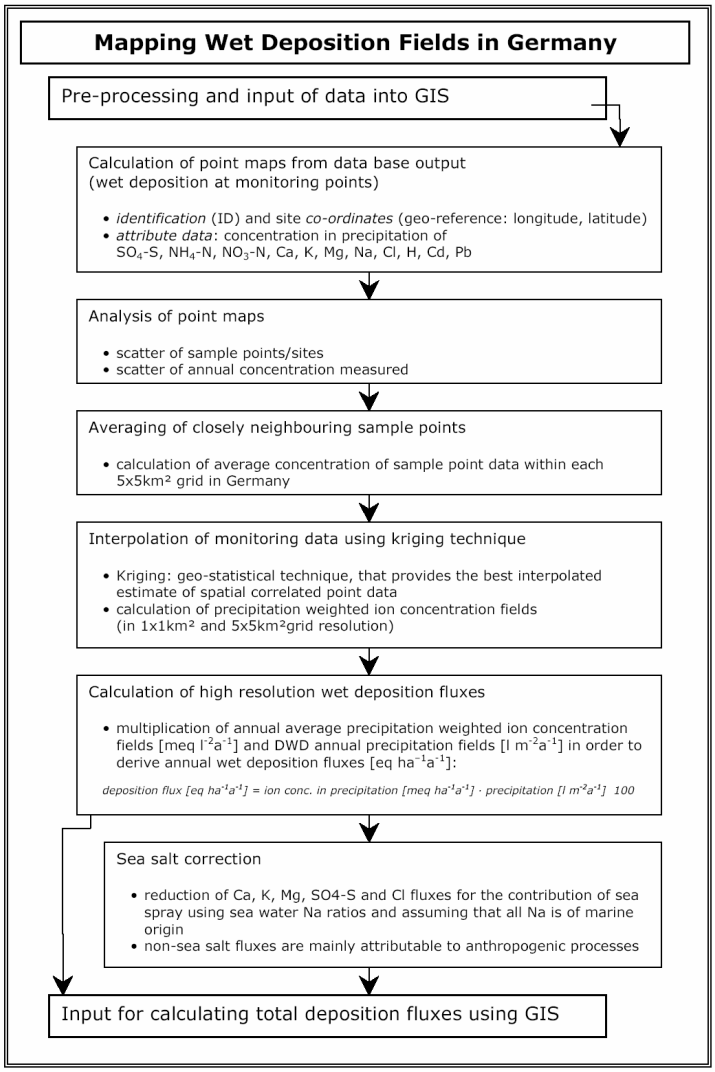

Figure 4.10: Outline of mapping wet deposition using GIS

The interpolated precipitation weighted annual ion concentration fields are, if necessary, resampled into 1x1km² grid maps and multiplied with a high resolution (1x1km²) precipitation map, provided by DWD. This DWD modelled maps of annual precipitation fields are derived using more than 3500 samples of the DWD precipitation monitoring

Since precipitation data show significant correlation to topography, regression coefficients between precipitation and topography (i.e. elevation, slope, land use) can be derived. By DWD modelling the precipitation data are reduced to a common reference level by using spatially variable regression functions. Then the reduced data are interpolated (in a 1x1km² grid) and subsequently recalculated into the real topography by using the regression functions in a 1x1km² grid map covering all Germany (MÜLLER-WESTERMEIER 1995).

The result of the intersection of fields of annual concentration in rainfall with the annual precipitation map is a 1x1km² wet deposition loads map, combining the maximum information on both spatially differentiated wet deposition and precipitation monitoring.

4.3.2 Quality of the wet deposition mapping results

An overview of consistency of the wet deposition mapping results for each year considered in this study is carried out by calculating ion balance maps. Within each grid of the maps the ion balance of all main components mapped is calculated (using Equation 4.1, Chapter 4.2.2). The outcome in this ion balance map then should show values more or less in the same range of the ion balance of input data. Moreover it is possible to get back ion balance values at those locations of monitoring plots where only incomplete data sets were provided for the wet deposition data base, or where not all main components are analysed from the sample, and only an interpolated estimate is substituting the missing values at this specific locations.

Figure 4.11 is presenting the mapping results as average sum of anions (SO_4^{2-}-S, NO_3^--N, and Cl^-) and cations

(NH_4^+-N, K^+, Ca^{2+}, Mg^{2+}, Na^+, and H^+), and the total sum of all these ions in Germany over the whole 18 year period from 1987 to 2004. In all years the average sum of anions and the average sum of cations are close together, though a small surplus of cations, compared to anions can be observed.

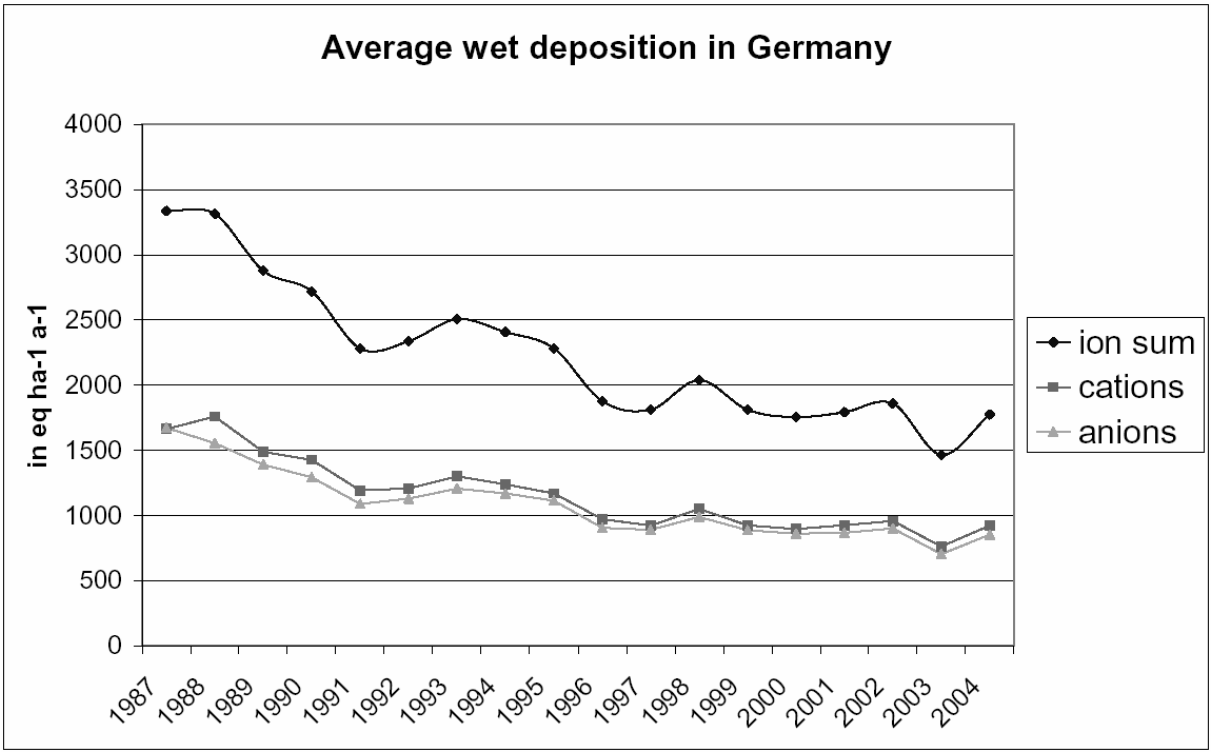

Figure 4.11: Average wet deposition of anions and cations 1987-2004

The ion balance calculated from the wet deposition maps of 1993 to 2004 using Eq. 4.1 (Chapter 4.2.2) is shown in Map 4.1. The range of the ion balance for the wet deposited main components in 1993-2004 shows satisfying results. Negative values (-) denote surplus of the respective anions, positive values (+) denote a surplus of the respective cations in the ion balance. Each year imbalances between -10% and +10% cover most parts of Germany. However, higher imbalances (+15% to over +20%) are found in some areas around and between individual sites where already higher ionic imbalances of the monitoring data were observed. Over time, notably higher imbalances above +20% are covering larger areas mainly in Bavaria, the south-eastern part of Germany.

The ion balance calculated using Eq. 4.4 (Chapter 4.2.2), where Ca^{2+}, K^+, and H^+ are not included, is shown in Map 4.2. The spatial pattern of high ion imbalances, with a surplus of anions of more than 20% over time continually diminishes. From the mid 1990ies onward imbalances are mainly ranging between ±10%, while in the south-western part and in some central and eastern parts of Germay a surplus of anions above 15% can be observed.

Only in the north-western part of Germany both approaches of calculating ion balances lead to imbalances mainly ranging between ±10%. In most of the other regions eather one or the other approach applied shows imbalances above 15%.

A site specific comparison between mapped and measured data has been carried out for wet deposition loads. The results of this comparison are shown for 1987-2004 in Table 4.8. This comparison mainly reflects the effect of data pre-processing, interpolation and intersection of wet concentration with the DWD precipitation map at the points of the open field wet deposition monitoring.

Table 4.8: Comparison of measured and mapped wet deposition loads 1987-2004

1987	SOx-S	NOy-N	NHx-N	Ca	K	Mg	H	Na	Cl
n	221	226	202	160	161	155	157	155	213
m	0.99	0.98	0.98	1.00	0.97	0.98	1.00	1.01	1.02
r	0.89	0.79	0.86	0.85	0.58	0.73	0.88	0.92	0.72
r^2	0.80	0.63	0.75	0.72	0.34	0.54	0.77	0.85	0.51
1988	**SOx -S**	**NOy-N**	**NHx-N**	**Ca**	**K**	**Mg**	**H**	**Na**	**Cl**
n	269	279	259	205	239	212	189	241	261
m	0.94	0.92	0.95	0.93	0.95	0.94	0.94	1.03	1.00
r	0.87	0.71	0.72	0.71	0.48	0.66	0.87	0.94	0.92
r^2	0.79	0.50	0.52	0.50	0.23	0.43	0.76	0.89	0.84
1989	**SOx -S**	**NOy-N**	**NHx-N**	**Ca**	**K**	**Mg**	**H**	**Na**	**Cl**
n	283	291	258	212	256	220	212	254	288
m	0.97	0.96	0.97	0.93	0.95	0.96	1.01	1.02	1.00
r	0.86	0.76	0.64	0.60	0.55	0.66	0.81	0.86	0.92
r^2	0.74	0.58	0.42	0.36	0.31	0.44	0.66	0.74	0.84
1990	**SOx -S**	**NOy-N**	**NHx-N**	**Ca**	**K**	**Mg**	**H**	**Na**	**Cl**
n	253	257	223	179	222	185	170	220	247
m	0.96	0.94	0.92	0.92	0.95	0.96	0.95	0.99	1.01
r	0.86	0.72	0.58	0.83	0.73	0.92	0.55	0.97	0.96
r^2	0.74	0.52	0.33	0.69	0.54	0.84	0.31	0.93	0.92
1991	**SOx -S**	**NOy-N**	**NHx-N**	**Ca**	**K**	**Mg**	**H**	**Na**	**Cl**
n	163	165	135	129	130	130	125	129	157
m	0.93	0.92	0.93	0.85	0.93	0.87	0.88	0.96	0.98
r	0.71	0.66	0.80	0.43	0.59	0.69	0.87	0.96	0.95
r^2	0.50	0.44	0.64	0.15	0.34	0.47	0.75	0.92	0.90
1992	**SOx -S**	**NOy-N**	**NHx-N**	**Ca**	**K**	**Mg**	**H**	**Na**	**Cl**
n	224	239	180	170	191	166	147	184	194
m	0.97	0.95	0.93	0.98	0.95	0.99	0.99	0.97	0.99
r	0.63	0.68	0.61	0.79	0.38	0.81	0.69	0.97	0.95
r^2	0.40	0.46	0.38	0.62	0.15	0.66	0.47	0.94	0.89
1993	**SOx -S**	**NOy-N**	**NHx-N**	**Ca**	**K**	**Mg**	**H**	**Na**	**Cl**
n	270	275	207	207	226	203	169	221	223
m	0.92	0.90	0.89	0.83	0.87	0.84	0.94	0.94	0.93
r	0.73	0.75	0.76	0.48	0.32	0.63	0.65	0.94	0.94
r^2	0.54	0.57	0.59	0.23	0.11	0.40	0.43	0.88	0.89
1994	**SOx -S**	**NOy-N**	**NHx-N**	**Ca**	**K**	**Mg**	**H**	**Na**	**Cl**
n	297	302	235	215	226	214	170	235	239
m	0.90	0.93	0.94	0.82	0.96	0.94	1.05	0.93	0.94
r	0.52	0.69	0.66	0.14	0.47	0.72	0.93	0.97	0.93
r^2	0.27	0.47	0.43	0.02	0.23	0.52	0.86	0.93	0.86
1995	**SOx -S**	**NOy-N**	**NHx-N**	**Ca**	**K**	**Mg**	**H**	**Na**	**Cl**
n	327	320	267	244	255	257	189	259	260
m	0.94	0.94	0.94	0.89	0.96	0.99	1.02	0.99	0.99
r	0.73	0.72	0.71	0.48	0.55	0.91	0.87	0.98	0.93
r^2	0.54	0.51	0.50	0.23	0.30	0.82	0.76	0.96	0.87
1996	**SOx -S**	**NOy-N**	**NHx-N**	**Ca**	**K**	**Mg**	**H**	**Na**	**Cl**
n	365	364	306	282	296	294	203	296	283
m	0.94	0.95	0.92	0.88	0.96	0.96	1.01	0.97	0.95
r	0.69	0.74	0.61	0.31	0.64	0.75	0.80	0.96	0.96
r^2	0.48	0.54	0.37	0.10	0.41	0.56	0.64	0.92	0.91
									…

1997	**SOx -S**	**NOy-N**	**NHx-N**	**Ca**	**K**	**Mg**	**H**	**Na**	**Cl**
n	350	347	296	296	289	304	212	299	293
m	0.93	0.95	0.93	0.86	0.87	0.96	1.05	0.93	0.93
r	0.62	0.73	0.66	0.22	0.67	0.80	0.83	0.96	0.95
r^2	0.39	0.53	0.44	0.05	0.45	0.63	0.69	0.92	0.90
1998	**SOx -S**	**NOy-N**	**NHx-N**	**Ca**	**K**	**Mg**	**H**	**Na**	**Cl**
n	388	384	335	307	294	316	248	299	305
m	0.92	0.94	0.91	0.87	0.89	0.94	1.04	0.95	0.94
r	0.71	0.79	0.67	0.19	0.44	0.77	0.82	0.92	0.91
r^2	0.50	0.63	0.44	0.03	0.19	0.59	0.68	0.84	0.83
1999	**SOx -S**	**NOy-N**	**NHx-N**	**Ca**	**K**	**Mg**	**H**	**Na**	**Cl**
n	401	401	353	315	318	323	322	315	315
m	0.92	0.92	0.91	0.88	0.88	0.91	0.98	0.94	0.93
r	0.75	0.78	0.71	0.59	0.40	0.79	0.83	0.96	0.95
r^2	0.56	0.61	0.51	0.35	0.16	0.62	0.70	0.92	0.90
2000	**SOx -S**	**NOy-N**	**NHx-N**	**Ca**	**K**	**Mg**	**H**	**Na**	**Cl**
n	381	381	328	302	300	311	299	301	301
m	0.95	0.96	0.94	0.88	0.92	0.94	1.05	0.97	0.97
r	0.78	0.78	0.73	0.46	0.52	0.67	0.78	0.96	0.95
r^2	0.61	0.61	0.53	0.21	0.28	0.45	0.61	0.91	0.91
2001	**SOx -S**	**NOy-N**	**NHx-N**	**Ca**	**K**	**Mg**	**H**	**Na**	**Cl**
n	379	376	331	327	319	336	266	297	298
m	0.91	0.92	0.87	0.86	0.86	0.92	0.99	0.92	0.92
r	0.73	0.77	0.59	0.40	0.44	0.73	0.81	0.95	0.95
r^2	0.54	0.59	0.35	0.16	0.20	0.54	0.65	0.90	0.91
2002	**SOx -S**	**NOy-N**	**NHx-N**	**Ca**	**K**	**Mg**	**H**	**Na**	**Cl**
n	400	403	351	298	296	302	262	304	297
m	0.93	0.91	0.90	0.89	0.87	0.94	0.99	0.94	0.94
r	0.73	0.71	0.57	0.47	0.41	0.72	0.83	0.96	0.97
r^2	0.53	0.50	0.33	0.22	0.17	0.52	0.68	0.93	0.94
2003	**SOx -S**	**NOy-N**	**NHx-N**	**Ca**	**K**	**Mg**	**H**	**Na**	**Cl**
n	424	427	378	313	315	321	272	318	326
m	0.95	0.94	0.94	0.93	0.87	0.95	1.06	0.94	0.94
r	0.71	0.67	0.64	0.37	0.34	0.63	0.76	0.94	0.95
r^2	0.51	0.45	0.41	0.14	0.12	0.40	0.59	0.88	0.90
2004	**SOx-S**	**NOy-N**	**NHx-N**	**Ca**	**K**	**Mg**	**H**	**Na**	**Cl**
n	343	344	333	264	249	262	221	255	271
m	0.94	0.91	0.90	0.87	0.94	0.95	1.07	0.96	0.96
r	0.86	0.73	0.56	0.24	0.51	0.80	0.78	0.95	0.97
r^2	0.74	0.53	0.32	0.06	0.26	0.64	0.60	0.90	0.93

n = number of points
m = slope of linear regression line
r = Pearson correlation coefficient
r^2 = coefficient of determination

4.4 Ion balance maps of main compound wet deposition fluxes in Germany 1993-2004

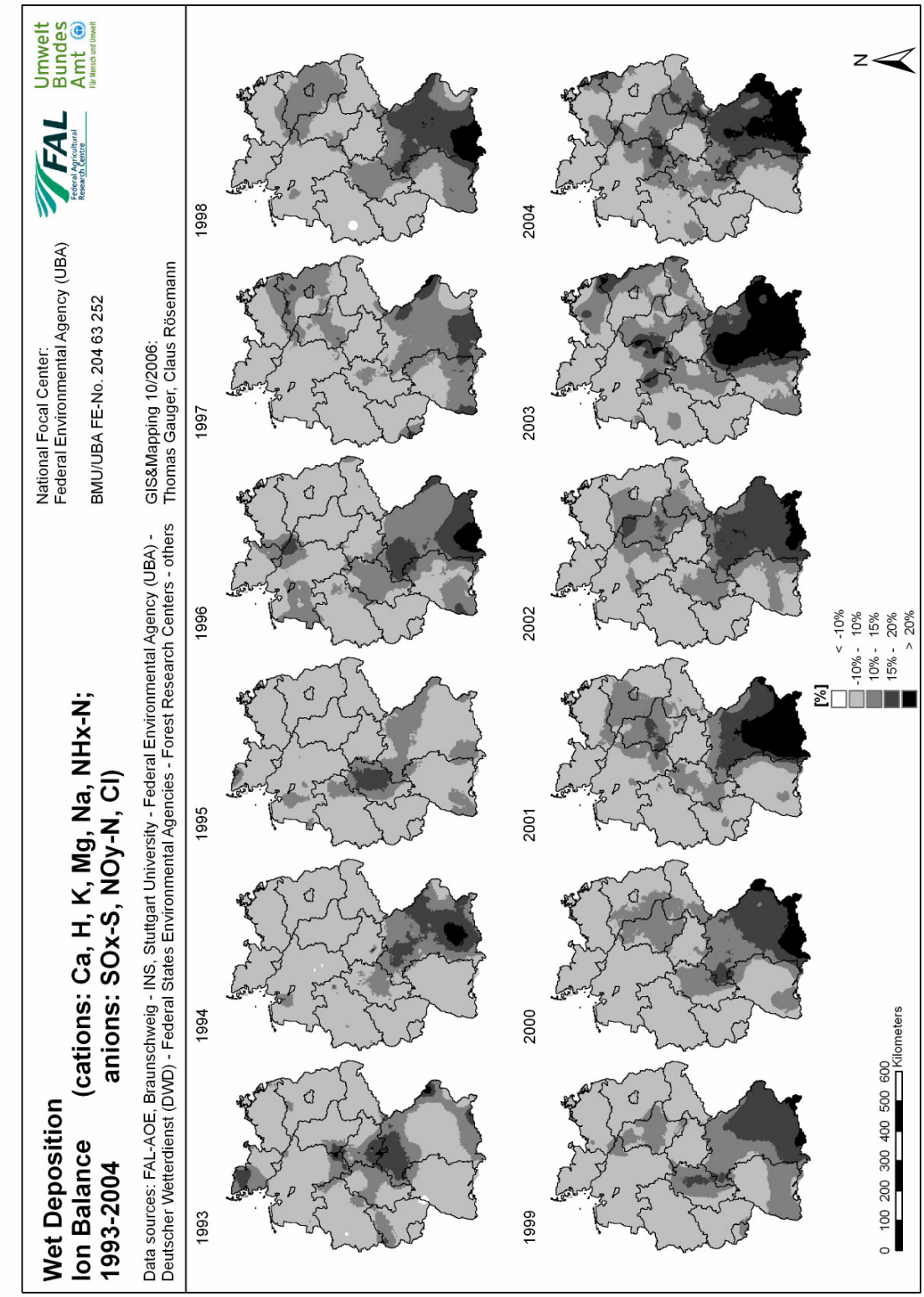

Map 4.1: Ion balance of 9 main components in precipitation 1993-2004

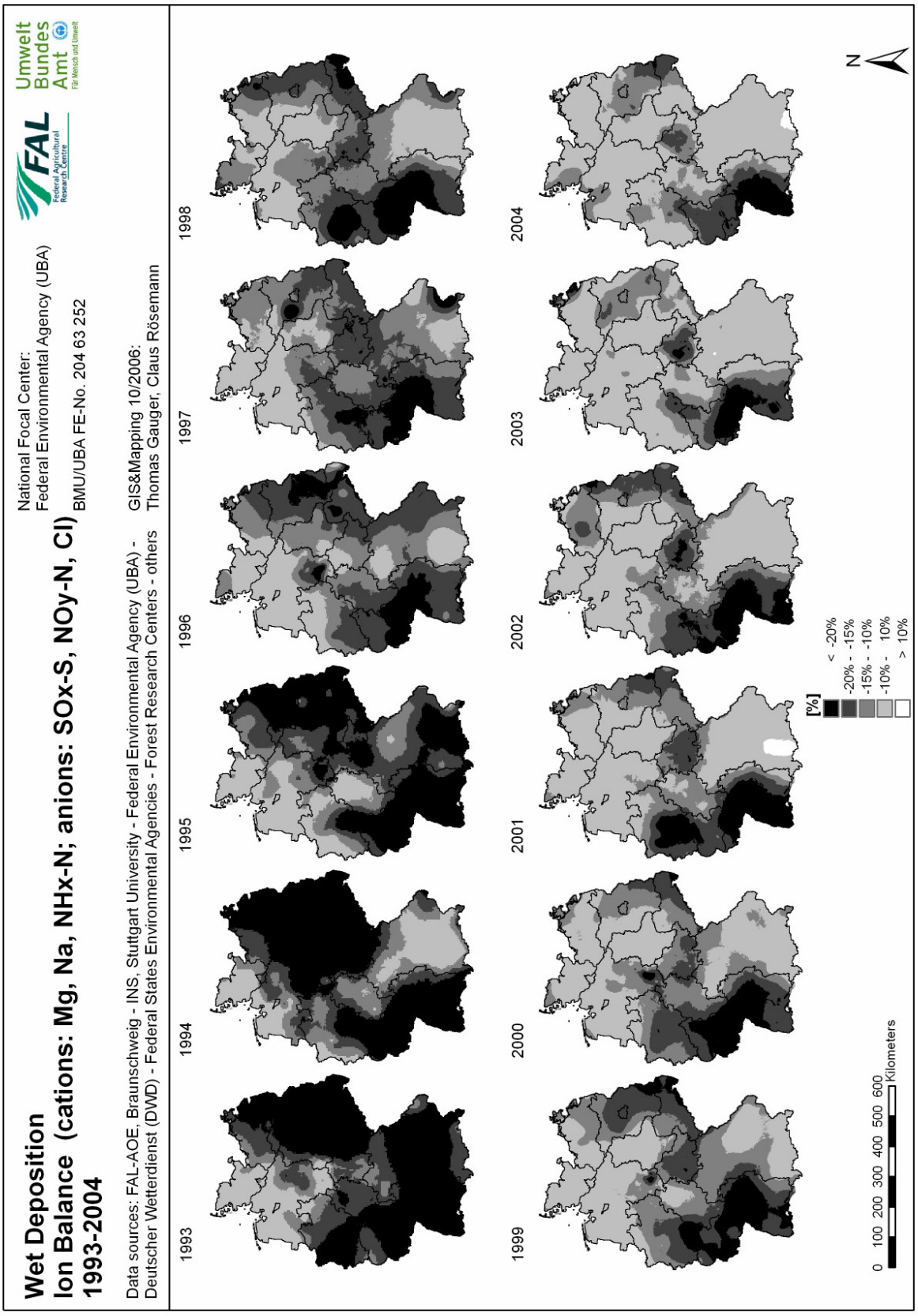

Map 4.2: Ion balance of 6 main components in precipitation 1993-2004

4.5 Wet deposition of heavy metals (Cd, Pb)

In general the same methods were applied for mapping wet deposition of Cd and Pb as for main components in precipitation (cf. Chapter 4.3, Figure 4.10).

Wet deposition data of the heavy metals lead (Pb) and cadmium (Cd) were provided from several institutions reponsible for deposition monitoring in Germany, or could be retrieved by download from the respective sites and reports in the internet (c.f Chapter 4.1.2, Table 4.1). The data acquisition mainly is aiming at gathering and including as many deposition data of heavy metals into the INS/FAL/UBA deposition database as possible. Hence all available data sets on Cd and Pb were compiled into the data base, which were derived from

- samples of main compound wet and bulk deposition, analysed also as 'screening data' of heavy metal deposition
- monitoring networks using Bergerhoff samplers for heavy metal analysis
- monitoring networks designed and equipped for special analysis of wet-only and bulk deposition of heavy metals

Precipitation analysis from samples of routinely working deposition monitoring networks in many cases also includes analysis of heavy metals. Not always special equipment is used in the field for heavy metal analysis. This additional heavy metal analysis using conventional deposition monitoring sites and equipment designed for analysis of main components in precipitation often is referred to as 'heavy metal screening'. In many aspects this is problematic, since underlying uncertainties are high with respect on possible contamination of the samples, exchange processes within the sample or even exchange with the sampler material, if standard plastic funnels and bottles are used, limited volume of the sample for multiple analysis, etc.

On the other hand, many networks for sampling airbourne heavy metal input are using Bergerhoff samplers, bucket samplers, which are recommended by some German standards (e.g. VDI-Richtlinie 2119, Blatt 2: "Messung partikelförmiger Niederschläge"). The Bergerhoff sampling method is problematic, since the definition of the physical characteristics of deposition into Bergerhoff samplers is difficult (DÄMMGEN&KÜSTERS 1992), and loss of collected material by blow-out frequently occurs (DÄMMGEN ET AL. 2005).

The third group of heavy metal monitoring networks is equipped with samplers designed for heavy metal analysis using inert funnels and bottles made of glass or stainless steel, and are explicitly designed for analysis of heavy metal wet or bulk deposition.

With respect to the data retrieved and the chemical analysis of the samples, two different approaches can be identified. Methods applied are eather aiming at total pulping of heavy metal content, or at analysis of the water soluble content of heavy metal bulk deposition. The latter mainly is used in monitoring networks aiming at water management research. At some neighbouring sites of two different monitoring networks in north-western Germany both analytical methods are used. It was tried to quantify the differences of both methods at those neighbouring sites. A preliminary comparison between the annual bulk deposition of Cd and Pb unfortunately showed that the results of total pulping content were lower than the water soluble content. Reasons for this unexpected result could not be found yet.

Table 4.9: Average ratio of wet-only and bulk fluxes of Cd and Pb used as correction factors in order to derive wet deposition from bulk deposition samples (GAUGER ET AL. 2000)

	Cd	**Pb**
simultaneous measurements, n =	12	11
average ratio wet-only / bulk	**0.73**	**0.71**
Maximum	1.00	0.93
Minimum	0.55	0.25
Standard deviation	0.14	0.20
Coefficient of variation [%]	19	28

As input to the INS/FAL/UBA wet deposition data base, however, all available data of Cd and Pb were used. Pre-processing of the data included correction of bulk deposition for wet-only fluxes using correction factors (Table 4.9) derived from parallel operating measurements of both bulk and wet-only samples in Germany (GAUGER ET AL 2000).

The amount of input data used for mapping is listed in Table 4.10. Due to the heterogenious approaches used within the different monitoring networks no quantitative overall quality check on the data population compiled in the database can be applied within this study. The data only were checked for high outliers using the "4-sigma-test" (SACHS, 1997, c.f. Chapter 4.2.2). All detected outliers in excess of the mean value +4 times the standard deviation of the population are excluded from further processing. In Table 4.10 the amount of data in the INS/FAL/UBA database is denoted 'available data', whereas 'after revision' denotes the amount of data after exclusion of high outliers from further processing.

Concentration of Cd and Pb in precipitation is used as input into GIS. In order to avoid clustered data in certain areas in Germany, the data of closey neighbouring sample plots where averaged within each 5x5km² grid cell. The amount of this data is denoted 'input data' in Table 4.10, specifying the data used for kriging application in order to derive fields of precipitation weighted annual mean ion concentrations of Cd and Pb. Once the concentration fields are mapped, wet deposition fluxes are calculated as the product of concentrations and the annual precipitation amount provided by Deutscher Wetterdienst (DWD) in 1x1km² grid resolution maps. The precipitation maps are modelled by DWD using a very large network of gauges (more than 3500 sample sites) as primary input (cf. Chapter 4.3.1).

As it is shown by the declining numbers from 'available data' over 'after revision' to 'input data' in Table 4.10 4-18% of the input data are identified as outliers and deleted from further processing. The amount of single input data diminishes to the rest of 78-65% of plots by averaging closely neighbouring sietes, which then are used to derive fields of wet deposition.

Table 4.10: Quantity of monitoring data used for mapping Cd and Pb wet deposition

	1994			1995			1996			1997			1998			1999		
	availabe data(1)	after revision (2)	input data(3)	availabe data[1]	after revision [2]	input data[3]	availabe data[1]	after revision [2]	input data[3]	availabe data[1]	after revision [2]	input data[3]	availabe data[1]	after revision [2]	input data[3]	availabe data[1]	after revision [2]	input data[3]
Pb	204	167	134	365	325	239	406	367	287	424	391	310	532	499	376	592	500	405
Cd	187	180	143	346	328	242	409	379	294	412	372	292	565	522	395	536	489	389
precip.			DWD map			DWD map			DWD map			DWD map			DWD map			DWD map
	2000			**2001**			**2002**			**2003**			**2004**					
	availabe data(1)	after revision (2)	input data(3)	availabe data[1]	after revision [2]	input data[3]	availabe data[1]	after revision [2]	input data[3]	availabe data[1]	after revision [2]	input data[3]	availabe data[1]	after revision [2]	input data[3]			
Pb	442	418	350	472	439	359	406	382	312	293	273	234	228	219	188			
Cd	453	420	347	470	438	354	424	382	309	309	277	233	241	224	189			
precip.			DWD map			DWD map			DWD map			DWD map			DWD map			DWD map

[1] = quantity of open field sampling data in the wet deposition data base

[2] = quantity of data after data revision (without outliers)

[3] = quantity of data input for mapping after averaging closely neighbouring sample points (within each 5x5km² grid cell)

In Table 4.11 the results of a comparison between the wet deposition fields and the measurements, corrected for the dry deposited contribution in bulk deposition, are shown. This comparison mainly reflects the effect of data pre-processing, interpolation and intersection of wet concentration with the DWD precipitation map at the points of the open field deposition monitoring.

Table 4.11: Comparison of measured and mapped Cd and Pb wet deposition loads 1994-2004

1994	Cd	Pb	1995	Cd	Pb
n	180	167	**n**	327	324
m	1.02	1.03	**m**	1.00	0.94
r	0.66	0.58	**r**	0.74	0.47
r²	0.44	0.33	**r²**	0.55	0.22
1996	**Cd**	**Pb**	**1997**	**Cd**	**Pb**
n	378	366	**n**	366	374
m	1.00	0.99	**m**	0.95	0.95
r	0.64	0.74	**r**	0.52	0.51
r²	0.41	0.54	**r²**	0.27	0.26
1998	**Cd**	**Pb**	**1999**	**Cd**	**Pb**
n	513	482	**n**	479	481
m	1.02	0.96	**m**	0.97	0.97
r	0.85	0.50	**r**	0.54	0.46
r²	0.72	0.25	**r²**	0.29	0.21
2000	**Cd**	**Pb**	**2001**	**Cd**	**Pb**
n	406	400	**n**	431	426
m	0.96	0.95	**m**	0.93	1.04
r	0.41	0.32	**r**	0.48	0.53
r²	0.17	0.10	**r²**	0.23	0.28
2002	**Cd**	**Pb**	**2003**	**Cd**	**Pb**
n	370	367	**n**	261	255
m	0.98	1.03	**m**	1.07	0.95
r	0.58	0.54	**r**	0.59	0.37
r²	0.33	0.30	**r²**	0.35	0.13
2004	**Cd**	**Pb**			
n	211	206			
m	1.06	1.05			
r	0.71	0.56			
r²	0.50	0.31			

n = number of points
m = slope of linear regression line
r = Pearson correlation coefficient
r² = coefficient of determination

5 Wet deposition mapping results

Claus Rösemann & Thomas Gauger
Federal Agricultural Research Centre, Institute of Agroecology (FAL-AOE), Bundesallee 50, D-38116 Braunschweig
Bundesforschungsanstalt für Landwirtschaft, Institut für Agrarökologie (FAL-AOE), Bundesallee 50, 38116 Braunschweig

Annual average wet deposition fluxes have been calculated and mapped for the 18 year time perod from 1987 to 2004. Samples of open field wet deposition of the major ions sulphur (SO_4-S), nitrate (NO_3-N) and ammonium (NH_4-N), sodium (Na), chlorine (Cl), protons (H), and the base cations calcium (Ca), magnesium (Mg), potassium (K) present in precipitation are used to map annual mean wet concentration fields using kriging technique. The concentration in precipitation is mapped in 5x5km² grid resolution for the years 1987 to 1995. From 1996 onward more samples of wet deposition are available. The scatter and amout of data allows applying kriging interpolation technique for a grid resolution of 1x1km². These precipitation weighted annual wet concentration fields (in meq ha^{-1} a^{-1}) are representing the annual mean patterns of concentration of all main wet deposited species over Germany. Wet deposition fluxes (wet deposition loads in eq ha^{-1} a^{-1}) are derived by multiplying the wet concentration fields with 1x1km² precipitation fields obtained from the German meteorological survey (Deutscher Wetterdienst, DWD).

In Table 5.1 and Figure 5.1 an overview is given on the mapping results. Table 5.1 shows the single mapping results for each species and for the years 1987 to 2004, given as average annual wet deposition loads in Germany. The sum of the major anions and cations as well as the result of the ion balance calculation is included. The difference between the sum of cations and anions is given as mean annual average of the not analysed fraction. Negative difference values are indicating annual mean anion surplus, whereas positive difference values would stand for annual mean cation surplus in the ion balance of all species taken into account.

Table 5.1: Average annual wet deposition of main compounds in precipitation 1987-2004

	1987	1988	1989	1990	1991	1992	1993	1994	1995
Na [eq ha^{-1} a^{-1}]	226	278	278	305	208	218	231	230	233
H [eq ha^{-1} a^{-1}]	420	354	311	298	266	278	271	259	244
Ca [eq ha^{-1} a^{-1}]	335	310	246	199	186	177	209	175	146
K [eq ha^{-1} a^{-1}]	51	40	41	43	34	41	39	34	38
Mg [eq ha^{-1} a^{-1}]	117	131	110	99	82	74	94	85	77
NH_4-N [eq ha^{-1} a^{-1}]	514	506	503	482	416	421	456	456	432
SO_4-S [eq ha^{-1} a^{-1}]	902	799	672	613	512	529	552	512	450
NO_3-N [eq ha^{-1} a^{-1}]	384	378	347	314	292	302	332	325	312
Cl [eq ha^{-1} a^{-1}]	312	378	300	321	233	239	244	275	268
Cations: (Na+H+Ca+K+NH_4-N) [eq ha^{-1} a^{-1}]	1664	1619	1489	1427	1192	1208	1301	1239	1170
Anions: (SO_4-S + NO_3-N + Cl) [eq ha^{-1} a^{-1}]	1599	1555	1319	1248	1038	1070	1128	1113	1030
Difference (=ion balance error) [eq ha^{-1} a^{-1}]	-65	-64	-170	-179	-154	-138	-172	-126	-140
Difference (=ion balance error) [%]	-2	-2	-6	-6	-6	-6	-7	-5	-6

	1996	1997	1998	1999	2000	2001	2002	2003	2004
Na [eq ha^{-1} a^{-1}]	146	166	194	184	154	172	173	147	194
H [eq ha^{-1} a^{-1}]	183	137	178	131	116	119	122	67	106
Ca [eq ha^{-1} a^{-1}]	126	143	151	136	143	138	141	134	133
K [eq ha^{-1} a^{-1}]	32	30	35	30	30	31	36	32	36
Mg [eq ha^{-1} a^{-1}]	61	63	73	64	59	60	62	53	65
NH_4-N [eq ha^{-1} a^{-1}]	423	384	419	379	393	406	425	331	389
SO_4-S [eq ha^{-1} a^{-1}]	358	327	359	297	294	283	306	221	262
NO_3-N [eq ha^{-1} a^{-1}]	287	265	301	283	285	288	294	227	276
Cl [eq ha^{-1} a^{-1}]	166	203	234	212	186	201	206	160	221
Cations: (Na+H+Ca+K+NH_4-N) [eq ha^{-1} a^{-1}]	971	922	1051	925	896	926	958	762	922
Anions: (SO_4-S + NO_3-N + Cl) [eq ha^{-1} a^{-1}]	811	795	893	792	765	772	805	608	759
Difference (=ion balance error) [eq ha^{-1} a^{-1}]	-160	-127	-158	-133	-131	-155	-153	-154	-164
Difference (=ion balance error) [%]	-8	-7	-8	-7	-7	-8	-8	-10	-9

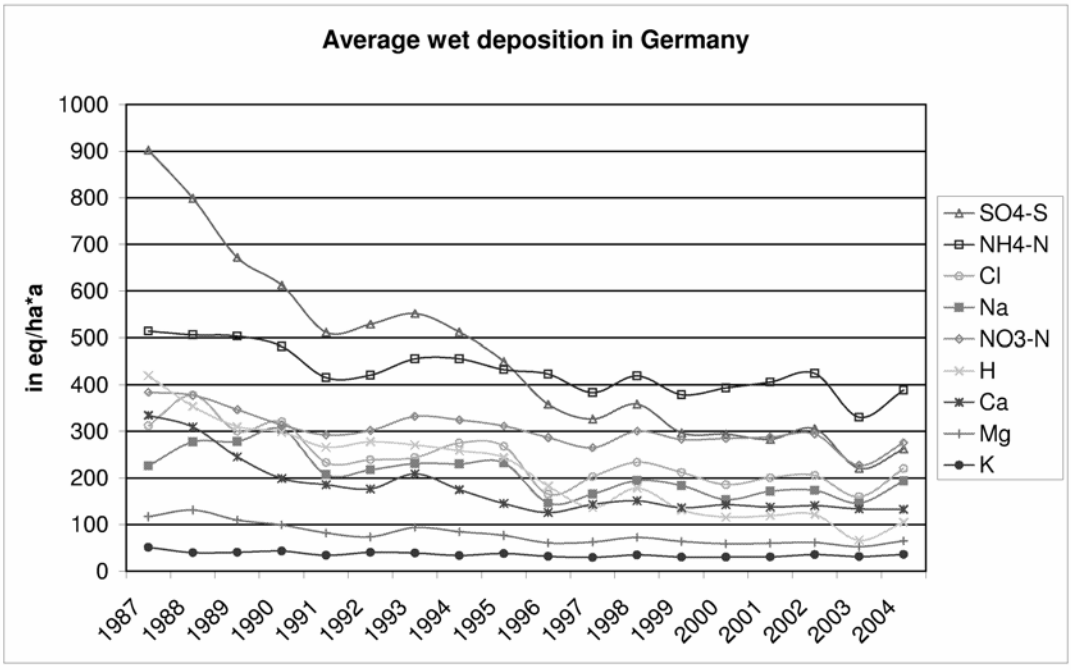

Figure 5.1: Average annual wet deposition of main compounds 1987–2004

The total average of the sum of all major compounds in wet deposition declined for about 51% between 1987 and 2004. This decline is dominated by the sharp fall of sulphur (SO_4-S), where the annual average wet

deposition load in 2004 is about 71% lower than in 1987 (Figure 5.1).

Remarkable in the graph (Figure 5.1) is the depression of almost all average wet fluxes of the single species in the year 2003. Only for base cations (Ca^{2+}, K^+, Mg^+) this is not very distinct. This phenomenon is due to the exceptional dry weather conditions in Germany that year.

The trends in Na^+ and Cl^- wet deposition are similar (Figure 5.1). Na^+ is assumed to be 100% of marine origin, and it is deposited together with chlorine as sea salt input. The curve of chlorine lies above the sodium line, which is due to slightly higher Cl^- fractions in sea water, compared to Na^+. Moreover the shape of both curves is not fully parallel, especially in 1987 and 1988. This indicates that Cl^- also originates from other sources than from sea spray only. The non-sea salt chloride deposition is assumed to be completely due to anthropogenic HCl emissions (ICP MODELLING AND MAPPING 1996, 2004). However, the oscillation of the Na^+ and Cl^- curves from year to year mainly reflects the variation in inland transport of sea salt from the German Bight (North Sea) by marine air masses, to a certain extent driven by autumn or winter time storms. These sea salt transport processes are varying each of the single years considered.

The wet deposition loads of H^+ declined by about 79% from 1987 to 2004. The shape of the H^+ curve (Figure 5.1) is on a much lower level almost parallel with the curve of sulphur wet deposition, i.e. the wet flux of H^+ and SO_4-S are to some extent correlated.

The annual variation of the average wet deposition of Na^+, Cl^- and H^+ (wet fluxes in eq ha^{-1} a^{-1}) in Table 5.2 is shown also as percentage change from the previous year, as well as over the whole time series mapped. There is no clear trend in Na^+ and Cl^- wet deposition. Rather big percentage differences up to more than ±30% from one year to the next, and the irregular sequence of positive or negative sign is indicating annual differences in inland sea salt transport as dominating process.

Table 5.2: Budgets of average annual wet deposition of Na, Cl, and H 1987-2004

	Na [eq ha^{-1} a^{-1}]	Change from previous year [%]	Cl [eq ha^{-1} a^{-1}]	Change from previous year [%]	H [eq ha^{-1} a^{-1}]	Change from previous year [%]
1987	226	- -	312	- -	420	- -
1988	278	+22.6	378	+21.1	354	-15.8
1989	278	+0.3	300	-20.6	311	-12.2
1990	305	+9.6	321	+6.9	298	-4.0
1991	208	-31.9	233	-27.3	266	-10.8
1992	218	+4.8	239	+2.6	278	+4.5
1993	231	+6.2	244	+2.0	271	-2.5
1994	230	-0.3	275	+12.8	259	-4.6
1995	233	+1.0	268	-2.7	244	-5.6
1996	146	-37.2	166	-38.1	183	-25.0
1997	166	+13.5	203	+22.6	137	-25.4
1998	194	+17.2	234	+15.0	178	+30.5
1999	184	-5.4	212	-9.3	131	-26.3
2000	154	-16.4	186	-12.3	116	-11.6
2001	172	+11.6	201	+7.9	119	+2.6
2002	173	+1.1	206	+2.4	122	+2.1
2003	147	-15.5	160	-22.2	67	-45.3
2004	194	+32.2	221	+37.9	106	+58.3
Change from 1987 to 2004 [%]		-14.4		-29.4		-74.9

Table 5.3: Budgets of average annual wet deposition of SO_4-S, NH_4-N, NO_3-N, and N 1987-2004

	SO_4-S [eq ha^{-1} a^{-1}]	Change from previous year [%]	NH_4-N [eq ha^{-1} a^{-1}]	Change from previous year [%]	NO_3-N [eq ha^{-1} a^{-1}]	Change from previous year [%]	N [eq ha^{-1} a^{-1}]	Change from previous year [%]
1987	902		514		384		899	
1988	799	-11.5	506	-1.5	378	-1.7	884	-1.6
1989	672	-15.9	503	-0.6	347	-8.1	850	-3.8
1990	613	-8.8	482	-4.3	314	-9.5	796	-6.4
1991	512	-16.5	416	-13.7	292	-6.9	708	-11.0
1992	529	+3.3	421	+1.3	302	+3.3	723	+2.1
1993	552	+4.4	456	+8.3	332	+10.1	788	+9.1
1994	512	-7.2	456	+0.0	325	-2.3	781	-0.9
1995	450	-12.2	432	-5.2	312	-4.1	744	-4.7
1996	358	-20.4	423	-2.1	287	-7.9	710	-4.5
1997	327	-8.8	384	-9.4	265	-7.6	649	-8.7
1998	359	+9.8	419	+9.3	301	+13.3	720	+11.0
1999	297	-17.2	379	-9.7	283	-6.0	662	-8.1
2000	294	-0.9	393	+3.8	285	+0.8	678	+2.6
2001	283	-3.9	406	+3.3	288	+1.0	694	+2.3
2002	306	+8.1	425	+4.6	294	+2.2	719	+3.6
2003	221	-27.7	331	-22.2	227	-22.7	558	-22.4
2004	262	+18.7	389	+17.6	276	+21.3	664	+19.1
Change from 1987 to 2004 [%]		-70.9		-24.4		-28.3		-26.1

The annual average NH_4-N and NO_3-N wet deposition flux 1987 to 2004 shows more or less parallel curves (Figure 5.1), which, over the whole time period, are only slightly moving downward. From 1991 on rather an oscillation of the mean NH_4-N wet flux of about 410 eq ha^{-1} a^{-1}, and of NO_3-N of about 290 eq ha^{-1} a^{-1},

respectively, can be observed (Table 5.3). The run of the NO_3-N curve over time, however, in most of the years can be found on an about 30% lower level than the NH_4-N curve.

The average wet flux of SO_4-S over Germany declined remarkably from 1987 to 1991 by about 43% and then again from 1993 to 1997 by about 41%. In 2004 the average wet deposition flux of SO_4-S over Germany is reduced to about one third of the average wet flux in 1987 (Table 5.3).

From 1996 on the NH_4-N curve lies above the SO_4-S curve (Figure 5.1), which illustrates that, with respect to the magnitude of average wet deposition loads over all Germany, NH_4-N is more and more becoming the most important acidifying compound. The annual average wet flux of total Nitrogen (N = NH_4-N + NO_3-N) between 1987 and 2004 declined by about 26%.

Table 5.4: Budgets of average annual wet deposition of Ca, Mg, K and BC 1987-2004

	Ca [eq ha^{-1} a^{-1}]	Change from previous year [%]	Mg [eq ha^{-1} a^{-1}]	Change from previous year [%]	K [eq ha^{-1} a^{-1}]	Change from previous year [%]	BC [eq ha^{-1} a^{-1}]	Change from previous year [%]
1987	335		117		51		503	
1988	310	-7.5	131	+11.8	40	-22.0	481	-4.4
1989	246	-20.7	110	-16.2	41	+1.6	396	-17.6
1990	199	-18.9	99	-9.7	43	+6.2	342	-13.7
1991	186	-6.7	82	-17.1	34	-20.5	303	-11.5
1992	177	-5.0	74	-10.3	41	+18.3	291	-3.8
1993	209	+18.4	94	+27.4	39	-3.2	343	+17.7
1994	175	-16.2	85	-9.9	34	-13.7	294	-14.2
1995	146	-16.9	77	-9.2	38	+11.6	261	-11.3
1996	126	-13.3	61	-21.1	32	-16.0	219	-16.0
1997	143	+13.7	63	+3.7	30	-6.6	236	+8.0
1998	151	+5.4	73	+15.5	35	+18.0	259	+9.7
1999	136	-9.9	64	-12.2	30	-13.8	230	-11.1
2000	143	+4.9	59	-7.4	30	+0.6	233	+0.9
2001	138	-3.6	60	+2.0	31	+1.5	229	-1.5
2002	141	+2.2	62	+2.2	36	+15.3	238	+3.9
2003	134	-5.0	53	-13.9	32	-11.3	218	-8.3
2004	133	-0.6	65	+22.8	36	+14.7	234	+7.3
Change from 1987 to 2004 [%]		-60.3		-44.5		-29.3		-53.4

The average wet deposition flux of base cations (BC = Ca^{2+} + Mg^{2+} + K) over the time period 1987 to 2004 show a more or less continuous decline in magnitude. The average BC wet flux declined by about 53% between 1987 and 2004 (c.f. Table 5.4 and Figure 5.1).

All of the tree base cations are aside Na^+, Cl^-, and SO_4-S main compounds of sea salt aerosols. Calcium (Ca^{2+}) to more than 90% originates from both terrestrial and anthropogenic emission sources, such as soil particulates and fly ash. Magnesium (Mg^{2+}) mainly, i.e. to more than 70%, originates from sea spray. Main terrestrial sources of Mg^{2+} are mineral particulates from soil, industry and lignite (brown coal) combustion. Potassium (K^+) is by more than 80% emitted from terrestrial and vegetation sources. Anthropogenic sources are emission by combustion, during fertilizer application and wind blown soil particulates. Naturally it is emitted from vegetation and sea spray. If very high K^+ content is analysed in bulk deposition samples it is indicating contamination by bird droppings.

The contribution of Ca^{2+} to the sum of base cations (BC) over the whole time scale mapped averages 61%. The respective share of Mg^{2+} in BC wet deposition is about 27%, of K^+ about 12%, respectively. The annual average wet deposition load of Ca^{2+} 2004 is about 60% lower than in 1987. Since 1995 no clear trend of reduction can be observed. The Ca^{2+} wet deposition flux from then on is rather oscillating around average 140 eq ha^{-1} a^{-1} (Table 5.4). Average Mg^{2+} wet deposition declined by about 45% from 1987 to 2004. Since 1996 no directed trend can be observed: Mg^{2+} mean annual wet flux over Germany is between 59 and 73 eq ha^{-1} a^{-1}. The annual average wet deposition flux of K^+ 2004 is about 29% lower than in 1987. Here also no clear trend can be observed. From 1988 onward the K^+ wet deposition flux over Germany is fluctuating between 30 and 41 eq ha^{-1} a^{-1}.

5.1 Wet deposition fluxes and trends of base cations (Na; Ca, K, and Mg)

The deposition of Sodium (Na^-) is assumed to be 100% of marine origin (ICP MODELLING AND MAPPING 1996, 2004, www.icpmapping.org). Sodium compounds are deposited as neutral salt and their elements do neither contribute to acidification nor to acid neutralisation. Na fluxes are mapped, because Na is used as a tracer for calculating the sea salt contribution to the wet flux of Ca^{2+}, K^+, Mg^+, Cl^- and SO_4-S^{2-} (cf. sea salt correction, Chapter 4.3.1). The marine compounds of these species are also deposited as neutral salt and thus are assumed not to be physiologically active within the receptor ecosystems.

The deposited sum of non-sea salt base cations ($BC_{(nss)} = Ca_{(nss)} + K_{(nss)} + Mg_{(nss)}$) is physiologically active. If not deposited as neutral salt, Ca^{2+}, K^+, and Mg^+ can improve the nutrient status with respect to eutrophication, and they counteract deposition of potential acid.

Following the Critical Load approach, anthropogenic base cation deposition should not be accounted for. The aim of the Convention on Long-range Transboundary Air Pollution (CLTRAP 1979) is to minimise emissions of acidifying compounds irrespective of other man made emissions. The emission abatement of acidifying compounds has to be derived from their effects alone. Thus it is not permissible to charge up base cations against acidifying compunds, if both are emitted from anthropogenic sources, even though those base cations would also buffer acidity. Only the deposited natural background level of base cations should be used as a magnitude counteracting man made acidifying input into ecosystems, because it has a relatively large continuity in time and space and can be assumed to be a quality of the ecosystems. Unfortunately there are no methods or data yet available (e.g. emission inventories of base cations) to clearly quantify all fractions of anthropogenic and natural deposition loads of base cations besides the sea salt fraction. Therefore the non-sea salt fraction (BC(nss)) is only attributable to natural and anthropogenic emission processes excluding sea spray. (ICP MODELING AND MAPPING 1996; GAUGER ET AL. 1997; KÖBLE & SPRANGER 1999, GAUGER ET AL. 2000, GAUGER ET AL.2002).

5.1.1 Wet deposition of sodium (Na)

In Figure 5.2 the map statistics of Sodium (Na) wet deposition in the years 1987 to 2004 in Germany is shown. A relatively large inter-annual variability of the median and mean wet deposition fluxes up to more than 30% from one year to the next can be observed. The highest mean and maximum annual wet deposition of Na is found in 1990.

Maps of wet deposition of Na 1993 to 2004 are presented in Map 5.3. The spatial pattern of high and low fluxes (Map 5.1) clearly reflects the marine origin of Na. Sodium wet deposition each year shows a regular spatial gradient with highest wet deposition loads at the coastal region of the North Sea (NW) and lowest wet deposition loads in continental most inland areas of Germany (SE). In inland areas only orographic obstacles (mountain areas and the alpine region) receive higher Na loads than their surrounding areas, due to elevation and long-range transport of marine air masses. The magnitude of annual sodium deposition in Germany mainly is due to the occurrence of storm events from north-west in winter time, where higher amounts of sea salt are transported inland (cf. UBA 1997). The highest peak of Na wet deposition occurs in 1990. This year storm events were observed in autumn, mainly over the western half of Germany.

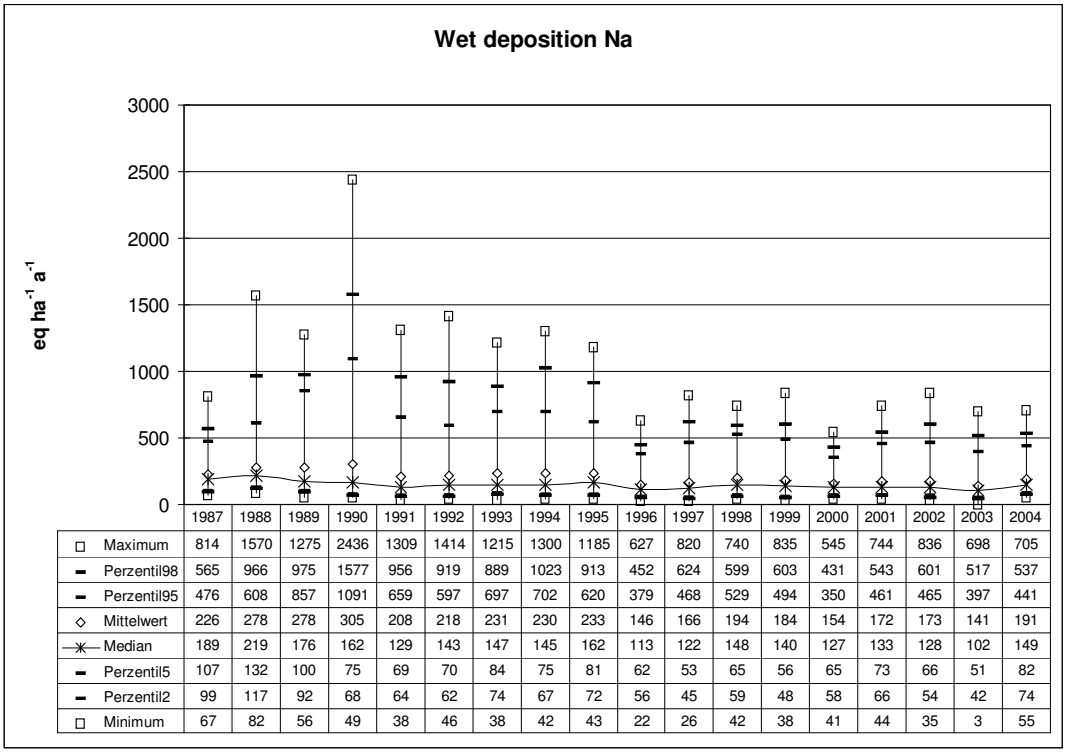

	1987	1988	1989	1990	1991	1992	1993	1994	1995	1996	1997	1998	1999	2000	2001	2002	2003	2004
Maximum	814	1570	1275	2436	1309	1414	1215	1300	1185	627	820	740	835	545	744	836	698	705
Perzentil98	565	966	975	1577	956	919	889	1023	913	452	624	599	603	431	543	601	517	537
Perzentil95	476	608	857	1091	659	597	697	702	620	379	468	529	494	350	461	465	397	441
Mittelwert	226	278	278	305	208	218	231	230	233	146	166	194	184	154	172	173	141	191
Median	189	219	176	162	129	143	147	145	162	113	122	148	140	127	133	128	102	149
Perzentil5	107	132	100	75	69	70	84	75	81	62	53	65	56	65	73	66	51	82
Perzentil2	99	117	92	68	64	62	74	67	72	56	45	59	48	58	66	54	42	74
Minimum	67	82	56	49	38	46	38	42	43	22	26	42	38	41	44	35	3	55

Figure 5.2: Statistical evaluation of annual sodium (Na) wet deposition 1987-2004

5.1.2 Wet deposition of non-sea salt calcium ($Ca_{(nss)}$)

From 1987 to 2004 average and median of non sea salt wet fluxes of Calcium ($Ca_{(nss)}$) declined by 62% and 54%, respectively. From 1996 onward mean wet fluxes about 130 eq ha^{-1} a^{-1} can be observed. Peak values show a steep decline, and the span between extreme values shrank from more than 1000 eq ha^{-1} a^{-1}in 1988 to a span of only 300 to 400 eq ha^{-1} a^{-1}. The decline of maxima can be attributed to emission reduction, which mainly took place since the decree on high-capacity firing plants (Großfeuerungsanlagen-Verordnung, GFAVO) entered into force. Due to the economic changes in the eastern part of Germany after 1989, old industrial complexes were refurbished and dust removal technique was applied in all Germany. This, in its graphical representation is shown in Map 5.2, where the 1993 to 2004 $Ca_{(nss)}$ wet deposition maps show patterns of higher deposition loads mainly over remote areas with highest precipitation rates.

The magnitude of the sea salt fraction of wet deposited calcium is listed in Table 5.5 as total sum on the whole area of Germany in kilo tons per year (kt), as flux in equivalents and kilo grammes per hectare per year (eq ha^{-1} a^{-1} and kg ha^{-1} a^{-1}), and as prercentage of the whole wet deposited species, respectively. Here again, as it is shown for the non-sea salt fraction of wet deposited Ca^{2+}, a discontinuous, but obvious decline of the absolute average wet sea salt calcium deposition flux can be observed. This discontinuous fluctuation of the mean wet fluxes, however, is due to the inland spread of sea spray originating mainly from the North Sea (cf. Sodium, Chapter 5.1.1). The average wet deposition load of sea salt Ca^{2+} ranges from 0.13 kg ha^{-1} a^{-1} in 1996 and 2003, respectively, to 0.27 kg ha^{-1} a^{-1} in 1990. In most of the years the average wet deposition load of sea salt Ca^{2+}in Germany is roughly about 0.2 kg ha^{-1} a^{-1}. The relative sea salt Ca share, shown as percentage of the total wet deposited Ca^{2+}, over the time period is slightly and, due to years like 1990 with more storms from north west, discontinuously rising from 3% (1987) to about 6% (2004). There are several natural and anthropogenic, local and remote sources of (measured) non-sea salt calcium in wet deposition. Thus uncertainties in the attribution to different emission sources are high, due to lacking data and research. The doubling of the fraction of sea salt Ca^{2+}, while the amount of deposited non-sea salt $Ca_{(nss)}$ is decreasing (cf. Figure 5.3), however, can possibly be interpreted as additional indication of continuing emission abatement of anthropogenic calcium.

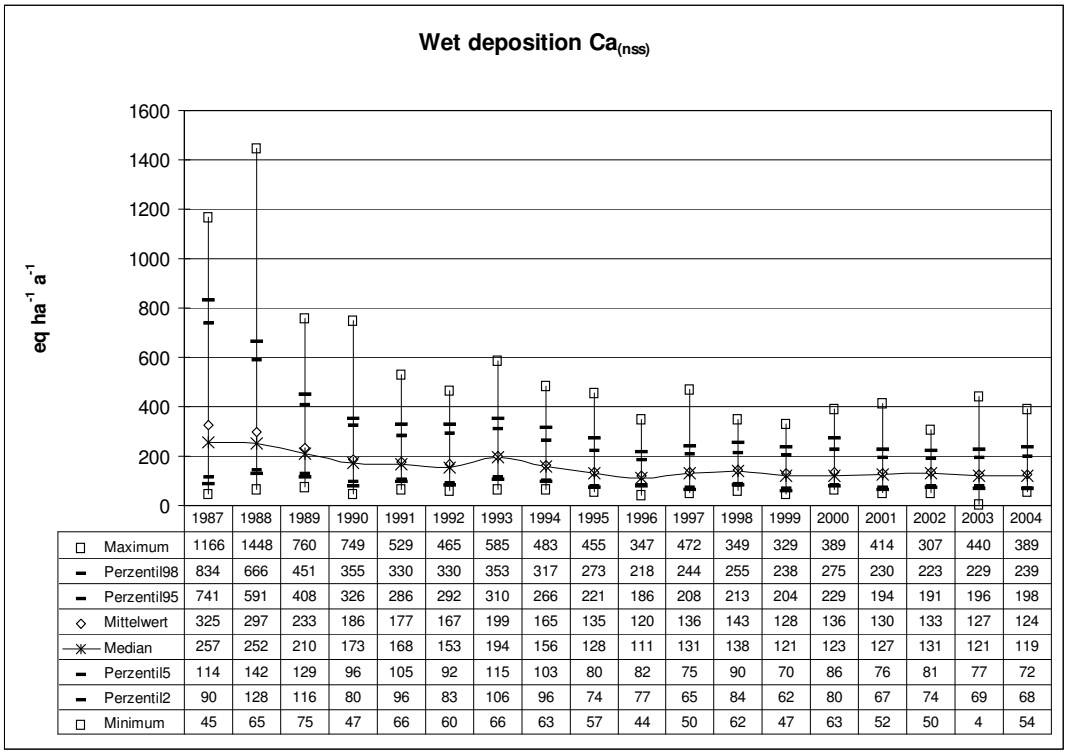

	1987	1988	1989	1990	1991	1992	1993	1994	1995	1996	1997	1998	1999	2000	2001	2002	2003	2004
Maximum	1166	1448	760	749	529	465	585	483	455	347	472	349	329	389	414	307	440	389
Perzentil98	834	666	451	355	330	330	353	317	273	218	244	255	238	275	230	223	229	239
Perzentil95	741	591	408	326	286	292	310	266	221	186	208	213	204	229	194	191	196	198
Mittelwert	325	297	233	186	177	167	199	165	135	120	136	143	128	136	130	133	127	124
Median	257	252	210	173	168	153	194	156	128	111	131	138	121	123	127	131	121	119
Perzentil5	114	142	129	96	105	92	115	103	80	82	75	90	70	86	76	81	77	72
Perzentil2	90	128	116	80	96	83	106	96	74	77	65	84	62	80	67	74	69	68
Minimum	45	65	75	47	66	60	66	63	57	44	50	62	47	63	52	50	4	54

Figure 5.3: Statistical evaluation of annual non-sea salt calcium ($Ca_{(nss)}$) wet deposition 1987-2004

Table 5.5: Average sea salt fraction of calcium wet deposition 1987-2004

	1987	1988	1989	1990	1991	1992	1993	1994	1995
in kt a^{-1}	7.1	8.7	8.8	9.6	6.5	6.9	7.3	7.3	7.3
in eq ha^{-1} a^{-1}	10.0	12.2	12.2	13.4	9.1	9.6	10.2	10.1	10.2
in kg ha^{-1} a^{-1}	0.20	0.24	0.25	0.27	0.18	0.19	0.20	0.20	0.21
Wet deposited sea salt fraction %	3.0	3.9	5.0	6.7	4.9	5.4	4.9	5.8	7.0

	1996	1997	1998	1999	2000	2001	2002	2003	2004
in kt a^{-1}	4.6	5.2	6.1	5.8	4.8	5.4	5.5	4.6	6.1
in eq ha^{-1} a^{-1}	6.4	7.3	8.6	8.1	6.8	7.6	7.6	6.5	8.5
in kg ha^{-1} a^{-1}	0.13	0.15	0.17	0.16	0.14	0.15	0.15	0.13	0.17
Wet deposited sea salt fraction %	5.1	5.1	5.7	5.9	4.7	5.5	5.4	4.8	6.4

5.1.3 Wet deposition of non-sea salt potassium ($K_{(nss)}$)

A weak trend of declining non sea salt ($K_{(nss)}$) wet deposition flux can be observed from 1987 to 1994 (Figure 5.4). Hereafter the average wet flux is fluctuating between 27 to 33 eq ha^{-1} a^{-1}. Over the whole time period median and mean of $K_{(nss)}$ wet deposition fluxes are diminishing by about 31% and 33%, respectively. This equals an absolute decrease of $K_{(nss)}$ total wet deposition flux on the whole area of Germany of about 20 kt from 65 kt a^{-1} 1987 to 45 kt a^{-1} in 2004. Maximum values (Figure 5.4) do not reflect a trend of decreasing $K_{(nss)}$ wet deposition.

Maps of wet deposition of $K_{(nss)}$ 1993 to 2004 are presented in Map 5.3. Wet $K_{(nss)}$ deposition loads above the annual average each year more or less distinct can be found in the Alps and in mountain regions which receive higher precipitation rates. In the single years considered, however, higher $K_{(nss)}$ deposition loads can also be observed over areas in other regions, partly dominated by agricultural activities. Sources of $K_{(nss)}$ are urban and industrial combustion, mineral fertiliser application, soil particulates and vegetation.

The sea salt fraction of K wet deposition (Table 5.6) from 1987 to 1995 (13% on average) is higher than from 1996 to 2004 (11% on average). The overall K sea salt fraction averages about 9% to 15% over the wole time

period considered.

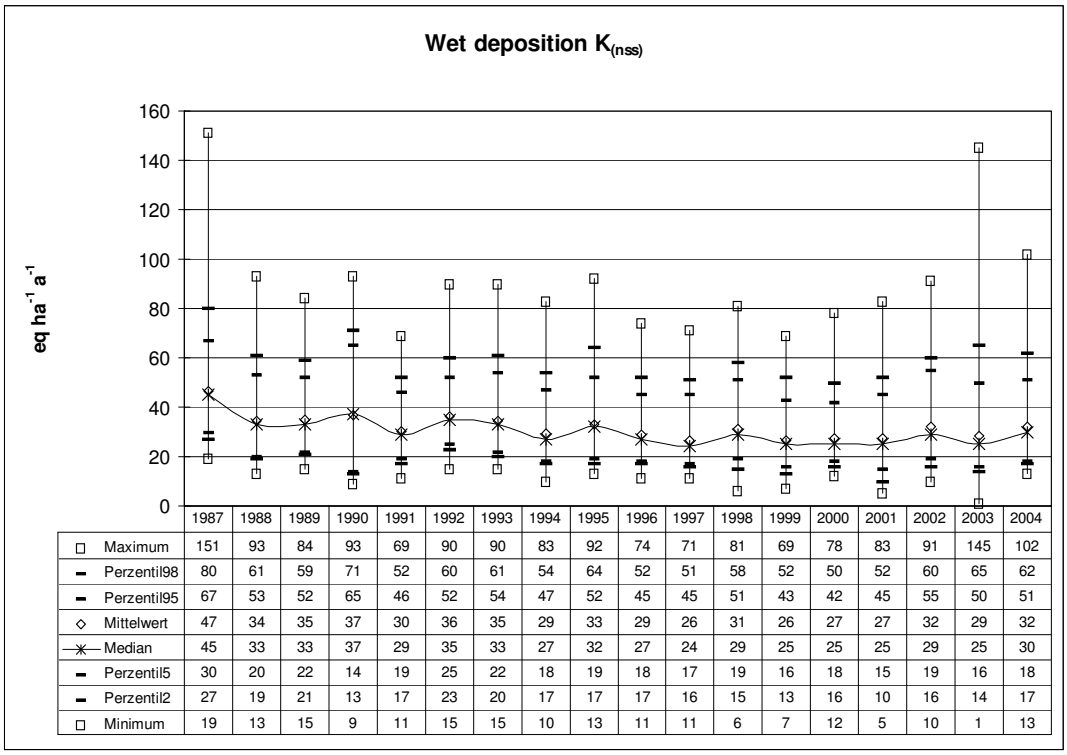

	1987	1988	1989	1990	1991	1992	1993	1994	1995	1996	1997	1998	1999	2000	2001	2002	2003	2004
Maximum	151	93	84	93	69	90	90	83	92	74	71	81	69	78	83	91	145	102
Perzentil98	80	61	59	71	52	60	61	54	64	52	51	58	52	50	52	60	65	62
Perzentil95	67	53	52	65	46	52	54	47	52	45	45	51	43	42	45	55	50	51
Mittelwert	47	34	35	37	30	36	35	29	33	29	26	31	26	27	27	32	29	32
Median	45	33	33	37	29	35	33	27	32	27	24	29	25	25	25	29	25	30
Perzentil5	30	20	22	14	19	25	22	18	19	18	17	19	16	18	15	19	16	18
Perzentil2	27	19	21	13	17	23	20	17	17	17	16	15	13	16	10	16	14	17
Minimum	19	13	15	9	11	15	15	10	13	11	11	6	7	12	5	10	1	13

Figure 5.4: Statistical evaluation of annual non-sea salt potassium ($K_{(nss)}$) wet deposition 1987-2004

Table 5.6: Average sea salt fraction of potassium wet deposition 1987-2004

	1987	1988	1989	1990	1991	1992	1993	1994	1995
in kt a^{-1}	6.6	8.1	8.2	8.9	6.1	6.4	6.8	6.8	6.8
in eq ha^{-1} a^{-1}	4.8	5.8	5.8	6.4	4.4	4.6	4.9	4.8	4.9
in kg ha^{-1} a^{-1}	0.19	0.23	0.23	0.25	0.17	0.18	0.19	0.19	0.19
Wet deposited sea salt fraction %	9.3	14.5	14.3	14.8	12.7	11.2	12.3	14.2	12.9

	1996	1997	1998	1999	2000	2001	2002	2003	2004
in kt a^{-1}	4.3	4.9	5.7	5.4	4.5	5.0	5.1	4.3	5.7
in eq ha^{-1} a^{-1}	3.1	3.5	4.1	3.9	3.2	3.6	3.6	3.1	4.1
in kg ha^{-1} a^{-1}	0.12	0.14	0.16	0.15	0.13	0.14	0.14	0.12	0.16
Wet deposited sea salt fraction %	9.6	11.7	11.6	12.7	10.6	11.7	10.2	9.7	11.2

5.1.4 Wet deposition of non-sea salt magnesium ($Mg_{(nss)}$)

Annual average wet flux of non sea salt Magnesium ($Mg_{(nss)}$) over the whole time period from 1987 to 2004 diminished by about 77% (Figure 5.5). From 1999 onward no significant decline can be observed. This equals an absolute decrease of 19 kt on whole Germany from 24 kt to only 5 kt (0.16 kg ha^{-1} a^{-1}) in 2004. Minima, 5th, and 2nd percentile in all the years except for 1988 are zero. This is an effect of the sea salt correction applied, taking Na as tracer (c.f. Chapter 4.3.2). From this result it can be concluded that on at least 5% of the total area of Germany all wet Mg flux originates from sea salt.

Spatal patterns of $Mg_{(nss)}$ wet deposition 1993 to 2004 are presented in Map 5.4. Main terrestrial sources of Mg are soil particulates, material extraction processes (dolomite) and industry, and lignite combustion. The decrease of $Mg_{(nss)}$ wet deposition loads over time, and the decline of maximum values can clearly be found in the maps.

The average sea salt fraction of Mg wet deposition (Table 5.7) accounts 53% (1987) to 81% (2004). The increase of the sea salt fraction is relatively continuous over the whole time period and reflects the corresponding

decrease of Mg from anthropogenic (and other) sources.

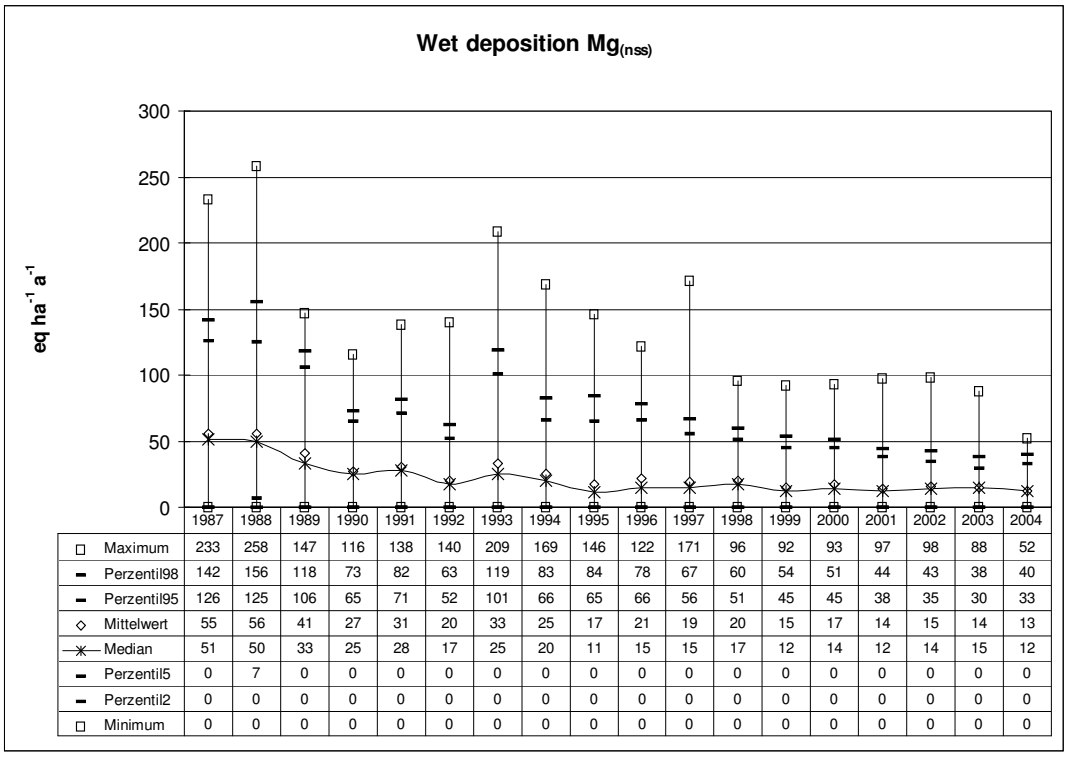

	1987	1988	1989	1990	1991	1992	1993	1994	1995	1996	1997	1998	1999	2000	2001	2002	2003	2004
Maximum	233	258	147	116	138	140	209	169	146	122	171	96	92	93	97	98	88	52
Perzentil98	142	156	118	73	82	63	119	83	84	78	67	60	54	51	44	43	38	40
Perzentil95	126	125	106	65	71	52	101	66	65	66	56	51	45	45	38	35	30	33
Mittelwert	55	56	41	27	31	20	33	25	17	21	19	20	15	17	14	15	14	13
Median	51	50	33	25	28	17	25	20	11	15	15	17	12	14	12	14	15	12
Perzentil5	0	7	0	0	0	0	0	0	0	0	0	0	0	0	0	0	0	0
Perzentil2	0	0	0	0	0	0	0	0	0	0	0	0	0	0	0	0	0	0
Minimum	0	0	0	0	0	0	0	0	0	0	0	0	0	0	0	0	0	0

Figure 5.5: Statistical evaluation of annual non-sea salt magnesium ($Mg_{(nss)}$) wet deposition 1987-2004

Table 5.7: Average sea salt fraction of magnesium wet deposition 1987-2004

	1987	1988	1989	1990	1991	1992	1993	1994	1995
in kt a^{-1}	26.8	32.8	30.1	31.4	22.3	23.3	26.6	25.8	26.0
in eq ha^{-1} a^{-1}	61.9	75.6	69.4	72.3	51.5	53.7	61.2	59.6	59.9
in kg ha^{-1} a^{-1}	0.75	0.92	0.84	0.88	0.63	0.65	0.74	0.72	0.73
Wet deposited sea salt fraction %	52.7	57.6	63.1	72.8	62.5	72.7	65.1	70.3	77.8
	1996	**1997**	**1998**	**1999**	**2000**	**2001**	**2002**	**2003**	**2004**
in kt a^{-1}	17.1	19.1	23.0	21.2	18.2	20.2	20.1	16.8	22.8
in eq ha^{-1} a^{-1}	39.3	44.1	53.0	48.8	41.9	46.6	46.3	38.7	52.6
in kg ha^{-1} a^{-1}	0.48	0.54	0.64	0.59	0.51	0.57	0.56	0.47	0.64
Wet deposited sea salt fraction %	64.7	70.0	72.8	76.4	70.9	77.2	75.0	72.9	80.8

5.1.5 Wet deposition of non-sea salt base cations ($BC_{(nss)} = Ca_{(nss)} + K_{(nss)} + Mg_{(nss)}$)

Average wet deposition flux of the sum of non-sea salt base cations ($BC_{(nss)} = Ca_{(nss)} + K_{(nss)} + Mg_{(nss)}$) within 1987 and 2004 decreased about 60% (mean), or 54% (median), respectively. From 1996 onward no significant decrease can be observed. Mean wet $BC_{(nss)}$ fluxes 1987 to 2004 declined by 231 eq ha^{-1} a^{-1} from 427 eq ha^{-1} a^{-1} to 169 eq ha^{-1} a^{-1}. In terms of the median of wet $BC_{(nss)}$ fluxes the decline equals 190 eq ha^{-1} a^{-1} , from 1987 351 eq ha^{-1} a^{-1} to 161 eq ha^{-1} a^{-1} in 2004.

The average percentage of sea salt BC ranges from 15% (1987) to 29% in 1995 (Table 5.8). $Ca_{(nss)}$ with average 75% is the dominating compound of the sum of $BC_{(nss)}$ (Table 5.9). The mean fraction of $K_{(nss)}$, and $Mg_{(nss)}$ of the sum of $BC_{(nss)}$ is 15% and 10%, respectively.

The spatial patterns of $BC_{(nss)}$ 1993 to 2004 are shown in Map 5.5.

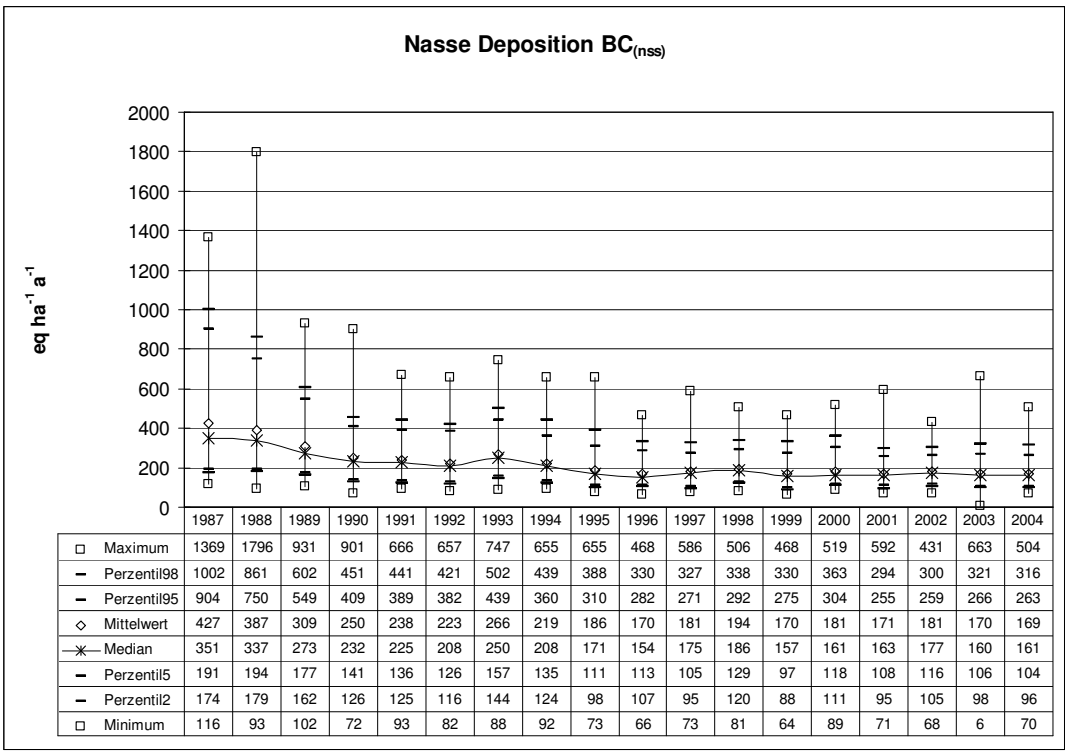

	1987	1988	1989	1990	1991	1992	1993	1994	1995	1996	1997	1998	1999	2000	2001	2002	2003	2004
Maximum	1369	1796	931	901	666	657	747	655	655	468	586	506	468	519	592	431	663	504
Perzentil98	1002	861	602	451	441	421	502	439	388	330	327	338	330	363	294	300	321	316
Perzentil95	904	750	549	409	389	382	439	360	310	282	271	292	275	304	255	259	266	263
Mittelwert	427	387	309	250	238	223	266	219	186	170	181	194	170	181	171	181	170	169
Median	351	337	273	232	225	208	250	208	171	154	175	186	157	161	163	177	160	161
Perzentil5	191	194	177	141	136	126	157	135	111	113	105	129	97	118	108	116	106	104
Perzentil2	174	179	162	126	125	116	144	124	98	107	95	120	88	111	95	105	98	96
Minimum	116	93	102	72	93	82	88	92	73	66	73	81	64	89	71	68	6	70

Figure 5.6: Statistical evaluation of annual non-sea salt base cations ($BC_{(nss)}$) wet deposition 1987-2004

Table 5.8: Average sea salt fraction of base cations wet deposition 1987-2004

	1987	1988	1989	1990	1991	1992	1993	1994	1995
in eq ha^{-1} a^{-1}	76.6	93.6	87.5	92.1	65.0	67.8	76.2	74.5	75.0
Wet deposited sea salt fraction %	15.2	19.5	22.1	27.0	21.5	23.3	22.3	25.4	28.8
	1996	**1997**	**1998**	**1999**	**2000**	**2001**	**2002**	**2003**	**2004**
in eq ha^{-1} a^{-1}	48.8	54.9	65.6	60.8	51.9	57.7	57.6	48.2	65.2
Wet deposited sea salt fraction %	22.3	23.2	25.3	26.4	22.3	25.2	24.2	22.1	27.8

Table 5.9: Average non-sea salt calcium ($Ca_{(nss)}$), potassium ($K_{(nss)}$) and magnesium ($Mg_{(nss)}$) fraction of the sum of wet deposited non-sea salt base cations ($BC_{(nss)}$) 1987-2004

	1987	1988	1989	1990	1991	1992	1993	1994	1995
Ca %	76.1	76.8	75.6	74.4	74.4	74.8	74.7	75.2	73.0
K %	10.9	8.8	11.3	14.8	12.6	16.2	13.0	13.3	17.8
Mg %	13.0	14.4	13.1	10.8	13.0	9.0	12.3	11.5	9.2
Total %	100	100	100	100	100	100	100	100	100
	1996	**1997**	**1998**	**1999**	**2000**	**2001**	**2002**	**2003**	**2004**
Ca %	70.4	75.1	73.7	75.5	75.4	76.0	73.7	74.8	73.6
K %	16.9	14.5	16.0	15.6	15.1	15.9	17.7	16.8	19.0
Mg %	12.6	10.4	10.2	8.9	9.5	8.0	8.5	8.4	7.4
Total %	100	100	100	100	100	100	100	100	100

5.2 Wet deposition fluxes and trends of nitrogen and acidifying compounds

In the majority of terrestrial ecosystems Nitrogen is the limiting factor for plant growth. Eutropication of ecosystems does occur when excess nitrogen (N) inputs, acting as a fertilizer, will result in nutrient imbalances, selective favoring of certain species at the expense of others, and in impoverishment of ecosystems. Atmospheric N inputs, caused by anthropogenic emission of oxidised Nitrogen (NO_Y-N) mainly from combustion processes and reduced Nitrogen (NH_X-N) mainly from agriculture, may affect the structure and function of natural and semi-natural ecosystems. Due to nutrient imbalances ecosystems more likely are affected by climatic stress and eutrophication can affect biodiversity due to stress caused by changes in chemical conditions.

Acidification of ecosystems is increased by both, the deposition of sulphur (S) and nitrogen (N). It affects soil depletion, leaching of nutrients, release of heavy metals, and contributes to forest damage (c.f. Chapter 2).

5.2.1 Wet deposition of non-sea salt sulphur (SO_4-$S_{(nss)}$)

Between 1987 and 2004 wet deposition of sulphur on average diminished by about 73% (median -70%). Over the whole area of Germany this equals a decline of about 364 kt from about 501 kt in 1987 to 137 kt in 2004. The average wet deposition flux declined from about 14 kg ha^{-1} a^{-1} in 1987 to about 4 kg ha^{-1} a^{-1} in 2004.

In contrary to the trend of base cations over time, the decline of SO_4-$S_{(nss)}$ can be observed over the whole period considered, though the decline is steep until 1997, due to emission reducion mainly driven by the GFAVO. From 1987 to 2004 the maximum values of SO_4-$S_{(nss)}$ wet deposition diminishes by 80%. From 1997 onward the declining trend is continuing on a lower level.The successful emission abatement can clearly be seen in the decline of the peak values (maximum, 98th and 95th percentile in Figure 5.7).

The sea salt fraction of average wet deposition load of sulphur (SO_4-S) ranges from 3% in 1987 to 8.9% in 2004 (Table 5.10). Though an interannual oscillation of the average sea salt contribution can be observed, there is a clear rising trend in the percentage of the sea salt contribution that can be attributed to the decline of anthropogenic emission. The annual average absolute fraction of sea salt SO_4-S ranges from 10 kt a^{-1} (in 1996) to 21 kt a^{-1} (in 1990). Until 1996 the absolute sea salt contribution sightly declining, and from 1997 onward it is variing around a level of about 11.5 kt a^{-1}.

The spatial patterns of SO_4-$S_{(nss)}$ wet deposition loads1993 to 2004 are shown in Map 5.6. The overall decline of peak values can clearly be observed over time. From 1993 onward the SO_4-$S_{(nss)}$ overall wet deposition is declining with the exception of the years 1998, and 2002.

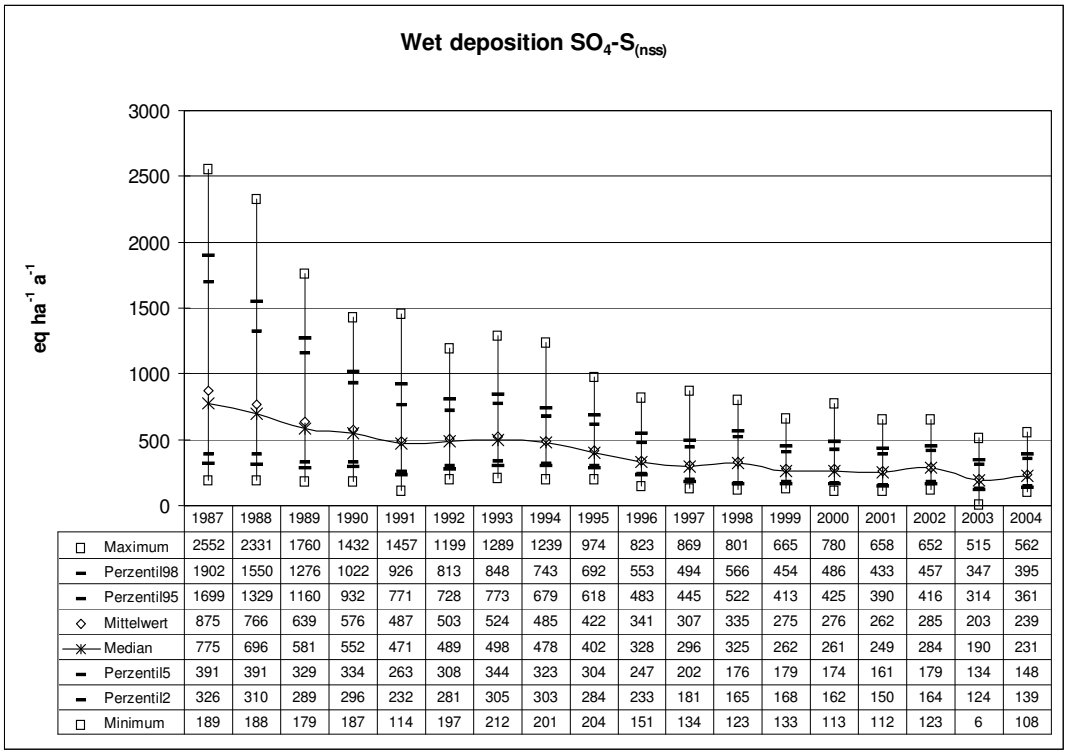

	1987	1988	1989	1990	1991	1992	1993	1994	1995	1996	1997	1998	1999	2000	2001	2002	2003	2004
Maximum	2552	2331	1760	1432	1457	1199	1289	1239	974	823	869	801	665	780	658	652	515	562
Perzentil98	1902	1550	1276	1022	926	813	848	743	692	553	494	566	454	486	433	457	347	395
Perzentil95	1699	1329	1160	932	771	728	773	679	618	483	445	522	413	425	390	416	314	361
Mittelwert	875	766	639	576	487	503	524	485	422	341	307	335	275	276	262	285	203	239
Median	775	696	581	552	471	489	498	478	402	328	296	325	262	261	249	284	190	231
Perzentil5	391	391	329	334	263	308	344	323	304	247	202	176	179	174	161	179	134	148
Perzentil2	326	310	289	296	232	281	305	303	284	233	181	165	168	162	150	164	124	139
Minimum	189	188	179	187	114	197	212	201	204	151	134	123	133	113	112	123	6	108

Figure 5.7: Statistical evaluation of annual non-sea salt sulphur (SO_4-$S_{(nss)}$) wet deposition 1987-2004

Table 5.10: Average sea salt fraction of sulphur wet deposition 1987-2004

	1987	1988	1989	1990	1991	1992	1993	1994	1995
in kt a^{-1}	15.5	19.1	19.1	21.0	14.3	14.9	15.9	15.8	16.0
in eq ha^{-1} a^{-1}	27.2	33.3	33.4	36.6	24.9	26.1	27.7	27.6	27.9
in kg ha^{-1} a^{-1}	0.44	0.53	0.54	0.59	0.40	0.42	0.44	0.44	0.45
Wet deposited sea salt fraction %	3.0	4.2	5.0	6.0	4.9	4.9	5.0	5.4	6.2
	1996	**1997**	**1998**	**1999**	**2000**	**2001**	**2002**	**2003**	**2004**
in kt a^{-1}	10.0	11.4	13.4	12.6	10.6	11.8	11.9	10.1	13.3
in eq ha^{-1} a^{-1}	17.5	19.9	23.3	22.1	18.5	20.6	20.8	17.6	23.3
in kg ha^{-1} a^{-1}	0.28	0.32	0.37	0.35	0.30	0.33	0.33	0.28	0.37
Wet deposited sea salt fraction %	4.9	6.1	6.5	7.4	6.3	7.3	6.8	8.0	8.9

5.2.2 Wet deposition of reduced nitrogen (NH_4-N)

Average wet deposition flux of reduced nitrogen (NH_4-N) declined by about 24% from 1987 to 2004, the median wet flux declined by 28%, respectively. The absolute wet deposition load on the whole area of Germany declined by about 63 kt from 257 kt in 1987 to 194 kt in 2004, which equals average 7.2 kg ha^{-1} a^{-1} and 5.44 kg ha^{-1} a^{-1}, respectively. The main decline can be observed until 1991. From 1992 onward the average wet fluxes of NH_4-N vary around 410 eq ha^{-1} a^{-1}, and median wet fluxes around 390 eq ha^{-1} a^{-1}. Also with respect to the peak values clearly no declining trend can be observed (Figure 5.8).

Spatial patterns of NH_4-N wet deposition loads from 1993 to 2004 are presented in Map 5.7. The maps show rather year to year variations then clear changes in the general spatial pattern. Areas with wet fluxes of NH_4-N above the annual average are mainly found in the north-western Part of Germany, and, less distinct, in some south-eastern parts of Germany. These regions mainly reflect the areas of higher density of animal husbandry. From 1993 onward areas with wet fluxes above 9 kg ha^{-1} a^{-1} are much less extended.
In 1993 and 1994 the same amount of NH_4-N is deposited wet in Germany, but the spatial trend is different. In 1993 higher wet fluxes are covering north-west Germany compared to 1994, while in 1994 higher NH_4-N wet deposition fluxes can be observed in Bavaria than in 1993. From 1994 to 1997 a slight fall of NH_4-N wet deposition can be found. In 1998 the spatial trend is quite similar as in 1993, while the total amount of NH_4-N wet deposition over Germany is almost at the level of 1996. From 1999 to 2002 NH_4-N wet deposition is slightly rising again up to a similar level as in 1996. In 2004 the spatial trend as well as the NH_4-N wet deposition level is almost the same as it was in 1997.

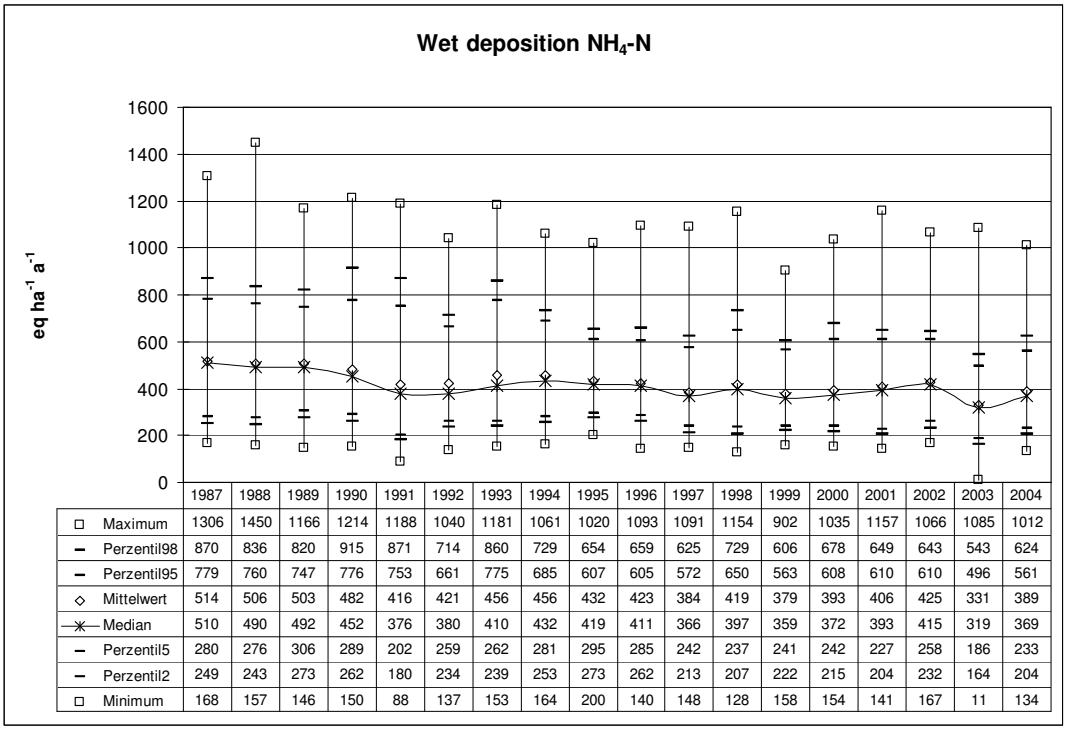

	1987	1988	1989	1990	1991	1992	1993	1994	1995	1996	1997	1998	1999	2000	2001	2002	2003	2004
Maximum	1306	1450	1166	1214	1188	1040	1181	1061	1020	1093	1091	1154	902	1035	1157	1066	1085	1012
Perzentil98	870	836	820	915	871	714	860	729	654	659	625	729	606	678	649	643	543	624
Perzentil95	779	760	747	776	753	661	775	685	607	605	572	650	563	608	610	610	496	561
Mittelwert	514	506	503	482	416	421	456	456	432	423	384	419	379	393	406	425	331	389
Median	510	490	492	452	376	380	410	432	419	411	366	397	359	372	393	415	319	369
Perzentil5	280	276	306	289	202	259	262	281	295	285	242	237	241	242	227	258	186	233
Perzentil2	249	243	273	262	180	234	239	253	273	262	213	207	222	215	204	232	164	204
Minimum	168	157	146	150	88	137	153	164	200	140	148	128	158	154	141	167	11	134

Figure 5.8: Statistical evaluation of annual reduced nitrogen (NH_4-N) wet deposition 1987-2004

5.2.3 Wet deposition of oxidised nitrogen (NO_3-N)

Annual average wet deposition of oxidised nitrogen from 1987 to 2004 declined by 28%, the median by about 29%. The total annual wet deposition load over Germany declined by about 54 kt from about 192 kt (5.4 kg ha^{-1} a^{-1}) in 1987 to 138 kt (3.9 kg ha^{-1} a^{-1}) in 2004. The main decline can be observed between 1987 and 1991. From 1992 onward the average wet deposition load varies around 290 eq ha^{-1} a^{-1} (4.0 kg ha^{-1} a^{-1}), the median around 280 eq ha^{-1} a^{-1} (3.9 kg ha^{-1} a^{-1}), respectively. Also with respect to the peak values no clear declining trend can be observed (Figure 5.9) since 1990.

The spatial patterns of NO_3-N wet deposition loads 1993 to 2004 are presented in Map 5.8. From 1993 to 1997 a decline of NO_3-N wet fluxes can be observed, whereas in 1998 average fluxes are again higher than in 1996. From 1999 onward average wet NO_3-N fluxes are slightly rising until 2003, the exceptional year showing lowest wet deposition. In 2004 NO_3-N wet deposition is slightly above the level of 1997, but showing a slightly different spatial trend.

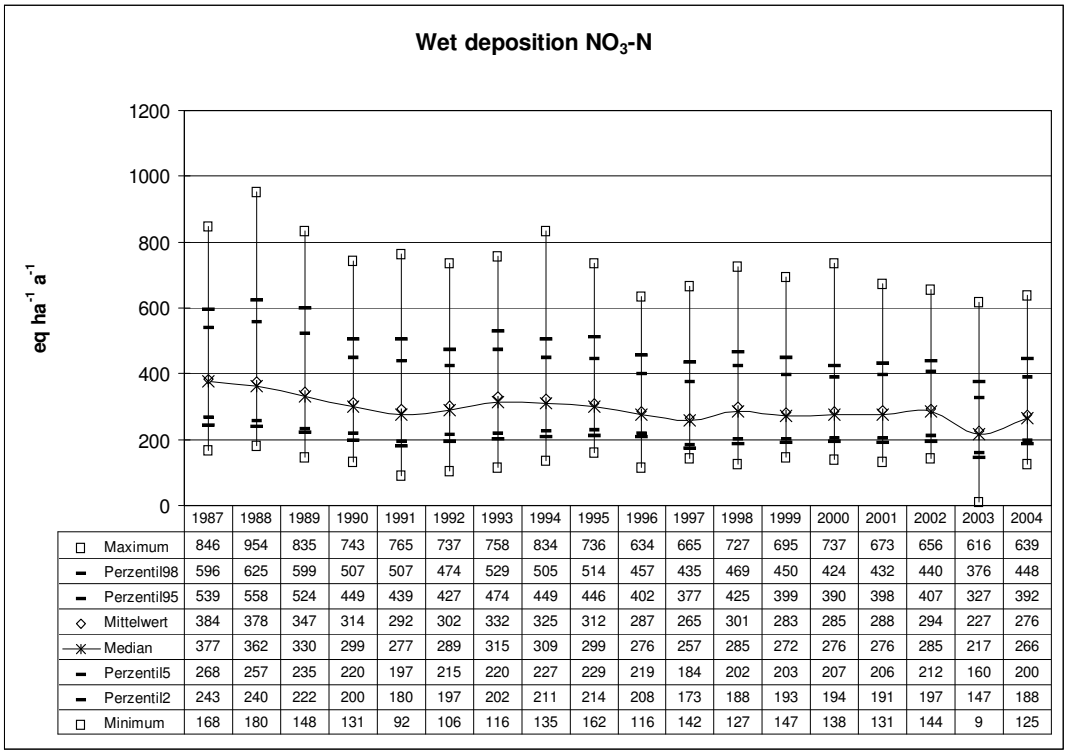

	1987	1988	1989	1990	1991	1992	1993	1994	1995	1996	1997	1998	1999	2000	2001	2002	2003	2004
Maximum	846	954	835	743	765	737	758	834	736	634	665	727	695	737	673	656	616	639
Perzentil98	596	625	599	507	507	474	529	505	514	457	435	469	450	424	432	440	376	448
Perzentil95	539	558	524	449	439	427	474	449	446	402	377	425	399	390	398	407	327	392
Mittelwert	384	378	347	314	292	302	332	325	312	287	265	301	283	285	288	294	227	276
Median	377	362	330	299	277	289	315	309	299	276	257	285	272	276	276	285	217	266
Perzentil5	268	257	235	220	197	215	220	227	229	219	184	202	203	207	206	212	160	200
Perzentil2	243	240	222	200	180	197	202	211	214	208	173	188	193	194	191	197	147	188
Minimum	168	180	148	131	92	106	116	135	162	116	142	127	147	138	131	144	9	125

Figure 5.9: Statistical evaluation of annual oxidised nitrogen (NO_3-N) wet deposition 1987-2004

5.2.4 Wet deposition of total nitrogen (N = NO_3-N + NH_4-N)

A straight trend in wet deposition of total Nitrogen, calculated as the sum of reduced and oxidised nitrogen, can hardly be found in the annual map statistics (Figure 5.10). A more or less obvious decline in the maximum wet deposition fluxes can be observed between 1987 and 2004. Average N wet deposition 2004 compared to 1987 shows about 26% lower wet fluxes. Median N wet deposition over the whole period mapped diminishes by about 30%. In 1987 average N wet deposition was about 449 kt N (12.6 kg ha^{-1} a^{-1}) in Gerrmany, whereas in 2004 the averae magnitude of N wet deposition was 332 kt (9.3 kg ha^{-1} a^{-1}), respectively.
The average fraction of reduced (NH_4-N) and oxdised nitrogen (NO_3-N) of wet deposited N is shown in Table 5.11, where the average wet flux of total N in Germany is composed by about 59% NH_4-N (ranging from 57.2% to 60.5%) and 41% NO_3-N (ranging from 39.5% to 42.8%) , respectively.

The spatial patterns of total N wet deposition loads 1993 to 2004 are presented in Map 5.9. From 1993 to 1997 a decline of N wet deposition loads can be observed. In 1998 the spatial trend is quite similar as it was in 1994, while the total amount of N wet deposition over Germany is slightly above the level of 1996. From 1999 to 2002 N wet deposition is slightly rising again up to a similar level as in 1996. In 2004 the spatial trend as well as the N wet deposition level is the same as it was in 1999.

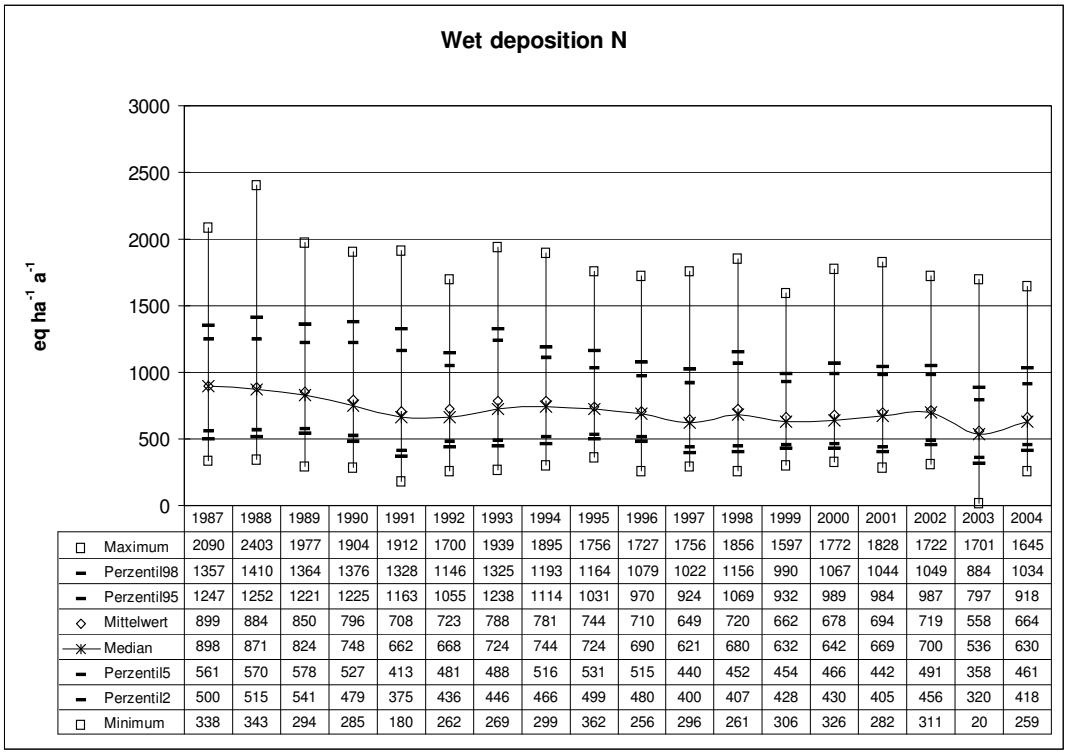

	1987	1988	1989	1990	1991	1992	1993	1994	1995	1996	1997	1998	1999	2000	2001	2002	2003	2004
Maximum	2090	2403	1977	1904	1912	1700	1939	1895	1756	1727	1756	1856	1597	1772	1828	1722	1701	1645
Perzentil98	1357	1410	1364	1376	1328	1146	1325	1193	1164	1079	1022	1156	990	1067	1044	1049	884	1034
Perzentil95	1247	1252	1221	1225	1163	1055	1238	1114	1031	970	924	1069	932	989	984	987	797	918
Mittelwert	899	884	850	796	708	723	788	781	744	710	649	720	662	678	694	719	558	664
Median	898	871	824	748	662	668	724	744	724	690	621	680	632	642	669	700	536	630
Perzentil5	561	570	578	527	413	481	488	516	531	515	440	452	454	466	442	491	358	461
Perzentil2	500	515	541	479	375	436	446	466	499	480	400	407	428	430	405	456	320	418
Minimum	338	343	294	285	180	262	269	299	362	256	296	261	306	326	282	311	20	259

Figure 5.10: Statistical evaluation of annual total nitrogen (N) wet deposition 1987-2004

Table 5.11: Average NH_4-N and NO_3-N fraction of wet deposited N 1987-2004

	1987	1988	1989	1990	1991	1992	1993	1994	1995
NH_4-N %	57.2	57.3	59.2	60.5	58.7	58.2	57.8	58.4	58.1
NO_3-N %	42.8	42.7	40.8	39.5	41.3	41.8	42.2	41.6	41.9
Total %	100	100	100	100	100	100	100	100	100
	1996	**1997**	**1998**	**1999**	**2000**	**2001**	**2002**	**2003**	**2004**
NH_4-N %	59.6	59.1	58.2	57.3	58.0	58.5	59.1	59.3	58.5
NO_3-N %	40.4	40.9	41.8	42.7	42.0	41.5	40.9	40.7	41.5
Total %	100	100	100	100	100	100	100	100	100

5.2.5 Wet deposition of non-sea salt chlorine ($Cl_{(nss)}$)

Chlorine mainly originates from sea spray (c.f. Table 5.11). Annual average non-sea salt chlorine ($Cl_{(nss)}$) wet deposition loads are relatively low in magnitude (c.f. Figure 5.11), the median of annual wet deposition of $Cl_{(nss)}$ in some cases even is zero. It is assumed, that wet deposition of non-sea salt chlorine is completely due to anthropogenic HCl emissions. Moreover it is assumed that dry deposition of HCl locally is relevant close to emission sources only. Hence $Cl_{(nss)}$ wet deposition is attributed to total deposition of anthropogenic chlorine.

Average $Cl_{(nss)}$ wet deposition 2004 is remarkable 80% lower than in 1987. In 1987 about 84 kt (2.4 kg ha^{-1} a^{-1}) $Cl_{(nss)}$ were with the wet flux in Germany, in 2004 only 17 kt (0.47 kg ha^{-1} a^{-1}; c.f. Figure 5.10). The annual percentage changes, however, are varying very much (Table 5.11), and hence a trend over the whole 18 years period can not be determined.

In the maps of annual average $Cl_{(nss)}$ wet deposition 1993 to 2004 (Map 5.10) rather different spatial patterns of low and spots of high value areas can be found than a trend within certain German regions.

The sea salt contribution to the wet flux of chlorine in Germany in 1987 is about 79%, whereas in 2004 it is about 94% (c.f. Table 5.12). From 1987 to 1993 a straigt trend of rising sea-salt contribution, and hence declining non sea-salt chlorine ($Cl_{(nss)}$) contribution can be observed. From 1994 onward the Cl sea salt fraction ranges from 90% to 97%. Assuming that $Cl_{(nss)}$ wet deposition is completely due to anthropogenic HCl emission,

the observed trends can be attributed to HCl emission abatement. Main anthropogenic sources of HCl are lgnite and waste combustion. Technical emission abatement of HCL mainly is done by flue gas purification.

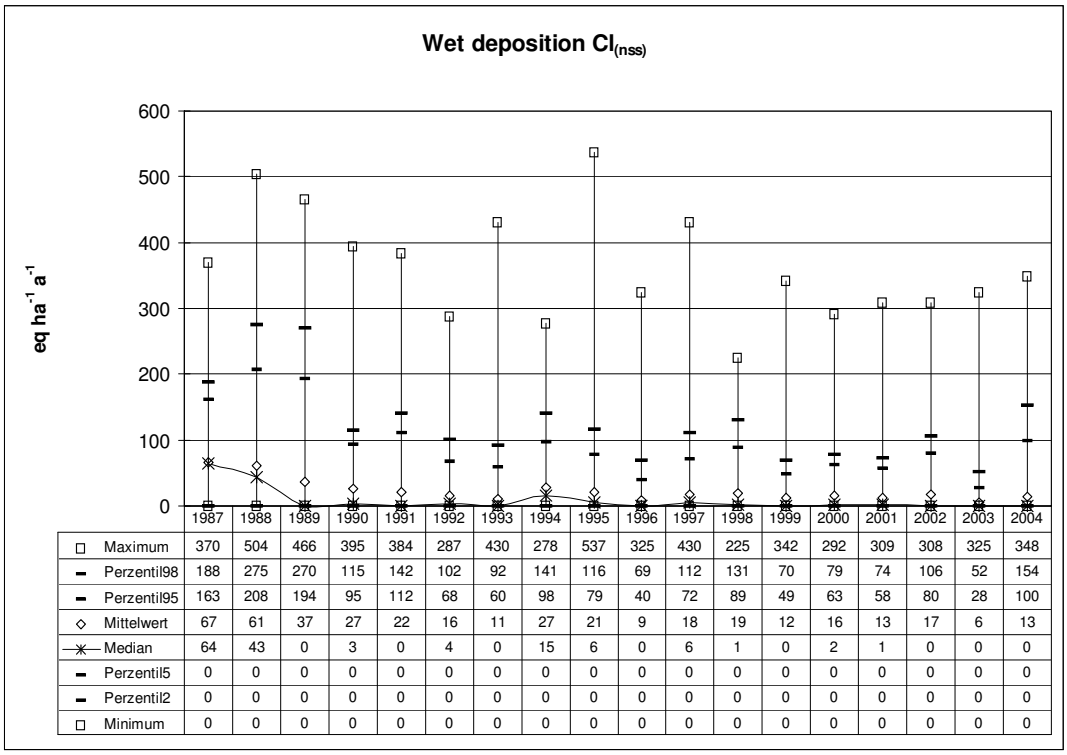

	1987	1988	1989	1990	1991	1992	1993	1994	1995	1996	1997	1998	1999	2000	2001	2002	2003	2004
Maximum	370	504	466	395	384	287	430	278	537	325	430	225	342	292	309	308	325	348
Perzentil98	188	275	270	115	142	102	92	141	116	69	112	131	70	79	74	106	52	154
Perzentil95	163	208	194	95	112	68	60	98	79	40	72	89	49	63	58	80	28	100
Mittelwert	67	61	37	27	22	16	11	27	21	9	18	19	12	16	13	17	6	13
Median	64	43	0	3	0	4	0	15	6	0	6	1	0	2	1	0	0	0
Perzentil5	0	0	0	0	0	0	0	0	0	0	0	0	0	0	0	0	0	0
Perzentil2	0	0	0	0	0	0	0	0	0	0	0	0	0	0	0	0	0	0
Minimum	0	0	0	0	0	0	0	0	0	0	0	0	0	0	0	0	0	0

Figure 5.11: Statistical evaluation of annual non-sea salt chlorine ($Cl_{(nss)}$)wet deposition 1987-2004

Table 5.12: Budgets of average non-sea salt wet deposition of Chlorine ($Cl_{(nss)}$) 1987-2004

Annual average $Cl_{(nss)}$ wet deposition	1987	1988	1989	1990	1991	1992	1993	1994	1995
Cl [eq ha^{-1} a^{-1}]	66.5	60.9	37.1	27.0	21.7	16.2	11.2	27.2	20.6
Change from previous year [%]		-8.4	-39.1	-27.1	-19.8	-25.1	-31.3	+143.8	-24.2
Annual average $Cl_{(nss)}$ wet deposition	**1996**	**1997**	**1998**	**1999**	**2000**	**2001**	**2002**	**2003**	**2004**
Cl [eq ha^{-1} a^{-1}]	8.5	17.8	19.5	12.3	16.4	12.8	17.0	5.7	13.4
Change from previous year [%]	-58.6	+108.4	+9.5	-36.9	+33.4	-22.2	+33.3	-66.8	+136.9
Change from 1987 to 2004 [%]									-79.9

Table 5.13: Average sea salt fraction of chlorine wet deposition 1987-2004

	1987	1988	1989	1990	1991	1992	1993	1994	1995
in kt a^{-1}	311.2	401.6	333.1	372.0	267.9	282.3	294.9	314.2	313.0
in eq ha^{-1} a^{-1}	245.87	317	263.2	293.9	211.6	223.1	233	248.2	247.3
in kg ha^{-1} a^{-1}	8.72	11.25	9.33	10.42	7.50	7.91	8.26	8.80	8.77
Wet deposited sea salt fraction %	78.7	83.9	87.6	91.6	90.7	93.2	95.4	90.1	92.3
	1996	**1997**	**1998**	**1999**	**2000**	**2001**	**2002**	**2003**	**2004**
in kt a^{-1}	199.0	234.6	271.1	252.8	214.7	238.0	238.7	195.3	262.2
in eq ha^{-1} a^{-1}	157.2	185.4	214.2	199.7	169.6	188	188.6	154.3	207.1
in kg ha^{-1} a^{-1}	5.57	6.57	7.59	7.08	6.01	6.66	6.68	5.47	7.34
Wet deposited sea salt fraction %	94.9	91.2	91.7	94.2	91.2	93.6	91.7	96.5	93.9

5.2.6 Wet deposition of potential acidity ($AC_{pot} = SO_4\text{-}S_{(nss)} + N + Cl_{(nss)}$)

Potential acidity (AC_{pot}) is defined as the sum of total nitrogen (N = NH_4-N + NO_3-N), non-sea salt sulphur (SO_4-$S_{(nss)}$), and non-sea salt chlorine ($Cl_{(nss)}$) (ICP MODELLING AND MAPPING 1996, 2004). Wet deposition of AC_{pot} declined by about 50% from 1987 to 2004 from 1840 eq ha^{-1} a^{-1} in 1987 to 917 eq ha^{-1} a^{-1} in 2004 (c.f. Figure 5.12 & 5.13). From 1997 ownard only a slight decline of potential acid wet deposition can be found. The straight decline between 1987 and 1997 mainly is due to the sharp decline in sulphur wet deposition (SO_4-$S_{(nss)}$) (Chapter 5.2.1). The main compound forming the wet flux of potential acidity over the whole time period considered is nitrogen (N) (Chapter 5.2.4).

In Table 5.14 the average fractions of wet deposited acidifying compounds are listed. The contribution of $Cl_{(nss)}$ is the smallest, ranging from about 0.7% to 3.6% in the different years considered. The contribution of $Cl_{(nss)}$ to potential acidity between 1987 and 1993 is declining rapidly from 3.6% to less than 1%, whereas the $Cl_{(nss)}$ contribution in the following years is about 1.5% ± 0.7%.

The fraction of SO_X-$S_{(nss)}$ is contributing by 48% to 26% with an continuous decline between 1987 and 2004. In contrast the contribution of total N to wet deposition of AC_{pot} is rising from 49% in 1987 to 73% in 2004. This is due to both, the fraction of reduced nitrogen (NH_4-N) and oxidised nitrogen (NO_Y-N), which show only slightly falling absolute values, and hence a rising relative contribution to AC_{pot} (c.f. Figure 5.12 and 5.13). From 1996 onward the NH_4-N fraction contributes more to potential acidity than the SO_4-$S_{(nss)}$ fraction, from 1999 onward also the NO_3-N fraction is above the SO_4-$S_{(nss)}$ fraction of wet flux potential acidity in Germany.

The spatial patterns of AC_{pot} in the single years 1993 to 2004 are presented in Map 5.11. The spatial trend in the single years considered as well as the trend over time is mainly following the trend of total N wet deposition, being the quantitatively dominating compound of potential acidity. AC_{pot} wet deposition above the average regularly can be found over regions in North and North-Western, and western Germany (Schleswig-Holstein, Niedersachsen, Northrhine-Westpalia), the alpine region in southern Germany, over higher mountain areas of the Black Forest, the Thuringen Forest, the Bavarian Forest, and the Ore Mountain, while peak values each year can be observed over the Harz mountain. Wet deposition of AC_{pot} at and below average fluxes can be found over most regions of Eastern Germany (Mecklenburg-Vorpommern, Brandenburg, Sachen-Anhalt, Thuringia, northern Saxony), over Saarland and Rhineland-Palatinate, and most parts of Baden-Württemberg and Bavaria and Hesse.

From 1993 to 1997 a decline of AC_{pot} wet deposition loads can be observed. In 1998 the spatial trend is quite similar as it was in 1995, while the total amount of AC_{pot} wet deposition over Germany is slightly above the level of 1996. From 1999 to 2002 AC_{pot} wet deposition is slightly rising again up to a similar level as in 1998. In 2004 the spatial trend is similar as it was from 1999 to 2002. The 2002 AC_{pot} wet deposition level has fallen below the level of 2002.

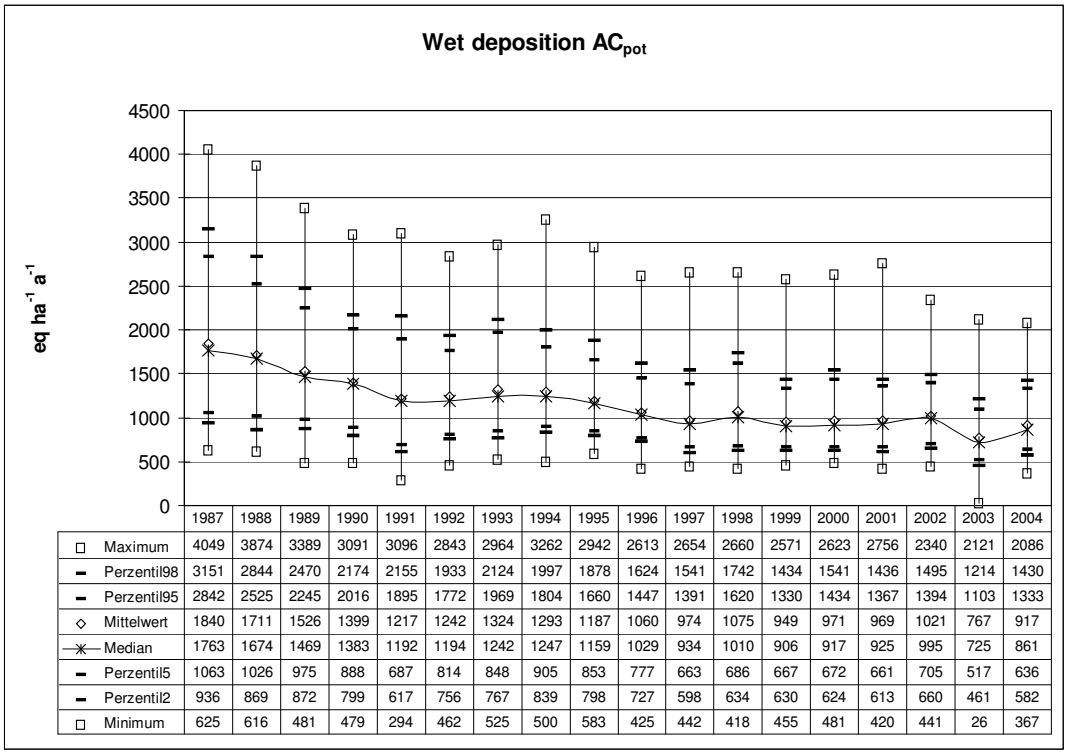

	1987	1988	1989	1990	1991	1992	1993	1994	1995	1996	1997	1998	1999	2000	2001	2002	2003	2004
Maximum	4049	3874	3389	3091	3096	2843	2964	3262	2942	2613	2654	2660	2571	2623	2756	2340	2121	2086
Perzentil98	3151	2844	2470	2174	2155	1933	2124	1997	1878	1624	1541	1742	1434	1541	1436	1495	1214	1430
Perzentil95	2842	2525	2245	2016	1895	1772	1969	1804	1660	1447	1391	1620	1330	1434	1367	1394	1103	1333
Mittelwert	1840	1711	1526	1399	1217	1242	1324	1293	1187	1060	974	1075	949	971	969	1021	767	917
Median	1763	1674	1469	1383	1192	1194	1242	1247	1159	1029	934	1010	906	917	925	995	725	861
Perzentil5	1063	1026	975	888	687	814	848	905	853	777	663	686	667	672	661	705	517	636
Perzentil2	936	869	872	799	617	756	767	839	798	727	598	634	630	624	613	660	461	582
Minimum	625	616	481	479	294	462	525	500	583	425	442	418	455	481	420	441	26	367

Figure 5.12: Statistical evaluation of annual potential acidity (AC_{pot}) wet deposition 1987-2004

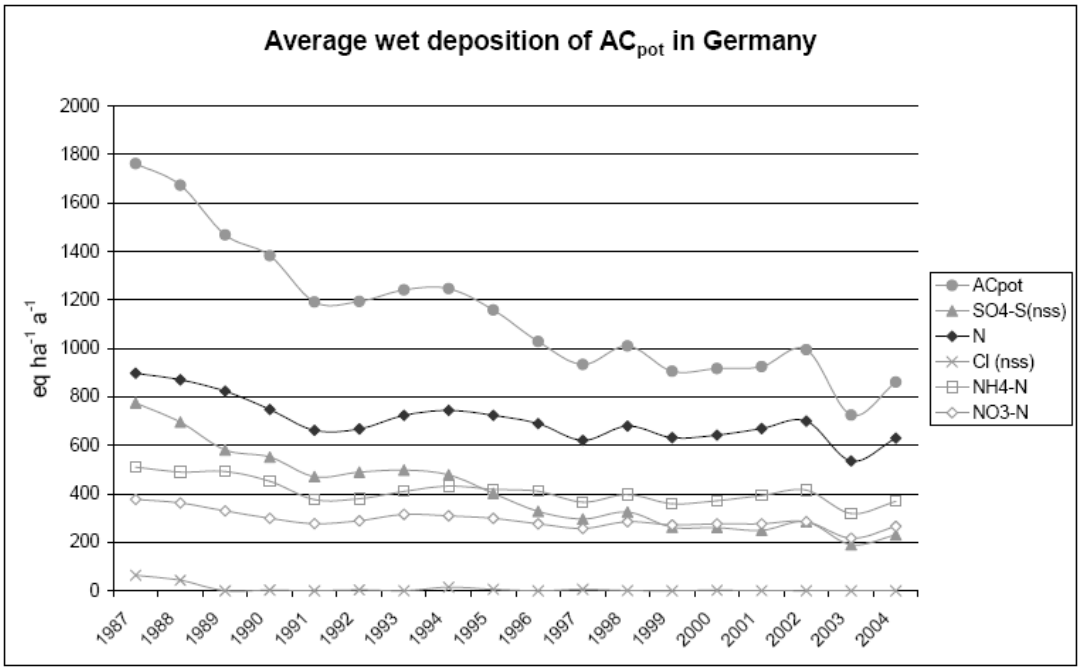

Figure 5.13: Average wet deposition of potential acidity (AC_{pot}) and its compounds 1987-2004

Table 5.14: Average fractions of acidifying compounds in wet deposition 1987-2004

Average fraction of ...	1987	1988	1989	1990	1991	1992	1993	1994	1995
SO_4-$S_{(nss)}$ [eq ha^{-1}]	875	766	639	576	487	503	524	485	422
SO_4-$S_{(nss)}$ [% of AC_{pot} wet deposition]	47.6	44.8	41.8	41.2	40.0	40.5	39.6	37.5	35.6
N [eq ha^{-1}]	899	884	850	796	708	723	788	781	744
N [% of AC_{pot} wet deposition]	48.8	51.7	55.7	56.9	58.2	58.2	59.6	60.4	62.7
$Cl_{(nss)}$ [eq ha^{-1}]	66.5	60.9	37.1	27.0	21.7	16.2	11.2	27.2	20.6
$Cl_{(nss)}$ [% of AC_{pot} wet deposition]	3.6	3.6	2.4	1.9	1.8	1.3	0.8	2.1	1.7
NH_4-N [eq ha^{-1}]	514	506	503	482	416	421	456	456	432
NH_4-N [% of AC_{pot} wet deposition]	27.9	29.6	33.0	34.4	34.2	33.9	34.4	35.3	36.4
NO_3-N [eq ha^{-1}]	384	378	347	314	292	302	333	325	312
NO_3-N [% of AC_{pot} wet deposition]	20.9	22.1	22.7	22.5	24.0	24.3	25.1	25.1	26.3

Average fraction of ...	1996	1997	1998	1999	2000	2001	2002	2003	2004
SO_4-$S_{(nss)}$ [eq ha^{-1}]	341	307	336	275	276	262	285	204	239
SO_4-$S_{(nss)}$ [% of AC_{pot} wet deposition]	32.2	31.5	31.2	29.0	28.4	27.1	27.9	26.5	26.1
N [eq ha^{-1}]	710	649	720	662	678	694	719	558	664
N [% of AC_{pot} wet deposition]	67.0	66.7	67.0	69.7	69.9	71.6	70.4	72.7	72.5
$Cl_{(nss)}$ [eq ha^{-1}]	8.5	17.8	19.5	12.3	16.4	12.8	17.0	5.7	13.4
$Cl_{(nss)}$ [% of AC_{pot} wet deposition]	0.8	1.8	1.8	1.3	1.7	1.3	1.7	0.7	1.5
NH_4-N [eq ha^{-1}]	423	384	419	379	393	406	425	331	389
NH_4-N [% of AC_{pot} wet deposition]	39.9	39.4	39.0	39.9	40.5	41.9	41.6	43.1	42.4
NO_3-N [eq ha^{-1}]	287	265	301	283	285	288	294	227	276
NO_3-N [% of AC_{pot} wet deposition]	27.1	27.3	28.0	29.8	29.4	29.7	28.8	29.6	30.1

5.2.7 Wet deposition of potential net acidity ($AC_{pot(net)} = SO_4\text{-}S_{(nss)} + N + Cl_{(nss)} - BC_{(nss)}$) and acid neutralisation ($= BC_{(nss)} \cdot 100 / AC_{pot}$ [%])

The sum of base cations ($BC_{(nss)} = Ca_{(nss)} + K_{(nss)} + Mg_{(nss)}$) is subtracted from potential acidity (AC_{pot}) in order to calculate potential net acidity ($AC_{pot(net)}$). By doing so, the potential of acid neutralisation is accounted for. Hence the wet deposition loads of $AC_{pot(net)}$ are lower than the wet deposition loads of AC_{pot}. The relative magnitudes of acid neutralisation by wet deposition of $BC_{(nss)}$ are presented in Figure 5.14. Wet flux acid neutralisation by the sum of non-sea salt base cations ($BC_{(nss)}$) on average ranges between 15% (1995) and 22% (1987, 1988, and 2003) of the average wet flux of potential acidity in Germany.

Annual average wet deposition of potential net acidity diminished by 47% from 1987 to 2004, the median by about 50%, respectively (Figure 5.15). Hence the mean changes in $AC_{pot(net)}$ wet deposition in Germany over time are in the same magitude as observed for AC_{pot} (Chapter 5.2.6).

The graphical representation of acid neutralisation in wet deposition from 1993 to 2004 is presented in Map 5.13.

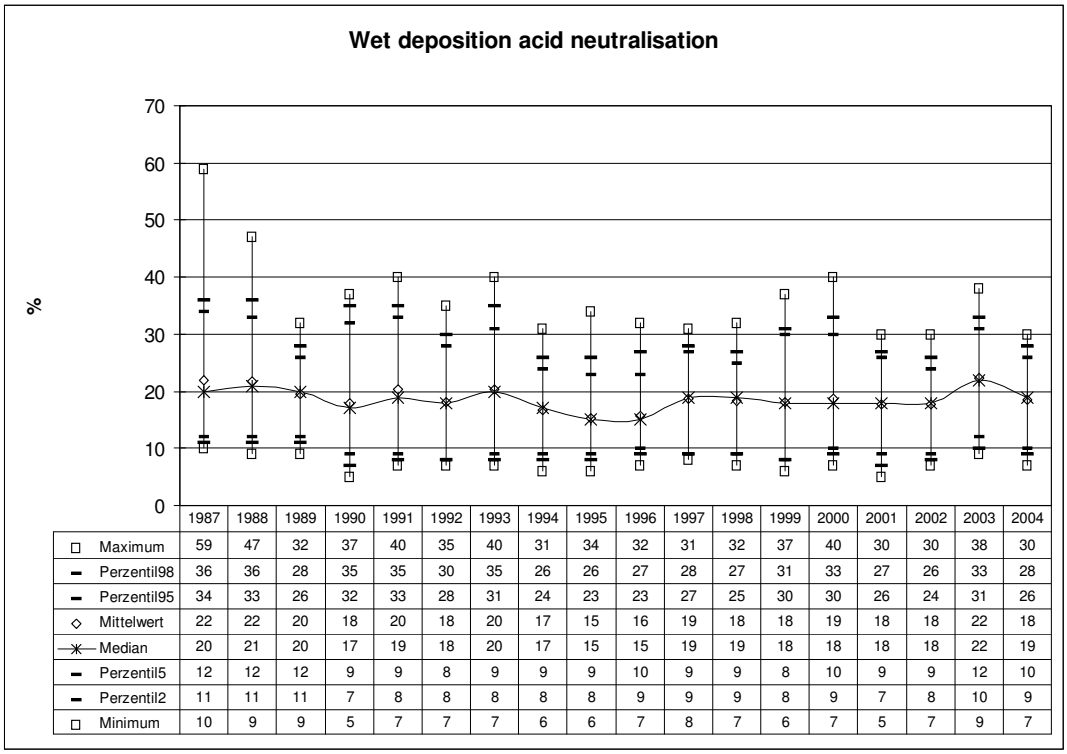

	1987	1988	1989	1990	1991	1992	1993	1994	1995	1996	1997	1998	1999	2000	2001	2002	2003	2004
Maximum	59	47	32	37	40	35	40	31	34	32	31	32	37	40	30	30	38	30
Perzentil98	36	36	28	35	35	30	35	26	26	27	28	27	31	33	27	26	33	28
Perzentil95	34	33	26	32	33	28	31	24	23	23	27	25	30	30	26	24	31	26
Mittelwert	22	22	20	18	20	18	20	17	15	16	19	18	18	19	18	18	22	18
Median	20	21	20	17	19	18	20	17	15	15	19	19	18	18	18	18	22	19
Perzentil5	12	12	12	9	9	8	9	9	9	10	9	9	8	10	9	9	12	10
Perzentil2	11	11	11	7	8	8	8	8	8	9	9	9	8	9	7	8	10	9
Minimum	10	9	9	5	7	7	7	6	6	7	8	7	6	7	5	7	9	7

Figure 5.14: Statistical evaluation of annual acid neutralisation in wet deposition 1987-2004

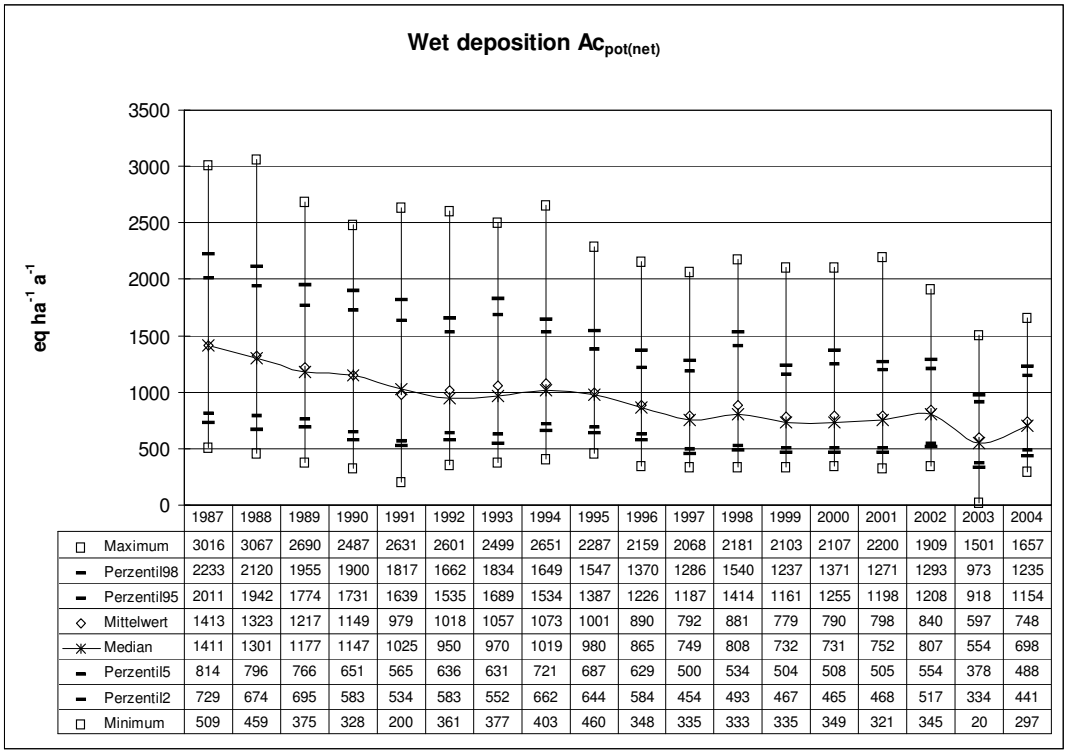

	1987	1988	1989	1990	1991	1992	1993	1994	1995	1996	1997	1998	1999	2000	2001	2002	2003	2004
Maximum	3016	3067	2690	2487	2631	2601	2499	2651	2287	2159	2068	2181	2103	2107	2200	1909	1501	1657
Perzentil98	2233	2120	1955	1900	1817	1662	1834	1649	1547	1370	1286	1540	1237	1371	1271	1293	973	1235
Perzentil95	2011	1942	1774	1731	1639	1535	1689	1534	1387	1226	1187	1414	1161	1255	1198	1208	918	1154
Mittelwert	1413	1323	1217	1149	979	1018	1057	1073	1001	890	792	881	779	790	798	840	597	748
Median	1411	1301	1177	1147	1025	950	970	1019	980	865	749	808	732	731	752	807	554	698
Perzentil5	814	796	766	651	565	636	631	721	687	629	500	534	504	508	505	554	378	488
Perzentil2	729	674	695	583	534	583	552	662	644	584	454	493	467	465	468	517	334	441
Minimum	509	459	375	328	200	361	377	403	460	348	335	333	335	349	321	345	20	297

Figure 5.15: Statistical evaluation of annual potential net acidity ($AC_{pot(net)}$) wet deposition 1987-2004

The spatial patterns of $AC_{pot(net)}$ 1993 to 2004 are presented in Map 5.12. The decline of peak values (Figure 5.15) are represented in the maps by obviously less high value areas, especially from 1993 to 1997. Regions with wet $AC_{pot(net)}$ fluxes above the average in the later years are found in north-western Germany, while in the other parts of Germany fluxes above the annual average are mainly restricted to small higher altitude mountain areas.

5.3 Wet deposition fluxes and trends of cadmium (Cd) and lead (Pb)

For mapping wet deposition fluxes of cadmium (Cd) and lead (Pb) the same methods were applied as for main compounds in precipitation (cf. Chapter 4.4). Wet deposition loads of heavy metals are much lower than wet deposition loads of main compounds in precipitation. Cd wet deposition loads are a factor of about 10000 lower than wet fluxes of main compounds, Pb wet fluxes are a factor of about 1000 lower, respectively. Hence enhanced errors and uncertainties may be expected, both in data of the samples used as input for calculation of wet deposition fields, and caused by application of the mapping procedure.

Annual average wet deposition fluxes of Cd and Pb are calculated and maped for the 11 years time period from 1994 to 2004. In Table 5.15 an overview is given on each year's average Cd and Pb wet deposition mapping results. The annual variation of average wet deposition fluxes is given as percentage change from the respective previous year. Cd average wet deposition fluxes from 1994 to 2004 declined by about 21%, average Pb wet fluxes declined by about 19%, respectively. The changes between one year and the next, however, are ranging up to ±30% for cadmium wet deposition, and from +19% to -14% for average Pb wet deposition flux, which is in the same order of magnitude as the changes are over the whole time period considered.

Table 5.15: Budgets of average annual wet deposition of Cd and Pb 1994-2004

	Cd [µeq $ha^{-1}a^{-1}$]	Cd [mg $ha^{-1}a^{-1}$]	change from previous year [%]	Pb [µeq $ha^{-1}a^{-1}$]	Pb [g $ha^{-1}a^{-1}$]	change from previous year [%]
1994	2097	118		25720	2.7	
1995	2016	113	-3.9	30545	3.2	+18.8
1996	1985	112	-1.5	29907	3.1	-2.1
1997	1408	79	-29.1	28682	3.0	-4.1
1998	1621	91	+15.2	29382	3.0	+2.4
1999	1615	91	-0.4	30498	3.2	+3.8
2000	1453	82	-10.1	27164	2.8	-10.9
2001	1534	86	+5.6	27259	2.8	+0.4
2002	1536	86	+0.1	27268	2.8	+0.0
2003	1263	71	-17.7	24216	2.5	-11.2
2004	1651	93	+30.6	20746	2.1	-14.3
change from 1994 to 2004 [%]			-21.3			-19.3

Table 5.16: Comparison of Cd and Pb wet deposition and emission data[1)] in Germany 1994-2004
([1)]UBA 2007 http://www.umweltbundesamt.de/emissionen/archiv/DE_2007_Tables_IV1A_1990_2005.zip)

	Cd wet deposition [t a^{-1}]	Cd emission [1)] [t a^{-1}]	Ratio: wet flux / emission	Pb wet deposition [t a^{-1}]	Pb emission [1)] [t a^{-1}]	Ratio: wet flux / emission
1994	4.2	2.3	1.64	95.1	405	0.23
1995	4.0	2.3	1.75	112.9	330	0.34
1996	4.0	2.2	1.78	110.6	330	0.50
1997	2.8	2.4	1.16	106.0	222	1.11
1998	3.3	2.2	1.45	108.6	96	1.16
1999	3.2	2.7	1.19	112.7	94	1.18
2000	2.9	2.4	1.20	100.4	96	0.98
2001	3.1	2.6	1.20	100.8	102	0.96
2002	3.1	2.7	1.13	100.8	105	0.95
2003	2.5	2.7	0.92	89.5	106	0.84
2004	3.3	2.7	1.27	76.7	107	0.70

5.3.1 Wet deposition of cadmium (Cd)

Between 1994 and 2004 wet deposition of cadmium (Cd) on average diminished by about 21% (median -35%). Over the whole area of Germany this equals a decline of about 0.9 t from about 4.2 t in 1994 to 3.3 t in 2004.

The average wet deposition flux declined from about 118 mg ha^{-1} a^{-1} in 1994 to about 93 mg ha^{-1} a^{-1} in 2004. The steepest fall in average Cd wet deposition flux (-29%) can be observed from 1996 to 1997 (Figure 5.16), when peak values as well as the average wet flux clearly declined. In 1998 again 15.2% higher average Cd wet fluxes can be found, and in the following years 1999 to 2002 the annual average wet deposition fluxes are remaining more or less on the same level. In 2003, the meteorologically exceptional dry year in the period, average Cd wet fluxes fall by about 17%, whereas in 2004 average wet deposition fluxes are almost at the same level as in 1998.

Maps of wet deposition of Cd 1994 to 2004 are presented in Map 5.14. The patterns of high and low wet deposition fluxes are relatively different over time. While the map statistics presented in Figure 5.16 are similar in 1998 and 2004, the spatial distribution of wet Cd input over Germany in these two years is quite different: in 1998 higher fluxes mainly can be observed in central germany, whereas in 2004 fluxes above the average mainly can be found in the south-western and estern most parts of Germany. Those annual differences in each year's spatial scatter of high and low wet Cd fluxes mainly are due to the analytical data provided from deposition measurement networks in the respective years.

As can be seen in the ratios above 1.0, calculated from wet flux and emission data in table 5.16, total wet deposition flux of Cd, wich is based upon monitoring data, in all of the years of the time period considered except 2003 is higher than the official total emission data reported to the UN ECE CLRTAP.

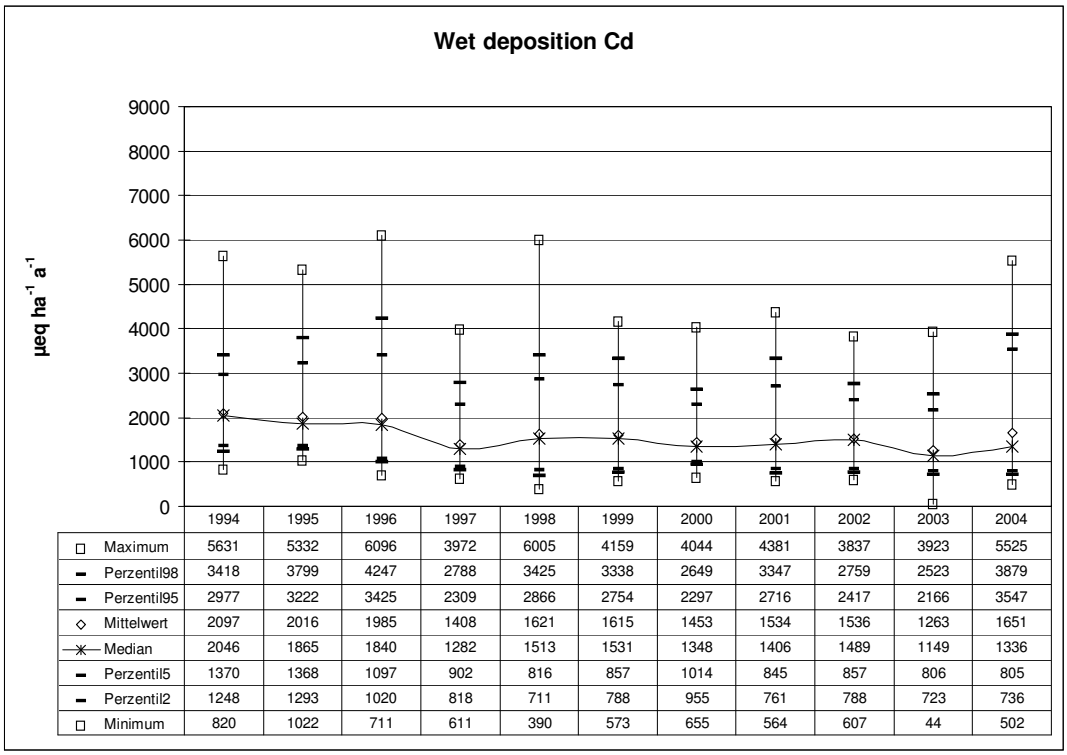

	1994	1995	1996	1997	1998	1999	2000	2001	2002	2003	2004
Maximum	5631	5332	6096	3972	6005	4159	4044	4381	3837	3923	5525
Perzentil98	3418	3799	4247	2788	3425	3338	2649	3347	2759	2523	3879
Perzentil95	2977	3222	3425	2309	2866	2754	2297	2716	2417	2166	3547
Mittelwert	2097	2016	1985	1408	1621	1615	1453	1534	1536	1263	1651
Median	2046	1865	1840	1282	1513	1531	1348	1406	1489	1149	1336
Perzentil5	1370	1368	1097	902	816	857	1014	845	857	806	805
Perzentil2	1248	1293	1020	818	711	788	955	761	788	723	736
Minimum	820	1022	711	611	390	573	655	564	607	44	502

Figure 5.16: Statistical evaluation of annual cadmium (Cd) wet deposition 1994-2004

5.3.2 Wet deposition of lead (Pb)

Wet deposition fluxes of lead (Pb) over Germany from 1995 to 2002 on average are almost on the same level of about 2.8 to 3.2 g ha^{-1} a^{-1} (Figure 5.17 and Table 5.15). Over the whole area of Germany this equals a total input of about 101 to about 113 t a^{-1} (cf. Table 5.16). From 1994 to 1995 average Pb wet deposition flux is rising by about 19%. From 2002 to 2004 average Pb wet deposition flux is falling by about 24%. Hence the decline from the first year mapped (1994) to the last (2004) is about 19%, which equals a decline of about 18.4 t a^{-1} from about 95.1 t a^{-1} (2.7 g ha^{-1} a^{-1}) in 1994 to 76.7 t a^{-1} (2.1 g ha^{-1} a^{-1}) in 2004.

The spatial pattern of Pb wet deposition fluxes over Germany is presented in Map 5.15. From 1995 to 2002 the spatial distribution of Pb wet deposition fluxes is quite similar, with much higher input than average mainly in the north-eastern part of Germany, and in some parts in south-western and southern Germany more or less close to the border to France and Austria.

The total wet deposition flux of Pb over Germany in 1997, 1998, and 1999 is higher than the official total emission data reported to the UN ECE CLRTAP (Table 5.16). This means, that the emission estimates are too

low. In 2000 to 2002 the wet deposition flux still is very close to the total emission amount, which also seems to be unrealistic. Only in 1994 to 1996 the wet Pb flux is less than 50% of the total emission in Germany.

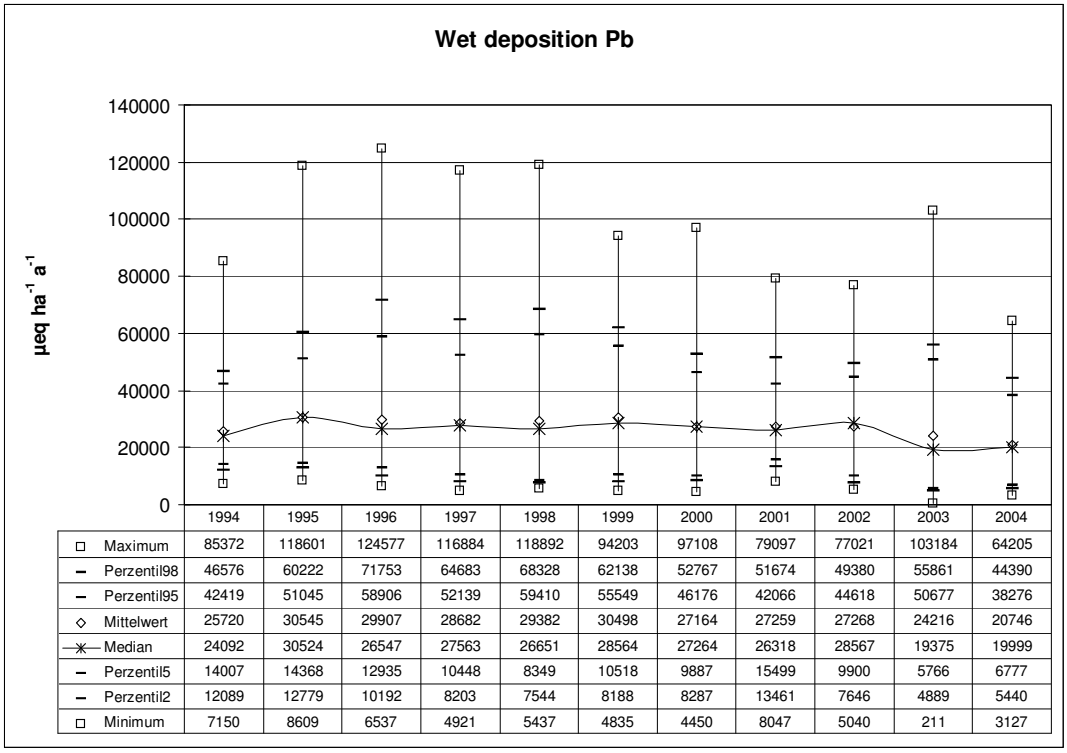

	1994	1995	1996	1997	1998	1999	2000	2001	2002	2003	2004
Maximum	85372	118601	124577	116884	118892	94203	97108	79097	77021	103184	64205
Perzentil98	46576	60222	71753	64683	68328	62138	52767	51674	49380	55861	44390
Perzentil95	42419	51045	58906	52139	59410	55549	46176	42066	44618	50677	38276
Mittelwert	25720	30545	29907	28682	29382	30498	27164	27259	27268	24216	20746
Median	24092	30524	26547	27563	26651	28564	27264	26318	28567	19375	19999
Perzentil5	14007	14368	12935	10448	8349	10518	9887	15499	9900	5766	6777
Perzentil2	12089	12779	10192	8203	7544	8188	8287	13461	7646	4889	5440
Minimum	7150	8609	6537	4921	5437	4835	4450	8047	5040	211	3127

Figure 5.17: Statistical evaluation of annual lead (Pb) wet deposition 1994-2004

5.4 Maps of wet deposition 1993-2004

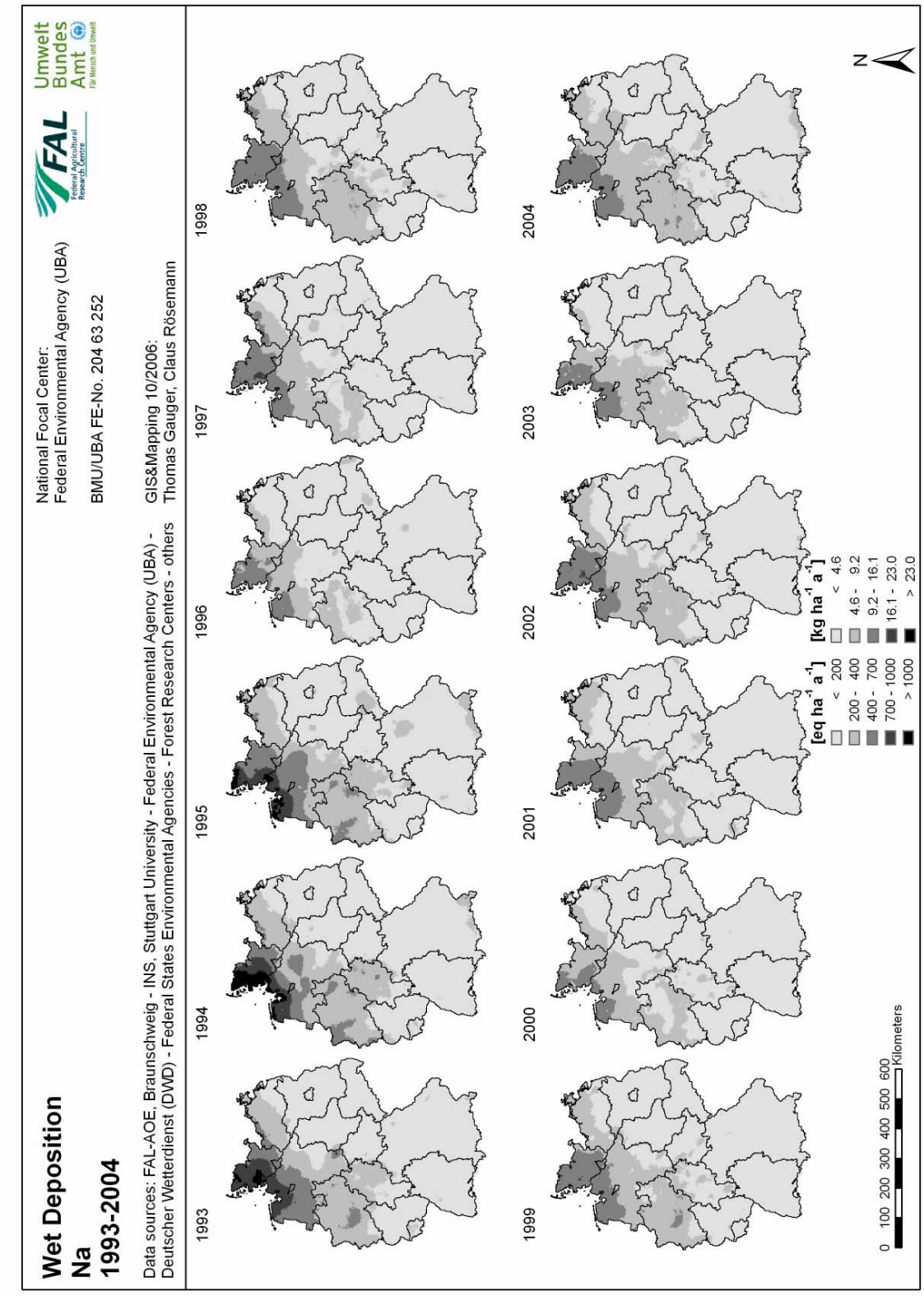

Map 5.1: Wet deposition of Na 1993-2004

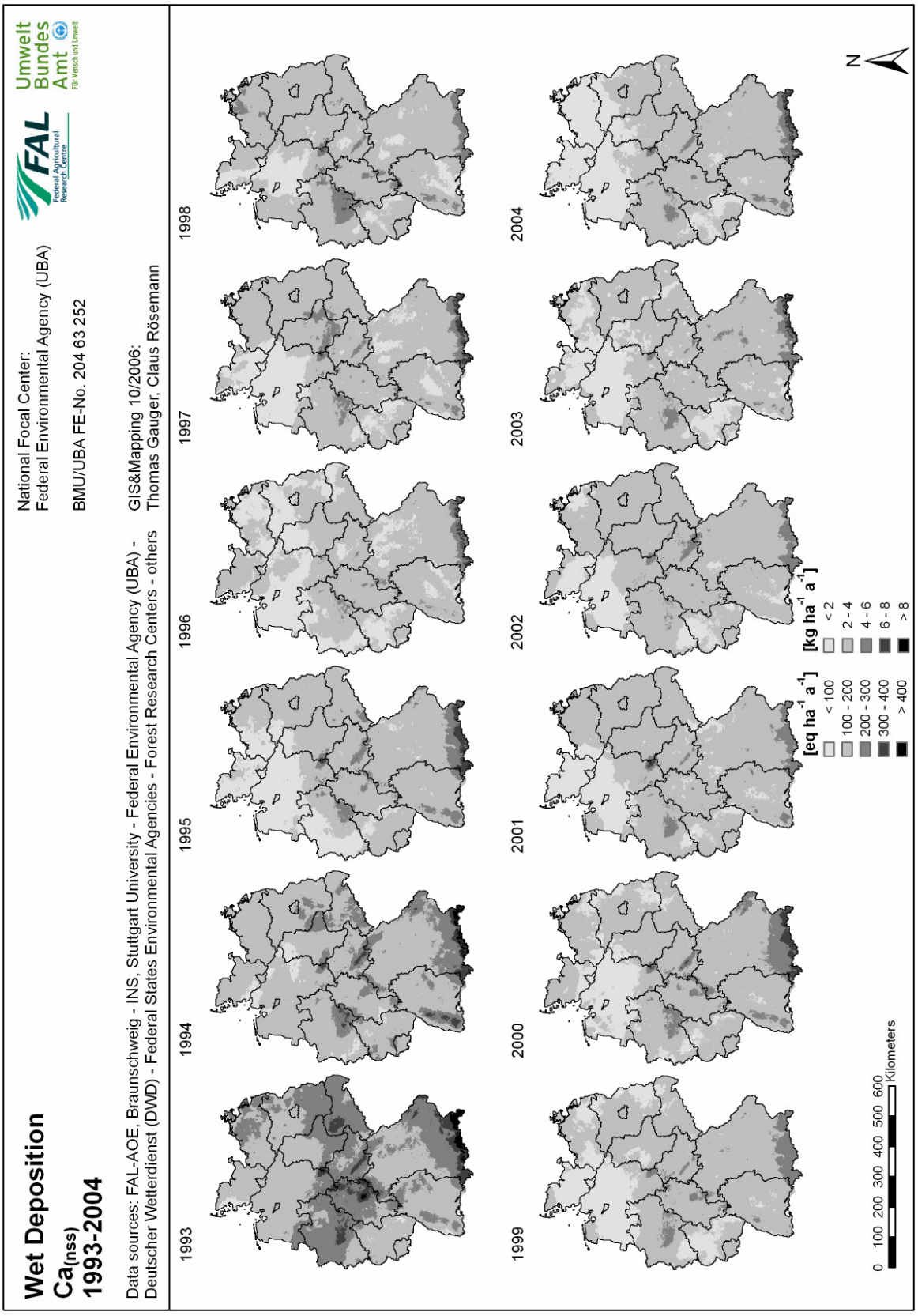

Map 5.2: Wet deposition of $Ca_{(nss)}$ 1993-2004

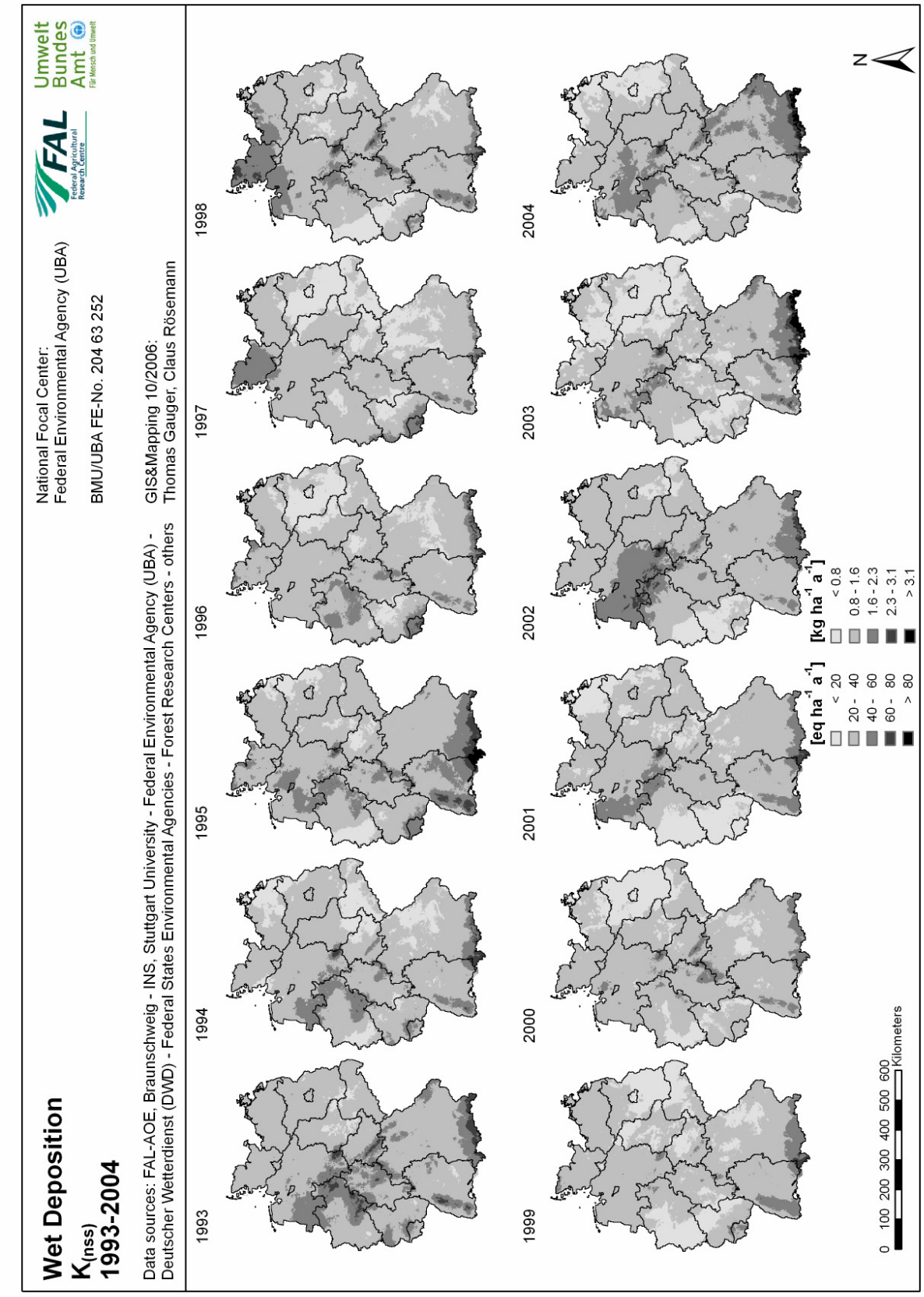

Map 5.3: Wet deposition of $K_{(nss)}$ 1993-2004

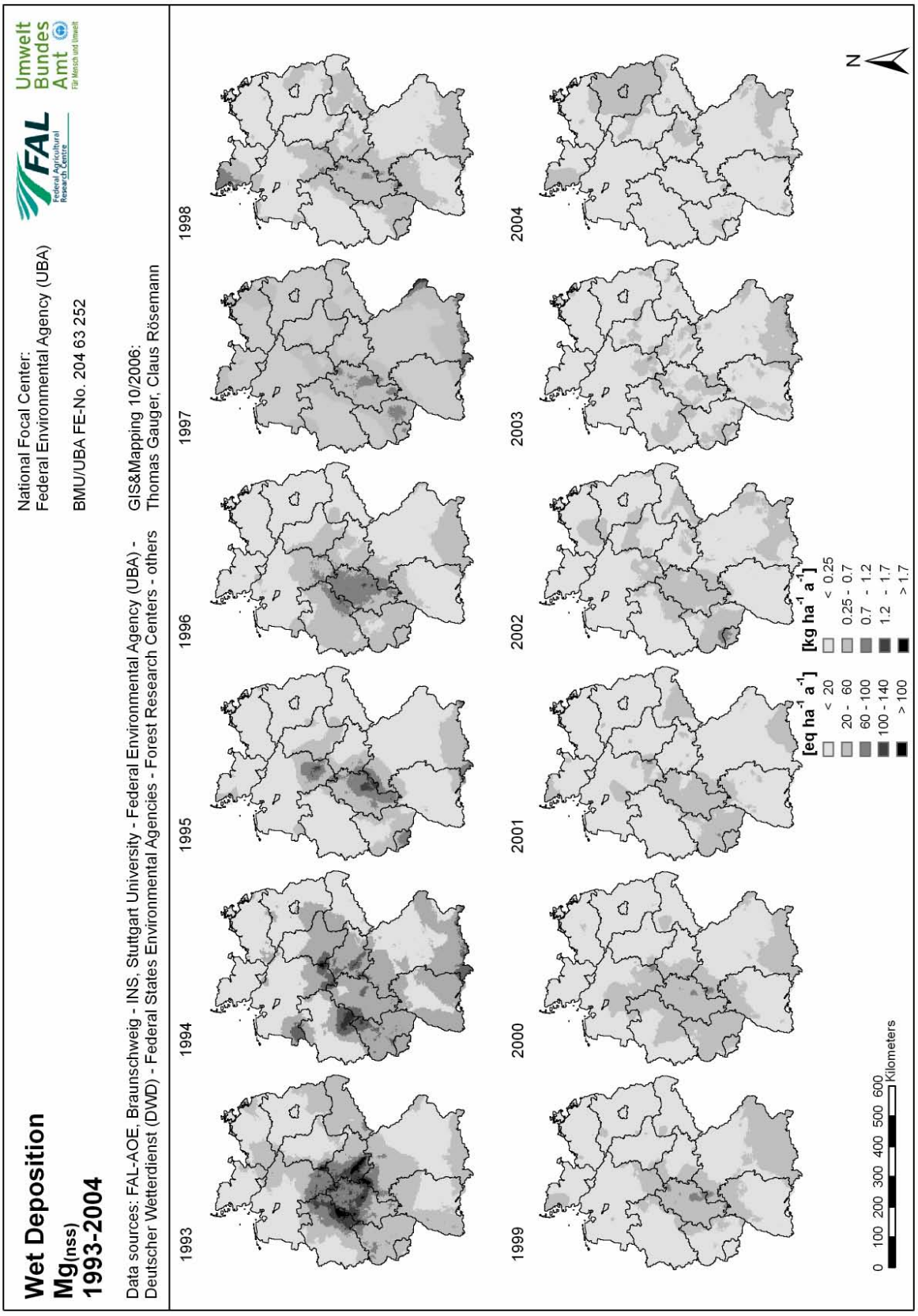

Map 5.4: Wet deposition of $Mg_{(nss)}$ 1993-2004

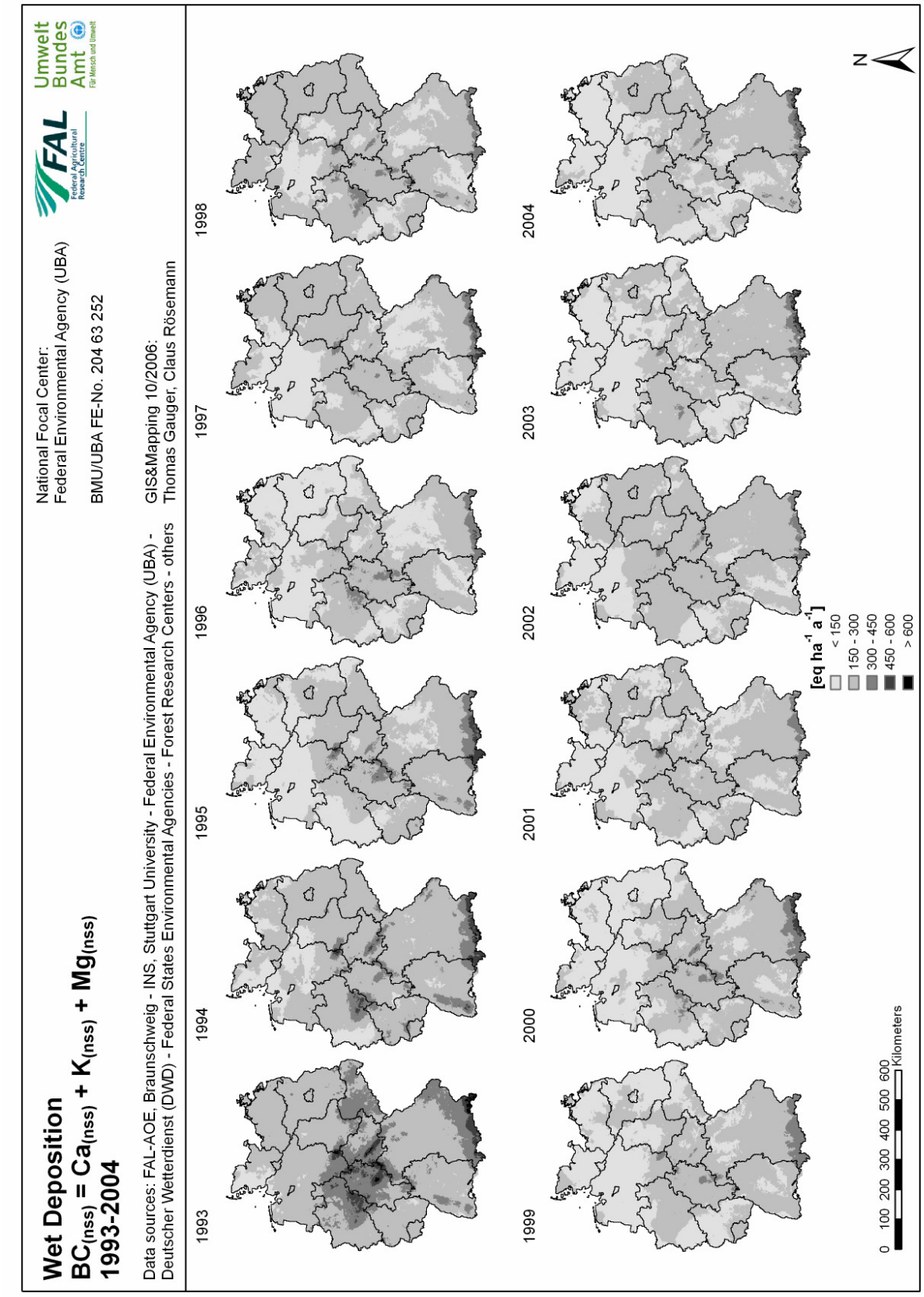

Map 5.5: Wet deposition of $BC_{(nss)}$ 1993-2004

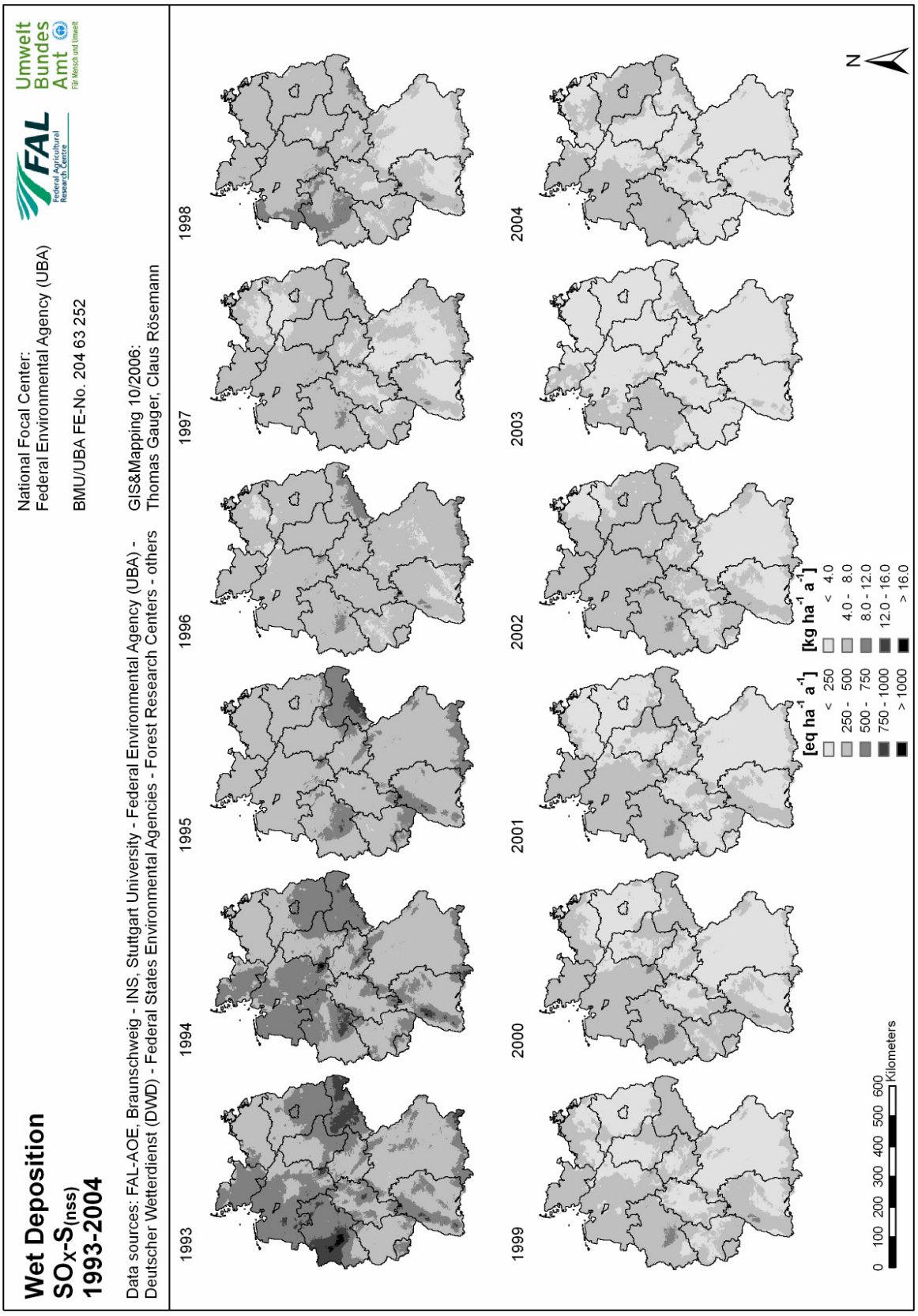

Map 5.6: Wet deposition of SO_4-$S_{(nss)}$ 1993-2004

Map 5.7: Wet deposition of NH_4-N 1993-2004

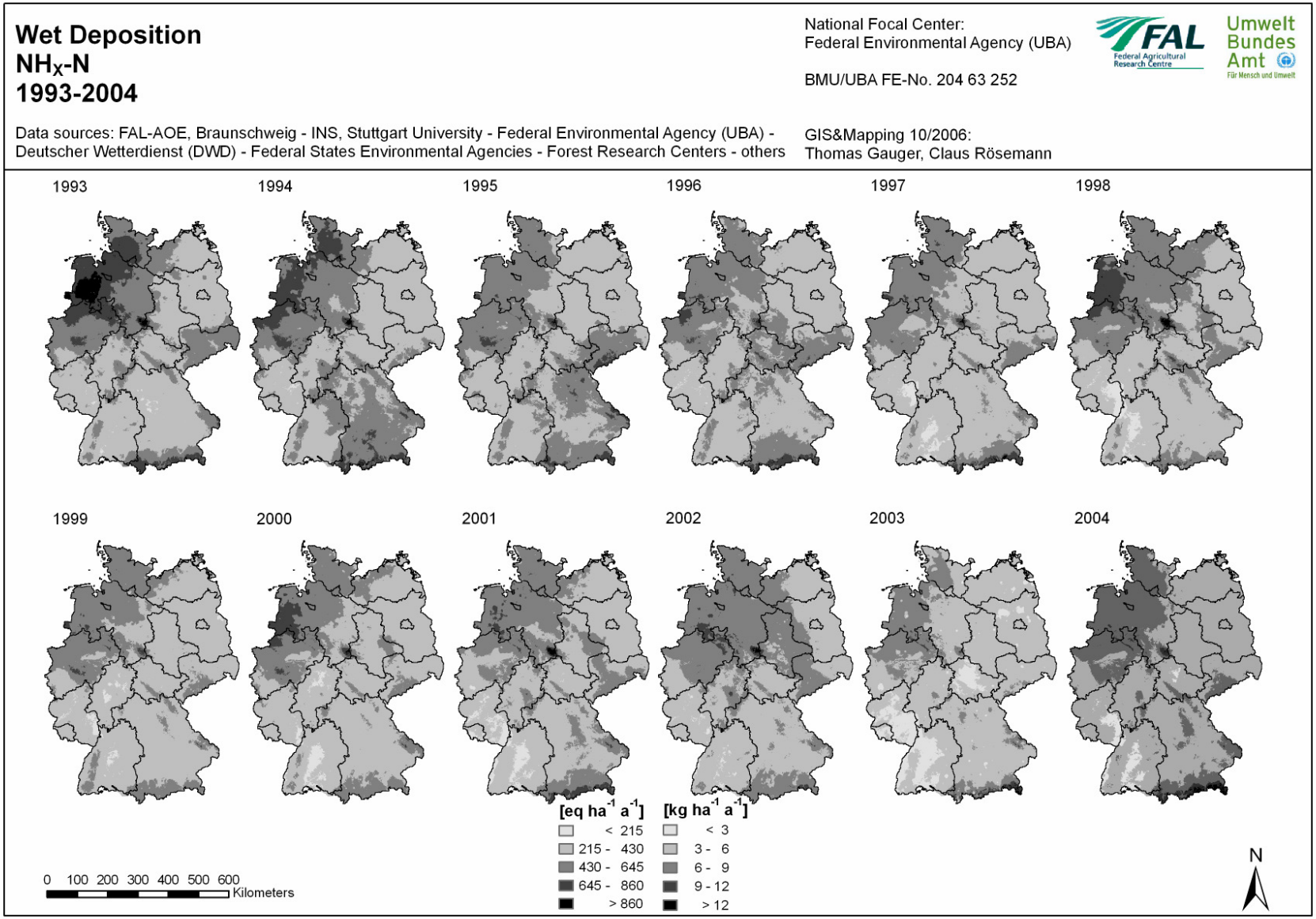

Map 5.8: Wet deposition of NO_3-N 1993-2004

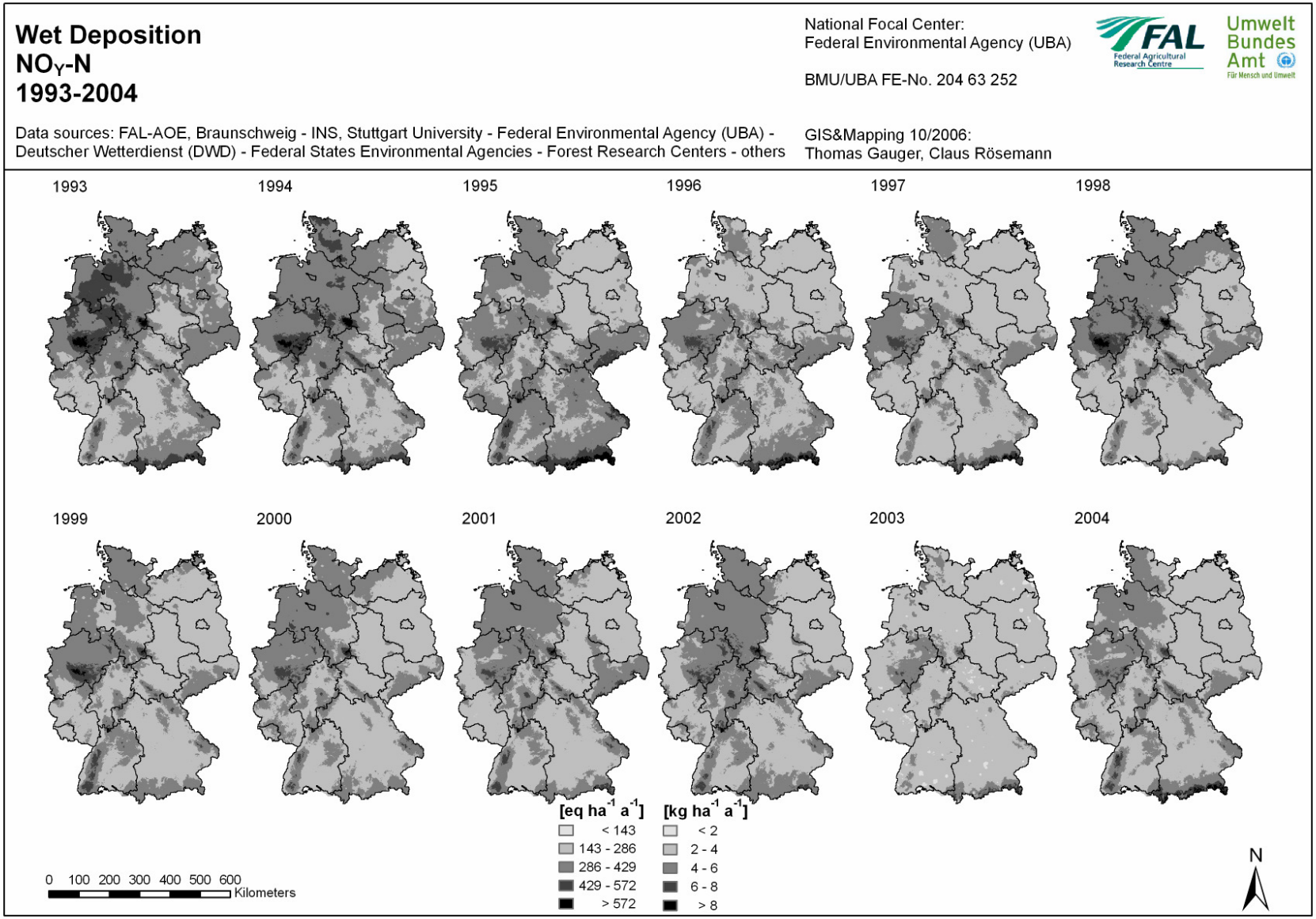

Map 5.9: Wet deposition of N 1993-2004

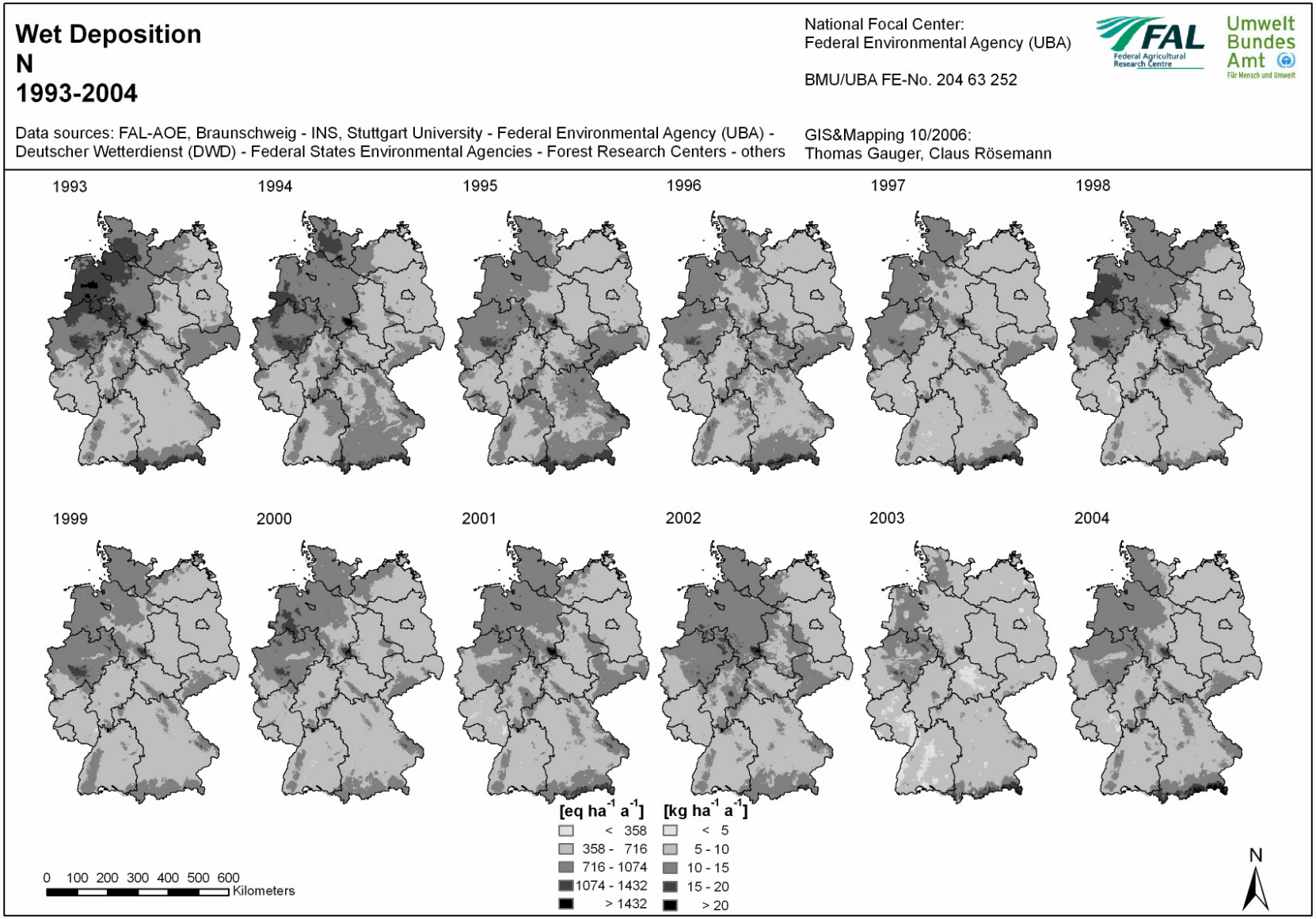

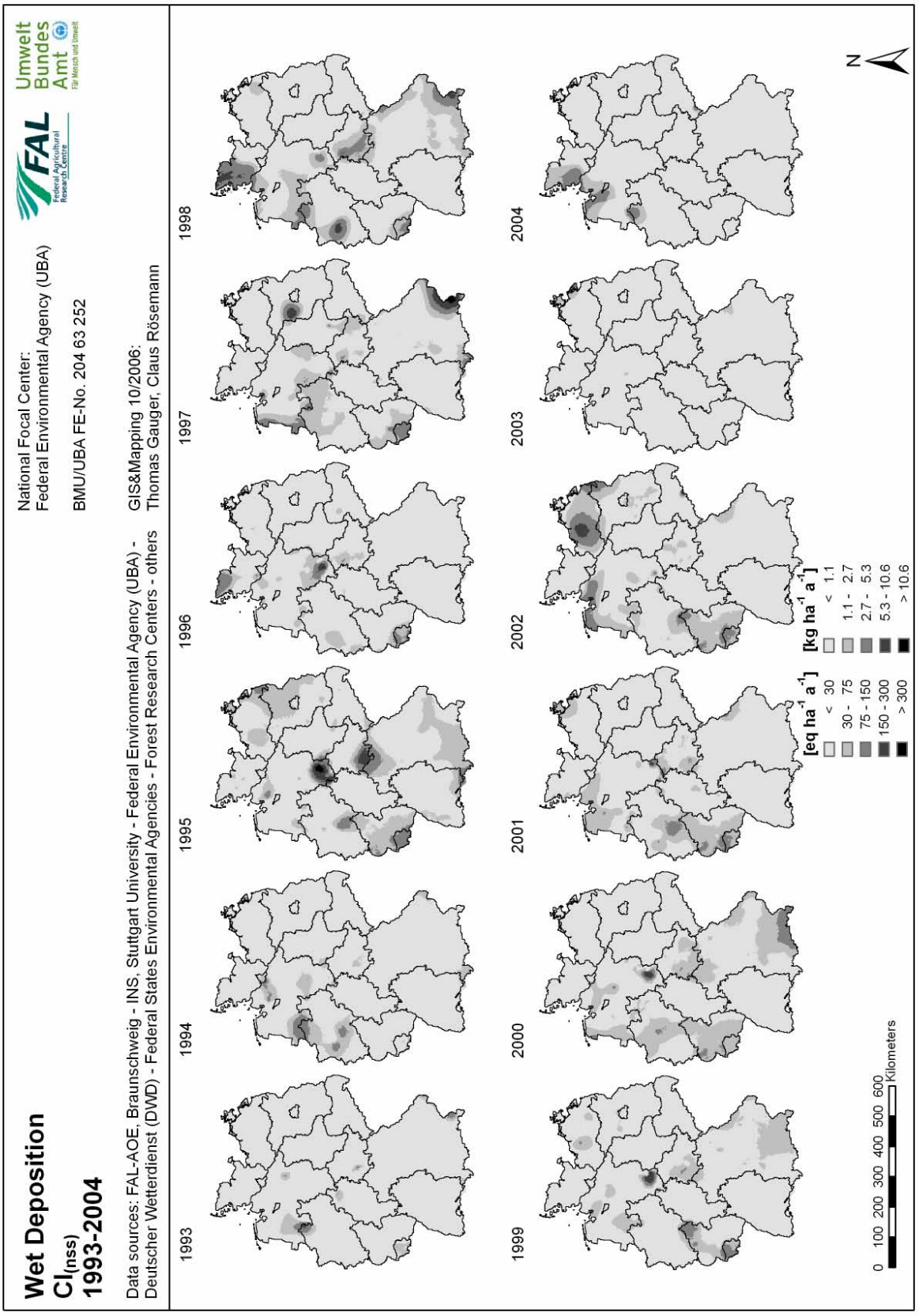

Map 5.10: Wet deposition of $Cl_{(nss)}$ 1993-2004

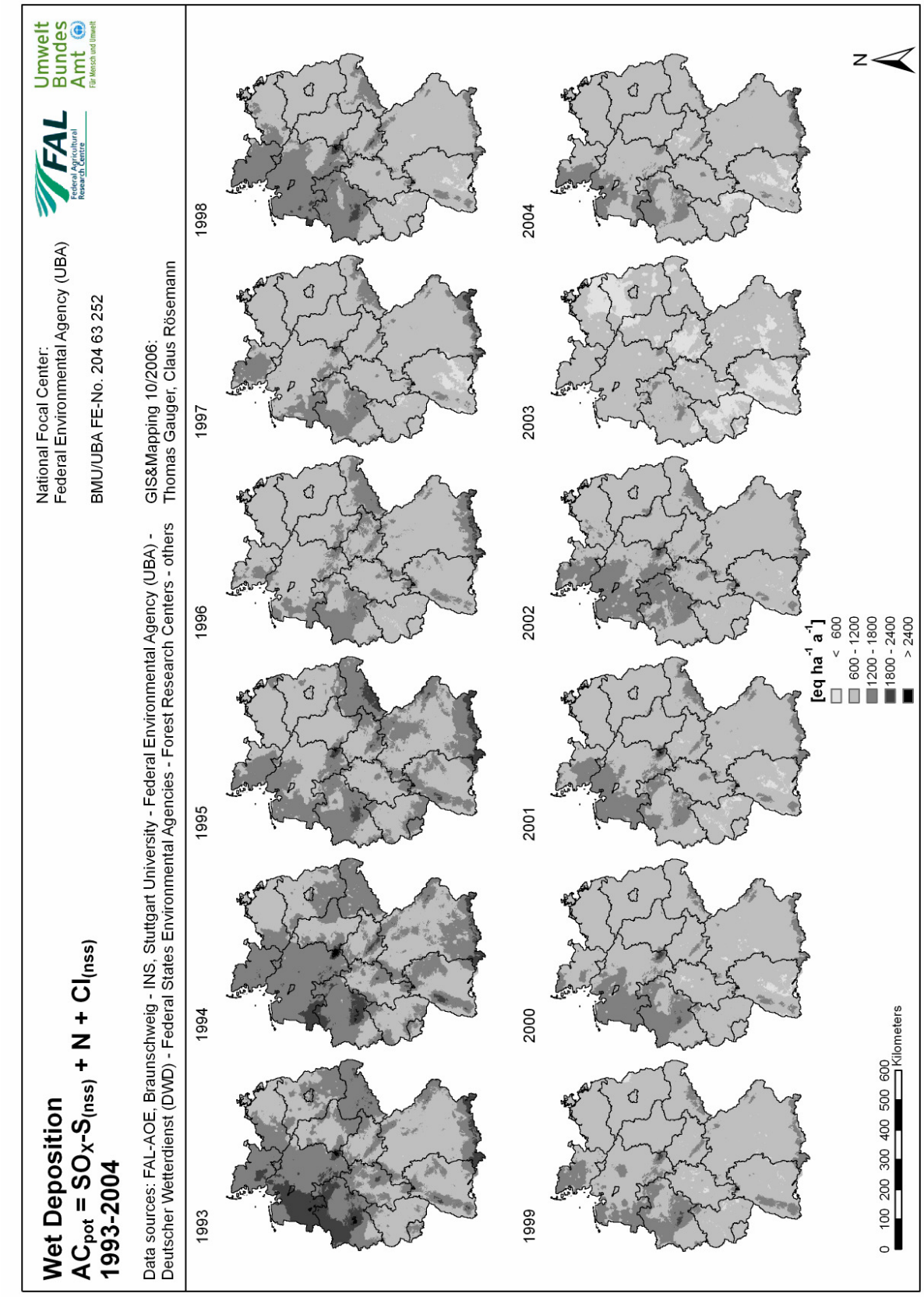

Map 5.11: Wet deposition of AC_{pot} 1993-2004

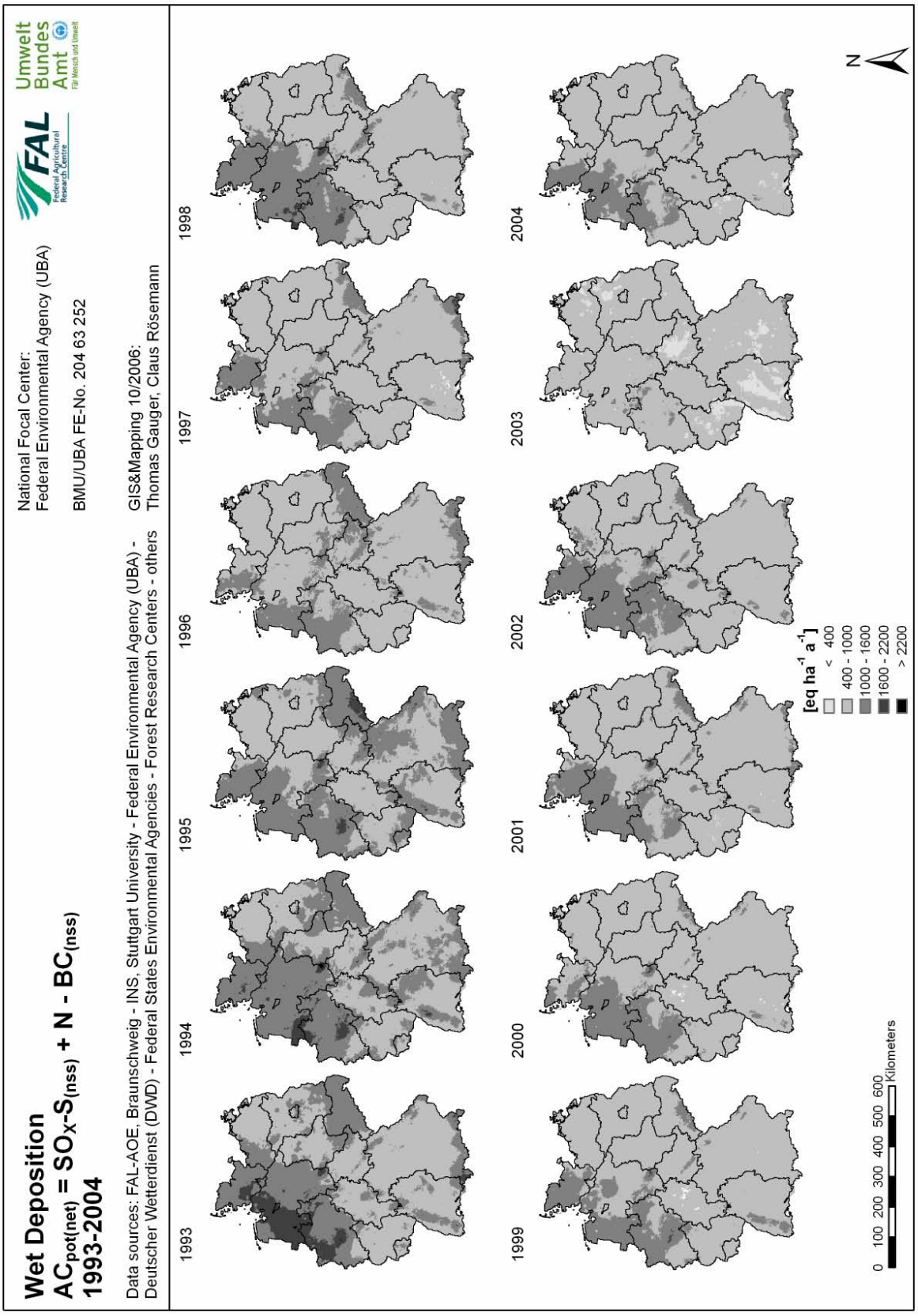

Map 5.12: Wet deposition of $AC_{pot(net)}$ 1993-2004

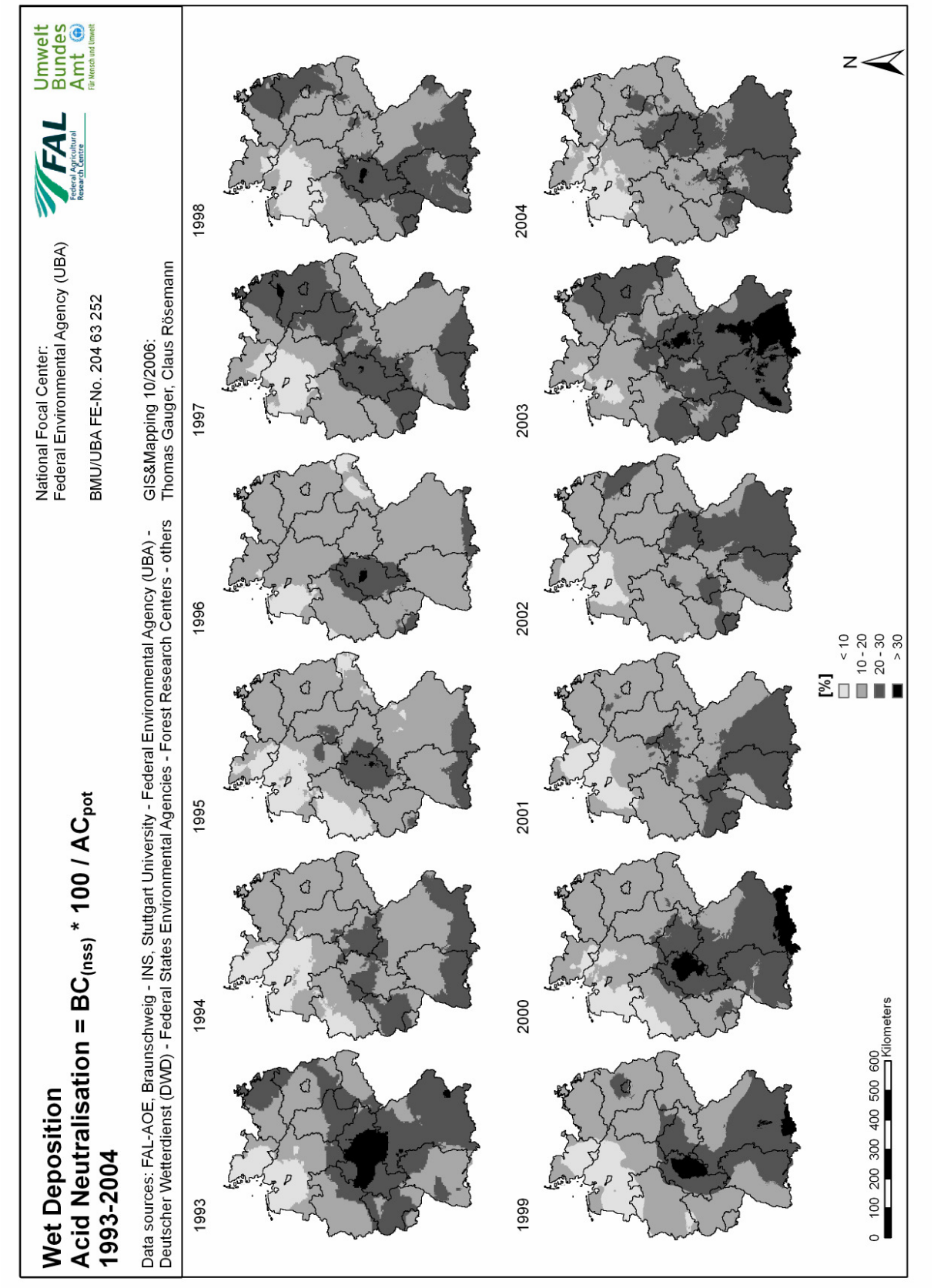

Map 5.13: Neutralisation of wet deposited AC_{pot} by $BC_{(nss)}$ 1993-2004

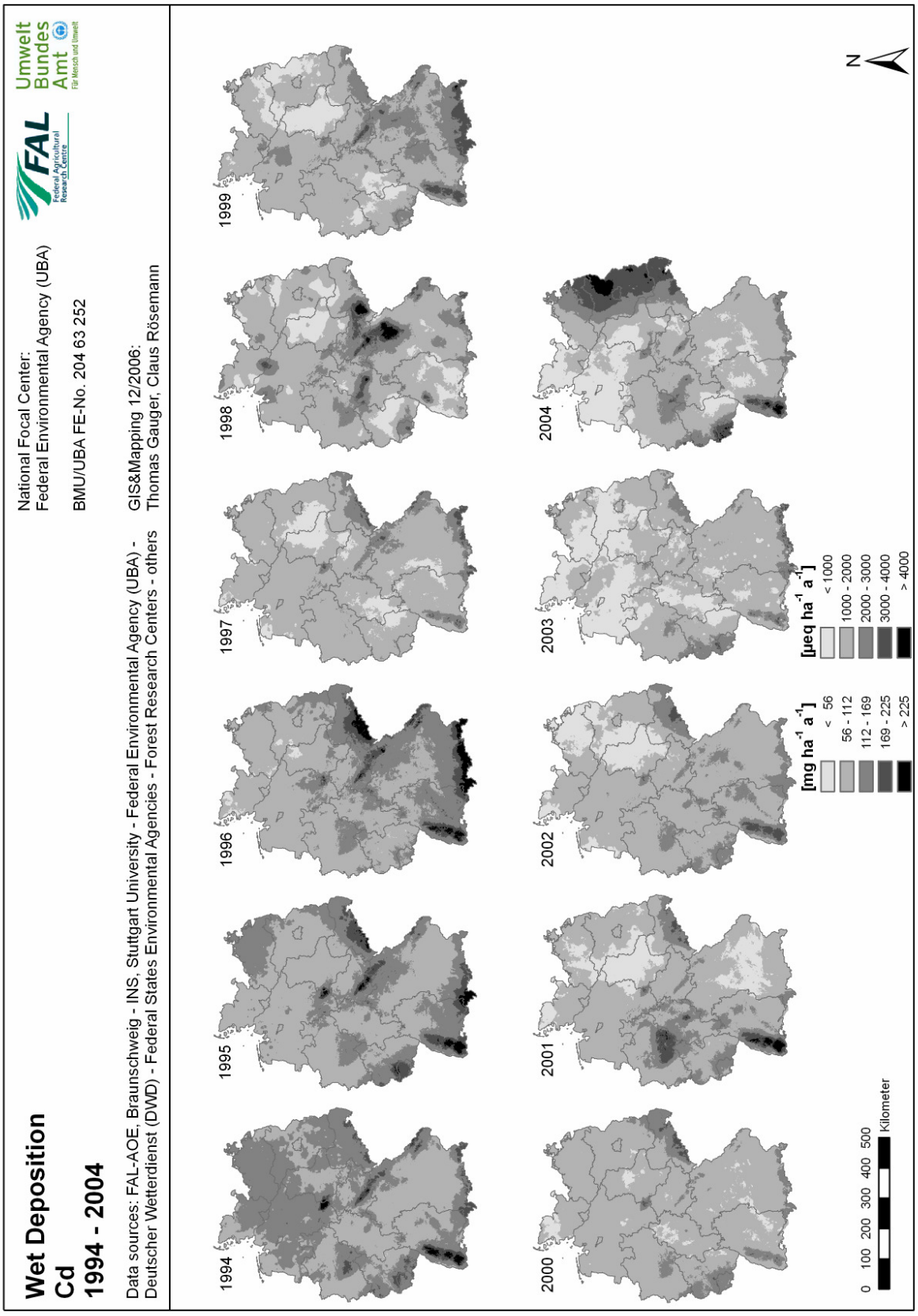

Map 5.14: Wet deposition of Cd 1994-2004

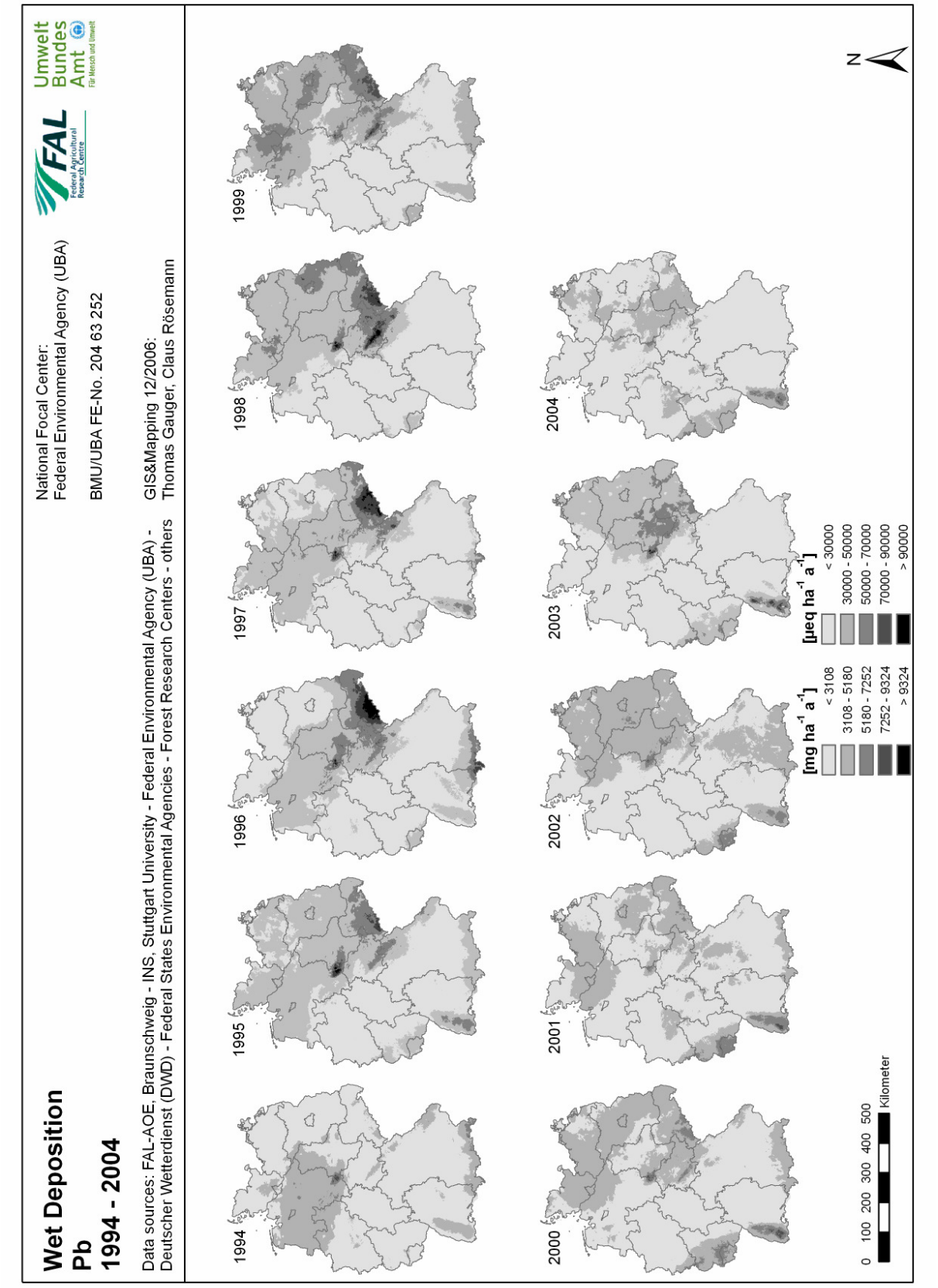

Map 5.15: Wet deposition of Pb 1994-2004

6 Mapping dry deposition

A.T. Vermeulen, A. Bleeker
Energy research Center of the Netherlands (ECN) - Biomass, Coal & Environmental Research, Air Quality & Climate Change, Petten, The Netherlands

6.1 General

The dry deposition of the components considered in this project is calculated by a model called the Integrated DEposition Model (IDEM), using the so called dry deposition inference method (ERISMAN, 1992; ERISMAN & BALDOCCHI, 1994; VAN PUL ET AL, 1992, 1995). The dry deposition sub-model that was built into IDEM is based on the DEPAC module. DEPAC stands for DEPosition of Acidifying Components. The IDEM model is built around this dry deposition scheme and integrates the retrieval of spatial data concerning land use etc., and time dependent data like meteorological and concentration data with the deposition calculations. The method followed is roughly the same as in the EDACS model that was used in previous projects (VAN PUL, 1995; BLEEKER ET AL., 2000), except for usage of different and higher resolution meteorological and modelled concentration data, an updated land-use map based on the CORINE-2000 data, some small changes and corrections in DEPAC, and the updated integrative viewer program to enable dissemination of the calculated data on CD. The outline of the IDEM model is presented in Figure 6.1.

Dry deposition fluxes are calculated in IDEM by calculation of dry deposition velocities and applying these on modelled concentrations for the same height. In the inference method it is assumed that a constant flux layer exists between a reference height and the surface. To fulfil this condition the air and the surface layer need to be in equilibrium, with no chemical reactions taking place in the surface layer and no advection. Only then the deposition flux at the reference height is equal to that at the surface. The reference height has to be chosen so that it lies within the surface layer and that the concentration at that height is not severely influenced by local deposition, so that using concentration data from a relatively coarse resolution model or measurement network is allowed. In IDEM and EDACS the reference height is taken at 50 m above ground level (ERISMAN, 1992).

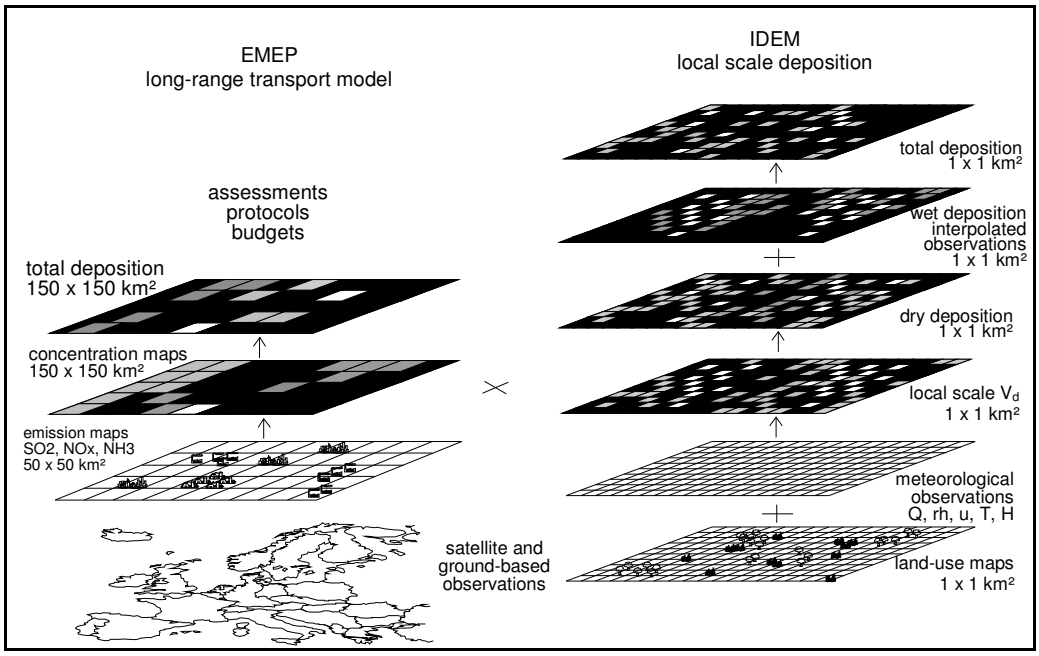

Figure 6.1: Outline of the EMEP and IDEM model (from BLEEKER ET AL. 2000, modified)

6.1.1 IDEM domain

The IDEM model domain for the calculations described in this report was a 1x1km² grid covering Germany. The grid consists of 750 data points in West-East direction and 1000 data points in North-South direction. IDEM was provided with land use data and data describing the German Federate State ('Bundesland') for each pixel in the previous version. The 6 land-use classes that were used in the previous version of IDEM, and the corresponding roughness lengths used per land use class are explained in Table 6.1. Table 6.2 shows the updated land-use classification based on the CORINE-2000 dataset, using 9 different land-use classes. The following 3 Land Use Types were added: *Pasture, Semi-natural* and *Other*. Furthermore in the new version IDEM the land-use

classification is given as a percentage for each of the 9 new land-use classes per 1x1 km grid cell. The resulting roughness length (z_0) of each 1x1 km grid cell is calculated as the logarithmic weighted average of the corresponding z_0's per land use class. Dry deposition fluxes and velocities are calculated for each grid cell for each land use class separately and afterwards the weighted average flux per cell is calculated and taken as the average flux for that grid cell.

The regional average tree heights ('TH') used to calculate roughness lengths of forests is listed in Table 6.3.

Table 6.1: IDEM land use types "1990"

Land use type	Roughness length (m)		Canopy height (m)
	Summer	winter	
Arable (agriculture)	0.1	0.05	0.5
Coniferous forest	0.085 x TH*		see Table 6.3
Deciduous forest	0.06 x TH*	0.09 x TH*	see Table 6.3
Mixed forest	0.085 x TH*		see Table 6.3
Water	0.0002		n.a.
Urban	1.0		n.a.
* TH = Tree Height (m); n.a. = not applicable			

Table 6.2: IDEM land use types "Corine2000"

Land use type	Roughness length (m)		Canopy height (m)
	summer	winter	
Arable (agriculture)	0.1	0.05	0.5
Coniferous forest	0.085 x TH*		see Table 6.3
Deciduous forest	0.06 x TH*	0.09 x TH*	see Table 6.3
Mixed forest	0.085 x TH*		see Table 6.3
Pasture	0.05	0.03	n.a.
Semi-natural	0.1		n.a.
Water	0.0002		n.a.
Urban	1.0		n.a.
Other	0.01		n.a.
* TH = Tree Height (m); n.a. = not applicable			

Table 6.3: Average tree height per tree type and per Bundesland

Federal States of Germany	Deciduous	Coniferous	Mixed
Brandenburg	19.3	14.6	15.3
Mecklenburg-West Pommerania	21.0	16.8	18.4
Saxony	17.1	15.2	15.6
Saxony-Anhalt	19.6	15.2	16.6
Thuringia	21.1	16.4	17.9
Schleswig-Holstein	19.3	16.4	18.0
Lower Saxony	17.7	14.8	15.9
Saarland	17.8	17.8	17.7
Rhineland-Palatinate	18.6	18.4	18.5
Hesse	21.8	19.8	20.8
Baden-Württemberg	21.6	22.1	21.7
Bavaria	18.2	21.0	20.2
North Rhine-Westphalia	18.7	17.4	18.1
Germany average	19.4	17.4	18.0

In Figure 6.2 the dominant land use categories following the Corine2000 classification scheme on the 1x1km² grid over Germany are shown.

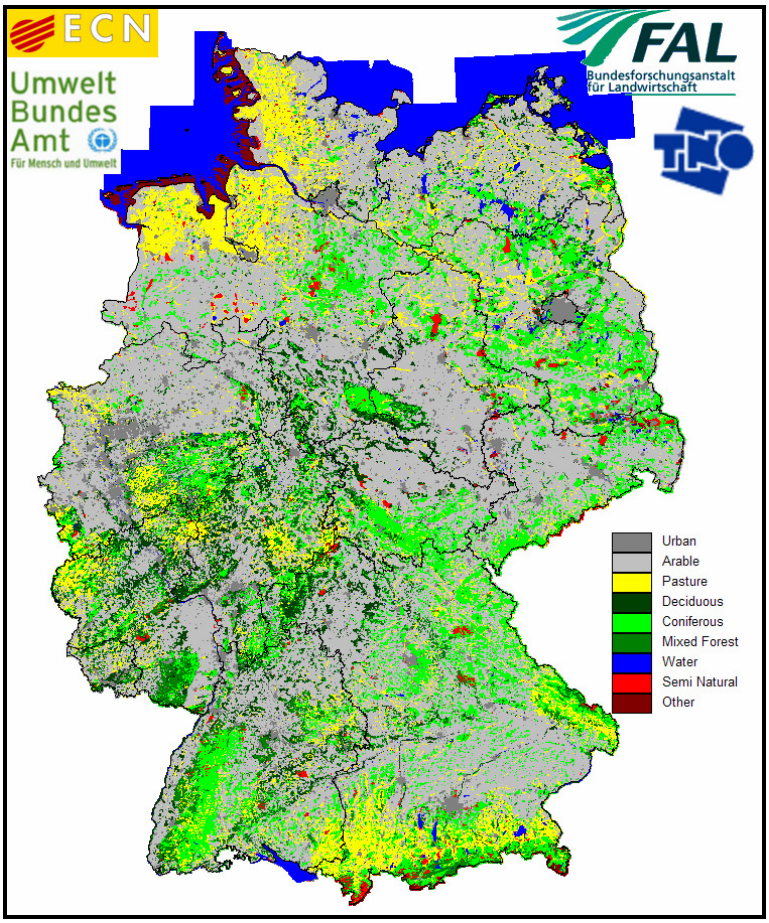

Figure 6.2: Dominant land use categories on the 1x1km² grid over Germany (source: Corine Land Cover2000)

6.1.2 IDEM components

In IDEM the dry deposition velocities are calculated for the following components:

- Ammonia; NH_3
- Ammonium; NH_4
- Sulphur dioxide; SO_2
- Sulphate (aerosol); SO_4
- Nitrogen monoxide; NO
- Nitrogen dioxide; NO_2
- Nitric Acid; HNO_3
- Nitrate aerosol; NO_3
- Base Cations; Na, Mg, Ca, K

The following definitions are used for certain groups of components:

- **NO_Y** = $NO+NO_2+HNO_3+NO_3$
- **NH_X =** NH_3+NH_4
- **SO_X =** SO_2+SO_4
- **Total Acid =** $NO_Y+NH_X+SO_X$
- **BC** = Ca+K+Mg

6.1.3 IDEM meteorological input

IDEM requires detailed meteorological input data. In the calculations described in this report, data was used from the ECMWF MARS (European Centre for Medium-Range Weather Forecasts Meteorological Archival Retrieval System) [http://www.ecmwf.int/] database. For the years 1995 and 1999-2001 re-analysed data was

used (ERA40). For the further period (2002-2004) the re-analysed data is not yet available, so the standard analysed fields from the MARS database were used. The resolution of the data is 0.5 by 0.5 degree longitude and latitude, which on average over Germany is approximately 35 km by 55.6 km. The time interval between the records is three hours. The data is stored in so called GRIB (GRId in Binary format) files. IDEM accesses these GRIB files directly using text index files to locate the requested data in the compressed binary GRIB data files. The de-assimilation of assimilated analysed data in the ECMWF databases is carried out by slightly modified software provided by Paul James [http://www.forst.tu-muenchen.de/EXT/LST/METEO/stohl/flextra/ecmwf_extr.html] .. The data fields required by IDEM are listed in Table 6.4.

Table 6.4: IDEM required fields in meteorological input

Abbreviation	*Description*	*Abbreviation*	*Description*
WU	Wind speed in EW direction at 10 m	**LSP**	Large scale precipitation
WV	Wind speed in NS direction at 10 m	**SD**	Snow depth
MSL	Atmospheric pressure at surface level	**GLRad**	Global radiation
T2	Temperature at 2 m height	**TCC**	Total cloud cover
HF	Sensible Heat flux	**SSWE**	Surface stress in WE direction
TS	Soil temperature	**SSNS**	Surface stress in NS direction
CVP	Convective precipitation		

Atmospheric stability is determined by mechanically induced turbulence caused by the friction of wind at the surface and thermally induced turbulence caused by cooling or heating of the surface by exchange of long wave (infrared) radiation. The thermal turbulence is expressed as a function of the sensible heat flux (HF), the mechanical turbulence is expressed as a function of the friction velocity (u_*). It is possible to derive the atmospheric stability from the ECMWF input, as this contains values for both Sensible Heat flux and friction velocity (through SSWE, SSNS; cf. Table 6.3). The values obtained are, however, values that are representative for the 0.5 by 0.5 degree grid cell. In IDEM we derive from wind speed, cloud cover, radiation and local surface roughness a localised version of the energy balance on the 1x1km² grid and use this in the dry deposition calculation scheme. The surface energy budget scheme from BELJAARS & HOLTSLAG (1990) is used in an optimised version. This leads to a presumably much higher accuracy then using the ECMWF values.

The IDEM model interpolates all meteorological data to the 1x1km² grid using weighted distance averaging. This avoids visual block effects in some of the calculated data when sharp gradients in for example wind speed exist between 0.5x0.5 degree meteorological grid data cells.

6.1.4 IDEM concentration input

The model can use concentration data in the latitude-longitude projection as well as in the EMEP projection. For the years 1995, 1997, and 1999-2004 data was obtained from the TNO LOTOS/EUROS Eulerian transport model, the data use has a resolution of 0.5x0.25 degree horizontal and 3 hours time resolution.

Also the concentration data for the calculations in this report is interpolated to the 1x1km² grid using weighted distance averaging. The concentration data is used by IDEM in the same native binary format in which the input files were provided by TNO.

6.1.5 IDEM dry deposition module: DEPAC

The approach followed in this project for estimating dry deposition velocity involves using larger scale atmospheric models and gridded fields of surface meteorological data to produce a regular grid of deposition velocity values.

Air quality models used to study acid deposition and photochemical oxidants contain modules to estimate dry deposition velocities. WESELY (1989) and WALMSLEY & WESELY (1996) described the model used within RADM (Regional Acid Deposition Model; CHANG ET AL., 1987), PADRO ET AL. (1991) evaluated the model included in ADOM (Acid Deposition and Oxidant Model; PLEIM ET AL., 1984; VENKATRAM ET AL., 1988) and VOLDNER ET AL. (1986) developed a dry deposition parameterisation for use in the Canadian Lagrangian acid deposition model. The ADOM and RADM dry deposition modules have appeared in several applications. For example, the RADM module has been adapted for the California Institute of Technology photochemistry airshed model (HARLEY ET AL., 1993), the Urban Airshed Model (UAM; SAI, 1996), studies involving the California Ozone Deposition Experiment (CODE; MASSMAN ET AL., 1994; PEDERSON ET AL., 1995), the Global CHemistry Model (GChM; LEUCKEN ET AL., 1991; BENKOVITZ ET AL., 1994), and EURopean Air Pollution Dispersion model system in western Europe (EURAD; HASS ET AL., 1995). The ADOM module has, for example, been used in the CALGRID photochemical oxidant model (YAMARTINO ET AL., 1992).

Several models have been developed in Europe. VAN PUL ET AL. (1995) described a model, EDACS (European Deposition of Acidifying Components on Small scale), that has been developed for routine estimates of dry deposition across a regular grid covering Europe. Meteorological inputs for this model are derived through interpolation of surface meteorological observations and land-use data that are provided on a 10x20km² grid. This work represents the first attempt to apply a model for routine estimation of spatially ($1/6^{o}$x$1/6^{o}$) and temporally (6h) resolved dry deposition that is suitable for combination with wet deposition measurements for determination of annual total deposition. EDACS and the Dutch Empirical Acid Deposition Model (DEADM) have been used with long-range modules to map modelled deposition amounts for sulphur and nitrogen compounds (e.g., ERISMAN & DRAAIJERS, 1995). Concern over the accuracy of estimates of particulate deposition has led to several experimental efforts (e.g., ERISMAN ET AL., 1997). In addition, dry deposition routines for general circulation models coupled with chemistry modules have been carried out for the European Centre HAmburg Model (ECHAM; GANZEVELD & LELIEVELD, 1995).

In areas that contain sharp contrasts in surface characteristics, edge effects, and hilly terrain, the assumptions inherent in the micrometeorological formulations that are commonly used in large-scale and site-specific models are questionable. In mountainous terrain or where patchy forest conditions exist, the approach of measuring the amounts and chemical composition of throughfall and stemflow in forests at specific sites is considered more reliable for some substances, especially sulphur, than the micrometeorological methods (DRAAIJERS ET AL., 1994; LOVETT, 1994; VELTKAMP & WYERS, 1997).

6.1.6 Theory of dry deposition parameterisation

Several articles have reviewed the state of the science in evaluating dry deposition (BALDOCCHI, 1993; ERISMAN ET AL., 1994b; ERISMAN & DRAAIJERS, 1995; RUIJGROK ET AL., 1995; WESELY & HICKS, 2000). WESELY AND HICKS (2000) indicated that although models have been improving and can perform well at specific sites under certain conditions, there remain many problems and more research is needed. In spite of these problems, given the necessary meteorological and surface/vegetative data, there are a number of models for estimating deposition velocity (V_d) that have been shown to produce reasonable results using currently available information.

Dry deposition processes for gaseous species are generally understood better than for particles. Several dry deposition model formulations have been reported in the literature. These include big-leaf models (HICKS ET AL., 1987; BALDOCCHI ET AL., 1987), multi-layer models (BALDOCCHI, 1988; MEYERS ET AL., 1998) and general dry deposition models (ERISMAN ET AL., 1996). Some of these models have been developed for estimating V_d at specific sites and are used within the framework of monitoring networks (CLARKE ET AL., 1997; MEYERS ET AL., 1991).

Computation of the dry deposition rate of a chemical species requires that the concentration c of the substance of interest is known through model computations or measurement. In most modelling schemes, the mass flux density F is found as

$$F = -V_d(z) \cdot c(z) \tag{6.1}$$

where $c(z)$ is the concentration at height z and V_d is the dry deposition velocity. Estimates of deposition velocities V_d constitute the primary output of dry deposition models, both for large-scale models and site-specific methods of inferring dry deposition from local observations of concentrations, meteorological conditions, and surface conditions (CHANG ET AL., 1987; VENKATRAM ET AL., 1988; MEYERS ET AL., 1991; GANZEVELD AND LELIEVELD, 1995). z is the reference height above the surface. If the surface is covered with vegetation, a zero-plane displacement is included: $z=z-d$. d is usually taken as 0.6-0.8 times the vegetation height (THOM, 1975). The absorbing surface is often assumed to have zero surface concentration and the flux is therefore viewed as being linearly dependent on atmospheric concentration. This holds only for depositing gases and not for gases that might be also emitted, such as NH_3 and NO. For these gases a nonzero surface concentration, a compensation point c_p, might exist, which can be higher than the ambient concentration, in which case the gas is emitted. For these gases the flux is estimated as

$$F = -V_d(z) \cdot [c(z) - c_p] \tag{6.2}$$

V_d provides a measure of conductivity of the atmosphere-surface combination for the gas and it is widely used to parameterise gas uptake at the ground surface (WESELY & ., 1977; HICKS ET AL., 1989; FOWLER ET AL., 1989). To describe the exchange of a range of gases and particles with very different chemical and physical properties, a common framework is provided, the resistance analogy (THOM, 1975; GARLAND, 1977; WESELY & HICKS, 1977; FOWLER, 1978; BALDOCCHI ET AL., 1987). In this framework, V_d is calculated as the inverse of three resistances:

$$V_d(z) = \frac{1}{R_a(z-d) + R_b + R_c} \tag{6.3}$$

The three resistances represent bulk properties of the lower atmosphere or surface. R_a, R_b and R_c must be described by parameterisations. Although this approach is practical, it can lead to oversimplification of the physical, chemical, and biological properties of the atmosphere or surface that affect deposition.

The term R_a represents the aerodynamic resistance above the surface for the turbulent layer. R_a is governed by micrometeorological parameters and has the same value for all substances. R_a depends mainly on the local atmospheric turbulence intensities. Turbulence may be generated through mechanical forces of friction with the underlying surface (forced convection) or through surface heating (buoyancy or free convection). Unless wind speed is very low, free convection is small compared to mechanical turbulence.

The term R_b represents the quasi-laminar resistance to transport through the thin layer of air in contact with surface elements, and is governed by diffusivity of the gaseous species and air viscosity. For surfaces with bluff roughness elements, values of R_b are considerably larger than for relatively permeable, uniform vegetative cover, and the appropriate formulations should be used (TUOVINEN ET AL., 1998).

Considerable variation from model to model is associated with the methods used to evaluate the surface or canopy resistance R_c for the receptor itself. R_c represents the capacity for a surface to act as a sink for a particular pollutant, and depends on the primary pathways for uptake such as diffusion through leaf stomata, uptake by the leaf cuticular membrane, and deposition to the soil surface. This makes R_c complicated, because it depends on the nature of the surface and how the sink capacities for specific surfaces vary as a function of the local microclimate.

The resistance analogy is not used for particles. For sub-micron particles, the transport through the boundary layer is more or less the same as for gases. However, transport of particles through the quasi-laminar layer can differ. Whereas gases are transported primarily through molecular diffusion, particle transport and deposition basically take place through sedimentation, interception, impaction, and/or Brownian diffusion. Sedimentation under the influence of gravity is especially significant for receptor surfaces with horizontally oriented components. Interception occurs if particles moving in the mean air motion pass sufficiently close to an obstacle to collide with it. Like interception, impaction occurs when there are changes in the direction of airflow, but unlike interception a particle subject to impaction leaves the air streamline and crosses the laminar boundary layer with inertial energy imparted from the mean airflow. The driving force for Brownian diffusion transport is the random thermal energy of molecules. Transport is a function of atmospheric conditions, characteristics of the depositing contaminant and the magnitude of the concentration gradient over the quasi-laminar layer (DAVIDSON AND WU, 1990).

Which type of transport process dominates is largely controlled by the size distribution of the particles (SEHMEL, 1980; SLINN, 1982). For particles with a diameter <0.1µm, deposition is controlled by diffusion, whereas deposition of particles with a diameter >10µm is more controlled by sedimentation. Deposition of particles with a diameter between 0.1 and 1µm is determined by the rates of impaction and interception and depends heavily on the turbulence intensity. To describe particle dry deposition, the terms $(R_b+R_c)^{-1}$ on the right-hand side of Equation (6.3) must be replaced with a surface deposition velocity or conductance, and gravitational settings must be handled properly.

Dry deposition models or modules require several types of inputs from observations or from simulations of atmospheric chemistry, meteorology, and surface conditions. To compute fluxes, the concentrations of the substances must be known. Inputs required from meteorological models are values of friction velocity u^*, atmospheric stability via the Monin-Obukhov length scale L, aerodynamic surface roughness z_0, and aerodynamic displacement height d. Most dry deposition models also need solar radiation or, preferably, photosynthetically active radiation; ambient air temperature at a specified height; and measures of surface wetness caused by rain and dewfall. All models require a description of surface conditions, but the level of detail depends on the model chosen. Descriptions could include broad land use categories, plant species, leaf area index (LAI), greenness as indicated by the normalised difference vegetation index, various measures of plant structure, amount of bare soil exposed, and soil pH.

6.1.7 Description of the land use information

The deposition velocity for each chemical species can differ by close to an order of magnitude between some landuse classes. In the daytime, SO_2 and O_3 have higher deposition velocities over surface types or canopy types with large leaf area indices (LAIs) due to uptake through the leaf stomata. This uptake is greater in the summer

or growing season compared to the autumn. The effect of canopy wetness on dry deposition velocities can be significant. Surface roughness also has an important role due to its influence on aerodynamic resistance. This is particularly noticeable for HNO_3 and SO_4^{2-}, for which stomata opening and closing is not important.

6.1.8 Aerodynamic and quasi-laminar boundary layer resistances

The atmospheric resistance to transport of gases across the constant flux layer is assumed to be similar to that of heat (e.g., HICKS ET AL., 1989). R_a is approximated following the procedures used by GARLAND (1978):

$$R_a(z-d) = \frac{1}{\kappa \cdot u*} \cdot \left[\ln\left(\frac{z-d}{z_o}\right) - \psi_h\left(\frac{z-d}{L}\right) + \psi_h\left(\frac{z_o}{L}\right) \right] \qquad (6.4)$$

in which κ is the Von Karman constant (0.4), u^* is the friction velocity, which is calculated from the output of the meteorological model, L is the Monin-Obukhov length, d is the displacement height and z_0 is the roughness length, which is defined independently for each land use and season category. $\psi_h[(z-d)/L]$ is the integrated stability function for heat. These can be estimated using procedures described in BELJAARS AND HOLTSLAG (1990). Under the same meteorological conditions, the aerodynamic resistance is the same for all gases and in fact also for aerosols. Only for aerosols with a radius > 5µm does the additional contribution of gravitational settling become significant. When the wind speed increases, the turbulence usually increases as well and consequently R_a becomes smaller.

The second atmospheric resistance component R_b is associated with transfer through the quasi-laminar layer in contact with the surface. The transport through the laminar boundary layer takes place for gases by molecular diffusion and for particles by several processes: Brownian diffusion, interception, impaction, and by transport under influence of gravitation. None of the processes for particles are as efficient as the molecular diffusion of gas molecules. This is because molecules are much smaller than aerosols and therefore have much higher velocities. For particles with radii <0.1µm Brownian diffusion is the most efficient process, whereas impaction and interception are relatively important for those with radii >1µm. For particles with radii between 0.1 and 1µm the transport through the laminar boundary layer is slowest (R_b is largest). The laminar boundary layer resistance is for most surface types more or less constant (forest, at sea for a wind speed < 3m/s) or decreases with wind speed (low vegetation).

R_b quantifies the way in which pollutant or heat transfer differs from momentum transfer in the immediate vicinity of the surface. The quasi-laminar layer resistance R_b can be approximated by the procedure presented by HICKS ET AL. (1987):

$$R_b = \frac{2}{\kappa \cdot u_*} \cdot \left(\frac{Sc}{\mathrm{Pr}}\right)^{2/3} \qquad (6.5)$$

where Sc and Pr are the Schmidt and Prandtl number, respectively. Pr is 0.72 and Sc is defined as $Sc = \upsilon / D_i$, with υ being the kinematic viscosity of air (0.15 $cm^2\ s^{-1}$) and D_i the molecular diffusivity of pollutant i and thus component specific. The Schmidt and Prandtl number correction in the equation for R_b is listed in Table 6.5 for different gases. Molecular and Brownian diffusivities for a selected range of pollutants, and the deduced values of Schmidt number are listed in Table 6.6. Usually R_b values are smaller than R_a and R_c. Over very rough surfaces such as forest canopies, however, R_a may approach small values and the accuracy of the R_b estimate becomes important. This is especially the case for trace gases with a small or zero surface resistance.

Table 6.5: Schmidt and Prandtl number correction in equation for R_b (HICKS ET AL., 1987) for different gaseous species, and the diffusion coefficient ratio of water to the pollutant i (PERRY, 1950)

Component	$D^*_{H_2O} / D_i$	$(Sc/Pr)^{2/3}$
SO_2	1.9	1.34
NO	1.5	1.14
NO_2	1.6	1.19
NH_3	1	0.87
HNO_2	1.7	1.24
HNO_3	1.9	1.34
HCl	1.5	1.14
PAN	2.8	1.73
H_2O	1	0.87
O_3	1.5	1.14

$^* D_{H_2O} = 2.27 \cdot 10^{-5} m^2 s^{-1}$

Table 6.6: Molecular (for gases) and Brownian (for particles) diffusivities (D; $cm^2\ s^{-1}$) for a range of pollutants, and the deduced values of Schmidt number (Sc). The viscosity of air is taken to be 0.15 $cm^2\ s^{-1}$. From HICKS ET AL. (1987)

Component	*D*	*Sc*
Gaseous species		
H_2	0.67	0.22
H_2O	0.22	0.68
O_2	0.17	0.88
CO_2	0.14	1.07
NO_2	0.14	1.07
O_3	0.14	1.07
HNO_3	0.12	1.25
SO_2	0.12	1.25
Particles (unit density)		
0.001 μm radius	$1.28\ 10^{-2}$	$1.17\ 10^{1}$
0.01	$1.35\ 10^{-4}$	$1.11\ 10^{3}$
0.1	$2.21\ 10^{-6}$	$6.79\ 10^{4}$
1	$1.27\ 10^{-7}$	$1.18\ 10^{6}$
10	$1.38\ 10^{-8}$	10^{7}

6.1.9 Surface resistance parameterisation for gases

The surface or canopy resistance R_c is the most difficult of the three resistances to describe, and is often the controlling resistance of deposition flux. The analytical description of R_c has been difficult since it involves physical, chemical and biological interaction of the pollutant with the deposition surface. Over a given area of land, numerous plant, soil, water, and other material surfaces are present, each with a characteristic resistance to the uptake of a given pollutant.

R_c values presented in the literature are primarily based on measurements of V_d and on chamber studies. By determining R_a and R_b from the meteorological measurements, R_c can be calculated as the residual resistance. Values of R_c can then be related to surface conditions, time of day, etc., yielding parameterisations. However, measurements using existing techniques are still neither accurate nor complete enough to obtain R_c values under most conditions. Furthermore, R_c is specific for a given combination of pollutants, type of vegetation and surface conditions, and measurements are available only for a limited number of combinations.

The surface resistance of gases consists of other resistances (Figure 6.3), either determined by the actual state of the receptor, or by a memory effect. R_c is a function of the canopy stomatal resistance R_{stom} and mesophyll resistance R_m; the canopy cuticle or external leaf resistance R_{ext}; the soil resistance R_{soil} and in-canopy resistance R_{inc}, and the resistance to surface waters or moorland pools R_{wat}. In turn, these resistances are affected by leaf area, stomatal physiology, soil and external leaf surface pH, and presence and chemistry of liquid drops and films. Based on values from the literature for the stomatal resistance (WESELY, 1989), and on estimated values for wet (due to rain and to an increase in relative humidity) and snow-covered surfaces, the following parameterisation (with the stomatal resistance, external leaf surface resistance and soil resistance acting in parallel) can be applied for routinely measured components (ERISMAN ET AL., 1994b):

vegetative surface:

$$R_c = \left[\frac{1}{R_{stom} + R_m} + \frac{1}{R_{inc} + R_{soil}} + \frac{1}{R_{ext}} \right]^{-1} \quad (6.6)$$

water surfaces:

$$R_c = R_{wat} \quad (6.7)$$

bare soil:

$$R_c = R_{soil} \quad (6.8)$$

snow cover:

$$R_c = R_{snow} \quad (6.9)$$

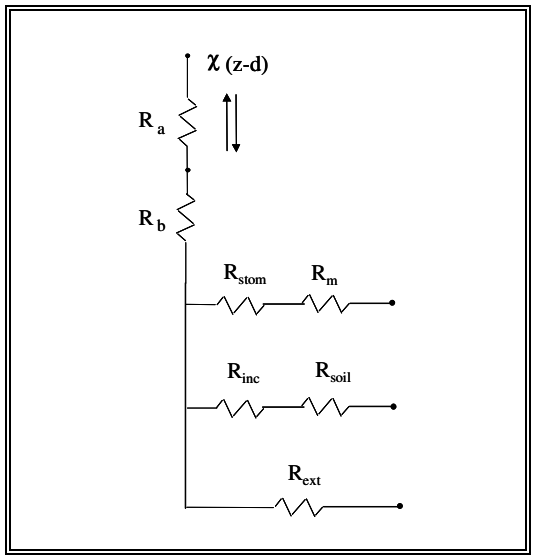

Figure 6.3: Resistance analogy approach in dry deposition models

Table 6.7 shows some surface resistance values for soil surfaces (R_{soil}), snow-covered surfaces (R_{snow}) and water surfaces (R_{wat}).

Table 6.7: Surface resistance values (s m^{-1}) for soil surfaces (R_{soil}), snow-covered surfaces (R_{snow}) and water surfaces (R_{wat}). From ERISMAN ET AL. (1994b)

Gas	Soil surfaces, R_{soil}		Water surfaces,	Soil or water	Snow-covered surfaces	
	Wet	Dry	R_{wat}	PH	R_{snow}	Temperature (°C)
SO_2 and	0	1000	0	>4	70 (2-T)	-1<T<1
HNO_2	500	R_{ext}	500	<4	500	T<-1
	250	Emission: 500		>8	70 (2-T)	-1<T<1
NH_3	0	50	500	<8	500	T<-1
	emission: 1000	emission:		----	2000	----
NO	2000	1000	0	----	2000	----
NO_2 and	0	1000	2000	>2	0	T>-5
PAN		0	2000		100	T<-5
HNO_3 and	500		0	----	2000	----
HCl		100	2000			
O_3						

It is not clear whether R_m is relevant at ambient concentrations (ERISMAN ET AL., 1994b). Therefore, they consider the sum of R_{stom} and R_m to be a new resistance R_{st}, a stomatally controlled resistance which would equal the true stomatal resistance R_{stom} if $R_m=0$. Similarly, they defined a new resistance $R_{fs}=R_{inc}+R_{soil}$, a non-stomatal resistance to express that the uptake could be either direct foliage uptake or soil uptake. Thus, Equation (6.6) reduces to

$$R_c = \frac{R_{st} \cdot R_{fs}}{R_{st} + R_{fs}} \tag{6.10}$$

Combining Equations (6.3) and (6.10) yields

$$\frac{1}{V_d} = R_a + R_b + \frac{R_{st} \cdot R_{fs}}{R_{st} + R_{fs}} \tag{6.11}$$

for daytime situations. During the night, when stomata are closed, $R_{st} = \infty$ is assumed and Equation (6.11) can be reduced to

$$\frac{1}{V_d} = R_a + R_b + R_{fs} \tag{6.12}$$

R_{cut} denotes local leaf cuticular resistance. In BROOK ET AL. (1999):

$$R_{cut}(SO_2) = R_{cut}(LUC, season); \tag{6.13}$$

$$R_{cut}(HNO_3) = 20\ sm^{-1}. \tag{6.14}$$

LUC denotes land use class. Under wet surface conditions after rainfall or dew R_{cut} is replaced by R_{wcut}, which denotes wet cuticle resistance. For SO_2, under wet/dew conditions it is assumed a constant value of 50 sm^{-1} for both dew-covered and rainfall conditions:

$$R_{wcut}(SO_2) = 50\ sm^{-1} \tag{6.15}$$

HNO_3 uptake is rapid regardless of wetness.
R_g denotes ground surface resistance, which varies depending upon whether the surface is soil, water or snow/ice and whether it is wet or dry.

$$R_g(SO_2) = 100\ sm^{-1} \tag{6.16}$$

$$R_g(HNO_3) = 20\ sm^{-1} \tag{6.17}$$

For all surface conditions (dry, wet or snow) a small value of 20 sm^{-1} is used for the ground resistance of HNO_3. For wet soil, a constant value of 100 sm^{-1} is used for SO_2. There is little information available for resistance over snow or ice surfaces. From the limited amount of data available (see BROOK ET AL., 1999) a value of 200 s m^{-1} is set for $R_g(SO_2)$ *for* snow covered surfaces:

$$R_g(SO_2) = 200\ sm^{-1} \tag{6.18}$$

Stomatal (R_{stom}) and mesophyll (R_m) resistances

Most gases enter plants through stomata. As gas molecules enter the leaf, deposition occurs as molecules react with the moist cells in the sub-stomatal cavity and the mesophyll. Stomatal resistance decreases hyperbolically with increasing light and increases linearly with increasing vapour pressure deficits (JARVIS, 1976). Soil water deficits cause stomata to close after some threshold deficit level is exceeded. Low and high temperatures cause stomatal closure; stomatal opening is optimal at a vegetation-specific temperature. Leaf age, nutrition and adaptation are other factors affecting stomatal resistance (JARVIS, 1976). Elevated exposure to SO_2 causes stomata to close, whereas exposure to both O_3 and NH_3 may increase stomatal opening. Stomatal resistance is different for different types of vegetation.

The stomatal resistance for water vapour, R_{stom}, is a function of the photosynthetically active radiation (*PAR*), air temperature (*T*), leaf water potential (ψ), vapour pressure deficit (*VPD*), and can be calculated using a scheme described by BALDOCCHI ET AL. (1987). This scheme is based on a model presented by JARVIS (1976) for the computation of the stomatal resistance to water vapour transfer of a leaf that is biologically and physically realistic. It is a multiplicative model which is expressed in terms of stomatal conductance (g_s), the inverse of R_{stom}. In this scheme the bulk leaf stomatal conductance is written as:

$$g_s = f(PAR) \cdot f(T) \cdot f(VPD) \cdot f(\psi) \tag{6.19}$$

Values of the functions *f(T), f(ψ)* and *f(VPD)* range from 0 to 1. *f(PAR)* is the influence of photosynthetically active radiation on the stomatal conductance, and depends on the LUC-dependent parameters of the minimum stomatal resistance, $R_s(min)$; the light response constant, b_{rs}, equal to the *PAR* flux density at twice the minimum stomatal resistance; the leaf area index, *LAI*; and variations in *PAR* (Table 6.8). The response of stomatal resistance to *PAR* is estimated using a rectangular hyperbola relationship (TURNER AND BEGG, 1974):

$$f(PAR) = \frac{1}{r_s(min)} \cdot \frac{1}{1 + b_{rs}(PAR)/PAR} \tag{6.20}$$

PAR is estimated as a fraction of the short-wave incoming radiation, *Q*:

$$PAR = 0.5 \cdot Q \tag{6.21}$$

Stomatal conductance increases with increasing temperature until a threshold temperature, after which it decreases. This dependence on temperature is the result of energy balance feedbacks between humidity and transpiration of the leaf (SCHULZE AND HALL, 1982) and the influence of temperature on enzymes associated with stomatal operation (JARVIS AND MORISON, 1981). The response of stomatal conductance to temperature (*T*) is computed using the relationship presented by JARVIS (1976):

$$f(T) = \left[\frac{T - T_{min}}{T_{opt} - T_{min}}\right] \cdot \left[\frac{T_{max} - T}{T_{max} - T_{opt}}\right]^{\beta} \tag{6.22}$$

where, according to JARVIS (1976), and ERISMAN ET AL. (1994b)

$$\beta = (T_{max} - T_{opt})/(T_{max} - T_{min}) \tag{6.23}$$

However, according to BALDOCCHI ET AL. (1987), and BROOK ET AL. (1999)

$$\beta = (T_{max} - T_{opt})/(T_{opt} - T_{min}) \tag{6.24}$$

$T_{min}(i)$, $T_{max}(i)$ indicates minimum and maximum temperatures at which stomatal closure occurs, and the optimum temperature $T_{opt}(i)$ indicates the temperature of maximum stomatal opening (Table 6.8).

The influence of vapour pressure deficit on stomatal conductance *f(VPD)* is represented by

$$f(VPD) = 1 - b_{vpd} \cdot VPD \tag{6.25}$$

b_{vpd} is a constant (Table 6.8), while *VPD*, vapour pressure deficit, is estimated from relative humidity *rh* (%) by (BELJAARS AND HOLTSLAG, 1990)

$$VPD = (1 - rh/100) \cdot es \tag{6.26}$$

es is the saturated water vapour pressure (mbar):

$$es = 6.1365 \cdot \exp\left(\frac{17.502 \cdot T}{240.97 + T}\right) \tag{6.27}$$

According to MONTEITH (1975), the saturated water vapour pressure *es* (in kPa) at temperature *t* (°C) can be calculated using:

$$\begin{aligned} es = {} & 0.611371893 + 0.044383935 \cdot t \\ & + 0.001398175 \cdot t^2 + 0.000029295 \cdot t^3 \\ & + 0.000000216 \cdot t^4 + 0.000000003 \cdot t^5 \end{aligned} \tag{6.28}$$

The bulk stomatal resistance is approximated with

$$R_{stom} = \frac{1}{LAI \cdot g_s} \tag{6.29}$$

which will lead to an overestimation of R_{stom} caused by partial shading of leaves (BALDOCCHI ET AL., 1987).

Modelling the stomatal resistance in a detailed manner is only possible if enough information is available. This might be a problem for the water potential and for the leaf area index *LAI*. For those regions where such data are not available the parameterisation for the stomatal resistance given by WESELY (1989) may be used. This parameterisation is derived from the method by BALDOCCHI ET AL. (1987) and only needs data for global radiation *Q* (W m^{-2}) and surface temperature T_s (°C):

$$R_{stom} = R_i \cdot \left\{1 + \left[\frac{200}{Q + 0.1}\right]^2\right\} \cdot \left\{\frac{400}{T_s \cdot (40 - T_s)}\right\} \tag{6.30}$$

Values for R_i can be obtained from a look-up table for different land use categories and seasons, as listed in

Table 6.9 (from WESELY, 1989).

Table 6.8: Constants used in ERISMAN ET AL. (1994b) to compute R_{stom} for several vegetation types (adopted from BALDOCCHI ET AL., 1987)

Variable	Units	Spruce	Oak	Corn	Soybean
R_s *(min)*	s m^{-1}	232	145	242	65
b_{rs}*(PAR)*	W m^{-2}	25	22	66	10
T_{min}	°C	-5	10	5	5
T_{max}	°C	35	45	45	45
T_{opt}	°C	9	24-32	22-25	25
b_{vpd}	k Pa^{-1}	-0.0026	0	0	0
ψ_o	M Pa	-2.1	-2.0	-0.8	-1.1

Table 6.9: Internal resistance (R_i) used in ERISMAN ET AL. (1994b) to compute the stomatal resistance for different seasons and land use types. Entities of -999 indicate that there is no air-surface exchange via that resistance pathway (adopted from WESELY, 1989)

Land use * / Seasonal Category	1	2	4	5	6	7	9	10
Midsummer with lush vegetation	-999	60	70	130	100	-999	80	100
Autumn with unharvested cropland	-999	-999	-999	250	500	-999	-999	-999
Late autumn after frost, no snow	-999	-999	-999	250	500	-999	-999	-999
Winter, snow on ground and subfreezing	-999	-999	-999	400	800	-999	-999	-999
Transitional spring with partially green short annuals	-999	120	140	250	190	-999	160	200

* (1) Urban land, (2) agricultural land, (4) deciduous forest, (5) coniferous forest, (6) mixed forest including wetland, (7) water, both salt and fresh, (9) non-forested wetland, (10) mixed agricultural and range land

After the passage through the stomatal opening, transfer of pollutant must take place between the gas phase of the stomatal cavity and the apoplast fluids. Parameterisations for R_m usually include a dependency on the Henry constant of the compound (e.g., WESELY, 1989). It was considered independent of land use class and season, and BALDOCCHI ET AL. (1987) estimated that R_m should be between 10 and 50 s m^{-1}. However, many water soluble compounds, such as HNO_3 and SO_2 are assumed to dissolve easily into the apoplast fluid due to a high or moderate (respectively) Henry coefficient and/or efficient conversion and transport after dissolution. Therefore R_m for HNO_3 and SO_2 (also for O_3) is generally assumed to be negligible (VOLDNER ET AL., 1986; WESELY, 1989, ERISMAN ET AL., 1994b; NOAA, 1997). For NH_3, R_m is usually also set to zero. This approximation may be well acceptable for unfertilised vegetation. However, it may be far from realistic if fertilisation causes a high ammonium content in the apoplast, leading to frequent and significant emissions. In that case, it may be necessary to account for R_m, unless the concentration in the stomata is estimated or calculated directly as a compensation point. In general, the mesophyll resistances R_m for all the gases are assumed to be zero, because of insufficient knowledge.

This general framework for the water vapour stomatal resistance can be used to describe stomatal uptake for each gas by correcting the R_{stom} using the ratio of the diffusion coefficient of the gas involved to that of water vapour (D_{H_2O} / D_i ; Table 6.5) and adding the mesophyll resistance:

$$R_{stom,x} = R_{stom} \cdot \frac{D_{H_2O}}{D_x} + R_m \qquad (6.31)$$

External leaf uptake *(R_{ext})*

Many studies have shown that the external leaf surface can act as an effective sink, especially for soluble gases at wet surfaces (HICKS ET AL., 1989; FOWLER ET AL., 1991; ERISMAN ET AL., 1993a, 1994a). Under some conditions the external leaf sink can be much larger than the stomatal uptake. When R_{ext} is negligible, R_c also becomes negligible, dominating the other resistances.

SO_2

SO_2 dry deposition is enhanced over wet surfaces (GARLAND & BRANSON, 1977; FOWLER & UNSWORTH, 1979; FOWLER, 1985; VERMETTEN ET AL., 1992; ERISMAN ET AL., 1993b; ERISMAN & WYERS, 1993). ERISMAN ET AL. (1994b) derived an R_{ext} parameterisation for wet surfaces (due to precipitation and an increase in relative humidity) of heather plants:

- during or just after precipitation:

$$R_{ext} = 1 \text{ s m-1} \tag{6.32}$$

- in all other cases:

$$R_{ext} = \begin{cases} 25000 \cdot e^{-0.0693 \cdot rh} & \text{rh} \le 81.3\% \\ 58 \cdot 10^{10} \cdot \text{e}^{-0.278 \cdot \text{rh}} & \text{rh} > 81.3\% \end{cases} \tag{6.33}$$

where *rh* is the relative humidity. The previous equation is applied to air temperatures above -1°C. Below this temperature it is assumed that surface uptake decreases and R_{ext} is set at 200 (-1>*T*>-5°C), or 500 (*T*<-5°C) s m^{-1}. R_{ext} will be zero for some hours after precipitation has stopped. This time limit varies with season and depends on environmental conditions. Drying of vegetation is approximated to take 2h during daytime in summer and 4h in winter. During night-time, vegetation is expected to be dry after 4h in summer and after 8h in winter (ERISMAN ET AL., 1993a).

NH_3

While most other gaseous pollutants have a consistently downward flux, NH_3 is both emitted from and deposited to land and water surfaces. For semi-natural vegetation, fluxes are usually directed to the surface, whereas fluxes are directed away from the surface over agricultural grassland treated with manure. For arable cropland fluxes may be bi-directional depending on atmospheric conditions and the stage in the cropping cycle (SUTTON, 1990). Nitrogen metabolism has been shown to produce NH_3 and as a result there is a compensation point (FARQUHAR ET AL., 1980) at which deposition might change into emission when ambient concentrations fall below the compensation concentration and vice versa.

To describe NH_3 exchange it is necessary to consider natural and managed vegetation separately. For managed vegetation the compensation point approach seems to be most promising for use in models. However, the current state of knowledge is insufficient to define canopy resistance terms or compensation points reliable over different surface types and under different environmental conditions relevant for model parameterisation (LÖVBLAD ET AL., 1993). Furthermore, the compensation point is expected to be a function of many (undefined) factors and not a constant value.

Ammonia generally deposits rapidly to semi-natural (unfertilised) ecosystems and forests. Results show R_c values mostly in the range of 0-50 s m^{-1} (DUYZER ET AL., 1987, 1992; SUTTON ET AL. 1992; ERISMAN ET AL., 1993b). There is a clear effect of canopy wetness and relative humidity on R_c values (ERISMAN & WYERS, 1993). Under very dry, warm conditions (*rh*<60%, *T*>15°C) deposition to the leaf surface may saturate, so that exchange is limited to uptake through stomata, even allowing for the possibility of emission at low ambient concentrations. In this context a larger R_c may be appropriate (~50 s m^{-1}). Table 6.10 shows some values for R_{ext} for NH_3, for different land use categories.

Table 6.10: R_{ext} for NH_3 (s m^{-1}) over different vegetation categories in Europe. Negative values for R_{ext} denote emission for estimating a net upward flux. From ERISMAN AND DRAAIJERS (1995)

Land use category		Day		Night	
		Dry	Wet	Dry	Wet
Pasture during grazing:	summer	-1000	-1000	1000	1000
	winter	50	20	100	20
Crops and ungrazed pasture:	summer	$-R_{stom}$	50	200	50
	winter	$-R_{stom}$	100	300	100
Semi-natural ecosystems and forests		-500	0	1000	0
Winter conditions: *T*>-1 °C, otherwise R_{ext}=200 s m^{-1} (-1>*T*>-5 °C) or R_{ext}=500 s m^{-1} (*T*<-5 °C)					

NO_X

A very small stomatal uptake might be observed for NO at ambient concentrations. Fluxes are, however, very low and uptake is therefore neglected (WESELY ET AL., 1989; LÖVBLAD & ERISMAN, 1992). Uptake of NO_2

seems to be under stomatal control with no internal resistance. In EUGSTER AND HESTERBERG (1996) it is addressed that, for deposition of NO_2, R_{ext} is assumed to be very large (FOWLER ET AL., 1991) and can be set to infinity. R_{ext} is set at 9999 s m^{-1}.

HNO_3

The difficulty of measuring nitric acid (HNO_3) concentrations at ambient levels has limited the number of flux measurements of these gases. Recent investigations, however, consistently show that for vegetative surfaces these gases deposit rapidly, with negligible surface resistances. Deposition of HNO_3 seems to be limited by the aerodynamic resistance only. For this gas the external surface resistance is found to be negligible: R_{ext} is set at 1 s m^{-1}.

In-canopy transport *(R_{inc})*

Deposition to canopies includes vegetation and soil. Early studies assumed that deposition to soils under vegetation was relatively small (5-10% of the total flux; FOWLER, 1978). Recent work shows that a substantial amount of material can be deposited to the soil below vegetation. This substantial transfer occurs because large-scale intermittent eddies are able to penetrate through the vegetation and transport material to the soil.

The in-canopy aerodynamic resistance R_{inc} for vegetation is modelled according to data from VAN PUL AND JACOBS (1993):

$$R_{inc} = \frac{b \cdot LAI \cdot h}{u*} \tag{6.34}$$

where *LAI* is the one-sided leaf area index (set to one for a deciduous forest in winter), *h* the vegetation height and *b* an empirical constant taken as 14 m^{-1}. The previous equation is only applied to tall vegetation. For low vegetation R_{inc} is assumed to be negligible. The resistance to uptake at the soil under the canopy R_{soil} is modelled similarly to the soil resistance to bare soils. This will probably underestimate uptake to surfaces under forests (partly) covered with vegetation. Parameters used for the calculation of R_{inc} are summarised in Table 6.11.

Table 6.11: Parameters for the calculation of R_{inc}, for simple vegetation classes by WILSON AND HENDERSON-SELLERS (1985) to translate OLSON ET AL. (1985).

Vegetation type	*LAI*	*b*	*h*
Desert	-9999	-9999	-9999
Tundra	6	-9999	-9999
Grassland	6	-9999	-9999
Grassland + shrub cover	6	-9999	-9999
Grassland + tree cover	6	-9999	-9999
Deciduous forest	5	14	20
Coniferous forest	5	14	20
Rain forest	-9999	-9999	-9999
Ice	-9999	-9999	-9999
Cultivation	5	14	1
Bog or marsh	-9999	-9999	-9999
Semi-desert	-9999	-9999	-9999
Bare soil	-9999	-9999	-9999
Water	-9999	-9999	-9999
Urban	-9999	-9999	-9999

Deposition to soil *(R_{soil})* and water surfaces *(R_{wat})*

SO_2

Deposition of SO_2 to soil decreases at a soil pH below 4 and increases with relative humidity (GARLAND, 1977). In SPRANGER ET AL. (1994) R_{soil} dependence on *pH* and relative humidity is calculated as

$$R_{soil} = e^{9.471 - 0.0235 \cdot rh - 0.578 \cdot pH} \tag{6.35}$$

When surface temperatures fall below zero or the surface is covered with snow, R_c values increase up to 200-500 s m^{-1}. The deposition of SO_2 to snow-covered surfaces depends on *pH*, snow temperature and probably the amount of SO_2 already scavenged by the snow pack. ERISMAN ET AL. (1994b) found the following relations for snow-covered surfaces:

R_{snow}=500 s m^{-1} at T<-1°C

R_{snow}=70(2-T) s m^{-1} at -1<T<1°C (6.36)

NH_3

Deposition of NH_3 to soil, snow and water surfaces is similar to that of SO_2, only the pH dependence is different. Resistances to unfertilised moist soils will be very small provided that the soil pH is below 7. Fertilised soils, or soils with a high ammonium content, will show emission fluxes, depending on the ambient concentration of NH_3. Resistances to water surfaces will be negligible if the water pH is below 7. Resistances to snow will be similar to that of SO_2 at pH<7. Resistances will increase rapidly above a pH of 7.

NO_X

For NO at ambient concentrations, emission from soils is observed more frequently than deposition. This emission, the result of microbial activity in the soil, is dependent on soil temperature, water content and ambient concentrations of NO (HICKS ET AL., 1989). Emissions are to be expected at locations with low ambient NO and NO_2 concentrations (<5ppb).
The surface resistance for NO_2 to soil surfaces is found to be about 1000-2000 sm^{-1} (WESELY, 1989). If the soil is covered by snow, the resistance will become even higher. Resistances of NO_2 to water surfaces are also expected to be high due to the low solubility of this gas.

HNO_3

Resistances to water surfaces (pH>2) and soils for HNO_3 are assumed to be negligible. A surface resistance for HNO_3 to snow surfaces at temperatures below –5°C is expected. Resistances for HNO_2 are assumed to follow those of SO_2.

R_{soil}, R_{snow} and R_{wat} values for different gases are summarised in Table 6.7.

Particles

The process of dry deposition of particles differs from that of gases in two respects:

- *Deposition depends on particle size since transfer to the surface involves Brownian diffusion, inertial impaction/interception and sedimentation (all of which are a strong function of particle size).*
- *Presumably the surface resistance for particles less than 10μm diameter (HICKS & GARLAND, 1983) is negligible small to all surfaces.*

For submicron particles, the transport through the boundary layer is more or less the same as for gases. However, transport of particles through the quasi-laminar layer can differ. For particles with a diameter <0.1μm, deposition is controlled by diffusion, whereas deposition of particles with a diameter >10μm is more controlled by sedimentation. Deposition of particles with a diameter between 0.1 and 1μm is determined by the rates of impaction and interception and depends heavily on the turbulence density.

RUIJGROK ET AL. (1997) proposed another parameterisation derived from measurements over a coniferous forest. In this approach, which is simplified from SLINN's (1982) model, V_d is not only a function of u_*, but also of relative humidity (rh) and surface wetness. Inclusion of rh allows accounting for particle growth under humid conditions and for reduced particle bounce when the canopy is wet. Dry deposition velocity is expressed as:

$$\frac{1}{V_d} = R_a + \frac{1}{V_{ds}} \tag{6.37}$$

where R_a is the aerodynamic resistance, which is the same as for gaseous species, and V_{ds} is the surface deposition velocity.

For tall canopies V_{ds} is parameterised by RUIJGROK ET AL. (1997) as

$$V_{ds} = E \cdot \frac{u_*^2}{u_h} \tag{6.38}$$

where u_h is the wind speed at the top of the canopy, which is obtained by extrapolating the logarithmic wind profile from Z_R to the canopy height h. u_h can be expressed as:

$$u_h = \frac{u_*}{k}\left(\ln\left(\frac{10\cdot z_0 - d}{z_0}\right) - \psi_h\left(\frac{10\cdot z_0 - d}{L}\right) + \psi_h\left(\frac{z_0}{L}\right)\right) \tag{6.39}$$

E is the total efficiency for canopy capture of particles, and is parameterised separately for dry and wet surfaces (RUIJGROK ET AL., 1997).

For dry surfaces, for SO_4^{2-} particles (BROOK ET AL., 1999):

$$E = \begin{cases} 0.005\,u_*^{0.28} & \text{rh} \le 80\% \\ 0.005\,u_*^{0.28}\cdot\left[1 + 0.18\cdot\exp\dfrac{rh-80}{20}\right] & \text{rh} > 80\% \end{cases} \tag{6.40}$$

For wet surfaces, for SO_4^{2-} particles (BROOK ET AL., 1999):

$$E = \begin{cases} 0.08\,u_*^{0.45} & \text{rh} \le 80\% \\ 0.08\,u_*^{0.45}\cdot\left[1 + 0.37\cdot\exp\dfrac{rh-80}{20}\right] & \text{rh} > 80\% \end{cases} \tag{6.41}$$

rh (relative humidity) is taken at the reference height.

ERISMAN AND DRAAIJERS (1995) used the following general form for the calculation of V_d:

$$V_d = \frac{1}{R_a + \dfrac{1}{V_{ds}}} + V_s \tag{6.42}$$

where V_s is the deposition velocity due to sedimentation, to represent deposition of large particles, and V_{ds} can be estimated from Equation (6.38). Relations for E for different components and conditions are given in Table 6.12. These were derived from model calculations and multiple regression analysis (ERISMAN & DRAAIJERS, 1995).

Table 6.12: Parameterisations of E values for different components and conditions. From ERISMAN AND DRAAIJERS (1995)

	Wet surface		Dry surface	
Compound	$rh \le 80\%$	$rh > 80\%$	$rh \le 80\%$	$rh > 80\%$
NH_4^+	$0.066\cdot u_*^{0.41}$	$0.066\cdot u_*^{0.41}\cdot\left[1+0.37\cdot e^{\frac{rh-80}{20}}\right]$	$0.05\cdot u_*^{0.23}$	$0.05\cdot u_*^{0.23}\cdot\left[1+0.18\cdot e^{\frac{rh-80}{20}}\right]$
SO_4^{2-}	$0.08\cdot u_*^{0.45}$	$0.08\cdot u_*^{0.45}\cdot\left[1+0.37\cdot e^{\frac{rh-80}{20}}\right]$	$0.05\cdot u_*^{0.28}$	$0.05\cdot u_*^{0.28}\cdot\left[1+0.18\cdot e^{\frac{rh-80}{20}}\right]$
NO_3^-	$0.10\cdot u_*^{0.43}$	$0.10\cdot u_*^{0.43}\cdot\left[1+0.37\cdot e^{\frac{rh-80}{20}}\right]$	$0.063\cdot u_*^{0.25}$	$0.063\cdot u_*^{0.25}\cdot\left[1+0.18\cdot e^{\frac{rh-80}{20}}\right]$
Na^+, Ca^{2+}, Mg^{2+}	$0.679\cdot u_*^{0.56}$	$0.679\cdot u_*^{0.56}\cdot\left[1+0.37\cdot e^{\frac{rh-80}{20}}\right]$	$0.14\cdot u_*^{0.12}$	$0.14\cdot u_*^{0.12}\cdot\left[1-0.09\cdot e^{\frac{rh-80}{20}}\right]$

For the large particles (Na^+, Ca^{2+}, Mg^{2+}) and for low vegetation (for all particles), the sedimentation velocity has to be added:

$$\begin{aligned} V_s &= 0.0067\ m\cdot s^{-1} && \text{rh} \le 80 \\ V_s &= 0.0067\cdot e^{\frac{0.0066\cdot rh}{1.058-rh}}\ m\cdot s^{-1} && \text{rh} > 80\% \end{aligned} \tag{6.43}$$

6.1.10 Dry deposition of the heavy metals cadmium (Cd) and lead (Pb)

Dry deposition velocities for aerosols are quite uncertain. As a good approximation we modelled the dry deposition rates for the heavy metals Cd and Pb through two separate size categories. For the fine aerosol (diameters < 2.5 µm) the deposition velocity is taken from that calculated for the sulphate aerosol ($V_{d\,(SO4,f)}$). The coarse fraction is given a deposition velocity equal to that of the base cations ($V_{d\,(CAT,f)}$). The same approximation is followed in the LOTOS-EUROS model and this model also gives the air concentration of the heavy metals

both in the fine ($C_{(fine,t)}$) and in the coarse aerosol ($C_{(coarse,t)}$). Therefore the total dry deposition flux for heavy metals at each time step (t) is given by:

$$F_{tot} = V_{d\,(SO4,\,t)} * C_{(fine,\,t)} + V_{d\,(CAT,\,t)} * C_{(coarse,\,t)} \qquad (6.44)$$

6.2 IDEM cloud deposition module

In mountainous and hilly regions cloud droplet deposition occurs frequently. This gives rise to another source of acidifying input to especially forest ecosystems, as these intercept cloud droplets very efficiently. In hilly regions low clouds occur more frequently then in the lower regions because of the upward movements of moist air, leading to so called orographic clouds, usually when moist oceanic air is pushed into the continent with westerly flows. The frequency with which these conditions exist in hilly regions is higher then the frequency of conditions in which radiative fog exists, a type of fog also known in lower regions. Radiative fog usually exists under low wind conditions, whereas orographic clouds usually are produced at moderate to high wind speeds with corresponding higher turbulent exchange.

Chemical composition of hill clouds and radiative fog has also been found to be quite different, with higher concentrations in radiative fog.

The presence of clouds on the more remote hilly forested regions is poorly described by measurements and/or models. In this project an attempt was made to use the best available meteorological information to obtain approximations of the mean Liquid Water Content (LWC) due to clouds in hilly regions, using the 0.5 by 0.5 degree ECMWF analysed data.

For this, vertical information on the LWC from the ECMWF model was obtained for the years 2000-2003. The data used provides 31 so called sigma layers, of which the first ten are in the lower 2500 meter above the mean surface height. Another input used was DTM (Digital Terrain Model; BGR 1998) data for Germany with a resolution of 1x1km².

In Figure 6.4 the used elevation map is shown.

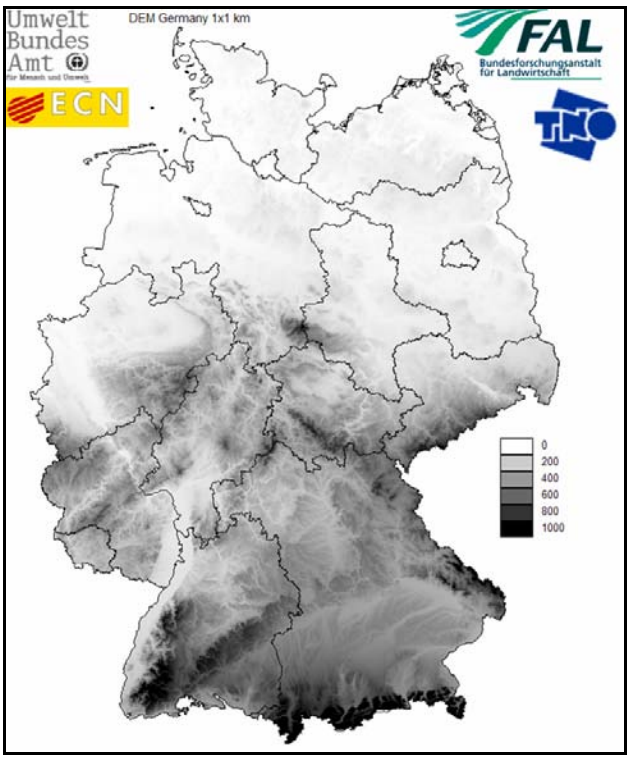

Figure 6.4: Digital elevation model on 1x1km² scale for Germany [in m ASL] (source: BGR 1998)

For each ECMWF grid cell the lowest height in the corresponding DTM cells was used as the base level of the sigma co-ordinates. Then for each time step in the LWC data (6 hours) the value of the LWC at the level of each 1x1km² grid cell was calculated by vertical interpolation of the sigma level values converted to height above surface using the standard atmosphere vertical pressure gradient. This leads to an average LWC per 1x1km² grid cell for the whole year.

In Figure 6.5 the resulting mean LWC for the 1x1km² grid is shown.

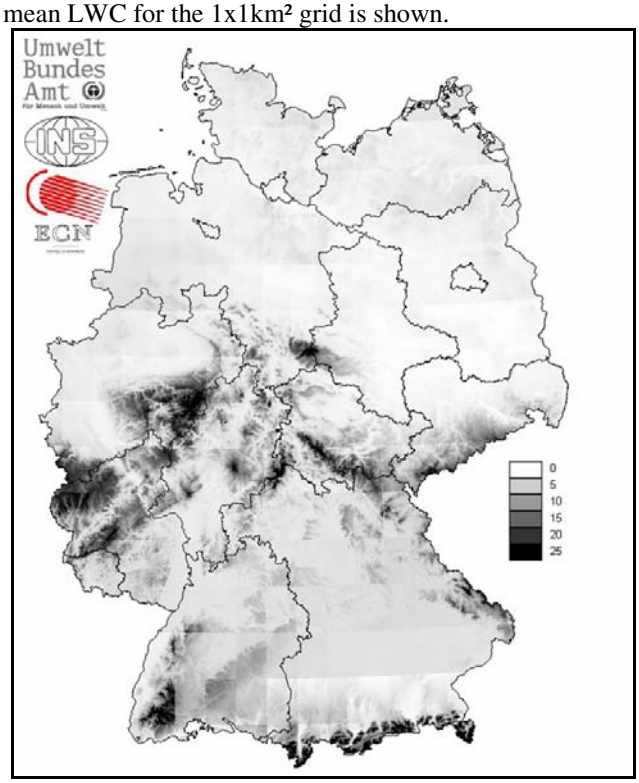

Figure 6.5: Mean LWC [g/kg] due to clouds over the year 1998 on the 1x1km² grid

The dry deposition rate and the deposition for fog/cloud droplets can be approximated by (REYNOLDS ET AL., 1997):

$$v_d = \frac{1}{r_a}$$

$$F = C_{cloud} * \frac{\sum_{t=1}^{n} LWC_t * v_{d_t}}{n} \qquad (6.45)$$

where C_{cloud} is the cloud water concentration of the compound studied. This cloud water concentration can be derived from a large number of observations of the ratio between rain water concentrations and cloud water concentrations as a function of height above sea level. To derive those factors the kriged rain water concentration data for 1993 from INS was used (BLEEKER ET AL., 2000). The best fit of the relationships between rain water concentration and cloud concentrations as a function of height as the values of the constants a and b in the next equation are shown in the next table (Table 6.13):

$$\frac{C_{cloud}}{C_{rain}} = a.z^b \qquad (6.46)$$

Table 6.13: Best fit for the values of constant a and b in Equation (6.46) used (BLEEKER ET AL., 2000)

Component	a	b
SO_4	341	-0.64
NO_3	912	-0.77
NH_4	25.6	-0.24
H	15.3	-0.24
Na	$9.1\ 10^5$	-1.90
Mg	$6.0\ 10^7$	-2.50
Ca	$1.3\ 10^5$	-1.60
K	$2.2\ 10^3$	-0.99
Cl	$3.0\ 10^6$	-2.09

As these functions lead to unrealistic high cloud water concentrations at heights below 250 ASL, so the procedure to derive cloud&fog deposition fluxes was only applied to areas above 250 m ASL.

The resulting estimated total acid deposition flux due to cloud&fog water deposition is shown in Figure 6.6, using the 2002 yearly product of v_{dt} and Liquid Water Content, the year average kriged rain water concentration for 2002 over Germany, all calculated in this project in the way described in this chapter. For the years outside the period 2000-2004 the mean yearly product of v_{dt} and Liquid Water Content for the period 2000-2004 was used to calculate the occult fluxes using the cloud concentrations for that particular year. This is due to data availability, since meteorological data for the years before 2000 could not be retrieved from ECMWF as for the years 2000 onward.

Table 6.14 shows the 2002 total acid fluxes by cloud deposition as a function of land use class and Bundesland.

As can be seen from Figure 6.6 the high elevation locations receive high fog water deposition fluxes because of the high mean LWC, but because the concentrations on the cloud water are calculated to be very low for the high sites, the total deposition per compound is low. Only for the middle high areas with heights between 250 and 750 meter significant cloud acid fluxes are calculated, these areas are of course also the most important forested regions of Germany. As can be seen clearly from Table 6.14 and Figure 6.6, forested regions receive up to 272 eq ha^{-1} a^{-1}, while the average over Germany is only 70 eq ha^{-1} a^{-1}.

Table 6.14: Annual average total acid deposition flux by cloud&fog deposition for the German Bundesländer with areas above 250 meter ASL [eq ha-1 a-1]

Land use class Federal States of Germany	Urban	Arable	Pasture	Deciduous Forest	Coniferous Forest	Mixed Forest	Water	Semi Natural	Other	Total Mean
Lower Saxony	12	7	8	72	43	56	11	11	- -	19
North Rhine-Westphalia	75	59	137	168	256	218	55	130	15	99
Hesse	84	117	151	179	225	188	24	193	121	147
Rhineland-Palatinate	83	90	138	136	187	152	18	123	- -	116
Baden-Wurttemberg	85	82	104	101	138	134	28	135	- -	103
Bavaria	62	60	83	104	105	123	27	117	149	84
Saarland	46	52	55	69	92	69	31	72	- -	57
Saxony	141	110	160	74	178	120	31	77	- -	124
Saxony -Anhalt	13	9	14	62	46	83	10	17	4	22
Thuringia	152	131	194	206	272	216	124	179	105	171
Germany	61	36	58	131	127	155	10	64	34	70

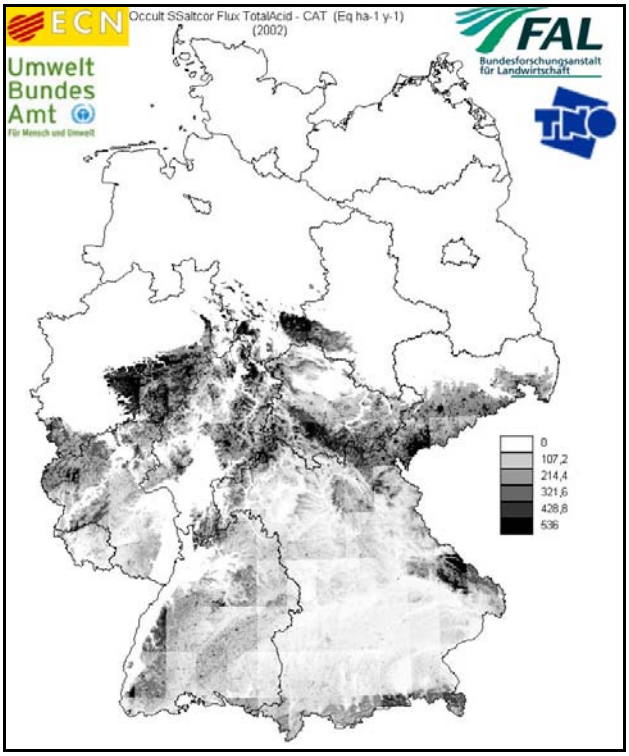

Figure 6.6: Total non-sea salt acid deposition by cloud water deposition in 2002 [eq ha^{-1} a^{-1}]

6.3 Dry deposition of base cations (Ca, K, Mg; Na)

Contrary to the other components SO_X, NO_Y and NH_X, no modelled or measured concentrations in air exist for base cations. As these components may contribute quite effectively to reducing the acidic input to ecosystems by their anion buffering capacity it is important to have a good estimate also of their dry deposition fluxes.

The concentrations in air of the base cations (Ca, K, Mg; Na) are derived indirectly using concentrations in rain water. As explained in Chapter 4 kriged maps have been produced in the framework of this project on a scale of 1x1km² over Germany for the acidifying components and the base cations. So called Scavenging Ratios (*SR*) have been applied to derive from these maps the concentration for the base cations. The scavenging ratio is simply expressed as:

$$SR = \rho \frac{C_{rain}}{C_{air}} \tag{6.47}$$

Where ρ is the density of air [g m^{-3}], C_{air} is the concentration in air [µg m^{-3}] and C_{rain} is the concentration in rain water [mg l^{-1}]. Alkaline particles usually fall in the size range between 0.1 and 2 µm. The *SR* depends on the mean mass diameter (*MMD* [µm]) of the particles (KANE ET AL, 1994):

$$SR = 188 * e^{0.227*MMD} \tag{6.48}$$

Combination of Equation 6.42 and Equation 6.43 yields a simple relationship between the concentration in air and that in rain.

The *MMD* of particles depends on many factors of which the most important one is the distance to the source as several processes like coagulation, condensation and uptake of humidity leads to growth of the *MMD* of particles over time. Also the concentration in rain water increases with the distance to the sources as in and below cloud scavenging increase with distance from the source. Assuming a simple linear relationship between the *MMD* and the concentration in rain several authors derived best-fit relationships. From DRAAIJERS ET AL. (1996) the following relationships were taken (Table 6.15):

Table 6.15: Best fit constants for the linear relationship between Mean Mass Diameter (MMD) and the concentrations in rain for the studied (base) cations Na, Mg, Ca and K

$MMD=A*C_{rain}+B$	*A*	*B*
Na	0.574	6.082
Mg	2.778	5.694
Ca	1.520	6.316
K	2.740	4.096

The procedure as sketched above will derive mean concentrations at the same time resolution as the data for the rain water concentration. In our case this is a resolution of one year. Therefore dry deposition fluxes of the base cations only could be calculated as year average values by applying the year averaged dry deposition rate for base cations on the year average concentration in air of these base cations as derived by scavenging ratios from year average rain water concentration.

7 Dry deposition mapping results

Thomas Gauger & Claus Rösemann
Federal Agricultural Research Centre, Institute of Agroecology (FAL-AOE), Bundesallee 50, D-38116 Braunschweig
Bundesforschungsanstalt für Landwirtschaft, Institut für Agrarökologie (FAL-AOE), Bundesallee 50, D-38116 Braunschweig

Dry deposition fluxes in this study are calculated in a high resolution grid (1x1km²) over Germany for the years 1995, 1997, and 1999 to 2004 using the inferential model IDEM (Integrated DEposition Model) as described in Chapter 6.

7.1 Dry deposition fluxes and trends of non-sea salt base cations ($BC_{(nss)}$)

Non-sea salt base cations ($BC_{(nss)}$) are calculated as the sum of non-sea salt Calcium ($Ca_{(nss)}$), non-sea salt Potassium ($K_{(nss)}$), and non-sea salt Magnesium ($Mg_{(nss)}$).

Over all years modelled in this study no trend in annual average dry deposition of $BC_{(nss)}$ in the period from 1995 to 2004 can be observed (cf. Figure 7.1). Compared to 1995 the $BC_{(nss)}$ dry deposition flux in 2004 is 7.3% higher. This lies within the range of changes between the single years of the time period considered (cf. Table 7.1). The $BC_{(nss)}$ dry deposition model estimates for the year 2003, however, are considerably out of range: The mean value of $BC_{(nss)}$ dry deposition in 2003 is about 3 times higher than in any of the other years (cf. Figure 7.1, Table 7.1).

Table 7.1: Budgets of average annual dry deposition of non-sea salt base cations 1995-2004

	$BC_{(nss)}$ [eq ha^{-1} a^{-1}]	% change from previous year
1995	352	
1996		
1997	403	+14.6
1998		
1999	330	-18.0
2000	367	+11.0
2001	338	-7.8
2002	326	-3.7
2003	984	+202.2
2004	377	-61.7
% change from 1995 to 2004		+7.3

In 2003 the weather conditions over Germany were exceptional dry. BC, and $BC_{(nss)}$ dry deposition fluxes are derived using the scavenging ratio approach. Air concentration of BC species is calculated from wet deposition monitoring data, namely from fields of concentration of base cations in precipitation (Chapter 6.3). In 2003 wet or bulk deposition monitoring was often hampered by the dry weather conditions that way that no or not much water was found in many samples exposed in the respective areas. This leads to relatively high concentrations in the samples and hence in the interpolated fields. The concentration fields of base cations in precipitation in 2003 on average showed about 30% higher values than in 2002 and 2004, which is exceptional high compared also to the other years considered. From this high concentration in precipitation high in-air concentration is calculated using the scavenging ratio approach. The application of deposition velocities in the usual way then leads to high deposition fluxes. Hence the exceptional high $BC_{(nss)}$ dry deposition estimates in 2003 must be seen as anomalous result, where the scavenging ratio approach is suitable only to a very limited extent, compared to the other years considered.

The spatial patterns of the dry deposition flux of $BC_{(nss)}$ 1995, 1997, and 1999 to 2004 are shown in Map 7.1. Patterns of highest deposition regularly can be found in bigger urban areas (e.g. Bremen, Hamburg, Berlin, Munich, Ruhr area, etc.) and over forested areas in the mountain range. This pattern of higher dry deposition fluxes of $BC_{(nss)}$ can be observed mainly in a stripe crossing Germany from northeast to the southwest.

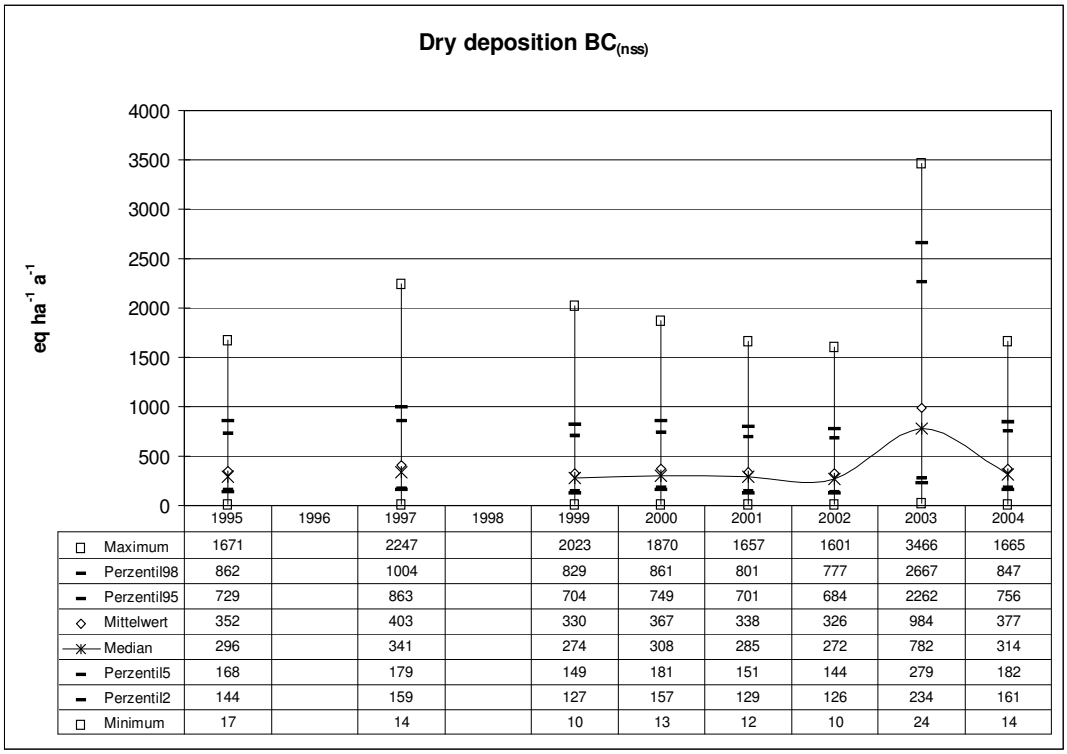

	1995	1996	1997	1998	1999	2000	2001	2002	2003	2004
Maximum	1671		2247		2023	1870	1657	1601	3466	1665
Perzentil98	862		1004		829	861	801	777	2667	847
Perzentil95	729		863		704	749	701	684	2262	756
Mittelwert	352		403		330	367	338	326	984	377
Median	296		341		274	308	285	272	782	314
Perzentil5	168		179		149	181	151	144	279	182
Perzentil2	144		159		127	157	129	126	234	161
Minimum	17		14		10	13	12	10	24	14

Figure 7.1: Statistical evaluation of annual non-sea salt base cations ($BC_{(nss)}$) dry deposition 1995-2004

7.2 Dry deposition fluxes and trends of acidifying compounds and nitrogen

Eutrophication occurs due to immoderate atmospheric input of nitrogen, which causes nutrient imbalances. Acidification is caused by deposition of both sulphur and nitrogen compounds. Average annual dry deposition 1995 to 2004 and the percentage changes for sulphur (SO_X-$S_{(nss)}$), reduced, oxidised and total nitrogen (NH_X-N, NO_Y-N, N), respectively, are shown in Table 7.2. Over the period from 1995 to 1999, the dry deposition of all acidifying compounds declined. In the following years this trend is stopped and while dry deposition of sulphur stays more or less at the same level, dry deposition fluxes of nitrogen compounds, especially for reduced nitrogen (NH_X-N) are slightly rising since 1999. However, this is no straight forward trend.

In 2003, the year with exceptional dry weather conditions, the model estimates for all acidifying compounds yield remarkably lower dry deposition fluxes than in 2002 and 2004, respectively. The results in 2003 are mainly artefacts that can be traced back to different meteorological data that were used when setting up emission inventories on the one hand, and, when air concentration and dry deposition is calculated on the other hand. Emission inventory calculation mainly uses long-term average meteorological data (e.g. of temperature) when emission densities are modelled. Air concentration and dry deposition modelling in this study makes use of actual meteorological data of each year. 2003 showed exceptional warm and dry weather conditions in Central Europe, which are not represented in long term average meteorology. This leads to unrealistic underestimates in the dry deposition model results.

1995 to 2004 budgets of average annual dry deposition of potential acidity (AC_{pot} = SO_X-$S_{(nss)}$ + N), potential net acidity ($AC_{pot(net)}$ = ACpot – $BC_{(nss)}$), and acid neutralisation by dry deposition of base cations ($BC_{(nss)}$ = Ca + K + Mg) are shown in Table 7.3.

Table 7.2: Budgets of average annual dry deposition of SO_X-$S_{(nss)}$, NH_X-N, NO_Y-N, and N 1995-2004

	SO_X-$S_{(nss)}$ [eq $ha^{-1}a^{-1}$]	% change from previous year	NH_X-N [eq $ha^{-1}a^{-1}$]	% change from previous year	NO_Y-N [eq $ha^{-1}a^{-1}$]	% change from previous year	N [eq $ha^{-1}a^{-1}$]	% change from previous year
1995	801		754		470		1225	
1996								
1997	555	-30.8	794	+5.2	436	-7.3	1231	+0.4
1998								
1999	377	-32.1	609	-23.3	361	-17.2	970	-21.2
2000	366	-2.7	711	+16.9	390	+8.2	1102	+13.6
2001	402	+9.6	768	+7.9	425	+9.0	1194	+8.3
2002	391	-2.7	760	-1.0	406	-4.5	1168	-2.2
2003	271	-30.6	562	-26.1	326	-19.7	889	-23.8
2004	429	+58.0	858	+52.7	439	+34.6	1298	+46.0
% change from 1995 to 2004		-46.5		+13.7		-6.5		+6.0

Table 7.3: Budgets of average annual dry deposition of AC_{pot}, $AC_{pot(net)}$, and acid neutralisation by $BC_{(nss)}$ 1995-2004

	AC_{pot} [eq ha^{-1} a^{-1}]	% change from previous year	$AC_{pot(net)}$ [eq ha^{-1} a^{-1}]	% change from previous year	$BC_{(nss)}$ [eq ha^{-1} a^{-1}]	% change from previous year	Acid neutralisation [%]
1995	2028		1676		352		19
1996							
1997	1786	-11.9	1383	-17.5	403	+14.6	25
1998							
1999	1348	-24.5	1017	-26.4	330	-18.0	27
2000	1470	+9.1	1103	+8.4	367	+11.0	27
2001	1597	+8.6	1259	+14.1	338	-7.8	23
2002	1560	-2.3	1234	-2.0	326	-3.7	23
2003	1162	-25.5	178	-85.6	984	+202.2	95
2004	1728	+48.8	1351	+661.0	377	-61.7	24
% change from 1995 to 2004		-14.8		-19.4		+7.3	

7.2.1 Dry deposition of non-sea salt sulphur (SO_X-$S_{(nss)}$)

From 1995 to 2004 annual average dry deposition of non-sea salt Sulphur (SO_X-$S_{(nss)}$) declines by about 46.5%. This decline is not due to a continuous trend over time. From 1995 to 1999 SO_X-$S_{(nss)}$ dry deposition fluxes over Germany diminished by about 47% from 801 eq ha^{-1} a^{-1} (12.8 kg $ha^{-1}a^{-1}$ or 460 kt a^{-1}, respectively) in 1995 to 377 eq ha^{-1} a^{-1} (6.0 kg $ha^{-1}a^{-1}$ or 216 kt a^{-1}, respectively) in 1999 (cf. Figure 7.2, Table 7.2). Whereas in 2004 average SO_X-$S_{(nss)}$ dry deposition estimates of about 429 eq ha^{-1} a^{-1} (6.9 kg $ha^{-1}a^{-1}$ or 246 kt a^{-1}) can be found, which are highest since 1999. Hence from 1999 to 2004 there is no trend over time in any direction traceable.

The spatial patterns of SO_X-$S_{(nss)}$ dry deposition are shown in Map 7.2. From the maps it can be seen that deposition declines in the years 1995 to 1999. In all maps presented the highest dry deposition can be found over the Ruhr basin region in western Germany, while lowest fluxes can regularly be observed in southern Germany.

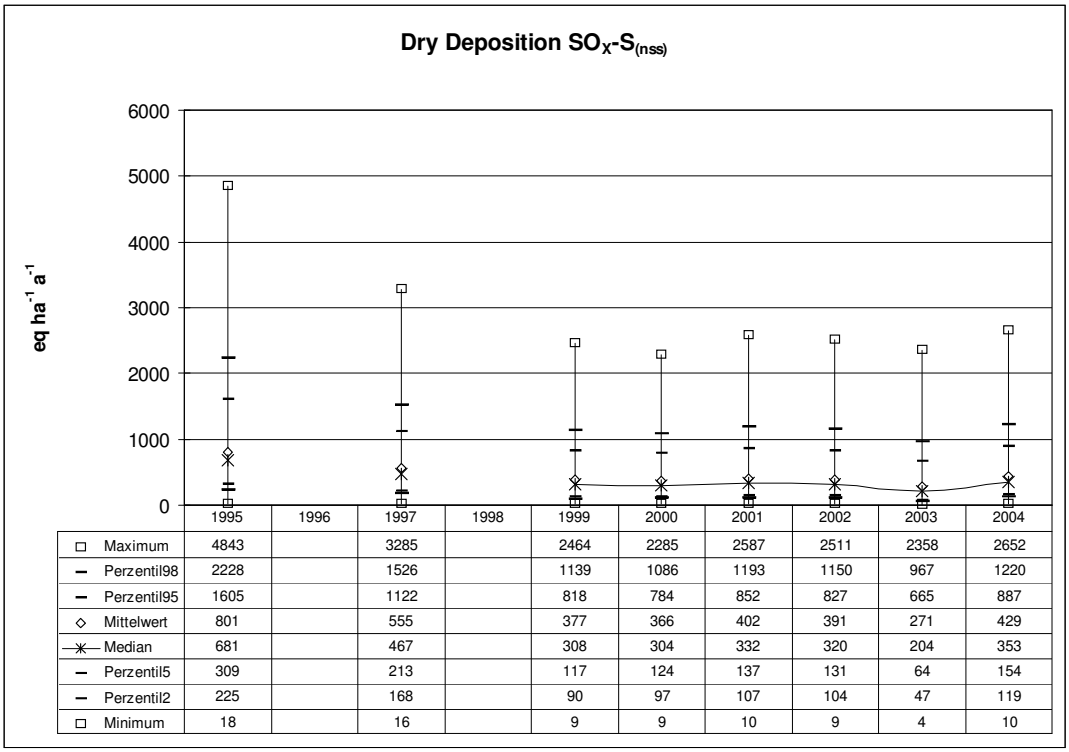

	1995	1996	1997	1998	1999	2000	2001	2002	2003	2004
Maximum	4843		3285		2464	2285	2587	2511	2358	2652
Perzentil98	2228		1526		1139	1086	1193	1150	967	1220
Perzentil95	1605		1122		818	784	852	827	665	887
Mittelwert	801		555		377	366	402	391	271	429
Median	681		467		308	304	332	320	204	353
Perzentil5	309		213		117	124	137	131	64	154
Perzentil2	225		168		90	97	107	104	47	119
Minimum	18		16		9	9	10	9	4	10

Figure 7.2: Statistical evaluation of annual non-sea salt sulphur (SOX-S(nss)) dry deposition 1995-2004

7.2.2 Dry deposition of reduced nitrogen (NH_X-N)

Map statistics of 1995 to 2004 dry deposition fluxes are shown in Figure 7.3. Though peak values diminished between 1995 and 2004, total dry deposited NH_X-N raised by about 13.7% from 378 kt a^{-1} (10.6 kg $ha^{-1}a^{-1}$) in 1995 to 430 kt a^{-1} (12.0 kg $ha^{-1}a^{-1}$) in 2004. Also no straight trend in dry deposition fluxes of NH_X-N from 1995 to 1999 can be found. From 1999 to 2002 modelled average NH_X-N dry deposition fluxes are slightly rising. From 2002 to 2003 a decline by about 26% can be observed (Table 7.2). The 2004 average NH_X-N dry deposition flux exceeds the 1995 average by about 1.4 kg ha^{-1} a^{-1} (100 eq ha^{-1} a^{-1}).

The overall spatial patterns of NH_X-N dry deposition are presented in Map7.3. Modelled dry deposition fluxes of NH_X-N in all years are highest in the north-western part of Germany, where regions with intensive animal husbandry can be found. Relative to other land use classes high dry deposition loads are found over forested areas scattered over the whole area of Germany and mainly situated in low mountain range areas further away from areas of high NH_X-N emission density.

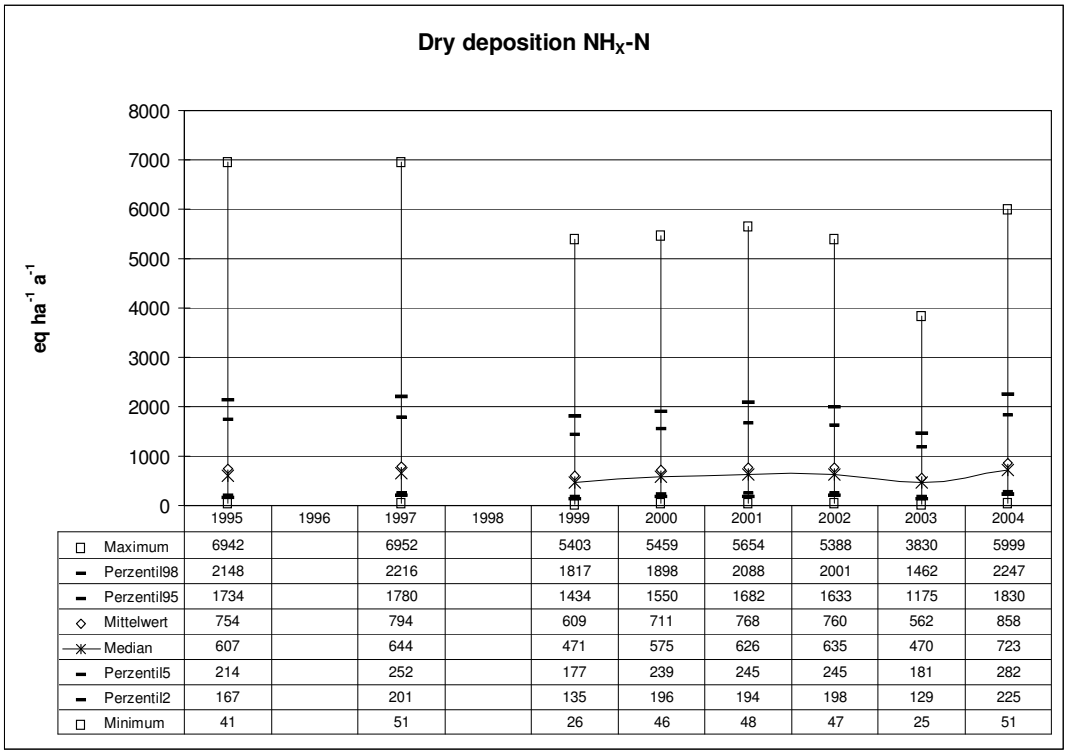

	1995	1996	1997	1998	1999	2000	2001	2002	2003	2004
Maximum	6942		6952		5403	5459	5654	5388	3830	5999
Perzentil98	2148		2216		1817	1898	2088	2001	1462	2247
Perzentil95	1734		1780		1434	1550	1682	1633	1175	1830
Mittelwert	754		794		609	711	768	760	562	858
Median	607		644		471	575	626	635	470	723
Perzentil5	214		252		177	239	245	245	181	282
Perzentil2	167		201		135	196	194	198	129	225
Minimum	41		51		26	46	48	47	25	51

Figure 7.3: Statistical evaluation of annual reduced nitrogen (NH_X-N) dry deposition 1995-2004

7.2.3 Dry deposition of oxidised nitrogen (NO_Y-N)

Map statistics of dry deposition of NO_Y-N are shown in Figure 7.4. From 1995 to 1999 average fluxes are declining by about 23%. From 1999 to 2004 increasing dry deposition fluxes can be observed with the exception of average dry NO_Y-N flux in 2003. In 2004 average dry deposition flux is about 6.5% lower than in 1995 (Table 7.2). Total amount of dry deposited NO_Y-N slightly declined from 236 kt a^{-1} (6.6 kg $ha^{-1}a^{-1}$) in 1995 to 220 kt a^{-1} (6.2 kg $ha^{-1}a^{-1}$) in 2004. Over the whole time period modelled no directed trend can be found. The rising peak values (figure 7.4) from 1999 to 2004 rather indicate rising dry deposition fluxes over time than stagnation or even decline.

Patterns of NO_Y-N dry deposition fluxes are presented in Map 7.4. Generally pronounced in the maps by high deposition loads are urban regions with high population densities, high energy production and consumption, as well as high traffic density. Small patterns with higher dry deposition fluxes than the surrounding areas are indicating higher fluxes into forested areas, which mainly are situated in higher altitude.

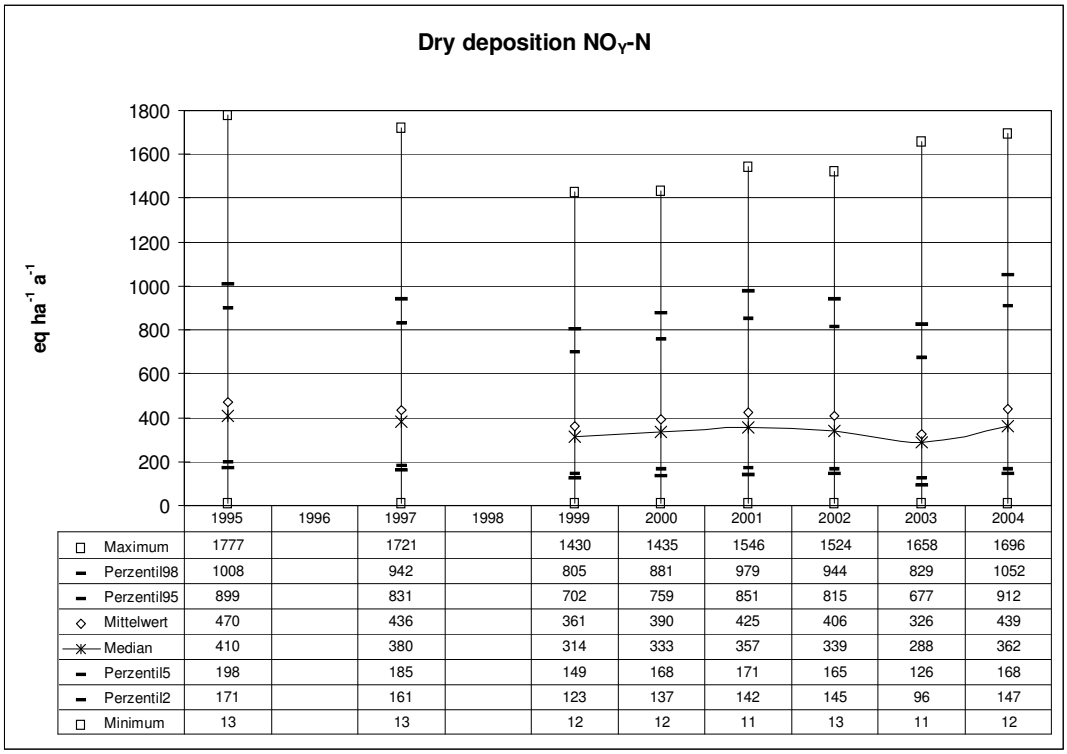

	1995	1996	1997	1998	1999	2000	2001	2002	2003	2004
Maximum	1777		1721		1430	1435	1546	1524	1658	1696
Perzentil98	1008		942		805	881	979	944	829	1052
Perzentil95	899		831		702	759	851	815	677	912
Mittelwert	470		436		361	390	425	406	326	439
Median	410		380		314	333	357	339	288	362
Perzentil5	198		185		149	168	171	165	126	168
Perzentil2	171		161		123	137	142	145	96	147
Minimum	13		13		12	12	11	13	11	12

Figure 7.4: Statistical evaluation of annual oxidised nitrogen (NO_Y-N) dry deposition 1995-2004

7.2.4 Dry deposition of total nitrogen (N = NH_X-N + NO_Y-N)

Dry deposition flux of total nitrogen (N) is the sum of reduced and oxidised nitrogen compounds (N = NH_X-N + NO_Y-N). From 1995 to 2004 N dry deposition fluxes increased by about 6.0% (Table 7.2, Figure 7.5). This is mainly due to the change of NH_X-N dry fluxes over time. Total amount of N dry fluxes declined by about 21% from 614 kt a^{-1} (17.2 kg $ha^{-1}a^{-1}$) in 1995 to 486 kt a^{-1} (13,6 kg $ha^{-1}a^{-1}$) in 1999. From 1999 N dry flux rises by about 25%, 165 kt a^{-1}, respectively, to 651 kt a^{-1} (18.2 kg $ha^{-1}a^{-1}$) in 2004. Over the whole time period no trend of decline can be observed.

Average contribution of NH_X-N and NO_Y-N to total N dry deposition fluxes for all years considered are listed in Table 7.4. The ratio between the two fractions over time is varying in the range of 4.5%. Reduced nitrogen amounts for almost two third of dry deposited total N. Though NH_X-N fraction of total N in 2004 is the highest, no directed trend of the NH_X-N or NO_Y-N fraction over time can be observed.

Spatial patterns of N dry deposition are presented in Map 7.5. The region with highest dry deposition of total nitrogen in all the years is located in the north-west of Germany. Regions with lower values are situated in the south-west of Germany (Rhineland-Palatinate, western parts of Baden-Württemberg) and in eastern Germany.

Table 7.4: Average NH_X-N and NO_Y-N fraction of dry deposited N 1995-2004

	1995	1996	1997	1998	1999	2000	2001	2002	2003	2004
NH_X-N [%]	61.6		64.6		62.8	64.6	64.3	65.2	63.2	66.1
NO_Y-N [%]	38.4		35.4		37.2	35.4	35.7	34.8	36.8	33.9

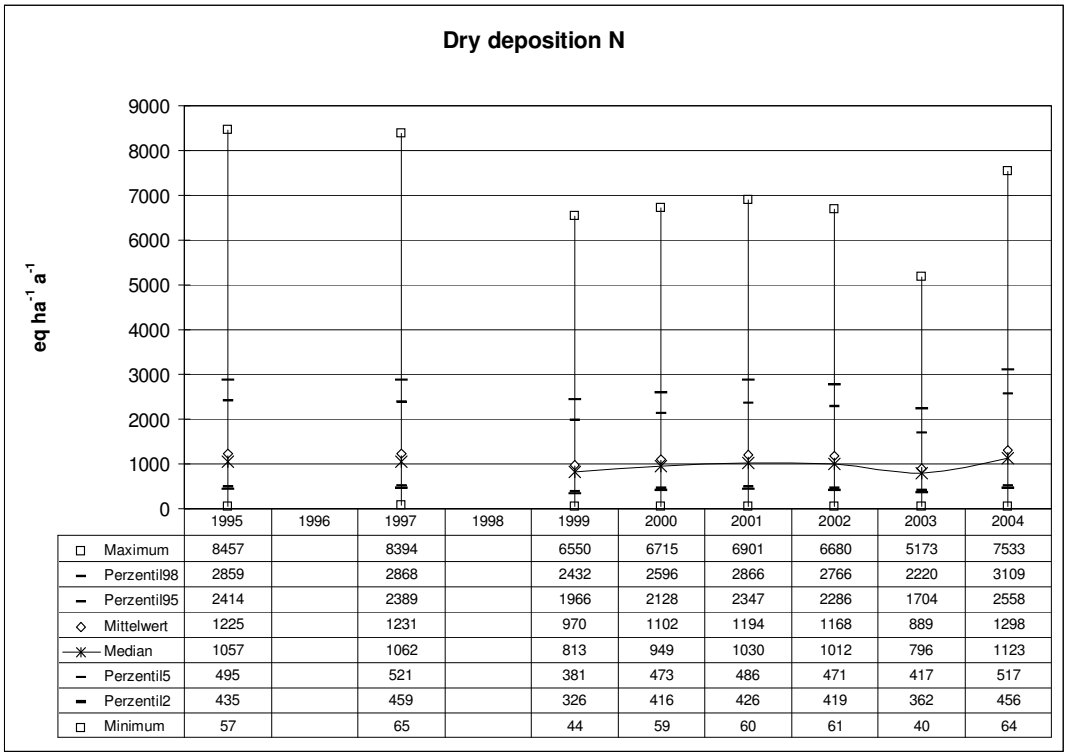

	1995	1996	1997	1998	1999	2000	2001	2002	2003	2004
Maximum	8457		8394		6550	6715	6901	6680	5173	7533
Perzentil98	2859		2868		2432	2596	2866	2766	2220	3109
Perzentil95	2414		2389		1966	2128	2347	2286	1704	2558
Mittelwert	1225		1231		970	1102	1194	1168	889	1298
Median	1057		1062		813	949	1030	1012	796	1123
Perzentil5	495		521		381	473	486	471	417	517
Perzentil2	435		459		326	416	426	419	362	456
Minimum	57		65		44	59	60	61	40	64

Figure 7.5: Statistical evaluation of annual total nitrogen (N) dry deposition 1995-2004

7.2.5 Dry deposition of potential acidity ($AC_{pot} = SO_X\text{-}S_{(nss)} + N$)

Dry deposition of potential acidity is the sum of non-sea salt sulphur and total nitrogen ($AC_{pot} = SO_X\text{-}S_{(nss)} + N$). Average dry deposition fluxes of AC_{pot} from 1995 to 2004 diminished by about 14.8% (cf. Table 7.3). This decline mainly can be attributed to the -46.5% change of $SO_X\text{-}S_{(nss)}$ dry deposition fluxes (c.f. Chapter 7.2.1) between1995 and 2004, whereas N dry deposition flux from 1995 to 2004 was rising by about 6%.

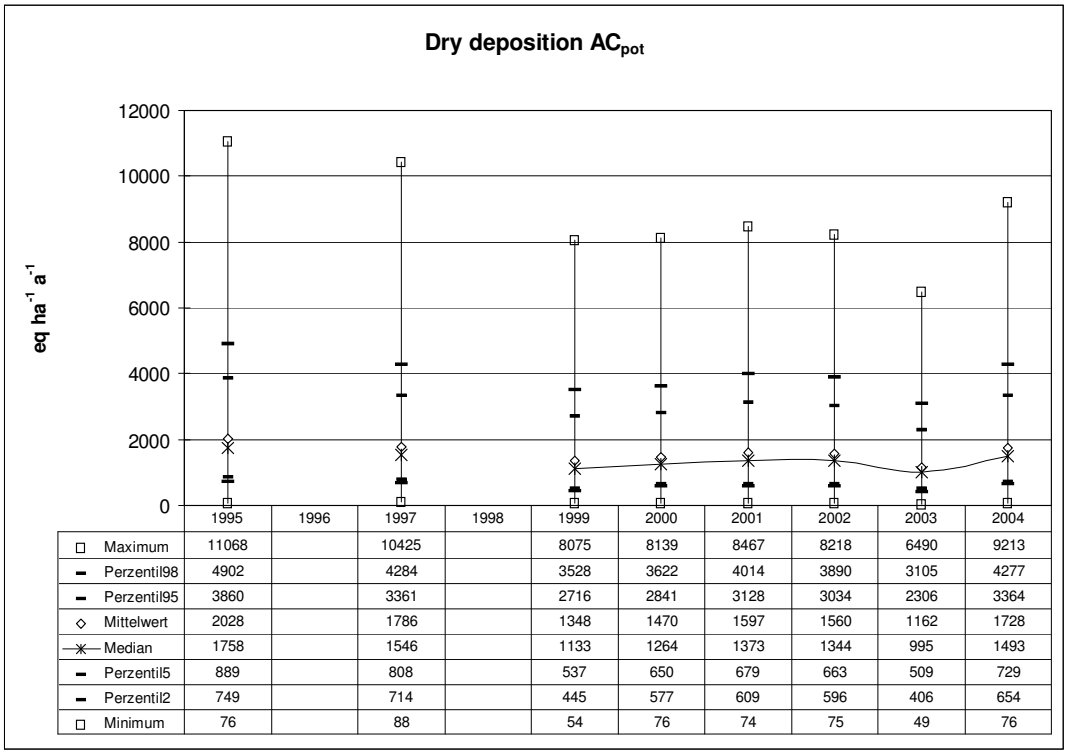

	1995	1996	1997	1998	1999	2000	2001	2002	2003	2004
Maximum	11068		10425		8075	8139	8467	8218	6490	9213
Perzentil98	4902		4284		3528	3622	4014	3890	3105	4277
Perzentil95	3860		3361		2716	2841	3128	3034	2306	3364
Mittelwert	2028		1786		1348	1470	1597	1560	1162	1728
Median	1758		1546		1133	1264	1373	1344	995	1493
Perzentil5	889		808		537	650	679	663	509	729
Perzentil2	749		714		445	577	609	596	406	654
Minimum	76		88		54	76	74	75	49	76

Figure 7.6: Statistical evaluation of annual potential acidity (AC_{pot}) dry deposition 1995-2004

Average fractions of the single compounds of dry fluxes of AC_{pot} in Germany 1995 to 2004 are listed in Table

7.5.
An overview of the average composition of the dry fluxes of AC_{pot} 1995 to 2004 is also given in Figure 7.7 on the basis of annual average dry deposition fluxes of NH_X-N, NO_Y-N, and SO_X-S in Germany. In 1995 SO_X-$S_{(nss)}$ is the main acidifying compound. From 1997 onward average dry NH_X-N flux is the dominating compound of AC_{pot}. From 2000 onward also NO_Y-N contributes more to AC_{pot} than SO_X-$S_{(nss)}$ does.

The spatial patterns of AC_{pot} dry deposition are presented in Map 7.6. The scatter of regions with higher and lower values resembles total N dry deposition maps (cf. Map 7.5), due to the major role of N as acidifying compound (cf. table 7.5).

Table 7.5: Average fractions of acidifying compounds of dry deposition 1995-2004

	1995	1996	1997	1998	1999	2000	2001	2002	2003	2004
SO_X-S [%]	39.5		31.1		27.9	24.9	25.2	25.1	23.4	24.8
NH_X-N [%]	37.2		44.4		45.1	48.4	48.1	48.7	48.4	49.6
NO_Y-N [%]	23.2		24.4		26.8	26.5	26.6	26.1	28.1	25.4
N [%]	60.4		68.9		72.0	75.0	74.8	74.9	76.5	75.1

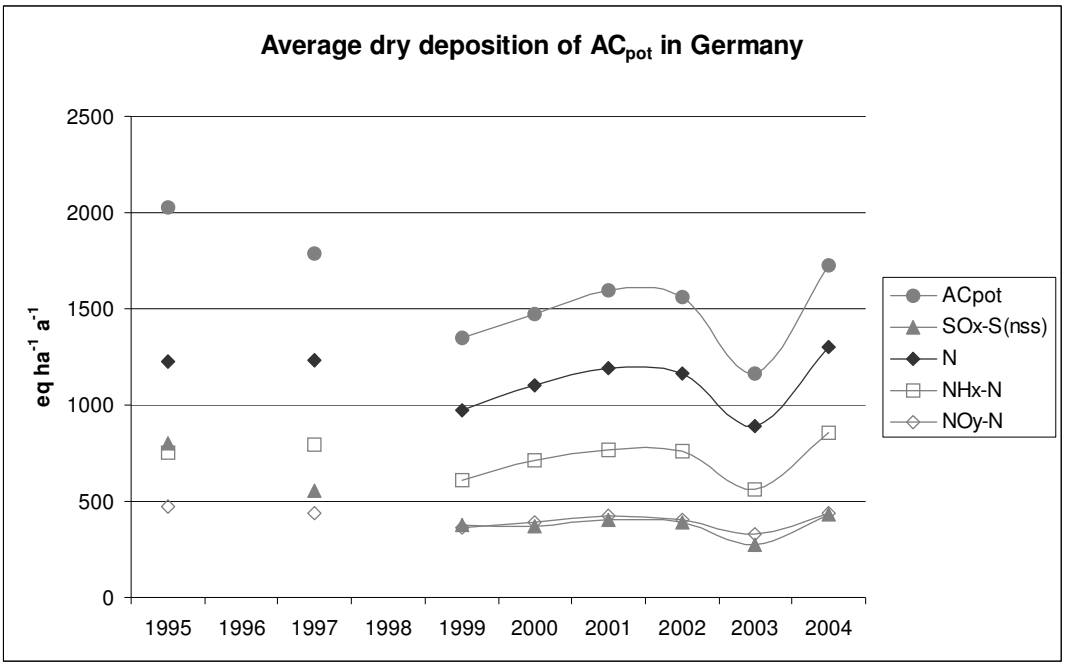

Figure 7.7: Average dry deposition of potential acidity (AC_{pot}) and its compounds 1995-2004

7.2.6 Dry deposition of potential net-acidity ($AC_{pot(net)} = SO_X$-$S_{(nss)} + N - BC_{(nss)}$) and acid neutralisation ($= BC_{(nss)} \cdot 100 / AC_{pot}$ [%])

Potential net acidity is calculated by subtracting the fluxes of non-sea salt base cations ($BC_{(nss)}$) from the sum of potential acidifying compounds (AC_{pot}) in order to account for potential acid neutralisation). Hence dry deposition loads of $AC_{pot(net)}$ generally are lower than dry deposition loads of AC_{pot} (cf. Figure 7.6 and 7.8).

Average dry deposition flux of $AC_{pot(net)}$ in 2004 is about 19.4% (about 322 eq ha^{-1} a^{-1}) lower compared to 1995 (Figure 7.8, Table 7.3).

Acid neutralisation by dry deposition of non-sea salt base cations ($BC_{(nss)}$) in the period 1995-2004 is shown in Figure 7.9. Neglecting the implausible results for the year 2003 (cf. Chapter 7.1) the annual average values of acid neutralisation are varying between 19% in 1995 and 27% in 1999 and 2000. The spatial patterns of $AC_{pot(net)}$ are shown in Map 7.7, the acid neutralisation by dry deposition of $BC_{(nss)}$ is presented in Map 7.8, respectively. Each year the highest values of $AC_{pot(net)}$ can be found in the north western Part of Germany. Hence acid neutralisation in this region is the lowest.

Budgets of average dry deposition of AC_{pot}, $AC_{pot(net)}$ and acid neutralisation by $BC_{(nss)}$ from 1995 to 2004 are listed in Table 7.5.

Irrespective the implausible results for 2003 (cf. Chapter 7.1), the downward trend of dry deposition of AC_{pot} and $AC_{pot(net)}$ from 1995 to 1999 from 2000 onward turned to a slightly rising trend until 2004 (cf. Figure 7.10). Since for non-sea salt base cations ($BC_{(nss)}$) no trend over the whole period considered (except 2003) can be found, the acid neutralisation is increasing until 2000 and a little decreasing the years after (cf. Table 7.5, and Figure 7.10).

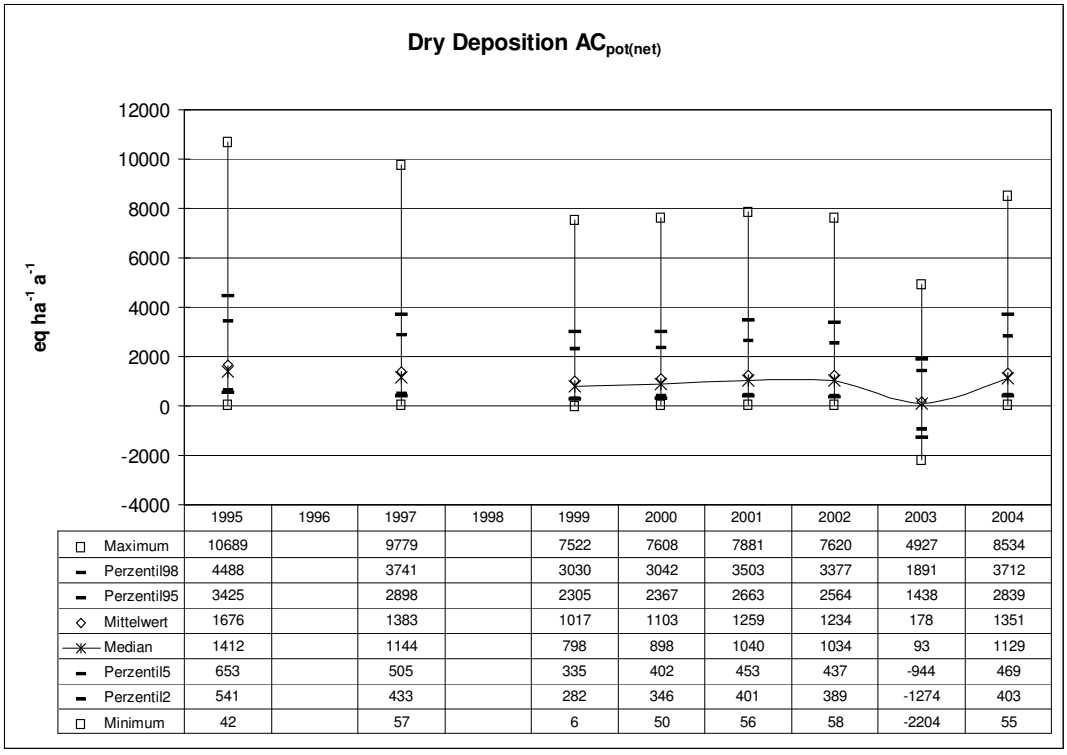

	1995	1996	1997	1998	1999	2000	2001	2002	2003	2004
Maximum	10689		9779		7522	7608	7881	7620	4927	8534
Perzentil98	4488		3741		3030	3042	3503	3377	1891	3712
Perzentil95	3425		2898		2305	2367	2663	2564	1438	2839
Mittelwert	1676		1383		1017	1103	1259	1234	178	1351
Median	1412		1144		798	898	1040	1034	93	1129
Perzentil5	653		505		335	402	453	437	-944	469
Perzentil2	541		433		282	346	401	389	-1274	403
Minimum	42		57		6	50	56	58	-2204	55

Figure 7.8: Statistical evaluation of annual potential net acidity ($AC_{pot(net)}$) dry deposition 1995-2004

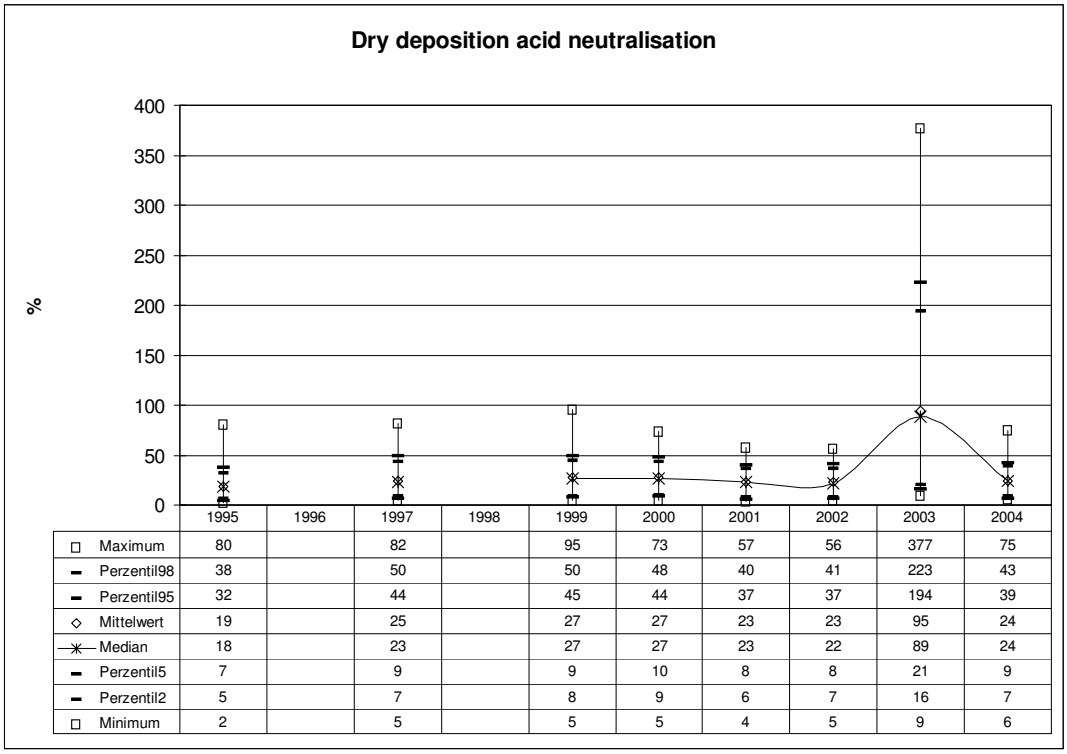

	1995	1996	1997	1998	1999	2000	2001	2002	2003	2004
Maximum	80		82		95	73	57	56	377	75
Perzentil98	38		50		50	48	40	41	223	43
Perzentil95	32		44		45	44	37	37	194	39
Mittelwert	19		25		27	27	23	23	95	24
Median	18		23		27	27	23	22	89	24
Perzentil5	7		9		9	10	8	8	21	9
Perzentil2	5		7		8	9	6	7	16	7
Minimum	2		5		5	5	4	5	9	6

Figure 7.9: Statistical evaluation of annual acid neutralisation in dry deposition 1995-2004

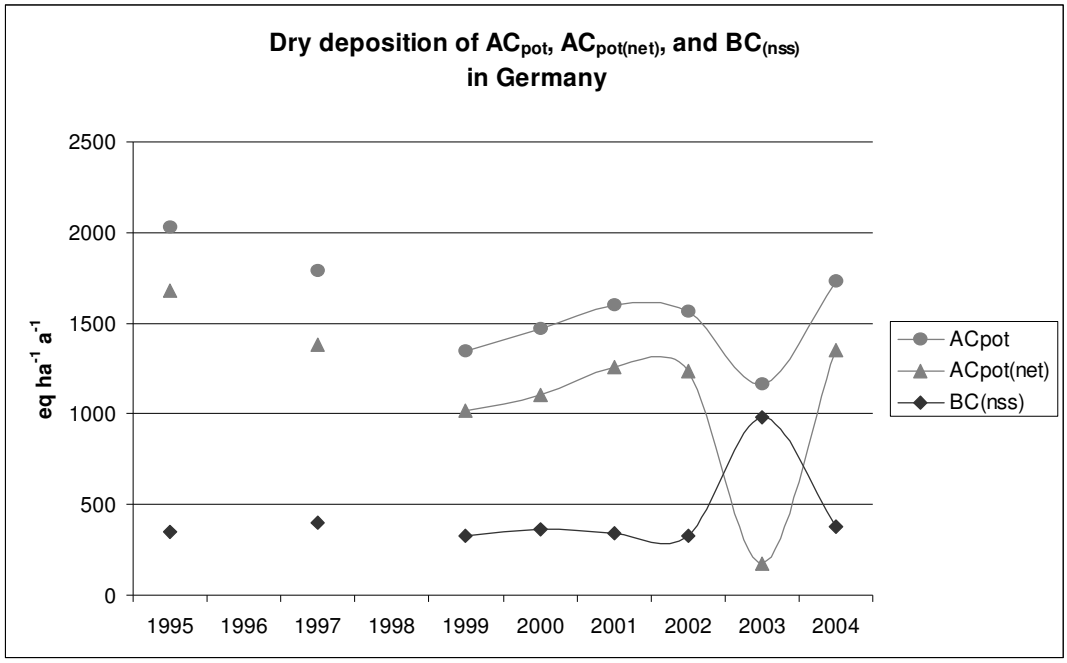

Figure 7.10: Average dry deposition of AC_{pot}, $AC_{pot(net)}$, and $BC_{(nss)}$ 1995-2004

7.3 Dry deposition fluxes of cadmium (Cd) and lead (Pb)

Dry deposition of the heavy metals cadmium (Cd) and lead (Pb) in this study is modelled by IDEM using LOTOS-EUROS air concentration estimates, derived using TNO emission inventory data (see Chapter 10.4 for further details). The preliminary modelled air concentrations are seriously underestimating respective measurements at EMEP sites for both Pb and Cd (Chapter 10.4.2). Dry deposition estimates presented here are very low compared e.g. to wet deposition measurements and mapping results (Chapter 5.3). The order of magnitude of preliminary dry deposition estimates for Pb on average over Germany is in the range of the dry deposited fraction collected with bulk deposition samplers (GAUGER ET AL. 2000). In the case of Cd dry deposition estimates it is even less than the dry contribution within the bulk deposition flux (Table 7.6).

Table 7.6: Order of magnitude of annual mean contribution of dry deposition in bulk precipitation fluxes (GAUGER ET AL. 2000) and preliminary dry deposition model estimates of Cd and Pb

Cd dry contribution to bulk deposition flux [ratio: dry flux/bulk flux]	Contribution of Cd dry deposition estimates to total flux [ratio: dry flux/(wet flux + dry flux)]	Pb dry contribution to bulk deposition flux [ratio: dry flux/bulk flux]	Contribution of Pb dry deposition estimates to total flux [ratio: dry flux/(wet flux + dry flux)]
0.27	0.16	0.29	0.32

Budgets of average annual dry deposition estimates, however, are shown in Table 7.7. It can be found that the differences in annual average dry deposition fluxes between the single years are quite high compared e.g. to the trends of main compound dry deposition estimates. The changes from one year to the next are ranging from about -36% to +131% for average Cd dry deposition flux, and for Pb from about -48% to about +151%.

In table 7.8 the dry fluxes of cadmium and lead are compared to the official emission data. Emission data for Cd over time are higher in the latest years (2.7 t a^{-1} in 2002 to 2004) than in the earliest year considered (2.3 t a^{-1} in 1995). The corresponding ratios between dry flux estimates and emission are ranging from 0.13 in 2002 to 0.34 in 1997.

Official emission data for Pb are declining over time. The steepest fall by 234 t a^{-1} is from 1995 to 1997. Form 1997 onward the emission totals are ranging from 94 t a^{-1} to 109 t a^{-1}. Ratios for Pb dry flux estimates and emission data are ranging from 0.11 in 1995 to 0.61 in 2004 (Table 7.8).

Table 7.7: Budgets of average annual dry deposition of Cd and Pb 1995-2004

	Cd [µeq $ha^{-1}a^{-1}$]	Cd [mg $ha^{-1}a^{-1}$]	change from previous year [%]	Pb [µeq $ha^{-1}a^{-1}$]	Pb [g $ha^{-1}a^{-1}$]	change from previous year [%]
1995	262	15		9831	1.02	
1996						
1997	411	23	+56.6	14424	1.49	+46.7
1998						
1999	324	18	-21.1	12149	1.26	-15.8
2000	299	17	-7.7	14434	1.50	+18.8
2001	285	16	-4.9	13725	1.42	-4.9
2002	181	10	-36.4	7135	0.74	-48.0
2003						
2004	418	23	+130.7	17874	1.85	+150.5
change from 1995 to 2004 [%]			+59.2			+81.8

Table 7.8: Comparison of Cd and Pb dry deposition and emission data[1)] in Germany 1995-2004
([1)]UBA 2007 http://www.umweltbundesamt.de/emissionen/archiv/DE_2007_Tables_IV1A_1990_2005.zip)

	Cd dry deposition [t a^{-1}]	Cd emission [1)] [t a^{-1}]	Ratio: dry flux / emission	Pb dry deposition [t a^{-1}]	Pb emission [1)] [t a^{-1}]	Ratio: dry flux / emission
1995	0.5	2.3	0.23	36.3	330	0.11
1996		2.2			222	
1997	0.8	2.4	0.34	53.3	96	0.56
1998		2.2			94	
1999	0.7	2.7	0.24	44.9	96	0.47
2000	0.6	2.4	0.25	53.4	102	0.52
2001	0.6	2.6	0.22	50.7	105	0.48
2002	0.4	2.7	0.13	26.4	106	0.25
2003		2.7			107	
2004	0.8	2.7	0.31	66.1	109	0.61

7.3.1 Dry deposition of cadmium (Cd)

Map statistics of dry Cd deposition fluxes 1995, 1997, 1999 to 2002 and 2004 are shown in Figure 7.11. For better visibility of the range of values the y-axis is logarithmic. Over the time period from 1995 to 2004 average estimates of dry deposition fluxes of Cd are varying from 181 µeq ha^{-1} a^{-1} (10 mg ha^{-1} a^{-1}) in 2002 to 418 µeq ha^{-1} a^{-1} (23 mg ha^{-1} a^{-1}) in 2004. The variation of Cd dry deposition fluxes from one year to the next is quite high (cf. Table 7.7).

The graphic representation of Cd dry deposition over time is shown in Map 7.9. The spatial scatter of the maps mainly shows Cd dry deposition fluxes above the respective annual averages around urban and industrial agglomeration areas in the northern half and western parts of Germany, whereas in southern Germany, and in the northern most parts of Germany lower fluxes than the average can be found.

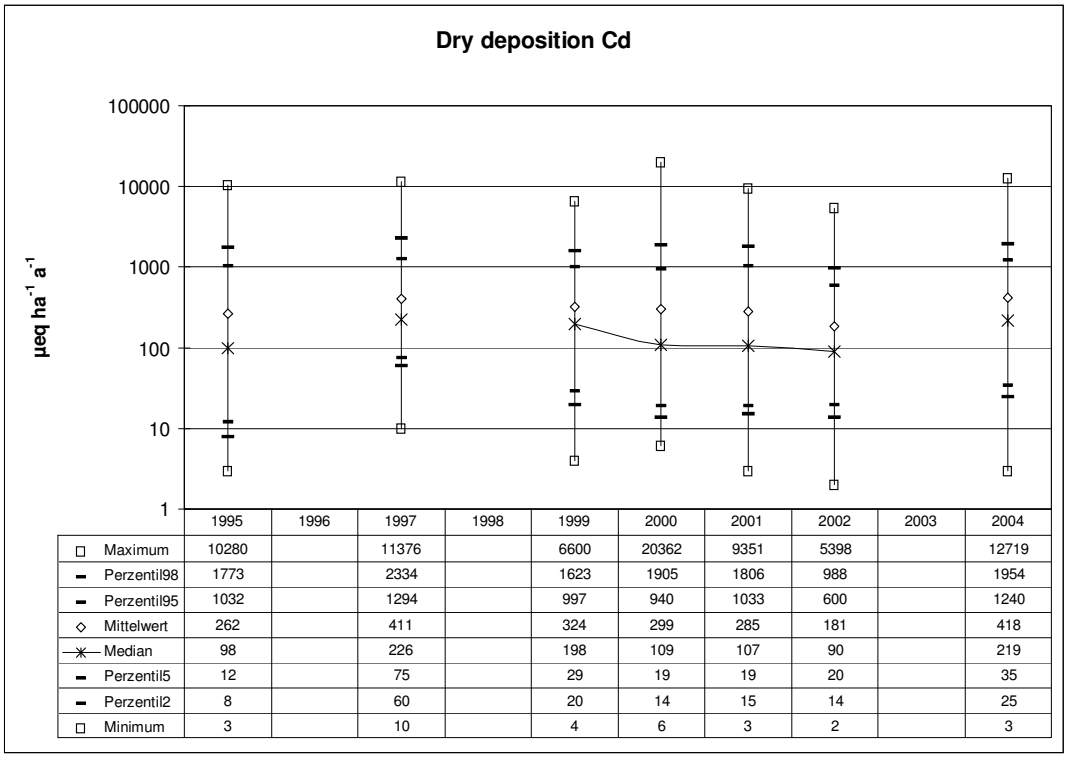

	1995	1996	1997	1998	1999	2000	2001	2002	2003	2004
Maximum	10280		11376		6600	20362	9351	5398		12719
Perzentil98	1773		2334		1623	1905	1806	988		1954
Perzentil95	1032		1294		997	940	1033	600		1240
Mittelwert	262		411		324	299	285	181		418
Median	98		226		198	109	107	90		219
Perzentil5	12		75		29	19	19	20		35
Perzentil2	8		60		20	14	15	14		25
Minimum	3		10		4	6	3	2		3

Figure 7.11: Statistical evaluation of annual cadmium (Cd) dry deposition 1995-2004

7.3.2 Dry deposition of lead (Pb)

Map statistics of dry Pb deposition fluxes 1995, 1997, 1999 to 2002 and 2004 are shown in Figure 7.12. As for Cd, the y-axis of the graph is logarithmic for better visibility of the range of values. Over the time period from 1995 to 2004 average estimates of dry deposition fluxes of Pb are varying from 7.4 meq ha^{-1} a^{-1} (0.74 g ha^{-1} a^{-1}) in 2002 to 17.8 meq ha^{-1} a^{-1} (1.85 g ha^{-1} a^{-1}) in 2004. The variation of Pb dry deposition fluxes from one year to the next is quite high and no directed trend can be observed (cf. Table 7.7).

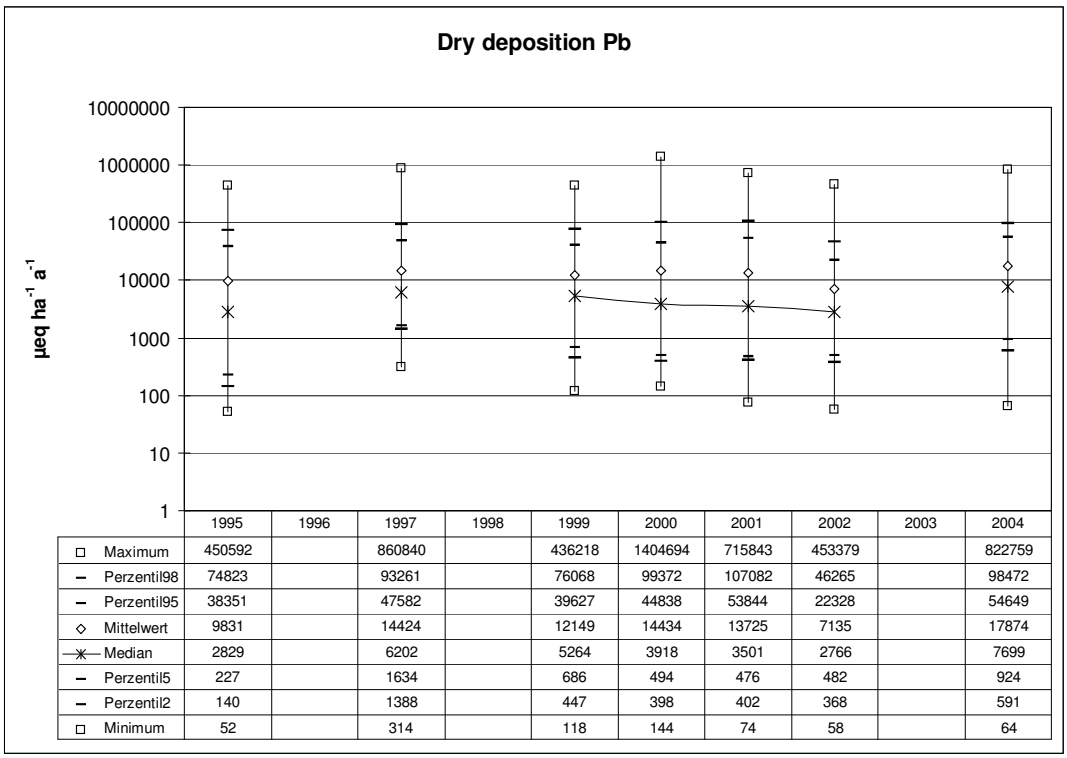

	1995	1996	1997	1998	1999	2000	2001	2002	2003	2004
Maximum	450592		860840		436218	1404694	715843	453379		822759
Perzentil98	74823		93261		76068	99372	107082	46265		98472
Perzentil95	38351		47582		39627	44838	53844	22328		54649
Mittelwert	9831		14424		12149	14434	13725	7135		17874
Median	2829		6202		5264	3918	3501	2766		7699
Perzentil5	227		1634		686	494	476	482		924
Perzentil2	140		1388		447	398	402	368		591
Minimum	52		314		118	144	74	58		64

Figure 7.11: Statistical evaluation of annual lead (Pb) dry deposition 1995-2004

The graphic representation of Pb dry deposition fields over time is shown in Map 7.10. The spatial scatter of the maps mainly shows Pb dry deposition fluxes above the respective annual averages over western parts of Germany and its northern and central parts. In south-eastern Germany and in the northern most parts of Germany lower fluxes than the average can be found. Spots of highest Pb dry deposition fluxes can be found over urban and industrial agglomerations, like Bremen, Hamburg, in the Saarland, the Ruhr region, and at the Hochrhein, in the south-western most part of Germany.

7.4 Maps of dry deposition 1995, 1997, 1999-2004

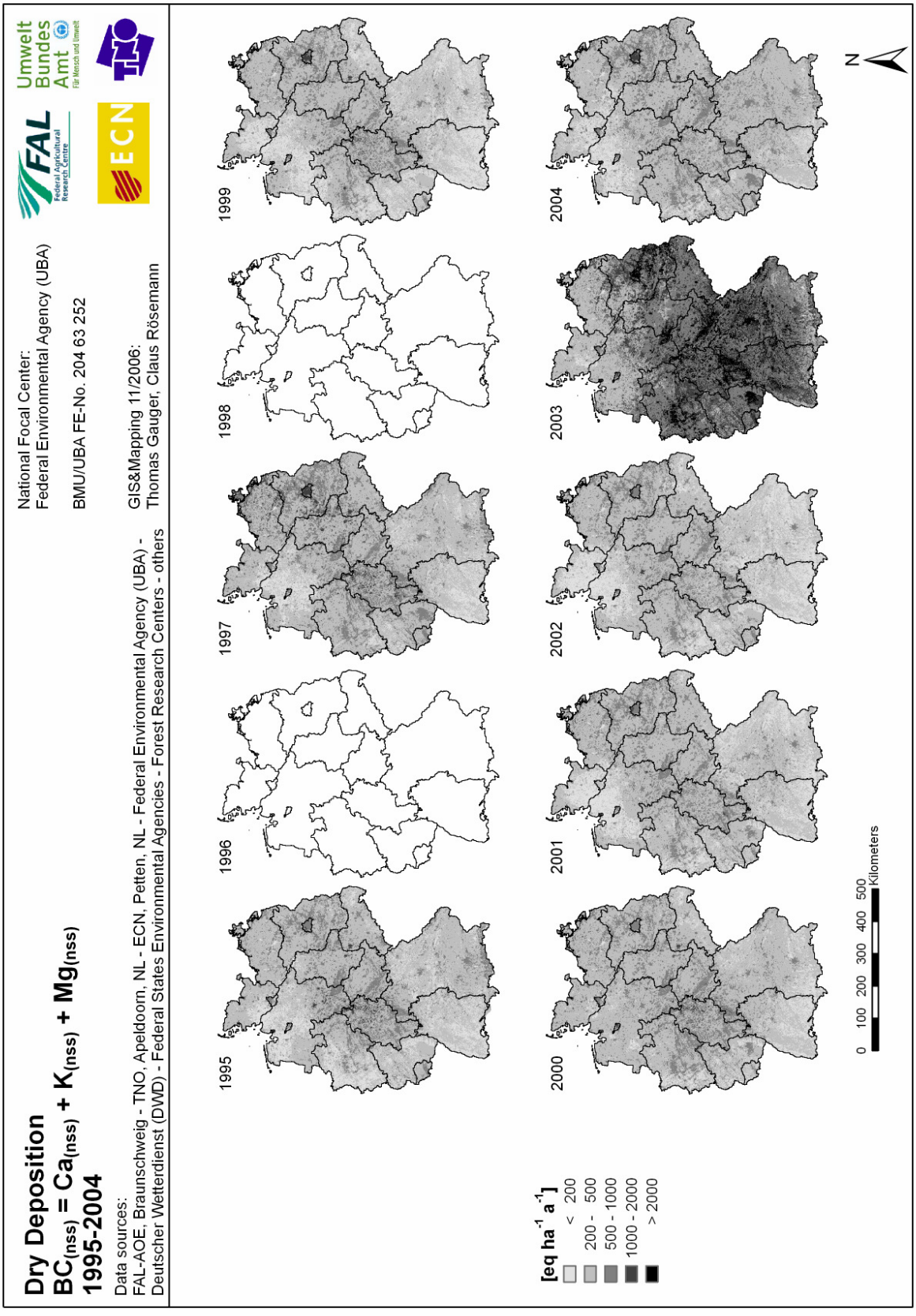

Map 7.1: Dry deposition of $BC_{(nss)}$ 1995-2004

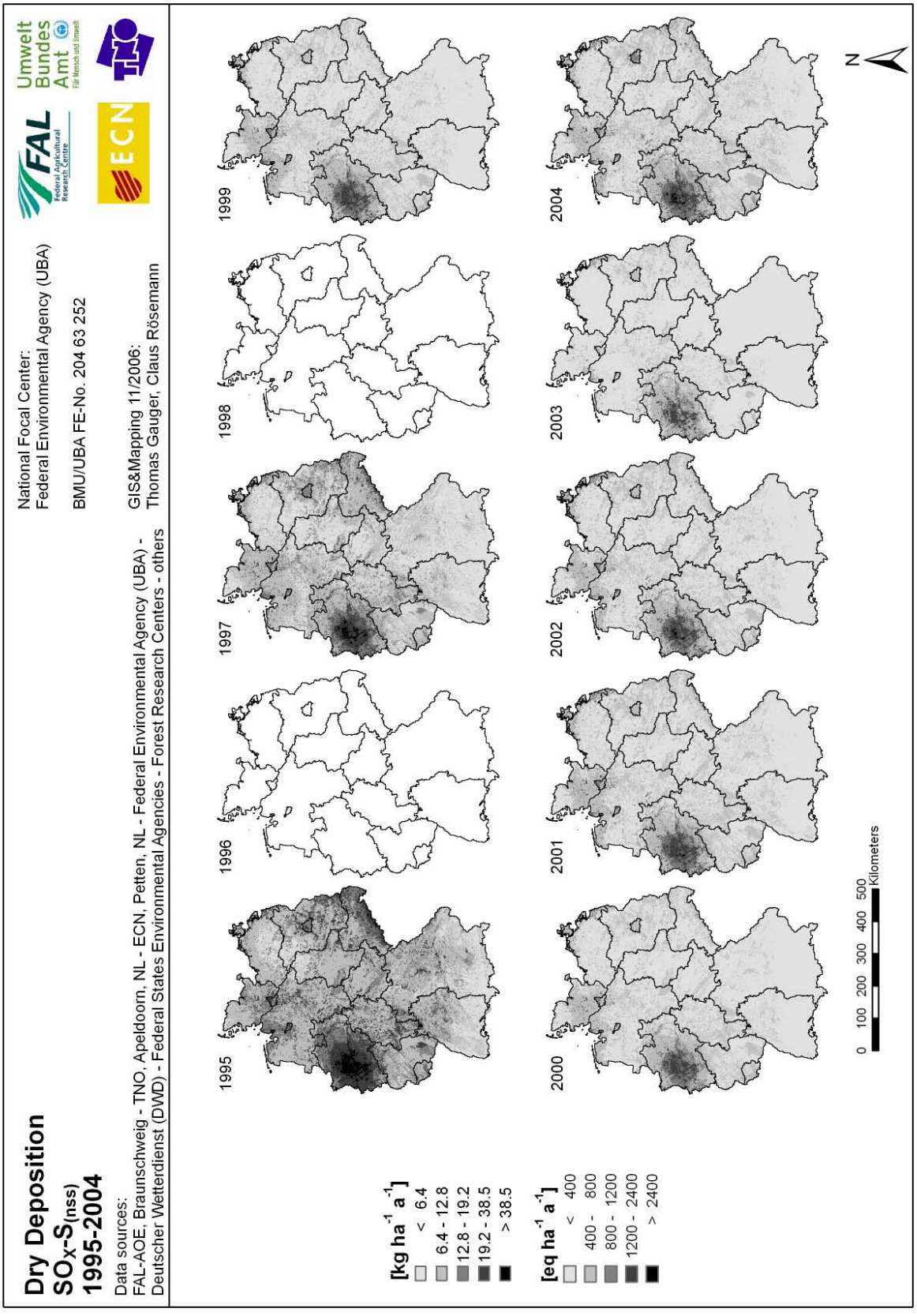

Map 7.2: Dry deposition of SO_X-$S_{(nss)}$ 1995-2004

Map 7.3: Dry deposition of NH_X-N 1995-2004

Dry Deposition
NH_X-N
1995-2004

Data sources:
FAL-AOE, Braunschweig - TNO, Apeldoorn, NL - ECN, Petten, NL - Federal Environmental Agency (UBA) - Deutscher Wetterdienst (DWD) - Federal States Environmental Agencies - Forest Research Centers - others

National Focal Center:
Federal Environmental Agency (UBA)

BMU/UBA FE-No. 204 63 252

GIS&Mapping 11/2006:
Thomas Gauger, Claus Rösemann

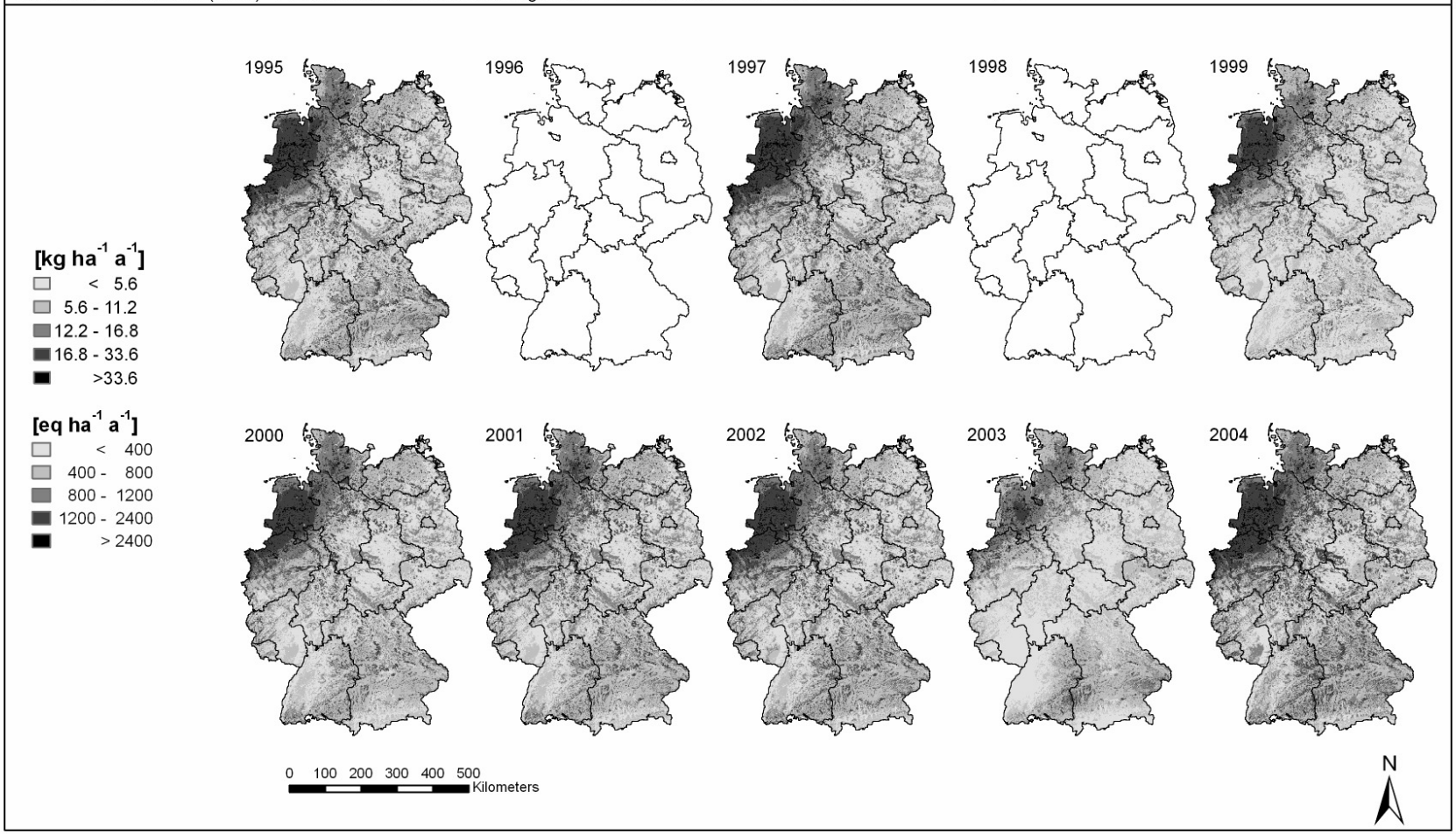

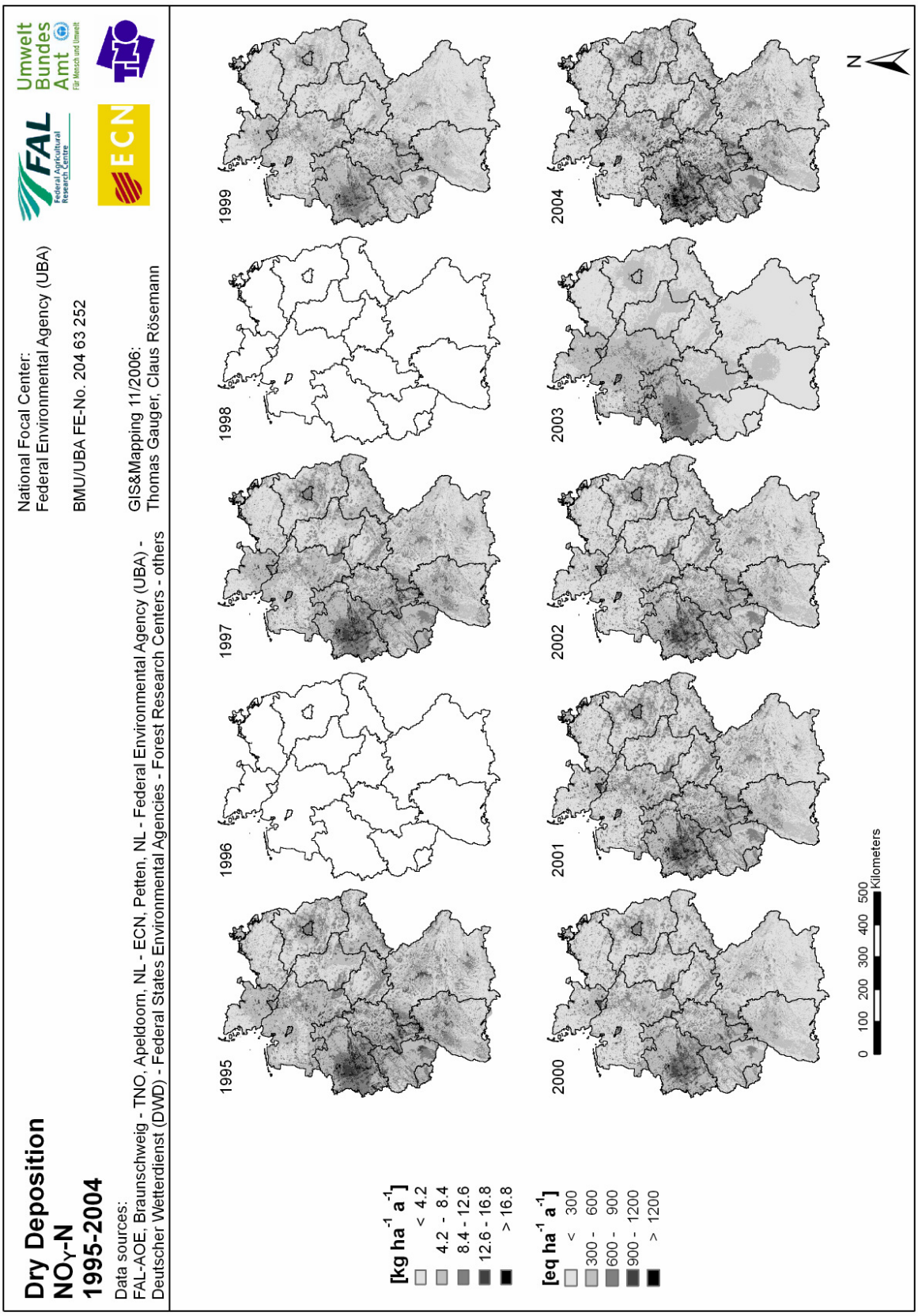

Map 7.4: Dry deposition of NO_Y-N 1995-2004

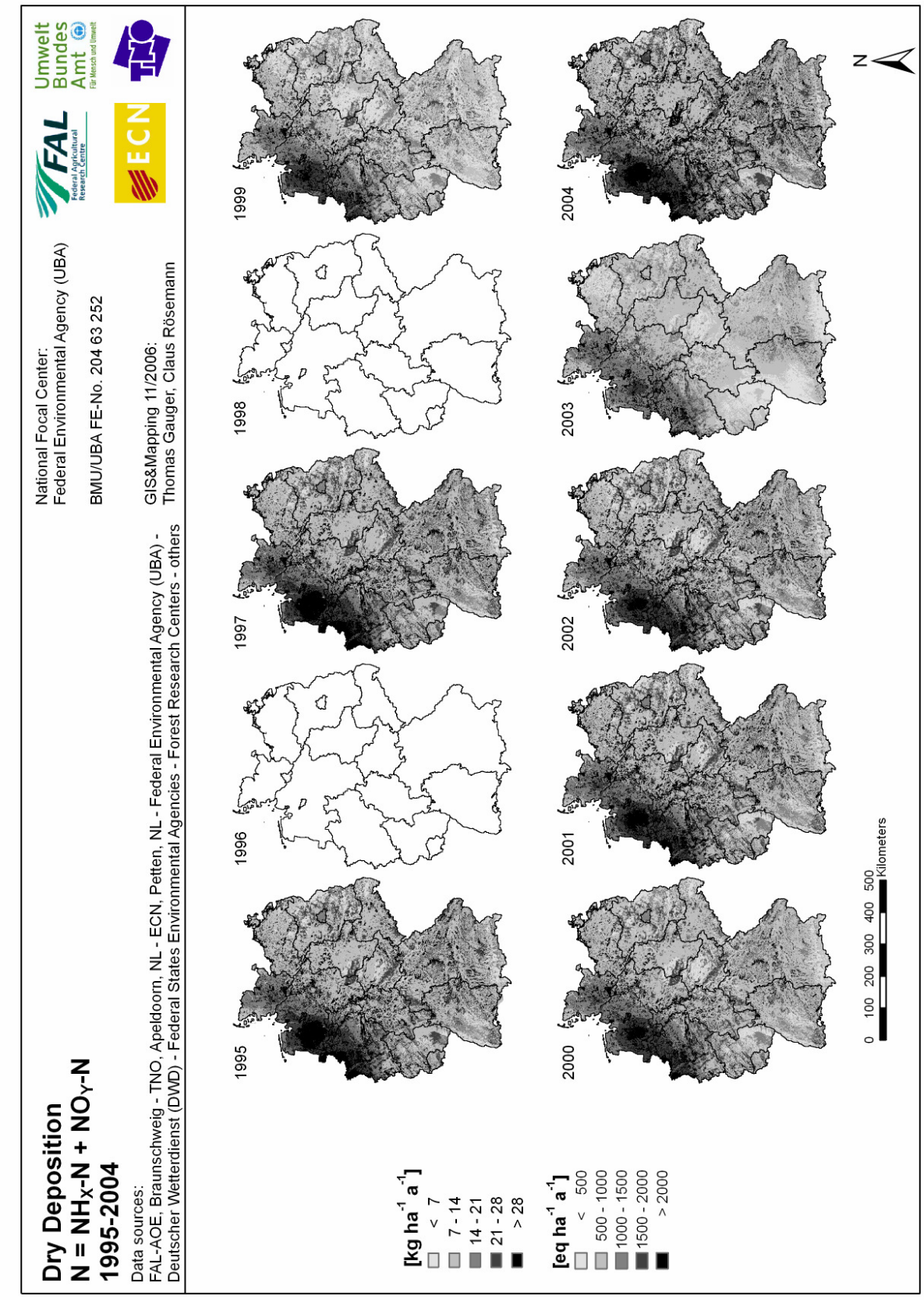

Map 7.5: Dry deposition of N 1995-2004

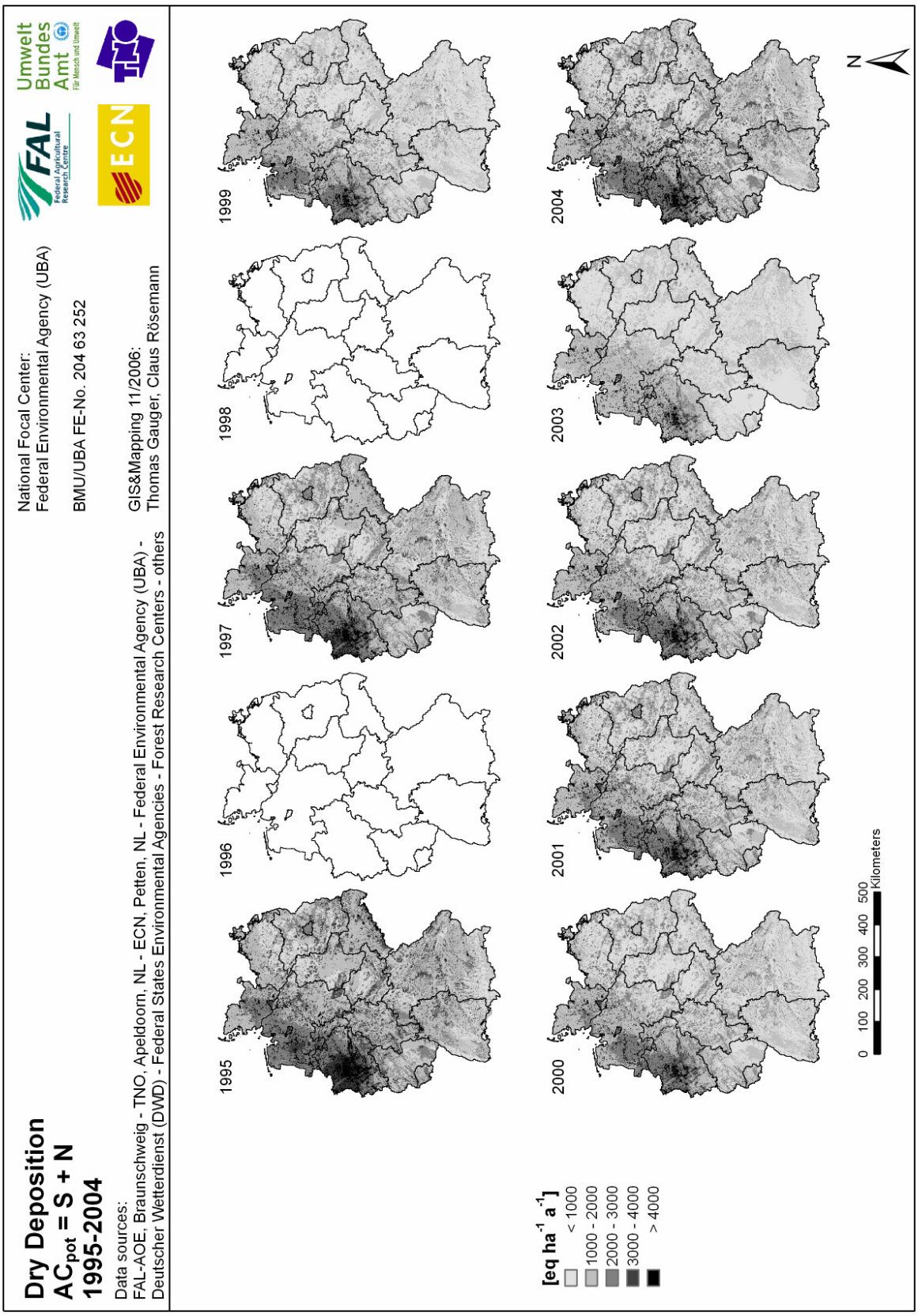

Map 7.6: Dry deposition of AC_{pot} 1995-2004

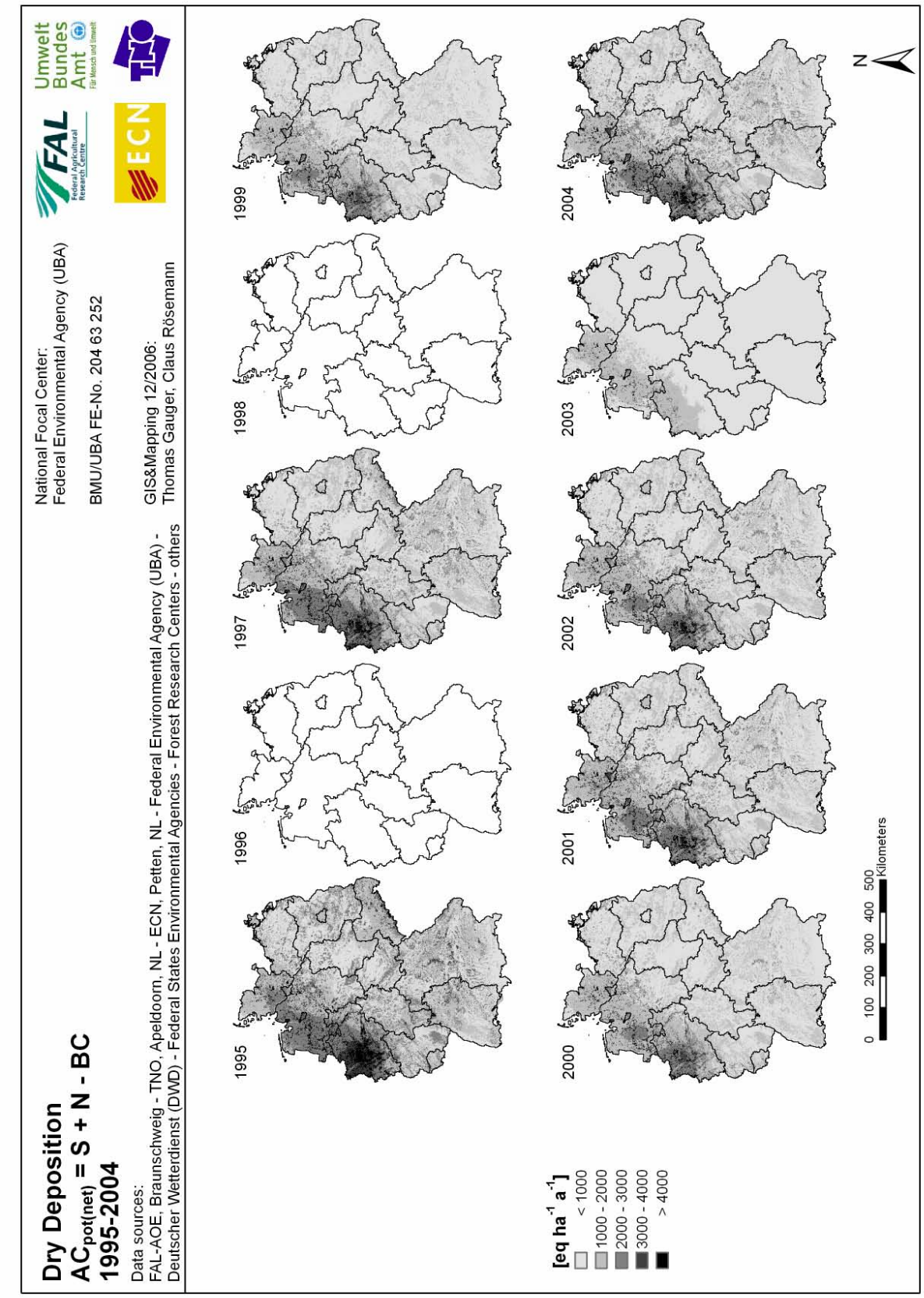

Map 7.7: Dry deposition of $AC_{pot(net)}$ 1995-2004

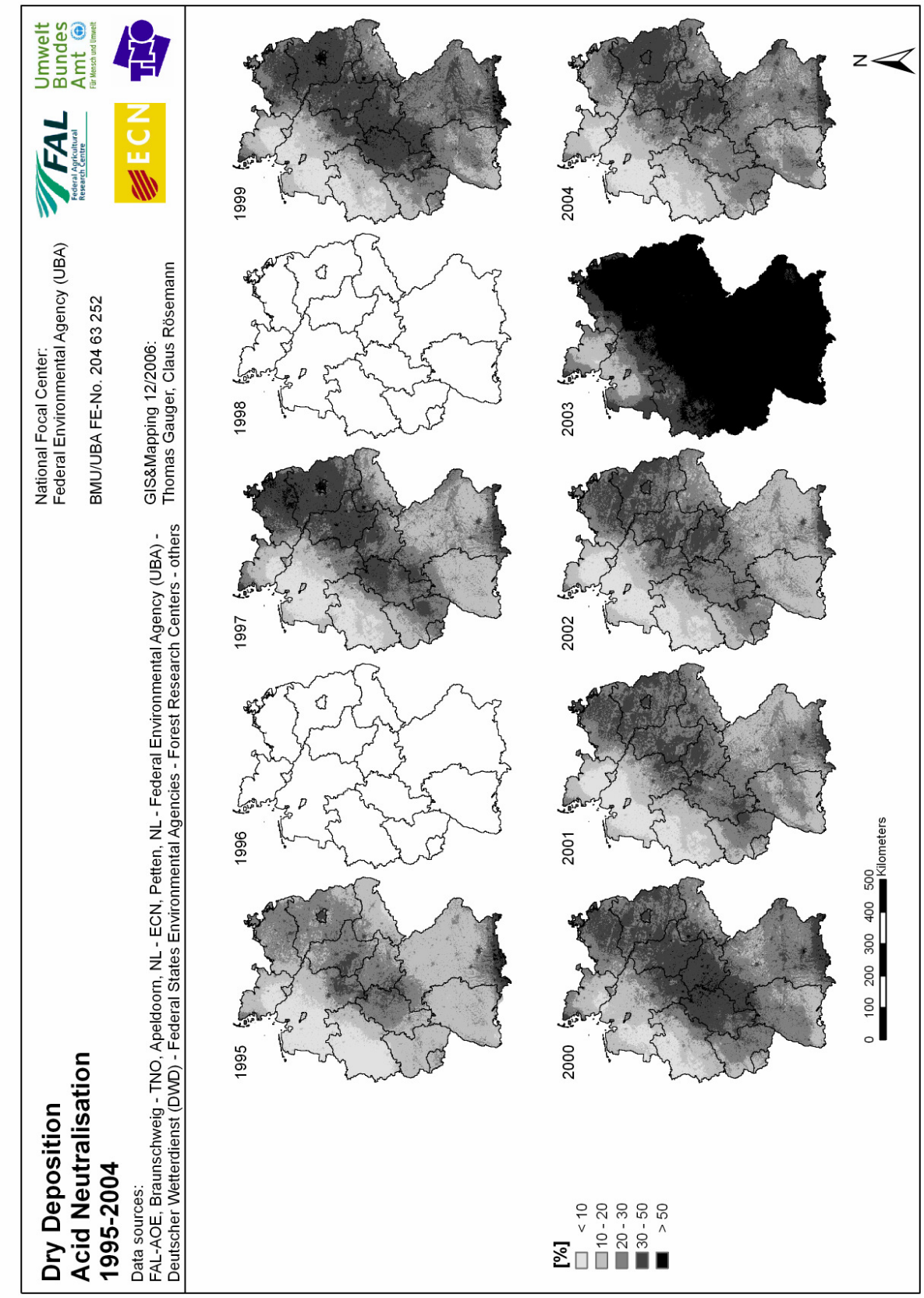

Map 7.8: Neutralisation of dry deposited AC_{pot} by $BC_{(nss)}$ 1995-2004

Map 7.9: Dry deposition of Cd 1995-2004

Dry Deposition
Cd
1995-2004

Data sources:
FAL-AOE, Braunschweig - TNO, Apeldoorn, NL - ECN, Petten, NL - Federal Environmental Agency (UBA) - Deutscher Wetterdienst (DWD) - Federal States Environmental Agencies - Forest Research Centers - others

National Focal Center:
Federal Environmental Agency (UBA)

BMU/UBA FE-No. 204 63 252

GIS&Mapping 06/2007:
Thomas Gauger, Claus Rösemann

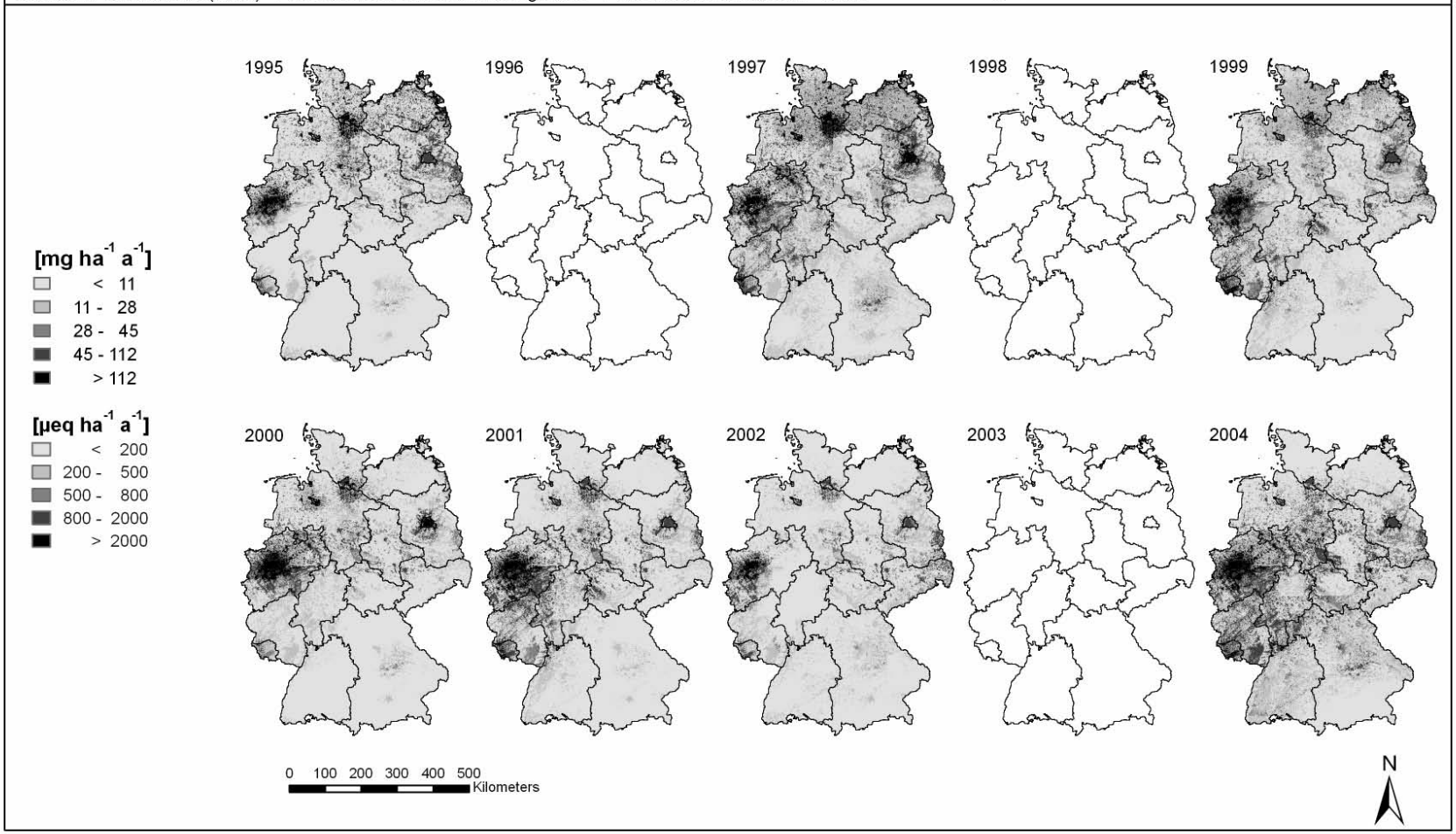

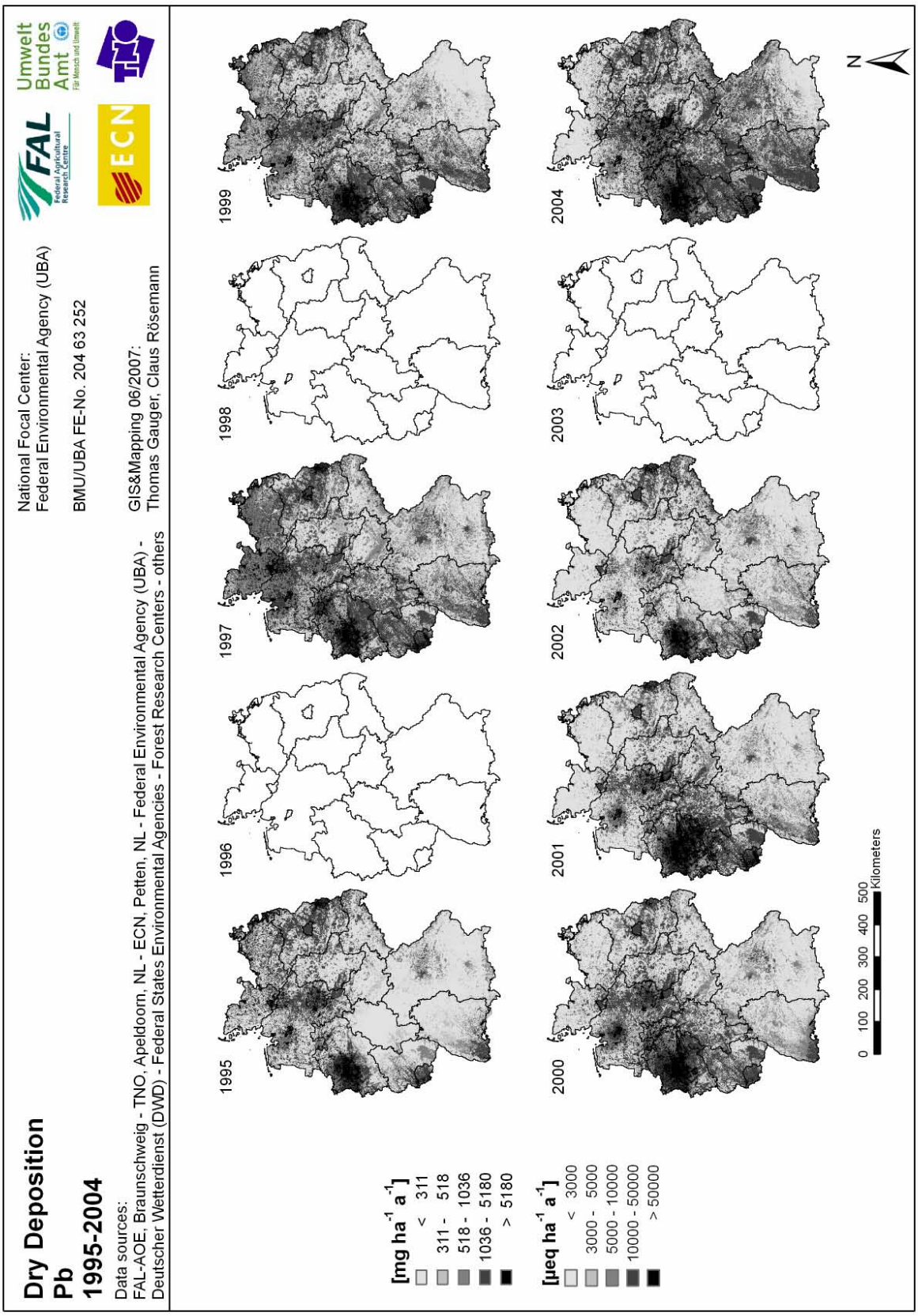

Map 7.10: Dry deposition of Pb 1995-2004

8 Cloud&fog deposition mapping results

Thomas Gauger & Claus Rösemann
Federal Agricultural Research Centre, Institute of Agroecology (FAL-AOE), Bundesallee 50, D-38116 Braunschweig
Bundesforschungsanstalt für Landwirtschaft, Institut für Agrarökologie (FAL-AOE), Bundesallee 50, D-38116 Braunschweig

The flux of cloud droplets and of droplets of radiative fog to the surface of exposed receptors in this study is termed cloud&fog (occult) deposition. Cloud&fog deposition, is calculated in a 1x1km² grid resolution for areas above 250m ASL in Germany. Hence it is modelled for about 46% of the terrestrial surface area of Germany. Estimates of cloud&fog deposition fluxes, however, are only applied for calculating total deposition of forested areas in Germany (cf. Chapter 9). The description of modelling procedures applied in order to calculate cloud&fog deposition fluxes using IDEM cloud deposition module can be found in Chapter 6.2.

8.1 Cloud&fog deposition fluxes and trends of non-sea salt base cations ($BC_{(nss)}$)

The sum of non-sea salt base cations ($BC_{(nss)}$) is calculated from non-sea salt Calcium ($Ca_{(nss)}$), non-sea salt Potassium ($K_{(nss)}$), and non-sea salt Magnesium ($Mg_{(nss)}$).

Over all years modelled no trend in any direction in annual average cloud&fog deposition of $BC_{(nss)}$ in the period from 1995 to 2004 can be found (cf. Figure 8.1).

Compared to 1995 average $BC_{(nss)}$ cloud&fog deposition flux in 2004 is 15.4% lower. This is within the range of changes between the single years of the time period considered (cf. Table 8.1). In 2003 average cloud&fog deposition flux is remarkable high. The mean value of $BC_{(nss)}$ cloud&fog deposition in 2003 is about 35% higher than the average of the other years.

Table 8.1: Budgets of average annual cloud&fog deposition of non-sea salt base cations 1995-2004

	$BC_{(nss)}$ [eq $ha^{-1}a^{-1}$]	% change from previous year
1995	27	
1996		
1997	30	+12.1
1998		
1999	25	-17.8
2000	28	+13.1
2001	32	+15.0
2002	35	+6.6
2003	44	+26.8
2004	23	-47.8
% change from 1995 to 2004		-15.4

The spatial patterns of the cloud&fog deposition flux of $BC_{(nss)}$ 1995, 1997, and 1999 to 2004 are shown in Map 8.1. Highest deposition regularly can be found in the forested low mountain ranges of the centre of Germany (mountains in Hesse, Thuringia; Harz in south western Lower Saxony).

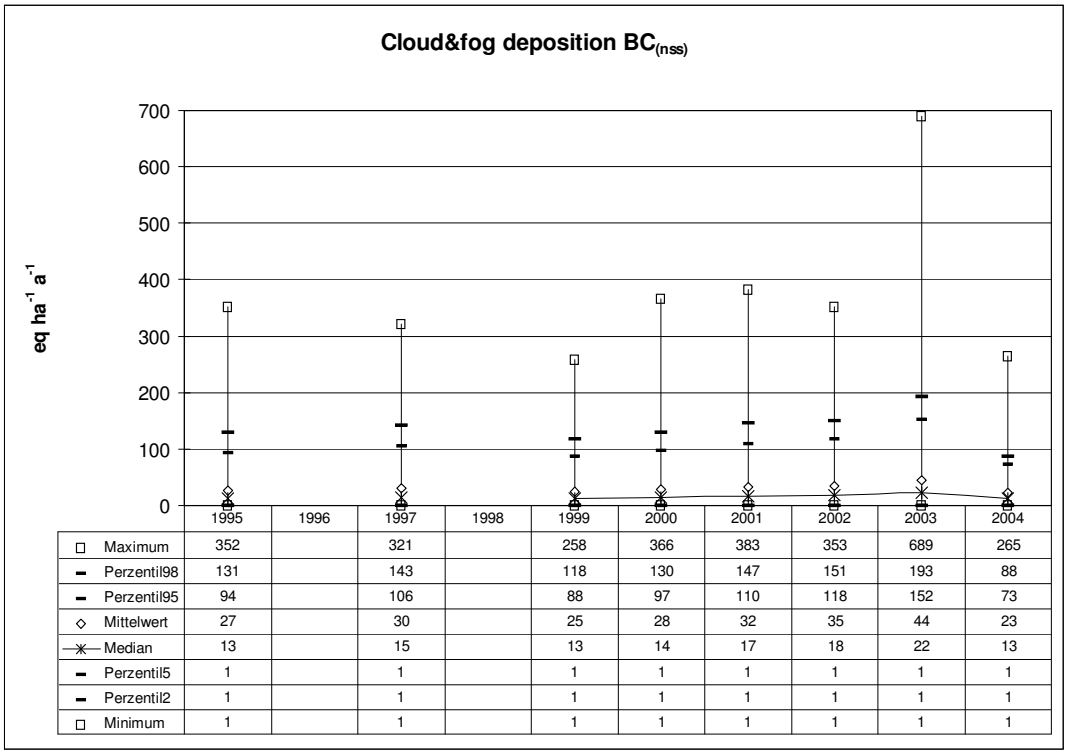

	1995	1996	1997	1998	1999	2000	2001	2002	2003	2004
Maximum	352		321		258	366	383	353	689	265
Perzentil98	131		143		118	130	147	151	193	88
Perzentil95	94		106		88	97	110	118	152	73
Mittelwert	27		30		25	28	32	35	44	23
Median	13		15		13	14	17	18	22	13
Perzentil5	1		1		1	1	1	1	1	1
Perzentil2	1		1		1	1	1	1	1	1
Minimum	1		1		1	1	1	1	1	1

Figure 8.1: Statistical evaluation of annual non-sea salt base cations ($BC_{(nss)}$) cloud&fog deposition 1995-2004

8.2 Cloud&fog deposition fluxes and trends of acidifying compounds and nitrogen

Acidification is caused by deposition loads of sulphur and nitrogen compounds. The atmospheric input of nitrogen, furthermore, causes nutrient imbalances and leads to eutrophication. Average annual cloud&fog deposition 1995 to 2004, and the percentage changes for sulphur (SO_X-$S_{(nss)}$), reduced, oxidised and total nitrogen (NH_X-N, NO_Y-N, N), respectively, are shown in Table 8.2. In the ten years period from 1995 to 2004 cloud&fog deposition of SO_X-$S_{(nss)}$ declined by 40%, while cloud&fog deposition of nitrogen (N) and its compounds 2004 is at the same level as in 1995.

Table 8.2: Budgets of average annual cloud&fog deposition of SO_X-$S_{(nss)}$, NH_X-N, NO_Y-N, and N 1995-2004

	SO_X-$S_{(nss)}$ [eq $ha^{-1}a^{-1}$]	% change from previous year	NH_X-N [eq $ha^{-1}a^{-1}$]	% change from previous year	NO_Y-N [eq $ha^{-1}a^{-1}$]	% change from previous year	N [eq $ha^{-1}a^{-1}$]	% change from previous year
1995	44		39		40		77	
1996								
1997	40	-8.5	42	+7.0	44	+8.9	83	+8.0
1998								
1999	32	-21.1	35	-17.4	39	-11.1	71	-14.6
2000	31	-1.5	36	+2.1	38	-1.2	71	+0.5
2001	40	+29.6	51	+42.9	53	+37.3	101	+41.0
2002	43	+7.4	52	+3.1	56	+5.9	105	+4.6
2003	45	+3.9	60	+14.7	62	+10.9	118	+12.6
2004	27	-41.2	38	-36.8	40	-34.6	76	-35.9
% change from 1995 to 2004		-39.6		-3.7		+0.8		-1.5

8.2.1 Cloud&fog deposition of non-sea salt sulphur (SO_X-$S_{(nss)}$)

Annual average cloud&fog deposition of non-sea salt Sulphur (SO_X-$S_{(nss)}$) from about 44 eq ha^{-1} a^{-1} (0.7 kg $ha^{-1}a^{-1}$ or 25.7 kt a^{-1}, respectively) in 1995 declines to about 31 eq ha^{-1} a^{-1} (0.5 kg $ha^{-1}a^{-1}$ or 17.8 kt a^{-1}, respectively) in 2000 (cf. Figure 8.2, Table 8.2). Although the modelled cloud&fog deposition data of 2004 is the lowest of all years considered, no directed trend over time can be found.

The spatial patterns of SO_X-$S_{(nss)}$ cloud&fog deposition are shown in Map 8.2. Highest deposition regularly can be found in the forested low mountain ranges in the centre of Germany (eastern North Rhine-Westphalia, Hesse, Thuringia, Harz Mountains).

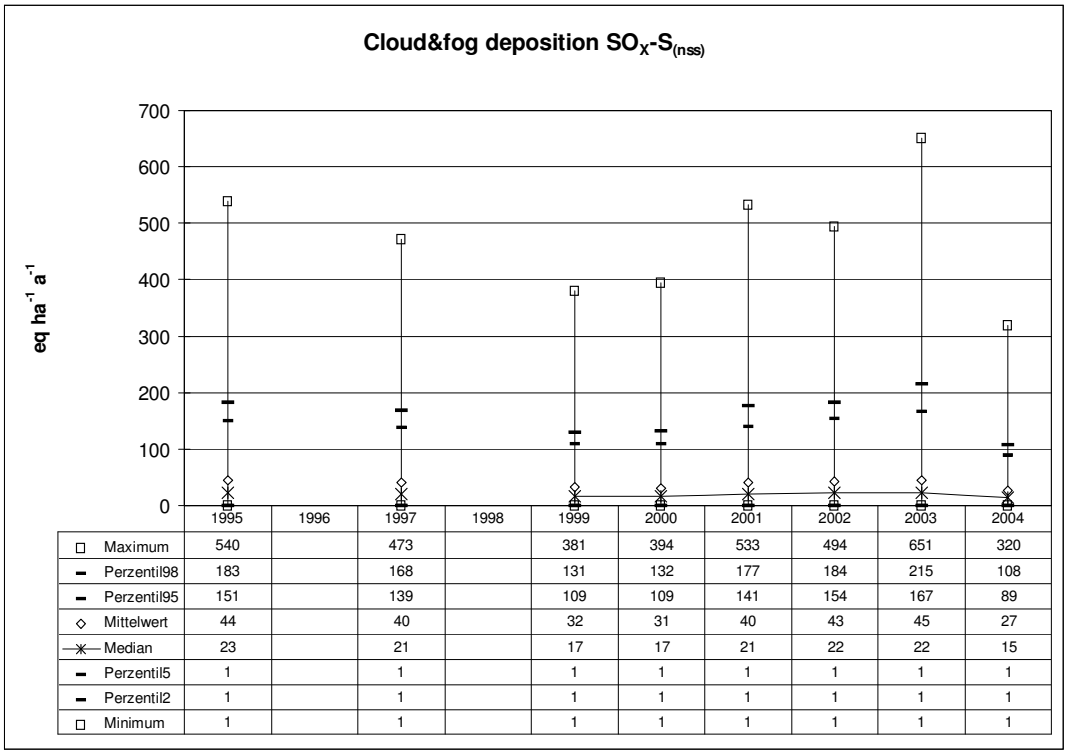

	1995	1996	1997	1998	1999	2000	2001	2002	2003	2004
Maximum	540		473		381	394	533	494	651	320
Perzentil98	183		168		131	132	177	184	215	108
Perzentil95	151		139		109	109	141	154	167	89
Mittelwert	44		40		32	31	40	43	45	27
Median	23		21		17	17	21	22	22	15
Perzentil5	1		1		1	1	1	1	1	1
Perzentil2	1		1		1	1	1	1	1	1
Minimum	1		1		1	1	1	1	1	1

Figure 8.2: Statistical evaluation of annual non-sea salt sulphur (SO_X-$S_{(nss)}$) cloud&fog deposition 1995-2004

8.2.2 Cloud&fog deposition of reduced nitrogen (NHX-N)

No trend of NH_X-N cloud&fog deposition fluxes from 1995 to 1999 can be observed. From 1999 onward average cloud&fog deposition fluxes are slightly rising, and in 2003 highest annual average deposition loads of about 60 eq $ha^{-1}a^{-1}$, 0.8 kg $ha^{-1}a^{-1}$, respectively, can be observed. Average cloud&fog deposition in 2004 (39 eq $ha^{-1}a^{-1}$ or 0.5 kg $ha^{-1}a^{-1}$, respectively) is about the same level as the mean value of 1995 data (38 eq $ha^{-1}a^{-1}$ or 0.5 kg $ha^{-1}a^{-1}$, respectively).

The overall spatial patterns of NH_X-N cloud&fog deposition are presented in Map 8.3. Highest modelled cloud&fog deposition fluxes of NH_X-N in all years considered can be found in forested low mountain ranges situated in central Germany, in the Bavarian Forest, and in the Alps.

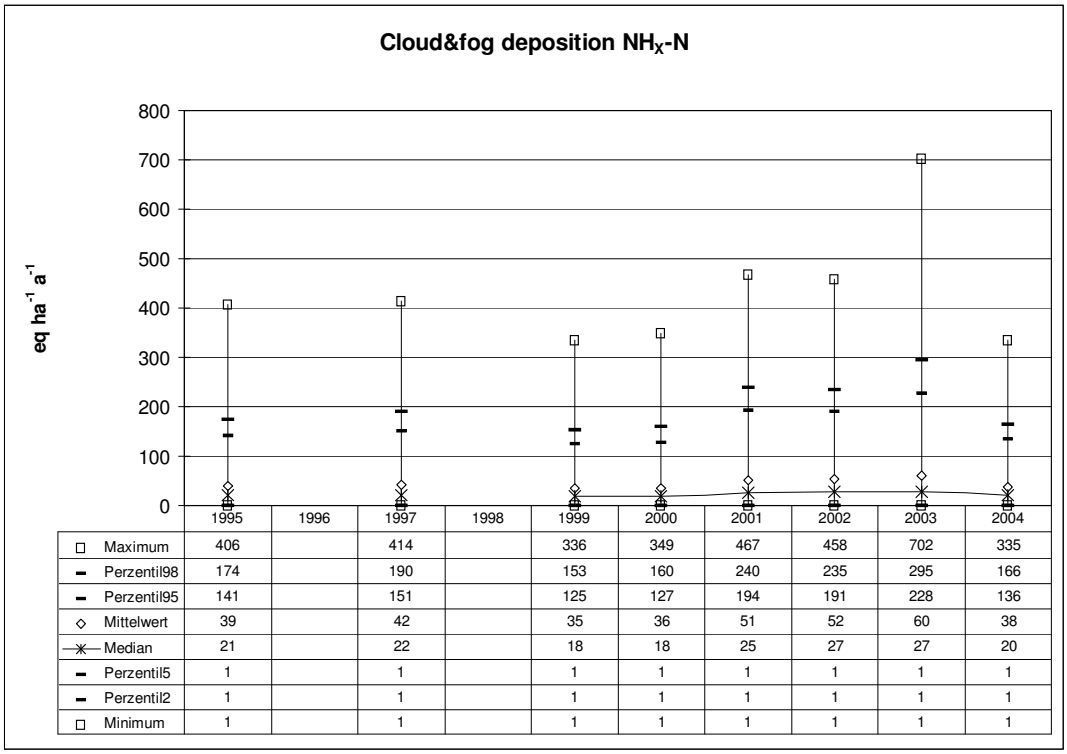

	1995	1996	1997	1998	1999	2000	2001	2002	2003	2004
Maximum	406		414		336	349	467	458	702	335
Perzentil98	174		190		153	160	240	235	295	166
Perzentil95	141		151		125	127	194	191	228	136
Mittelwert	39		42		35	36	51	52	60	38
Median	21		22		18	18	25	27	27	20
Perzentil5	1		1		1	1	1	1	1	1
Perzentil2	1		1		1	1	1	1	1	1
Minimum	1		1		1	1	1	1	1	1

Figure 8.3: Statistical evaluation of annual reduced nitrogen (NHX-N) cloud&fog deposition 1995-2004

8.2.3 Cloud&fog deposition of oxidised nitrogen (NO_Y-N)

In general cloud&fog deposition fluxes of oxidised nitrogen (NO_Y-N) are almost at the same level as cloud&fog deposition of reduced nitrogen (NH_X-N). In every year considered annual average NO_Y-N cloud&fog flux is only about 1 to 4 eq $ha^{-1}a^{-1}$ above the respective annual average NH_X-N flux. The spatial patterns of cloud&fog deposition fluxes of reduced and oxidised nitrogen over Germany are very similar (c.f. Map 8.3 and 8.4).

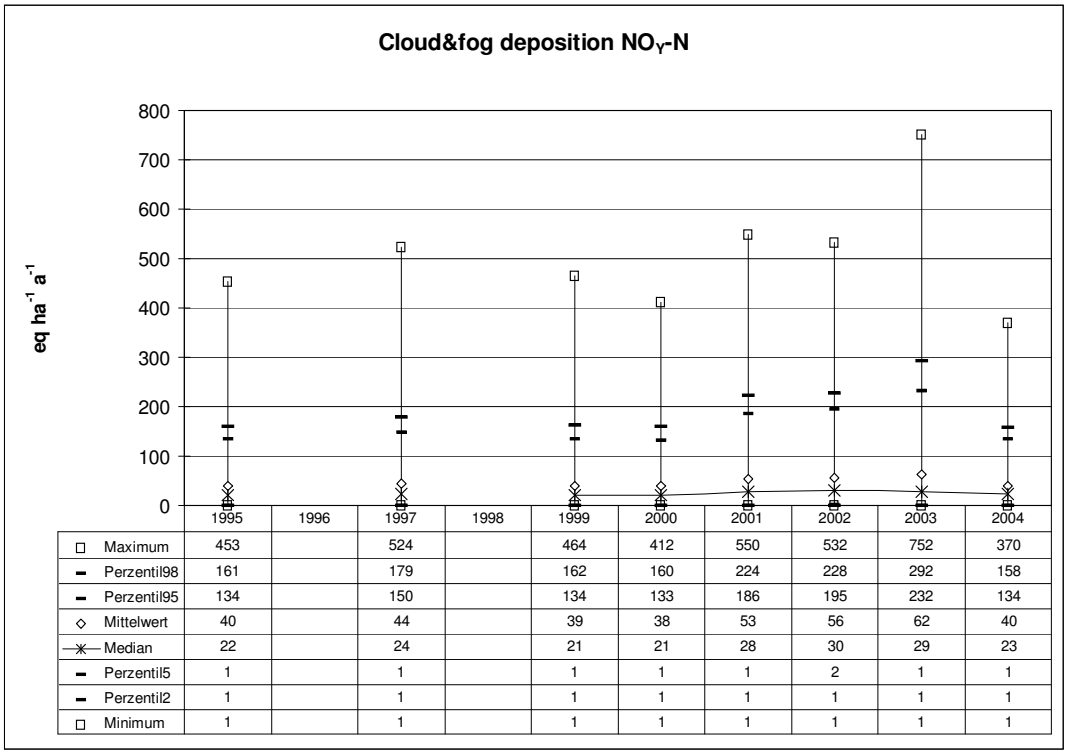

	1995	1996	1997	1998	1999	2000	2001	2002	2003	2004
Maximum	453		524		464	412	550	532	752	370
Perzentil98	161		179		162	160	224	228	292	158
Perzentil95	134		150		134	133	186	195	232	134
Mittelwert	40		44		39	38	53	56	62	40
Median	22		24		21	21	28	30	29	23
Perzentil5	1		1		1	1	1	2	1	1
Perzentil2	1		1		1	1	1	1	1	1
Minimum	1		1		1	1	1	1	1	1

Figure 8.4: Statistical evaluation of annual oxidised nitrogen (NO_Y-N) cloud&fog deposition 1995-2004

8.2.4 Cloud&fog deposition of total nitrogen (N = NH_X-N + NO_Y-N)

Since cloud&fog deposition of reduced (NH_X-N) and oxidised nitrogen (NO_Y-N) in each year considered are very similar, both horizontally, and as the order of magnitude of the cloud&fog deposition loads is concerned, total nitrogen (N) cloud&fog deposition flux, calculated as the sum of the two compounds, over time shows the same changes and spatial patterns.

From 1995 to 1999 no trend can be observed, whereas from 2000 to 2003 increasing average cloud&fog deposition fluxes can be found. In 2003 average cloud&fog flux over Germany is 118 eq $ha^{-1}a^{-1}$, 1.7 kg $ha^{-1}a^{-1}$ or 59.2 kt a^{-1}, respectively. From 2003 to 2004 a 36% decline of average cloud&fog deposition loads to about the same level as in 1995 can be observed. In 2004 average N cloud&fog flux is about 76 eq $ha^{-1}a^{-1}$, 1.1 kg $ha^{-1}a^{-1}$ or 38.1 kt a^{-1}, respectively (Figure 8.5).

The average fractions of reduced and oxidised nitrogen to total nitrogen cloud&fog deposition fluxes are listed in Table 8.3. Over time the ratio between the two fractions is varying only to small extent (in the range of 2.2%), and each compound contributes by about 50% to total nitrogen.
Graphs of modelled cloud&fog deposition fluxes of total nitrogen are presented in Map 8.5. Like in Map 8.3 and 8.4, highest cloud&fog deposition fluxes in Germany can be observed over forested low mountain ranges in the centre of Germany, in the Bavarian Forest, and in the Alps.

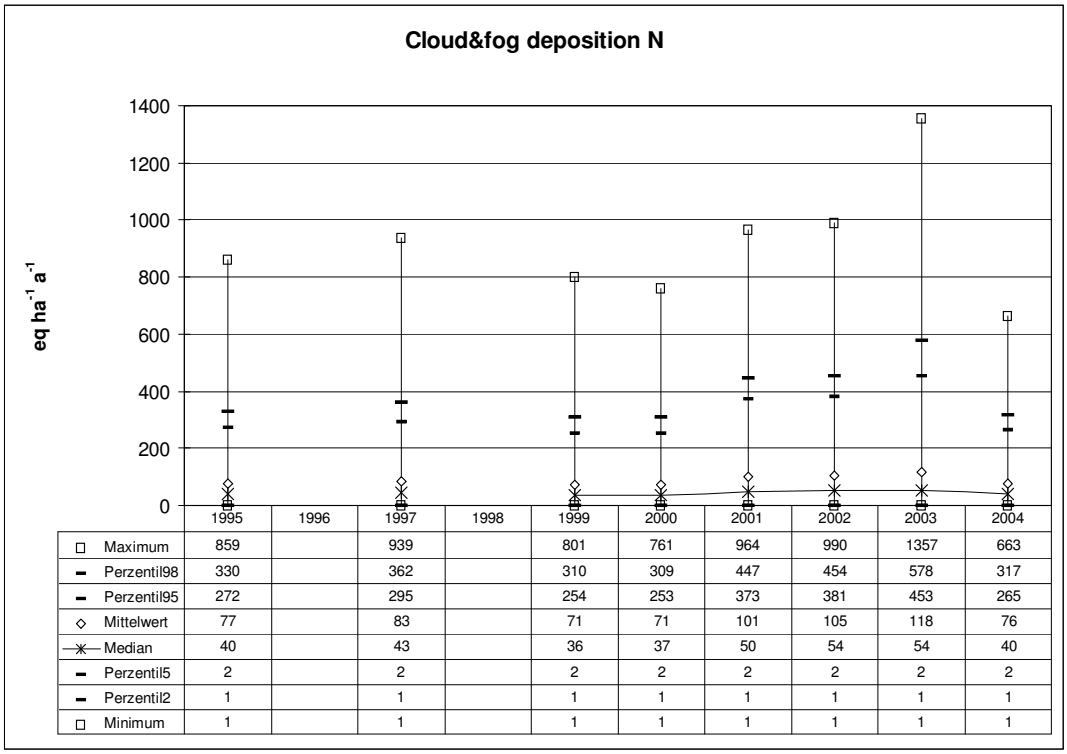

	1995	1996	1997	1998	1999	2000	2001	2002	2003	2004
Maximum	859		939		801	761	964	990	1357	663
Perzentil98	330		362		310	309	447	454	578	317
Perzentil95	272		295		254	253	373	381	453	265
Mittelwert	77		83		71	71	101	105	118	76
Median	40		43		36	37	50	54	54	40
Perzentil5	2		2		2	2	2	2	2	2
Perzentil2	1		1		1	1	1	1	1	1
Minimum	1		1		1	1	1	1	1	1

Figure 8.5: Statistical evaluation of annual total nitrogen (N) cloud&fog deposition 1995-2004

Table 8.3: Average NH_X-N and NO_Y-N fraction of cloud&fog deposited N 1995 to 2004

	1995	1996	1997	1998	1999	2000	2001	2002	2003	2004
NH_X-N [%]	49.5		49.1		47.3	48.1	49.1	48.4	49.2	48.4
NO_Y-N [%]	50.5		50.9		52.7	51.9	50.9	51.6	50.8	51.6

8.2.5 Cloud&fog deposition of potential acidity (AC_{pot} = SO_X-$S_{(nss)}$ + N)

Cloud&fog deposition of potential acidity is calculated as the sum of non-sea salt sulphur and total nitrogen (AC_{pot} = SO_X-$S_{(nss)}$ + N). Average cloud&fog deposition fluxes of AC_{pot} from 1995 to 2004 have diminished by about 15.6% (cf. Table 8.4 and Figure 8.7). The decline is only due to the reduction of sulphur deposition because the average cloud&fog deposition of nitrogen in 2004 approximates the data of 1995 (cf. Table 8.2 and Figure 8.7).

The average fractions of the single compound cloud&fog fluxes of AC_{pot} in Germany 1995 to 2004 are listed in Table 8.4. Total N cloud&fog deposition flux in 1995 is contributing by little less than about two third (64%) to cloud&fog AC_{pot} flux in Germany, SO_X-$S_{(nss)}$ is contributing little more than one third (36%). In 2004 about one quarter of cloud&fog AC_{pot} flux is formed by SO_X-$S_{(nss)}$, while three quarters are due to the total N cloud&fog flux.

Table 8.4: Average fractions of acidifying compounds of cloud&fog deposition 1995-2004

	1995	1996	1997	1998	1999	2000	2001	2002	2003	2004
SO_X-S [%]	36		32		30	29	28	28	27	25
N [%]	64		68		70	71	72	72	73	75
NH_X-N [%]	32		33		33	34	35	35	36	36
NO_Y-N [%]	32		35		37	37	37	37	37	39

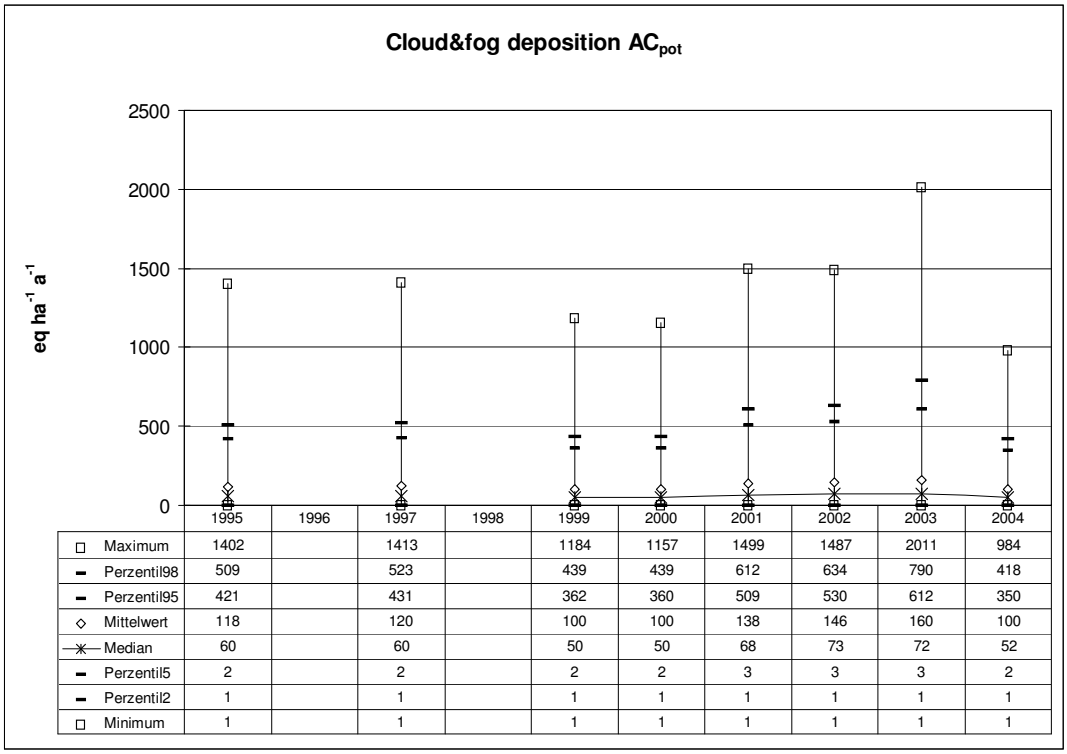

	1995	1996	1997	1998	1999	2000	2001	2002	2003	2004
Maximum	1402		1413		1184	1157	1499	1487	2011	984
Perzentil98	509		523		439	439	612	634	790	418
Perzentil95	421		431		362	360	509	530	612	350
Mittelwert	118		120		100	100	138	146	160	100
Median	60		60		50	50	68	73	72	52
Perzentil5	2		2		2	2	3	3	3	2
Perzentil2	1		1		1	1	1	1	1	1
Minimum	1		1		1	1	1	1	1	1

Figure 8.6: Statistical evaluation of annual potential acidity (AC_{pot}) cloud&fog deposition 1995-2004

A graphic overview of the annual average composition of the cloud&fog fluxes of AC_{pot} in Germany 1995 to 2004 is shown in Figure 8.7 on the basis of annual average cloud&fog fluxes of NH_X-N, NO_Y-N, and SO_X-$S_{(nss)}$. In 1995 SO_X-$S_{(nss)}$ is the main acidifying compound. From 1997 onward the contribution of SO_X-$S_{(nss)}$ to AC_{pot} is the least one, while annual average NO_Y-N cloud&fog flux is the dominating compound of $AC_{(pot)}$. From 1997 onward also annual average NH_X-N cloud&fog flux contributes more to AC_{pot} than SO_X-$S_{(nss)}$ does.

The spatial patterns of AC_{pot} cloud&fog deposition are presented in Map 8.6. The scatter of regions with higher or lower fluxes than average resembles that of total N cloud&fog deposition maps for the respective years (cf. Map 8.5), due to the dominating role of N as acidifying compound.

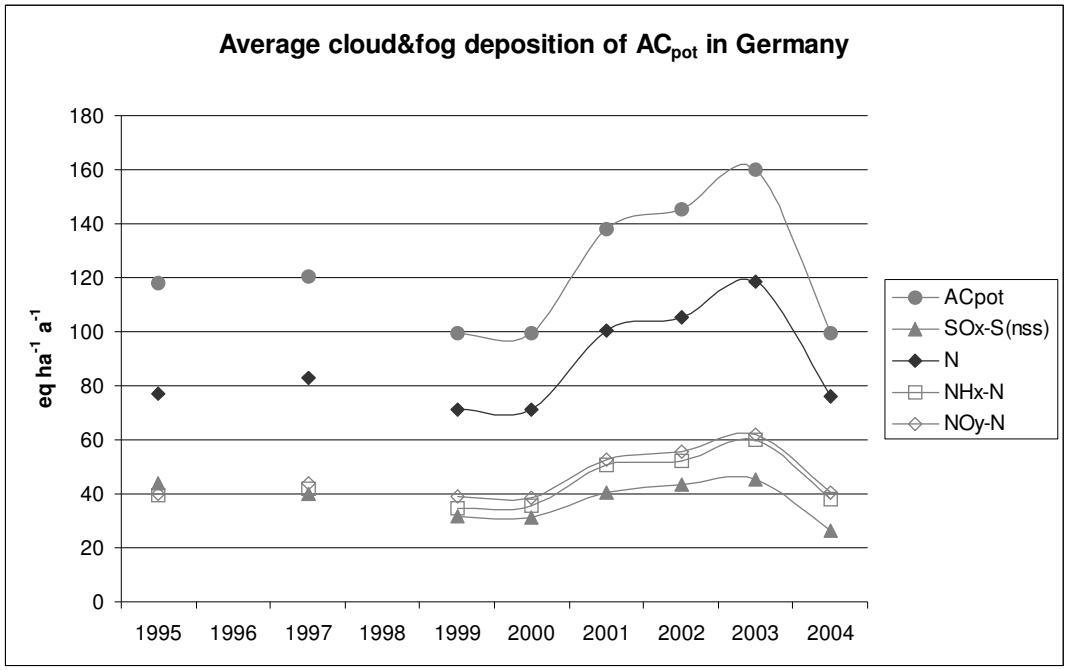

Figure 8.7: Average cloud&fog deposition of potential acidity (AC_{pot}) and its compounds 1995-2004

8.2.6 Cloud&fog deposition of potential net-acidity (ACpot(net) = SOX-S(nss) + N – BC(nss)) and acid neutralisation (= BC(nss) · 100 / ACpot [%])

Potential net-acidity is calculated by subtracting the fluxes of non-sea salt base cations ($BC_{(nss)}$) from the sum of potential acidifying compounds (AC_{pot}) in order to account for potential acid neutralisation. Hence cloud&fog deposition loads of $AC_{pot(net)}$ are lower than cloud&fog deposition loads of AC_{pot}.

The difference between the average cloud&fog deposition of $AC_{pot(net)}$ in 1995 and 2004 is a 15.8% (about 15 eq ha^{-1} a^{-1}) lower flux (Figure 8.8, Table 8.5).

Acid neutralisation by cloud&fog deposition of non-sea salt base cations ($BC_{(nss)}$) in the period 1995 to 2004 is shown in Figure 8.9. The annual average values of acid neutralisation are varying from 20% in 1995 up to 28% in 2003. The spatial patterns of $AC_{pot(net)}$ are shown in Map 8.7, the acid neutralisation by cloud&fog deposition of $BC_{(nss)}$ is presented in Map 8.8, respectively. The highest values of $AC_{pot(net)}$ can be found in the forested low mountain ranges in the centre of Germany and near the border to the Czech Republic in the Ore Mountains and in the Bavarian Forest. Hence acid neutralisation in these regions is lowest (cf. Map 8.8).

Budgets of average cloud&fog deposition of AC_{pot}, $AC_{pot(net)}$ and acid neutralisation by $BC_{(nss)}$ from 1995 to 2004 are listed in Table 8.5.

An overview on annual average AC_{pot}, $AC_{pot(net)}$, and $BC_{(nss)}$ cloud&fog fluxes over Germany 1995 to 2004 is given in Figure 8.10. Over the time period considered lowest annual average cloud&fog fluxes of $BC_{(nss)}$ can be observed in 1999 (25 eq ha^{-1} a^{-1}), lowest annual average cloud&fog flux of AC_{pot} (100 eq ha^{-1} a^{-1}) and $AC_{pot(net)}$ (74 eq ha^{-1} a^{-1}) in 2000, respectively (cf. Table 8.5). From 2000 to 2003 increasing average cloud&fog fluxes of AC_{pot} and $AC_{pot(net)}$ can be observed. In 2004 average cloud&fog flux of AC_{pot} and of $AC_{pot(net)}$ can be found on the same level as in 1999 (100 eq ha^{-1} a^{-1} and 79 eq ha^{-1} a^{-1}, respectively).

Since acid neutralisation depends on both, the flux of $BC_{(nss)}$ (cf. Map 8.1) and the flux of AC_{pot} (cf. Map 8.6), spatial patterns of acid neutralisation (cf. Map 8.8) are not matching the spatial patterns of $BC_{(nss)}$.

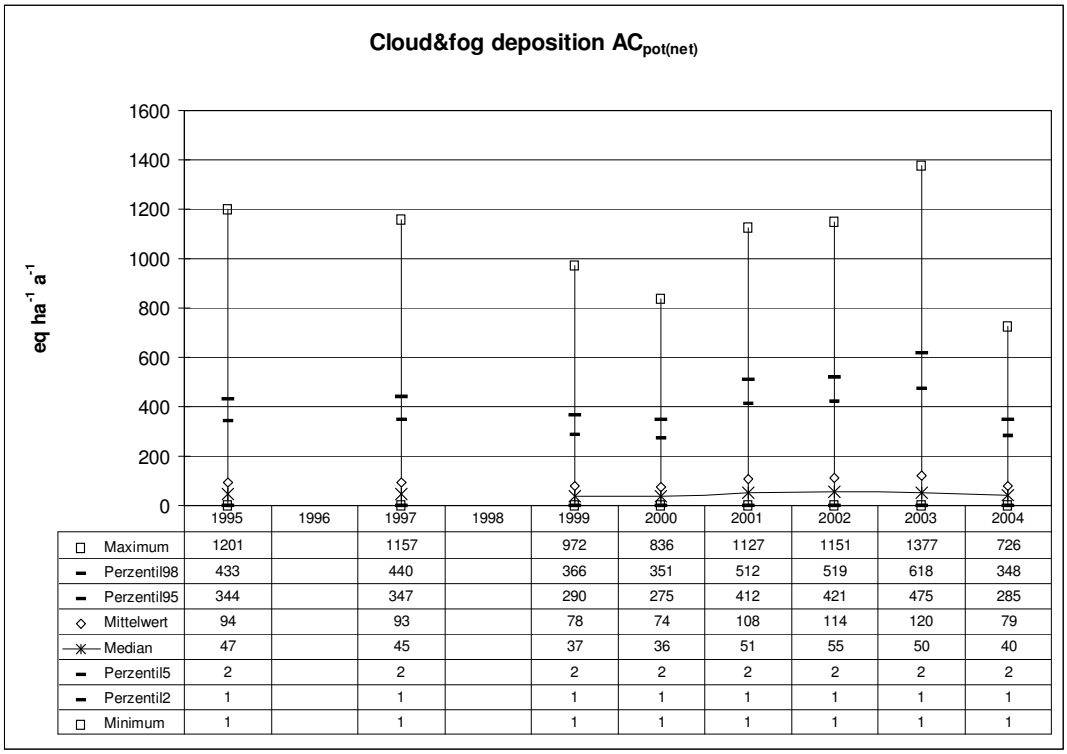

	1995	1996	1997	1998	1999	2000	2001	2002	2003	2004
Maximum	1201		1157		972	836	1127	1151	1377	726
Perzentil98	433		440		366	351	512	519	618	348
Perzentil95	344		347		290	275	412	421	475	285
Mittelwert	94		93		78	74	108	114	120	79
Median	47		45		37	36	51	55	50	40
Perzentil5	2		2		2	2	2	2	2	2
Perzentil2	1		1		1	1	1	1	1	1
Minimum	1		1		1	1	1	1	1	1

Figure 8.8: Statistical evaluation of annual potential net acidity ($AC_{pot(net)}$) cloud&fog deposition 1995-2004

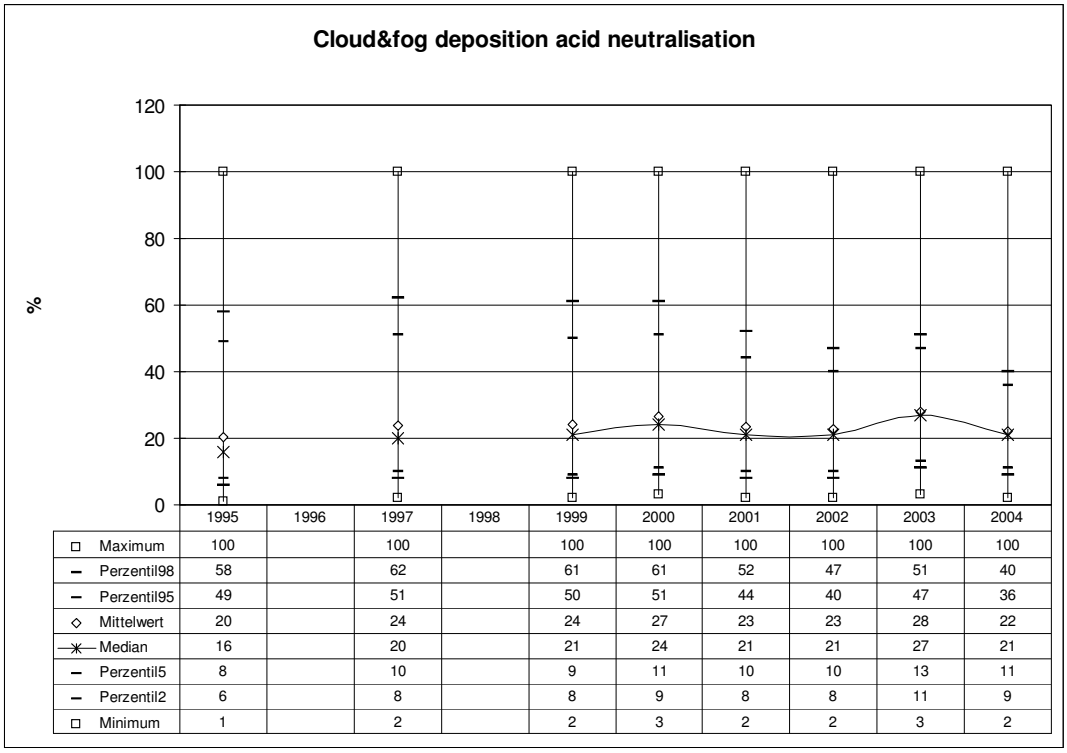

	1995	1996	1997	1998	1999	2000	2001	2002	2003	2004
Maximum	100		100		100	100	100	100	100	100
Perzentil98	58		62		61	61	52	47	51	40
Perzentil95	49		51		50	51	44	40	47	36
Mittelwert	20		24		24	27	23	23	28	22
Median	16		20		21	24	21	21	27	21
Perzentil5	8		10		9	11	10	10	13	11
Perzentil2	6		8		8	9	8	8	11	9
Minimum	1		2		2	3	2	2	3	2

Figure 8.9: Statistical evaluation of annual acid neutralisation in cloud&fog deposition 1995-2004

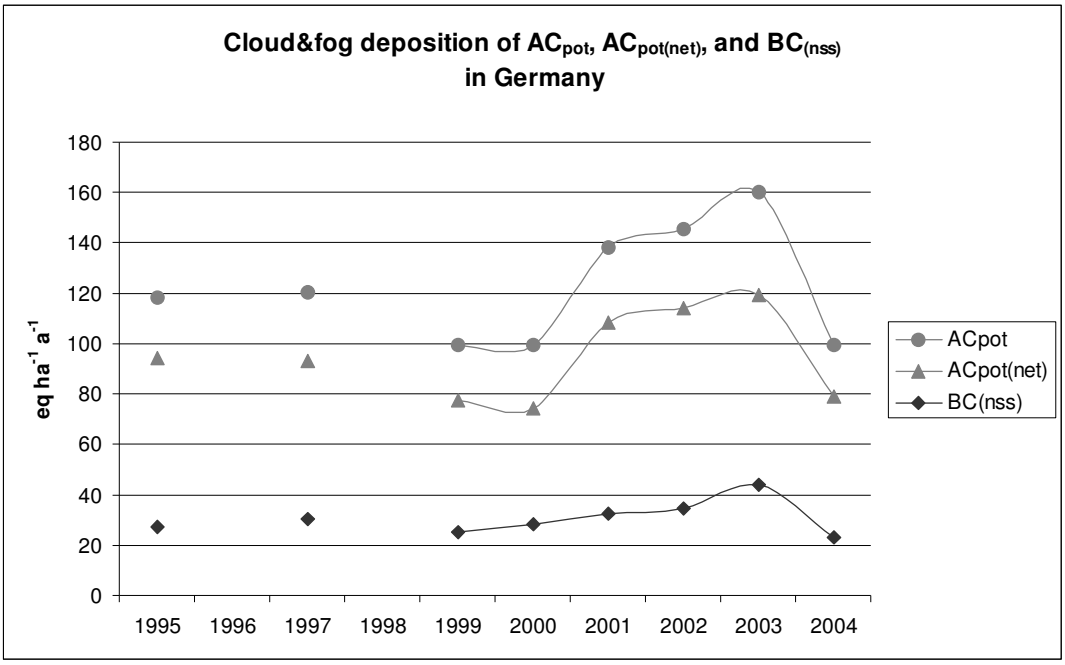

Figure 8.10: Average cloud&fog deposition of AC_{pot}, $AC_{pot(net)}$, and $BC_{(nss)}$ 1995-2004

Table 8.5: Budgets of average annual cloud&fog deposition of AC_{pot}, $AC_{pot(net)}$, and acid neutralisation by $BC_{(nss)}$ 1995-2004

	AC_{pot} [eq $ha^{-1}a^{-1}$]	% change from previous year	$AC_{pot(net)}$ [eq $ha^{-1}a^{-1}$]	% change from previous year	$BC_{(nss)}$ [eq $ha^{-1}a^{-1}$]	% change from previous year	Acid neu-tralisation [%]
1995	118		94		27		20
1996							
1997	120	+1.9	93	-1.0	30	+12.1	24
1998							
1999	100	-17.2	78	-16.6	25	-17.8	24
2000	100	-0.1	74	-4.2	28	+13.1	27
2001	138	+38.5	108	+45.8	32	+15.0	23
2002	146	+5.5	114	+5.1	35	+6.6	23
2003	160	+9.9	120	+5.0	44	+26.8	28
2004	100	-37.7	79	-33.8	23	-47.8	22
% change from 1995 to 2004		-15.6		-15.8		-15.4	

8.3 Maps of cloud&fog deposition 1995, 1997, 1999-2004

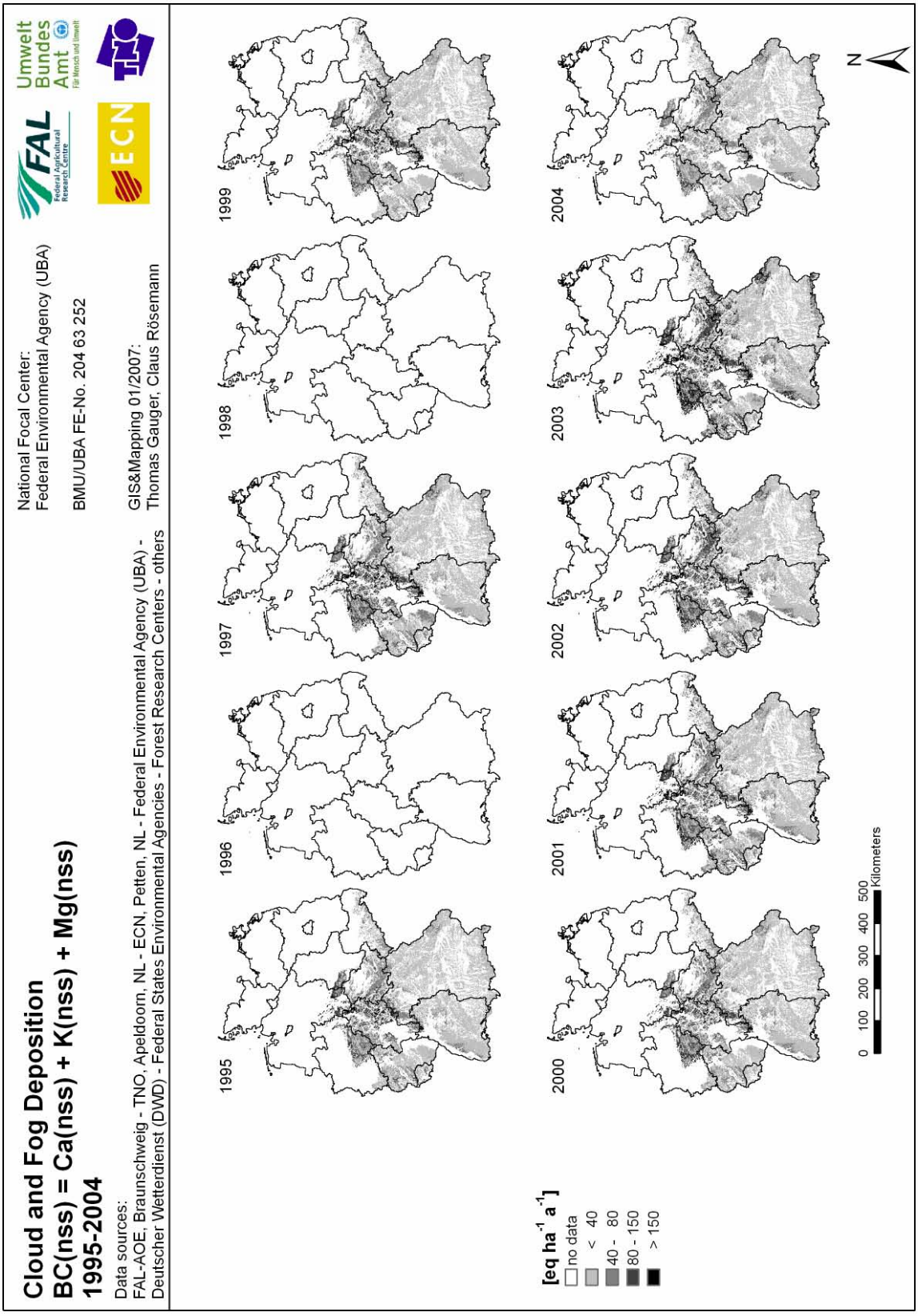

Map 8.1: Cloud&fog deposition of $BC_{(nss)}$ 1995-2004

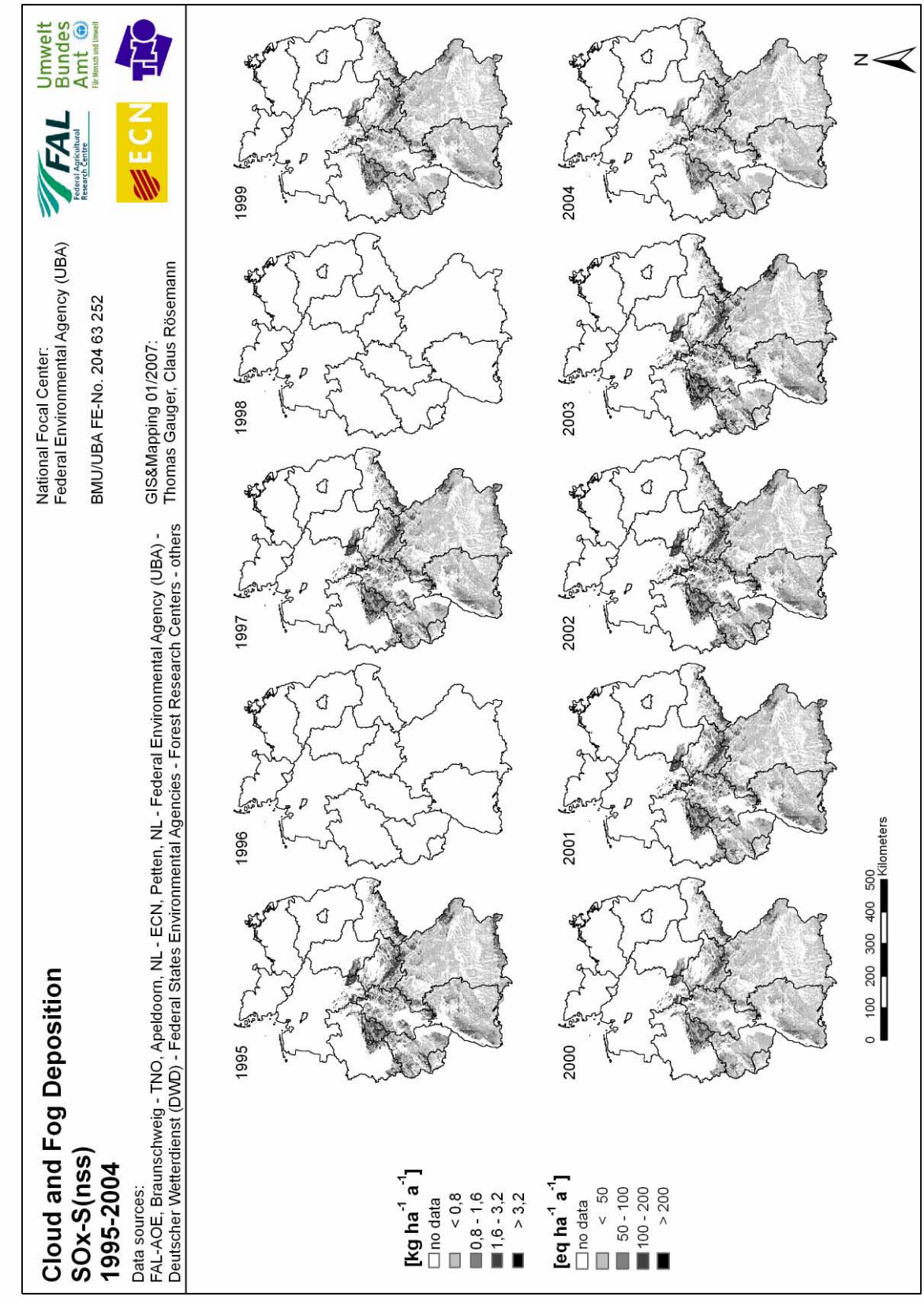

Map 8.2: Cloud&fog deposition of SO_X-$S_{(nss)}$ 1995-2004

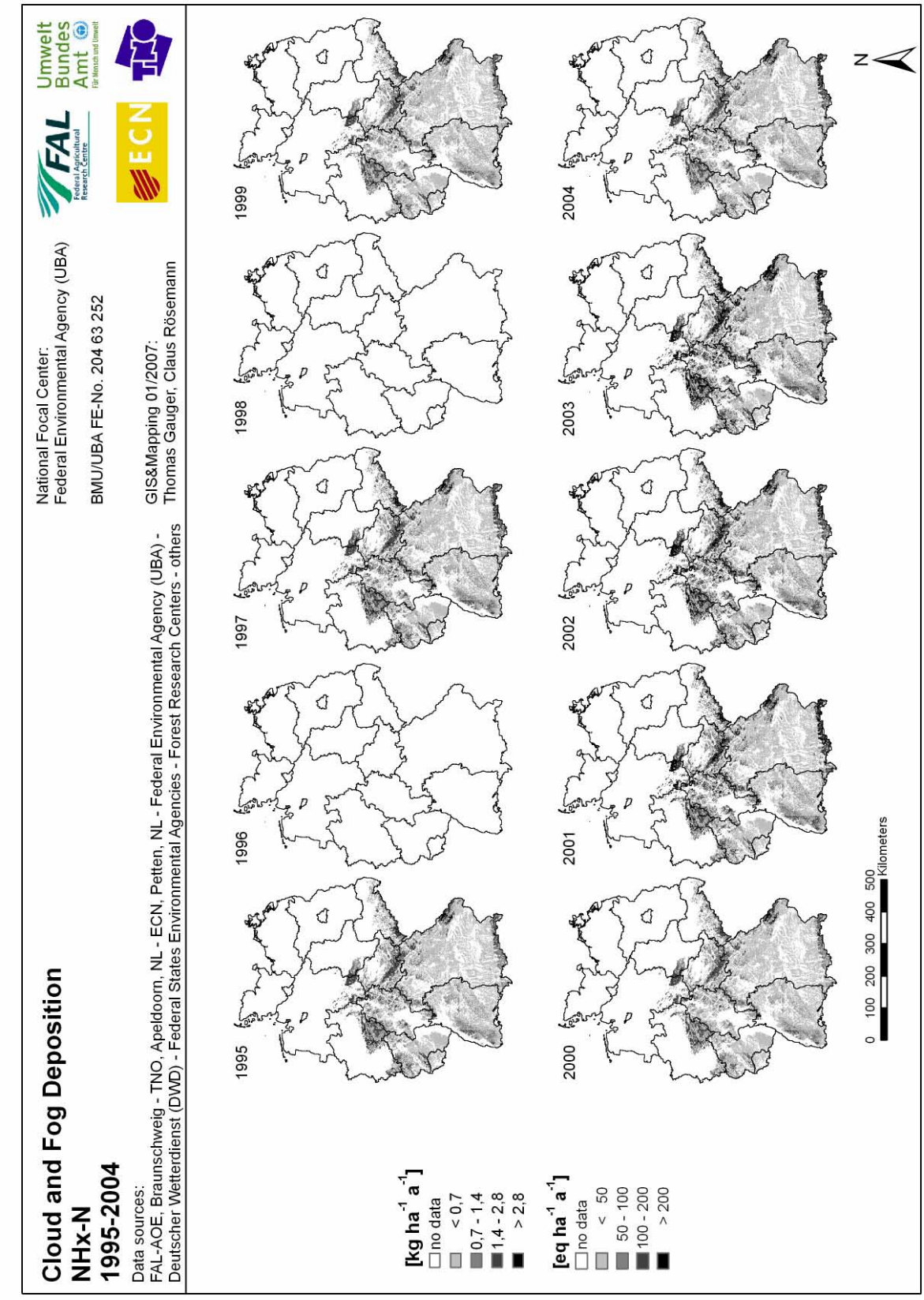

Map 8.3: Cloud&fog deposition of NH_X-N 1995-2004

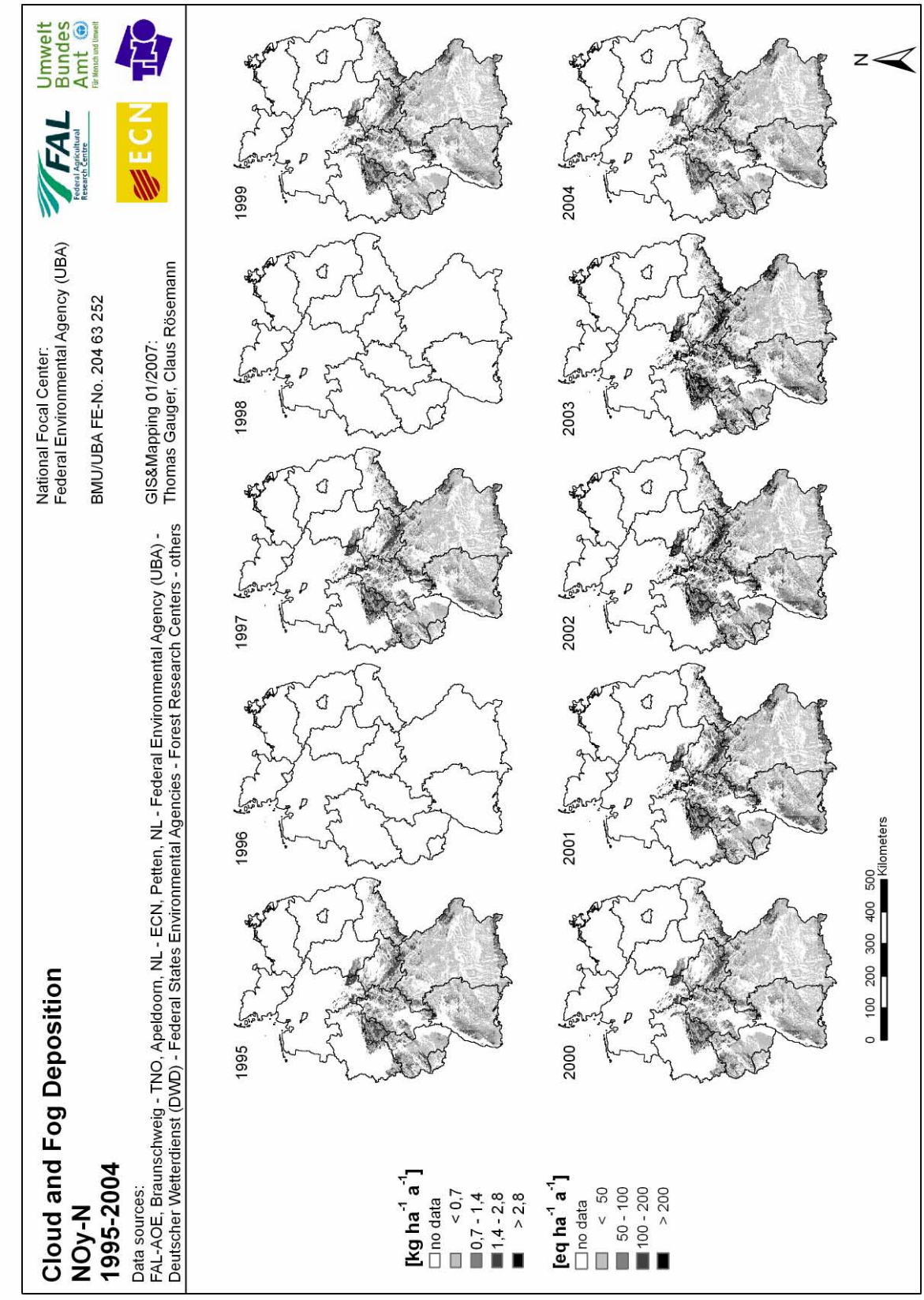

Map 8.4: Cloud&fog deposition of NO_Y-N 1995-2004

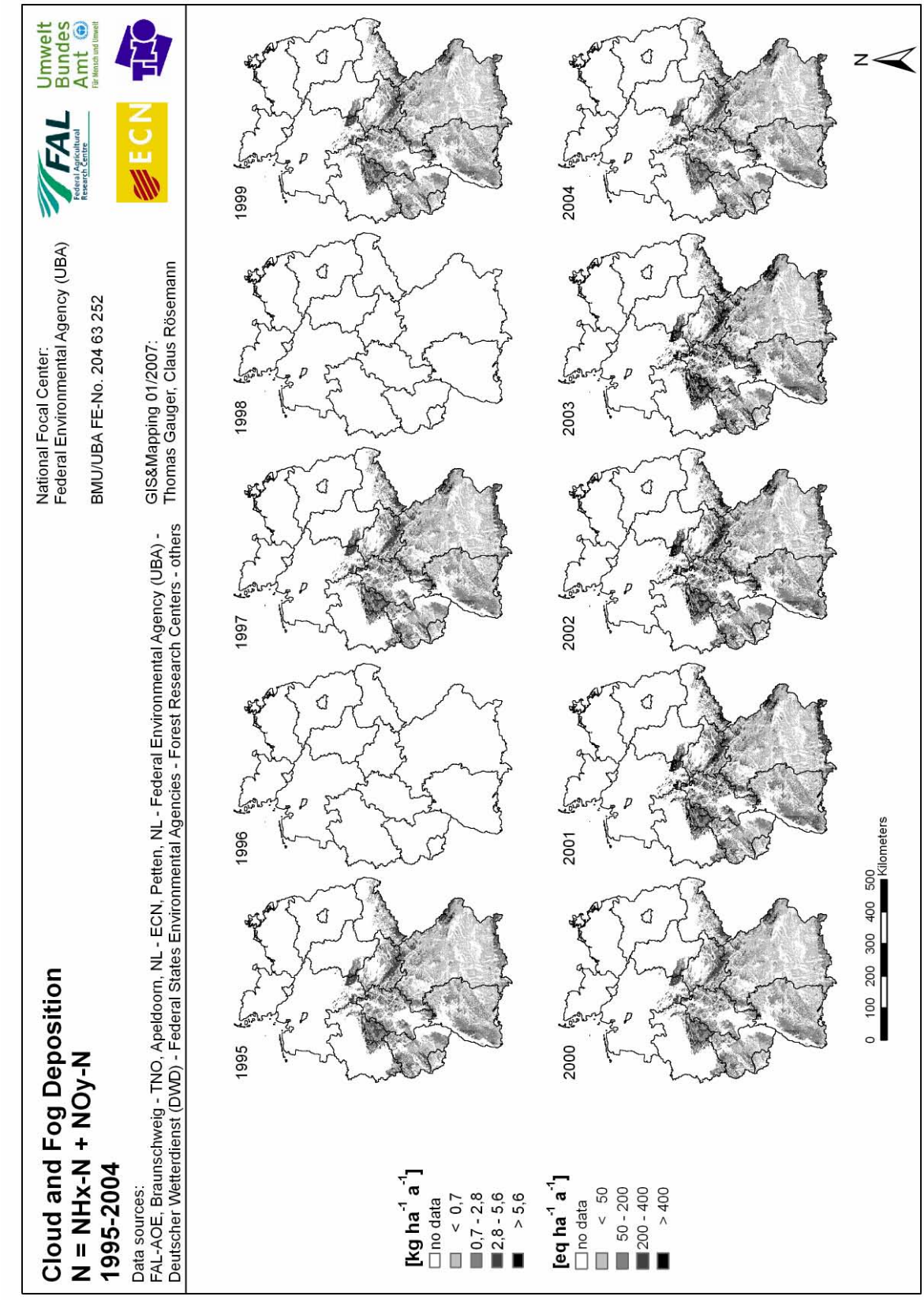

Map 8.5: Cloud&fog deposition of N 1995-2004

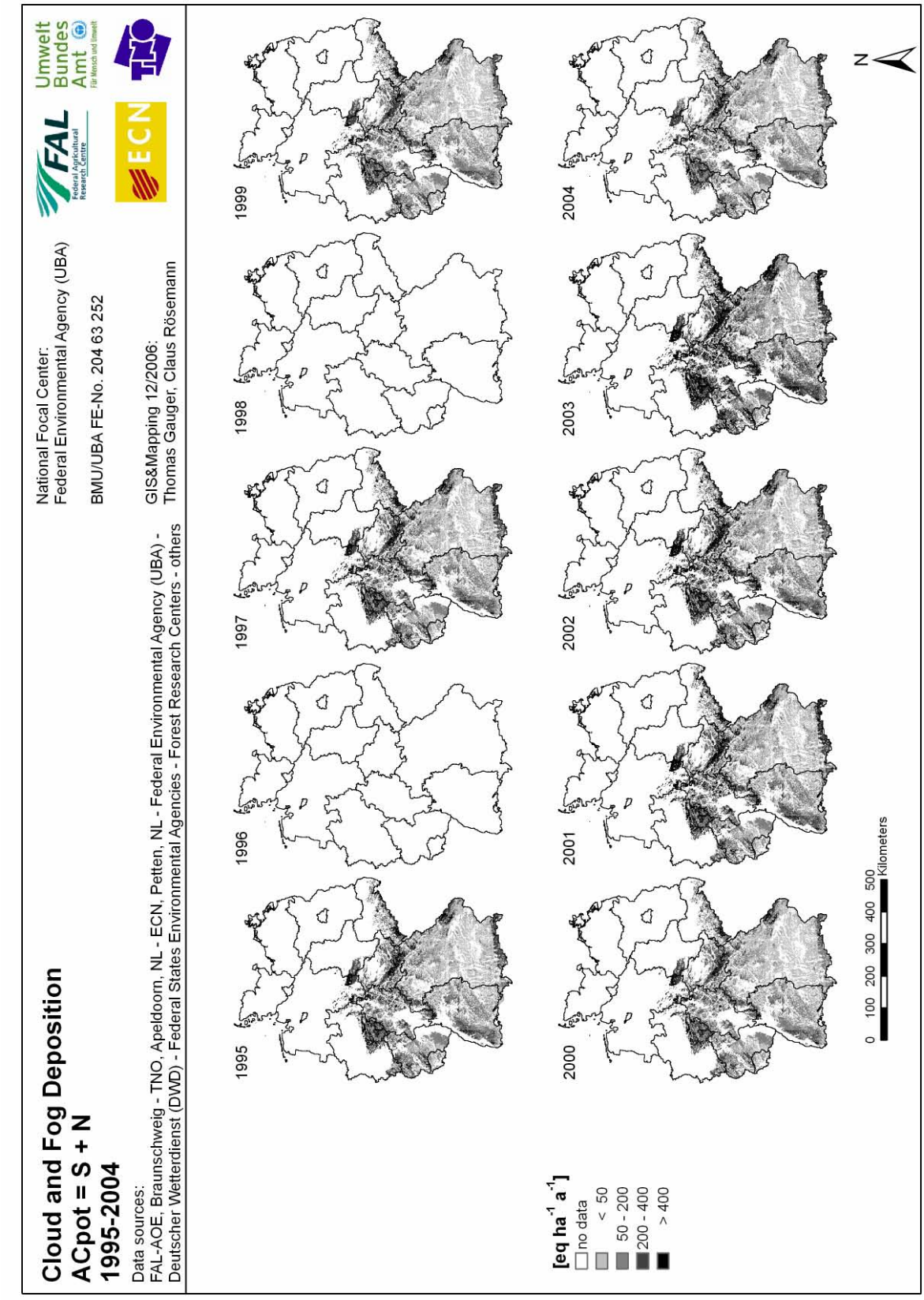

Map 8.6: Cloud&fog deposition of AC_{pot} 1995-2004

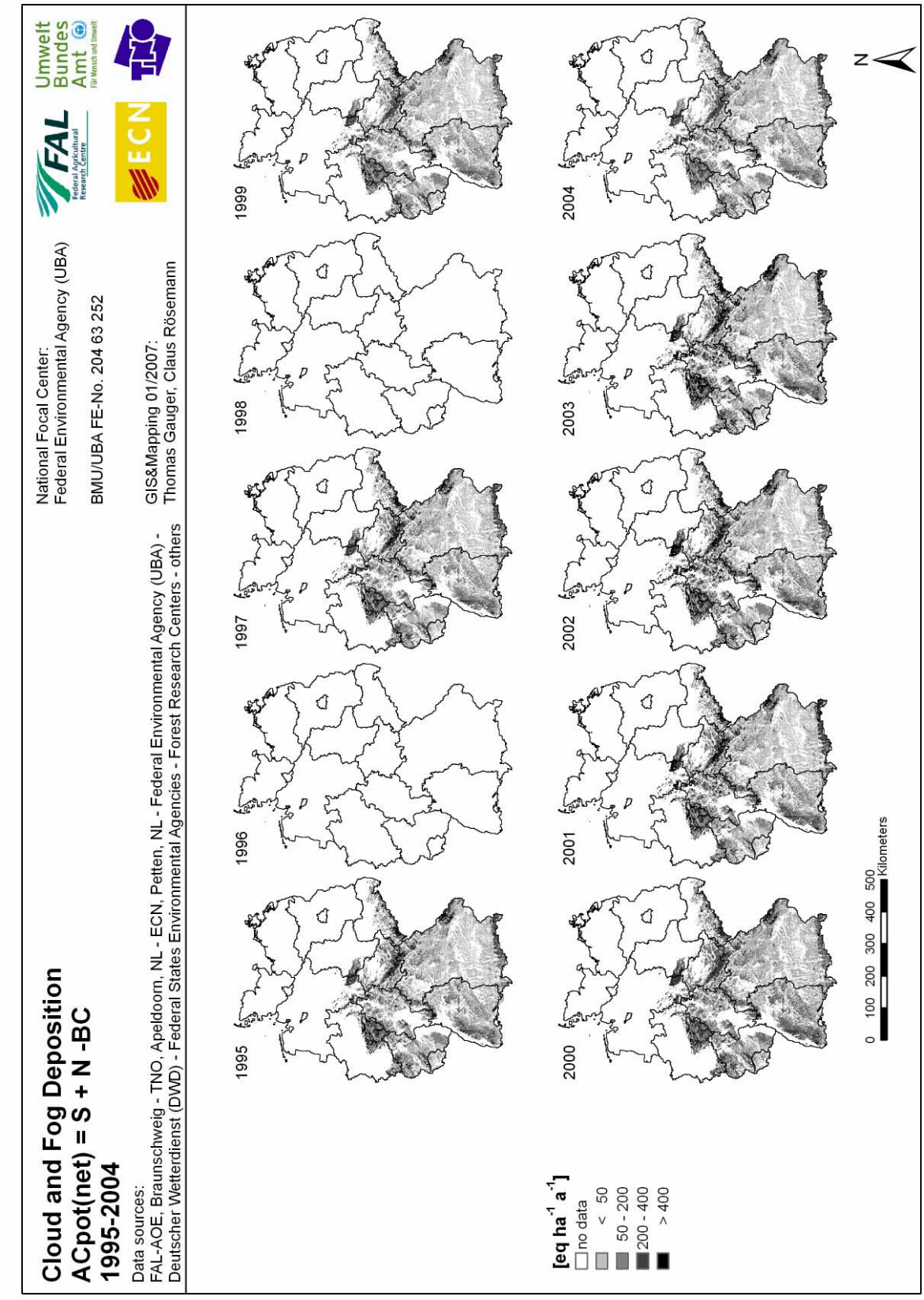

Map 8.7: Cloud&fog deposition of $AC_{pot(net)}$ 1995-2004

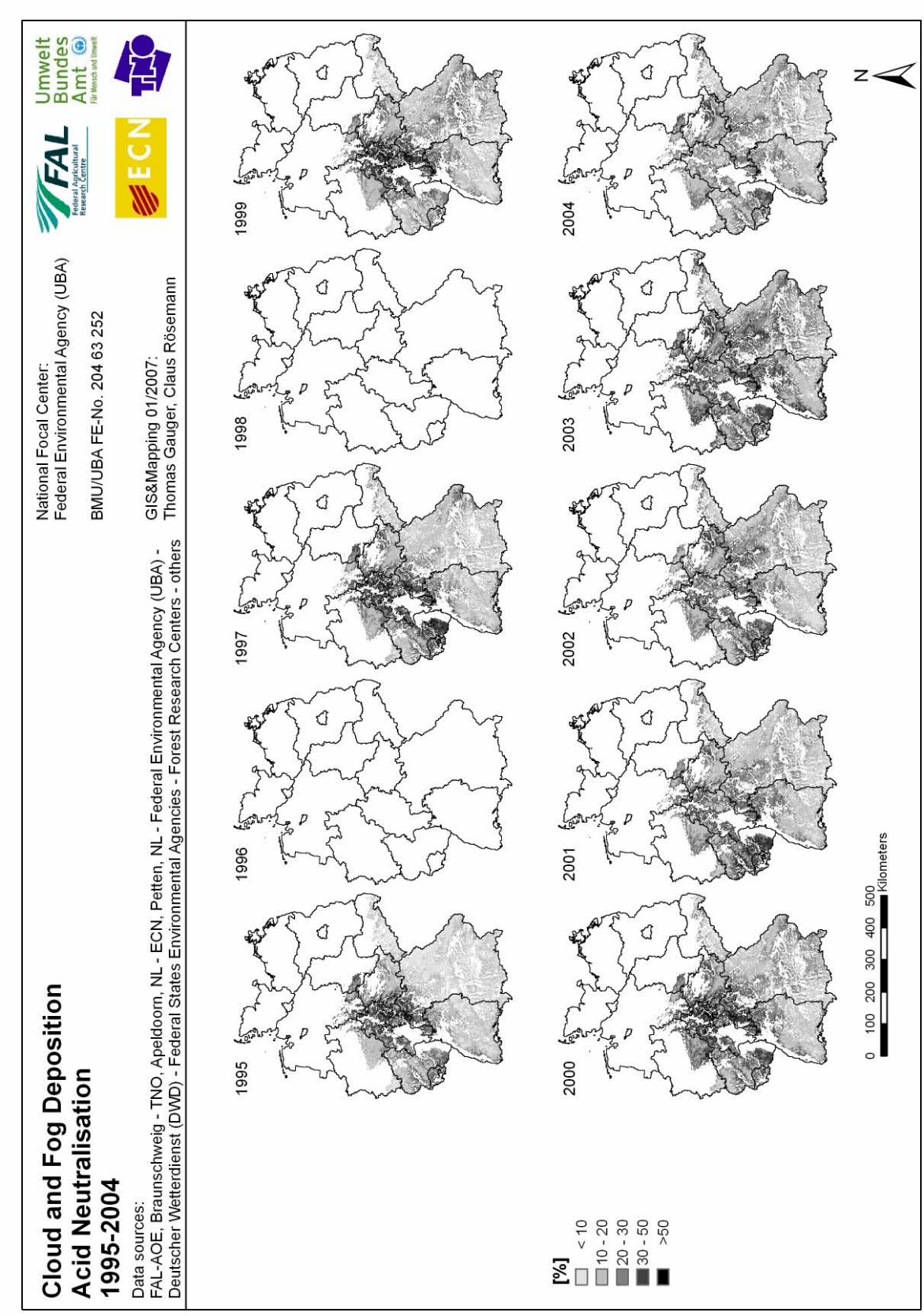

Map 8.8: Neutralisation of cloud&fog deposited AC_{pot} by $BC_{(nss)}$ 1995-2004

9 Total deposition mapping results

Thomas Gauger & Claus Rösemann
Federal Agricultural Research Centre, Institute of Agroecology (FAL-AOE), Bundesallee 50, D-38116 Braunschweig
Bundesforschungsanstalt für Landwirtschaft, Institut für Agrarökologie (FAL-AOE), Bundesallee 50, D-38116 Braunschweig

Maps of total deposition in this study are calculated as the sum of wet, dry, and cloud&fog deposition fluxes. Dry and wet deposition model estimates are covering the whole inland area of Germany. Estimates of cloud&fog deposition fluxes are only modelled for areas above 250m ASL, and in this study it is only applied to total deposition of forested areas, since cloud&fog deposition, with average fluxes far below 1% of total deposition rates, is negligible for other land use classes.

Main results of the total deposition mapping calculations are presented in the following sub Chapters 9.1 and 9.2. The graphical representation of modelled total deposition data sets (maps) are shown in Chapter 9.3.

An extensive description of methods applied for mapping wet deposition can be found in Chapter 4, main results of wet deposition mapping procedures are shown in Chapter 5 of this report. The description of modelling procedures applied in order to calculate dry and occult (cloud&fog) deposition fluxes using the IDEM model can be found in Chapter 6, main results of dry deposition fluxes are described in Chapter 7, main results of modelling cloud&fog deposition are shown in Chapter 8.

9.1 Total deposition fluxes and trends of non-sea salt base cations ($BC_{(nss)}$)

The sum of non-sea salt base cations ($BC_{(nss)}$) is calculated from non-sea salt calcium ($Ca_{(nss)}$), non-sea salt potassium ($K_{(nss)}$), and non-sea salt magnesium ($Mg_{(nss)}$). Average total deposition of non-sea salt base cations ($BC_{(nss)}$) over the whole time period considered can be found on a rather constant level ranging from 508 eq ha^{-1} a^{-1} in 1999 to 595 eq ha^{-1} a^{-1} in 1997 (cf. Figure 9.1). An exception is the year 2003 due to anomalous dry deposition results (cf. Chapter 7.1). Compared to the other years considered the 2003 average $BC_{(nss)}$ total deposition flux is higher by a factor of two.

In Map 9.1 the spatial patterns of total deposition of $BC_{(nss)}$ are presented. Areas receiving highest deposition fluxes like in the $BC_{(nss)}$ dry deposition map (cf. Map 7.1) can be found at some bigger agglomerations (Berlin, Munich) and in forested areas mainly in central Germany (Hesse and surrounding regions). High total deposition fluxes of non-sea salt base cations mainly due to the wet deposition flux can be observed in the Alpine region.

Table 9.1 shows that the amount of the wet deposited fraction of $BC_{(nss)}$ 2003 is in line with the other years, whereas the dry deposited fraction in 2003 exceeds the average of the other years by a factor of three. In general over the whole area of Germany and over the whole period 1995 to 2004 about one third of non-sea salt base cations are deposited with the wet deposition flux and two thirds are deposited dry (cf. Figure 9.2). In 2003 the ratio is 14.5% to 84%. Cloud&fog deposition on average only contributes by about 1.7% to average total deposition. This seems to be a negligible share, but as forested areas in medium range altitude are concerned (250m to 750m ASL), the absolute amount of cloud&fog water deposition is significant (cf. Chapter 6.2). The fraction of cloud&fog $BC_{(nss)}$ deposition flux in some forested areas can be up to about 10% of the total $BC_{(nss)}$ deposition flux.

In Figure 9.2 the average contribution of wet, dry, and cloud&fog deposition flux to $BC_{(nss)}$ total deposition per land use class is shown.

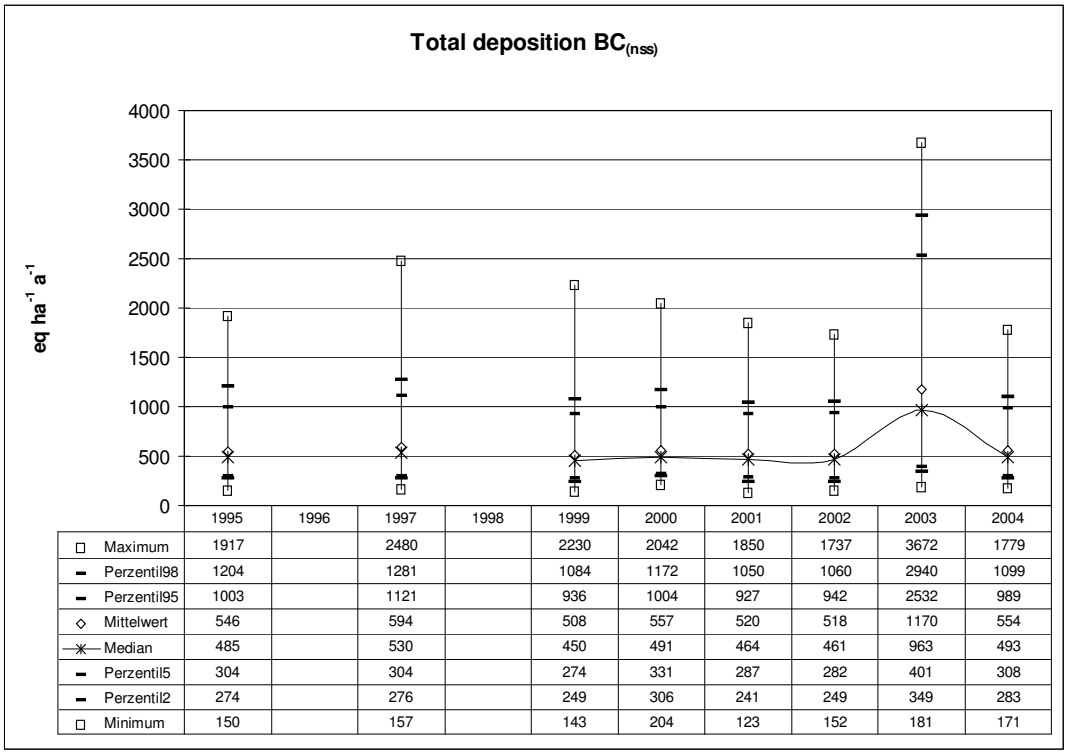

	1995	1996	1997	1998	1999	2000	2001	2002	2003	2004
Maximum	1917		2480		2230	2042	1850	1737	3672	1779
Perzentil98	1204		1281		1084	1172	1050	1060	2940	1099
Perzentil95	1003		1121		936	1004	927	942	2532	989
Mittelwert	546		594		508	557	520	518	1170	554
Median	485		530		450	491	464	461	963	493
Perzentil5	304		304		274	331	287	282	401	308
Perzentil2	274		276		249	306	241	249	349	283
Minimum	150		157		143	204	123	152	181	171

Figure 9.1: Statistical evaluation of annual non-sea salt base cations ($BC_{(nss)}$) total deposition 1995-2004

Table 9.1: Average wet, dry, and cloud&fog fraction of $BC_{(nss)}$ total deposition 1995-2004

	1995	1996	1997	1998	1999	2000	2001	2002	2003	2004
$BC_{(nss)}$ wet flux [eq ha^{-1} a^{-1}]	186	170	181	194	170	181	171	181	170	169
$BC_{(nss)}$ wet fraction [%]	34.0%		30.5%		33.4%	32.5%	32.9%	34.9%	14.6%	30.5%
$BC_{(nss)}$ dry flux [eq ha^{-1} a^{-1}]	352		403		330	367	338	326	984	377
$BC_{(nss)}$ dry fraction [%]	64.4%		67.8%		65.0%	65.9%	65.0%	62.9%	84.1%	68.1%
$BC_{(nss)}$ wet + dry flux [%]	98.4%		98.3%		98.4%	98.3%	97.9%	97.8%	98.7%	98.6%
$BC_{(nss)}$ cloud&fog fraction [%]	1.6%		1.7%		1.6%	1.7%	2.1%	2.2%	1.3%	1.4%

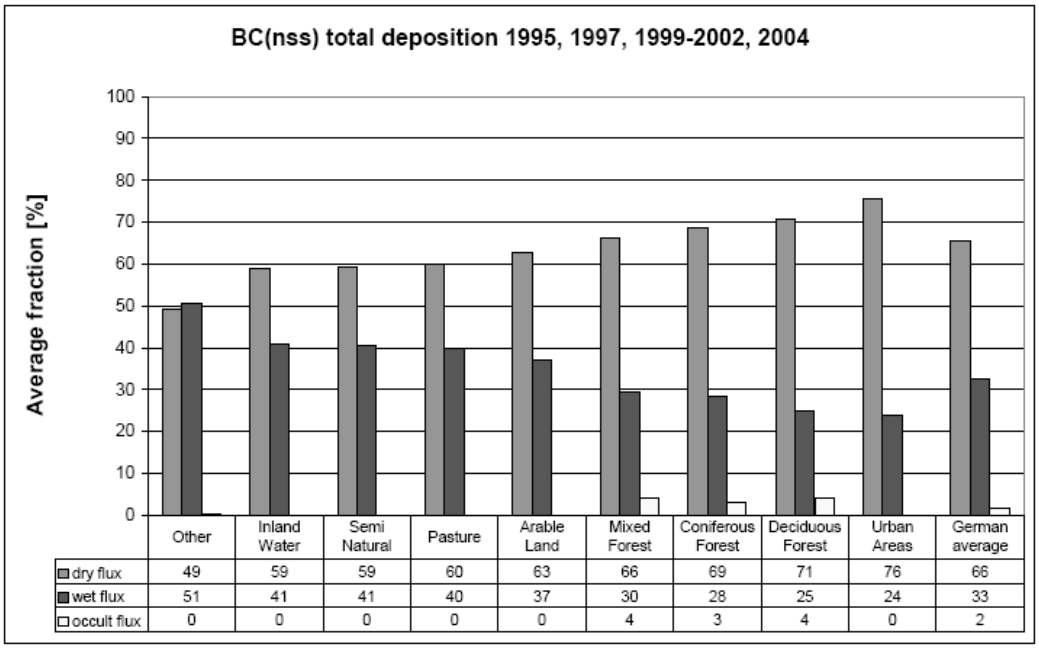

	Other	Inland Water	Semi Natural	Pasture	Arable Land	Mixed Forest	Coniferous Forest	Deciduous Forest	Urban Areas	German average
dry flux	49	59	59	60	63	66	69	71	76	66
wet flux	51	41	41	40	37	30	28	25	24	33
occult flux	0	0	0	0	0	4	3	4	0	2

Figure 9.2: Average fraction of wet, dry, and cloud&fog flux contributing to $BC_{(nss)}$ total deposition into different land use classes 1995-2004 (2003 data not considered here)

9.2 Total deposition fluxes and trends of acidifying compounds and nitrogen

Eutrophication occurs due to atmospheric input of nitrogen, which causes nutrient imbalances, while acidification is caused by deposition loads of sulphur and nitrogen compounds. Average annual total deposition 1995 to 2004 and the percentage changes for sulphur (SO_X-$S_{(nss)}$), reduced, oxidised, and total nitrogen (NH_X-N, NO_Y-N, N), respectively, are shown in Table 9.2. From 1995 to 1999 total deposition of all acidifying compounds declined, mainly pronounced in the case of SO_X-$S_{(nss)}$, not as obvious as nitrogen compounds are concerned.

Table 9.2: Budgets of annual average total deposition of SO_X-$S_{(nss)}$, NH_X-N, NO_Y-N, and N 1995-2004

	SO_X-$S_{(nss)}$ [eq $ha^{-1}a^{-1}$]	% change from previous year	NH_X-N [eq $ha^{-1}a^{-1}$]	% change from previous year	NO_Y-N [eq $ha^{-1}a^{-1}$]	% change from previous year	N [eq $ha^{-1}a^{-1}$]	% change from previous year
1995	1238		1200		794		1995	
1996								
1997	874	-29.3	1191	-0.7	715	-10.0	1908	-4.4
1998								
1999	661	-24.4	998	-16.2	656	-8.3	1656	-13.2
2000	652	-1.4	1116	+11.8	688	+4.9	1805	+9.0
2001	677	+3.8	1191	+6.7	731	+6.2	1923	+6.5
2002	690	+1.9	1202	+1.0	719	-1.6	1923	±0.0
2003	489	-29.1	912	-24.1	574	-20.2	1488	-22.6
2004	676	+38.2	1259	+38.0	728	+26.8	1988	+33.7
% change from 1995 to 2004		-45.4		+4.9		-8.3		-0.3

The following years this trend is stopped, and while total deposition of sulphur stays more or less at the same level, total deposition of nitrogen compounds slightly tends to increase. In contradiction to total deposition of base cations 2003, for all acidifying compounds a reduction of total deposition compared to the previous year 2002 can be noticed. In the ten years period considered (1995 to 2004) the total deposition of SO_X-$S_{(nss)}$ declined by about 45%, while total deposition of total nitrogen and its compounds in 2004 is at the same level as it was in 1995.

9.2.1 Total deposition of non-sea salt sulphur (SO_X-$S_{(nss)}$)

Annual average total deposition of non-sea salt Sulphur SO_X-$S_{(nss)}$ declines 1995 to 1999 by about 47% from about 1238 eq ha^{-1} a^{-1} (19.8 kg $ha^{-1}a^{-1}$ or 710 kt a^{-1}, respectively) in 1995 to about 661 eq ha^{-1} a^{-1} (10.6 kg $ha^{-1}a^{-1}$ or 380 kt a^{-1}, respectively) in 1999 (cf. Figure 9.3, Table 9.2). Peak values and 98th and 95th percentiles are significantly decreasing during this time period. For the period after 1999 there is no downward trend detectable any more. The amounts of all statistic values are stagnating with the exception of the year 2003 which shows a temporally decline of all statistics presented (cf. Figure 9.3).

The average contribution of wet and dry deposition to total deposition of SO_X-$S_{(nss)}$ 1995 to 2004 is listed in Table 9.3. On average over the whole ten year time period wet deposition contributes by about 38.8% , and dry deposition by about 59.5% to total deposition of non-sea salt sulphur. The remaining percentages of about on average 1.7% are due to cloud&fog deposition.

In Figure 9.4 the average contribution of wet, dry, and cloud&fog deposition flux to SO_X-$S_{(nss)}$ total deposition per land use class is shown. Cloud&fog deposition is contributing by 3% to 4% to total deposition into forested areas. In some forested regions, e.g. in Thuringia, the cloud&fog flux is contributing up to more than 9.5% to SO_X-$S_{(nss)}$ total deposition. The dry deposition in all of the land use classes except for the class “other”, in which dunes and other sparsely vegetated ecosystems are pooled, is the dominating flux contributing to SO_X-$S_{(nss)}$ total deposition.

The spatial patterns of SO_X-$S_{(nss)}$ total deposition are illustrated in Map 9.2. From the maps it clearly can be seen that deposition declines in the years 1995 to 1999. In all maps presented highest total deposition fluxes covering an area of bigger extent can be found over the Ruhr basin in western Germany.

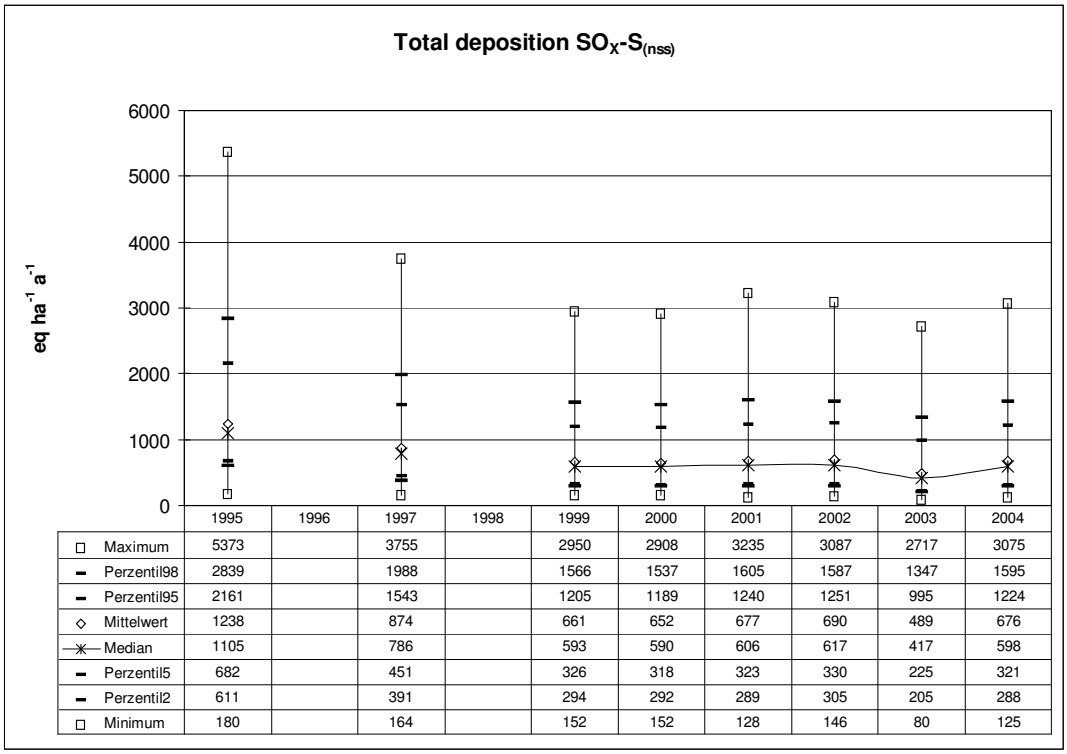

	1995	1996	1997	1998	1999	2000	2001	2002	2003	2004
Maximum	5373		3755		2950	2908	3235	3087	2717	3075
Perzentil98	2839		1988		1566	1537	1605	1587	1347	1595
Perzentil95	2161		1543		1205	1189	1240	1251	995	1224
Mittelwert	1238		874		661	652	677	690	489	676
Median	1105		786		593	590	606	617	417	598
Perzentil5	682		451		326	318	323	330	225	321
Perzentil2	611		391		294	292	289	305	205	288
Minimum	180		164		152	152	128	146	80	125

Figure 9.3: Statistical evaluation of annual non-sea salt sulphur (SO_X-$S_{(nss)}$) total deposition 1995-2004

Table 9.3: Average wet, dry, and cloud&fog fraction of SO_X-$S_{(nss)}$ total deposition 1995-2004

	1995	1996	1997	1998	1999	2000	2001	2002	2003	2004
SO_X-$S_{(nss)}$ wet flux [eq ha^{-1} a^{-1}]	422	341	307	335	275	276	262	285	203	239
SO_X-$S_{(nss)}$ wet fraction [%]	34.1%		35.1%		41.6%	42.3%	38.7%	41.3%	41.6%	35.4%
SO_X-$S_{(nss)}$ dry flux [eq ha^{-1} a^{-1}]	801		555		377	366	402	391	271	429
SO_X-$S_{(nss)}$ dry fraction [%]	64.8%		63.4%		56.9%	56.2%	59.3%	56.7%	55.5%	63.4%
SO_X-$S_{(nss)}$ wet + dry flux [%]	98.9%		98.5%		98.5%	98.5%	98.1%	98.0%	97.1%	98.8%
SO_X-$S_{(nss)}$ cloud&fog fraction [%]	1.1%		1.5%		1.5%	1.5%	1.9%	2.0%	2.9%	1.2%

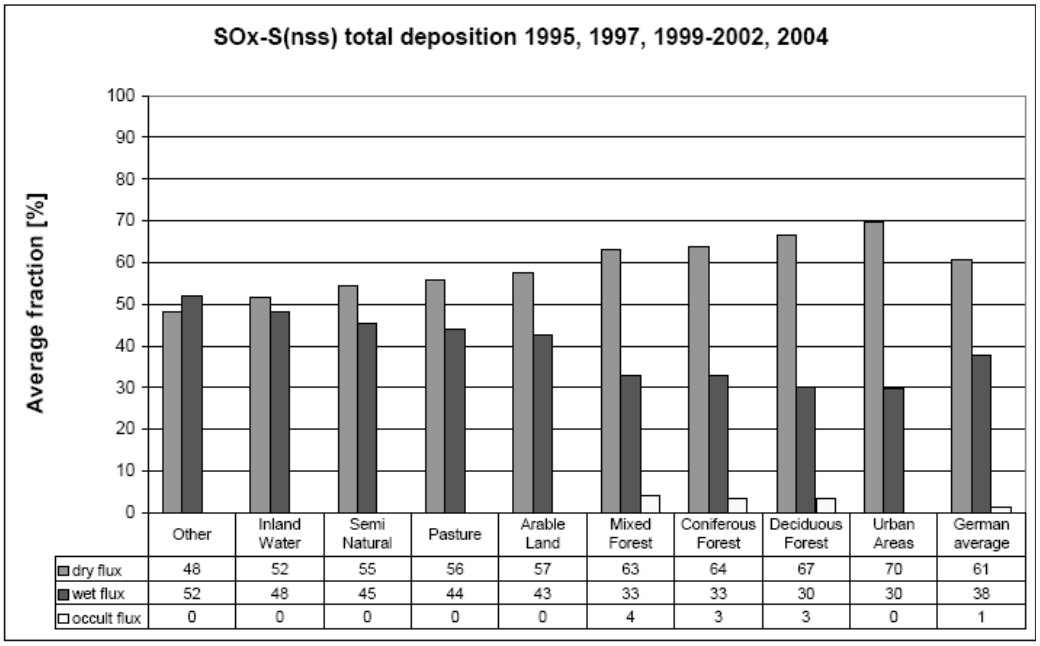

	Other	Inland Water	Semi Natural	Pasture	Arable Land	Mixed Forest	Coniferous Forest	Deciduous Forest	Urban Areas	German average
dry flux	48	52	55	56	57	63	64	67	70	61
wet flux	52	48	45	44	43	33	33	30	30	38
occult flux	0	0	0	0	0	4	3	3	0	1

Figure 9.4: Average fraction of wet, dry, and cloud&fog flux contributing to SO_X-$S_{(nss)}$ total deposition into different land use classes 1995-2004 (2003 data not considered here)

9.2.2 Total deposition of reduced nitrogen (NH_X-N)

Annual average total deposition of reduced nitrogen (NH_X-N) in Germany in 1995 is about 1200 eq ha^{-1} a^{-1} (16.8 kg $ha^{-1}a^{-1}$ or 600 kt a^{-1}, respectively), in 2004 about 1259 eq ha^{-1} a^{-1} (16.9 kg $ha^{-1}a^{-1}$ or 630 kt a^{-1}, respectively). Hence no declining trend, but slightly rising NH_X-N total deposition loads over time can be found from 1995 to 2004 (cf. Figure 9.5). From 1999 onward only peak values declined compared to the previous years 1995 and 1997.

In Table 9.4 the annual average contribution of wet, dry, and cloud&fog deposition fluxes to NH_X-N total deposition 1995 to 2004 is shown. The mean fraction of the wet deposition flux contributing to total deposition is about 34.7%, average dry flux fraction is about 64%, and average cloud&fog flux fraction 1.3%, respectively. The inter-annual percentages of the wet and dry flux are varying within the range of about 7%. No straight trend of rising or falling contribution of any fraction to NH_X-N total deposition can be found.

In Figure 9.6 the average contribution of wet, dry, and cloud&fog deposition flux to NH_X-N total deposition per land use class is shown. Cloud&fog deposition is contributing by 2% to 3% to total deposition into forested areas. In some forested regions, e.g. in Thuringia, the cloud&fog flux is contributing up to more than 6% to NH_X-N total deposition.

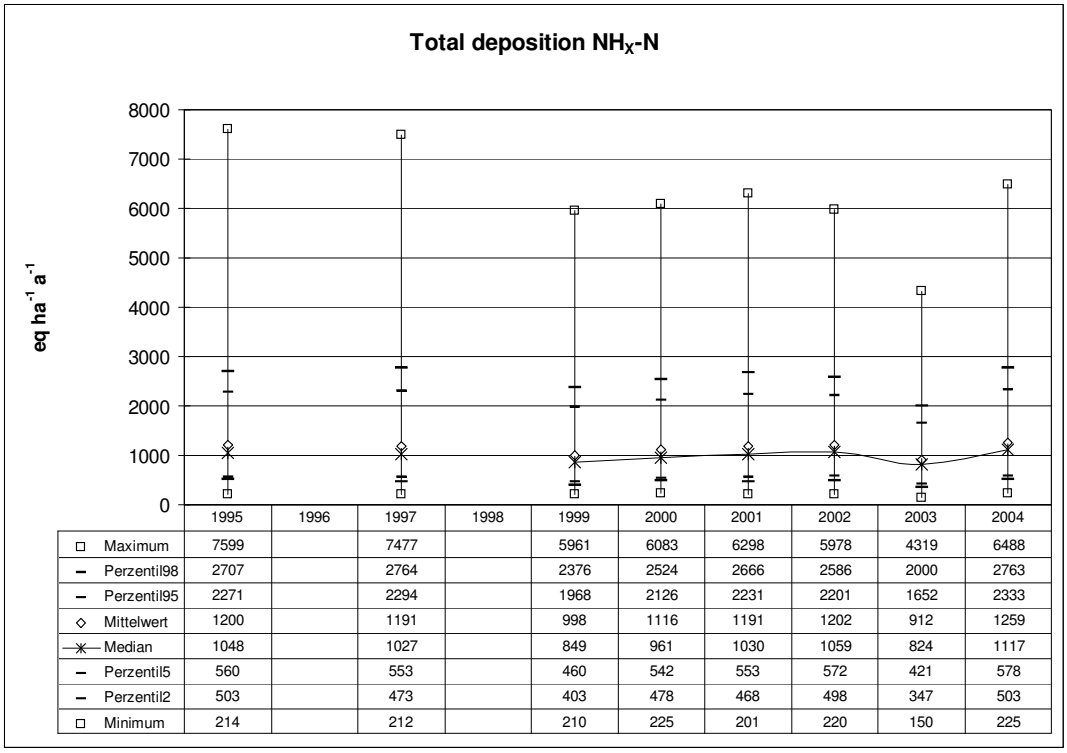

	1995	1996	1997	1998	1999	2000	2001	2002	2003	2004
Maximum	7599		7477		5961	6083	6298	5978	4319	6488
Perzentil98	2707		2764		2376	2524	2666	2586	2000	2763
Perzentil95	2271		2294		1968	2126	2231	2201	1652	2333
Mittelwert	1200		1191		998	1116	1191	1202	912	1259
Median	1048		1027		849	961	1030	1059	824	1117
Perzentil5	560		553		460	542	553	572	421	578
Perzentil2	503		473		403	478	468	498	347	503
Minimum	214		212		210	225	201	220	150	225

Figure 9.5: Statistical evaluation of annual reduced nitrogen (NH_X-N) total deposition 1995-2004

Table 9.4: Average wet, dry, and cloud&fog fraction of NH_X-N total deposition 1995-2004

	1995	1996	1997	1998	1999	2000	2001	2002	2003	2004
NH_X-N wet flux [eq $ha^{-1}a^{-1}$]	432	423	384	419	379	393	406	425	331	389
NH_X-N wet fraction [%]	36.0%		32.2%		37.9%	35.2%	34.1%	35.3%	36.2%	30.9%
NH_X-N dry flux [eq $ha^{-1}a^{-1}$]	754		794		609	711	768	760	562	858
NH_X-N dry fraction [%]	62.9%		66.6%		60.9%	63.7%	64.5%	63.2%	61.6%	68.2%
NH_X-N wet + dry flux [%]	98.9%		98.8%		98.9%	99.0%	98.6%	98.6%	97.8%	99.0%
NH_X-N cloud&fog fraction [%]	1.1%		1.2%		1.1%	1.0%	1.4%	1.4%	2.2%	1.0%

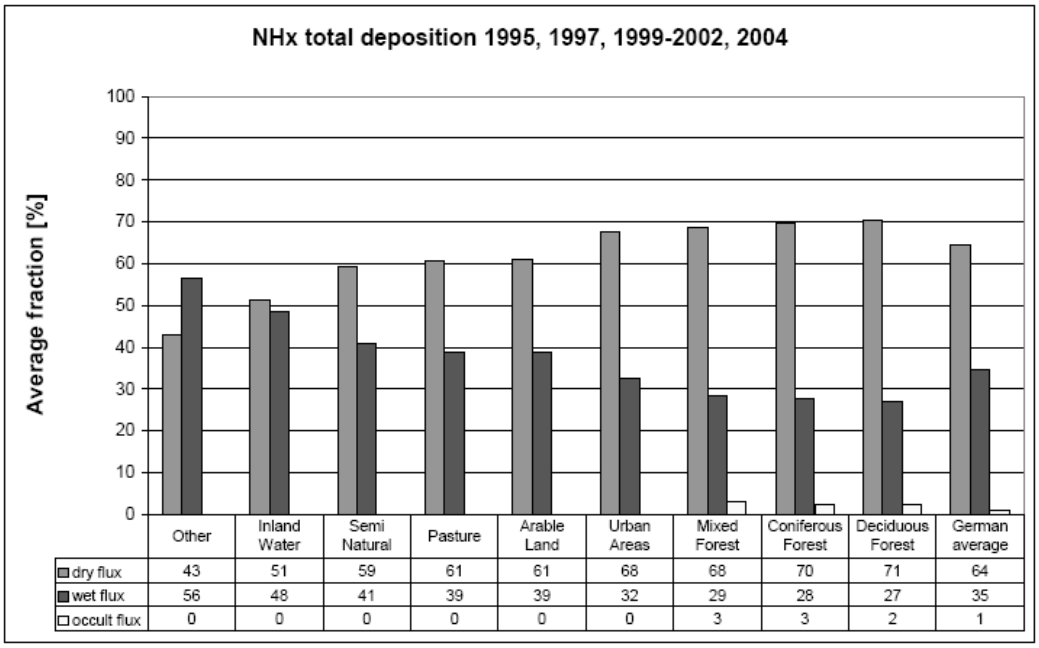

	Other	Inland Water	Semi Natural	Pasture	Arable Land	Urban Areas	Mixed Forest	Coniferous Forest	Deciduous Forest	German average
dry flux	43	51	59	61	61	68	68	70	71	64
wet flux	56	48	41	39	39	32	29	28	27	35
occult flux	0	0	0	0	0	0	3	3	2	1

Figure 9.6: Average fraction of wet, dry, and cloud&fog flux contributing to NHX-N total deposition into different land use classes 1995-2004 (2003 data not considered here)

The spatial patterns of total deposition of reduced nitrogen are presented in Map 9.3. In the north-west region of Germany high fluxes above the annual average in all years considered can be observed. Here emission source areas with intensive animal husbandry can be found. Relatively lower than average total deposition fluxes regularly can be observed in the regions from south-west Germany over central Germany to the Baltic Sea. In Bavaria the total deposition of reduced Nitrogen is a little higher than the mean value. Locally high NH_X-N total deposition can be found over small patterns of forested areas, which are receiving more reduced nitrogen with the dry deposition flux than neighbouring areas of other non-urban land use.

9.2.3 Total deposition of oxidised nitrogen (NO_Y-N)

Between 1995 and 1999 a decline of about 17% of total deposition of oxidised nitrogen (NO_Y-N) can be observed (cf. Table 9.2). From 1999 onward a reversal of this trend can be found. With the exception of the year 2003 annual average NO_Y-N total deposition loads over Germany are increasing. In 2004 the average of the modelled data is about 8.3% lower than in 1995 but peak values (95^{th} and 98^{th} percentile) are at the same level as the corresponding statistics of total deposition of oxidised nitrogen in 1995 (cf. Figure 9.7). According to the results shown in the map statistics of Figure 9.7 the total amount of total deposited NO_Y-N declined from about 398 kt a^{-1} (11.1 kg $ha^{-1}a^{-1}$) in 1995 to about 365 kt a^{-1} (10.2 kg $ha^{-1}a^{-1}$) in 2004. Changes of average NO_Y-N total deposition fluxes between each year considered are in the range of about 10% (with the exception of the year 2003), and hence relatively small (c.f. Table 9.2).

The contributions of wet, dry, and cloud&fog deposition fluxes to total deposition of NO_Y-N are shown in Table 9.5. The mean fraction of wet deposition over the whole time period is about 39.8%. The NO_Y-N dry deposition flux contributes on average by about 58% to total deposition. Cloud&fog deposition contributes by about 2.2% to total deposition. From 1999 onward the contribution of wet deposition is slightly falling from 43.1% to 37.9% in 2004, the dry fraction is rising accordingly from 55% in 1999 to about 60.3% in 2004.

In Figure 9.7 the average contribution of wet, dry, and cloud&fog deposition flux to NO_Y-N total deposition per land use class is shown. Cloud&fog deposition is contributing by 4% to 5% to total deposition into forested areas. In some forested regions the cloud&fog flux is contributing up to more than 6% to 8% (Hesse, Rhineland-Palatinate, North Rhine-Westphalia), or even up to more than 10% (Thuringia), to NO_Y-N total deposition.

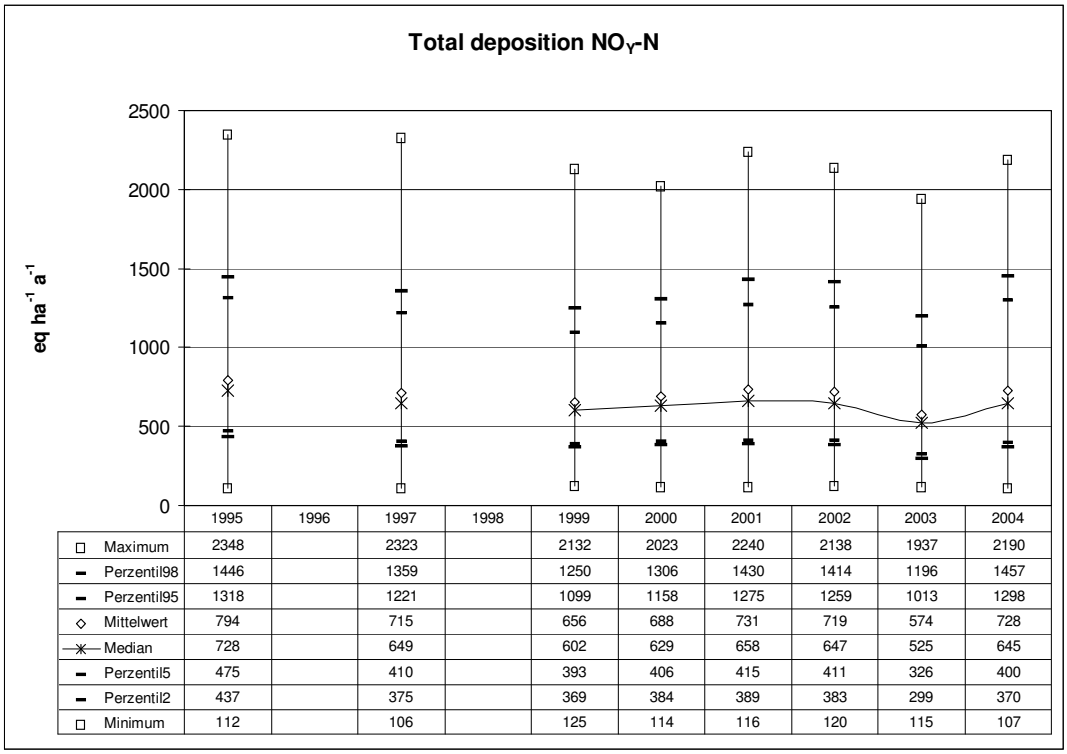

	1995	1996	1997	1998	1999	2000	2001	2002	2003	2004
Maximum	2348		2323		2132	2023	2240	2138	1937	2190
Perzentil98	1446		1359		1250	1306	1430	1414	1196	1457
Perzentil95	1318		1221		1099	1158	1275	1259	1013	1298
Mittelwert	794		715		656	688	731	719	574	728
Median	728		649		602	629	658	647	525	645
Perzentil5	475		410		393	406	415	411	326	400
Perzentil2	437		375		369	384	389	383	299	370
Minimum	112		106		125	114	116	120	115	107

Figure 9.7: Statistical evaluation of annual oxidised nitrogen (NO_Y-N) total deposition 1995-2004

Table 9.5: Average wet, dry, and cloud&fog fraction of NO_Y-N total deposition 1995-2004

	1995	1996	1997	1998	1999	2000	2001	2002	2003	2004
NO_Y-N wet flux [eq $ha^{-1}a^{-1}$]	312	287	265	301	283	285	288	294	227	276
NO_Y-N wet fraction [%]	39.2%		37.1%		43.1%	41.5%	39.4%	40.9%	39.6%	37.9%
NO_Y-N dry flux [eq $ha^{-1}a^{-1}$]	470		436		361	390	425	406	326	439
NO_Y-N dry fraction [%]	59.1%		60.9%		55.0%	56.7%	58.2%	56.5%	56.9%	60.3%
NO_Y-N wet + dry flux [%]	98.4%		98.0%		98.1%	98.2%	97.6%	97.4%	96.5%	98.2%
NO_Y-N cloud&fog fraction [%]	1.6%		2.0%		1.9%	1.8%	2.4%	2.6%	3.5%	1.8%

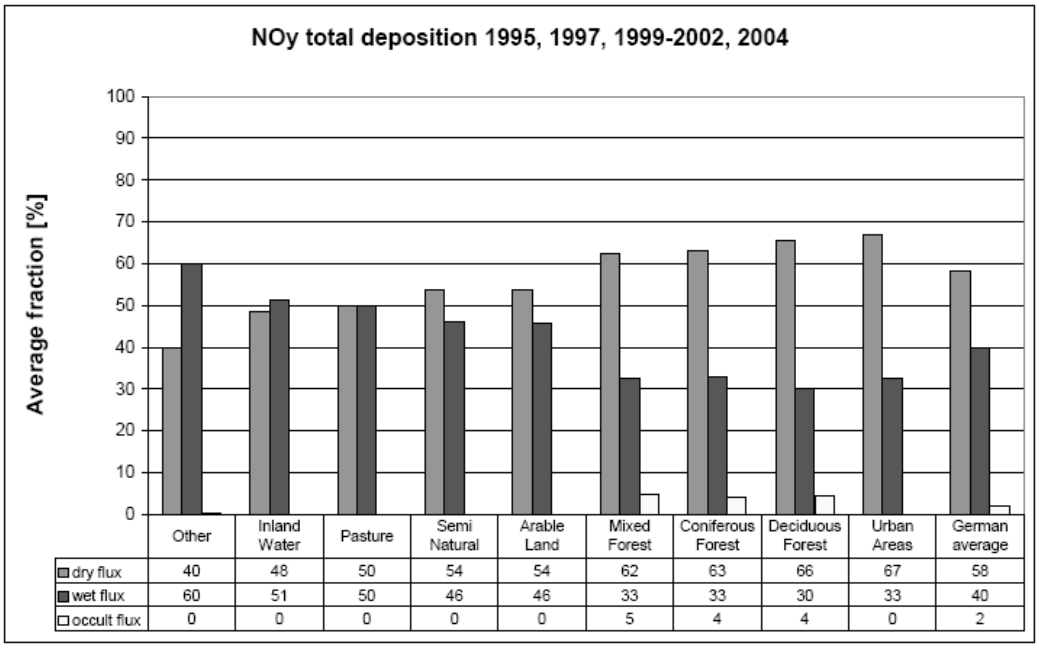

	Other	Inland Water	Pasture	Semi Natural	Arable Land	Mixed Forest	Coniferous Forest	Deciduous Forest	Urban Areas	German average
dry flux	40	48	50	54	54	62	63	66	67	58
wet flux	60	51	50	46	46	33	33	30	33	40
occult flux	0	0	0	0	0	5	4	4	0	2

Figure 9.8: Average fraction of wet, dry, and cloud&fog flux contributing to NO_Y-N total deposition into different land use classes 1995-2004 (2003 data not considered here)

The spatial patterns of NO_Y-N total deposition fluxes are presented in Map 9.4. Generally pronounced in the maps by high deposition loads are urban regions (highest total deposition fluxes are occurring in the Ruhr Basin) and forested areas situated in medium range altitude mountains (Harz, Thuringian Forest, Rheinisches Schiefergebirge). The moderately high deposition of oxidised nitrogen in the Black Forest and the Alps mainly is due to relatively high wet deposition fluxes.

9.2.4 Total deposition of total nitrogen (N = NH_X-N + NO_Y-N)

Total deposition of total nitrogen is calculated as sum of total deposited reduced and oxidised nitrogen (N = NH_X-N + NO_Y-N). The amount of average total deposition of nitrogen in Germany, both in 1995 and in 2004 is almost at the same level (cf. Figure 9.9). From 1995 to 1999 a decrease of about 170 kt N total deposition load can be observed. From 1999 to 2004 an increase of about 167 kt N total deposition load can be found. Hence a decline of only 0.3% from 1995 to 2004 N total deposition can be found over the whole time period considered (cf. Table 9.2). The total amount of N total deposition first declined from 1000 kt a^{-1} (27.9 kg $ha^{-1}a^{-1}$) in 1995 to 830 kt a^{-1} (23.2 kg $ha^{-1}a^{-1}$) in 1999 and then rises up to 997 kt a^{-1} (27.9 kg $ha^{-1}a^{-1}$). The slightly rising trend from 1999 to 2004 is only interrupted by the exceptionally low total deposition in 2003, due to the anomalous climate conditions that year.

Average wet and dry deposition fluxes of total N deposition 1995 to 2004 are listed in Table 9.6. Average contribution of the wet flux to total N deposition over the whole period is about 36.7%, whereas 61.7% of total deposition of N is due to the dry deposition flux, and an average fraction of 1.7% is due to the N cloud&fog deposition flux into forested areas in medium range mountains (above 250m ASL). Highest contribution of wet deposition can be found in 1999 with 40.0%, lowest in 2004 with 33.4%.

In Figure 9.10 the average contribution of wet, dry, and cloud&fog deposition flux to N total deposition per land use class is shown. Cloud&fog deposition on average per land use class is contributing by 3% to 4% to total deposition into forested areas. In some forested regions the cloud&fog flux is contributing up to 7% (Hesse), or up to more than 10% (Thuringia), to N total deposition.

Dry deposition flux is contributing to more than 50% to N total deposition in all land use classes except inland water bodies and "other" ecosystems, the class pooling up sparsely vegetated rocks and dunes.

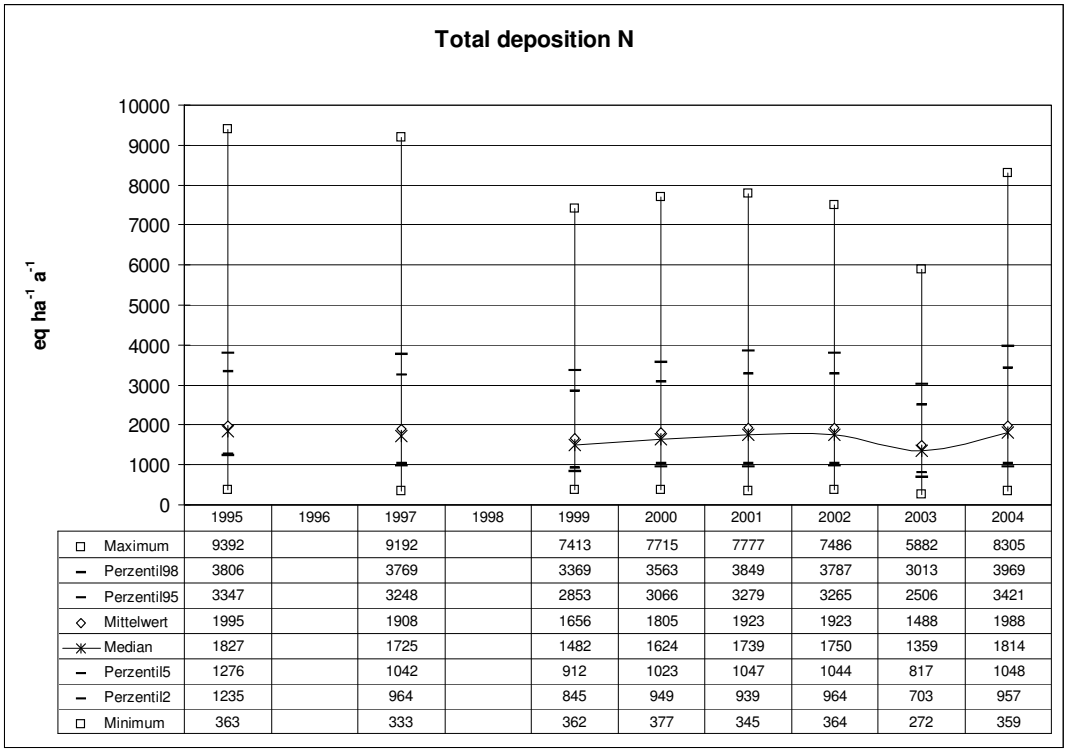

	1995	1996	1997	1998	1999	2000	2001	2002	2003	2004
Maximum	9392		9192		7413	7715	7777	7486	5882	8305
Perzentil98	3806		3769		3369	3563	3849	3787	3013	3969
Perzentil95	3347		3248		2853	3066	3279	3265	2506	3421
Mittelwert	1995		1908		1656	1805	1923	1923	1488	1988
Median	1827		1725		1482	1624	1739	1750	1359	1814
Perzentil5	1276		1042		912	1023	1047	1044	817	1048
Perzentil2	1235		964		845	949	939	964	703	957
Minimum	363		333		362	377	345	364	272	359

Figure 9.9: Statistical evaluation of annual total nitrogen (N) total deposition 1995-2004

Table 9.6: Average wet, dry, and cloud&fog fraction of N total deposition 1995-2004

	1995	1996	1997	1998	1999	2000	2001	2002	2003	2004
N wet flux [eq $ha^{-1}a^{-1}$]	744	710	649	720	662	678	694	719	558	664
N wet fraction [%]	37.3%		34.0%		40.0%	37.6%	36.1%	37.4%	37.5%	33.4%
N dry flux [eq $ha^{-1}a^{-1}$]	1225		1231		970	1102	1194	1168	889	1298
N dry faction [%]	61.4%		64.5%		58.6%	61.1%	62.1%	60.7%	59.8%	65.3%
N wet + dry flux [%]	98.7%		98.5%		98.6%	98.7%	98.2%	98.1%	97.3%	98.7%
N cloud&fog fraction [%]	1.3%		1.5%		1.45	1.3%	1.8%	1.9%	2.7%	1.3%

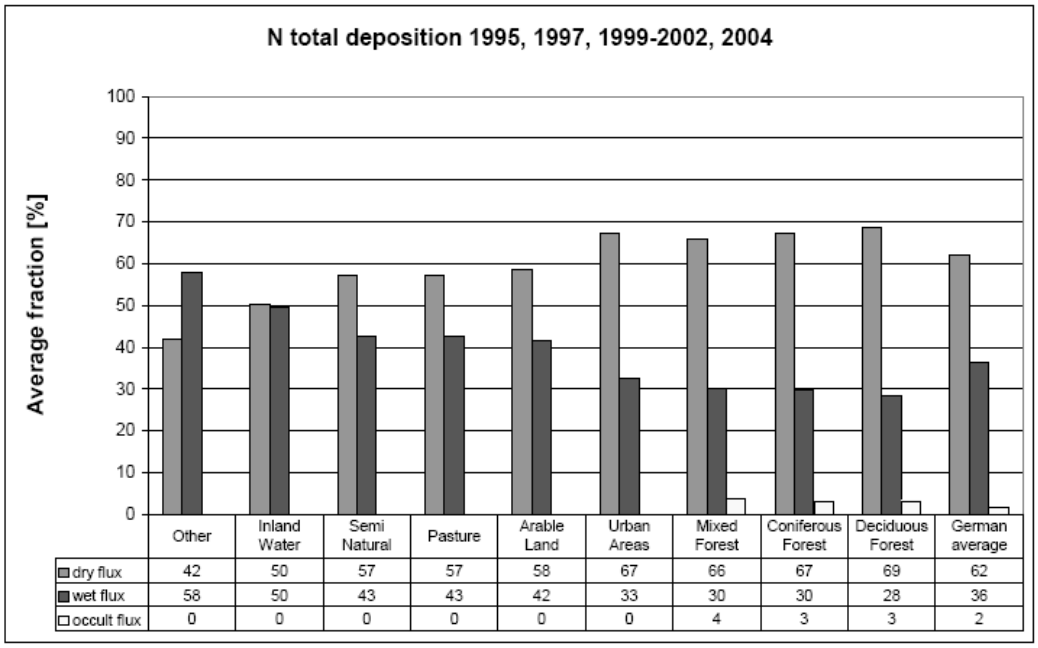

Figure 9.10: Average fraction of wet, dry, and cloud&fog flux contributing to N total deposition into different land use classes 1995-2004 (2003 data not considered here)

The average fractions of reduced (NH_X-N) and oxidised nitrogen (NO_Y-N) to nitrogen (N) total deposition are listed in Table 9.7. The ratio between the two fractions is varying only to a small extent (about 3.4%). On average NH_X-N is contributing 62% to N total deposition, NO_Y-N is contributing by average 38%, respectively. The highest contribution of NO_Y-N to N total deposition can be found in 1995 (39.8%) and the lowest contribution in 2004 (36.6%). However, there is no clear trend over time detectable of either an increasing or decreasing NH_X-N or NO_Y-N fraction contributing to N total deposition.

Table 9.7: Average NH_X-N and NO_Y-N fraction of total deposited N 1995-2004

	1995	1996	1997	1998	1999	2000	2001	2002	2003	2004
NH_X-N [eq $ha^{-1}a^{-1}$]	1200		1191		998	1116	1191	1202	912	1259
NH_X-N [%]	60.2%		62.5%		60.4%	61.9%	62.0%	62.6%	61.4%	63.4%
NO_Y-N [eq $ha^{-1}a^{-1}$]	794		715		656	688	731	719	574	728
NO_Y-N [%]	39.8%		37.5%		39.6%	38.1%	38.0%	37.4%	38.6%	36.6%

The spatial patterns of N total deposition are presented in Map 9.5. The region with highest total deposition of total nitrogen in all years mapped can be found in the north-western part of Germany. This is mainly due to high level total deposition of reduced nitrogen. Regions with comparably lower deposition loads can mainly be found in south-western Germany (Rhineland-Palatinate, western parts of Baden-Württemberg) and in eastern Germany (Berlin, Brandenburg, Saxony-Anhalt, northern Saxony, and eastern Mecklenburg-Western Pomerania).

9.2.5 Total deposition of potential acidity (ACpot = SO_X-$S_{(nss)}$ + N)

Total deposition of potential acidity (AC_{pot}) is calculated as the sum of wet, dry, and cloud&fog deposition of non-sea salt sulphur and total nitrogen (AC_{pot} = SO_X-$S_{(nss)}$ + N). The average total deposition fluxes of AC_{pot} from 1995 to 2004 have diminished by about 17.6% (cf. Table 9.8 and Figure 9.11). The decline is mainly due to the relatively high sulphur total deposition in 1995, and the declining deposition loads in the following years. From 1995 to 2004 a -45.4% change of SO_X-$S_{(nss)}$ total deposition fluxes over Germany can be observed (c.f. Chapter 9.2.1, and Table 9.2). Overall N total deposition on the contrary in 2004 is almost at the same level as it was in 1995 (c.f. Chapter 9.2.4, and Table 9.2).

In Table 9.9 the average contribution of the wet and dry deposition fluxes to total deposition of AC_{pot} is shown. Over the whole period 1995 to 2004 wet deposition contributes to about 37.7% and dry deposition to about 61.2% to the AC_{pot} total deposition flux. Cloud&fog deposition fluxes into forested areas (above 250m ASL) on average over the whole area mapped are contributing additional 1.1%. Highest average contribution of wet deposition to total deposition of AC_{pot} can be found in 1999 (40.9%), lowest average contribution in 2004 (34.4%). There is, however, no straight-line trend over time of a decrease in the wet deposition fraction of AC_{pot} total deposition, or of an increase of the dry fraction of AC_{pot} total deposition, and vice versa.

An overview of the average composition of the total deposition fluxes of AC_{pot} 1995 to 2004 is given in Figure 9.12 on the basis of annual average total deposition fluxes of NH_X-N, NO_Y-N, and SO_X-S in Germany. In 1995 sulphur is the main acidifying compound. From 2000 onward the contribution of sulphur to AC_{pot} is the least one. From 1997 onward average NH_X-N total deposition flux is the dominating compound of AC_{pot} total deposition. From 2000 onward also NO_Y-N contributes more to AC_{pot} total deposition than SO_X-$S_{(nss)}$ does.

Table 9.8: Budgets of average annual total deposition of AC_{pot}, $AC_{pot(net)}$, and acid neutralisation by $BC_{(nss)}$ 1995-2004

	AC_{pot} [eq $ha^{-1}a^{-1}$]	% change from previous year	$AC_{pot(net)}$ [eq $ha^{-1}a^{-1}$]	% change from previous year	$BC_{(nss)}$ [eq $ha^{-1}a^{-1}$]	% change from previous year	Acid neutrali-sation [%]
1995	3234		2690		546		17
1996							
1997	2784	-13.9	2190	-18.6	594	+8.9	22
1998							
1999	2318	-16.7	1810	-17.3	508	-14.5	23
2000	2458	+6.0	1902	+5.1	557	+9.5	24
2001	2601	+5.8	2081	+9.4	520	-6.5	21
2002	2614	+0.5	2096	+0.7	518	-0.5	20
2003	1978	-24.3	808	-61.4	1170	+126.0	62
2004	2666	+34.8	2113	+161.4	554	-52.7	22
% change from 1995 to 2004		-17.6		-21.5		1.5	

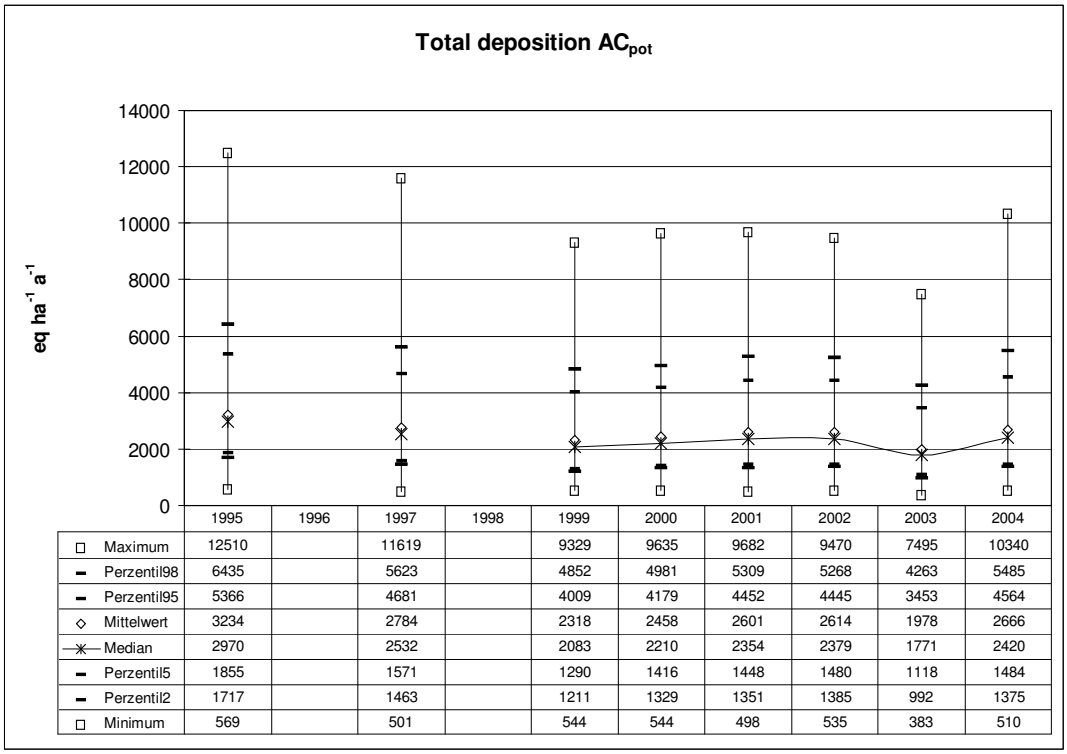

	1995	1996	1997	1998	1999	2000	2001	2002	2003	2004
Maximum	12510		11619		9329	9635	9682	9470	7495	10340
Perzentil98	6435		5623		4852	4981	5309	5268	4263	5485
Perzentil95	5366		4681		4009	4179	4452	4445	3453	4564
Mittelwert	3234		2784		2318	2458	2601	2614	1978	2666
Median	2970		2532		2083	2210	2354	2379	1771	2420
Perzentil5	1855		1571		1290	1416	1448	1480	1118	1484
Perzentil2	1717		1463		1211	1329	1351	1385	992	1375
Minimum	569		501		544	544	498	535	383	510

Figure 9.11: Statistical evaluation of annual potential acidity (AC_{pot}) total deposition 1995-2004

Table 9.9: Average wet, dry, and cloud&fog fraction of AC_{pot} total deposition 1995-2004

	1995	1996	1997	1998	1999	2000	2001	2002	2003	2004
AC_{pot} wet flux [eq ha^{-1}a^{-1}]	1187	1060	974	1075	949	971	969	1021	767	917
AC_{pot} wet fraction [%]	36.7%		35.0%		40.9%	39.5%	37.3%	39.1%	38.8%	34.4%
AC_{pot} dry flux [eq ha^{-1}a^{-1}]	2028		1786		1348	1470	1597	1560	1162	1728
AC_{pot} dry fraction [%]	62.7%		64.2%		58.1%	59.8%	61.4%	59.7%	58.7%	64.8%
AC_{pot} wet + dry flux [%]	99.4%		99.1%		99.1%	99.3%	98.7%	98.7%	97.5%	99.25
AC_{pot} cloud&fog fraction [%]	0.6%		0.9%		0.9%	0.7%	1.3%	1.3%	2.5%	0.8%

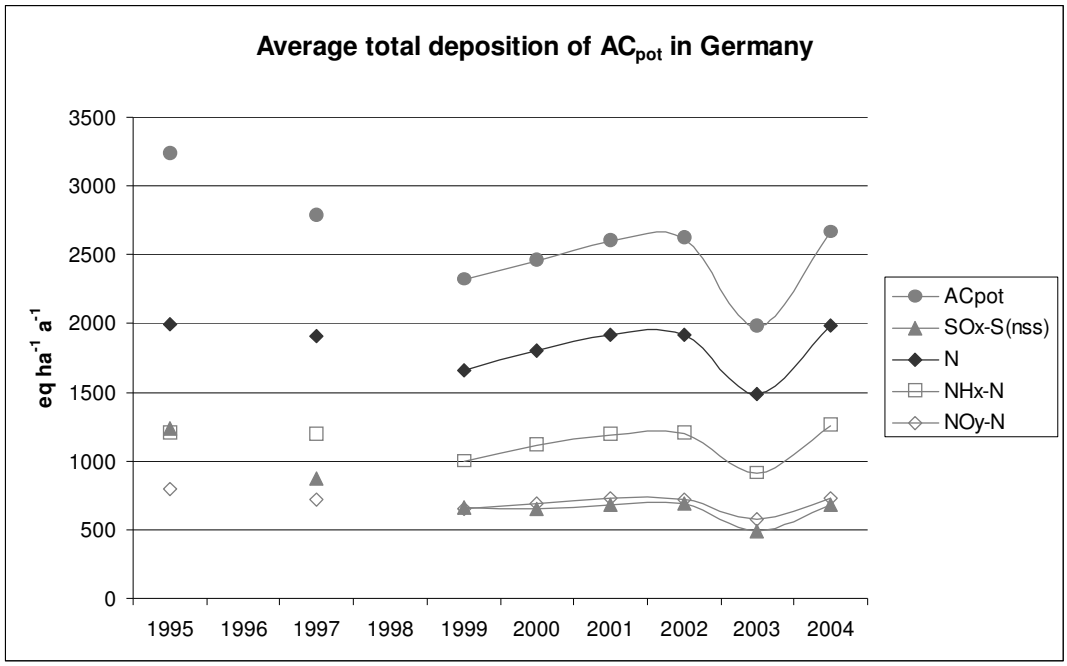

Figure 9.12: Average total deposition of potential acidity (AC_{pot}) and its compounds 1995 to 2004

The average fractions of the single compounds of AC_{pot} are additionally listed in Table 9.10. It clearly can be seen, that the contribution of N species to potential acidity has risen by about 13% from about 62% in 1995 to about 75% in 2004.

Table 9.10: Average fractions of acidifying compounds of total deposition 1995-2004

	1995	1996	1997	1998	1999	2000	2001	2002	2003	2004
SO_X-S [%]	38.3%		31.4%		28.5%	26.5%	26.0%	26.4%	24.7%	25.4%
N [%]	61.7%		68.5%		71.4%	73.4%	73.9%	73.6%	75.2%	74.6%
NH_X-N [%]	37.1%		42.8%		43.1%	45.4%	45.8%	46.0%	46.1%	47.2%
NO_Y-N [%]	24.6%		25.7%		28.3%	28.0%	28.1%	27.5%	29.0%	27.3%

The spatial patterns of AC_{pot} dry deposition are presented in Map 9.6. The patterns of AC_{pot} total deposition fluxes above and below average mainly resemble the patterns of N total deposition, the main acidifying compound in the time period mapped (cf. Map 9.5).

9.2.6 Total deposition of potential net-acidity ($AC_{pot(net)} = SO_X\text{-}S_{(nss)} + N - BC_{(nss)}$) and acid neutralisation ($= BC_{(nss)} \cdot 100 / AC_{pot}$ [%])

Potential net acidity ($AC_{pot(net)}$) is calculated by subtracting the fluxes of non-sea salt base cations ($BC_{(nss)}$) from the sum of potential acidifying compounds (AC_{pot}) in order to account for potential acid neutralisation. Hence total deposition loads of $AC_{pot(net)}$ generally are lower than total deposition loads of AC_{pot}.

The difference of average total deposition of $AC_{pot(net)}$ in 1995 compared to 2004 is a 577 eq $ha^{-1}a^{-1}$ (21.5%) lower total deposition flux (cf. Figure 9.13, Table 9.8). In 1999 compared to 1995 an about 880 eq $ha^{-1}a^{-1}$ (32.7%) lower $AC_{pot(net)}$ total flux can be found. This mainly is due to the -47% decline of total deposition of SO_X-S (cf. Chapter 9.2.5, Table 9.2), while N total deposition 1995 to 1999 declined by about 17%, and neutralising $BC_{(nss)}$ total deposition only declined by about 7% on average.

Budgets of average total deposition of AC_{pot} , $AC_{pot(net)}$, and acid neutralisation by $BC_{(nss)}$ within the ten years period considered are listed in Table 9.8. The extremely high acid neutralisation in 2003 (on average 64%, with a range from 9% to 267%; cf. Figure 9.14) is due to the implausible results for $BC_{(nss)}$ dry deposition (cf. Chapter 7.1).

Map statistics of acid neutralisation by deposition of $BC_{(nss)}$ is shown in Figure 9.14. The results for 2003 are clearly proven to be implausible. Hence they are excluded from further consideration. Average acid neutralisation ranges from 17% in 1995 to 24% in 2000. From 1997 on average acid neutralisation is above 20%. In the single years considered acid neutralisation over Germany is ranging from minimum 3% in 1995 to maximum 66% in 1997 (Figure 9.14).

In Figure 9.15 average total deposition of AC_{pot}, $AC_{pot(net)}$, and $BC_{(nss)}$ over time is presented. Three different sections can be distinguished in the graph (1) from 1995 to 1999 a sharp decline of average AC_{pot} (-28%) and $AC_{pot(net)}$ (-33%) can be found, (2) the depression of AC_{pot} and $AC_{pot(net)}$ in 2003 due to implausible high estimates of BC(nss), (3) from 1999 to 2004 (when 2003 results are omitted) a slightly increasing trend of average AC_{pot} and $AC_{pot(net)}$. In 2004 average total deposition of AC_{pot} and $AC_{pot(net)}$ are at about 96% of the total deposition level of AC_{pot} and $AC_{pot(net)}$ in 1997. $BC_{(nss)}$ total deposition on average over the whole time period considered is at a level of 542 eq ha^{-1} a^{-1} (± less than 10%), when 2003 results are omitted.

The spatial patterns of $AC_{pot(net)}$ are shown in Map 9.7, acid neutralisation by dry deposition of $BC_{(nss)}$ is presented in Map 9.8, respectively. Each year highest total deposition of $AC_{pot(net)}$ can be found over those areas, where patterns of total deposition of all, total deposition of NH_X-N (cf. Map 9.3), total deposition of NO_Y-N (cf. Map 9.4), and total deposition of $SO_X\text{-}S_{(nss)}$ (cf. Map 9.2) above the respective average can be found. This mainly is in the north-western part of Germany. Acid neutralisation by $BC_{(nss)}$ total deposition in these regions only is at about 10% to 20% (cf. Map 9.8).

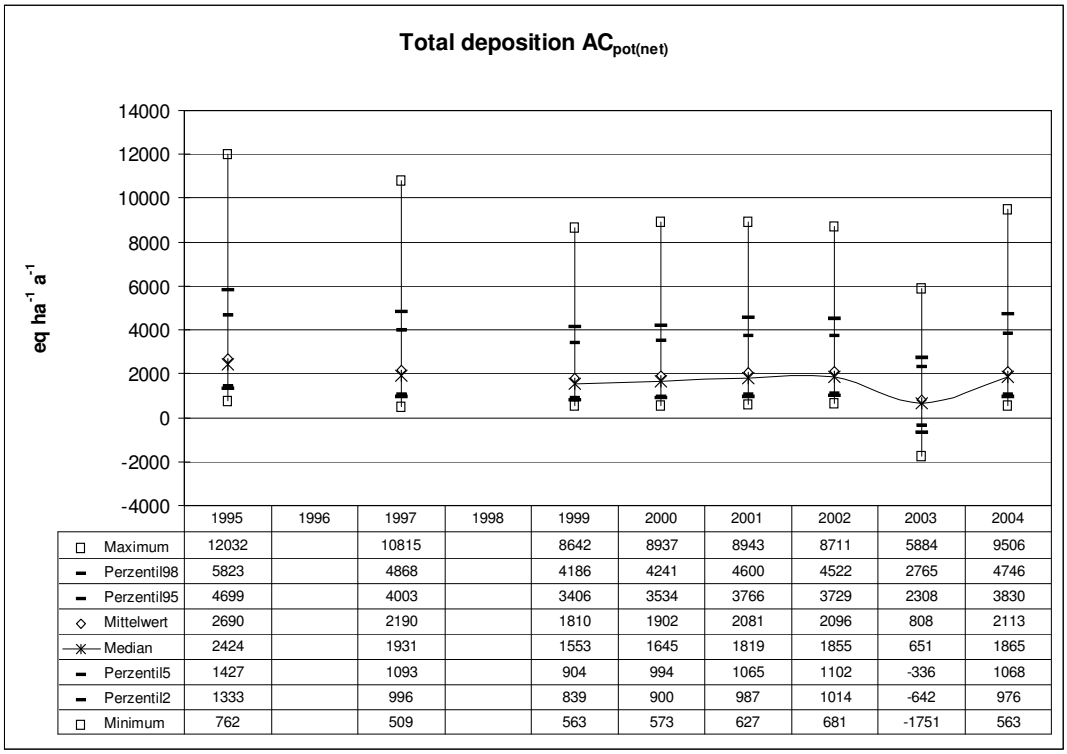

	1995	1996	1997	1998	1999	2000	2001	2002	2003	2004
Maximum	12032		10815		8642	8937	8943	8711	5884	9506
Perzentil98	5823		4868		4186	4241	4600	4522	2765	4746
Perzentil95	4699		4003		3406	3534	3766	3729	2308	3830
Mittelwert	2690		2190		1810	1902	2081	2096	808	2113
Median	2424		1931		1553	1645	1819	1855	651	1865
Perzentil5	1427		1093		904	994	1065	1102	-336	1068
Perzentil2	1333		996		839	900	987	1014	-642	976
Minimum	762		509		563	573	627	681	-1751	563

Figure 9.13: Statistical evaluation of annual potential net acidity ($AC_{pot(net)}$) total deposition 1995-2004

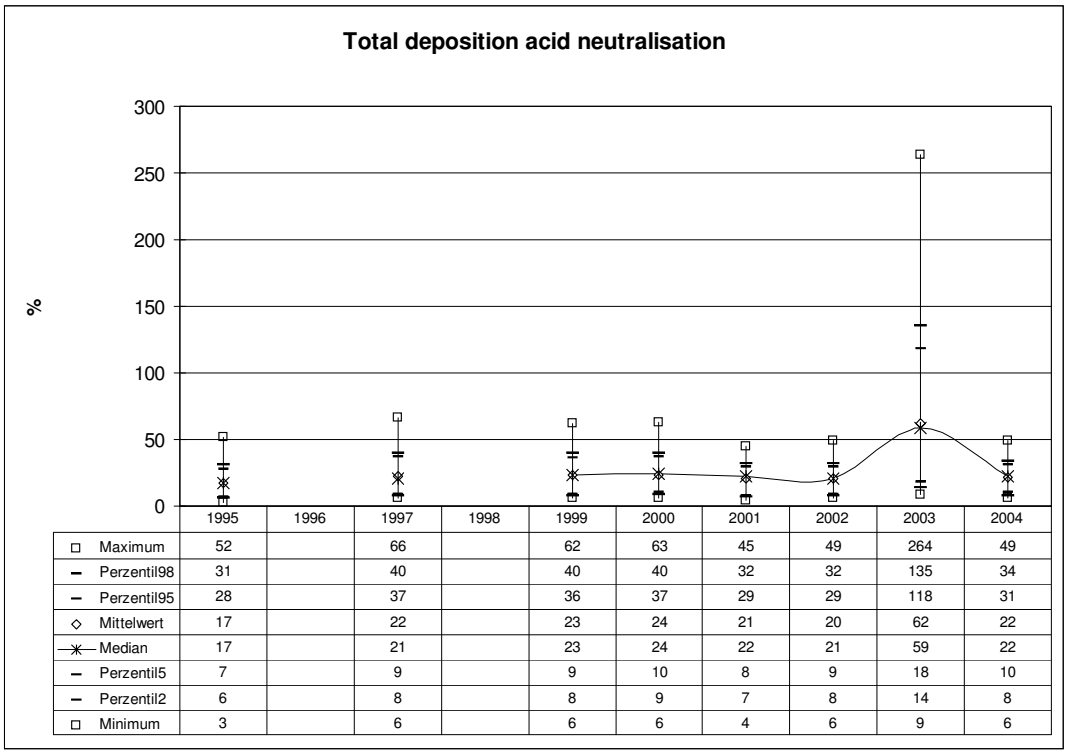

	1995	1996	1997	1998	1999	2000	2001	2002	2003	2004
Maximum	52		66		62	63	45	49	264	49
Perzentil98	31		40		40	40	32	32	135	34
Perzentil95	28		37		36	37	29	29	118	31
Mittelwert	17		22		23	24	21	20	62	22
Median	17		21		23	24	22	21	59	22
Perzentil5	7		9		9	10	8	9	18	10
Perzentil2	6		8		8	9	7	8	14	8
Minimum	3		6		6	6	4	6	9	6

Figure 9.14: Statistical evaluation of annual acid neutralisation in total deposition 1995-2004

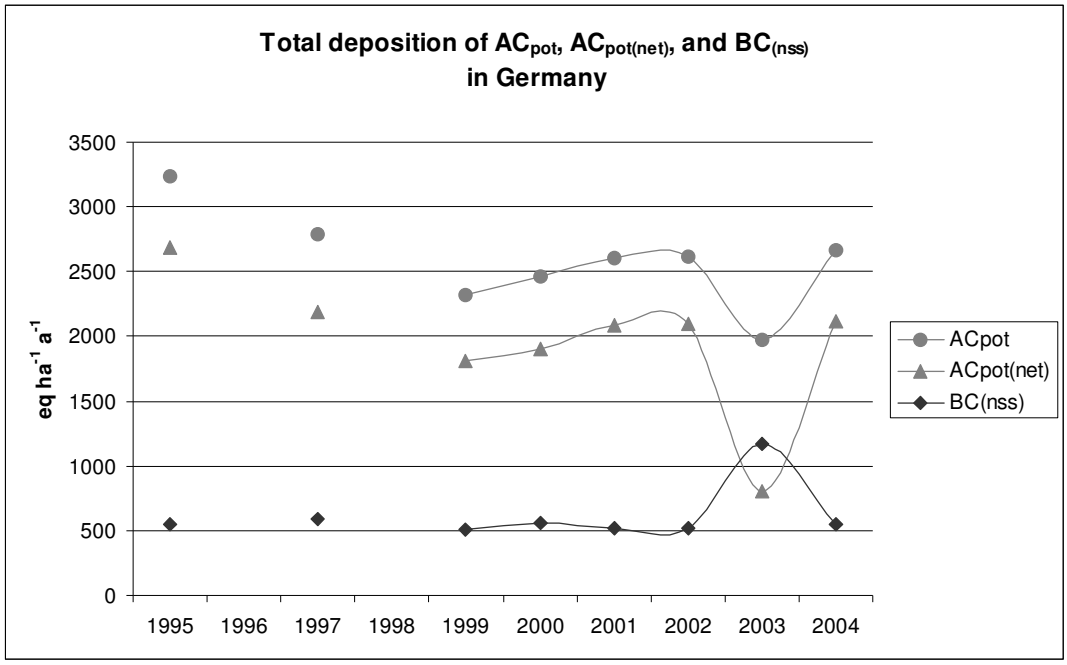

Figure 9.15: Average total deposition of AC_{pot}, $AC_{pot(net)}$, and $BC_{(nss)}$ 1995-2004

9.3 Total deposition fluxes of cadmium (Cd) and lead (Pb)

Total deposition fluxes of the heavy metals cadmium (Cd) and lead (Pb) are calculated as the sum of the respective wet (cf. Chapter 5.3) and dry deposition flux (cf. Chapter 7.3). Budgets of annual average total deposition of Cd and Pb are presented in Table 9.11. The variation between the years, is given as percentage change from the respective previous year, and over the whole time period considered. Cd average total deposition fluxes from 1995 to 2004 declined by about 9.1%, average Pb total deposition fluxes declined by about 4.3%, respectively. This is mainly due to the trend in wet deposition, which is the dominating flux of the preliminary estimates of heavy metal total deposition.

Table 9.11: Budgets of average annual total deposition of Cd and Pb 1995-2004

	Cd [µeq $ha^{-1}a^{-1}$]	Cd [mg $ha^{-1}a^{-1}$]	change from previous year [%]	Pb [µeq $ha^{-1}a^{-1}$]	Pb [g $ha^{-1}a^{-1}$]	change from previous year [%]
1995	2277	128		40367	4.18	
1996						
1997	1819	102	-20.1	43098	4.46	+6.8
1998						
1999	1939	109	+6.6	42639	4.42	-1.1
2000	1753	99	-9.6	41613	4.31	-2.4
2001	1819	102	+3.8	41007	4.25	-1.5
2002	1717	96	-5.6	34407	3.56	-16.1
2003						
2004	2069	116	+20.5	38648	4.00	+12.3
change from 1995 to 2004 [%]			-9.1			-4.3

The contribution of wet and dry deposition fluxes to total deposition of Cd and Pb, given as ratio of both fluxes, is presented in Table 9.12. The comparison of the magnitude of each flux in the single years considered for Cd clearly shows that the wet flux is the dominating fraction of this preliminary total deposition estimates, being more than a factor of 3 to more than 8 times higher than the estimates of the Cd dry deposition fluxes. The contribution of wet deposition to total Pb flux in 2004 is only 16% higher than the dry deposition estimates, while in the other years the Pb wet deposition flux is about a factor of 1.9 to 3.8 higher than the contribution of the dry deposition flux to total deposition. This is mainly due to an underestimation of dry deposition fluxes, and

can be traced back over the chain of model application within this study to serious underestimates of Cd and Pb air concentration and underlying emission inventory data (see Chapter 10.4 for further details).

Table 9.12: Comparison of Cd and Pb dry and wet deposition mapping results 1995-2004

	Cd wet deposition [t a^{-1}]	Cd dry deposition [t a^{-1}]	Ratio: wet flux / dry flux	Pb wet deposition [t a^{-1}]	Pb dry deposition [t a^{-1}]	Ratio: wet flux / dry flux
1995	4.0	0.5	7.68	112.9	36.3	3.11
1996						
1997	2.8	0.8	3.42	106.0	53.3	1.99
1998						
1999	3.2	0.7	4.98	112.7	44.9	2.51
2000	2.9	0.6	4.85	100.4	53.4	1.88
2001	3.1	0.6	5.39	100.8	50.7	1.99
2002	3.1	0.4	8.48	100.8	26.4	3.82
2003	2.5			89.5		
2004	3.3	0.8	3.95	76.7	66.1	1.16

The total deposition estimates and official emission inventory data are presented in Table 9.13. Annual totals of Cd and Pb deposition flux and emission data are compared by the ratio of both in the respective years. Cd total deposition flux in all years considered is higher than the national total emission by about 26% (2002) to 98% (1995). While Cd total deposition estimates over the whole time period is in the range of 3.4 t a^{-1} to 4.6 t a^{-1} the Cd national total emission ranges from 2.2 t a^{-1} to 2.7 t a^{-1}. Pb total deposition estimates in 1995 are 149 t a^{-1} wich is about 55% lower than the official national total emission of 330 t a^{-1}. From 1997 onward the national total emission ranges from 96 ta^{-1} to 109 t a^{-1}, wich is mor than one third less than in 1995, whereas average Pb total deposition estimates 1997 to 2004 are at about 20% to 67% higher than the emission data (Table 9.13).

The differences between national totals in official emission data and the total deposition mapping results can mainly be traced back to higher wet deposition fluxes, which are fully based on monitoring data (cf. Chapter 5.3). Moreover TNO emission data are used as basic input for modelling air concentration with LOTOS-EUROS, which are slightly higher than the official emission inventories for heavy metals (cf. Chapter 10.4), but the LOTOS-EUROS air concentration data are seriously underestimating monitoring data (cf. Chapter 10.4.2). This yields underestimation of dry deposition fluxes of Cd and Pb (cf. Chapter 7.3). Hence the preliminary total deposition estimates presented here are underestimating expected real fluxes into ecosystems, because presently available emission estimates for the heavy metals Cd and Pb are too low.

Table 9.13: Comparison of Cd and Pb total deposition and emission data[1)] in Germany 1995-2004
([1)]UBA 2007 http://www.umweltbundesamt.de/emissionen/archiv/DE_2007_Tables_IV1A_1990_2005.zip)

	Cd total deposition [t a^{-1}]	Cd emission [1)] [t a^{-1}]	Ratio: total flux / emission	Pb total deposition [t a^{-1}]	Pb emission [1)] [t a^{-1}]	Ratio: total flux / emission
1995	4.6	2.3	1.98	149	330	0.45
1996		2.2			222	
1997	3.6	2.4	1.50	159	96	1.67
1998		2.2			94	
1999	3.9	2.7	1.42	158	96	1.65
2000	3.5	2.4	1.45	154	102	1.51
2001	3.6	2.6	1.43	152	105	1.44
2002	3.4	2.7	1.26	127	106	1.20
2003		2.7			107	
2004	4.1	2.7	1.52	143	109	1.52

9.3.1 Total deposition of cadmium (Cd)

Cd total deposition map statistics are presented in Figure 9.16. Over the time period from 1995 to 2004 average estimates of total deposition fluxes of Cd are ranging from 1717 µeq $ha^{-1}a^{-1}$ (96 mg $ha^{-1}a^{-1}$) in 2002 to 2277 µeq $ha^{-1}a^{-1}$ (128 mg $ha^{-1}a^{-1}$) in 1995. In 2004 mean flux of Cd total deposition is 2069 µeq $ha^{-1}a^{-1}$ (116 mg $ha^{-1}a^{-1}$),

which is the second highest result within all years considered. The variation between the modelled years is ranging between about ±20% (Table 9.11). The steepest fall of Cd total deposition fluxes (-20%) can be observed from 1995 to 1997, the highest increase (+21%) from 2002 to 2004. Between 1997 and 2002 the average Cd total deposition flux is on a level of about 102 mg $ha^{-1}a^{-1}$ (1809 µeq $ha^{-1}a^{-1}$), with annual variations ranging from about +7 to about –10% (cf. Table 9.11). From the first year 1995 to the last year (2004) considered in this study, a decline of average total deposition of Cd by 9.1% can be found.

The graphical representation of total deposition fluxes of Cd 1995 to 2004 is presented in Map 9.9. The spatial scatter in each of the maps shows peak deposition fluxes either over higher altitude mountain regions, mainly situated in the southern parts of Germany, or over urban-industrial agglomerations. The latter is mainly du to high estimates of dry deposition fluxes, the former is mainly due to high wet deposition estimates, since those mountain areas are receiving higher precipitation rates.

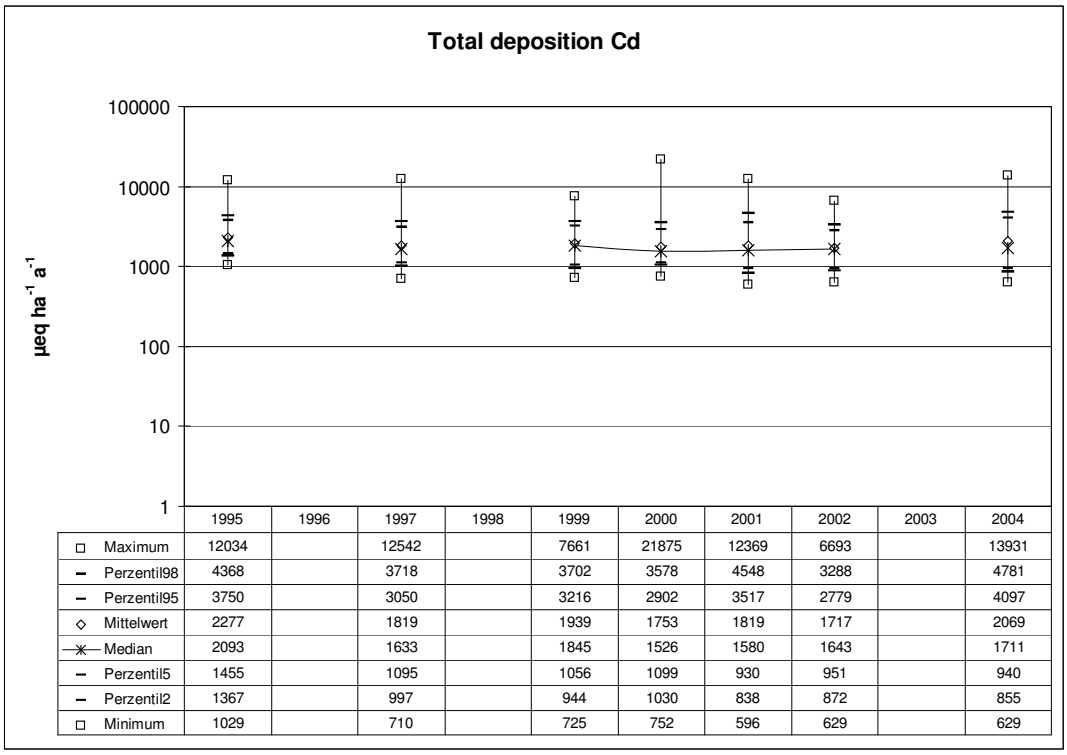

	1995	1996	1997	1998	1999	2000	2001	2002	2003	2004
Maximum	12034		12542		7661	21875	12369	6693		13931
Perzentil98	4368		3718		3702	3578	4548	3288		4781
Perzentil95	3750		3050		3216	2902	3517	2779		4097
Mittelwert	2277		1819		1939	1753	1819	1717		2069
Median	2093		1633		1845	1526	1580	1643		1711
Perzentil5	1455		1095		1056	1099	930	951		940
Perzentil2	1367		997		944	1030	838	872		855
Minimum	1029		710		725	752	596	629		629

Figure 9.16: Statistical evaluation of annual cadmium (Cd) total deposition 1995-2004 (note the logarithmic scale)

9.3.2 Total deposition of lead (Pb)

Map statistics of Pb total deposition estimates are presented in Figure 9.17. Maximum annual average Pb total deposition fluxes can be observed in 1997 with about 4.46 g $ha^{-1}a^{-1}$ (43.1 meq $ha^{-1}a^{-1}$), lowest fluxes with about 3.56 g $ha^{-1}a^{-1}$ (34.4 meq $ha^{-1}a^{-1}$) in 2002. In 2004 average Pb total deposition flux is about 4.0 g $ha^{-1}a^{-1}$ (38.7 meq $ha^{-1}a^{-1}$), which is the second lowest estimate within the time period considered. The variation between the single years is ranging between about -16% and +12%. The steepest decline of Pb total deposition fluxes (-16%) can be observed from 2001 to 2002, the highest increase (+12%) from 2002 to 2004 (cf. Table 9.11). The latter is mainly due to rising dry deposition estimates (cf. Chapter 7.3), while wet deposition fluxes at the same time are falling (cf. Chapter 5.3). From 1995 to 2004 annual average Pb total deposition estimates are falling by about 4.3%.

The graphical representation of Pb total deposition fluxes over time from 1995 to 2004 is presented in Map 9.10. In the spatial patterns of the maps peak deposition fluxes mainly can be found over the urban-industrial agglomerations in western Germany (Ruhr Area, Saarland, Bremen, Hamburg, Berlin). Generally lower Pb total deposition fluxes can be found the southern half of Germany, except in the area of the Black Forest, where higher Pb total deposition fluxes than average can be observed.

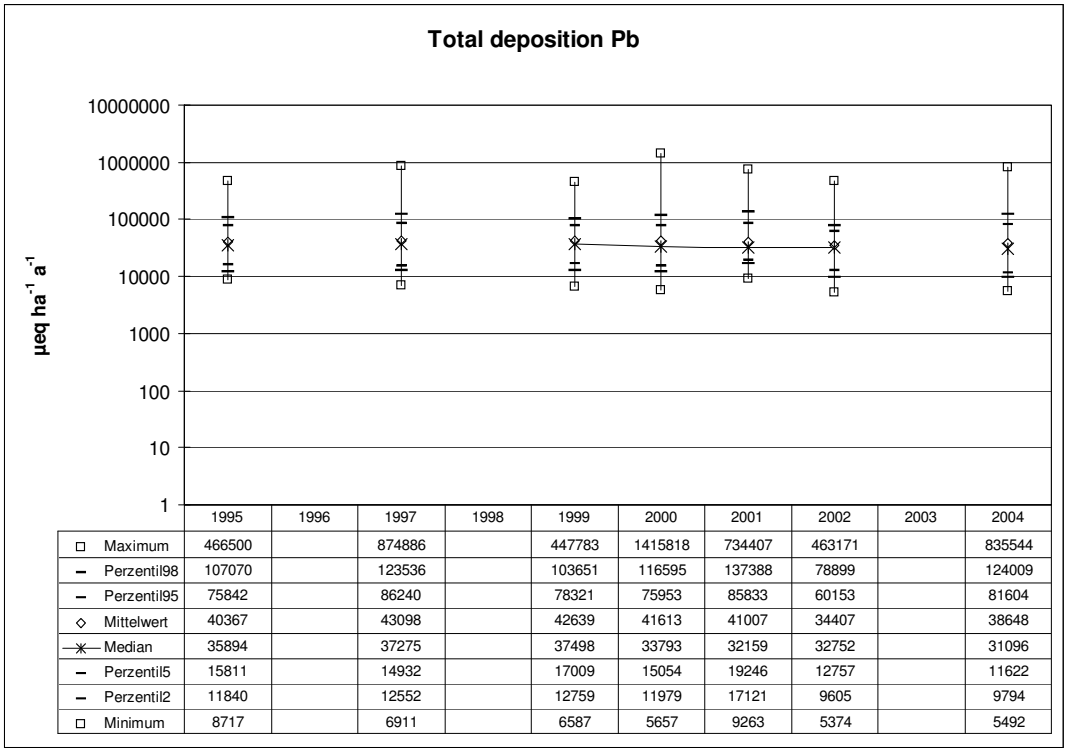

	1995	1996	1997	1998	1999	2000	2001	2002	2003	2004
Maximum	466500		874886		447783	1415818	734407	463171		835544
Perzentil98	107070		123536		103651	116595	137388	78899		124009
Perzentil95	75842		86240		78321	75953	85833	60153		81604
Mittelwert	40367		43098		42639	41613	41007	34407		38648
Median	35894		37275		37498	33793	32159	32752		31096
Perzentil5	15811		14932		17009	15054	19246	12757		11622
Perzentil2	11840		12552		12759	11979	17121	9605		9794
Minimum	8717		6911		6587	5657	9263	5374		5492

Figure 9.17: Statistical evaluation of annual lead (Pb) total deposition 1995-2004 (note the logarithmic scale)

9.4 Comparison of German and EMEP total deposition data of NO_Y-N, NH_X-N, and SO_X-S

A comparison between German and EMEP estimates of total deposition of oxidised nitrogen (NO_Y-N), reduced nitrogen (NH_X-N), total N, and oxidised non-sea salt sulphur (SO_X-$S_{(nss)}$) for 2004 was carried out. The latest available EMEP "WebDab Unified Model Results 2006" deposition data, calculated for the EMEP Status Report 1/2006 (http://www.emep.int/publ/common_publications.html) were retrieved from the UNECE/EMEP air-quality database (http://webdab.emep.int/Unified_Model_Results/).

The following data processing had to be carried out in order to calculate the comparison of national and EMEP total deposition estimates over Germany:

- EMEP 50x50km² grid data covering Germany have been projected in the German project's standard projection
- German model output of dry and wet deposition fluxes were used in order to calculate total deposition in-line with EMEP calculation of total deposition
- German deposition estimates were calculated as averages into the shape of the EMEP 50x50km² grid
- EMEP and German total deposition estimates were compared by calculating the differences and ratios of both

Here the deposition estimates of both, the EMEP model and the results of the German high resolution model approach, as well as the outcome of the comparison in detail is presented. The graphical representation of the EMEP and German total deposition model estimates for NO_Y-N, NH_X-N, total N, and SO_X-$S_{(nss)}$ 2004 and the result of the comparisons are presented in Figure 9.18 to 9.21. For both, the visual comparison and the calculated differences and ratio between EMEP and national deposition estimates, the EMEP grid was used.

In this exercise national high resolution maps in 1x1km² grid resolution are compared to EMEP 50x50km² maps on the same spatial and temporal scale, assuming that on average both model results should result in similar deposition fluxes. The comparison of the 2004 total deposition fluxes, calculated as average for 199 EMEP 50x50km² grid cells over Germany, shows higher deposition estimates for all air pollutants carrying out the German modelling approach.

However,
- for NO_Y-N total deposition German estimates are about 32% higher,
- for NH_X-N total deposition German estimates are about 45% higher,

- for total N deposition German estimates are about 40% higher,
- for SO_X-S total deposition German estimates are about 34% higher,

compared to the corresponding EMEP model results.

In Figure 9.22 and Figure 9.33 map statistics of the relative and absolute comparison between EMEP and national model results for the single compounds (NO_Y-N, NH_X-N, N, SO_X-S) and the single fluxes considered (wet, dry and total deposition loads) are presented.

NO_Y-N total deposition estimates

The spatial trend of the German and EMEP NO_Y-N total deposition is shown in Figure 9.18. The patterns of EMEP and German total NO_Y-N deposition estimates (Figure 9.18, left side) clearly show lower EMEP deposition fluxes (lighter colour) than the German total deposition result (darker map), though the spatial trend of both maps is similar as the distribution of higher deposition fluxes, which mainly can be found over western parts of Germany, and lower estimates, mainly over regions in eastern and southern Germany, is concerned.

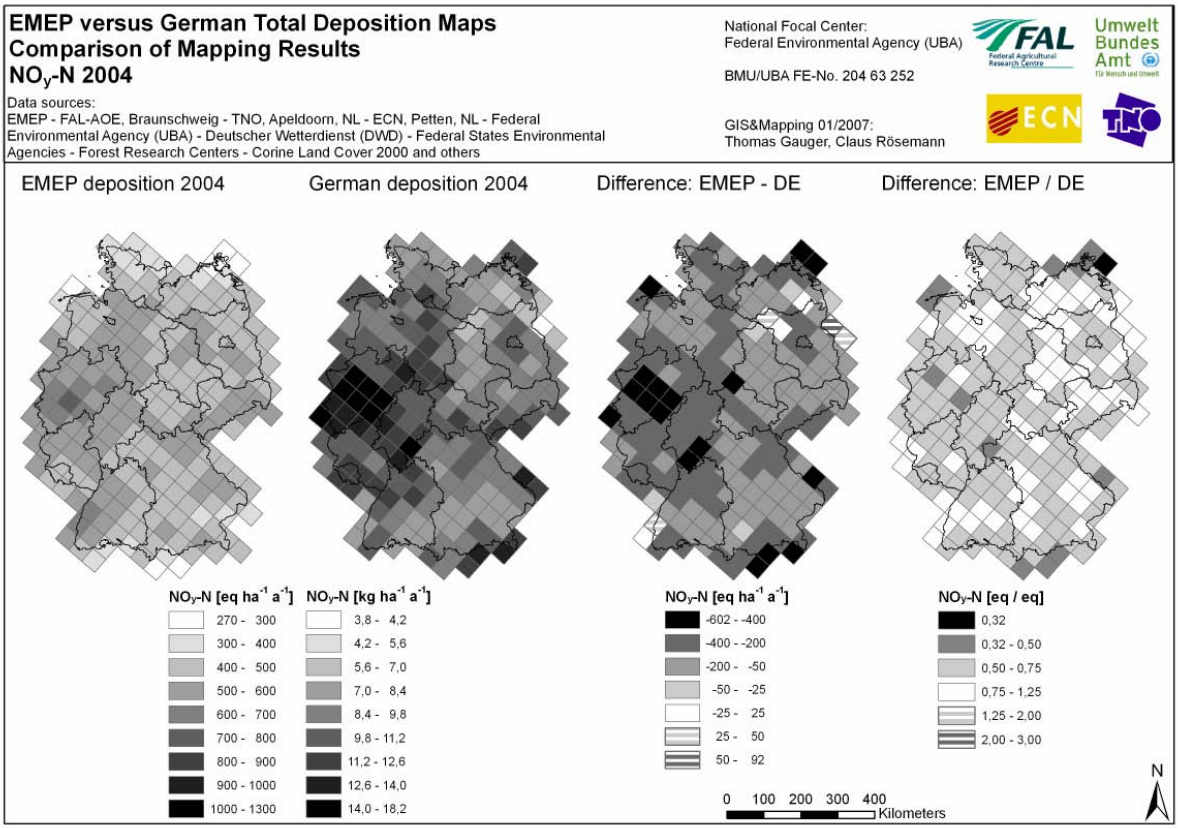

Figure 9.18: German and EMEP Total deposition of NO_Y-N 2004

The absolute differences between EMEP and German NO_Y-N total deposition estimates are ranging from about 1.3 kg ha^{-1} a^{-1} (93 eq ha^{-1} a^{-1}) higher EMEP results per EMEP grid cell over Germany to about 8.4 kg ha^{-1} a^{-1} (602 eq ha^{-1} a^{-1}) higher German estimates of NO_Y-N (Figure 9.18). Over all Germany an average difference of about 3.2 kg ha^{-1} a^{-1} (228 eq ha^{-1} a^{-1}) higher German estimates for total NO_Y-N deposition can be found. This equals an about 32% higher national NO_Y-N total deposition estimate compared to the EMEP model estimate for Germany.

NH_X-N total deposition estimates

In Figure 9.19 the EMEP and German estimates of NH_X-N 2004 total deposition as well as the comparison of both model results is shown. In the EMEP model estimates as well as in the German model results highest deposition fluxes can be found over the main source areas in the north-western part of Germany, whereas the north-eastern and central parts of Germany are receiving lower NH_X-N fluxes and a secondary peak area can be found over southern Germany. The national modelling and mapping result, however, on average is about 45% higher than the EMEP result. Highest differences between both estimates can be found over north-western Germany and in some parts of south-eastern Germany.

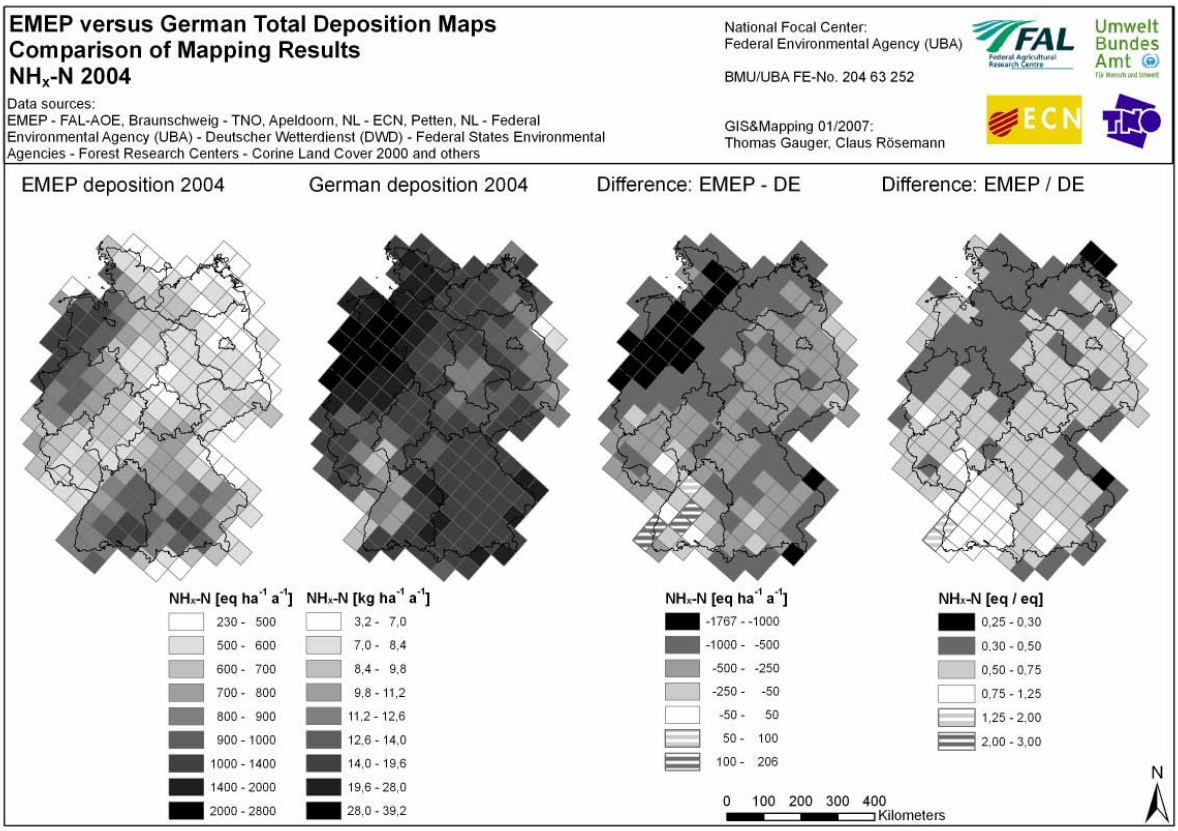

Figure 9.19: German and EMEP Total deposition of NH_X-N 2004

The maximum deviation between EMEP and the German NH_X-N total deposition estimates is ranging from a 2.9 kg ha^{-1} a^{-1} (206 eq ha^{-1} a^{-1}) higher EMEP estimate over south-western Germany to a 24.8 kg ha^{-1} a^{-1} (1767 eq ha^{-1} a^{-1}) higher national result, that can be found in north-western Germany. On average over Germany the differences are showing an about 7.9 kg ha^{-1} a^{-1} (562 eq ha^{-1} a^{-1}) higher national estimate of NH_X-N total deposition.

N total deposition estimates

Total deposition of total nitrogen is the sum of reduced (NH_X-N) and oxidised nitrogen (NO_Y-N) fluxes, where NH_X-N quantitatively contributes most to total nitrogen (N) total deposition fluxes. In case of the EMEP 2004 estimates NH_X-N on average is contributing by 59%, NO_Y-N by about 41% to N total deposition. The national model result is slightly different with NH_X-N contributing 64%, NO_Y-N by about 36% to N total deposition in 2004 over Germany. The spatial patterns and the comparison of both model estimates are shown in Figure 9.20. In the EMEP estimates N total deposition above the average of 1166 eq ha^{-1} a^{-1} (16.3 kg ha^{-1} a^{-1}) can be found over north-western and southern Germany, whereas N total deposition below average fluxes can mainly be observed over north-eastern and central Germany.

The average N total deposition flux of the national model estimate in 50x50km² EMEP grid resolution is about 27.4 kg ha^{-1} a^{-1} (1958 eq ha^{-1} a^{-1}), and hence 40% higher than the average EMEP result, which in the graphical representation (Figure 9.20) clearly can be seen in the darker colour of the German deposition map. N total deposition fluxes above the respective average model estimate, however, in both maps can be found in 47 identical 50x50km² grid cells, and N total deposition fluxes below the respective average model estimate can be found in 72 of 199 identical 50x50km² grid cells, which is indicating to some extend similar spatial trends of both estimates.

The differences of both N total deposition estimates within all 50x50km² grid cells considered are ranging from 3.4 kg ha^{-1} a^{-1} (246 eq ha^{-1} a^{-1}) higher EMEP deposition in south-western Germany to a 28.4 kg ha^{-1} a^{-1} (2013 eq ha^{-1} a^{-1}) higher national result in north-western Germany. In only 7 of the grid cells higher EMEP than German N total deposition estimates can be found. Highest relative divergence between both model estimates (above 50%) can be observed in northern and north-western Germany, and in some border grids in south eastern Germany, whereas the relative differences are low (±25%) in several grids over south-western and southern Germany (Figure 9.20).

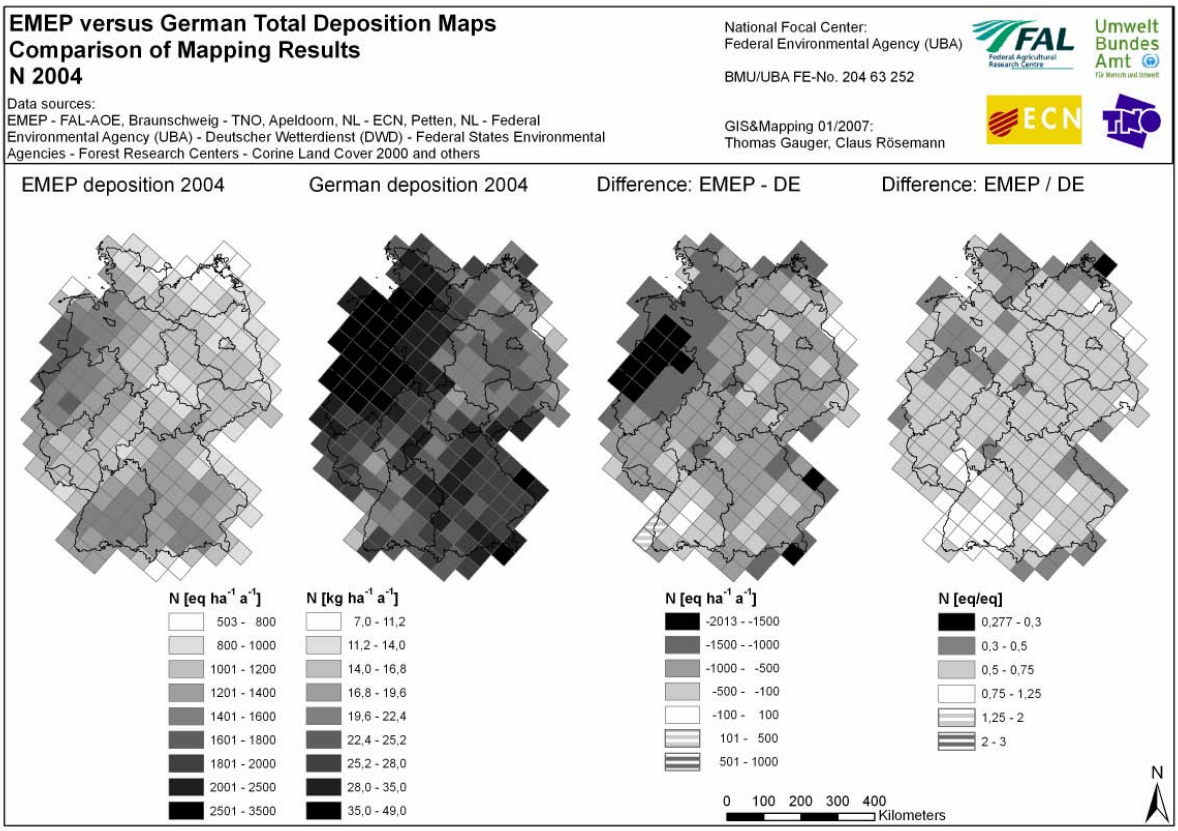

Figure 9.20: German and EMEP total deposition of N 2004

SO_X-S total deposition estimates

EMEP and German 50x50km² model estimates of total deposition fluxes of oxidised sulphur (SO_X-S) from anthropogenic sources are shown and compared to each other in Figure 9.21. Highest average SO_X-S total deposition fluxes in EMEP estimates for 2004 can be observed in western Germany (North Rhine-Westphalia) in eastern Germany (at the border between Saxony and the Czech Republic), and in the north (at the German Bight). In the national model estimates this regions also are receiving highest SO_X-S total deposition fluxes.

Obviously the lighter colour of the EMEP estimates presented in Figure 9.21, in contrast to the German estimates, is indicating that the national model estimates are higher than the respective EMEP results. The EMEP average SO_X-S total deposition flux over Germany in this 50x50km² grid maps is about 7.1 kg ha^{-1} a^{-1} (446 eq ha^{-1} a^{-1}), ranging from minimum 2.8 kg ha^{-1} a^{-1} (175 eq ha^{-1} a^{-1}) to maximum 13.2 kg ha^{-1} a^{-1} (826 eq ha^{-1} a^{-1}). The respective national estimates of average SO_X-S total deposition fluxes on average are 34% higher, ranging from 5.0 kg ha^{-1} a^{-1} (314 eq ha^{-1} a^{-1}) to maximum 30.3 kg ha^{-1} a^{-1} (1890 eq ha^{-1} a^{-1}), with an overall average of 10.8 kg ha^{-1} a^{-1} (673 eq ha^{-1} a^{-1}).

The spatial trend of both model results, however, to some extend is comparing well. Both approaches are showing SO_X-S total deposition fluxes above the respective average on 61 and below the respective average on 69 of 199 identical 50x50km² grids.

Highest absolute and relative differences between EMEP and national model estimates can be found over western Germany (Ruhr area, North Rhine-Westphalia), and at some bordering grids at the coastline of the North Sea and the Baltic Sea. The lowest deviation of both approaches for SO_X-S total deposition mainly can be found in southern Germany.

The differences of both SO_X-S total deposition estimates within all 50x50km² grid cells considered are ranging from 2.5 kg ha^{-1} a^{-1} (153 eq ha^{-1} a^{-1}) higher EMEP deposition in south-western Germany to a 18.6 kg ha^{-1} a^{-1} (1158 eq ha^{-1} a^{-1}) higher national result over western Germany. In 13 of all 50x50km² grid cells higher EMEP than German N total deposition estimates can be found. Highest relative divergence between both model estimates (above 50%) can be observed in western, north-western, and north-eastern most parts of Germany, whereas low relative differences (±25%) in several grids mainly over in the southern half of Germany can be found (Figure 9.21).

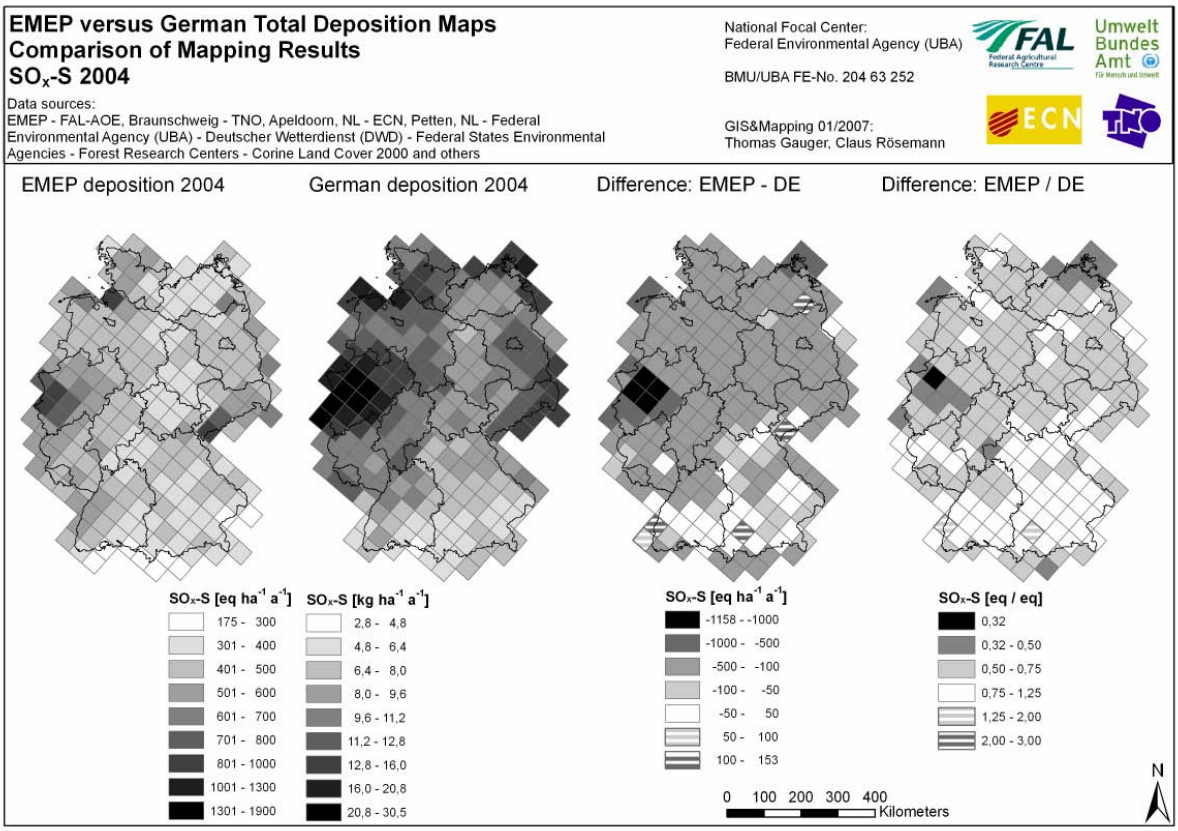

Figure 9.21: German and EMEP Total deposition of SO_X-$S_{(nss)}$ 2004

Differences with respect to single contributing fluxes of EMEP and German total deposition estimates

Figure 9.22 shows the relative differences for wet, dry and total deposition fluxes of EMEP and the German model output mapped for 199 EMEP 50x50km² grid cells over Germany, for SO_X-S, NO_Y-N, NH_X-N and total N. Differences signed negative (-) indicate higher results of the German high resolution model estimates, whereas positive differences indicate higher deposition fluxes from the EMEP model. Maxima, minima and mean values of the 199 grid cells' differences are also listed.

The national model estimates in most cases are higher than EMEP model results. Slightly higher average EMEP deposition fluxes are found for SO_X-S wet deposition (4% higher) and for wet deposition of NO_Y-N (1% higher than German estimates). All other deposition fluxes the German model results are on average higher than the EMEP estimates: 50% higher total deposition of SO_X-S, 140% higher dry deposition of SO_X-S, 71% higher total deposition of N, 2% higher wet deposition of N, 6% higher wet deposition of NH_X-N, 175% higher dry deposition of N, 128% higher dry deposition of NO_Y-N, and 215% higher dry deposition of NH_X-N (Figure 9.22).

The ranges of absolute difference (in kg ha^{-1} a^{-1}) between the national and EMEP deposition estimates are presented in Figure 9.23. Here the relevance of the differences with regard to eutrophication and acidification effects of the deposition estimates becomes more obvious than in relative differences (cf. Figure 9.22).

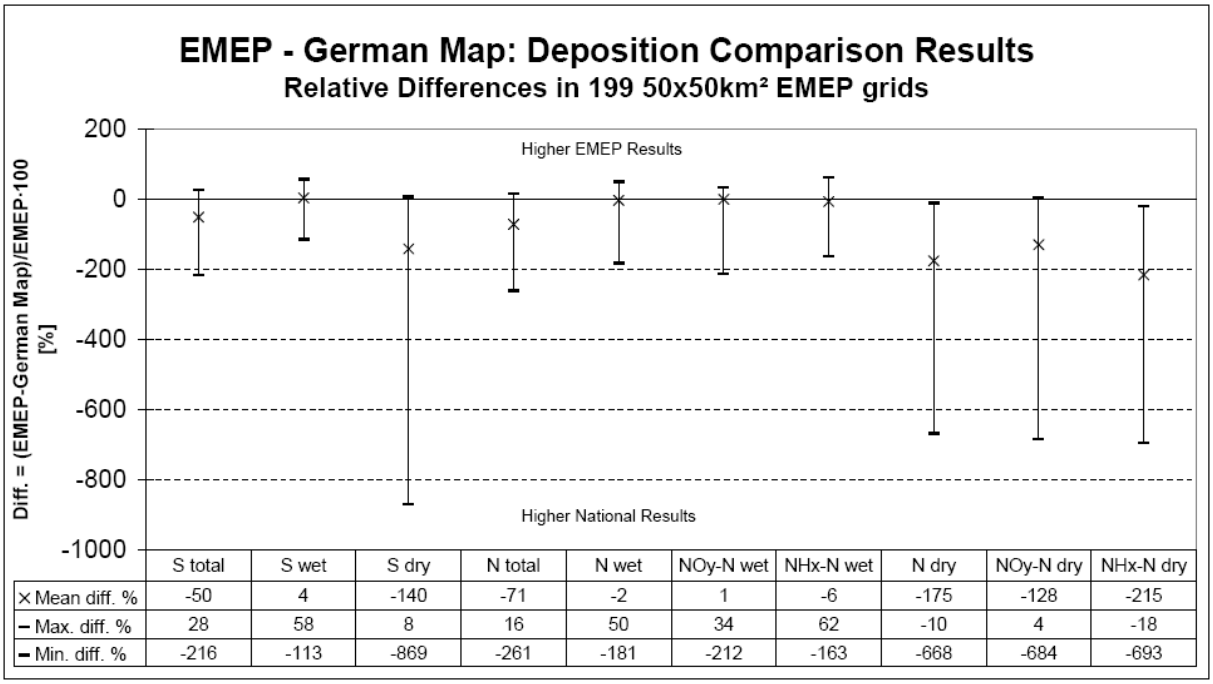

	S total	S wet	S dry	N total	N wet	NOy-N wet	NHx-N wet	N dry	NOy-N dry	NHx-N dry
× Mean diff. %	-50	4	-140	-71	-2	1	-6	-175	-128	-215
– Max. diff. %	28	58	8	16	50	34	62	-10	4	-18
– Min. diff. %	-216	-113	-869	-261	-181	-212	-163	-668	-684	-693

Figure 9.22: Relative differences between EMEP and German total deposition estimates 2004 [%]

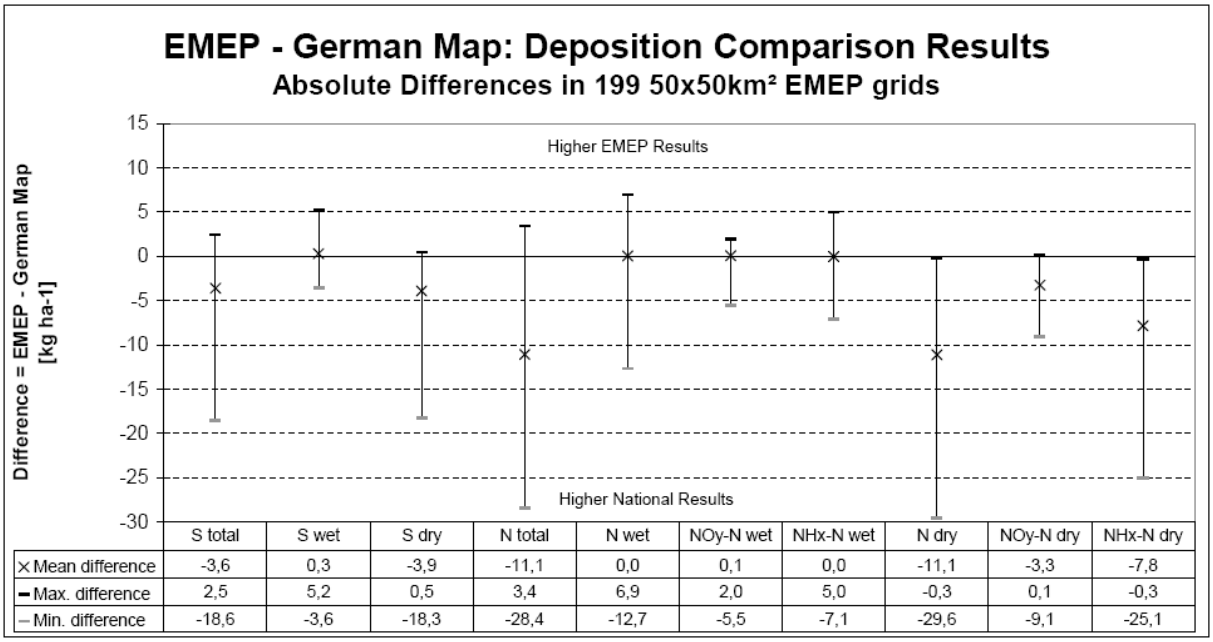

	S total	S wet	S dry	N total	N wet	NOy-N wet	NHx-N wet	N dry	NOy-N dry	NHx-N dry
× Mean difference	-3,6	0,3	-3,9	-11,1	0,0	0,1	0,0	-11,1	-3,3	-7,8
– Max. difference	2,5	5,2	0,5	3,4	6,9	2,0	5,0	-0,3	0,1	-0,3
– Min. difference	-18,6	-3,6	-18,3	-28,4	-12,7	-5,5	-7,1	-29,6	-9,1	-25,1

Figure 9.23: Absolute differences between EMEP and German total deposition estimates 2004 [kg ha^{-1} a^{-1}]

Table 9.14: Results and differences between EMEP and German 2004 deposition estimates for SO_X-S, total N, NO_Y-N and NH_X-N calculated in 199 50x50km² EMEP grids covering Germany

Species	Mean [eq ha^{-1} a^{-1}]	Mean [eq ha^{-1} a^{-1}]	Deviation [%]	Contribution of Wet Deposition Flux		Contribution of Dry Deposition Flux	
Total Deposition	EMEP	German Map	EMEP / German Map	EMEP	German Map	EMEP	German Map
SO_x-S	446	673	66%	59%	36%	41%	64%
N	1166	1958	60%	59%	35%	41%	65%
NO_y-N	483	712	68%	60%	40%	40%	60%
NH_x-N	683	1245	55%	59%	32%	41%	68%

In Table 9.14 a synopsis of average total deposition of both model approaches, as well as the respective contribution of wet and dry fluxes for sulphur and nitrogen species is presented. The average share of the dry and

wet fluxes to total deposition clearly shows that in the German approach dry deposition contributes to total deposition to a higher extent (average 60% to 68%) than in the EMEP model approach (average 40 to 41%). In the comparison presented here no comparison with measurements was carried out, but a few measurements of wet and dry deposition in Central Europe (Germany, Switzerland) can be found (Table 9.15), which indicate that the relative share of dry deposition fluxes of N and S species into different receptor systems is higher than the respective share of wet deposition. This is in line with the German modelling and mapping result and contradicts the EMEP result with its higher average wet than dry fluxes of S and N species over Germany.

Table 9.15: Contribution of wet and dry deposition derived by measurements in Central Europe

Species	Contribution of Wet Deposition	Contribution of Dry Deposition	Land Use	Location	Source
N total deposition	33%	67%	semi-natural (grassland)	Merenschwand near Zürich	Hesterberg et al. 1996
N total deposition	32%	68%	pine forest	Augustendorf, NW Germany	Mohr et al. 2005
N total deposition	24%	76%	agrarian area	Braunschweig	Dämmgen et al. (n.p.)
S total deposition	21%	79%	pine forest	Augustendorf, NW Germany	Mohr et al. 2005

The differences in the results of the two approaches are

- on average 3.6 kg ha^{-1} a^{-1} higher estimates of *SO_x-S total deposition* by the German method, ranging from 2.5 kg ha^{-1} a^{-1} higher EMEP model output to 18.6 kg ha^{-1} a^{-1} higher German model output in the single grids. The latter mainly is a result of the 0.3 to 18.3 kg ha^{-1} a^{-1} (17 to 113 eq ha^{-1} a^{-1}) lower estimates of *SO_x-S dry deposition* by EMEP compared to the German estimates, which can be found in 197 of 199 cells over Germany.
- almost identical average estimates of *SO_x-S wet deposition.* On average EMEP results of SO_x-S wet deposition are only slightly (0.3 kg ha^{-1} a^{-1}) higher, the range of divergence in the single grids however, is ranging from a 5.2 kg ha^{-1} a^{-1} higher EMEP result to a 3.6 kg ha^{-1} a^{-1} higher German model result
- on average 11.1 kg ha^{-1} a^{-1} higher estimates of *N total deposition* by the German method with a range in the single grids from a 3,4 kg ha^{-1} a^{-1} higher EMEP result to a 28.4 kg ha^{-1} a^{-1} higher national result
- on average identical estimates of *N wet deposition* by both the EMEP and the German method (± 0 kg ha^{-1} a^{-1}). In the single grids, however, a range from 6.9 kg ha^{-1} a^{-1} higher EMEP result to 12.7 kg ha^{-1} a^{-1} higher national result in the single grids can be observed
- on average 11.1 kg ha^{-1} a^{-1} higher German estimates of *N dry deposition* as a result of 0.3 kg ha^{-1} a^{-1} to 29.6 kg ha^{-1} a^{-1} higher national estimates in the 199 single grids compared
- almost the same results for *NO_y-N wet deposition* estimates by both model approaches with on average a slightly higher (0. 1 kg ha^{-1} a^{-1}) German result in the single grids, however, a range from 2.0 kg ha^{-1} a^{-1} higher EMEP result to 5.5 kg ha^{-1} a^{-1} higher national result in the single grids can be found
- average 3.3 kg ha^{-1} a^{-1} higher estimates of *NO_y-N dry deposition* by the German model. The range of the difference in the single grids lies between a 0.1 kg ha^{-1} a^{-1} lower and 9.1 kg ha^{-1} a^{-1} higher estimates of the German model in the single 50x50 km² grids
- on average identical estimates of *NH_x-N wet deposition* estimates (± 0 kg ha^{-1} a^{-1}). In the single grids, however, a range from 5.0 kg ha^{-1} a^{-1} higher EMEP result to 7.1 kg ha^{-1} a^{-1} higher national result in the single grids can be found
- on average 7.8 kg ha^{-1} a^{-1} higher German *NH_x-N dry deposition* estimates than the EMEP result. The single grids show a range from 0.3 kg ha^{-1} a^{-1} to a 25.1 kg ha^{-1} a^{-1} higher national result

The differences between the EMEP and the German model results are highest for dry deposition estimates of nitrogen species and sulphur, whereas wet deposition estimates are in best agreement within this exercise. The estimates of the wet deposition fluxes in the German method is based upon widespread networks of deposition and precipitation monitoring, which leads to reliable mapping results, as far as accuracy and reliability of the input data quality can be assumed. The national approach to derive wet deposition maps using deposition measurements is basically different to the EMEP model approach. The remarkable low difference of EMEP estimates to the compared national average wet deposition results calculated for the EMEP 50x50 km² grids indicates that the EMEP model results for SO_X-S as well as for N, NO_Y-N,and NH_X-N are showing no general over- or underestimate of this fluxes.

With respect to dry deposition fluxes, EMEP model results are much lower than the German model result. This

is mainly true for SO_X-S and NH_X-N dry deposition over areas with high emission density. The comparison of NO_Y-N dry deposition estimates also shows lower EMEP estimates compared to the German model result, but the differences can not be clearly attributed to certain areas.

In Table 9.16 the national total emission in Germany 2004 and the summarised deposition fluxes are listed. From this it can be seen, that the EMEP model estimates for total deposition of SO_X-S and NH_X-N are higher than the German inland emission of the respective species in 2004, whereas the German model predicts higher total deposition and hence net import of SO_X-S and NH_X-N inland.

Table 9.16: Emission totals and average wet, dry, and total deposition flux in the German and EMEP model result for 2004 [in Gg a^{-1}= kt a^{-1}]

2004 data comparison		**SOx-S**	**NOy-N**	**NHx-N**	**N**
Emission in Germany	*national total [kt a^{-1}]*	***296***	***480***	***514***	***994***
Deposition German Model	wet flux [kt a^{-1}]	122	142	201	343
	dry flux [kt a^{-1}]	216	215	424	640
	total flux [kt a^{-1}]	**387**	**357**	**625**	**983**
EMEP Model, Germany	wet flux [kt a^{-1}]	149	145	200	345
	dry flux [kt a^{-1}]	107	98	143	241
	total flux [kt a^{-1}]	**256**	**242**	**343**	**585**
EMEP-German model	*mean diff. total flux [kt a^{-1}]*	*-131*	*-115*	*-282*	*-398*
EMEP/Geman model	*mean deviation total flux [%]*	*66%*	*68%*	*55%*	*60%*

Discussion and conclusions

Higher national dry deposition estimates may be attributed to higher air concentration estimates derived by the LOTOS-EUROS model (cf. Chapter 10), and used as input to the IDEM deposition model. With respect to dry deposition estimates further analysis is needed to clearly identify reasons for the differences in the national and EMEP estimates. Possible causes for the discrepancy in dry deposition rates of oxidised sulphur, reduced and oxidised nitrogen may lie in different receptor information, meteorological data, different scale of model input and calculated output resolution, respectively, and in differences in parameterisation of the dry deposition processes in the respective model.

The main findings of the comparison carried out here are partly matching the findings of other and more detailed comparison exercises and model evaluations between EMEP and national modelling results, e.g. in The Netherlands (VELDERS ET AL. 2003, VAN DEN BROEK ET AL. 2008), and comparisons with measurements (e.g. SIMPSON ET AL. 2006), respectively.

The findings in SIMPSON ET AL. 2006, among others, consist of a description of EMEP modelled and observed contributions of wet and dry deposition of NH_X-N and NO_Y-N in 2000 over a forest plot in the Netherlands (Speulderbos). These data are with 65% dry and 35% wet deposition of N observed, and 76% dry and 24% wet deposition of N modelled, respectively, in good agreement. This unfortunately does not hold for the averaged 2004 EMEP data over Germany used for comparison here (cf. Table 9.14).

The main findings in VELDERS ET AL. 2003, where several aspects of the EMEP Unified model are compared to the OPS model with regard to deposition parameterisation, concentration, and deposition data for the year 2000, are

with regard to Emission data:

- Absence of changes over time in the geographical distribution of emissions (in Germany, The Netherlands, Poland) used in the EMEP model have been found, having effects on the spatial distribution of modelled air concentration and resulting in discrepancies to measurements.

with regard to the contribution of national emission to deposition (source receptor relation)

- Contribution of national emission to deposition in the Netherlands is always higher in national OPS estimates than in the EMEP model output. The latter, compared to observations, underestimates air concentration and/or dry deposition due to lower deposition velocities (v_d). Generally underestimates of air concentration may be traced back to overestimates of deposition (velocity) and vice versa. If both air concentration and dry deposition is underestimated a mismatch in the balance of in air species might be

the reason, resulting in overestimates of transport abroad (as found for EMEP modelled NH_X, NO_Y in The Netherlands).

with regard to the balance of concentration and deposition data:

- EMEP dry deposition estimates of nitrogen species are much lower than national results in the Netherlands.
- The parameterisation of deposition velocities in the EMEP model is inconsistent with respect to co-deposition of SO_2 and NH_3.
- Discrepancies in the dry deposition formulation between EMEP and the DEPAC module (used in the OPS model as well as in LOTOS-EUROS and IDEM) with dry deposition velocities having strong impact on model outcome regarding transport, deposition, and air concentration.
- EMEP modelled NO_X and NH_3 air concentration is 30% to 40% lower than measurements.
- Good agreement between modelled and measured wet deposition.

VAN DEN BROEK ET AL. (2008) described a

- mismatch between air concentration and deposition of NH_3 over fertilised grassland in the Netherlands. OPS modelled air concentration is too low compared with measurements, because dry deposition (loss from the atmosphere) is too high. Here the parameterisation of R_c, the canopy or surface resistance, is too low, compared to measurements. This is contrary to the EMEP model, where the parameterisation yields higher R_c, hence lower deposition velocities (v_d), lower dry deposition fluxes, and higher air concentration of NH_3.

The following conclusions can be drawn from the comparison exercise:

- The emission data used as input for both, EMEP and the German approach for modelling deposition loads are in the same order of magnitude, as far as national totals of sulphur, reduced, and oxidised nitrogen in Germany are concerned (Table 9.16; Klein & Benedictow 2006, UBA 2007). The allocation of emissions within Germany has not been compared in this exercise. It can be assumed, however, that the sub-regional distribution of emission density is different in the EMEP model compared to the Geman modelling approach, since the respective emission data used in the German modelling approach are using higher spatial resolution (cf. Chapter 10.2.3), and the pre-processing of emission data may be different within both modelling approaches. Further investigation would be needed to resolve this issue.
- Almost identical average estimates of wet deposition for S and N were found in the presented comparison exercise. This is in line with the findings in other comparisons with EMEP data (VELDERS ET AL. 2003, SIMPSON ET AL. 2006).
- Highest deviation is found for dry deposition estimates of N and S compounds, and hence for total (wet + dry) deposition estimates. EMEP modelling results are remarkably lower than the German modelling results. From measurements of wet and dry deposition it is indicated, that the EMEP model underestimates the contribution of dry deposition flux to total deposition (cf. Table 9.14 and 9.15). Since dry deposition loads in chemical transport models are the product of deposition velocity (v_d) and air concentration, an underestimate of the dry deposition flux may be attributed to underestimated effective deposition velocitiy, which leads to overestimates of air concentration (cf. VELDERS ET AL. 2003). Low deposition fluxes and high air concentration estimates on the other hand are leading to greater transport distances and deposition further away from the source areas.This also may result in higher export rates and deposition outside Germany. The comparison of national total emission and total deposition (c.f. Table 9.16) is indicating net export of SO_X-S and NH_X-N as a result of the EMEP model estimates for 2004, which is contradicted by the outcome of the German modelling, where the balance between emission and total deposition results in a net import of SO_X-S and NH_X-N.
- Lower inland total deposition fluxes calculated by the EMEP model also result in lower exceedance of critical loads in Germany compared to the respective German model outcome. On average 11 kg ha^{-1} a^{-1} lower N total deposition in Germany calculated by EMEP may result in approximately 50% lower average exceedances of critical loads for nitrogen ($CL_{(nut)}N$) compared to the national estimates (cf. NAGEL ET AL. in Part 2 of this report).

In the comparison of the EMEP and national model only annual aveaged depositopn fluxes of 2004 are compared. The differences found between the two model results strongly give reason for further analyses. Severe deviations in air concentration, transport and critical load exceedances predicted on the base of modelled deposition estimates are indicated. A more throughgoing comparison of national and EMEP model results is intended to be carried out in the German follow-up research project BMU/UBA 370764200.

9.5 *Maps of total deposition 1995, 1997, 1999-2004*

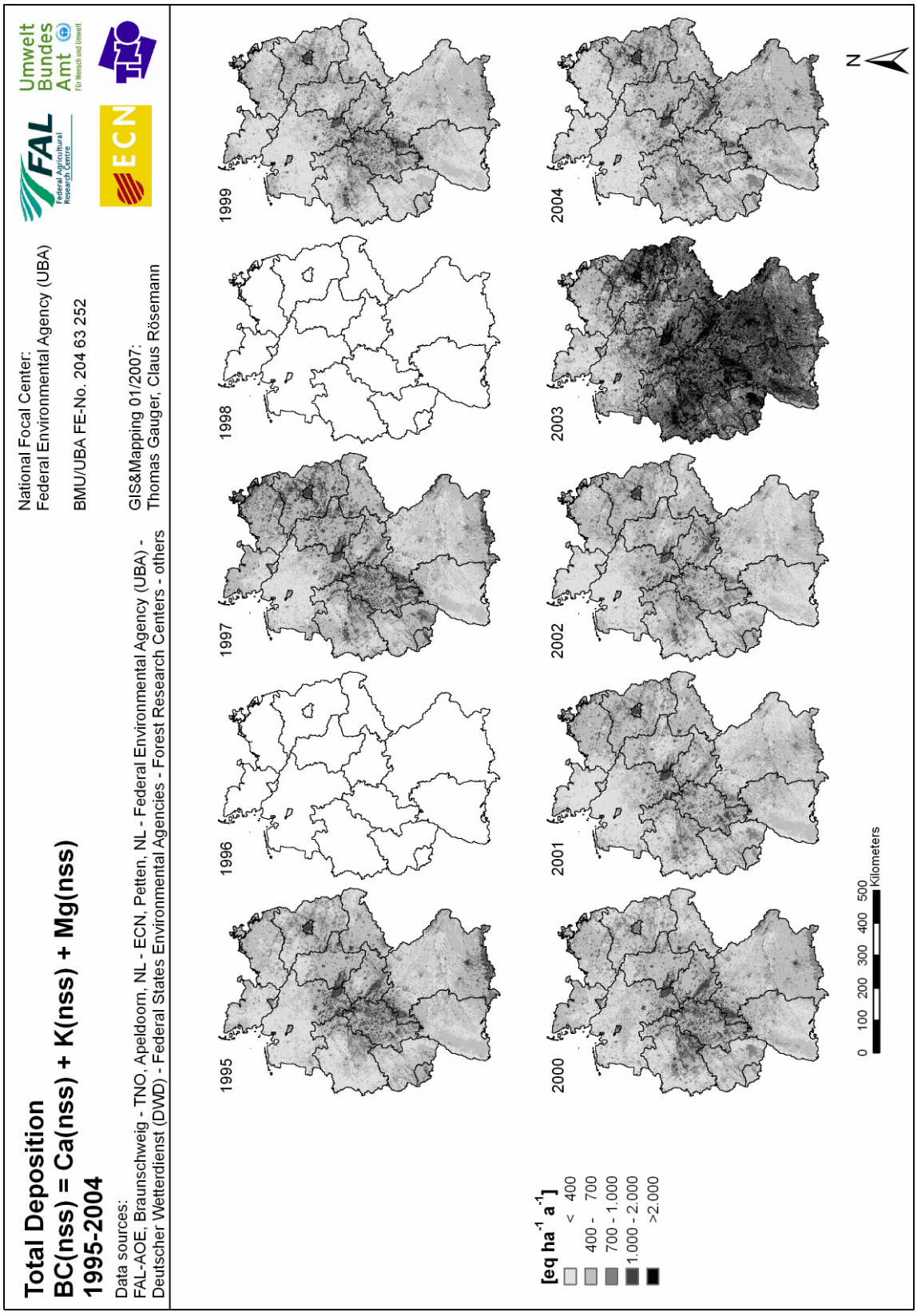

Map 9.1: Total deposition of $BC_{(nss)}$ 1995-2004

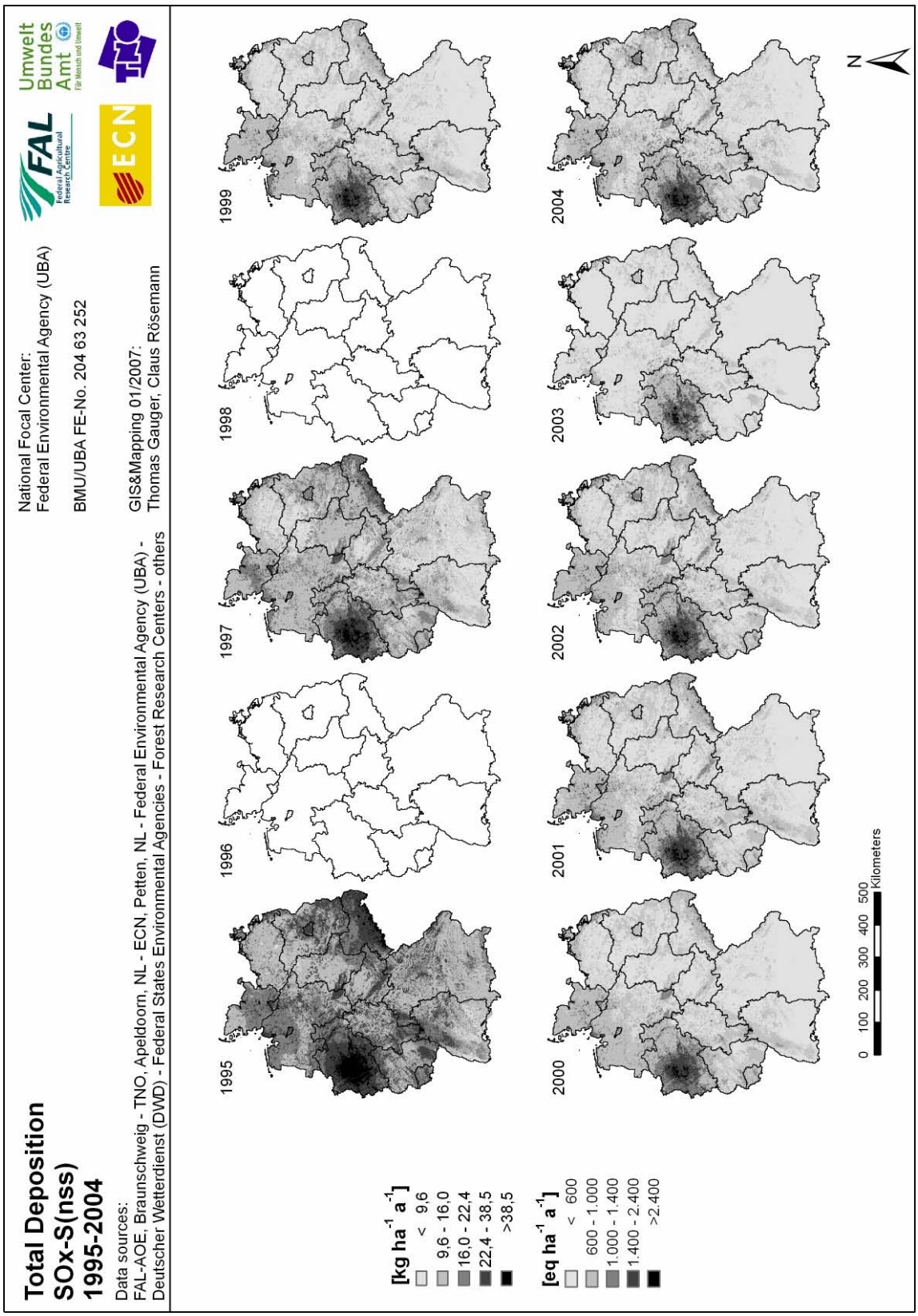

Map 9.2: Total deposition of SO_X-$S_{(nss)}$ 1995-2004

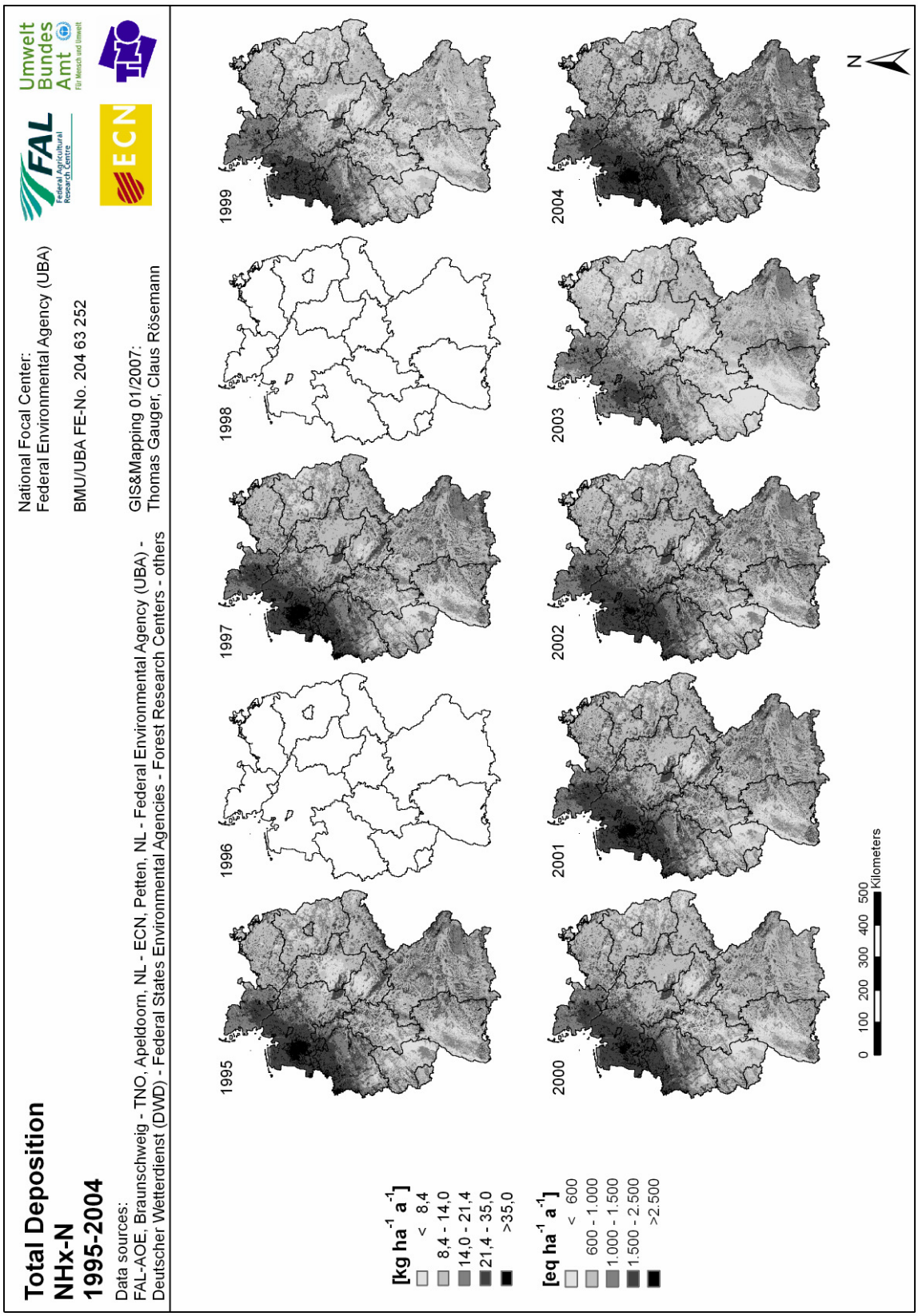

Map 9.3: Total deposition of NH_X-N 1995-2004

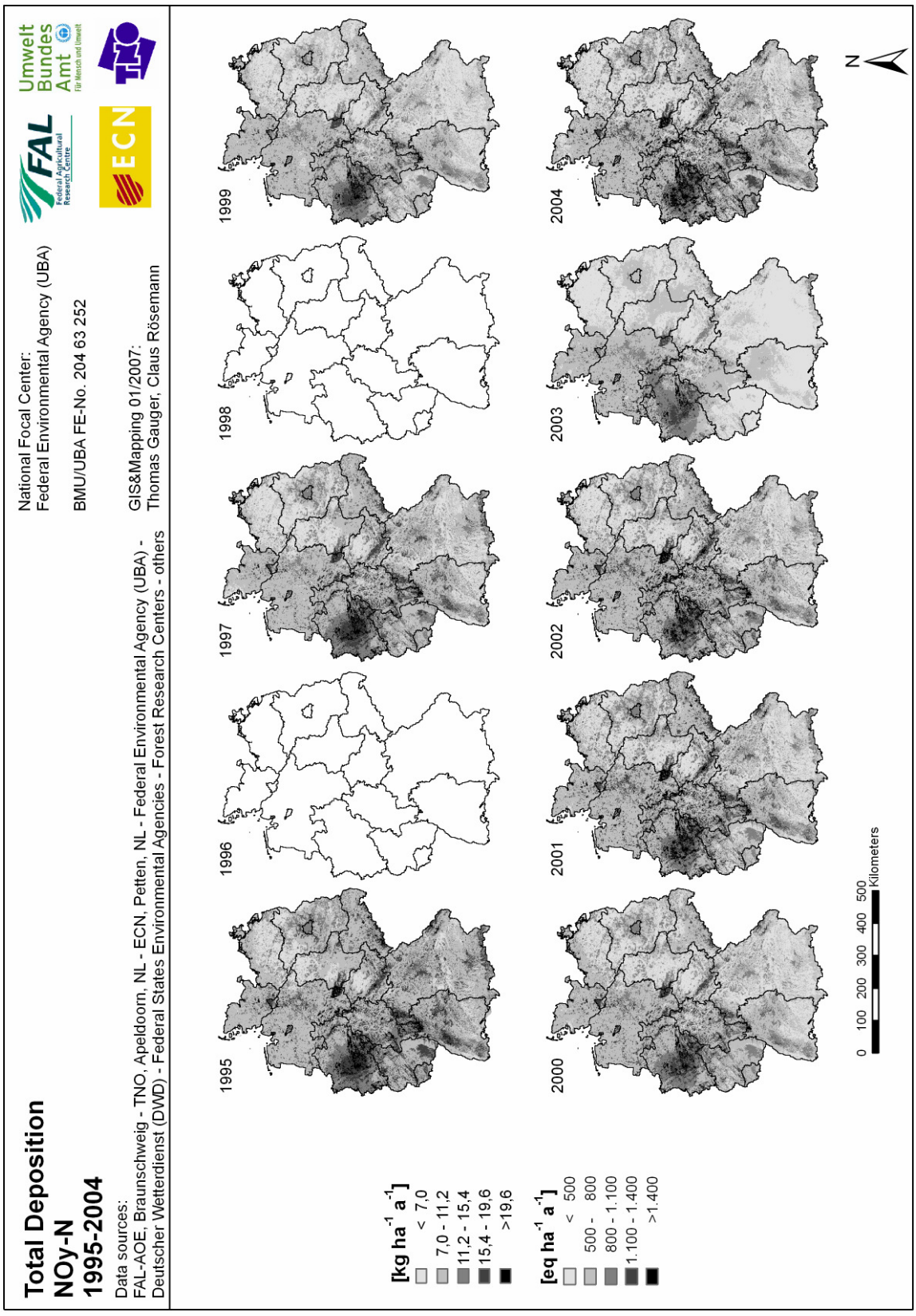

Map 9.4: Total deposition of NO_Y-N 1995-2004

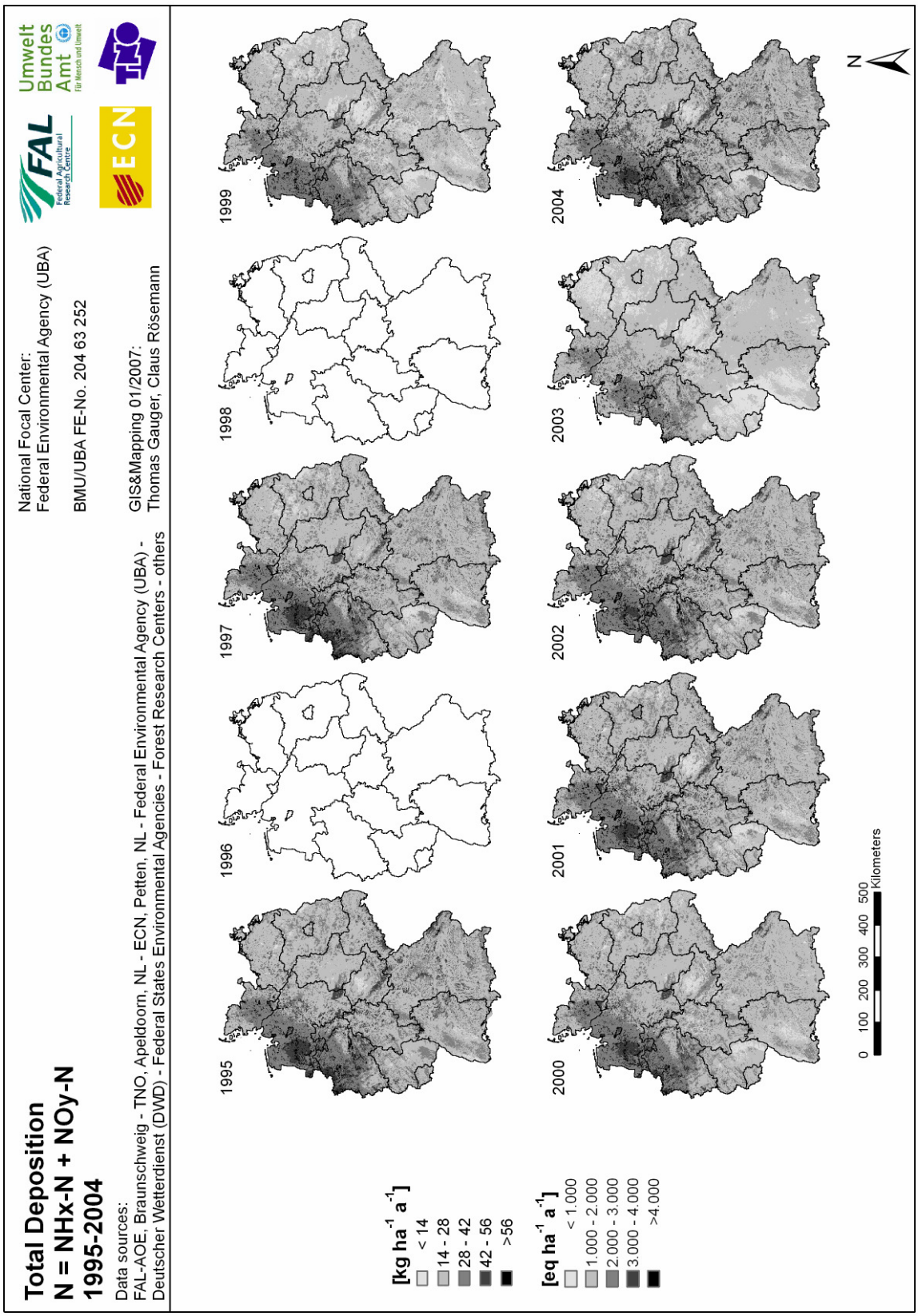

Map 9.5: Total deposition of N 1995-2004

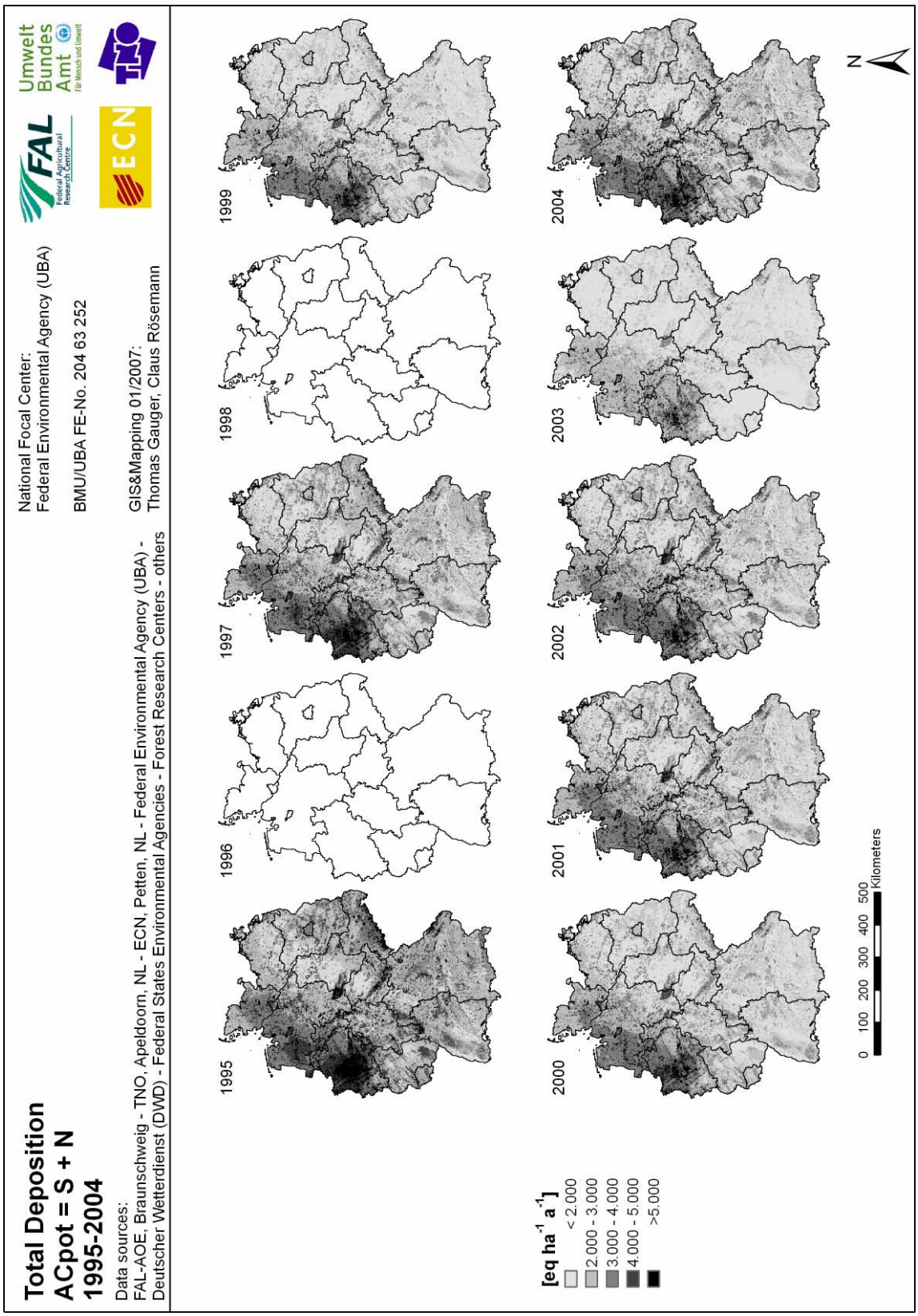

Map 9.6: Total deposition of AC_{pot} 1995-2004

Map 9.7: Total deposition of $AC_{pot(net)}$ 1995-2004

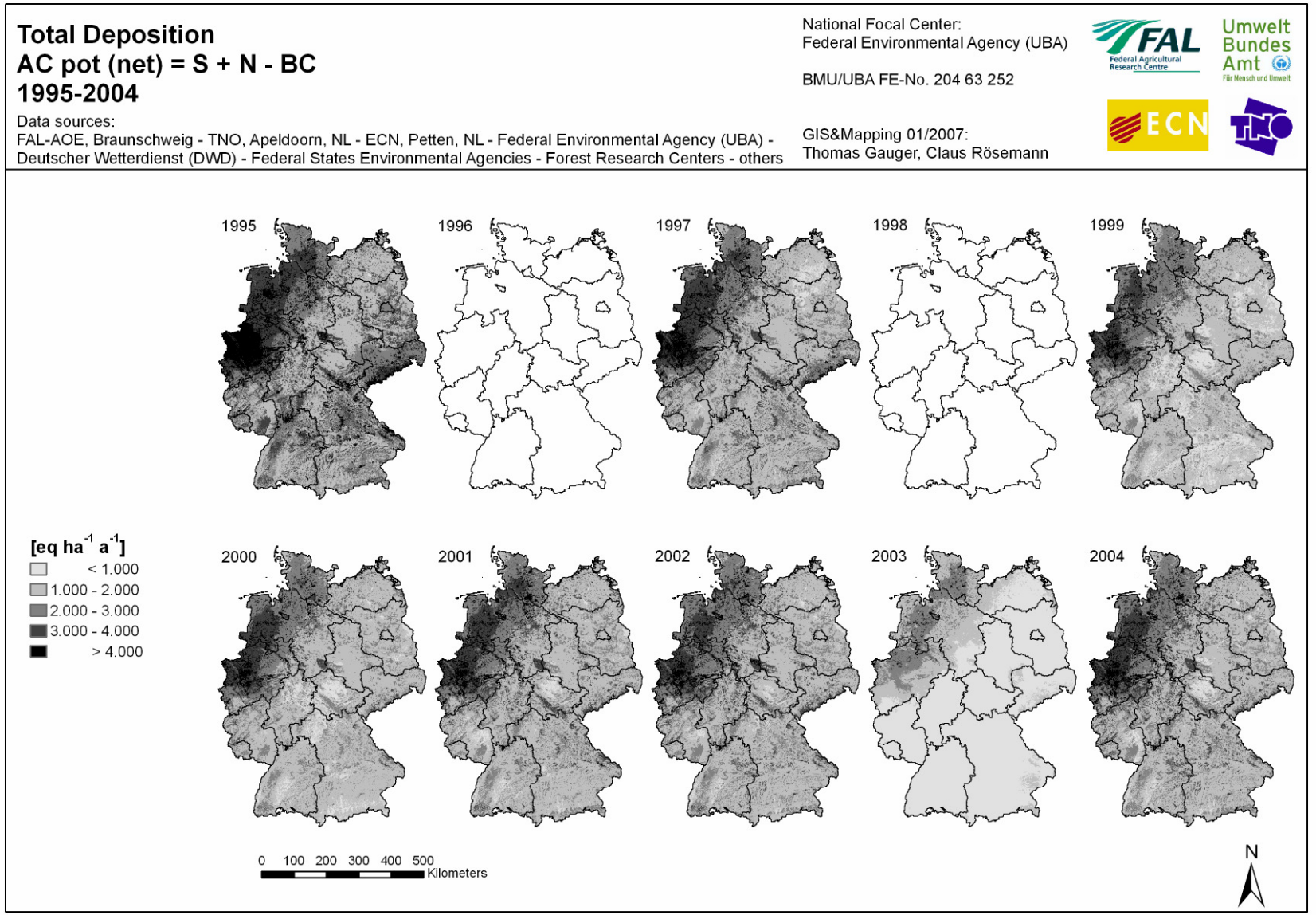

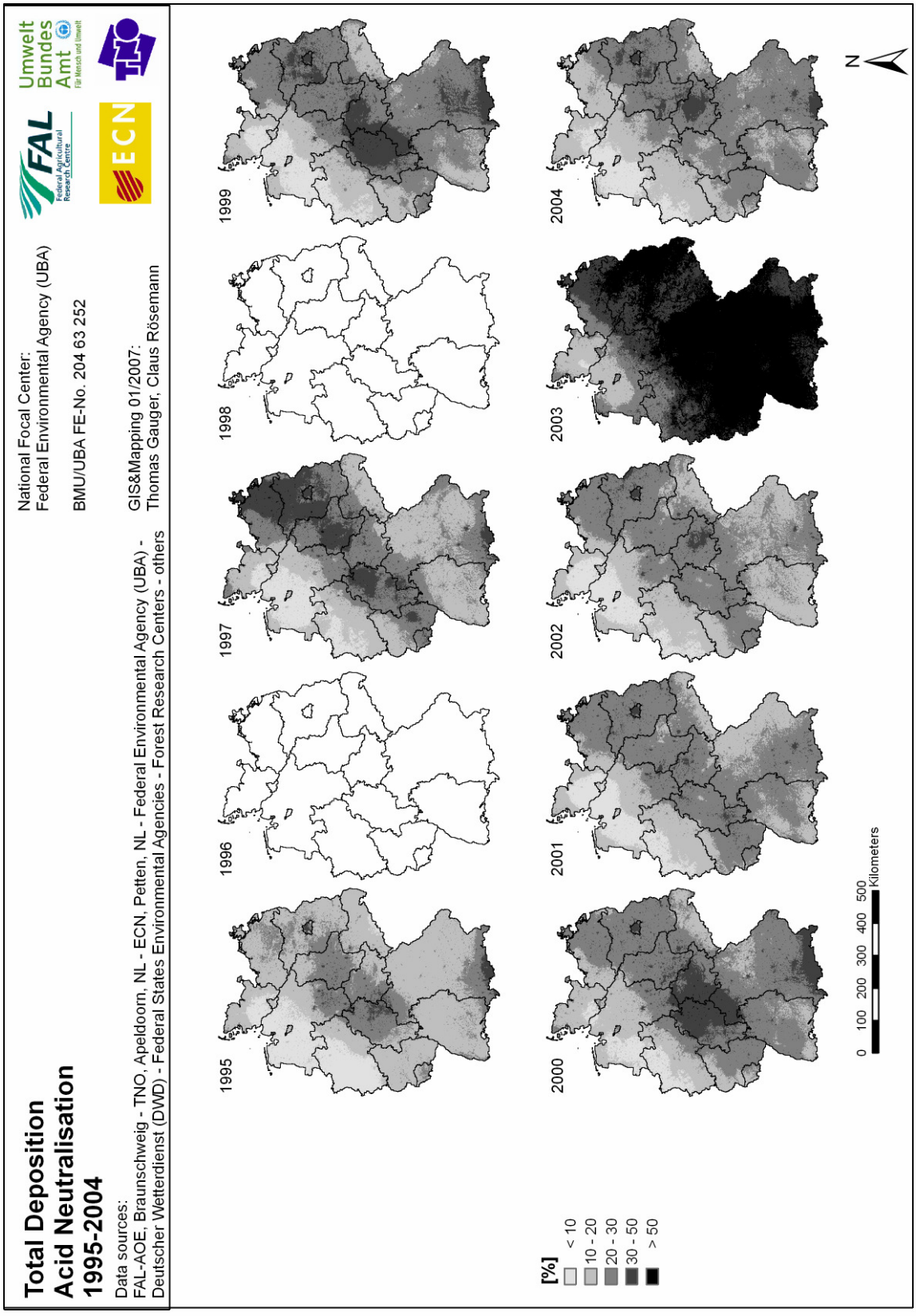

Map 9.8: Neutralisation of total deposited AC_{pot} by $BC_{(nss)}$ 1995-2004

Map 9.9: Total deposition of Cd 1995-2004

Total Deposition
Cd
1995-2004

Data sources:
FAL-AOE, Braunschweig - TNO, Apeldoorn, NL - ECN, Petten, NL - Federal Environmental Agency (UBA) - Deutscher Wetterdienst (DWD) - Federal States Environmental Agencies - Forest Research Centers - others

National Focal Center:
Federal Environmental Agency (UBA)

BMU/UBA FE-No. 204 63 252

GIS&Mapping 06/2007:
Thomas Gauger, Claus Rösemann

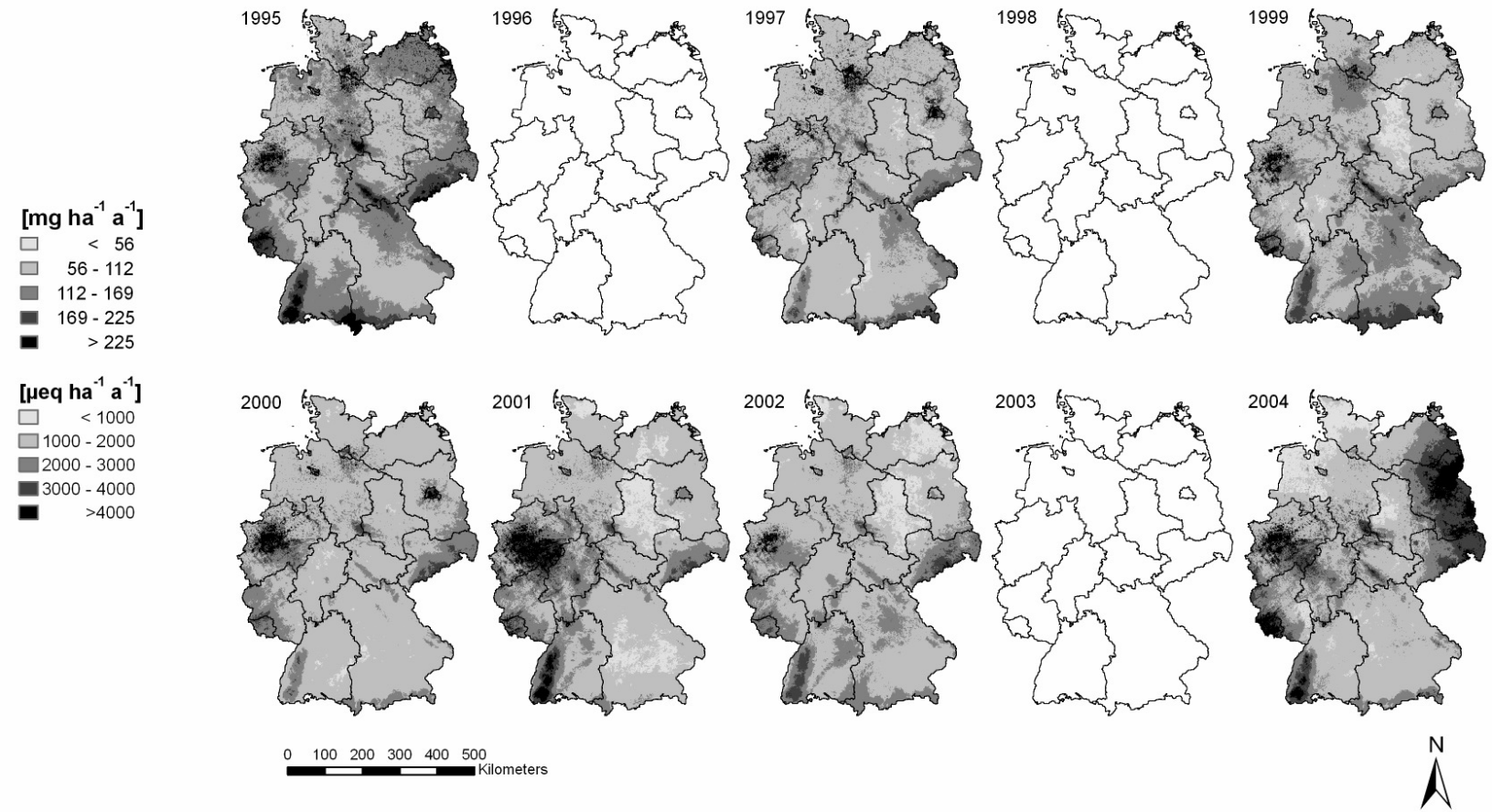

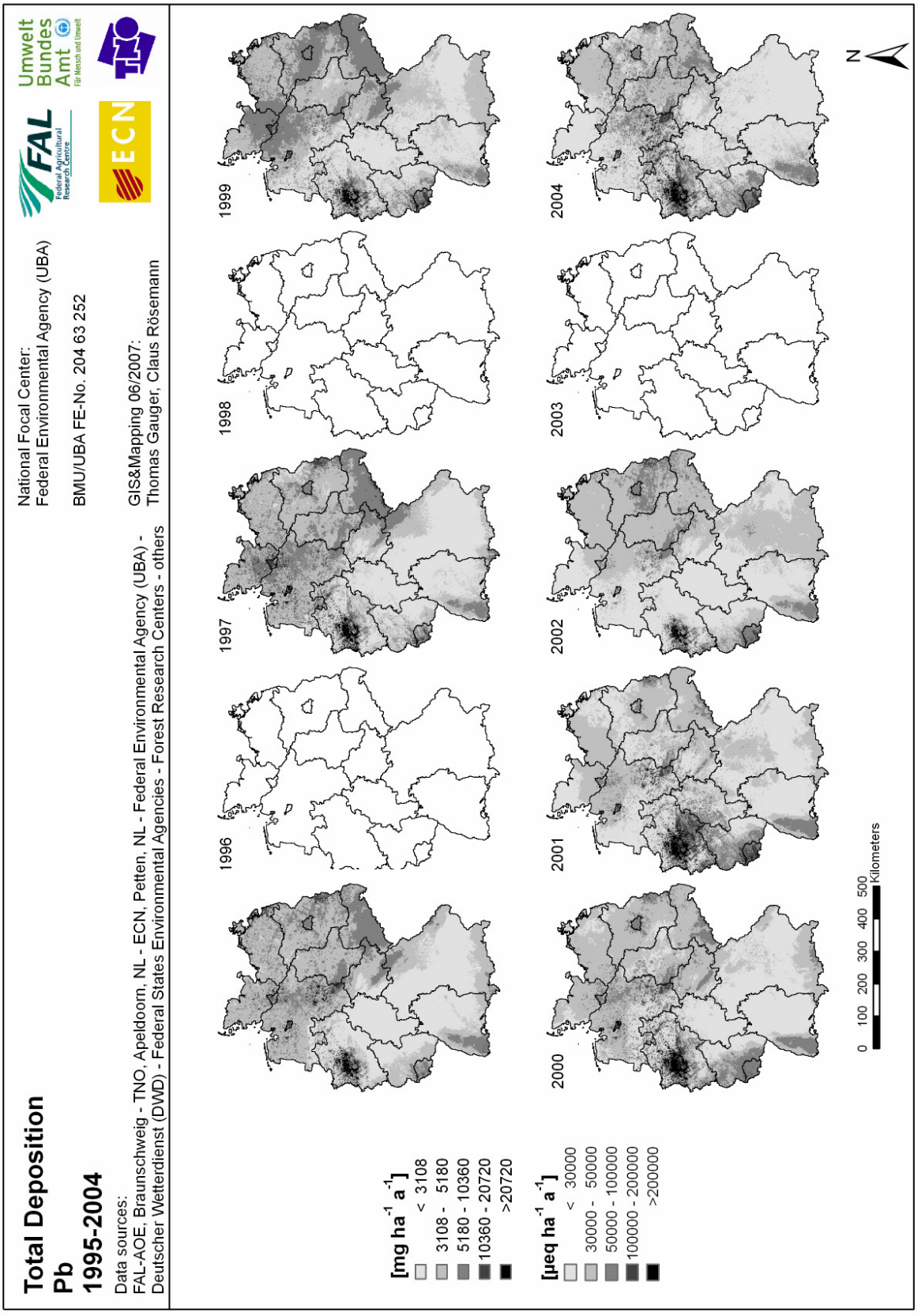

Map 9.10: Total deposition of Pb 1995-2004

10 Modelling the air concentrations of acidifying components and heavy metals

M. Schaap, R.M.A. Timmermans, P.J.H. Builtjes and J.H. Duyzer
Netherlands Organisation for Applied Scientific Research (TNO-B&O), Department of Environmental Quality, Apeldoorn, The Netherlands

10.1 Introduction

To calculate the dry deposition of the components considered in this project concentration data are needed for the domain that is covered by the Integrated DEposition Model (IDEM). In this study the LOTOS-EUROS model has been employed to calculate the distribution of these species on an about 25x25 km^2 (0.50 x 0.25 lat-lon) grid over Germany and the rest of Europe. LOTOS-EUROS is a product of the integration of the TNO model LOTOS (BUILTJES, 1992; HASS ET AL., 1997; SCHAAP ET AL., 2004a) and the RIVM model EUROS (MATTHIJSEN ET AL., 2002). The model is of intermediate complexity in the sense that the relevant processes are parameterised in such a way that the computational demands are modest enabling hour-by-hour calculations over extended periods of one or more years within acceptable CPU time, even on a workstation or a PC. LOTOS and EUROS were originally developed and used as a photo-oxidant model (BUILTJES, 1992; HASS ET AL., 1997; ROEMER, 2003). LOTOS has been used to simulate the inorganic secondary aerosols SO_4, NH_4 and NO_3 (SCHAAP ET AL., 2004a; 2004b) and carbonaceous aerosols (SCHAAP ET AL., 2004c). The combined model has been used and compared to other models in the EURODELTA exercise (e.g. VAN LOON ET AL., 2007).

The LOTOS-EUROS modelling system can be applied for the following components:

- Oxidants: O3, VOC's, NO_x, HNO_3, etc
- Secondary inorganic aerosol (SIA): SO_4, NO_3, NH_4
- Secondary organic aerosol (SOA) from terpenes
- Primary aerosol: PM2.5, PM10-2.5, Black Carbon (BC), sea salt.
- Heavy metals: Cd, Pb and other non-volatile metals
- POP's: BaP… etc.

Below we present an overview of the LOTOS-EUROS modelling system. For an extensive description and details we refer to the documentation of the model (SCHAAP ET AL., 2005). In chapter 10.3-10.5 we present the results for acidifying components, heavy metals and sea salt.

10.2 The LOTOS-EUROS modelling system

In this chapter we describe the general features of the LOTOS-EUROS model system. Within the course of the project we have performed two developments to the model code:

- inclusion of a surface layer
- update of the parameterisation of the dry deposition.

The inclusion of the surface layer was aimed to better describe the fate of primary components. Further, the dry deposition scheme was updated to be in line with the deposition modelling performed by ECN. Below we first describe the general features of the model. Afterwards we shortly address the improvements to the code.

10.2.1 Domain

The master domain of LOTOS-EUROS is bound at 35° and 70° North and 10° West and 60° East. The projection is normal longitude-latitude and the standard grid resolution is 0.50° longitude x 0.25° latitude, approximately 25x25 km^2. By means of a control file the actual domain for a simulation can be set as long as it falls within the master domain as specified above. In addition, it is possible to in- or decrease the resolution up to a factor 8 and 2, respectively.

In the vertical there are three dynamic layers and an optional surface layer. The model extends in vertical direction to 3.5 km above sea level. The lowest dynamic layer is the mixing layer, followed by two reservoir layers. The height of the mixing layer is part of the diagnostic meteorological input data. The height of the reservoir layers is determined by the difference between ceiling (3.5 km) and mixing layer height. Both layers are equally thick with a minimum of 50m. In some cases when the mixing layer extends near or above 3500 m the top of the model exceeds the 3500 m according to the above mentioned description. Optionally, a surface layer with a fixed depth of 25 m can be included in the model. The latter feature was added during the project and is discussed in some more detail below.

10.2.2 Processes

The main prognostic equation in the LOTOS-EUROS model is the continuity equation that describes the change in time of the concentration of a component as a result of transport and diffusion, chemistry, dry and wet deposition, emissions and entrainment. In the model the continuity equation is solved by means of operator splitting. The time step is split in two parts in which the concentration changes are calculated in order for the first half and in reverse order for the second half.

Transport

The transport consists of advection in 3 dimensions, horizontal and vertical diffusion, and entrainment. The advection is driven by meteorological fields which are input every 3 hours. The vertical wind speed is calculated by the model as a result of the divergence/convergence of the horizontal wind fields. The recently improved and highly-accurate, monotonic advection scheme developed by WALCEK (2000) is used to solve the system. The number of steps within the advection scheme is chosen such that the Courant restriction is fulfilled.

Entrainment is determined by the growth of the mixing layer during the day. Each hour the vertical structure of the model is adjusted to the new mixing layer depth. After the new structure is set the pollutant concentrations are redistributed using linear interpolation.

The horizontal diffusion is described with a horizontal eddy diffusion coefficient following the approach by LIU AND DURRAN (1977). Vertical diffusion is described using the standard K_z-theory. The K_z values are calculated within the stability parameterisation (see below). Vertical exchange is calculated employing the new integral scheme by YAMARTINO ET AL. (2004).

Chemistry

In this study the gas phase photochemistry in LOTOS-EUROS is described using a modified version of the CBM-IV mechanism (WHITTEN ET AL., 1980). The mechanism was tested against the results of a comparison presented by POPPE ET AL. (1996) and found to be in good agreement with the results presented for the other mechanisms. The photolysis rates are calculated following POPPE ET AL. (1996). The chemistry scheme further includes gas phase and heterogeneous reactions leading to secondary aerosol formation.

The reaction of N_2O_5 on aerosol surfaces has been proposed to play an important role in tropospheric chemistry (DENTENER AND CRUTZEN, 1993). This reaction is a source for nitric acid during night time, whereas during the day the NO_3 radical is readily photolysed. We parameterised this reaction following DENTENER AND CRUTZEN (1993). In this parameterisation a Whitby size distribution is assumed for the dry aerosol. The wet aerosol size distribution is calculated using the aerosol associated water obtained from the aerosol thermodynamics module (see below). The reaction probability of N_2O_5 on the aerosol surface has been determined for various solutions. Reaction probabilities between 0.01 and 0.2 were found (JACOB, 2000 and references therein). A study by MENTEL ET AL. (1999) indicates values at the lower part of this range. Therefore, we use a probability of γ = 0.05, which is somewhat lower than the generally used recommendation by JACOB (2000). In the polluted lower troposphere of Europe, however, the hydrolysis on the aerosol surfaces is fast, with lifetimes of N_2O_5 less than an hour (DENTENER AND CRUTZEN, 1993). Therefore the exact value of γ is not determining the results strongly. Due to the limited availability on cloud information, we neglect the role of clouds on the hydrolysis of N_2O_5, which may also contribute to nitric acid formation. However, due to the very fast reaction of N_2O_5 on aerosol in polluted Europe, the role of clouds on N_2O_5 hydrolysis is probably less important.

The ISORROPIA thermodynamic equilibrium module (NENES ET AL., 1998) is used to describe the equilibrium between gaseous nitric acid, ammonia and particulate ammonium nitrate and ammonium sulphate and aerosol water. In this study we assume equilibrium between the aerosol and gas phase at all times. For sub-micron aerosol this equilibrium assumption is valid in most cases, but it may not be valid for coarse fraction aerosol (MENG AND SEINFELD, 1996). However, since our model does currently not on a regular basis incorporates sea salt or dust, which are sinks for gaseous nitric acid, the results of our equilibrium calculations over marine and arid regions should not be overinterpreted (ZHANG ET AL., 2001).

It is important to give a good representation of sulphate formation, since sulphate competes for the ammonia available to combine with nitric acid. Most models that represent a direct coupling of sulphur chemistry with photochemistry underestimate sulphate levels in winter in Europe. This feature can probably be explained by a lack of model calculated oxidants or missing reactions (KASIBHATLA ET AL., 1997). Therefore, in addition to the gas phase reaction of OH with SO_2 we represent additional oxidation pathways in clouds with a simple first order reaction constant (*Rk*), which is calculated as function of relative humidity (%) and cloud cover (ε):

$$Rk = 8.3e\text{-}5 \cdot (1 + 2 \cdot \varepsilon) \quad (s\text{-}1),\ for\ RH < 90\ \% \qquad (10.1)$$

$$Rk = 8.3e\text{-}5 \cdot (1 + 2 \cdot \varepsilon) \cdot [1.0 + 0.1 \cdot (RH - 90.0)] \quad (s\text{-}1),\ for\ RH \geq 90\ \% \qquad (10.2)$$

This parameterisation is similar to that used by TARRASON AND IVERSEN (1998). It enhances the oxidation rate under cool and humid conditions. With cloud cover and relative humidity of 100 % the associated time scale is approximately one hour. Under humid conditions, the relative humidity in the model is frequently higher than 90% during the night. Model results using this parameterisation agree significantly better with observational data than results calculated using a reaction scheme that considers explicit cloud chemistry.

Wet deposition and boundary conditions

Wet deposition is calculated using simple coefficients for below cloud scavenging (DE LEEUW ET AL., 1988). Since in-cloud scavenging is not accounted for, calculated concentrations in rainwater are underestimated (SCHAAP ET AL., 2004).

Boundary conditions for O_3, NO_X and VOC in LOTOS are obtained from the 2D global Isaksen model (ROEMER, 1995). For sulphate we use a boundary condition of 0.7 µg m^{-3} as deduced from measurements. Measurements show that sulphate is completely neutralized over remote areas in Europe (KERMINEN ET AL., 2001). Therefore, we assume the imported sulphate to be fully neutralized by ammonium. Ammonium nitrate at the model boundaries was assumed to be zero. This assumption is probably valid for the west, north and south boundaries where the nitrate concentrations in air are very low or associated with sea salt and dust (KERMINEN ET AL., 2001, KOUVARAKIS ET AL., 2002). At the eastern boundary, however, the assumed boundary conditions and, hence, the model results for both nitrate and sulphate are highly uncertain and we therefore decided to present results only west of 30 ^{0}E.

10.2.3 Input data

Meteorology

The LOTOS-EUROS system is presently driven by 3-hourly meteorological data. These include 3D fields for wind direction, wind speed, temperature, humidity and density, substantiated by 2-d gridded fields of mixing layer height, precipitation rates, cloud cover and several boundary layer and surface variables. The standard meteorological data are produced at the Free University of Berlin employing a diagnostic meteorological analysis system based on an optimum interpolation procedure on isentropic surfaces. The system utilizes all available synoptic surface and upper air data (KERSCHBAUMER AND REIMER, 2003). Also, meteorological data obtained from ECMWF can be used to force the model.

Emissions

The anthropogenic emissions are a combination of the TNO emission database for the base year 2000 (VISSCHEDIJK AND DENIER VAN DER GON ET AL., 2005) and the official emission data as reported by EMEP. For each source category (Snap 1) and each country, we have scaled the country totals of the TNO emission database to those of the official emissions. Hence, we use the official emission totals as used within the LRTAP protocol but we benefit from the higher resolution of the TNO emission database (0.25 x 0.125 degrees longitude-latitude). The annual emission totals are broken down to hourly emission estimates using time factors for the emissions strength variation over the months, days of the week and the hours of the day (BUILTJES ET AL., 2003). In LOTOS-EUROS biogenic isoprene emissions are calculated following VELDT (1991) using the actual meteorological data. In addition, sea salt emissions are parameterised following MONAHAN ET AL. (1986) from the wind speed at ten meters.

Land use

The land use data used in LOTOS-EUROS are derived from the 1.1 x 1.1 km^2 resolution land use database PELINDA (DE BOER ET AL., 2000) and the IIASA database for Russia (STOLBOVOI AND MCCALLUM, 2002). From these databases the surface fraction covered by the land use classes used in the dry deposition module has been calculated for each cell in the domain (NIJENHUIS AND GROTEN, 1999).

10.2.4 Surface layer

To improve the representation of primary pollutants we have added a surface layer of 25 m deep to the model description during the project. The code was set-up such that the surface layer is optional. Meteorological input was generated to support simulations with the surface layer.

Inclusion of the surface layer implies that there is an additional interface for wich the transfer of pollutants needs

to be described. The new model structure is shown in figure 10.1 and illustrates that the surface layer may be very shallow compared to the boundary layer. Such situations are common in summer during the daytime. Standard theory used to describe the vertical diffusion between the model layers is given by:

$$F = Kz\ dC/dz \tag{10.3}$$

The *Kz* value is calculated by using standard similarity theory profiles. However, the correct *dC/dz* poses a problem. Using the mid-points of each cell and the layer averaged concentration causes a very small gradient in cases with a deep boundary layer which would suppress vertical diffusion. This approach is not valid under the assumption that the boundary layer is relatively well mixed and a better way to describe the *dC/dz* needs to be found. We have implemented a scheme developed by YAMARTINO ET AL. (2004) that assesses the depth that is associated with the gradient as function of stability parameters.

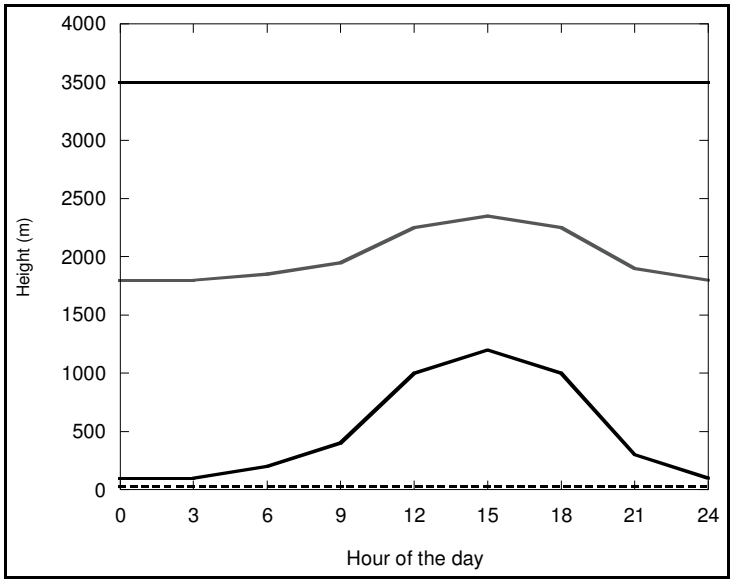

Figure 10.1: A schematic of the vertical structure of LOTOS-EUROS over a day

10.2.5 Dry deposition

Dry deposition was implemented following the same approach as it is used for dry deposition modelling in this study. A detailed description on the dry deposition parameterisation used is given in Chapter 6.1.6 to 6.1.9 of this report.

10.3 Modelled concentrations of acidifying components over Germany and Europe the LOTOS-EUROS modelling system

10.3.1 Emission data

The anthropogenic emission inventories of SO_x, NO_x, NM-VOC, CO, CH_4, NH_3 used in this study are a combination of the TNO emission database (VISSCHEDIJK AND DENIER VAN DER GON ET AL., 2005) and the EMEP emissions for 1995-2003. For each source category (Snap 1) and each country, we have scaled the country totals of the TNO emission database to those of the CAFE baseline emissions. Hence, we use the official emission totals as used within the LRTAP protocol but we benefit from the higher resolution of the TNO emission database (0.25 x 0.125 degrees longitude-latitude).

The temporal variation of the emissions is represented by time factors. For each source category a monthly factor breaks down the annual total into monthly value. This value is divided by a factor for the day of the week (i.e. Monday, Tuesday etc.) and finally by a factor for the hour of the day (local time). Except for ammonia, these factors are obtained from the TROTREP project (BUILTJES ET AL., 2003). In comparison with the emissions of SO_X, NO_X, and VOC, the emission of ammonia is uncertain and not as well understood. Ammonia emissions in Europe are for the largest part (80-95 %) associated with agricultural activities (VAN DER HOEK, 1998). The seasonal variation in ammonia emissions is uncertain and may differ regionally as function of farming procedures and climatic conditions. The seasonal variation in the ammonia emissions is modelled based on experimental data representative for the Netherlands as shown in Figure 10.2 (BOGAARD AND DUYZER, 1997). The seasonal variation shows a distinct maximum in March and a slight maximum in August due to the

application of manure on top of a function that roughly scales with duration of daylight. Following ASMAN (2001) we assumed a diurnal cycle in the emission with half the average value at midnight and twice the average at noon.

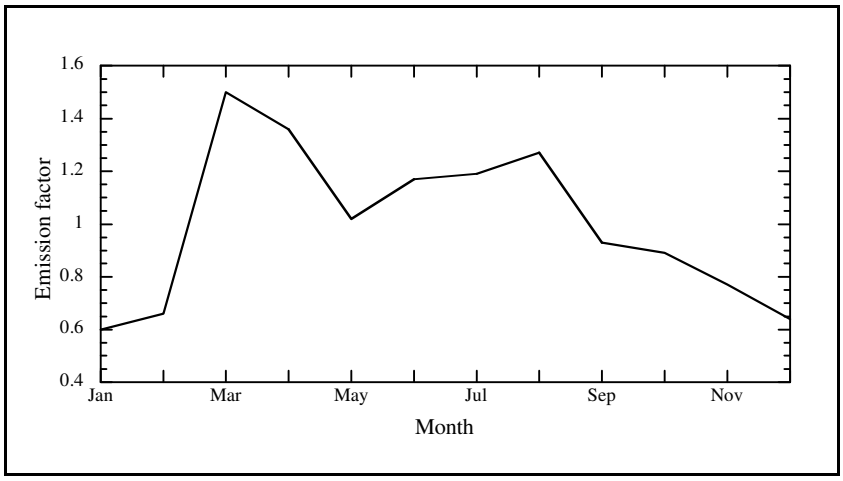

Figure 10.2: Monthly emission factor for ammonia (source: Bogaard and Duyzer, 1997)

Exchange, emission or deposition, of ammonia depends on the compensation point, which refers to the situation in which the ammonia concentration in air is in equilibrium with the vegetation. Assessing the compensation point of ammonia is not possible for many surfaces (ASMAN, 2001). In addition, the presence of a compensation point is probably most important in relatively remote regions away from the main sources. Close to sources ammonia exchange will be dominated by deposition. We can therefore safely describe emission and deposition separately.

Due to the emissions there is a large vertical gradient of ammonia concentrations in the source areas with highest concentrations near the ground. However, in our model the emissions are completely vertically mixed over the first layer. We may therefore underestimate the effective dry deposition of ammonia close to the sources. To account for this effect ASMAN AND JANSSEN (1987) and DENTENER AND CRUTZEN (1994) lowered the 'effective' emissions in their model by 25 %, assuming that this part of the emission was removed on sub grid scales. JANSSEN AND ASMAN (1988) argued that by uniformly lowering the ammonia emission, ammonium formation could be underestimated and more sophisticated correction factors were proposed. These correction factors would be highly variable depending on region, the surface roughness downwind of the sources, availability of acidic precursors, meteorological conditions and the history of the air parcel (e.g. ASMAN, 1998). Much of this information is not available in our model and therefore no correction factors are used in this study.

10.3.2 Modelled fields

In Figure 10.3 and 10.4 we show examples of the modelled distributions of acidifying components over Europe and Germany for 1995 and 2001, respectively. The annual average concentrations of NO and NO_2 maximise over densely populated areas. The Ruhr-area and large cities such as Berlin are recognised in the distributions. For SO_2 the maxima are found in industrial areas (Ruhr area) and the shipping tracks at sea. Sulphate concentrations show a large scale pattern over Europe with highest concentrations over south-eastern Europe. Over Germany a minimum is calculated over the southern part of the country. The higher concentrations in the West, North and East are explained by the densely populated and industrialised area in the Benelux and the Ruhr area, shipping and the influence of Eastern Europe, respectively.

High ammonia concentrations are found there where the emissions are high as well. For Germany this means that the concentrations in the Northwest of the country are particularly high (average concentrations above 5 $\mu g\ m^{-3}$). A secondary maximum can be observed over the southern Bundeslaender, e.g. Bavaria. Nitrate concentrations show a similar distribution over Germany, although the gradients are less than for ammonia. The similarity in the distributions can be explained by the semi-volatile character of ammonium nitrate. In summer high ammonia levels are needed to maintain the equilibrium between the gas and aerosol phase and hence nitrate is only stable in areas with high ammonia concentrations. In winter ammonium nitrate is stable and is more evenly distributed over the country. Nitric acid concentrations show a field which is anti-correlated to that of ammonia. The reason is that the nitric acid in the high ammonia regions is in the form of particulate nitrate whereas it is in the gas phase in low ammonia areas. Ammonium is present as ammonium sulphate and ammonium nitrate. Hence, the distribution resembles that of the combined sulphate and nitrate.

The modelled fields for 1995, 1997 and 1999 to 2004 were delivered to ECN for deposition calculations. For this

purpose, files with 3 hourly data were generated by sampling the results of the model calculations.

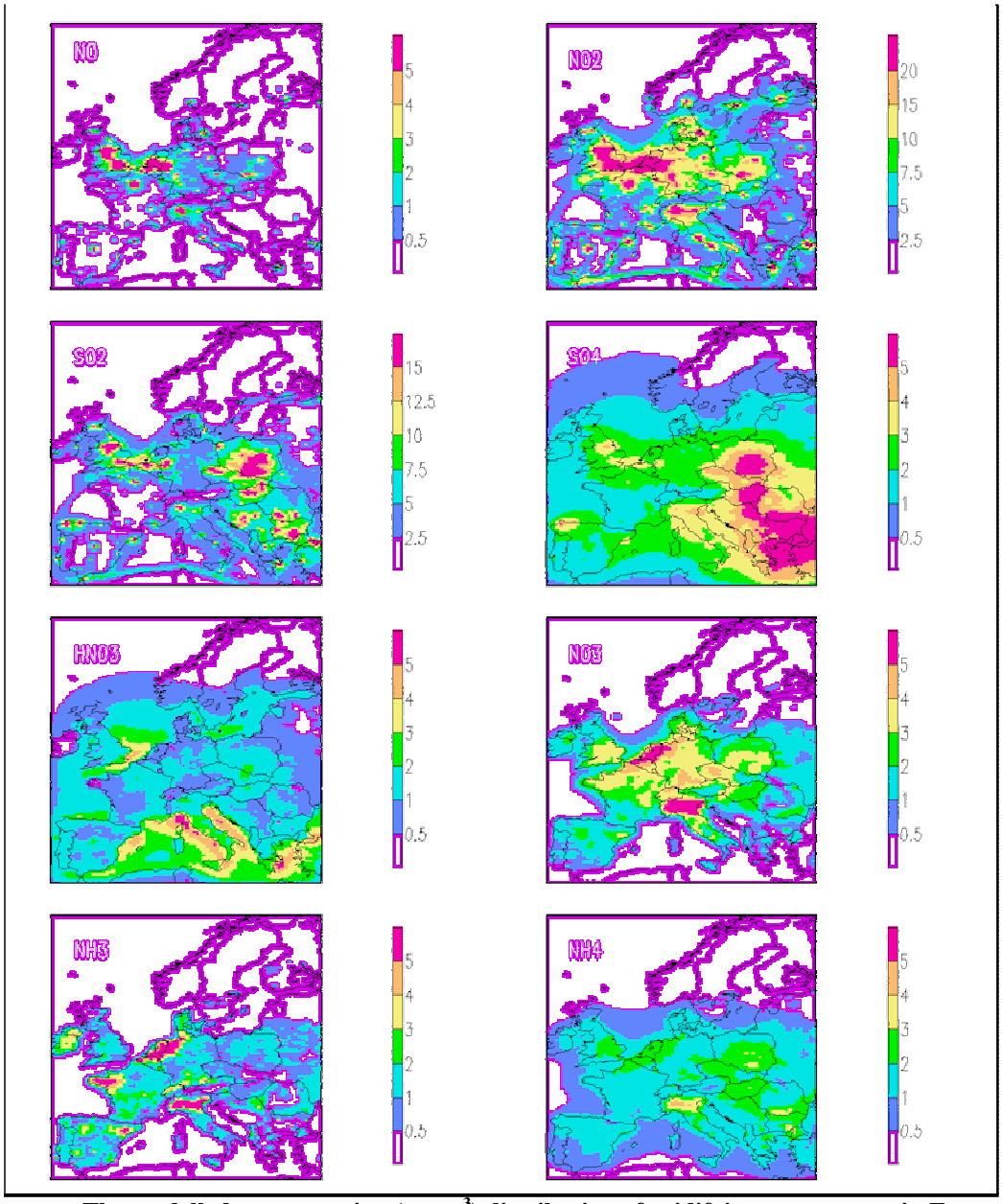

Figure 10.3: The modelled concentration (µg m^{-3}) distribution of acidifying components in Europe for 1995

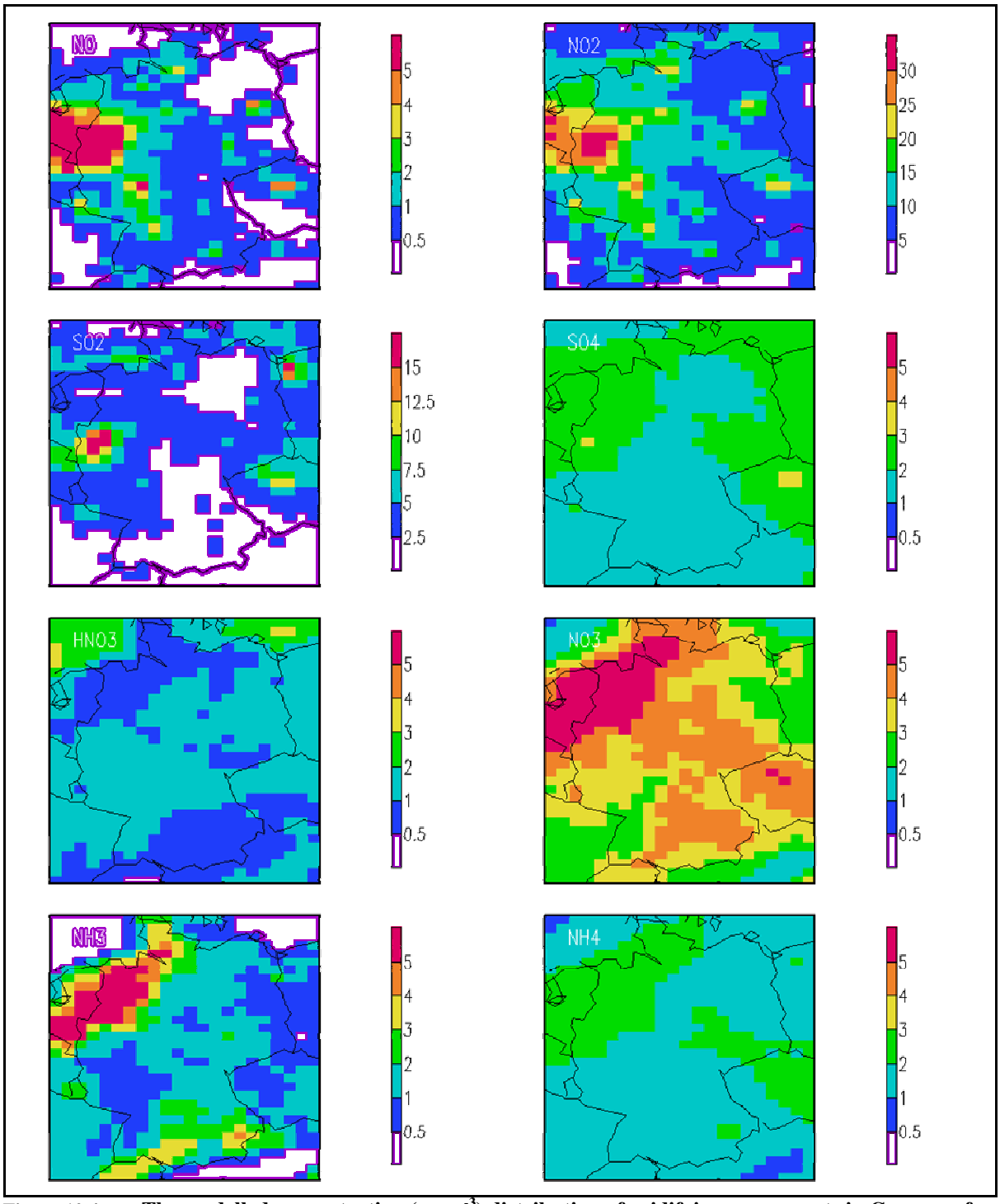

Figure 10.4: The modelled concentration (µg m^{-3}) distribution of acidifying components in Germany for 2001

10.3.3 Validation

In this chapter we compare the modelled concentrations to observations in Germany and the rest of Europe.

Approach

The model results of LOTOS-EUROS are compared to concentrations observed at regional background stations. Observations of SIA and its precursors used in this study are gathered from the EMEP database (www.emep.int). Furthermore, we used data from IfT and FAL for several locations in Germany. Mountain stations were excluded from the analysis. The data for nitrate and ammonium were screened as the measurements of these compounds are prone to artefacts (SCHAAP ET AL., 2002; 2004b). Nitrate data obtained with cellulose filters were interpreted as total nitrate. Aerosol nitrate data from inert filters were used in this study, although we are aware that they are

prone to losses at temperatures above about 20 degrees Celsius. Total nitrate and ammonium data which were not obtained in a single measurement set-up were disregarded. As the spatial coverage for aerosol nitrate and ammonium is low, all stations were included in the analysis. Hence, results for these components are biased to a few stations. Below, we use the EMEP codes for all stations used in the validation. The station codes, names and location are listed in Annex 1.

Note that the modelled concentration data in this study are representative for the surface layer of 25 m and not for measurement height. Due to the removal of species at the surface a concentration gradient exists from the surface layer to the surface. For species with a fast dry deposition rate, e.g. nitric acid, the gradient is quite strong causing substantially lower concentrations at measurement height compared to those in the surface layer. For species with a small dry deposition velocity such as sulphate this effect is negligible. In this chapter we present an overview of the validation results.

Sulphur dioxide and sulphate

The comparison against observations for SO_2 reveals that the model slightly overpredicts the SO_2 concentration at the German regional background sites. This is consistent with the picture throughout Europe (See Fig 10.5). A number of sites in Europe show a high overestimation by the model. These stations have in common that they are located along coast lines with shipping activities nearby. Hence, the influence of ship emissions may be overestimated. The temporal evolution of SO_2 concentrations at Zingst is shown in Figure 10.7. The temporal correlation is about 0.5 and indicates that events are often captured although the magnitude is not always represented well.

During the project the high predicted SO_2 concentrations in the Ruhr area were noticed. For this reason local measurements data were collected to compare the data to in more detail. The comparison for 2002 is shown in Figure 10.6. The comparison includes more than 700 stations available for rural, sub-urban, urban, and industrial sites. Bearing in mind that the model predicts an average concentration over 25x25 km^2 and the range of station types used here we expect a fair amount of scatter, which is indeed the case. However, we can use the data to get an impression of the quality of the modelled concentration ranges. For example, in the low concentration range the model slightly overestimates, which is in accordance with the regional UBA stations. There are only a few grid cells with high modelled concentrations (due to large point sources). For example, the highest concentration in a cell (located over Duisburg) is about 18 µg m^{-3}. It happens to be that there are 6 monitoring stations in this 25x25km^2 area with concentrations between 6 and 23µg/m^3. These measurements indicate the range of concentrations possible in a single model cell due to local emissions. Furthermore, the modelled values are not unrealistic. However, this exercise shows that in source areas the comparison between point measurements and cell averages is very difficult due to representativity issues. Hence, we use the rural UBA stations for validation in this study.

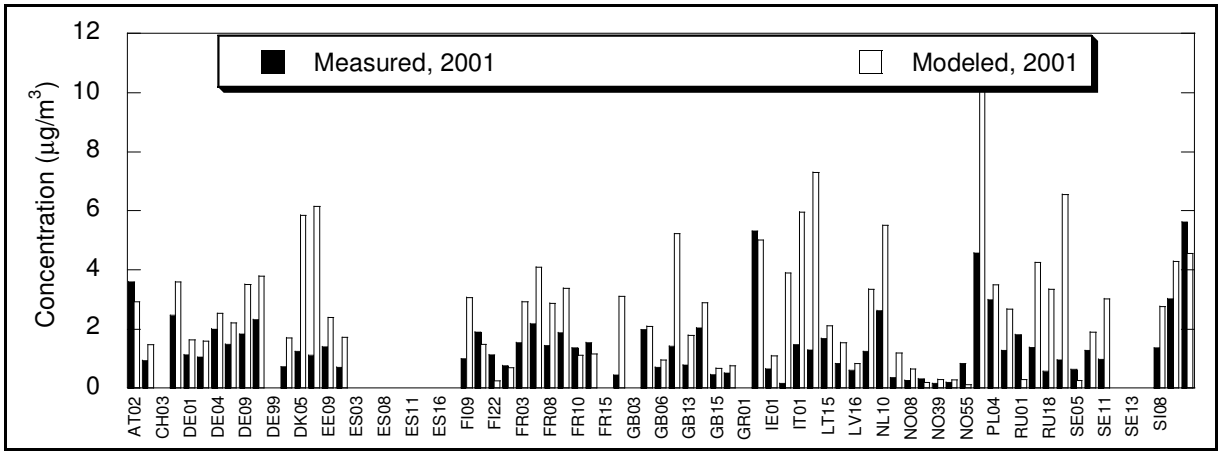

Figure 10.5: Comparison of measured and modelled annual average SO_2 concentrations for 2001 in Europe

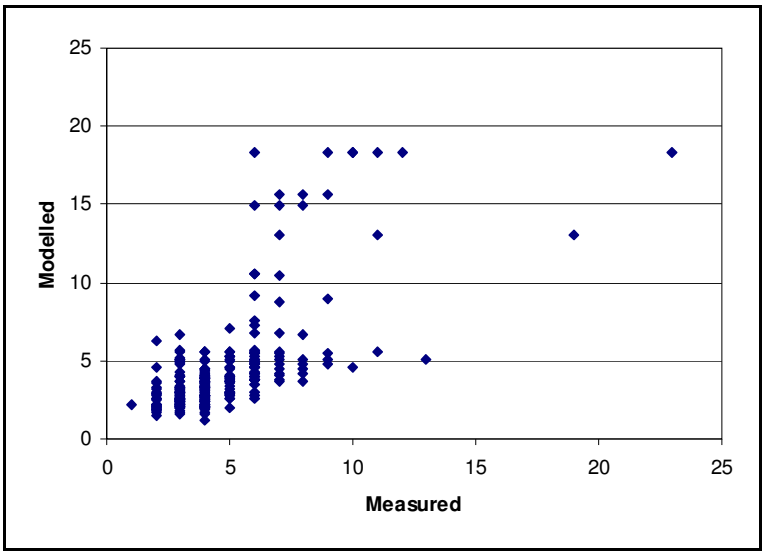

Figure 10.6: **Comparison between modelled and measured SO_2 concentrations for 2002 [µg m^{-3}]**

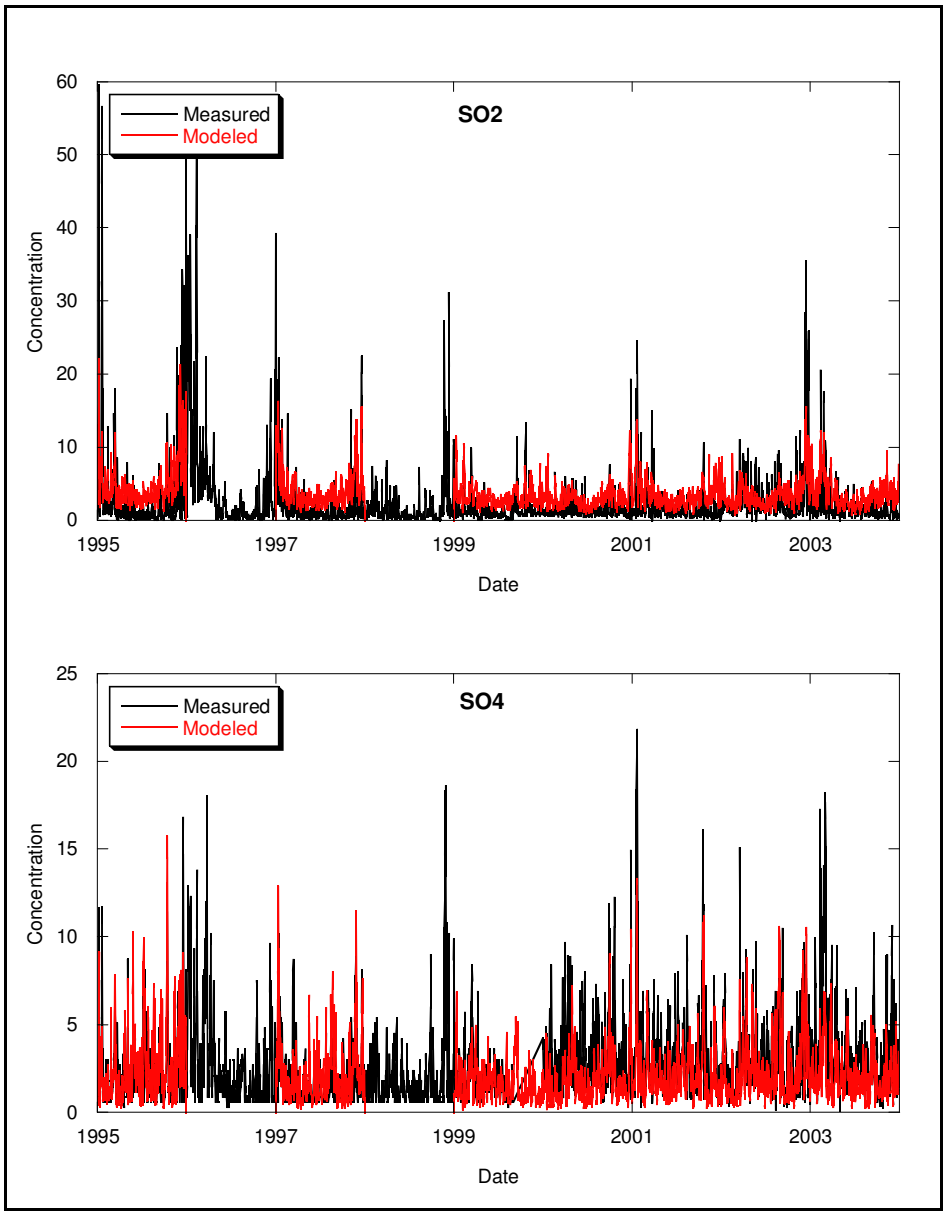

Figure 10.7: **The measured and modelled temporal variation of SO_2 and SO_4 at Zingst (DE09) [µg m^{-3}]**

The verification exercise for sulphate is shown in two pictures (lower part of Figure 10.7; 10.8, and 10.9). For 1995, 1997 and the first half of 1999 the modelled data compare favourably with measured data. However, from 2000 onwards the sulphate concentrations are underestimated by about 30%. This is caused by the UBA sulphate measurements that show consistently higher concentrations after summer 1999. The data after 1999 appear to be more inline with the data from research stations such as Braunschweig and Melpitz. This hints at too low observations before 1999.

Temporal correlation coefficients are mostly fine (between 0.6 and 0.7) but for some years somewhat lower values are found (Table 10.1). The correct timing of events is illustrated in Figure 10.9 where we zoom into 2002 and 2003 for Zingst. Although the timing compares favourably, the magnitude of the episodes is underestimated. The largest episode took place in February 2003, when sulphate levels exceed 15µg m^{-3}. This event is also present in the modelled time series but the model only simulates 7µg m^{-3}. The event was characterised by very high stability and low wind speeds. Based on this study we speculate that the relatively coarse model resolution above the boundary layer may have caused too much dilution of stack emissions (of SO_2) causing an underestimation of sulphate levels in stable conditions.

Inspection of the European data reveals that the large scale variability in the sulphate distribution is well reproduced by the model.

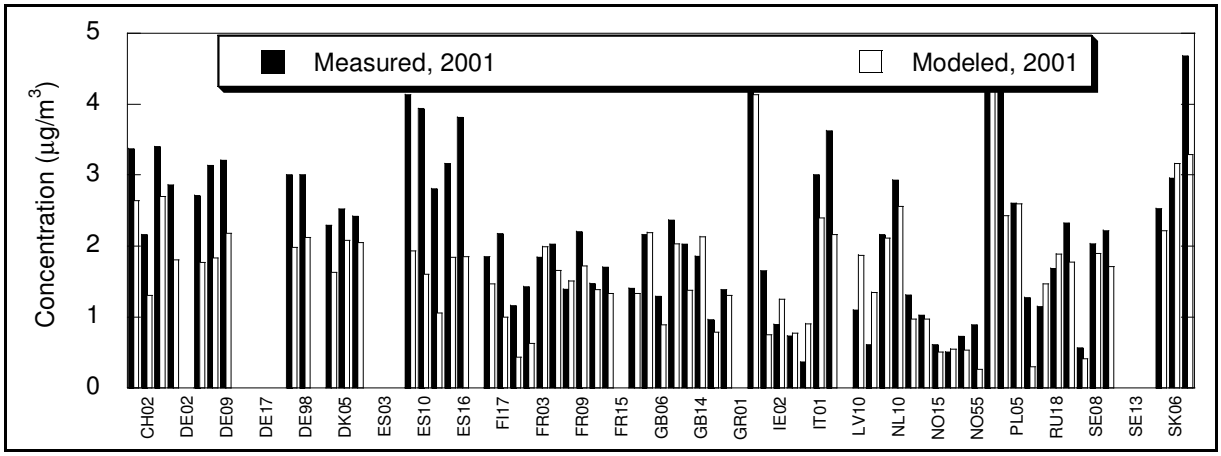

Figure 10.8: Comparison of measured and modelled annual average SO_4 concentrations for 2001 in Europe

Table 10.1: Measured and modelled average SO_4 concentrations [µg m^{-3}] over the German monitoring stations. Also given is the temporal correlation based on daily data and the number of stations ('nstat') that contribute to the average

SO_4	Meas	model	correlation	nstat
1995	3.0	2.9	0.60	11
1997	2.8	2.2	0.61	7
1999	2.7	1.6	0.42	7
2000	3.1	1.8	0.58	3
2001	3.0	2.0	0.66	6
2002	3.1	2.2	0.66	5
2003	3.5	2.0	0.55	5

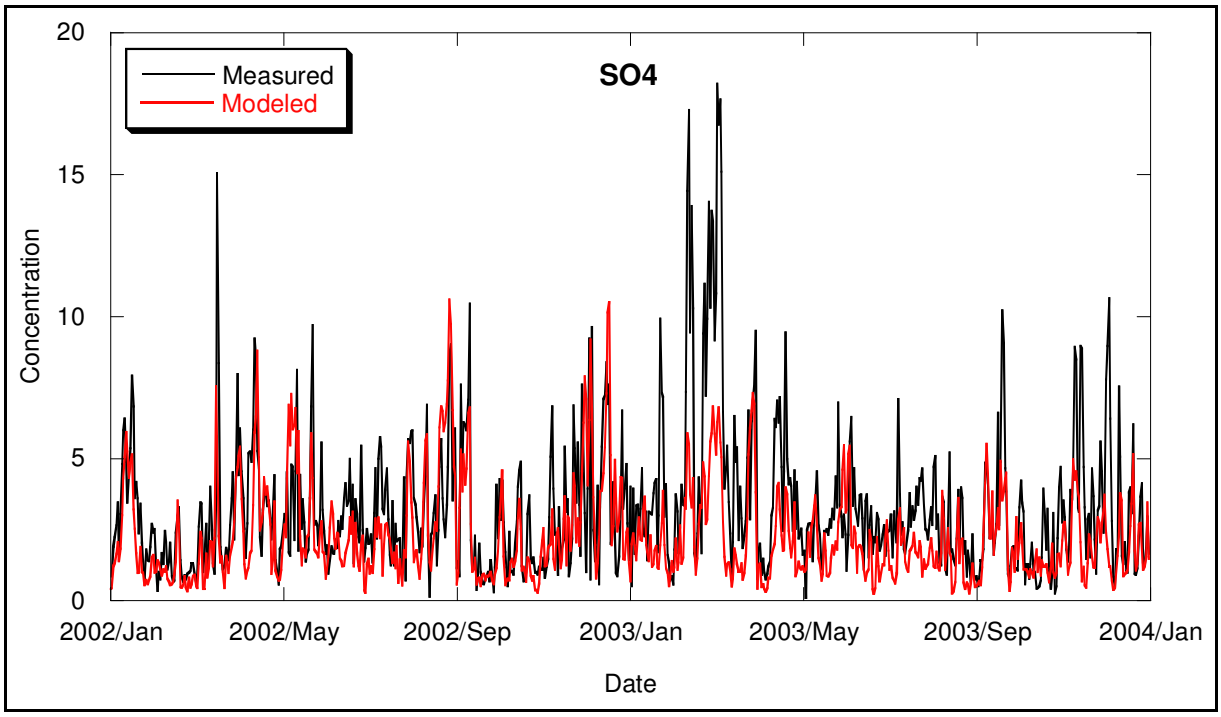

Figure 10.9: **The measured and modelled temporal variation of SO_4 at Zingst (DE09) for 2002 and 2003 [µg m^{-3}]**

Total nitrate, nitrate and nitric acid

Aerosol nitrate is difficult to measure due to the volatile character of ammonium nitrate and the reactivity of nitric acid. For monitoring purposes simple techniques are employed to measure total nitrate (TNO), the sum of particulate nitrate (NO_3) and nitric acid (HNO_3). The validation for total nitrate shows that the European fields are generally well reproduced by the model (Figure 10.10). In Germany total nitrate is measured since the 1999. In Figure 10.13 we show the time series for the monitoring station Zingst. The model captures the seasonal variation as well as single events rather well. On average the temporal correlation is over 0.6 on average, which is representative for the other stations (see table 10.2).

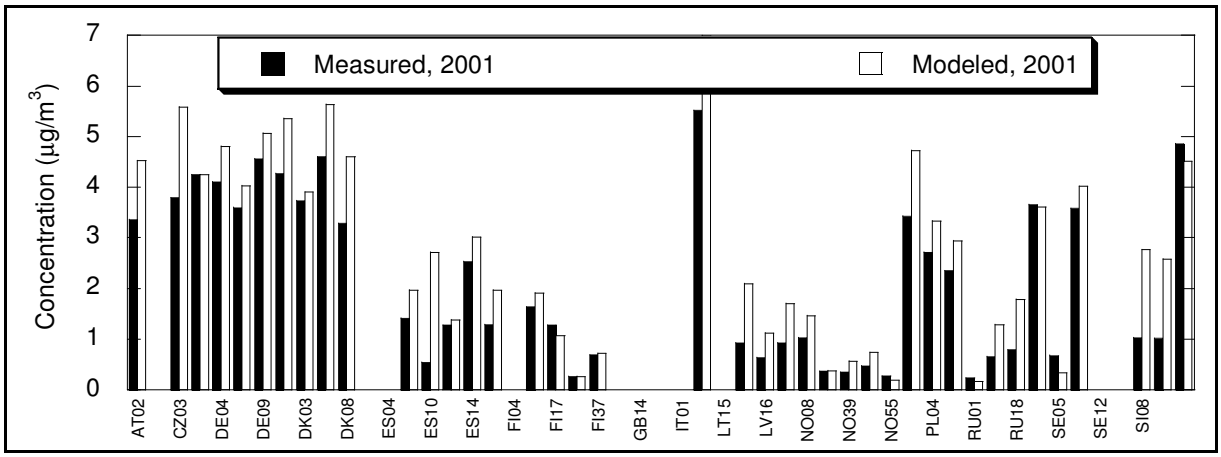

Figure 10.10: **Comparison of measured and modelled annual average TNO concentrations for 2001 in Europe**

Table 10.2: Measured and modelled average total nitrate (TNO) and nitrate (NO_3) concentrations over the German monitoring stations [µg m^{-3}]. Also given is the temporal correlation based on daily data and the number of stations (nstat) that contribute to the average

TNO	Meas	model	correlation	nstat	NO_3	Meas	model	correlation	nstat
1995				0	1995	3.0	2.5	0.53	2
1997				0	1997	3.7	2.7	0.62	2
1999	4.4	3.1	0.61	1	1999	3.5	2.5	0.59	2
2000	4.3	4.2	0.49	3	2000	3.2	3.4	0.43	1
2001	4.2	4.7	0.57	5	2001	3.6	4.0	0.56	2
2002	4.4	4.9	0.66	5	2002	3.5	4.2	0.63	1
2003	6.0	4.9	0.69	5	2003	4.5	4.1	0.60	1

The European perspective is summarised in Figure 10.11 for 2001. Note that the validation for nitrate is limited to only a few countries. For instance, for Germany, aerosol nitrate has been measured at Melpitz and at several sites by FAL. For these selected countries the model is able to reproduce the large scale pattern. However, for the Netherlands the model yields a significant overestimation. Looking in more detail, it shows that the overestimation is low in the mid-nineties and growing towards the end of the simulation period. As the nitrate maximum in Germany is located in the northwest the measurement data by FAL were also examined for this region (Linden, see Fig 10.12). The measurements performed by FAL are obtained with denuder filter packs. These techniques sample the nitric acid quantitatively prior to the aerosol sampling and sample the aerosol nitrate using a total nitrate method. These techniques are the proper way to measure nitrate, though not commonly applied due to the labour intensity of the method. In Linden (and Braunschweig) the seasonal variation with a spring maximum and a summer minimum are well captured by the model. However, the exact timing of the month in which the concentrations maximise is not correct for Linden. This has to do with the assumptions on the timing of manure applications to the land. Furthermore, the summer concentrations are overestimated by 1-1.5µg m^{-3}. This summer overestimation is also observed for the sites in the Netherlands.

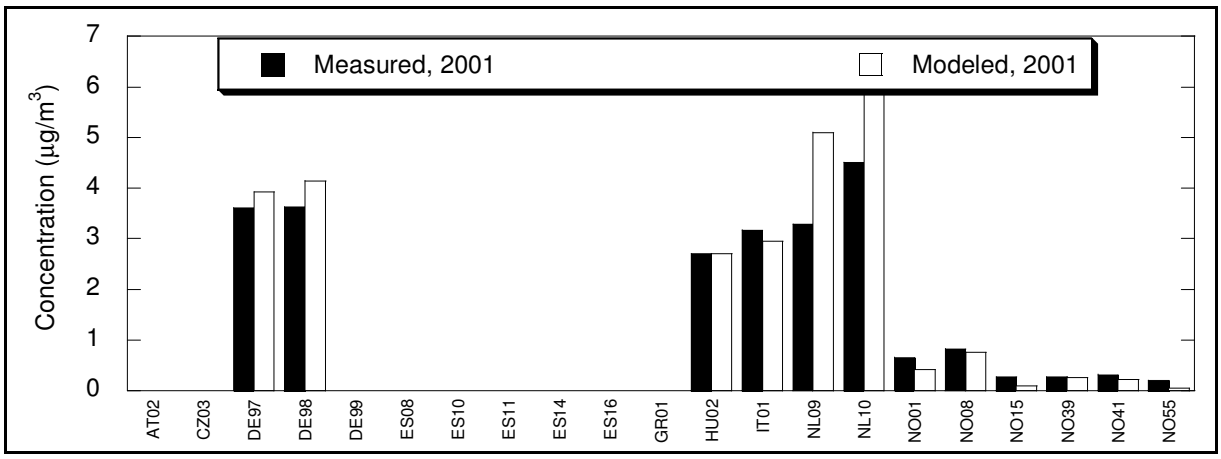

Figure 10.11: Comparison of measured and modelled annual average aerosol nitrate concentrations for 2001 in Europe

Nitric acid concentrations are compared to the FAL data in Figure 10.12. The seasonal variation in nitric acid can be explained by an effective transfer to the aerosol phase in winter due to the stability of ammonium nitrate in combination with a higher total availability of ammonia compared to nitrate (nitrate limiting ammonium nitrate formation) and more efficient photo-chemistry in combination with an unstable ammonium nitrate (higher partial pressure of ammonia) in summer. As the modelled concentrations are surface layer averages we expect the model should ideally overestimate the measured concentrations due to the effectively lower concentrations at measuring height due to dry deposition. This is indeed the case in summer but not in winter. Moreover, it seems that the stability of ammonium nitrate in the model is too high in winter and too low in summer. Such a conclusion is not valid at this moment as there is a strong diurnal cycle in both nitric acid and nitrate levels, especially in summer. Hence, these cycles need to be evaluated to improve the modelling of nitrate in the atmosphere.

In short, the modelled levels in nitrate and nitric acid show similar magnitudes and tendencies as measured in reality. However, a more detailed comparison reveals that the modelling of the nitrate species is uncertain. A more detailed study towards the partitioning of nitrate in the gas and aerosol phase in different parts of the

country appears to be very useful. Such a study should be directed to reveal the diurnal cycles of nitrate in regions with different ammonia regimes.

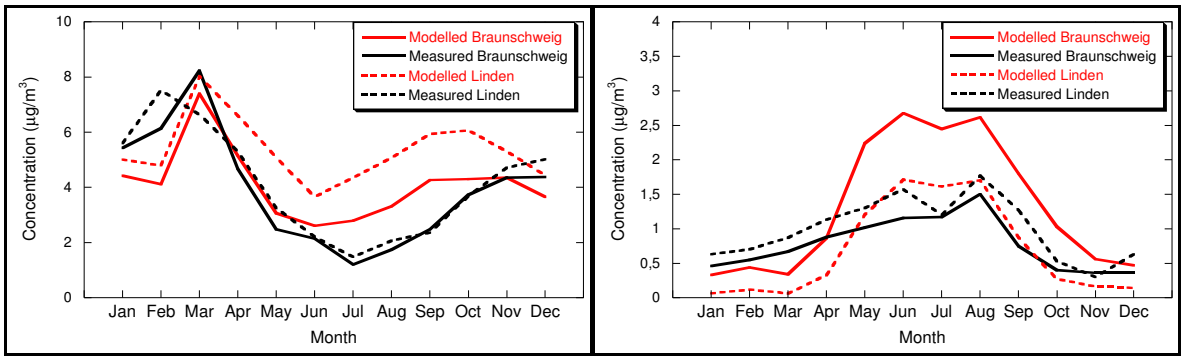

Figure 10.12: Comparison of the seasonal cycle of aerosol nitrate and nitric acid to observations at Braunschweig and Linden. The data represent a two-three year period each

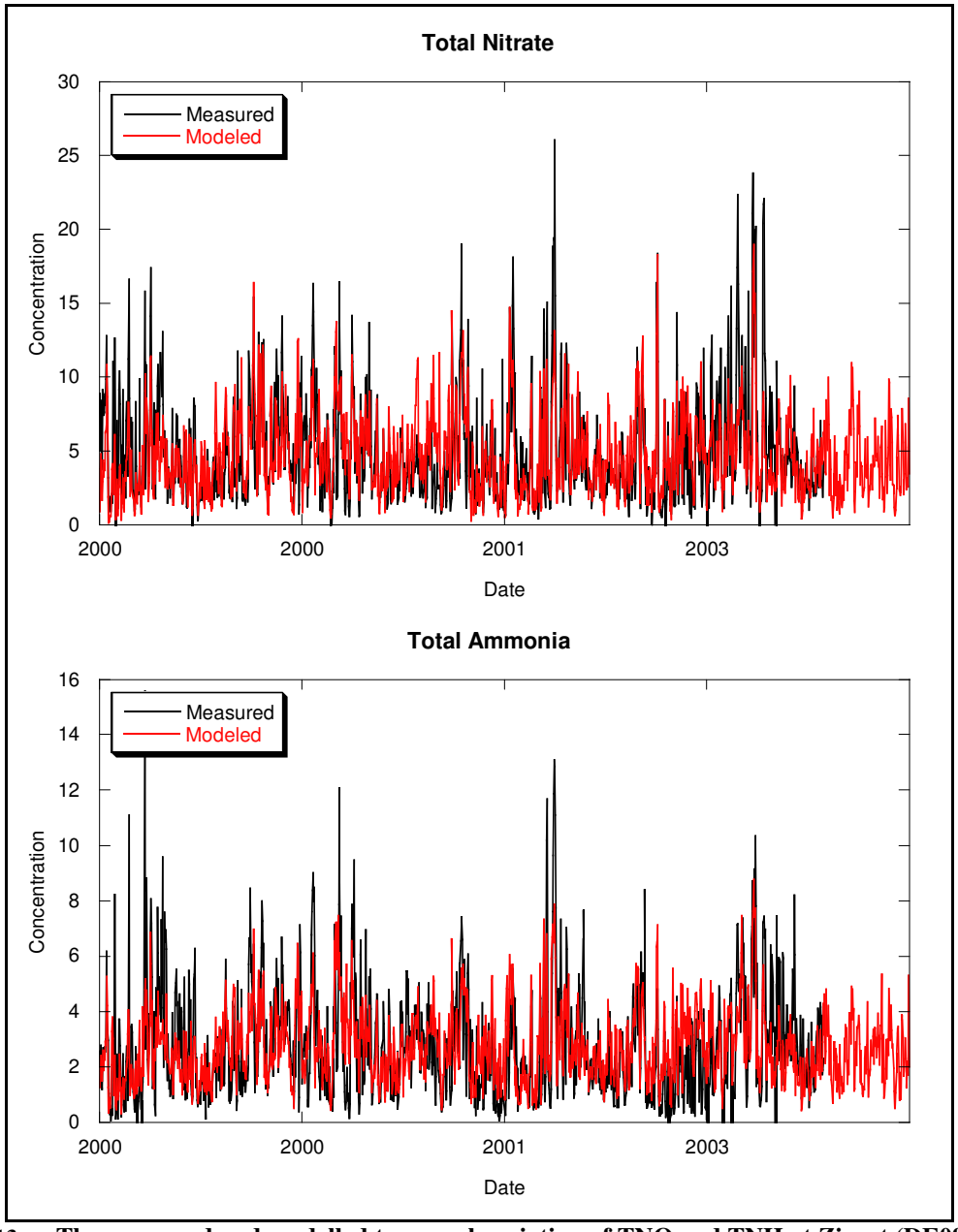

Figure 10.13: The measured and modelled temporal variation of TNO and TNH at Zingst (DE09) for 2000 to 2003 [µg m^{-3}]

Total ammonia, ammonium and ammonia

Total ammonia (TNH), the sum of ammonia and ammonium, is measured in Germany and a number of other countries since 2000. At the rural background EMEP sites in Germany the modelled total ammonium concentrations are in agreement with the observations (see Figure 10.14; Table 10.3). The nice spatial correlation shows that the model is able to capture the large scale variability in ammonia levels in Europe. The relatively nice comparison is caused by the dominant fraction of ammonium in total ammonia at background sites. The temporal correlation is on average 0.44 (-0.17 to 0.77) for all stations in Europe and about 0.6 for the German stations, which is not very good. The temporal correlation is somewhat less than for total nitrate and ammonium. The latter can explained by the primary nature of ammonia.

In source areas the ammonia concentrations are underestimated significantly by the model (see Table 10.4). For example, at Vredepeel or Braunschweig we underestimate by a factor 3. Also, the temporal correlation is low. This is not a surprise given the resolution of the model and the siting of the stations. The stations are located in agricultural areas with large ammonia emissions. Simulations on a higher resolution are needed. Now, comparing regional model results for sites located in agricultural areas is as if one compares a model result of NO_X to a measurement in the center of a large city.

The model results of ammonium aerosol concentrations are in better agreement with measurements than for ammonia both with respect to absolute levels and short term variations. This secondary component dry deposits only slowly and is more determined by long range transport and therefore easier to model on a large scale. Ammonium neutralizes both sulphate and nitrate. Hence, the distribution as well as the seasonal variation reflects the combined signal of sulphate and that of nitrate. Daily correlation coefficients are in the same range as well.

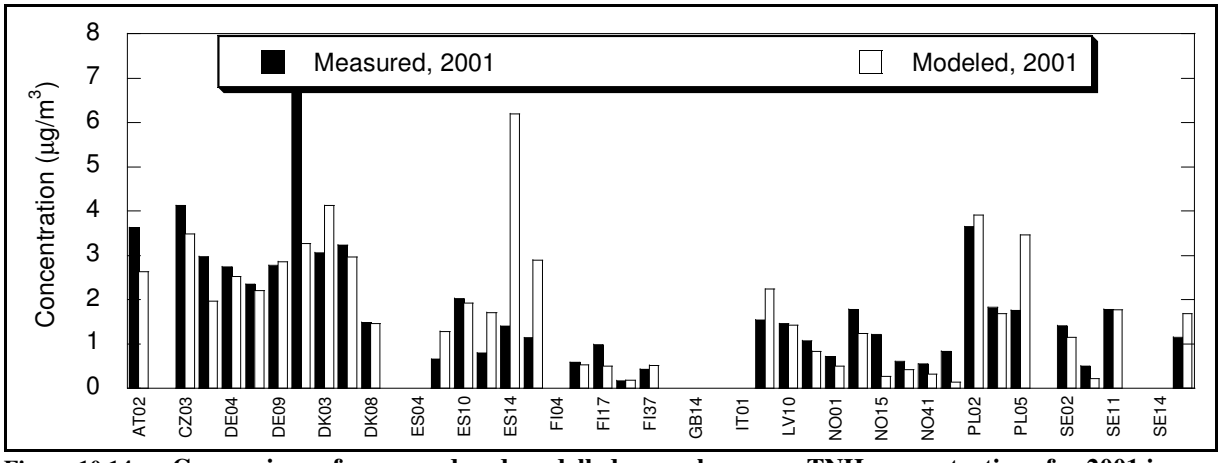

Figure 10.14: Comparison of measured and modelled annual average TNH concentrations for 2001 in Europe

Table 10.3: Measured and modelled average total ammonia (TNH) concentrations [µg m^{-3}] over the German monitoring stations. Also given is the temporal correlation based on daily data and the number of stations ('nstat') that contribute to the average

TNH	Meas	model	corellation	nstat	NH_4	Meas	model	corellation	nstat
1995				0	1995	3.0	2.1	0.66	2
1997				0	1997	2.6	1.7	0.65	2
1999				0	1999	2.2	1.3	0.62	2
2000	2.5	2.3	0.53	2	2000	2.2	1.6	0.51	1
2001	2.7	2.4	0.59	4	2001	2.2	1.9	0.62	2
2002	2.5	2.6	0.61	4	2002	2.4	2.1	0.59	1
2003	3.2	2.7	0.60	4	2003	2.8	2.0	0.54	1

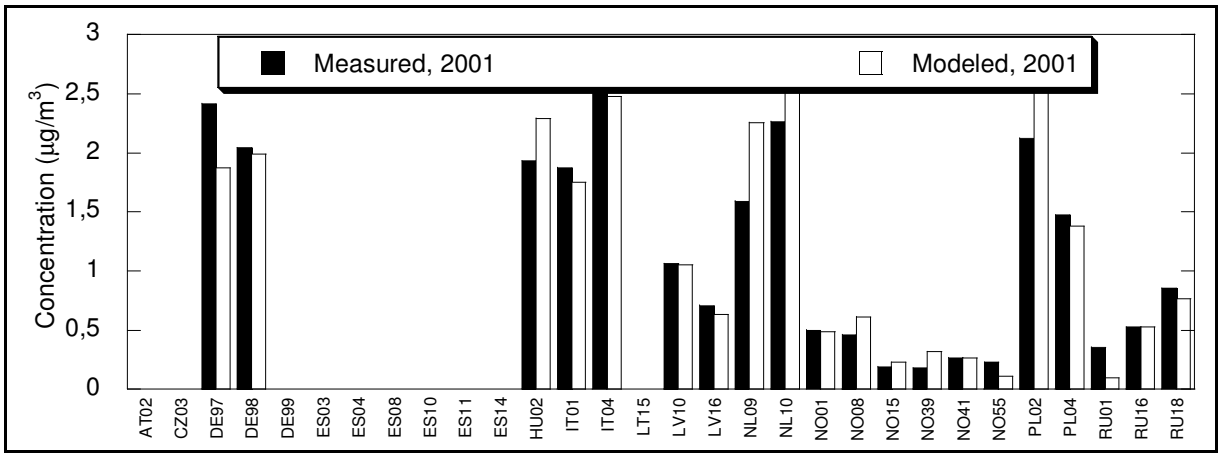

Figure 10.15: Comparison of measured and modelled annual average aerosol ammonium concentrations for 2001 in Europe

Table 10.4: Measured and modelled average ammonia (NH_3) concentrations [µg m^{-3}] at Müncheberg (before 2000) and Braunschweig (after 2000). Also given is the temporal correlation based on daily data

NH_3	Meas	model	correlation
1995	1.9	0.7	0.22
1997	2.9	0.8	0.35
1999	6.9	1.1	0.20
2000			
2001	5.4	1.4	0.14
2002	6.0	1.4	0.22
2003	6.6	1.6	0.25

10.3.4 Conclusions

The following conclusions can be drawn from this exercise.

- We have calculated the distribution of acidifying components over Germany for eight years.
- We have successfully implemented a model description for a shallow surface layer.
- The performance of the model for the secondary inorganic aerosols, nitrogen oxides and sulphur dioxide is state of the art.
- The model underestimates ammonia in agricultural areas whereas the modelled total availability of reduced N at the German EMEP sites is in line with the measured values.
- For all components the model performance is similar or better compared to that of the Unified EMEP model or other regional models in Europe (see van Loon et al., 2005)
- Except for ammonia in source regions, no biases larger than a factor of two were identified and all components show correlation coefficients of about 0.6.

Improvements to the modelling exercise can be obtained by:

Improving the model description:

- Develop or use existing modules for the timing of ammonia emissions as function of meteorology, compensation point and agricultural practice.
- Extensive validation: for a number of species (sea salt, ammonia, nitric acid, nitrate, base cations, etc) the availability of data through normal channels is so sparse that a targeted action appears to be required. Spatial representativity (for ammonia) should play a key role in this exercise.
- Investigating a more intensive coupling to meteorological input data from ECMWF. A number of parameters are available (e.g. snow cover, some stability parameters) but are not used as input to the model.
- Detailed studies regarding the partitioning of nitrate and ammonium over the gaseous and particulate phase with emphasis on the diurnal cycle.
- Coupling of sea salt and nitrogen/sulphur chemistry (for calculation of sodium nitrate in coastal regions).

Performing simulations on a higher resolution such as 6x6 km² over Germany (one way zoom). Especially for primary pollutants a better representation of the gradients is expected.

Applying data assimilation to obtain a best guess for the ambient concentrations of components with a large observational database. This could be done for sulphur dioxide, sulphate and possibly nitrogen oxides

Applying plume-in-grid algorithms (not available for LOTOS-EUROS at the moment) for a better representation in source areas. These approached allow for the explicit calculation of plumes from point sources (e.g. stables). Although not straightforward to implement, a considerable improvement of the primary components and especially ammonia is expected.

Prepare simulations for the period before 1995. This work would need a revision of the spatial allocation of the emissions for these years as the emissions in Eastern Germany have changed significantly over that period.

10.4 Modelled heavy metal concentrations over Germany and Europe

10.4.1 Model set-up

In this study we developed the code to perform simulations for lead and cadmium with LOTOS-EUROS. Although a large part of the modelling is similar as for primary particulate matter a number of modules were adjusted for heavy metals. Especially, the model input and interfaces needed to be changed. In this section we present the model set-up for heavy metals. As the atmospheric lifetime of particles and thus metals depends on its size, we distinguish between fine and coarse mode heavy metals in the model. Following PM, the fine mode includes all particles smaller than 2.5µm and the coarse mode all particles larger than 2.5µm up to 10µm.

Anthropogenic emissions

Large sources for heavy metals are the non-Ferro industry and combustion processes. Many of the sources are very specific for one metal. In this study we focus on Cadmium and Lead. Emissions from these metals are taken from the TNO emission inventory (DENIER VAN DER GON ET AL., 2005). DENIER VAN DER GON ET AL. (2005) estimated the emissions of these heavy metals combining the TNO activity database with emissions factors. The emission totals per mayor source category and country were scaled to the officially reported emissions by the member states of the European Union. Hence, official totals are used in combination with the detailed spatial distribution.

In Table 10.5 we summarise the emissions for the year 2000 with detailed source attribution given for Germany.

The emissions were distributed on the LOTOS grid of 0.5°x0.25° lon-lat. The spatial distribution of the emissions is shown in Figure 10.16. We have used these heavy metal emissions for 2000 for all model simulations

Table 10.5: Heavy Metal emissions for Europe (DENIER VAN DER GON ET AL., 2005)

Sector	Cd	Hg	Pb	As	Cr	Cu	Ni	Se	Zn
Public heat and power	*1056*	*16101*	*13742*	*14405*	*10409*	*4524*	*31861*	*9166*	*122204*
Residential, commercial and other	*2149*	*1490*	*11268*	*1804*	*3904*	*7052*	*6647*	*177*	*25382*
Industry	*14976*	*16218*	*534656*	*17260*	*40311*	*84910*	*199874*	*20093*	*961801*
Solvent and product use									
Road transport	*882*		*397*		*3996*	*102940*	*5046*	*544*	*209760*
Non-Road transport	*11*	*14*	*11686*	*58*	*54*	*53976*	*79*	*61*	*997*
Waste disposal	*1987*	*22190*	*15894*	*993*	*14899*	*19866*	*3973*	*258*	*337723*
Agriculture									
Total	**21062**	**56014**	**587643**	**34520**	**73574**	**273268**	**247481**	**30299**	**1657867**

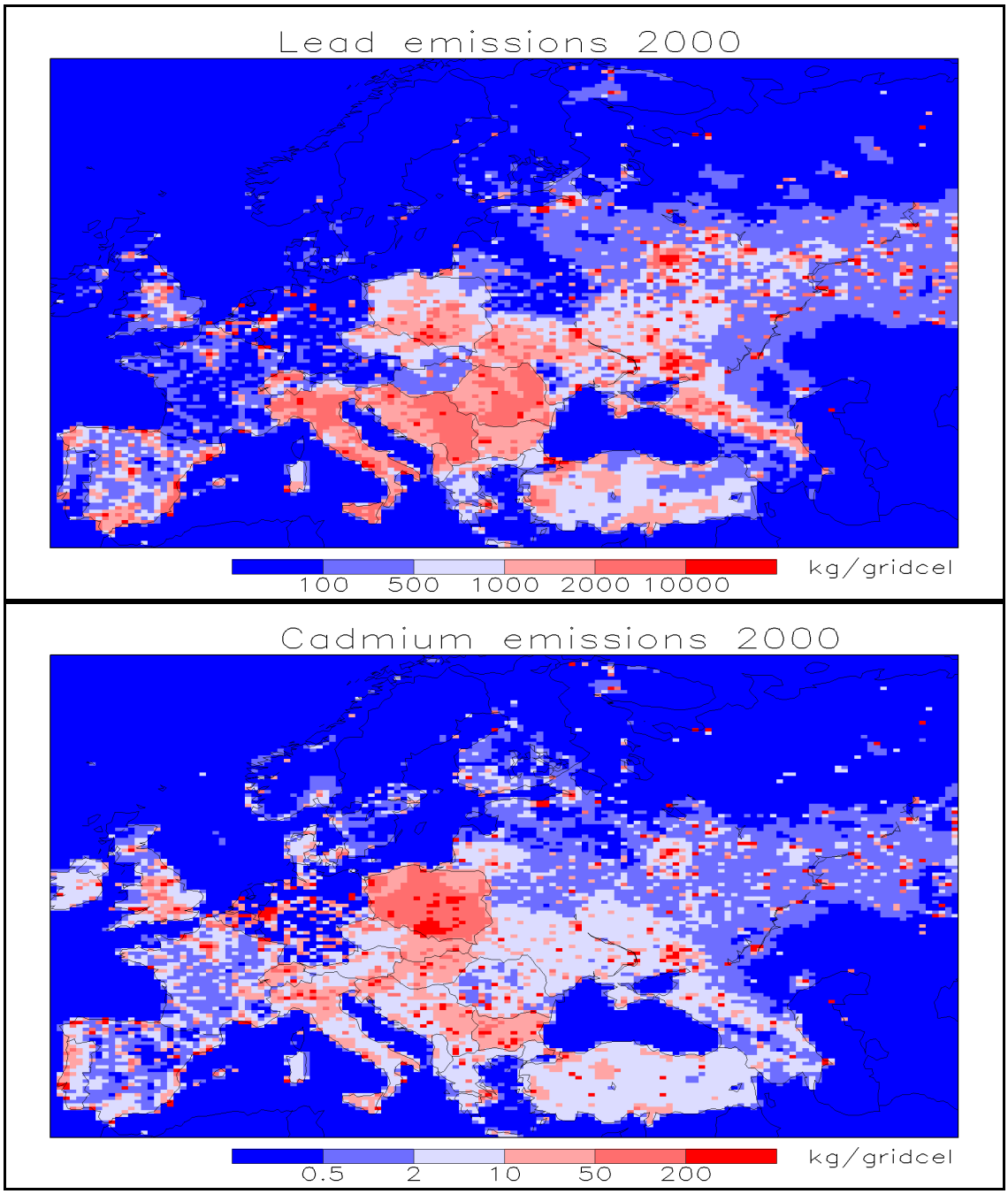

Figure 10.16: Distribution of the emissions of lead and cadmium in 2000 (in kg/gridcell of 0.5°x0.25°)

Natural emissions

Besides anthropogenic sources, heavy metals are also emitted from several natural sources (e.g. volcanoes, forest fires and wind blown dust). Furthermore anthropogenic pollutants can be re-emitted after being deposited at the Earth's surface. The re-suspension emissions are included in the model as natural emissions.

The natural emissions are chosen in accordance with the natural emissions in the EMEP/MSCE-HM model (TRAVNIKOV AND ILYIN, 2005). In this model the natural lead and cadmium emission fluxes are uniformly distributed over the sea and land surfaces and are parameterized as to fit the measured background concentrations. In the LOTOS-EUROS model we use the exact same values, i.e. lead 160 g km^{-2} a^{-1} and cadmium 8 g km^{-2} a^{-1} from sea surfaces, and lead 220 g km^{-2} a^{-1} and cadmium 12 g km^{-2} a^{-1} from soils. In the presence of snow cover the emissions are set to zero. It is assumed that 90% of all naturally emitted lead and cadmium is in the coarse mode and 10% in the fine mode.

Boundary conditions

For both lead and cadmium we use prescribed boundary conditions at the north, south, west, east and top of our model domain. The values are chosen in agreement with the prescribed boundary conditions used in the regional EMEP/MSCE-HM model (Travnikov and Ilyin, 2005), which in turn are based on measurement data.

Measured background concentrations of lead and cadmium in the ambient air in Europe lie mostly within the range 0.3-3 and 0.02 and 0.1ng m^{-3}. Lowest values are found in Northern Europe and over the Atlantic. High values are found over industrial regions. Table 10.6 presents the prescribed lead and cadmium boundary conditions used within LOTOS-EUROS, from which 90% is in the coarse mode and 10% in the fine mode.

Due to their relatively short residence time, the boundary conditions for lead and cadmium will not have a large influence on the concentrations in the centre of our domain. However, the boundary conditions can have influence close to the boundaries.

Table 10.6: Prescribed boundary conditions

	Lead (ng/m^3)	Cadmium (ng/m^3)
North	0.6	0.02
South	1.5	0.04
West	1	0.03
East	2	0.05
Top	0.1	0.003

Initial conditions

The initial conditions are derived by interpolation of the boundary conditions.

Deposition

The (wet and dry) deposition of fine and coarse heavy metals is treated in the same way as deposition of respectively $PM_{2.5}$ and PM_{10}.

10.4.2 Model results and validation

Lead and cadmium distributions

Figure 10.17 shows the annual mean distributions for lead (left plot) and cadmium (right plot) for the year 2000 as calculated using the LOTOS-EUROS model. Lead concentrations at rural background concentrations range between 1 and 7ng m^{-3}. Only in areas with a large concentration of sources higher concentrations are modelled. Cd is less abundant in the atmosphere than lead. Modelled concentrations of Cd are typically between 0.1 in rural areas and 1ng m^{-3}in source areas.

Figure 10.18 shows the concentrations measured at different EMEP stations averaged over the year 2000. A comparison between modelled concentrations and measurements performed at several EMEP stations revealed that the model values for both cadmium and lead are well below the measured concentrations. The underestimation is on average a factor 3.3 and reaches up to a factor 8 for some specific sites (see Table 10.7). For Germany the underestimation for lead is close to the average values. Overall, the differences are larger for lead than for cadmium. The latter could not be assessed for Germany as there are no Cd data available.

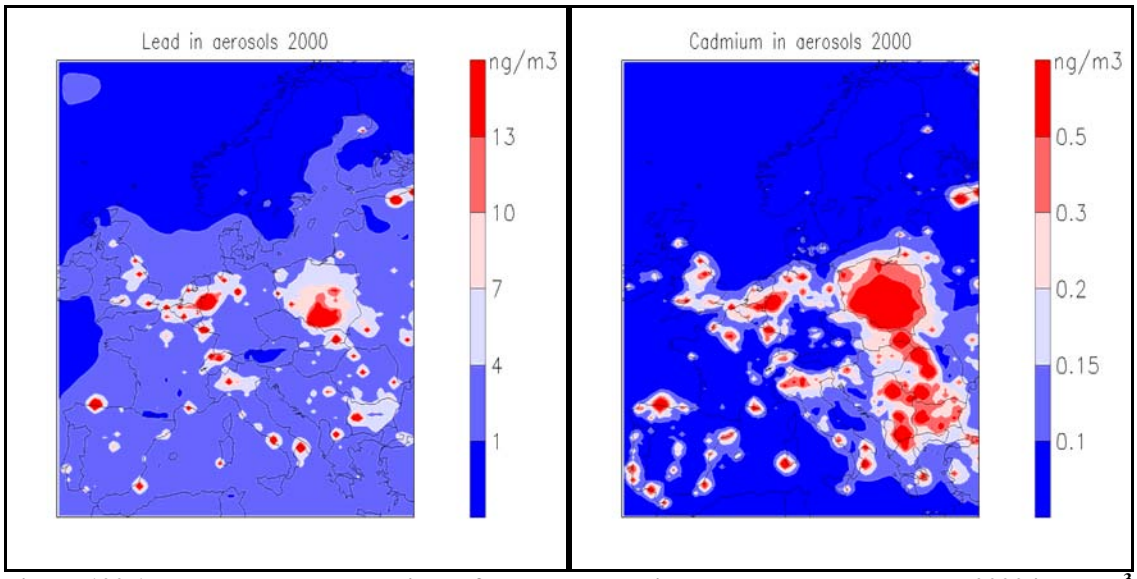

Figure 100.17: Modelled concentrations of lead and cadmium averaged over the year 2000 in ng m^{-3}

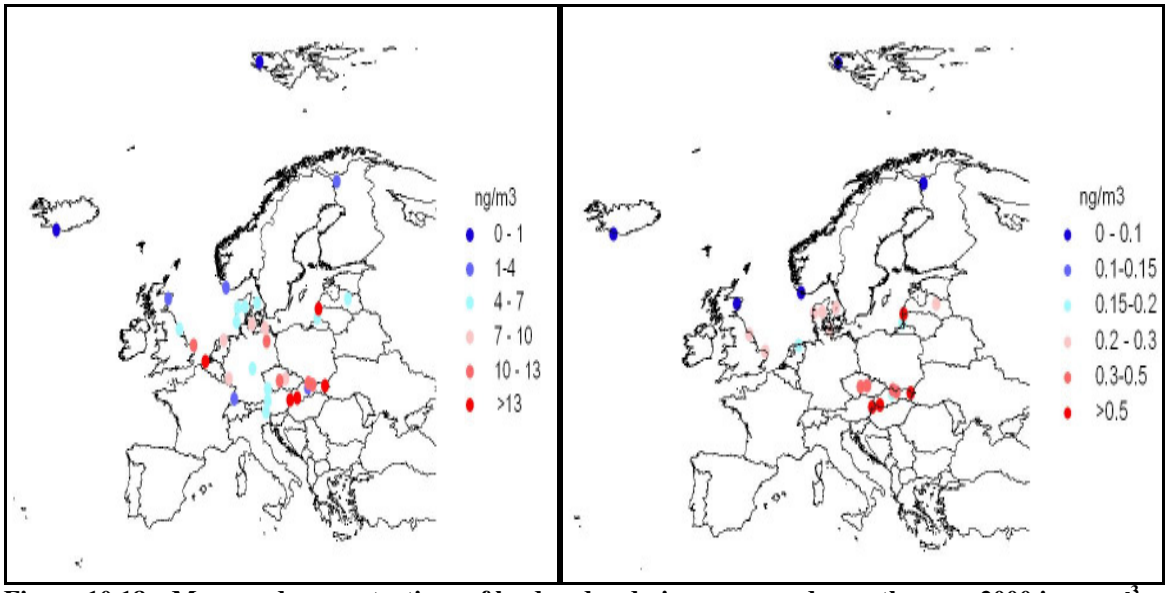

Figure 10.18: Measured concentrations of lead and cadmium averaged over the year 2000 in ng m^{-3}

Table 10.7: Difference factor between EMEP measurements and LOTOS-EUROS modelled concentrations

Station	Country	EMEP/LE Lead	EMEP/LE cadmium
AT02	Austria	7.71	3.65
AT04	Austria	5.37	-
AT05	Austria	3.21	-
BE04	Belgium	7.59	-
CZ01	Czech Republic	5.01	2.79
CZ03	Czech Republic	5.76	3.01
DE01	Germany	3.84	-
DE03	Germany	0.68	-
DE04	Germany	2.32	-
DE05	Germany	3.57	-
DE07	Germany	7.02	-
DE08	Germany	5.26	-
DE09	Germany	4.62	-
DK03	Denmark	4.13	3.32
DK05	Denmark	4.20	3.00
DK08	Denmark	3.61	2.93
DK31	Denmark	3.78	3.84
FI96	Finland	2.80	2.05
GB14	Great-Britain	1.53	1.27
GB90	Great-Britain	4.83	2.57
GB91	Great-Britain	1.89	0.93
LT15	Lithuania	1.73	0.84
LV10	Latvia	8.25	4.36
LV16	Latvia	5.49	3.79
NL09	Netherlands	3.35	1.78
NO99	Norway	3.24	1.70
SK02	Slovakia	1.10	0.72
SK04	Slovakia	2.23	1.09
SK05	Slovakia	1.75	1.02
SK06	Slovakia	4.26	1.77
SK07	Slovakia	5.38	2.67

Time series

Four EMEP stations in Denmark provide daily measurements of lead and cadmium. These daily measurements have been compared to daily values from the LOTOS-EUROS model. The correlation between both datasets for these four stations is presented Table 10.8.

Table 10.8: Correlation between daily EMEP measurements and LOTOS-EUROS modelled concentrations

Station	Cadmium	Lead
DK03	0.16	0.48
DK05	0.43	0.51
DK08	0.33	0.55
DK31	0.30	0.58

Figures 10.19 and 10.20 show the time series for lead and cadmium for the Danish station closest to Germany: DK05 (Keldsnor). The LOTOS-EUROS lead concentrations are multiplied by 4 and the LOTOS-EUROS cadmium concentrations by 3 to better compare the variability in model and measurements. The seasonal variability is well captured by the model and some of the peaks are well represented. However, for a majority of the observed peak values the model severely underestimates the concentrations or does not show a peak at all. Clearly, an important source or process is missing in the model as is also indicated by the correlation coefficients.

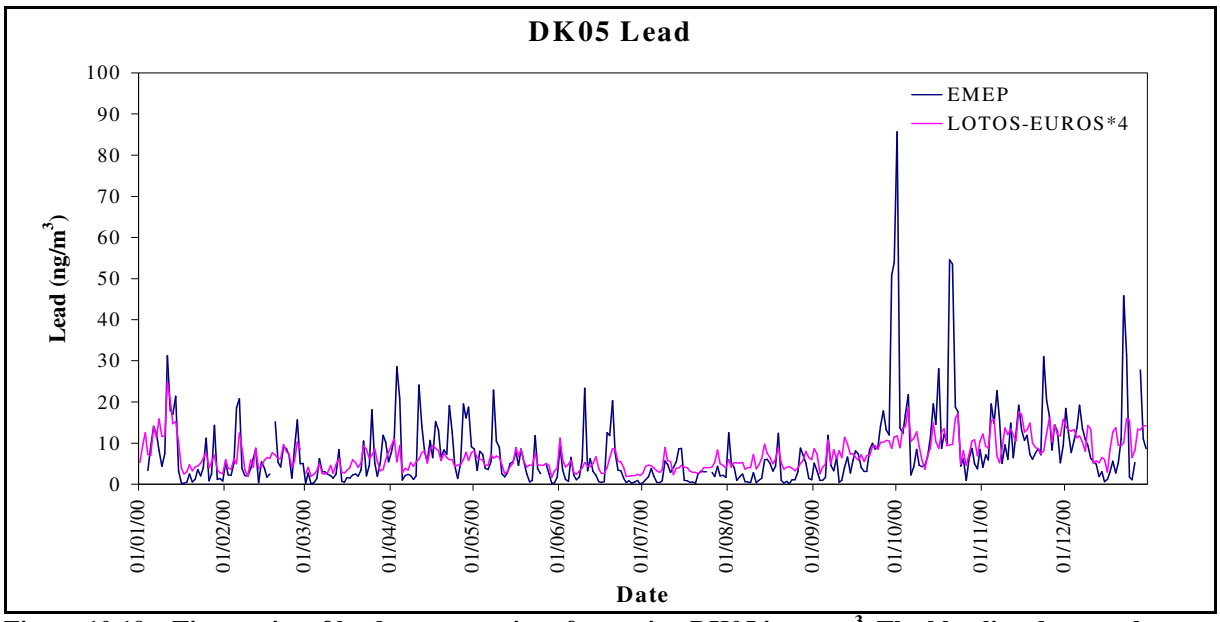

Figure 10.19: Time series of lead concentrations for station DK05 in ng m^{-3}. The blue line denotes the EMEP measurements and the pink line the LOTOS-EUROS values multiplied by 4

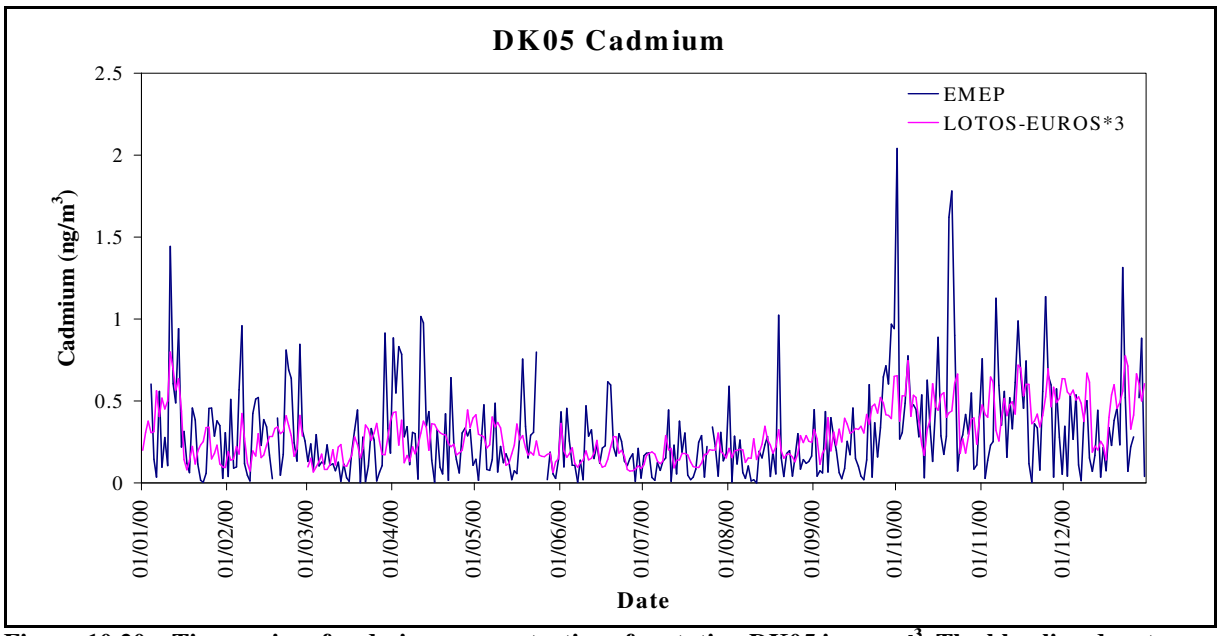

Figure 10.20: Time series of cadmium concentrations for station DK05 in ng m^{-3}. The blue line denotes the EMEP measurements and the pink line the LOTOS-EUROS values multiplied by 3

The LOTOS-EUROS model clearly shows lead and cadmium concentrations that are well below observed concentrations. This discrepancy has also been observed between other models and observations (e.g. ILYIN ET AL. 2005) and is believed to be largely due to the high level of uncertainty of emission data. For this reasons we compare the results of this simulation to that of a simulation with emissions obtained from the ongoing EU-FP6 project ESPREME below.

10.4.3 Comparison to results with ESPREME emissions

In this section we compare the official emission database to that obtained from the EU-FP6 project ESPREME and assess the impact of these databases.

Table 10.9: Comparison between the official TNO emission estimates (tons) and the official and expert estimates by the ESPREME project

Code	Country	Cd			Pb		
		TNO_off	Esp_off	Esp_exp	TNO_off	Esp_off	Esp_exp
ALB	Albania	0.2	0.6	0.4	43.2	24.0	24.4
AUT	Austria	1.4	1.4	5.7	13.9	13.9	64.1
BEL	Belgium	2.8	2.3	13.5	133.8	123.0	268.8
BGR	Bulgaria	11.0	11.0	12.9	214.1	213.4	163.6
BIH	Bosnia and Herzegovina	1.7	0.3	1.8	96.9	5.0	15.4
BLR	Belarus	1.4	1.4	2.3	51.0	46.1	146.7
CHE	Switzerland	2.2	2.2	4.9	113.6	113.6	107.0
CYP	Cyprus	0.0	0.2	0.9	47.1	74.0	40.6
CZE	Czech Republic	2.8	2.9	13.2	107.7	107.7	185.9
DEU	Germany	21.1	11.0	66.3	587.6	632.0	942.4
DNK	Denmark	1.0	0.7	3.6	9.6	7.0	38.5
ESP	Spain	15.0	19.8	33.0	904.2	672.5	787.3
EST	Estonia	0.7	0.7	1.7	40.7	40.7	21.3
FIN	Finland	1.4	1.4	5.7	37.5	37.5	94.9
FRA	France	10.5	11.5	42.3	234.1	196.0	520.3
GBR	United Kingdom	7.2	7.2	36.1	192.8	192.8	571.1
GRC	Greece	2.8	3.0	9.9	132.4	470.0	311.2
HRV	Croatia	1.0	1.0	2.1	146.9	146.9	153.9
HUN	Hungary	2.7	2.7	5.2	38.7	37.0	69.4
IRL	Ireland	1.3	2.0	4.1	8.7	83.0	97.8
ITA	Italy	11.1	29.9	55.2	908.9	2173.8	1919.2
LTU	Lithuania	1.4	1.4	0.8	16.1	15.9	16.5
LUX	Luxembourg	0.1	0.1	1.2	3.4	1.6	30.6
LVA	Latvia	0.6	0.6	0.6	8.2	8.4	14.5
MDA	Republic of Moldova	0.4	0.1	0.2	3.2	11.2	10.3
MKD	Former Yugoslav Republic of Macedonia	9.8	0.2	0.9	87.0	3.0	9.7
NLD	Netherlands	1.2	1.2	10.7	44.1	44.1	183.0
NOR	Norway	0.7	0.7	3.7	6.0	6.0	33.2
POL	Poland	50.4	50.4	39.4	647.5	647.5	437.1
PRT	Portugal	3.2	3.0	7.5	39.0	365.0	198.1
ROM	Romania	17.4	21.0	13.8	604.4	510.0	541.7
SVK	Slovak Republic	7.2	7.2	6.6	74.3	74.3	69.7
SVN	Slovenia	1.5	1.5	1.9	37.5	37.2	43.6
SWE	Sweden	0.4	0.9	6.0	11.8	15.4	105.2
TUR	Turkey	16.6	0.2	26.7	764.9	427.0	650.9
UKR	Ukraine	23.7	10.5	33.7	1703.2	663.1	740.9
YUG	Federal Republic of Yugoslavia	8.7	6.0	8.7	299.8	331.0	340.2
	Total	243	218	483	8414	8571	9969

The comparison of the emission databases presented here is not exhaustive but should be interpreted as a first scan of the data. A full comparison is out of the scope of the project and would mean a substantial effort (the devil is in the details). More importantly, the data needed for such an exercise are not yet available. The following remarks can be made on the comparison between the emission data.

- ESPREME does not cover total UNECE area. Hence, we focus our analysis on the countries included in the modelling domain (see Table 10.9).

- Since both projects accept official emission estimates as the “correct” estimate which overrules the expert estimate the differences in the emission estimates are fairly small (see Table 10.9)

- The official databases by both ESPREME and TNO are in very good agreement with each other. This can be interpreted as a quality control as they should reflect official data. The major discrepancies in the official databases for Pb and Cd are found in the Ukraine, Greece, Portugal and Italy. These

discrepancies are mostly due to differences in expert estimates for some sectors/countries where no country data were available.

- We only analyzed the differences at the national total. The difference in the sector apportionment may be somewhat larger as TNO completed estimates for sectors where countries did not report emissions.

- The TNO project did not have time allocated for updating emission factors (as they would have largely been overruled anyway). ESPREME invested in this part of emission estimation methodology so they may have a more up-to-date emission factor set. The impact for the official database is limited as the country estimates overrule the expert estimates.

- The expert estimates by the ESPREME project are much higher than the official emission data. For Cadmium and Lead the expert emissions are respectively ~120 % and ~15% higher than the official database. For single countries the differences may be much larger. For Germany the difference for Cd is a factor 3 where the Pb emissions are a factor 1.6 higher. Overall, the expert emissions in Western Europe are higher whereas the emissions in Eastern Europe are lower than the official ones. Unfortunately, TNO did not generate an expert emission database to compare with.

Clearly, the large differences between the expert and the official emissions would have a large impact on the modelled concentrations. The effects have been assessed in a sensitivity simulation. For this simulation we have scaled the gridded official emission database to the totals of the expert estimates (by country). Hence, we have updated the emission strength but not the distribution over the countries which we expect to shift as it is probably only a few sectors that have large differences in emissions. The results should therefore be interpreted as indicative.

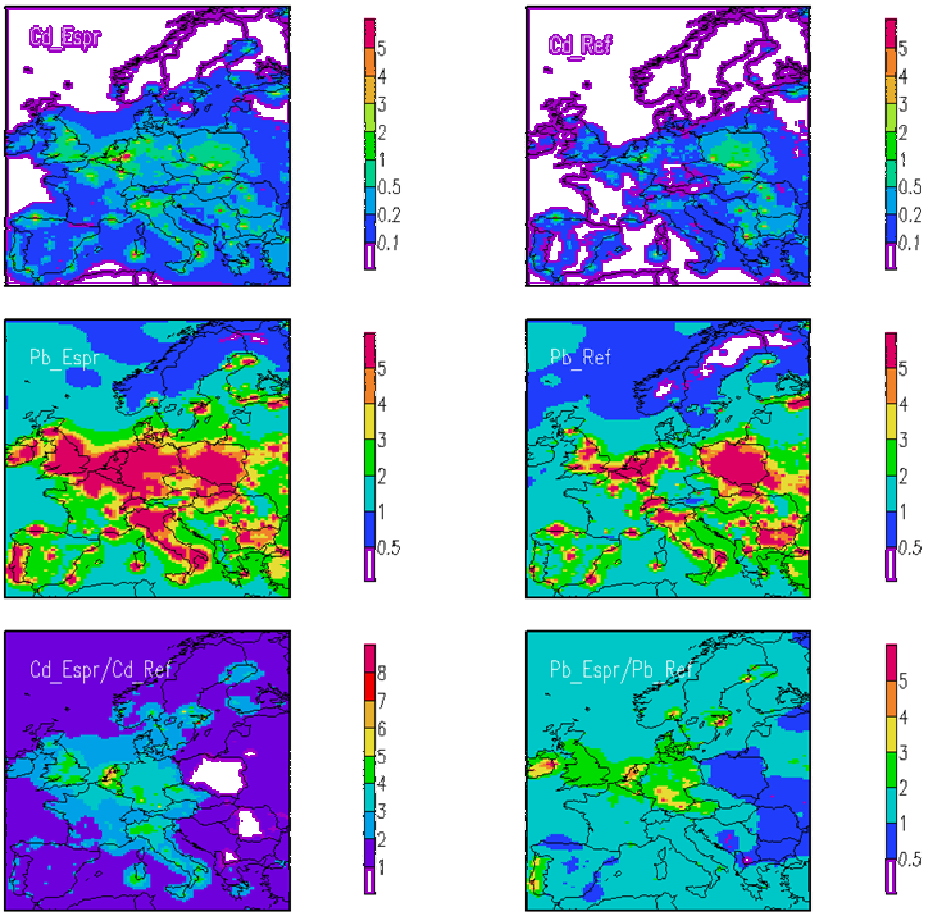

Figure 10.21: Comparison between modelled Cd (upper panels) and Pb (middle panels) concentrations using the ESPREME expert data and the TNO official database. The relative increase is shown in the lower panels

In Figure 10.21 the concentration fields using the official and the expert emissions are compared. For Cadmium

the concentrations due to the expert estimates increase by a factor 2-4 over north-western Europe, whereas they are only slightly higher in Spain and lower in eastern Europe. For lead a similar pattern arises with concentration increases of a factor 2-3 in north-western Europe. In some areas, like southern Germany the increase is even larger. However, small scale details are uncertain due to the uncertainties in the scaling of the emissions. The gap between modelled and measured concentrations is largely reduced, although an underestimation remains.

The huge difference in the model results indicates that a thorough analysis of the emission estimates is needed. Moreover, the differences indicate that for heavy metals important sources have been neglected in the past. A recent example is copper emissions from brake wear (traffic). These emissions, previously neglected, were estimated by HULSKOTTE ET AL. (2006) to equal the total amount of copper in the official emission data. They also showed that the existing gap between model and measurements for this component could be closed by using new data. They concluded that especially non-exhaust emissions from road traffic deserve more scientific research to support cost-effective international reduction programs of diffuse emissions from metals to the environment such a copper, zinc, antimony and lead.

10.4.4 Conclusions

The following conclusions can be drawn from this exercise.

- We have extended the LOTOS-EUROS model to perform simulations for Heavy Metals (excluding Mercury).
- Using the official database the levels of Cd and Pb are largely underestimated.
- The emission data are the most likely cause for this discrepancy.
- The official emission databases by both ESPREME and TNO are in very good agreement with each other.
- The expert estimates by the ESPREME project are much higher than the official emission data (~120 % and ~15% for Cd and Pb, respectively).
- For Cadmium and Lead the modelled concentrations due to the expert estimates increase by a factor 2-4 over north-western Europe, whereas they decrease over eastern Europe.
- The huge difference in the model results indicates that a thorough analysis of the emission estimates is needed.
- Non-exhaust emissions from road traffic deserve more scientific research to support cost-effective international reduction programs of diffuse emissions from metals to the environment such a copper, zinc, antimony and lead.

The implication for deposition mapping is that reliable concentration fields based on widely acknowledged data are not yet available. Moreover, it is expected that emission estimates may be updated frequently over the next years as there is a certain momentum in Europe to investigate the systematic underestimation of the simulated HM levels.

10.4.5 Outlook

This study has revealed large biases between modelled and measured concentrations of heavy metals. Furthermore, the comparison between official and expert emissions shows that there are large differences in these estimates. Hence, future work should be aimed to reduce the uncertainty in model-predicted concentrations/depositions and work towards (further) gap-closure of modelled / observed concentrations. We propose two ways of pursuing this goal, which should ideally be followed simultaneously. The first is directly via an analysis of emission estimates/factors. The second is based on an analysis of concentration data and inverse modelling.

Bottom-up through Emissions

A detailed comparison between the official and expert emissions by ESPREME should be performed to investigate the scientific basis/reasons of the large differences. A lot of the data needed for this is probably available through ESPREME. An evaluation of emission estimates of the sectors with the largest differences and of the most uncertain source contributions should be performed.

Top down through an integrated analysis of observations and model predictions in time and space

Several independent lines of investigation are initiated and subsequently integrated to achieve the goal outlined above.

1a Trend analysis of measured HM (wet) deposition data in one or more countries with relative accessible data of relative good quality (e.g. Germany, Netherlands, and UK).

1b Trend analysis of HM emission data in one or more countries matching the above made selection.
2 Model / trajectory analysis to separate source regions of modelled / observed concentration data, including an inverse modelling exercise.

Integration to address the question of uncertainty reduction and constraining of possible explanations of observed patterns through analysis of collected data, describe discrepancies between various HMs and processes e.g.

- Emission HM_X may show a decrease over time whereas emission of HM_Y remains constant – this indicates different sources are responsible
- How well do trends in activities and technologies match with emissions e.g. increasing trends in road transport, increased end-of-pipe measures for LCPs
- Deposition of HM_X may not reflect the trend in emission HM_X – missing sources? Resuspension and delay in effect?

Results: Hypotheses that may explain the observed patterns and propose verification / falsification routes, Including possible over/underestimated sources or source regions. Targeted uncertainty reduction and gap-closure to be defined based on results of the hypotheses.

10.5 Modelled sea salt concentrations over Germany and Europe

10.5.1 Modelled sodium distribution

The primary aerosol distributions modelled by LOTOS-EUROS also encompass the sea salt distribution, which is represented by sodium (Na^+) concentrations. Sodium is chosen as it is conserved as a sea salt tracer, in contrast to chloride. Chloride can be driven out of the aerosol phase when nitric acid or sulphuric acid condense on the sea salt particles and the more stable sodium nitrate or sulphate is formed. Hence, chloride is not conserved and is not suited to be used as a tracer for sea salt. To account for the difference in life time a separation is made between coarse (>2.5µm < 10µm) and fine (<2.5µm) mode Na^+.

Figure 10.22 shows the modelled annual averaged concentration fields for coarse and fine Na^+ for 2001. The modelled sodium concentrations are high over the open ocean. The concentrations are higher over the Atlantic Ocean compared to the Mediterranean Sea which can be explained by the higher wind speeds that generally occur over the open ocean. The sodium concentrations drop off fast over land. In coastal areas of northern Germany modelled concentrations range between 1 and 1.5µg m^{-3}. South of the line between Luxemburg and Stralsund the concentrations are modelled to be very low.

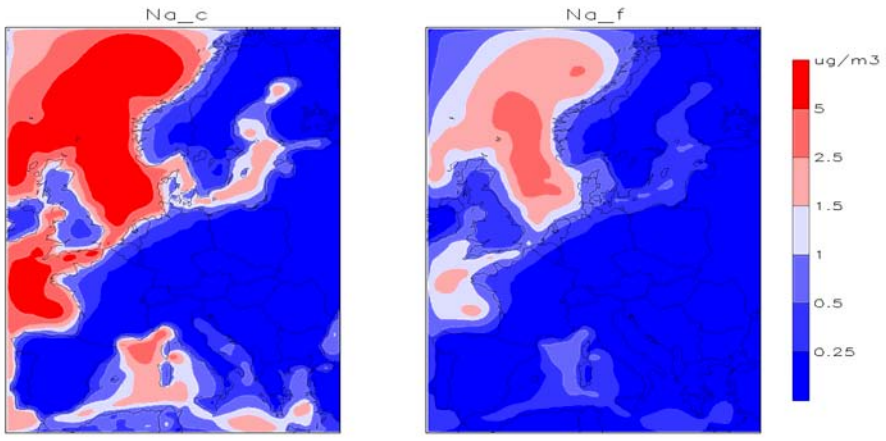

Figure 10.22: Distributions of coarse and fine Na^+ for 2001 (in µg m^{-3})

10.5.2 Validation

The availability of monitoring data for sodium concentrations in air is very limited. Moreover, they are not readily available for Germany. The modelled total (coarse and fine) Na^+ concentrations are compared to the corresponding daily measurements from 3 Danish EMEP stations and 5 Norwegian EMEP stations in Table 10.10. For all stations modelled values are higher than those observed. The difference between model and observations is larger for the Norwegian stations than for the Danish stations. The correlation coefficients are mostly well above 0.5. In Figure 10.23 modelled and observed Na^+ concentrations at the Danish station Tange are plotted for the year 2001. The variability in the observed concentrations is well captured by the model, which

is reflected in a high correlation coefficient of 0.67. However, most observed peak values are overestimated by the model causing the positive bias between LOTOS-EUROS and the observations.

We also compared our model results to a few observations obtained in campaigns in the Netherlands and Germany (see table 10.12). The modelled concentrations are within 30% of the observed ones for these studies.

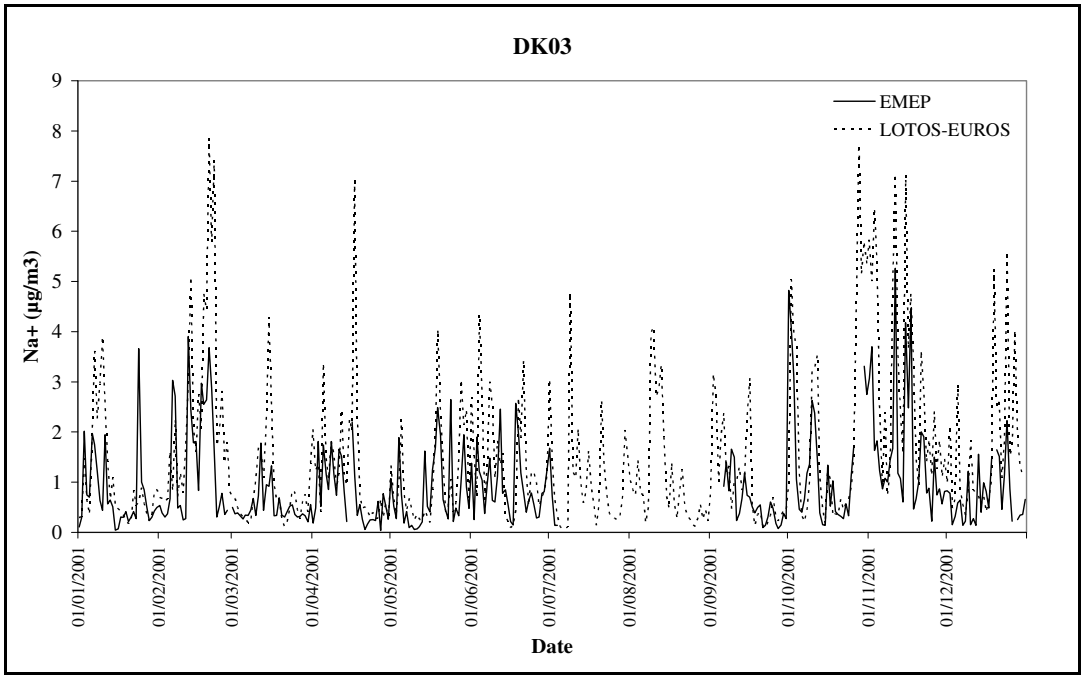

Figure 10.23: Comparison of modelled and observed Na+ concentrations at EMEP station Tange (DK03) in Denmark. The solid line indicates the observations. The dashed line indicates the modelled values by LOTOS-EUROS

Table 10.10: Averaged Na^+ concentrations in µg m^{-3} from both observations and model and correlation between the modelled and observed daily concentrations

EMEP Stations	***Period***	***Coincidences***	***Observation***	***Model***	***Correlation***
DK03	*2001*	*296*	*0.96*	*1.50*	*0.67*
DK05	*2001*	*341*	*1.44*	*1.64*	*0.29*
DK08	*2001*	*346*	*1.40*	*2.36*	*0.66*
NO01	*2001*	*357*	*0.33*	*1.08*	*0.57*
NO08	*2001*	*360*	*0.32*	*1.57*	*0.65*
NO15	*2001*	*365*	*0.26*	*1.25*	*0.56*
NO39	*2001*	*353*	*0.15*	*1.16*	*0.51*
NO41	*2001*	*350*	*0.09*	*0.37*	*0.21*
Extra stations	***Period of observation***	***Coincidences***	***Observation***	***Model (2001)***	***Reference for observations***
Cabauw (NL)	*Winter 2000*	*~140*	*0.81*	*1.00 (whole year)* *0.71 (Jan-March)*	*Weijers et al. 2002*
Speuld (NL)	*1995*	*~340*	*0.79*	*1.11*	*Erisman et al. 1996*
Duisburg (D)	*2002-2003*	*~360*	*0.66*	*0.50*	*Quass et al. 2004*
Augustendorf-Linden	*2001-2003*		*0.4-0.6*	*0.7*	*Daemmgen et al, 2006*

10.5.3 Discussion

The largest uncertainty in the modelling of sea salt is associated with the calculation of the source strength. The different emission parameterisations yield different emission fluxes up to a factor of three for the widely used ones, though larger differences exist when all flux parameterisations are taken into account. Hence, an uncertainty analysis should encompass the most widely used ones in combination with the dependency on the meteorological input.

Our results are comparable to the results from a comparison study by FOLTESCU ET AL. (2005) between the MATCH model and EMEP observations. The overestimation of the peak concentrations may be related to the relatively large uncertainty associated with the wind speed dependent emission strength of sea salt particles.

Further, our model assumes a coarse mode size distribution which may not be representative for the size distribution directly after emission, which may yield an underestimation of the deposition (of the largest particles) in the source regions. The orography around the Norwegian stations may largely explain the less favourable comparison between modelled and measured concentrations than in Denmark.

The results shown here only comprise a few stations. To allow a better evaluation of the model, a more extensive validation is needed. However, data for Germany and other European countries are sparse. We expect that an extensive literature study should be performed to compile a reasonably large data set to compare the model results to.

10.5.4 Other base cations

During the project we have also made a considerable effort to incorporate soil derived base cations into the modelling system. During the project, however, the direction of the work was altered to investigate, among other things, the underestimation of the heavy metals in the modelling system. As a consequence, the base cation development was not continued. Estimates for anthropogenic emissions and an emission module for wind-generated emissions from bare soil have been implemented and are ready to contribute to a future exercise.

10.6 Final remarks

This report presents an overview of the modelling activities to generate maps of dry deposition fluxes over Germany. The concentration data obtained from modelling activities with LOTOS-EUROS are input to the more detailed dry deposition modelling at ECN. We have delivered the bulk concentrations for the surface layer to the IDEM modelling on a three hour time resolution.

11 Agricultural emissions of acidifying and eutrophying species

Ulrich Dämmgen
Federal Agricultural Research Centre, Institute of Agroecology (FAL-AOE), Bundesallee 50, D-38116 Braunschweig
Bundesforschungsanstalt für Landwirtschaft, Institut für Agrarökologie (FAL-AOE), Bundesallee 50, 38116 Braunschweig

11.1 German national agricultural emission inventories

National emission inventories have to be provided both for the Convention on Long Range Transport of Air Pollutants (LRTAP) within the United Nations Economic Committee for Europe's activities concerning the reduction of atmospheric pollution, and for the United Nations Framework Convention on Climate Change (UNFCCC). The two conventions deal with different species (LRTAP: SO_2, CO, NO and NO_2, NH_3, CH_4, NMVOCs, POPs, heavy metals, particulate matter; UNFCCC: CO_2, CH_4, N_2O, F-gases). However, these may originate from the same sources. Hence the assessment of such emissions should make use of a methodological approach which integrates the two guidance documents provided by the Conventions (EMEP/CORINAIR, 2002; IPCC, 1996, 2000) in particular in those cases where emissions of two or more species are depending on one another. In particular, this has to be considered for the emissions of nitrogen species in animal husbandry. In line with other nations in Northwest Europe, Germany has developed and applied a procedure which considers as much as possible the flows of energy, carbon and nitrogen through agricultural production systems. The approach is described in detail in DÄMMGEN ET AL. (2007). Important facts concerning the resolution of the emission categories, the choice of methods, the resolution in space, and the accuracy are given below.

11.1.1 Source categories, activity data and emission assessment

A source category or subcategory comprises sources or sinks which exhibit the same structure and properties, such as feeding, performance or housing. The emissions from each category or subcategory are described using the respective activity data (animal numbers, fertiliser applied, cropped area, etc.) and an emission factor or function.

If a mass flow description of the emitting process cannot be provided, emission factors are used. If they are taken from the guidance documents (default emission factors), the procedure is called a simpler (EMEP/CORINAIR) or Tier 1 (IPCC) method. If the respective national emission factors are available or if emission factors can be deduced from national data (e.g. feed intake) the method is considered improved. Whenever emissions can be treated using the energy or mass flow approach, the method is called detailed (EMEP/CORINAIR) or Tier 2 (IPCC), respectively[1].

Detailed methods may differentiate between regions and normally require regional data for performance, feed, the frequency distribution of housing types, storage facilities etc. In such cases, the effective emission factor (implied emission factor IEF: IEF = emission/activity) is likely to vary with time.

Most emitting processes are temperature dependent, whereas some vary with precipitation, others with wind speed. Emission calculations reflect this, whenever national data are used which were obtained under the climatic conditions in Germany or a neighbouring country. For some emission factors, temperature zones have to be taken into account. However, the factors derived reflect the mean climate and ignore weather peculiarities.

At present, the resolution in time is always 1 a. The resolution in space is depending on the availability of activity data. Whenever a comprehensive census was performed, the resolution is based on rural districts for all activities except goats and buffalo, pesticide use and liming. Figures A and B illustrate the importance of spatial resolution of IEFs and the development of IEFs with time, for dairy cows and NH_3 emissions.

Table 11.1 gives an overview on the categories, the method used to derive emissions and the respective resolution in space.

[1] Note: The definition of Tiers both within EMEP/CORINAIR and IPCC is ambiguous at present (2006).

Table 11.1: Emission categories, methods applied and resolution in space

Source category	CH_4	CO_2	NM VOC	NH_3	N_2O	NO	N_2	PM
Emissions from systems with fertiliser								
Application of mineral fertiliser		D, RD	S, RD	D, RD	S, RD	S, RD		
Application of animal manures					S, RD	S, RD	S, RD	
Application of sewage sludge					S, RD			
Managed histosols					S, RD			
Methane deposition	I, RD							
NMVOC emissions from crops			S, RD					
Emission of particulate matter (PM10) from arable land								S, RD
Emissionen from system without fertiliser								
Biological N fixiation: legums				I, RD	I, RD	I, RD		
Animal grazing				S, RD	S, RD	E, RD		
Crop residues					I, RD	I, RD		
Indirect emissions resulting from deposition of reactive N originating in agriculture					S, RD			
Indirect emissions resulting from leaching and run-off of nitrogen in agricultural production systems					S, FS			
Emissions from enteric fermentation								
Dairy cattle	D, RD							
Other cattle (calves, heifers, male beef cattle, suckler cows, mature males)	D, RD							
Pigs (sows, weaners, fattening pigs, boars)	D, RD							
Sheep	S, RD							
Goats	S, FR							
Horses	S, RD							
Buffalo	S, FS							
Emissions from manure management (including emissions from houses, storage and application of manures)								
Dairy cattle	D, RD		S, RD	D, RD				S, RD
Other cattle (calves, heifers, male beef cattle, suckler cows, mature males)	D, RD		S, RD	D, RD				S, RD
Pigs (sows, weaners, fattening pigs, boars)	D, RD		S, RD	D, RD				S, RD
Sheep	S, RD		S, RD	D, RD				
Goats	S, FR			I, FR				
Horses	S, RD			I, RD				
Buffalo	S, FS			I, FS				
Leaying hens	D, RD		S, RD	D, RD				S, RD
Broilers	S, RD		S, RD	I, RD				S, RD
Pullets	D, RD		S, RD	I, RD				
Geese	S, RD		S, RD	I, RD				
Ducks	S, RD		S, RD	I, RD				
Turkeys	S, RD		S, RD	I, RD				
Fur animals				S, FS	S, FS	S, FS		
Animal manures imported				S, FR				
Pesticides and liming								
Pesticides			S, FR					
Limestone		D, FS						

Methods applied: S: simpler, I. improved; D: detailed.
Resolution in space: RD: rural district; FS: Federal State; FR: Federal Republic

In principle, detailed methodologies result in different emission factors for each category in each year and each

district, if the input data have the adequate resolution. Figure 11.1 shows a comparatively high resolution for the overall (implied) emission factor for dairy cows and 2003. As the frequency distribution of grazing, housing, storage and application can only be estimated for Federal States, the boundaries of these regions can be identified.

Figure 11.2 illustrates the influence of the years where a general census was made. The 1994 step in Mecklenburg-Western Pomerania and the 2003 step in Bavaria are clearly identified, indicating that the distributions are kept constant for the period till the next general census.

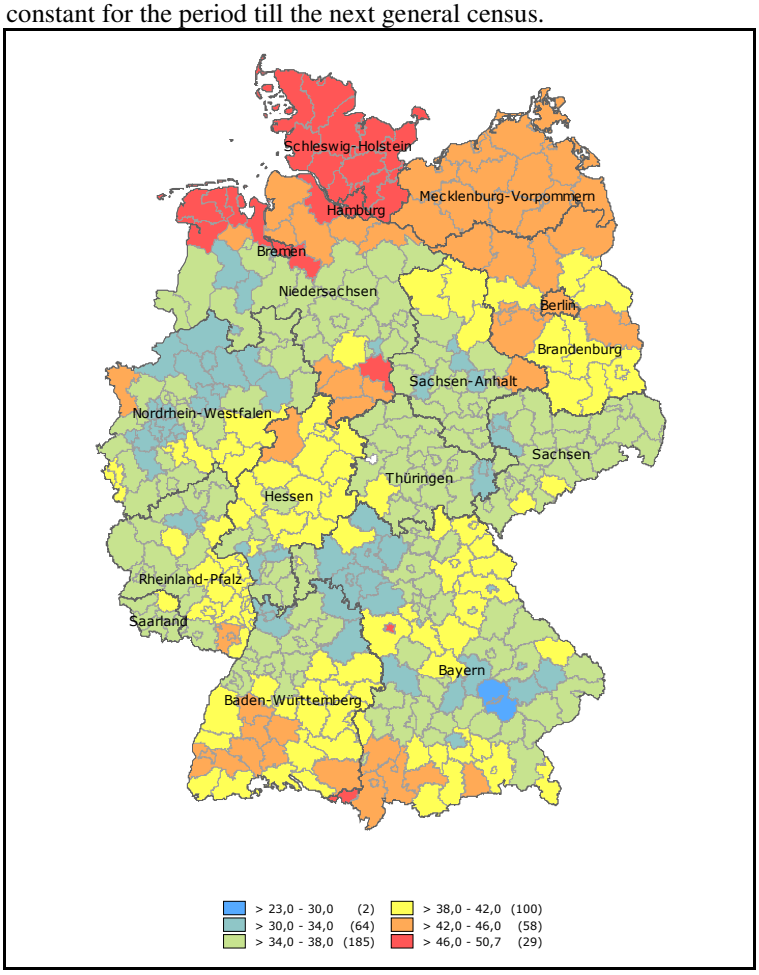

Figure 11.1: Resolution in space of the NH_3 implied emission factors for dairy cows, 2003

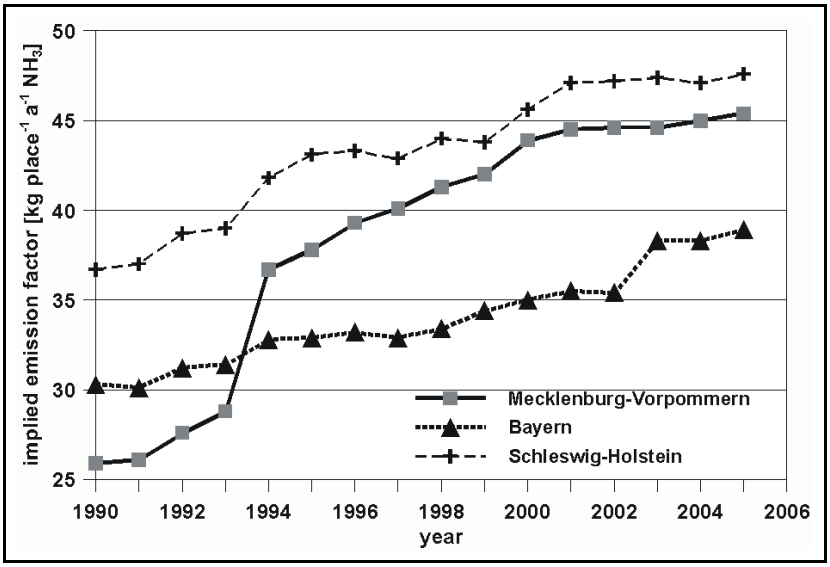

Figure 11.2: Time series of overall (implied) NH_3 emission factors for dairy cows in Mecklenburg-Western Pomerania, Bavaria and Schleswig-Holstein

11.1.2 Origin of data and data flow

The emission calculation programme GAS-EM makes use of officially available animal census and land use data, which are provided by the German Statistical offices. In some cases, the data provided do not match the source categories and have to be transformed. Occasionally, data gaps have to be closed. The animal numbers are reported every forth year for each rural district. However, the number given is the number of animals owned by a farmer in the respective rural district. The animals themselves may be housed in a different rural district. However, this fact is considered negligible. The same applies to the application of animal manures. As any other information is missing, it is assumed that the total amount of animal manures is applied in the rural district for which the animals are reported.

Data describing the frequency distributions housing, manure storage and manure application are modelled in RAUMIS, using a combination of official data, specially arranged surveys and expert knowledge.

Information is also gathered from publications of the various German experimental farms, research institutes, breeders' and producers' societies, feed producers, and publications in scientific and agronomic journals. Unpublished theses and personal communications are used. Each data set used is referenced in DÄMMGEN ET AL. (2007).

A detailed overview of the data flow of the German agricultural emission reporting from data sources over model application and its products to data bases, results and services is given in Figure 11.3.

Abbreviations and acronyms in Figure 11.3: StatBA: Statistisches Bundesamt (Federal Statistical Office); StatLÄ: Statistische Landesämter (Statistical Officies of the German Federal States); DWD: Deutscher Wetterdienst (German Weather Service); RAUMIS: Regionalisiertes Agrar- und UmweltInformationsSystem für Deutschland (regionalized information system for agriculture and environment in Germany); GAS-EM: Gaseous Emissions calculations tool; FAL: Bundesforschungsanstalt für Landwirtschaft (Federal Agricultural Research Centre); UBA: Umweltbundesamt (Federal Environment Agency); ZSE: Zentrales System Emissionen (Central Emissions System); BMELV: Bundesministerium für Ernährung, Landwirtschaft und Verbraucherschutz (Federal Ministry for Nutrition, Agriculture and Consumer Protection); IIASA: Internationales Institut für Angewandte Systemanalyse (International Institute of Applied Systems Analysis).

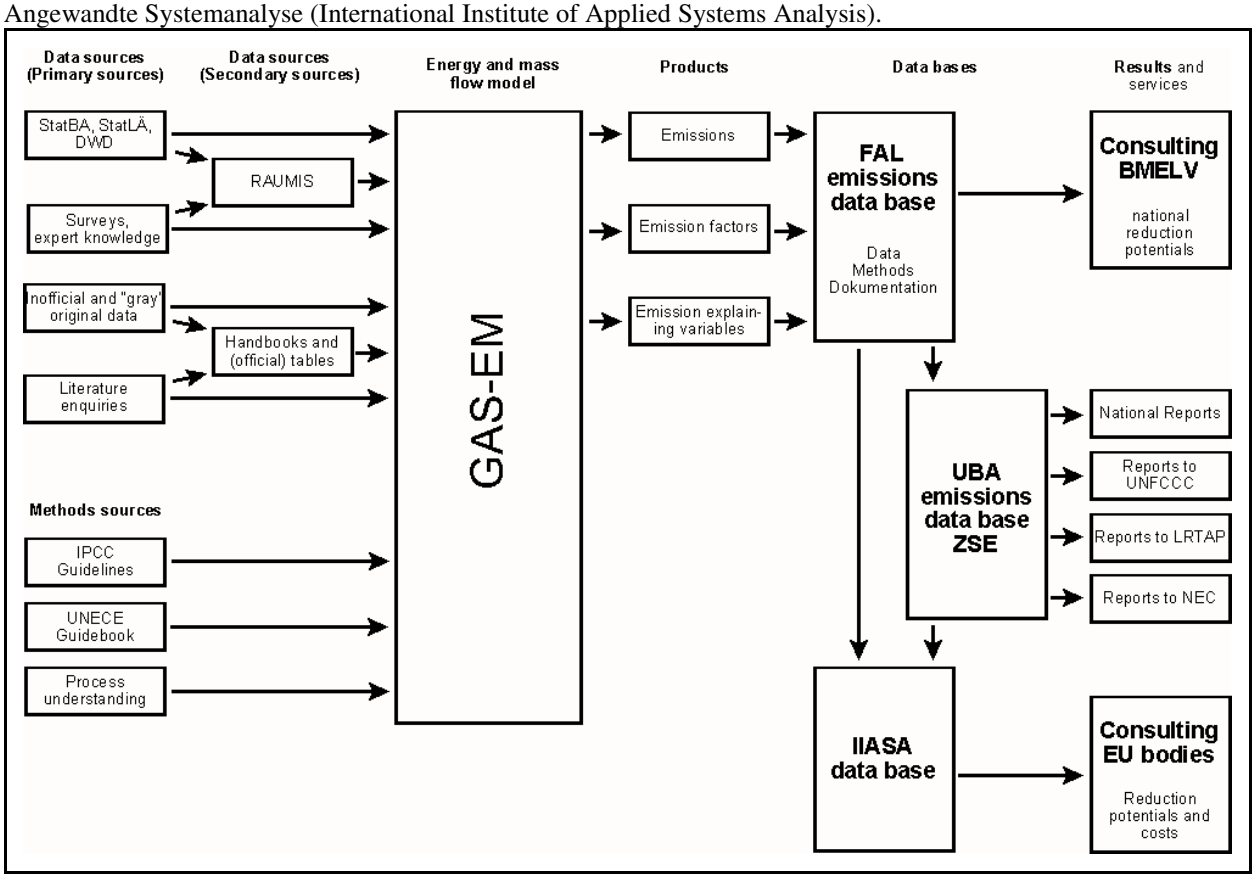

Figure 11.3: Data flow in German agricultural emission reporting (Dämmgen et al., 2006).

11.1.3 Updates

The agricultural emission inventory is calculated every year using the latest data sets available. In the past, the agricultural census provided animal numbers for rural districts for every second year (1990, 1992, 1994, 1996, 1999, 2001, 2003, and 2005). Complete land use surveys are available on the district level for 1992, 1996, 1999 and 2003. These are not only used to calculate emissions directly, but – in conjunction with inquiries – are used to establish the frequency distributions of important emission explaining variables.

The Atmospheric Emission Inventory Guidebook is updated whenever the need is felt and the state of knowledge allows for it. Care is taken that it is in line with the proposals made in the UN ECE Framework Advisory Code of Good Agricultural Practice for Reducing Ammonia Emissions.

A programme jointly financed by the German Federal Ministries of Nutrition, Agriculture and Consumer Protection and the Environment and Nuclear Safety commences in early 2007 to improve the data base for agricultural emission inventories with emphasis on NH_3.

11.1.4 Transparency

According to the rules communicated by the conventions, Excel sheets have to be used to calculate and report emissions. In combination with the additional information provided in DÄMMGEN ET AL. (2007), each calculation step can be traced. As the amount of data is huge and the calculation sheets are rather complex, transparency is guaranteed in principle only. In practice, the system is too complex to be analysed and checked in detail by outsiders, unless they devote sufficient time and energy.

11.1.5 Completeness

The German agricultural emission inventory is considered complete by the international bodies reviewing both the greenhouse gases and the air pollutants. However, it does not cover biogas production from slurry nor from energy crops due to lack of information. At present, the number of installations may be known, but the amount of biomass converted is yet unknown, and so is the efficiency (or leakage) of the systems in operation.

11.1.6 Consistency

Both LRTAP and UNFCCC reporting require the provision of time series. In order to identify emission reductions, these series have to be achieved using the same methodology for the whole time span between 1990 and the year of reporting. The German agricultural inventory is consistent in principle. However, emissions from fur animals are reported for 2000 only, emissions from buffalo have been reported since 2000. Both categories are negligible with respect to the overall emissions.

Whenever a method is updated, it is applied to the whole time series and recalculations are made to guarantee consistency.

11.1.7 Comparability

In order to avoid distortions of markets, emission inventories have to be constructed in a way that makes them comparable to other European countries. This can be achieved (a) by strictly following the guidance documents and (b) by international comparisons of methods and data. The German agricultural emission inventory was reviewed twice so far without giving reason for complaints. In Northwest Europe, the EAGER group [2] cooperates to harmonize calculation methods and to check the data achieved in national inventories. The emission inventory compares German implied emission factors with those of the neighbouring countries wherever possible.

11.1.8 Accuracy

The reporting procedures require a statement on the uncertainty of any data used in the calculation procedure. Uncertainties have to be reported for the activity data as well as for the emission factors.

In Germany, the assessment of animal numbers is based on a survey which excludes minor farms and any animals that are not kept on farm enterprises. Thus, animal numbers are underestimated in principle. However, the bias is thought to be smaller than 5 % for cattle, pigs and poultry. The numbers of horses in the official is likely to underestimate the true number by 100 %.

[2] EAGER – European Agricultural Gaseous Emissions Inventory Researchers Network (EAGER, 2005)

Due to lack of better data, the uncertainties for emission factors referred to in the guidance documents are taken to be valid for Germany. Even if a largely mechanistic model like the IPCC model for enteric fermentation is used, modelled emission deviate from measured emissions and from those of other largely mechanistic models (see KEBREAB ET AL., 2006). Most emission factors and partial emission factors used are national means. They are mainly considered to have stochastic uncertainties in the order of magnitude of 20 %. However, it should be noted that emission factors are based on measurements in environments which are "cleaner" than average conditions on producing farms. At least for NH_3 emission factors, it is likely that emission factors are biased and underestimate emissions. The order of magnitude is unknown; is it thought to be small.

Emission factors normally reflect the mean situation in a nation with respect to major emission explaining variables as well as climate. Any spatial disaggregation – however plausible – is likely to increase the uncertainty on a regional scale. This is true for emissions of N_2O, NO and N_2 in particular. As GAS-EM includes emissions of these species in the mass flow, they also influence NH_3 emissions. However, this is a source of uncertainty in straw based systems only. On average, similar emission factors will be observed in Germany.

Despite its uncertainties, the German agricultural emission inventory reflects the state of the art.

11.1.9 Results

Agriculture is the major source of ammonia (Figure 11.4); all other sources (including the chemical industry) contribute less than the order of magnitude assumed for the uncertainties of emissions from cattle.

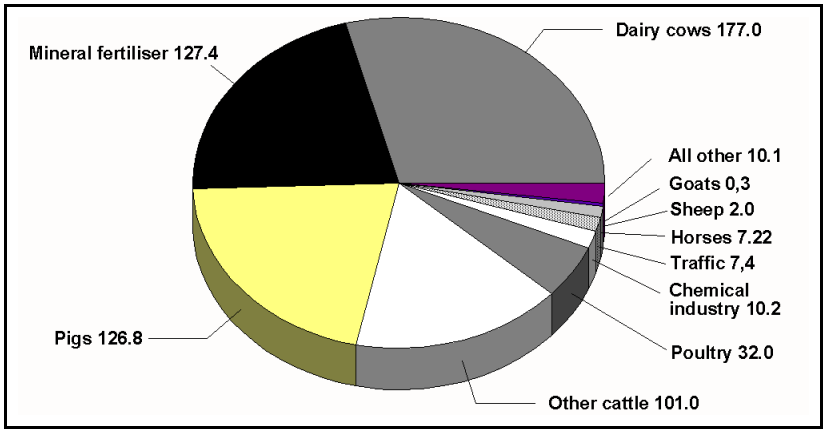

Figure 11.4: Contribution of the various sources of NH_3 to the national total emission [in Gg a^{-1}=kt a^{-1}]

Figures 11.5 and 11.6 illustrate the development of national NH_3 emissions in Germany. Emissions are dominated by cattle and pig husbandry as well as mineral fertiliser application. All other sources are minor on the national scale.

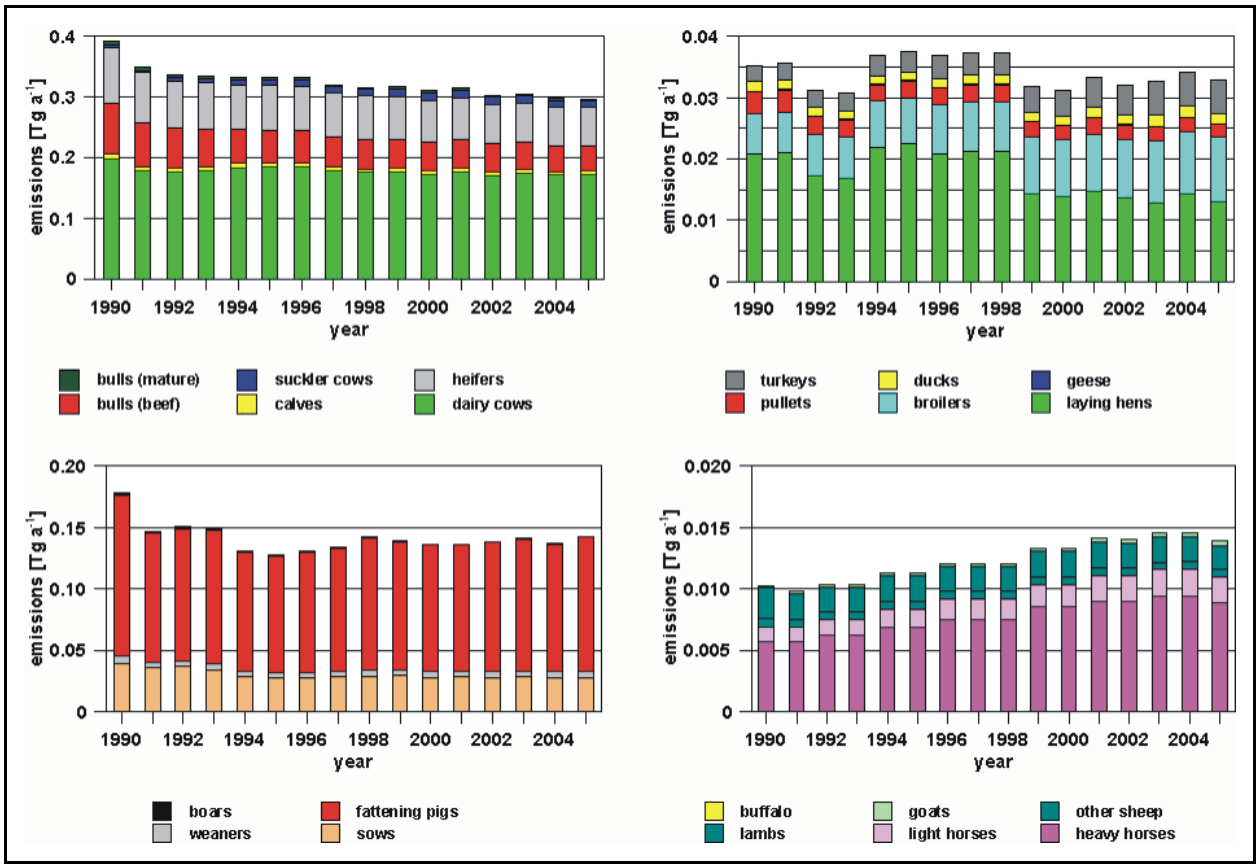

Figure 111.5: Time series of NH_3 emissions from German animal husbandry. Note the different scales!

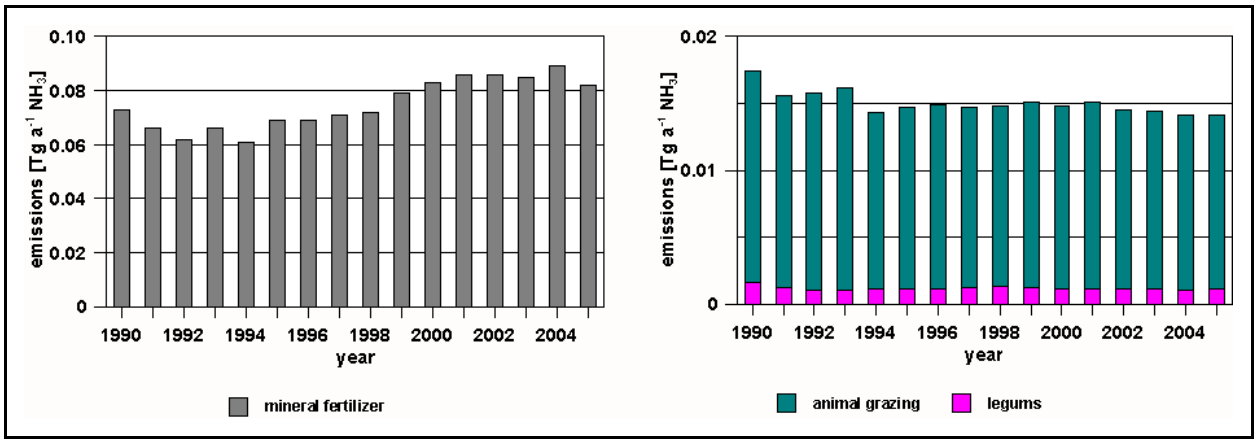

Figure 11.6: Time series of NH_3 emissions from plants and soils (note the different scales!)

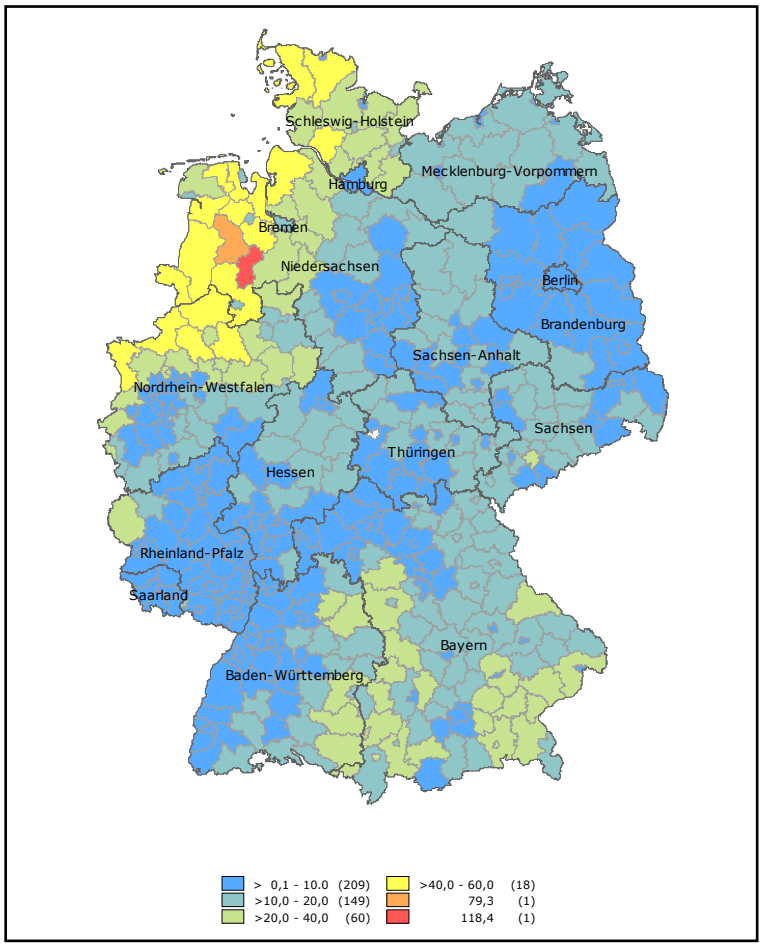

Figure 11.7: Overall NH_3 emission densities for 2003 as calculated with GAS-EM. Emission densities in kg ha^{-1} a^{-1} NH_3

As Fig. 11.7 indicates, NH_3 emissions are a regional rather than a national problem. Whereas emissions from cattle dominate the situation almost everywhere, emissions from pigs and poultry have the biggest share in the Weser-Ems region in Northwest Germany.

12 References

Anshelm F, Gauger Th, Schuster H, Droste-Franke B, Friedrich R, Reichert Th (2003) Kartierung von Materialschäden in Deutschland. Forschungsvorhaben im Auftrag des BMU/UBA, FE-Nr. 201 43 205. Institut für Navigation der Universität Stuttgart

Adelman ZE (1999) A re-evaluation of the Carbon Bond-IV photochemical mechanism. M.Sc. thesis, Department of Environmental Sciences and Engineering, School of Public Health, University of North Carolina, USA

Asman WAH (1992) Ammonia emissions in Europe: Updated emission and emission variations. RIVM, Bilthoven, The Netherlands. Report no. 228471008

Asman, WAH (2001) Modelling the atmospheric transport and deposition of ammonia and ammonium: an overview with special reference to Denmark, Atmos. Environ., 35, 1969-1983

Asman WAH (1998) Factors influencing local dry deposition of gases with special reference to ammonia, Atmos. Environ., 32, 415-421

Asman WAH and Janssen AJ (1987) A long-range transport model for ammonia and ammonium for Europe, Atmos. Environ., 21, 2099-2119

Asman WAH and van Jaarsveld JA (1992) A variable-resolution transport model applied for NH_X for Europe. Atmospheric Environment 26A: 445-464

Baart AC and Diederen HSMA (1991) Calculation of the atmospheric deposition of 29 contaminants to the Rhine catchment area. TNO, Delft, The Netherlands. TNO Report R 91/219

Baldocchi DD (1988) A multi-layer model for estimating sulfur dioxide deposition to a deciduous oak forest canopy. Atmospheric Environment 22: 869-884

Baldocchi Baldocchi DD (1993) Deposition of gaseous sulfur compounds to vegetation. In Sulfur Nutrition and Assimilation and Higher Plants (eds. Kok LJ et al.), pp. 271-293, SGP Academic, The Hague, The Netherlands

Baldocchi DD, Hicks BB and Camara P (1987) A canopy stomatal resistance model for gaseous deposition to vegetated surfaces. Atmospheric Environment 21: 91-101

Baldocchi DD, Hicks BB, Meyers TP (1988) Measuring biosphere-atmosphere exchanges of biologically related gases with micrometeorological methods. Ecology 69, 1331-1340

Beljaars ACM and Holtslag AAM (1990) Description of a software library for the calculation of surface fluxes. Environmental Software, 5: 60-68

Benkovitz C.M, Berkowitz CM, Easter RC, Nemesure S, Wagner R and Schwartz SE (1994) Sulfate over the North Atlantic and adjacent continental regions: evaluation for October and November 1986 using a three-dimensional model driven by observation-derived meteorology. Journal of Geophysical Research 99: 20725-20756

BGR (1998) Digitales Höhenmodell. Bundesanstalt für Geologie und Rohstoffe, Hannover.

Bleeker A, Draaijers GPJ, Klap JM and van Jaarsveld JA (2000) Deposition of acidifying components and base cations in Germany in the period 1987-1995. Bilthoven, RIVM, report no. 722108027. 124 p.

BMU/UBA 370764200 Assessment, Prognosis, and Rewiew of Deposition Loads and their Effects in Gemany / Erfassung, Prognose und Bewertung von Stoffeinträgen und deren Wirkungen in Deutschland. Research project carried out on behalf of BMU/UBA / Forschungsvorhaben im Auftrag des BMU/UBA FE-Nr. 370764200. [http://www.mapesi.de/]

Bogaard A, and Duyzer J (1997) Een vergelijking tussen resultaten van metingen en berekeningen van de concentratie van ammoniak in de buienlucht op een schaal kleiner dan5 kilometer, TNO-report, TNO-MEP-R97/423, Apeldoorn, The Netherlands

Branding A (1997) Die Bedeutung der atmosphärischen Deposition für die Forst- und Agrarökosysteme der Bornhöveder Seenkette. Dissertation im Geographischen Insitut d. Univ. Kiel. EcoSys. Suppl. Bd. 14, Vorabdruck. 117 p

Brook JR, Zhang L, Di-Giovanni F and Padro J (1999) Description and evaluation of a model of deposition velocities for routine estimates of air pollutant dry deposition over North America. Part I: model development. Atmospheric Environment 33: 5037-5051

Builtjes PJH (1992) The LOTOS-Long Term Ozone Simulation-project Summary Rep. TNO Rep. TNO-MW-R92/240, Apeldoorn, The Netherlands

Builtjes PJH, van Loon M, Schaap M, Teeuwisse S, Visschedijk AJH, Bloos JP (2003) Poject on the modelling and verification of ozone reduction strategies: contribution of TNO-MEP. O-report, MEP-R2003/166, Apeldoorn, The Netherlands

CCE (2001) Modelling and Mapping of Critical Thresholds in Europe. Status Report 2001. Edited by: Posch M, de Smet PAM, Hettelingh JP, Downing RJ. Coordination Center for Effects (CCE). National Institute of Public Health and the Environment, Bilthoven, The Netherlands. RIVM Report No. 259101010. ISBN No. 96-9690-092-7 [http://www.rivm.nl/cce/Images/SR01_tcm42-16441.pdf]

CCE (2003) Status Report 2003: Germany. National Institute of Public Health and the Environment, Bilthoven, The Netherlands. RIVM Report 259101013. p. 81-85. [http://www.rivm.nl/cce/Images/SR03-DE_tcm42-16628.pdf]

CCE (2005) Critical Loads of Cadmium, Lead and Mercury in Europe Critical Loads of Cadmium, Lead and Mercury in Europe, Collaborative Report by CCE and EMEP MSC-E, RIVM Report No. 259101015, ISBN No. 90-6960-119-2, Bilthoven, Netherlands. [http://www.rivm.nl/cce/] [http://www.rivm.nl/cce/Images/1382_tcm42-43234.pdf]

Chang JC, Brost RA, Isaksen ISA, Madronich P, Middleton P, Stockwell WR and Walcek CJ (1987) A three-dimensional Eulerian acid deposition model: physical concepts and formulation. Journal of Geophysical Research 92, 14681-14700.

Clarke JF, Edgerton ES and Martin BE (1997) Dry deposition calculations for the clean air status and trends network. Atmospheric Environment 21: 3667-3678

Dämmgen et al. (n.p) Results of deposition measurements at FAL-AOE in Braunschweig 2001-2003. Messfeld Agrarökologie, Dämmgen, unveröffentlicht / not published

Dämmgen U (2006) Atmospheric nitrogen dynamics in Hesse, Germany: Creating the data base – 1. Bulk deposition of acidifying and eutrophying species. Landbauforschung Völkenrode 3/4 2006 (56). 117-138

Dämmgen U, Döhler H, Lüttich M, Eurich-Menden B, Osterburg B, Haenel H-D, Döring U, Strogies M (2006) Die Analyse von Stickstoff-Flüssen in der Landwirtschaft zum Zweck der Politikberatung – Eine Übersicht über Datenflüsse und Datenmanagement. Teil 1. Emissionen. Landbauforschung Völkenrode Special Issue 291, 5-10

Dämmgen U, Erisman JW, Cape JN, Grünhage L, Fowler D (2005) Practical considerations for addressing uncertainties in monitoring bulk deposition. Environmental Pollution 134. 535-548

Dämmgen U, Küsters A (1992) Vergleich von Depositionssammlern der Typen ‚Osnabrück' und ‚Rrotenkamp'. Schlussbericht für das Niedersächsische Landesamt für Wasser und Abfall, Hildesheim. Technische Universität Braunschweig, Institut für Geographie und Geologie.37 S.

Dämmgen U, Lüttich M, Haenel H-D, Döhler H, Eurich-Menden B, Osterburg B (2007) Calculations of Emissions from German Agriculture - National Emission Inventory Report (NIR) 2007 for 2005. In preparation

Dämmgen U (ed.) (1996) Untersuchungen zum chemischen Klima in Südostniedersachsen. Arbeiten des Teilprojektes A10 Stoffflüsse in der bodennahen Atmosphäre des Sonderforschungsbereichs 179 Wasser- und Stoffdynamik in Agrar-Ökosystemen. Landbauforschung Völkenrode, Sonderheft 170. 333 S.

Dämmgen U. (ed.) (2000). Versauernde und eutrophierende Luftverschmutzung in Nordost-Brandenburg. Landbauforschung Völkenrode, Sonderheft 213. 152 p

Davidson CI and Wu YL (1990) Dry deposition of particles and vapors. In Acidic Precipitation (eds. S.E. Lindberg, A.L. Page and S.A. Norton), vol. 3. Springer-Verlag, New York

de Boer M, de Vente J, Mücher CA, Nijenhuis W and Thunnissen HAM (2000) Land cover monitoring. An approach towards pan European land cover classification and change detection. NRSP-2, Proj. 4.2/DE-03

de Leeuw FAAM, van Rheineck Leyssius HJ, van den Hout KD, Diederen HSMA, Berens M, Asman WAH (1988) A lagrangian long-range transport model with non-linear atmospheric chemistry: MPA-model. TNO rapport R87/344, RIVM Report 228471004, National Institute of Public Health and the Environment, Bilthoven, The Netherlands. 72 p (in Dutch)

Denier van der Gon HAC, van het Bolscher M, Visschedijk AJH, Zandveld PYJ (2005) Study to the effectiveness of the UNECE Heavy Metals Protocol and costs of possible additional measures Phase I: Estimation of emission reduction resulting from the implementation of the HM Protocol, TNO report B&O-A R 2005/193. Apeldoorn, The Netherlands

Dentener FJ and Crutzen PJ (1993) Reaction of N_2O_5 on tropospheric aerosols: Impact on the global distributions of NO_X, O_3, and OH. J. Geophys. Res., 7149-7163

Dentener FJ and Crutzen PJ (1994) A three-dimensional model of the global ammonia cycle, J. Atmos. Chem., 19, 331-369

de Vries W, Reinds GJ, van der Salm C, Draaiers GPJ, Bleeker A, Erisman JW, Auée J, Gundersen P, Kristensen HL, van Dobben H, de Zwart D, Derome J, Voogd JCM, Vel EM (2001) Intensive Monitoring of Forest Ecosystems in Europe. Technical Report 2001. UN/ECE and EC, Geneva and Brussels, Forest Intensive Monitoring Coordinating Institute, 177 pp

Draaijers GPJ, Erisman JW (1995) A canopy budget model to estimate atmospheric deposition from throughfall measurements. Water Air and Soil Pollution 85: 122-134

Draaijers GPJ, van Ek R, Beuten W (1994) Atmospheric deposition in complex forest landscapes. Boundary-Layer Meteorology 69: 343-366

Draaijers GPJ, Erisman JW, Spranger T, Vel E (1998). Quality and uncertainty aspects of forest deposition estimation using throughfall, stemflow and precipitation measurements. TNO-report TNO-MEP–R 98/093, Apeldoorn, The Netherlands, 73 p

Draaijers GPJ, van Leeuwen EP, de Jong PGH, Erisman JW (1996a) Deposition of base cations in Europe and its role in acid neutralization and forest nutrition. RIVM, Bilthoven, The Netherlands. Report no. 722108017

Draaijers GPJ, Erisman JW, Spranger T, Wyers GP (1996b) The application of throughfall measurements for atmospheric deposition monitoring. Athmospheric Environment 30(19): 3349-3361

Duyzer JH, Bouman AMM, van Aalst RM, Diederen HSMA (1987) Assessment of dry deposition of NH_3 and NH_4^+ over natural terrains. In: Proceedings of the EURASAP Symposium on Ammonia and Acidification. Bilthoven, The Netherlands, 13-15 April 1987

Duyzer JH, Verhagen HLM, Westrate JH, Bosveld FC, Vermetten AWM (1992) The dry deposition of ammonia onto a Douglas fir forest in the Netherlands. Environmental Pollution 75: 3-13

EAGER (2005) European Agricultural Gaseous Emissions Inventory Researchers Network (EAGER). [http://www.eager.ch/index.htm]

EMEP/CORINAIR (2002) Joint EMEP/CORINAIR Atmospheric Emission Inventory Guidebook. 3rd ed., EEA, Copenhagen. [http://reports.eea.eu.int/EMEPCORINAIR3/en/page019.html]

Erisman JW (1992) Atmospheric deposition of acidifying compounds in The Netherlands. Ph.D. thesis, University of Utrecht, The Netherlands

Erisman JW and Baldocchi DD (1994). Modelling dry deposition of SO_2. Tellus, 46B: 159-171

Erisman JW and Draaijers GPJ (1995) Atmospheric deposition in relation to acidification and eutrophication. Studies in Environmental Science, 63, Elsevier, Amsterdam

Erisman JW and Wyers GP (1993) On the interaction between deposition of SO_2 and NH_3. Atmospheric Environment, 27A: 1937-1949

Erisman JW, van Elzakker BG, Mennen M (1990) Dry deposition of SO_2 over grassland and heather vegetation in the Netherlands. RIVM, Bilthoven, The Netherlands. Report no. 723001004

Erisman JW, Versluis AH, Verplanke TAJW, de Haan D, Anink D, van Elzakker BG, Mennen MG, van Aalst RM (1993a) Monitoring dry deposition of SO2 in the Netherlands. Atmospheric Environment, 27A: 1153-1161

Erisman JW, Mennen M, Hogenkamp J, Kemkers E, Goedhart D, van Pul A, Boermans J. (1993b) Dry deposition over the Speulder forest. Proceedings of the CEC/BIATEX workshop, Aveiro, Portugal, 4-7 May 1993

Erisman JW, Potma C, Draaijers GPJ, van Leeuwen EP, van Pul WAJ (1994a) A generalised description of the deposition of acidifying pollutants on a small scale in Europe. Proceedings EUROTRAC symposium on Transport and transformation of pollutants in the Troposphere, Garmisch Partenkirchen, 11-15 April 1994

Erisman JW, van Pul A, Wyers P (1994b) Parameterization of surface resistance for the quantification of atmospheric deposition of acidifying pollutants and ozone. Atmospheric Environment 28(16), 2595-2607

Erisman JW, Potma C, Draaijers GPJ, Duyzer JH, Hofschreuder P, van Leeuwen N, Römer FG, Ruijgrok W, Wyers GP (1994c). Contribution of aerosol deposition to atmospheric deposition and soil loads onto forests. Final Report of the Aerosol Project executed within the third phase of the Dutch Priority Programme on acidification. RIVM Report no. 722108005. National Institute of Public Health and the Environment (RIVM), Bilthoven, The Netherlands

Erisman JW, Mennen MG, Fowler D, Flechard CR, Spindler G, Grüner A, Duyzer JH, Ruigrok W, Wyers GP (1996). Towards development of a deposition monitoring network for air pollution of Europe. RIVM Report no. 722108015, National Institute of Public Health and the Environment, Bilthoven, The Netherlands, April 1996

Erisman JW, Mennen MG, Fowler D, Flechard CR, Spindler G, Grüner A, Duyzer JH, Ruigrok W, Wyers GP (1997). Deposition monitoring in Europe. Environ. Monit. and Assessment 53: 279-295

ESPREME: Estimation of willingness-to-pay to reduce risks of exposure to heavy metals and cost-benefit analysis for reducing heavy metals occurrence in Europe [http://espreme.ier.uni-stuttgart.de]

Eugster W and Hesterberg R. (1996) Transfer resistances of NO2 determined from eddy correlation flux measurements over a litter meadow at a rural site on the swiss plateau. Atmospheric Environment 30(8): 1247-1254

Farquhar GD, Firth PM, Wetselaar R, Wier B (1980) On the gaseous exchange of ammonia between leaves and the environment: determination of the ammonia compensation point. Plant Physiol. 66: 710-714.

Foltescu VL, Pryor SC, Bennet C (2005) Sea salt generation, dispersion and removal on the regional scale. Atmospheric Environment, Vol. 39, pp.2123-2133

Fowler D (1978) Dry deposition of SO2 on agricultural crops. Atmospheric Environment, 12: 369-373

Fowler D (1985) Dry deposition of SO2 onto plant canopies. In Sulfur dioxide and vegetation (Eds. Winner, W.E., Mooney, H.A. and Goldstein, R.A.). Stanford University Press, California. pp. 75-95

Fowler D and Unsworth MH (1979) Turbulent transfer of sulfur dioxide to wheat crop. Quarterly Journal of the Royal Meteorological Society 105: 767-784

Fowler D, Cape JN, Unsworth MH (1989) Deposition of atmospheric pollutants on forests. Phil. Trans. R. Soc. Lond. B324: 247-265

Fowler D, Duyzer JH, Baldocchi DD (1991) Inputs of trace gases, particles and cloud droplets to terrestrial surfaces. Proc. R. Soc. Edinburgh 97B: 35-59

Franken G, Puhlmann M, Duijnisveld WHM, Böttcher J, Strebel O (1997) Auswirkungen saurer atmosphärischer Depositionen bei Nadelwald auf Stoffanlieferung an das Grundwasser und Stoffumsetzungen in einem Aquifer aus basenarmen Sanden (Fallstudie Modellgebiet Fuhrberger Feld). Wasserforschung. Forschungsbericht 102 02 629. Im Auftrag des Umweltbundesamtes. 272 S.

Ganzeveld L and Lelieveld J (1995) Dry deposition parameterization in a chemistry general circulation model and its influence on the distribution of reactive trace gases. Journal of Geophysical Research 100, 20999-21012

Garland JA (1977) The dry deposition of sulfur dioxide to land and water surfaces. Proc. R. Soc. Lond. A354: 245-268

Garland JA (1978) Dry and wet removal of sulfur from the atmosphere. Atmospheric Environment 12: 349

Garland JA and Branson JR (1977) The deposition of sulfur fioxide to pine forest assessed by a radioactive tracer method. Tellus 29, 445-454

Gauger Th, Köble R Smiatek G (1997) Kartierung kritischer Belastungskonzentrationen und –raten für empfindliche Ökosysteme in der Bundesrepublik Deutschland und anderen ECE-Ländern. Endbericht zum Forschungsvorhaben 106 01 061 im Auftrag des Umweltbundesamtes. Institut für Navigation der Universität Stuttgart. - Teil 1: Deposition Loads. 126 p, Teil 2: Critical Levels. 75 p, Teil 3: Informationssystem CANDIS. 27 p

Gauger Th, Anshelm F, Köble R (2000) Kritische Luftschadstoff-Konzentrationen und Eintragsraten sowie ihre Überschreitung für Wald und Agrarökosysteme sowie naturnahe waldfreie Ökosysteme. Forschungsvorhaben im Auftrag des BMU/UBA, FE-Nr. 297 85 079. Institut für Navigation, Universität Stuttgart. Teil 1: Deposition Loads. 140 p. - Teil 2: Critical Levels. 57 p. [http://www.nav.uni-stuttgart.de/navigation/forschung/critical_loads]

Gauger Th, Anshelm F, Schuster H, Draaijers GPJ, Bleeker A, Erisman JW, Vermeulen AT, Nagel HD (2002) Kartierung ökosystembezogener Langzeittrends atmosphärischer Stoffeinträge und Luftschadstoffkonzentrationen in Deutschland und deren Vergleich mit Critical Loads und Critical Levels. Forschungsvorhaben im Auftrag des BMU/UBA, FE-Nr. 299 42 210. Institut für Navigation, Univ. Stuttgart. [http://www.nav.uni-stuttgart.de/navigation/forschung/critical_loads/]

Gauger Th (2005) Nationale Luftreinhaltestrategie – Umsetzung von EU-Anforderungen; Teilvorhaben 02: Aufbereitung, Nutzung und Weiterentwicklung nationaler, hochauflösender Datensätze zu Konzentrationen und Depositionen von Luftschadstoffen. Forschungsvorhaben im Auftrag des BMU/UBA, FE-Nr. 203 43 257/02. FAL-AOE, Braunschweig. 23 S. Text + 54 S. Anhang

Gravenhorst G, Kreilein K, Schnitzler K-G, Ibrom A, Nützmann E (2000) Trockene und nasse Deposition von Spurenstoffen in der Atmosphäre. In Gudreian G (ed.) Handbuch der Umweltveränderungen und Ökotoxikologie. Bd. 1B: Atmosphäre - Aerosol/ Multiphasenchemie – Ausbreitung und Deposition von Spurenstoffen – Auswirkungen auf Strahlung und Klima. Springer-Verlag. Berlin, Heidelberg, New York. 147-247.

Grünhage L, Dämmgen U, Hertstein U, Jäger HJ (1993) Response of grassland ecosystem to air pollutants: I – Experimental concept and site of the Braunschweig Grassland Investigation Program. Environmental Pollution 81. 163–171

Harley RA, Russell AG, McRae GJ, Cass GR. Seinfeld JH (1993) Photochemical modeling of the Southern California Air Quality Study. Environmental Science and Technology 27: 378-388.

Hass H, Jakobs HJ, Memmesheimer M (1995) Analysis of a regional model (EURAD) near surface gas concentration predictions using observations from networks. Meteorology and Atmospheric Physics 57: 173-200.

Hass H, van Loon M, Kessler C, Stern R, Matthijsen J, Sauter F, Zlatev Z, Langner J, Foltescu V, Schaap M (2003) Aerosol modelling: Results and Intercomparison from European Regional –scale modelling systems. Special Rep. EUROTRAC-2 ISS, München.

Hesterberg R, Blatter A, Fahrni M, Rosset M, Neftel A, Eugster W, Wanner H (1996) Deposition of Nitrogen-Containing Compounds to an Extensively Managed Grassland in Central Switzerland. Environmental Pollution 91 1 (1996), pp. 21–34

Hicks BB, Baldocchi DD, Meyers TP, Hosker RP Jr., Matt DR (1987) A preliminary multiple resistance routine for deriving dry deposition velocities from measured quantities. Water Air and Soil Pollution, 36: 311-330.

Hicks, B.B. and Garland, J.A. (1983) Overview and suggestions for future research on dry deopsition. Precipitation Scavenging, dry deposition and resuspension (ed. Pruppacher, Semonin and Slinn), Elsevier, New York: 1429-1432.

Hicks BB and Lenschow DH (eds.) (1989) Global Tropospheric Chemistry, Chemical Fluxes in the Global Atmosphere. Report prepared for the National Center for Atmospheric Research Boulder, CO.

Hicks BB, Baldocchi DD, Meyers TP, Hosker RP Jr,, Matt DR (1987) A preliminary multiple resistance routine for deriving dry deposition velocities from measured quantities. Water Air Soil Pollut. 36, 311-330

ICP Modelling and Mapping (1996) Manual on Methodologies and Criteria for Mapping Critical Levels/Loads and geographical areas where they are exceeded. UBA-Texte 71/96 [http://www.umweltdaten.de/uid/manual/manual_mapping.pdf]

ICP Modelling and Mapping (2002) [http://www.icpmapping.org/]

ICP Modelling and Mapping (2004): Manual on Methodologies and Criteria for Mapping Critical Levels/Loads and geographical areas where they are exceeded. UBA-Texte 52/[http://www.icpmapping.org/]

Ihle P, Bieber E, Kallweit D (2001) Das Depositionsmessnetz des Umweltbundesamtes (Aufbau, Betrieb, Ergebnisse). In: Ihle P [Hrsg.] Atmosphärische Depositionen in der Bundesrepublik Deutschland. Teubner Stuttgart, Leipzig, Wiesbaden. 13-73

Ilyin I and Travnikov O (2005) Modelling of Heavy Metal Airborne Pollution in Europe: Evaluation of the Model Performance. Meteorological Synthesizing Centre – East, EMEP/MSC-E Technical Report 8/2005, August 2005 [http://www.emep.int/publ/emep2005_publications.html]

IPCC – Intergovernmental Panel on Climate Change (1996) Revised 1996 IPCC Guidelines for National Greenhouse Gas Inventories. Vol. 3. Greenhouse Gas Inventory Reference Manual. IPCC WGI Technical Support Unit, Bracknell

IPCC – Intergovernmental Panel on Climate Change (2000) Good Practice Guidance and Uncertainty Measurement in National Greenhouse Gas Inventories. IPCC National Greenhouse Gas Inventories programme. Technical Support Unit. Hayama

Jacob DJ (2000) Heterogeneous chemistry and tropospheric ozone, Atmospheric Environment, 34, 2131-2159

Janssen AJ and Asman, WAH (1988) Effective removal parameters in long-range air pollution transport models, Atmospheric Environment, 22, 359-367

Jarvis PG, James GB, Landsberg JJ (1976) Coniferous forest. In J.L. Monteith (ed.), Vegetation and the atmosphere –2. Academic Press, New York

Jarvis PG and Morison JIL (1981) The control of transpiration and photosynthesis by stomata. In Stomatal Physiology (ed. Jarvis, P.G. and Mansfield, T.A.). Cambridge Univ. Press, Cambridge. pp. 248-279

Jensen-Huß K (1990) Raumzeitliche Analyse atmospärischer Stoffeinträge in Schleswig-Holstein und deren ökologische Bewertung. Dissertation an d. Math.-Naturwiss. Fakultät d. Chr.-Albr.-Universität zu Kiel. 212 p

Kallweit D (1997) Geeignete Sammelverfahren zur Erfassung von Depositionen und Anwendung im UBA-Messnetz. In: Landesanstalt für Umweltschutz Baden-Württemberg (Hrsg.): Ermittlung atmosphärischer Stoffeinträge in den Boden. Nutzung neuer Sammel- und Nachweisverfahren. Fachgespräch am 27.11.1996 in Karlsruhe. Handbuch Boden 5: 41-47

Kane MM, Rendell AR, Jickells TD (1994) Atmospheric scavenging processes over the North Sea. Atmospheric Environment, 28: 2523-2530

Kebreab E, France J, McBride BW, Odongo N, Bannink A, Mills JAN, Dijkstra J (2006) Evaluation of Models to Predict Methane Emissions from Enteric Fermentation in North American Dairy Cattle. In: Kebreab E, Dijkstra J, Bannink A, Gerrits WFF, France J (eds.) Nutrient Digestion and Utilization in Farm Animals. Modelling Approaches. CAB International, pg. 299-313

Kerminen VM, Hillamo R, Teinila K, Pakkanen T, Allegrini I, Sparapani R (2001) Ion balances of size-resolved tropospheric aerosol samples: implications for the acidity and atmospheric processing of aerosols, Atmos. Environ., 35 (31), 5255-5265

Kerschbaumer A and Reimer E (2003) Preparation of Meteorological input data for the RCG-model, UBA-Rep. 299 432 46, Free Univ. Berlin Inst for Meteorology (in German)

Khasibatla P, Chameides WL, Duncan B, Houyoux M, Jang C, Mathur R, Odman T, Xiu A (1997) Impact of inert organic nitrate formation on ground-level ozone in a regional air quality modelusing the carbon bond mechanism 4. Geophysical Research Letters, 24, 3205-3208

Klein H and Benedictow A (2006) Transboundary air pollution by main pollutants (S, N, O3) and PM. Germany. MSC-W Data Note 1/2006. Date: December 2006. METEOROLOGISK INSTITUTT. Norwegian Meteorological Institute. EMEP/MSC-W. Data Note 2006. ISSN 1890-0003. [http://www.emep.org]

Köble R und Spranger T (1999) Definition und Kartierungsmethoden. In Nagel HD und Gregor HD [Hrsg.]: Ökologische Belastungsgrenzen – Critical Loads & Levels. Ein internationales Konzept für die Luftreinhaltepolitik. Springer-Verlag.

Kouvarakis G, Doukelis Y, Mihalopoulos N, Rapsomanikis S, Sciare J, Blumthaler M (2002) Chemical, physical, and optical characterization of aerosols during PAUR II experiment, J Geophys Res., 107(D18), 8141, doi:10.1029/2000JD000291

Krupa SV (2002) Sampling and physico-chemical analysis of precipitation: a review. Environmental Pollution 120, 565–594.

Leucken DJ, Berkowitz CM, Easter RC (1991) Use of a three-dimensional cloud-chemistry model to study the transatlantic transport of soluble sulfur species. Journal of Geophysical Research 96: 22477-22490

Liu MK and Durran D (1977) Development of a regional air pollution model and its application to the Northern Great Plains. US-EPA (EPA-908/1-77-001)

Logan J (1998) An analysis of ozonesonde data for the troposphere, recommendations for testing 3-D models and development of a gridded climatology for tropospheric ozone, J. Geophys. Res. 104, 16, 1998

Lövblad G, Erisman JW, Fowler D (eds.) (1993) Models and methods for the quantification of atmospheric input to ecosystems. Proceedings of an international workshop on the deposition of acidifying substances, Göteborg (Sweden), 3-6 November 1992. The Nordic Council of Ministers. Copenhagen. Report No. Nord 1993:573

Lövblad G and Erisman JW (1992) Deposition of nitrogen in Europe. In Proc. Critical Loads for Nitrogen, Lökeberg, Sweden, 6-10 April 1992 (eds. Grennfelt, P. and Thörnelöf, E.), Nordic Council of Ministers, Copenhagen, Denmark. Report no. Nord 1992:41

Lovett GM (1994) Atmospheric deposition of nutrients and pollutants in North America: An ecological perspective. Ecological Applications 4: 629-650

Lux W (1993) Das PROGRAMM "Biologische Umweltkontrolle durch Waldökosysteme" (Teil 1). Umweltbehörde Hamburg, Fachamt für ökologische Forst- u. Landwirtschaft. Institut für Bodenkunde, Hamburg. 53 p

Massman WJ, Pederson J, Delany A, Grantz D, den Hartog G, Neumann HH, Oncley SP, Pearson R Jr., Shaw RH (1994) An evaluation of the regional acid deposition model surface module for ozone uptake at three sites in the San Joaquin Valley of California. Journal of Geophysical Research 99: 8281-8294

Meng Z and Seinfeld JH (1996) Timescales to achieve atmospheric gas-aerosol equilibrium for volatile species, Atmos. Environ., 30, 2889-2900

Mentel TF, Sohn M, Wahner A (1999) Nitrate effect in the heterogeneous hydrolysis of dinitrogen pentoxide on aqueous aerosols, Phys. Chem. Chem. Phys., 1, 5451-5457

Meyers TP, Finklestein P, Clarke J, Ellestad T, Sims PF (1998) A multi-layer model for inferring dry deposition using standard meteorological measurements. Journal of Geophysical Research 103, 22645-22661

Meyers TP, Hicks BB, Hosker RP, Womack JD, Satterfield LC (1991) Dry deposition inferential measurement techniques-II. Seasonal and annual deposition rates of sulfur and nitrate. Atmospheric Environment 25A: 2361-2370

Mohr K, Meesenburg H, Horváth B, Meiwes KJ, Schaaf S, Dämmgen U (2005) Bestimmung von Ammoniak-Einträgen aus der Luft und deren Wirkungen auf Waldökosysteme (ANSWER-Projekt). Schlussbericht. BMU/UBA 200 88 213. Oldenburg, Göttingen und Braunschweig, März 2005. Landbauforschung Völkenrode. Sonderheft 279. 113 S.

Monahan EC, Spiel DE, Davidson KL (1986) A model of marine aerosol generation via whitecaps and wave disruption. In Oceanic Whitecaps and their role in air/sea exchange, edited by Monahan EC and Mac Niocaill G, pp. 167-174, D. Reidel, Norwell, Mass., USA

Monteith JL (1975) Vegetation and the atmosphere. Academic Press, London, England

Müller-Westermeier G (1995) Numerisches Verfahren zur Erstellung klimatologischer Karten. Berichte des Deutschen Wetterdienstes (DWD), Nr. 193. Offenbach. 18 S.

Nagel HD, Gregor HD [Eds.] (1999) Ökologische Belastungsgrenzen – Critical Loads & Levels. Ein internationales Konzept für die Luftreinhaltepolitik. Springer-Verlag. 320 S.

Nagel HD, Becker R, Eitner H, Kunze F, Schlutow A, Schütze G (2000) Kartierung von Critical Loads von Säure, eutrophierendem Stickstoff, POP's und Schwermetallen in Waldökosysteme und naturnahe waldfreie Ökosysteme zur Unterstützung von UN/ECE-Protokollen. Abschlussbericht zum F/E-Vorhaben 297 730 11 des Umweltbundesamtes, Berlin.

Nagel HD, Becker R, Eitner H, Kunze F, Schlutow A, Schütze G (2002) Kartierung von Critical Loads für Säure und Stickstoff. Zwischenbericht zum F&E-Vorhaben 200 85 212 im Auftrag des Umweltbundesamtes

NEGTAP (2001) Transboundary Air Pollutin: Acidification, Eutrophication and Ground-Level Ozone in the UK. Report prepared by the National Expert Group on Transboundary Air Pollution at CEH Edinbourgh on behalf of the UK Department for Environment, Food and Rural Affairs, Scottish Executive, The National Assembly for Wales/Cynulliad Cenedlaethol Cymru, Department Of the Environment in North Ireland.314 p. [http://www.nbu.ac.uk/negtap/]

Nenes A, Pilinis C, Pandis SN (1998) Isorropia: A new thermodynamic model for multiphase multicomponent inorganic aerosols, Aquatic Geochemistry, 4, 123-152

Nenes A, Pilinis C, Pandis SN (1999) Continued Development and Testing of a New Thermodynamic Aerosol Module for Urban and Regional Air Quality Models, Atmos. Env., Vol. 33 , pp.1553-1560

NOAA (1997) NOAA library of input data for 'Big-leaf' and 'Multi-layer' models. ATDD, NOAA, Oak Ridge, Tennessee

Olson JS, Watts JA, Allison LJ (1985) Major World Ecosystem Complexes Ranked by Carbon in Live Vegetation: A Database NDP017, Carbon Dioxide Information Center, Oak Ridge Laboratory, Oak Ridge, Tennessee

Padro J, den Hartog G, Neumann HH (1991) An investigation of the ADOM dry deposition module using summertime O3 measurements above a deciduous forest. Atmospheric Environment 25A: 1689-1704

Pederson JR, Massman WJ, Mahrt L, Delany A, Oncley S, den Hartog G, Neumann HH, Mickle RE, Shaw RH, Paw UKT, Grantz DA, MacPherson JI, Desjardins R, Schuepp PH, Pearson R Jr., Arcado TE (1995) California Ozone Deposition Experiment: methods, results, and opportunities. Atmospheric Environment 29: 3115-3132

Perry JH (ed.) (1950) Chemical Engineers Handbook. 3rd edn. McGraw-Hill, New York

Pleim JE, Venkatram A, Yamartino R (1984) ADOM/TADAP Model Development Program. The Dry Deposition Module, vol. 4. Ontario Ministry of the Environment, Rexdale, Canada

Poppe D, Andersson-Sköld Y, Baart A, Builtjes PJH, Das M, Fiedler F, Hov O, Kirchner F, Kuhn M, Makar PA, Milford JB, Roemer MGM, Ruhnke R, Simpson D, Stockwell WR, Strand A, Vogel B, Vogel H (1996) Gas-phase reactions in atmospheric chemistry and transport models: a model intercomparison. Eurotrac report. ISS, Garmisch-Partenkirchen.

Reynolds B, Fowler D, Smith RI, Hall JR (1997) Atmospheric inputs and catchment solute fluxes for major ions in five Welsh upland catchments. Journal of Hydrology, 194: 305-329

Roemer M (1995) The tropospheric budgets and trends of methane, carbon monoxide and ozone on a global scale. TNO-publication P95/035, Delft, The Netherlands

Roemer M, Beekmann M, Bergström R, Boersen G, Feldmann H, Flatøy F, Honore C, Langner J, Jonson JE, Matthijsen J, Memmesheimer M, Simpson D, Smeets P, Solberg S, Stern R, Stevenson D, Zandveld P, Zlatev, Z (2003) Ozone trends according to ten dispersion models, Special Rep. EUROTRAC-2 ISS , München

Ruijgrok W, Davidson CI, Nicholson KW (1995) Dry deposition of particles. Implications and recommendations for mapping of deposition over Europe. Tellus 47B, 587-601

Ruijgrok W, Tieben H, Eisinga P (1997) The dry deposition of particles to a forest canopy: a comparison of model and experimental results. Atmospheric Environment 31: 399-415

Sachs L (1989) Angewandte Statistik. Anwendung statistischer Methoden. Springer-Verlag. Berlin, Heidelberg, New York, Tokyo. 552 S

Sachs L (1997) Angewandte Statistik. Anwendung statistischer Methoden. 8., völlig neu bearb. und erw. Aufl. Springer-Verlag. Berlin, Heidelberg, New York

Sager (1997) Die Niedersclagsbeschaffenheits-Richtlinie der Länderarbeitsgemeinschaft Wasser (LAWA). In Landesanstalt für Umweltschutz Baden-Württemberg (ed): Ermittlung atmosphärischer Stoffeinträge in den Boden. Nutzung neuer Sammel- und Nachweisverfahren. Fachgespräch am 27.11.1996 in Karlsruhe. Handbuch Boden 5: pp. 56-64 [http://www.xfaweb.baden-wuerttemberg.de/bofaweb/print/mzb05.pdf]

SAI (1996) User's Guide to the Variable-Grid Urban Airshed Model (UAM-V). SYSAPP-96-95/27r, Systems Applications International, San Rafael, CA

Sandnes H (1993) Calculated budgets for airborne acidifying components in Europe, 1985, 1987, 1988. 1989, 1990, 1991 and 1992. EMEP report 1/93. MSC-West, Oslo, Norway

Schaap M, Mueller K, ten Brink HM (2002) Constructing the European aerosol nitrate concentration field from quality analysed data, Atmos. Environ,, 36 (8), 1323-1335

Schaap M, van Loon M, ten Brink HM, Dentener FD, Builtjes PJH (2004a) 'Secondary inorganic aerosol simulations for Europe with special attention to nitrate', Atmos. Phys. Chem., Vol. 4, pp.857-874

Schaap M, Spindler G, Schulz M, Acker K, Maenhaut W, Berner A, Wieprecht W, Streit N, Mueller K, Brüggemann E, Putaud JP, Puxbaum H, Baltensperger U, ten Brink HM (2004b) Artefacts in the sampling of nitrate studied in the "INTERCOMP" campaigns of EUROTRAC-AEROSOL, Atmos. Environ., 48, 6487-6496

Schaap M, Denier Van Der Gon HAC, Dentener FJ, Visschedijk AJH, van Loon M, Ten Brink HM, Putaud JP, Guillaume B, Liousse C, Builtjes PJH (2004c) Anthropogenic Black Carbon and Fine Aerosol Distribution over Europe. J. Geophys. Res., Vol. 109, D18201, doi: 10.1029/2003JD004330.

Schaap M, Roemer M, Sauter F, Boersen G, Timmermans R, Builtjes PJH (2005) LOTOS-EUROS Documentation, TNO report B&O 2005/297, TNO, Apeldoorn, The Netherlands.

Schimmig CG (1991) Wasser-, Luft-, Nähr- und Schadstoffdynamik charakteristischer Böden Schleswig-Holsteins. Dissertation. Schriftenr. Nr. 13 aus dem Institut für Pflanzenern. und Bodenkunde der Chr.-Albr.-Universität zu Kiel. 163 S

Schulze ED and Hall AE (1982) Stomatal responses, water loss and CO2 assimilation rates of plants in contrasting environments. In Encyclopedia of Plant Physiology, vol 12B (ed. Lange OL, Nobel PS, Osmond CB, Ziegler H), pp. 181-230. Springer, Berlin

Sehmel GA (1980) Particle and gas dry deposition: a review. Atmospheric Environment 14: 983-1011

Simon KH, Westendorff K (1991) Stoffeinträge mit dem Niederschlag in Kiefernbestände des norddeutschen Tieflandes in den Jahren 1985-1989. Beitr. Forstwissenschaft 25, 4. pp. 177-180

Simpson D, Fagerli H., Jonson J, Tsyro S, Wind P, Tuovinen JP, (2003a) EMEP MSC-W Report 1/2003, Transboundary Acidification, Eutrophication and Ground Level Ozone in Europe. Part I. The EMEP unified Eulerian model. Model description. The Norwegian Meteorological Institute, Oslo, Norway

Simpson D, Fagerli H, Solberg S, Ås W, (2003b) EMEP Report 1/2003, Transboundary Acidification, Eutrophication and Ground Level Ozone in Europe. Part II. Unified EMEP Model Performance. The Norwegian Meteorological Institute, Oslo, Norway

Simpson D, Butterbach-Bahl K, Fagerli H, Kesik M, Skiba U, Tang S (2006) Deposition and emissions of reactive nitrogen over European forests: A modelling study Atm. Env. 40. 2006. p 5712-5726

Slinn WGN (1982) Predictions for particle deposition to vegetative surfaces. Atmospheric Environment 16, 1785-1794

Spranger T (1992) Erfassung und ökosystemare Bewertung der atmosphärischen Deposition und weiterer oberirdischer Stoffeinflüsse im Bereich der Bornhöveder Seenkette. EcoSys, Beiträge zur Ökosystemforschung. Suppl. Bd. 4. 153 S

Spranger T, Hollwurtel E, Poetzsch-Heffter F, Branding A (1994) Dry deposition Estimates from Two Different Inferential Models as compared to Net Throughfall Measurements. A contribution to the subproject BIATEX. In Proceedings of EUROTRAC Symposium '94 (ed. P.M. Borrell et al.), SPB Academic Publishing bv, The Hague, The Netherlands. pp. 615-619

Spranger T, Kunze F, Gauger Th, Nagel HD, Bleeker A, Draaijers G (2001) Critical Loads Exceedances in Germany and their Difference on the Scale of Input Data. Water, Air, and Soil Pollution. Focus 1. 2001: 335-351

Stolbovoi V and McCallum I (2002) CD-ROM "Land Resources of Russia", International Institute for Applied Systems Analysis and the Russian Academy of Science, Laxenburg, Austria

Sutton MA (1990) The surface-atmosphere exchange of ammonia. Ph. D. thesis, University of Ëdinburgh, Scotland

Sutton MA, Moncrieff JB, Fowler D (1992) Deposition of atmospheric ammonia to moorlands. Environ. Pollut. 75: 15-24

Thom AS (1975) Momentum, mass and heat exchange of plant communities. In Vegetation and Atmosphere. Ed Monteith JL. Academic Press, London. pp. 58-109

Travnikov O and Ilyin I (2005), Regional model MSCE-HM of heavy metal transboundary air pollution in Europe, EMEP/MSC-E Technical report 6/2005 [http://www.msceast.org/publications.html]

Tuovinen JP, Aurela M, Laurila T (1998) Resistances to ozone deposition to flark fen in the northern aapa mire zone. Journal of Geophysical Research 103, 16953-16966

Turner NC and Begg JE (1974) Stomatal behavior and water status of maize, sorghum and tobacco under field conditions. I: at high soil water potential. Plant Physiol. 51: 31-36

UBA (1996) Manual on Methodologies and Criteria for Mapping Critical Levels/Loads and geographical areas where they are exceeded. UBA-Texte 71/96. [http://www.umweltbundesamt.de/mapping/]

UBA (1997) Ergebnisse täglicher Niederschlagsanalysen in Deutschland von 1982 bis 1995. UBA-Texte 10/97. Umweltbundesamt Berlin. 452 S. und Anhang.

UBA (2007) Berichterstattung 2007 unter dem Übereinkommen über weiträumige grenzüberschreitende Luftverschmutzung (UN ECE-CLRTAP). Inventartabellen im New Reporting Format (NFR). NFR 2007 (XLS in ZIP, circa 970 kB) [http://www.umweltbundesamt.de/emissionen/archiv/DE_2007_Tables_IV1A_1990_2005.zip]

Ulrich B (1983) Interaction of forest canopies with atmospheric constituents: SO_2, alkali and earth alkali cations and chloride. In Ulrich B. and J. Pankrath (eds), Effects of accumulation of air pollutants in forest ecosystems, Reidel, Dordrecht, The Netherlands: 33-45

Ulrich B (1991) Rechenweg zur Schätzung der Flüsse in Waldökosystemen. Identifizierung der sie bedingten Prozesse. Berichte des Forschungszentrums Waldökosysteme, Reihe B, Bd. 24: 204-210

van den Broek MMP, Sauter F, van Pul WAJ, van Jaarsveld H (2008) Modelled and measured ammonia concentrations over The Netherlands - The effect of dry deposition parameterization. Presentation at NitroEurope IP Open Science Conference Reactive Nitrogen and the European Greenhouse Gas Balance 20th - 21st February 2008 at Het Pand, Ghent, Belgium [http://nitrogen.ceh.ac.uk/conference2008/presentations.html]

van den Hout KD (ed.) (1994) The Impact of atmospheric deposition of non-acidifying compounds on the air quality of European forest soils and the North Sea. Main report of the ESQUAD project. Delft, The Netherlands. TNO report R93/329

van Jaarsveld JA (1989) A model approach for assessing transport and deposition of acidifying components on different spatial scales. In: Changing composition of the Troposphere: Special environmental report no.17. Geneva, Swizerland. WMO-no. 724. p. 197-204

van Jaarsveld JA (1990) An Operational atmosferic transport model for Priority Substances; specification and instructions for use. RIVM, Bilthoven, The Netherlands. Report no. 222501002.

van Jaarsveld JA (1995) Modelling the long-term atmospheric behaviour of polluants on various spatial scales. Ph.D. thesis. University of Utrecht, The Neterlands. RIVM, Bilthoven, The Netherlands. Report no. 722501005

van Jaarsveld JA, van Aalst RM, Onderdelinden D (1986) Deposition of metals from the atmosphere into the North Sea: model calculations. RIVM, Bilthoven, The Netherlands. Report no. 842015002

van Loon M, Roemer M, Builtjes PJH (2004) Model intercomparison in the framework of the review of the Unified EMEP model, TNO-Rep. R 2004/282, Apeldoorn, The Netherlands

van Loon M, Vautard R, Schaap M, Bergström R, Bessagnet B, Brandt B, Builtjes PJH, Christensen JH, Cuvelier K, Graf A, Jonson JE, Krol M, Langner J, Roberts P, Rouil L, Stern R, Tarrasón L, Thunis P, Vignati P, White L, Wind P (2007) Evaluation of long-term ozone simulations from seven regional air quality models and their ensemble average, Atmospheric Environment, 41 (10), 2083-2097

van Pul, WAJ and Jacobs AFG (1993) The conductance of a maize crop and the underlying soil to ozone under various environmental conditions. Boundary Layer Met.

van Pul WAJ, Erisman JW, van Jaarsveld JA, de Leeuw FAAM (1992) High resolution assessment of acid deposition fluxes. In Acidification Research, Evaluation and policy applications (edited by T. Schneider), Studies in Environmental Science, Elsevier, Amsterdam

van Pul WAJ, Potma C, van Leeuwen EP, Draaijers GPJ, Erisman JW (1995) EDACS: European Deposition maps of Acidifying Components on a Small scale. Model description and results. RIVM report no. 722401005, National Institute of Public Health and the Environment, Bilthoven, The Netherlands

Velders GJM, de Waal ES, van Jaarsveld JA, Ruiter JF (2003) The RIVM-MNP contribution to the evaluation of the EMEP Unifed (Eulerian) model. RIVM report 500037002 / 2003. 32 p

Veldt, C (1991) The use of biogenic VOC measurements in emission inventories. MT-TNO Rep 91-323, 1991.

Veltkamp AC and Wyers GP (1997) The contribution of root-derived sulfur to sulfate in throughfall in a Douglas fir forest. Atmospheric Environment 31: 1385-1391

Venkatram A, Karamchandi PK, Misra PK (1988). Testing a comprehensive acid deposition model. Atmospheric Environment 22: 737-747

Vermetten AWM, Hofschreuder P, Duyzer JH, Diederen HSMA, Bosveld FC, Bouten W (1992) Dry deposition of SO2 onto a stand of Douglas fir: the influence of canopy wetness. In Proceedings of the 5th IPSASEP-conference, Richland WA, USA, June 15-19, 1991 (eds. Schwartz, S.E. and Slinn, W.G.N.), Hemisphere Publishing Corporation, Washington. pp. 1403-1414

Visschedijk AJH and Denier van der Gon HAC (2005) Gridded European anthropogenic emission data for NO_X, SO_X, NMVOC, NH_3, CO, PPM10, PPM2.5 and CH_4 for the year 2000', TNO-Report B&O-A R 2005/106

Voldner E C, Barrie LA, Sirois A (1986) A literature review of dry deposition of oxides of sulphur and nitrogen with emphasis on long-range transport modeling in North America. Atmospheric Environment 20: 2101-2123

Walcek CJ (2000) Minor flux adjustment near mixing ratio extremes for simplified yet highly accurate monotonic calculation of tracer advection, J. Geophy. Res., Vol. 105, D7, pp.9335-9348

Walmsley JL and Wesely ML (1996) Modification of coded parameterizations of surface resistances to gaseous dry deposition. Atmospheric Environment 30: 1181-1188

Warmenhoven JP, Duiser JA, de Leu LTh, Veldt C (1989) The contribution of the input from the atmosphere to the contamination of the North Sea and the Dutch Wadden Sea. TNO, Delft, The Netherlands. TNO Report R 89/349A

Wesely ML (1989) Parameterization of surface resistances to gaseous dry deposition in regional-scale numerical models. Atmospheric Environment 23, 1293-1304

Wesely ML and Hicks BB (1977) Some factors that affect the deposition rates of sulfur dioxide and similar gases on vegetation. J. Air Pollut. Control Assoc. 27: 1110-1116

Wesely ML and Hicks BB (2000) A review of the current status of knowledge on dry deposition. Atmospheric Environment 34, 2261-2282

Wesely ML, Sisteron DL, Hart RL, Drapapcho DL, Lee IY (1989) Observations of nitric oxide fluxes over grass. J. atmos. Chem. 9: 447-463

Whitten G, Hogo H, Killus J (1980) The Carbon Bond Mechanism for photochemical smog. Env. Sci. Techn., Vol. 14, pp.14690-14700

Wilson MF and HendersonSellers A (1985) A Global Archive of Land Cover and Soils Data for Use in General Circulation Climate Models. Journal of Climatology, vol. 5: 119143

Yamartino RJ, Flemming J, Stern RM (2004) Adaption of analytic diffusivity formulations to eulerian grid model layers finite thickness, 27th ITM on Air Pollution Modelling and its Application. Banff, Canada, October 24-29, 2004

Yamartino RJ, Scire JS, Carmichael GR, Chang YS (1992) The CALGRID mesoscale photochemical grid model-I. Model evaluation. Atmospheric Environment 26A: 1493-1512

Zhang Y, Seigneur C, Seinfeld JH, Jacobson M, Clegg SL, Binkowski FS (2000) A comparative review of inorganic aerosol thermodynamic equilibrium modules: differences, and their likely causes, Atmospheric Environment, 34, 117

Acronyms of wet deposition data sources

BFH-BAR: Bundesforschungsanstalt für Holz- und Forstwirtschaft; Eberswalde (Simon&Westendorff)
BGR: Bundesanstalt für Geowissenschaften und Rohstoffe; Hannover (FRANKEN ET AL.)
BLFU: Bayerische Landesanstalt für Umweltschutz; Schloss Steinhausen, Kulmbach
BLFU: Bayerische Landesanstalt für Umweltschutz (former BLFW: Bayerisches Landesamt für Wasserwirtschaft), München
BLWF: Bayerische Landesanstalt für Wald- und Forstwirtschaft, Abt. Forsthydrologie; Freising
CGU: Èeský geologický ústav [Tschechischer Geologischer Dienst; Czech Geological Survey]; Prag, Tschechien
CHMI: Czech Hydrometeorological Institute; Prag, Tschechien
DDR-MD: Meteorologischer Dienst der DDR (via SLUG)
DWD: Deutscher Wetterdienst, Meteorologisches Observatorium Hohenpeißenberg
FAL: Bundesforschundsanstalt für Landwirtschaft, FAL-AOE, Braunschweig (former Institut für agrarrelevante Klimaforschung; Müncheberg und Braunschweig) (DÄMMGEN ET AL.)
FAWF-RP: Forschungsanstalt für Waldökologie und Forstwirtschaft, Rheinland-Pfalz (former Forstliche Versuchsanstalt Rheinland-Pfalz, FVA-RP) Abt. Waldschutz; Trippstadt
FhG: Fraunhofer Gesellschaft für Umweltchemie und Ökotoxikologie, Schmallenberg, Grafschaft
FPA-SB: Forstplanungsanstalt des Saarlandes; Saarbrücken/Univ. des Saarlandes, ZFU, AG-Forst; Duttweiler/Saarbrücken
FVA-BW: Forstliche Versuchs- und Forschungsanstalt Baden-Württemberg; Freiburg i. B.
FVA-RP: Forstliche Versuchsanstalt Rheinland-Pfalz, Abt. Waldschutz; Trippstadt; jetzt: FAWF-RP
FVFA-ST: Forstliche Versuchs- und Forschungsanstalt; Flechtingen
GIOS: Glowny Inspektorat Ochrony Srodowiska (GIOS), Departament Monitoringu, Wrozlaw, Polen
HBUAVCR: Hydrobiologicky ustav AV CR (HBU), Akademie ved Ceske republiky (AV CR) [Hydrobiologisches Institut der Akademie der Wissenschaften der Tschechischen Republik]; Ceske Budejovice, Tschechien
HLFUG: Hessische Landesanstalt für Umwelt und Geologie, Wiesbaden
HLFWW: Hessische Landesanstalt f. Forsteinrichtung, Waldforschung und Waldökologie; Hannoversch Münden
IFER: Ústav pro výzkum lesních ekosystému, s.r.o. [Institute of Forest Ecosystem Research, Ltd. - Institut für Forstökosysytemforschung], Jílové u Prahy, Tschechien
IFT: Institut für Troposphärenforschung e.V., Abt. Chemie; Leipzig
IMGW: Institute of Meteorology and Water Management, (IMGW), Wroclaw Branch, Polen
LAFOP-BB: Landesanstalt für Forstplanung, Brandenburg; Potsdam
LAFOP-MV: Landesamt für Forstplanung; Schwerin
LANU-SH: Landesamt für Natur und Umwelt des Landes Schleswig-Holstein, Abteilung Gewässer; Flintbeck (former Landesamt für Wasserhaushalt und Küsten, LaWaKü, Kiel)
LAUN-MV: Landesamt für Umwelt und Natur, Abt. Immissionsschutz; Güstrow-Gülzow
LFU-BW: Landesanstalt für Umweltschutz Baden-Württemberg, Ref. 31 Luftreinhaltung Klima; Karlsruhe
LfU-ST: Landesamt für Umweltschutz Sachsen-Anhalt, Abt.5, Halle
LANUV-NW: Das Landesamt für Natur, Umwelt und Verbraucherschutz Nordrhein-Westfalen [former LÖBF/LAFAO-NW (former LÖLF): Landesanstalt für Ökologie, Bodenordnung und Forsten/Landesamt für Agrarordnung Dez. Bioindikation, Biomonitoring; Recklinghausen], Abteilung 2, Naturschutz, Landschaftspflege; 25 Monitoring, Effizienzkontrolle in Naturschutz und Landschaftspflege]
LANUV-NW: Das Landesamt für Natur, Umwelt und Verbraucherschutz Nordrhein-Westfalen [former: LUA-NW: Landesanstalt für Umweltschutz (former LIS), Nordrhein-Westfalen, Abt. 3; Essen], Abteilung 3, Umweltwirkungen, Umwelt- und Verbraucherschutzberichterstattung, Umweltbildung; 31 Umweltwirkungen auf Mensch, Pflanze und Materialien; Gerüche
LUA-BB: Landesumweltamt Brandenburg, Abteilung ÖNW Ökologie, Naturschutz, Wasser; Ö 3 Umweltbeobachtung, Ökotoxikologie
TLWJF: Thüringer Landesanstalt für Wald, Jagd und Fischerei; Gotha (former Thüringer Landesanstalt für Wald und Forstwirtschaft, LWF-TN)
NFVA: Niedersächsische Forstliche Versuchsanstalt, Abt. Umweltkontrolle; Göttingen
NLÖ-H: Niedersächsisches Landesamt für Ökologie, Dez.63 Luftreinhaltung, Dr. K.-P. Giesen; Hannover
NLÖ-HI: Niedersächsisches Landesamt für Ökologie, Abt. 6 Immissionsschutz; Hildesheim
SenV-B.: Senatsverwaltung für Stadtentwicklung und Umweltschutz, Abt. III A 31; Berlin
SLAF: Sächsische Landesanstalt für Forsten; Graupa
SLFL: Sächsische Landesanstalt für Landwirtschaft, Fb. 4, Pflanzliche Erzeugung, Ref. 41, Pflanzenbau, Leipzig
SLUG: Sächsische Landesanstalt für Umwelt und Geologie, Abt. L1 Luft-Lärm-Strahlen; Radebeul
STUA-SH (former GAA-SH): Staatliches Umweltamt Itzehoe, Lufthygienische Überwachung Schleswig-Holstein, former Gewerbeaufsichtsamt Schleswig-Holstein, Dez. Luftqualitätsüberwachung
TLL: Thüringer Landesanstalt für Landwirtschaft, Abteilung 700: Agrarökologie, Ackerbau und Grünland, Jena
TLWJF: Thüringer Landesanstalt für Wald, Jagd und Fischerei, Gotha (former Landesanstalt für Wald und Forstwirtschaft, Gotha LWF-TN)
TU Wien: Technische Universität Wien, Institut für Analytische Chemie, Abt. Umweltanalytik
TU-DD: Technische Universität Dresden, Institut für Pflanzen- und Holzchemie; Tharandt
TU-FRE: TU Bergakademie Freiberg, IÖZ, Freiberg
UBA-b (bulk): Umweltbundesamt, Fg. II 6,5 Meßnetz-Datenzentrale; Langen (former in Berlin)
UBA-wo (wet-only): Umweltbundesamt, Fg. II 6.5; Meßnetz-Datenzentrale; Langen
UFZ: Umweltforschungszentrum Leipzig-Halle GmbH, Sektion Analytik; Leipzig
Univ. F: Universität Frankfurt, Zentrum für Umweltforschung (ZUF)

Univ. HH: Freie und Hansestadt Hamburg - Umweltbehörde, Amt für Naturschutz und Landschaftspflege / Universität Hamburg, Institut für Bodenkunde (LUX)
Univ. KI: Christian-Albrechts-Universität Kiel, Öklologie-Zentrum (JENSEN-HUß; SCHIMMING; SPRANGER; BRANDING)
VULHM: Výzkumny ústav lesního hospodáøský a myslivosti [Forschungsinstitut für Forst und Wildmanagement], Prag, Tschechien
VUV: Výzkumny ústav vodohospodáøský T.G.M. [Forschungsinstitut für Wasserwirtschaft T.G.M], Ostrava, Tschechien

Authors

Corresponding author:
Thomas Gauger, Federal Agricultural Research Centre, Institute of Agroecology (FAL-AOE), Braunschweig
New address since 10/2007:
Institute of Navigation, Universität Stuttgart (INS), Breitscheidstraße 2, 70174 Stuttgart, Germany
e-mail: gauger@nav.uni-stuttgart.de; tel. +49-711-685-8-4177; www.nav.uni-stuttgart.de

Hans-Dieter Haenel, Federal Agricultural Research Centre, Institute of Agroecology (FAL-AOE), Braunschweig; Bundesallee 50, 38116 Braunschweig, Germany
since 2008: Johann Heinrich von Thünen-Institut, Federal Research Institute for Rural Areas, Forestry and Fisheries, Institute of Agricultural Climate Research (vTI-AK), Bundesallee 50, 38116 Braunschweig, Germany
e-mail: dieter.haenel@vti.bund.de

Claus Rösemann, Federal Agricultural Research Centre, Institute of Agroecology (FAL-AOE), Braunschweig; Bundesallee 50, 38116 Braunschweig, Germany
since 2008: Johann Heinrich von Thünen-Institut, Federal Research Institute for Rural Areas, Forestry and Fisheries, Institute of Agricultural Climate Research (vTI-AK), Bundesallee 50, 38116 Braunschweig, Germany
e-mail: claus.roesemann@vti.bund.de

Ulrich Dämmgen, Federal Agricultural Research Centre, Institute of Agroecology (FAL-AOE), Braunschweig; Bundesallee 50, 38116 Braunschweig, Germany
since 2008: Johann Heinrich von Thünen-Institut, Federal Research Institute for Rural Areas, Forestry and Fisheries, Institute of Agricultural Climate Research (vTI-AK), Bundesallee 50, 38116 Braunschweig, Germany
e-mail: daemmgen@vti.bund.de

Albert Bleeker, Energy research Center of the Netherlands (ECN) - Biomass, Coal & Environmental Research, Air Quality & Climate Change, P.O. Box 1, 1755 ZG Petten, The Netherlands
e-mail: a.bleeker@ecn.nl

Jan Willem Erisman, Energy research Center of the Netherlands (ECN) - Biomass, Coal & Environmental Research, Air Quality & Climate Change, P.O. Box 1, 1755 ZG Petten, The Netherlands
e-mail: erisman@ecn.nl

Alex T. Vermeulen, Energy research Center of the Netherlands (ECN) - Biomass, Coal & Environmental Research, Air Quality & Climate Change, P.O. Box 1, 1755 ZG Petten, The Netherlands
e-mail: a.vermeulen@ecn.nl

Martijn Schaap, Netherlands Organisation for Applied Scientific Research (TNO-B&O), Department of Environmental Quality, P.O Box 80015, 3508 TA Utrecht, The Netherlands
e-mail: martijn.schaap@tno.nl

R.M.A Timmermanns, Netherlands Organisation for Applied Scientific Research (TNO-B&O), Department of Environmental Quality, P.O Box 80015, 3508 TA Utrecht, The Netherlands

Peter J. H. Builtjes, Netherlands Organisation for Applied Scientific Research (TNO-B&O), Department of Environmental Quality, P.O Box 80015, 3508 TA Utrecht, The Netherlands
e-mail: peter.builtjes@tno.nl

Jan H. Duyzer, Netherlands Organisation for Applied Scientific Research (TNO-B&O), Department of Environmental Quality, P.O Box 80015, 3508 TA Utrecht, The Netherlands
e-mail: j.h.duyzer@tno.nl